frontiers | Research Topics

Gene regulation of fungal secondary metabolism

Edited by
Wenbing Yin, Hee-Soo Park and Pinmei Wang

Coordinated by
Wenjie Wang

Published in
Frontiers in Microbiology

FRONTIERS EBOOK COPYRIGHT STATEMENT

The copyright in the text of individual articles in this ebook is the property of their respective authors or their respective institutions or funders. The copyright in graphics and images within each article may be subject to copyright of other parties. In both cases this is subject to a license granted to Frontiers.

The compilation of articles constituting this ebook is the property of Frontiers.

Each article within this ebook, and the ebook itself, are published under the most recent version of the Creative Commons CC-BY licence. The version current at the date of publication of this ebook is CC-BY 4.0. If the CC-BY licence is updated, the licence granted by Frontiers is automatically updated to the new version.

When exercising any right under the CC-BY licence, Frontiers must be attributed as the original publisher of the article or ebook, as applicable.

Authors have the responsibility of ensuring that any graphics or other materials which are the property of others may be included in the CC-BY licence, but this should be checked before relying on the CC-BY licence to reproduce those materials. Any copyright notices relating to those materials must be complied with.

Copyright and source acknowledgement notices may not be removed and must be displayed in any copy, derivative work or partial copy which includes the elements in question.

All copyright, and all rights therein, are protected by national and international copyright laws. The above represents a summary only. For further information please read Frontiers' Conditions for Website Use and Copyright Statement, and the applicable CC-BY licence.

ISSN 1664-8714
ISBN 978-2-8325-3371-0
DOI 10.3389/978-2-8325-3371-0

About Frontiers

Frontiers is more than just an open access publisher of scholarly articles: it is a pioneering approach to the world of academia, radically improving the way scholarly research is managed. The grand vision of Frontiers is a world where all people have an equal opportunity to seek, share and generate knowledge. Frontiers provides immediate and permanent online open access to all its publications, but this alone is not enough to realize our grand goals.

Frontiers journal series

The Frontiers journal series is a multi-tier and interdisciplinary set of open-access, online journals, promising a paradigm shift from the current review, selection and dissemination processes in academic publishing. All Frontiers journals are driven by researchers for researchers; therefore, they constitute a service to the scholarly community. At the same time, the *Frontiers journal series* operates on a revolutionary invention, the tiered publishing system, initially addressing specific communities of scholars, and gradually climbing up to broader public understanding, thus serving the interests of the lay society, too.

Dedication to quality

Each Frontiers article is a landmark of the highest quality, thanks to genuinely collaborative interactions between authors and review editors, who include some of the world's best academicians. Research must be certified by peers before entering a stream of knowledge that may eventually reach the public - and shape society; therefore, Frontiers only applies the most rigorous and unbiased reviews. Frontiers revolutionizes research publishing by freely delivering the most outstanding research, evaluated with no bias from both the academic and social point of view. By applying the most advanced information technologies, Frontiers is catapulting scholarly publishing into a new generation.

What are Frontiers Research Topics?

Frontiers Research Topics are very popular trademarks of the *Frontiers journals series*: they are collections of at least ten articles, all centered on a particular subject. With their unique mix of varied contributions from Original Research to Review Articles, Frontiers Research Topics unify the most influential researchers, the latest key findings and historical advances in a hot research area.

Find out more on how to host your own Frontiers Research Topic or contribute to one as an author by contacting the Frontiers editorial office: frontiersin.org/about/contact

Gene regulation of fungal secondary metabolism

Topic editors

Wenbing Yin — Institute of Microbiology, Chinese Academy of Sciences (CAS), China

Hee-Soo Park — Kyungpook National University, Republic of Korea

Pinmei Wang — Zhejiang University, China

Topic coordinator

Wenjie Wang — Zhejiang Gongshang University, China

Citation

Yin, W., Park, H.-S., Wang, P., Wang, W., eds. (2023). *Gene regulation of fungal secondary metabolism*. Lausanne: Frontiers Media SA.

doi: 10.3389/978-2-8325-3371-0

Table of contents

frontiers | Frontiers in Microbiology

TYPE Editorial
PUBLISHED 15 August 2023
DOI 10.3389/fmicb.2023.1260849

Check for updates

OPEN ACCESS

EDITED AND REVIEWED BY
Biswarup Mukhopadhyay,
Virginia Tech, United States

*CORRESPONDENCE
Pinmei Wang
✉ wangpinmei@zju.edu.cn
Wen-Bing Yin
✉ yinwb@im.ac.cn

RECEIVED 18 July 2023
ACCEPTED 07 August 2023
PUBLISHED 15 August 2023

CITATION
Wang P, Park H-S, Wang W and Yin W-B (2023) Editorial: Gene regulation of fungal secondary metabolism. *Front. Microbiol.* 14:1260849. doi: 10.3389/fmicb.2023.1260849

COPYRIGHT
© 2023 Wang, Park, Wang and Yin. This is an open-access article distributed under the terms of the Creative Commons Attribution License (CC BY). The use, distribution or reproduction in other forums is permitted, provided the original author(s) and the copyright owner(s) are credited and that the original publication in this journal is cited, in accordance with accepted academic practice. No use, distribution or reproduction is permitted which does not comply with these terms.

Editorial: Gene regulation of fungal secondary metabolism

Pinmei Wang[1]*, Hee-Soo Park[2], Wenjie Wang[3] and Wen-Bing Yin[4]*

[1]Ocean College, Zhejiang University, Zhoushan, China, [2]School of Food Science and Biotechnology, Kyungpook National University, Daegu, Republic of Korea, [3]School of Food Science and Biotechnology, Zhejiang Gongshang University, Hangzhou, China, [4]State Key Laboratory of Mycology, Institute of Microbiology, Chinese Academy of Sciences, Beijing, China

KEYWORDS

gene regulation, transcription factors, fungal secondary metabolism, biosynthesis, secondary metabolites

Editorial on the Research Topic
Gene regulation of fungal secondary metabolism

Fungi are prolific producers of secondary metabolites (SMs), which encompass a wide range of low-molecular-mass compounds. These SMs serve essential functions such as defense against pathogens, inhibition of competing microorganisms, and intercellular communication (Keller, 2019; Yu et al., 2023). Therefore, SMs usually possess dual roles, hazardous mycotoxins (e.g., aflatoxin and patulin), and valuable pharmaceuticals (e.g., penicillin and lovastatin) (Wang et al., 2021b). Surprisingly, genome mining studies have unveiled that the potential of fungi to synthesize SMs has been greatly underestimated, as numerous of biosynthetic gene clusters (BGCs) remain silent or cryptic under laboratory culture conditions (Brakhage, 2013; Wang et al., 2021b). Transcription factors (TFs) play an essential regulatory role in the expression of SM genes (Yin and Keller, 2011; Keller, 2019; Wang et al., 2021a). In recent years, researchers have actively explored the gene regulation mechanism of fungal secondary metabolism by using the methods of genetics, molecular biology and biochemistry (Wang et al., 2022; Zhang et al., 2022; Wei et al., 2023). The aim of this Research Topic is to gain a better understanding of the regulatory elements and network of fungal SMs, providing genetic approaches to manipulate fungal secondary metabolism to produce novel compounds with beneficial properties for medicine, agriculture, and other applications.

This Research Topic contains one review paper and eight original research articles. Deng et al. review article presents a comprehensive summary of perylenequinones (PQs) with literatures spanning from 1967 to 2022. As photosensitizers, PQs have been applied in various fields, including medical, food, agricultural and manufacturing fields. The authors not only collected information of the sources, structure diversity and biological activities of PQs, but also the biosynthetic pathways and regulation mechanism. Besides, strategies are given to enhance PQ production and quality, including modulating regulatory mechanisms, coordinating signal-response pathways, constructing heterologous production platforms, and applying physical and chemical methods to stimulate biosynthesis.

Three research articles investigate the gene regulation of ganoderma triterpenoids (GTs) biosynthesis in *Ganoderma lucidum* and *Ganoderma lingzhi*, both of which are traditional Chinese medicines. GTs exhibit a variety of biological activities, and their biosynthesis is regulated through a complex interplay between environmental and genetic factors. Meng et al. employed a comprehensive approach involving transcriptome and metabolome analyses to investigate the transcription factors (TFs) involved in ganoderic acid (GA) biosynthesis in different developmental stages of *G. lucidum*. By comparing gene expression patterns, they identified that homeobox transcription factor and velvet family protein were responsible for GA biosynthesis, and provided a model for the involvement of TFs in GA biosynthesis during fruiting body formation. The research article by Luo et al. describes an essential function of the well-known methyltransferase LaeA in the regulation of GA in basidiomycete fungus *G. lingzhi*. The results of *laeA* gene deletion and overexpression suggested that LaeA could regulate the expression of GA biosynthetic genes and asexual sporulation. The study by Xu et al. focused on understanding how *G. lucidum* responds to methyl jasmonate, an important elicitor in inducing the production of triterpenes and the biomass of mycelia. Transcriptomic analysis allowed researchers to identify positive and negative transcription factors of GTs that response to methyl jasmonate, and a negative regulator gene *Glmhr1* was found. The study provides new insights into the molecular mechanisms underlying the response of *G. lucidum* to fungal hormones and may facilitate the development of new strategies for enhancing the production of bioactive compounds.

Other two studies explored the role of BcLAE1 and Bcfrp1 in the regulation of abscisic acid (ABA) biosynthesis and growth of *Botrytis cinerea*. The study conducted by Wei et al. demonstrated the significant role of the methyltransferase BcLAE1 in epigenetic regulation of ABA biosynthesis in *B. cinerea*. Chen et al. elucidated the positive role and molecular mechanism of an F-box protein Bcfrp1 in regulating ABA biosynthesis and fungal growth. These studies provide valuable insights into the molecular mechanisms involving the regulation of ABA biosynthesis in *B. cinerea*.

Additionally, two separate investigations have provided knowledge about the mechanisms governing microbe-microbe interactions and plant-microbe interactions, respectively. Brault et al. conducted a study revealing the crucial role of Sib proteins (Sib1, Sib2, and Sib3) in facilitating iron acquisition and cross-feeding interaction between *Schizosaccharomyces pombe* and *Saccharomyces cerevisiae*. These proteins are responsible for the transport of ferrichrome, and their knockout disrupted the transport process and hindered cross-feeding. In another article by Wu et al., they investigated the production and distribution of flavonoids by the endophytic fungus *Aspergillus* sp. Gbtc 2, which was isolated from the root of *Ginkgo biloba*. Through LC-MS analysis, they identified flavonoid metabolites and discovered a unique distribution pattern of these compounds, both intracellularly and extracellularly, within the fungus Gbtc 2. This research expands our understanding of the potential application of endophytic fungi in the industrial flavonoid production. In the study conducted by Wang et al., genomic alterations in *Fusarium proliferatum* strains were examined to understand their role in adaptation and fumonisin production. Through their analysis, a total of 121 distinct genomic loci were identified, implicating 85 potential genes involved in adaptation to diverse environments and fumonisin B1 (FB1) production. Notably, five candidate genes were identified as being closely associated with FB1 production.

The articles within this Research Topic collectively highlight the significance of gene regulation in the biosynthesis of secondary metabolites in fungi. By investigating the regulatory mechanisms governing these processes, researchers can attain a comprehensive comprehension of the molecular mechanisms underlying fungal secondary metabolism. Moreover, these studies enable the identification of potential targets for genetic engineering, aiming to augment the production of bioactive compounds by these organisms. Such findings carry significant implications across various fields including medicine, agriculture, and biotechnology, as they contribute to the exploration and development of novel bioactive compounds of interest.

Author contributions

PW: Writing—original draft. H-SP: Writing—review and editing. WW: Writing—review and editing. W-BY: Writing—review and editing.

Funding

This research was supported in part by National Natural Science Foundation of China (32170066), the Key Laboratory of Tropical Marine Ecosystem and Bioresource, MNR (2022QN02) and Hainan Provincial Joint Project of Sanya Yazhou Bay Science and Technology City (420LH004), Key Research Program of Frontier Sciences, Chinese Academy of Sciences (ZDBS-LY-SM016), Biological Resources Program, Chinese Academy of Sciences (KFJ-BRP-009-005), and National Research Foundation of Korea (NRF) grant (NRF-2020R1C1C1004473).

Conflict of interest

The authors declare that the research was conducted in the absence of any commercial or financial relationships that could be construed as a potential conflict of interest.

The author(s) declared that they were an editorial board member of Frontiers, at the time of submission. This had no impact on the peer review process and the final decision.

Publisher's note

All claims expressed in this article are solely those of the authors and do not necessarily represent those of their affiliated organizations, or those of the publisher, the editors and the reviewers. Any product that may be evaluated in this article, or claim that may be made by its manufacturer, is not guaranteed or endorsed by the publisher.

References

Brakhage, A.A. (2013). Regulation of fungal secondary metabolism. *Nat. Rev. Microbiol.* 11, 21–32. doi: 10.1038/nrmicro2916

Keller, N.P. (2019). Fungal secondary metabolism: regulation, function and drug discovery. *Nat. Rev. Microbiol.* 17, 167–180. doi: 10.1038/s41579-018-0121-1

Wang, G., Ran, H., Fan, J., Keller, N.P., Liu, Z., Wu, F., et al. (2022). Fungal-fungal cocultivation leads to widespread secondary metabolite alteration requiring the partial loss-of-function VeA1 protein. *Sci. Adv.* 8, eabo6094. doi: 10.1126/sciadv.abo6094

Wang, W., Yu, Y., Keller, N.P., and Wang, P. (2021a). Presence, mode of action, and application of pathway specific transcription factors in *Aspergillus* biosynthetic gene clusters. *Int. J. Mol. Sci.* 22, 8709. doi: 10.3390/ijms22168709

Wang, W.J., Drott, M., Greco, C., Luciano-Rosario, D., Wang, P.M., and Keller, N.P. (2021b). Transcription factor repurposing offers insights into evolution of biosynthetic gene cluster regulation. *Mbio* 12, 10–1128. doi: 10.1128/mBio.01399-21

Wei, P.L., Fan, J., Yu, J., Ma, Z., Guo, X., Keller, N.P., et al. (2023). Quantitative characterization of filamentous fungal promoters on a single-cell resolution to discover cryptic natural products. *Sci. China Life Sci.* 66, 848–860. doi: 10.1007/s11427-022-2175-0

Yin, W., and Keller, N.P. (2011). Transcriptional regulatory elements in fungal secondary metabolism. *J. Microbiol.* 49, 329–339. doi: 10.1007/s12275-011-1009-1

Yu, W., Pei, R., Zhou, J., Zeng, B., Tu, Y., and He, B. (2023). Molecular regulation of fungal secondary metabolism. *World J. Microbiol. Biotechnol.* 39, 204. doi: 10.1007/s11274-023-03649-6

Zhang, H., Li, Z., Zhou, S., Li, S.M., Ran, H., Song, Z., et al. (2022). A fungal NRPS-PKS enzyme catalyses the formation of the flavonoid naringenin. *Nat. Commun.* 13, 6361. doi: 10.1038/s41467-022-34150-7

frontiers | Frontiers in Microbiology

TYPE Original Research
PUBLISHED 19 July 2022
DOI 10.3389/fmicb.2022.962853

Check for updates

OPEN ACCESS

EDITED BY
Hee-Soo Park,
Kyungpook National University,
South Korea

REVIEWED BY
Charles Hoffman,
Boston College, United States
Makoto Kawamukai,
Shimane University, Japan

*CORRESPONDENCE
Simon Labbé
Simon.Labbe@USherbrooke.ca

SPECIALTY SECTION
This article was submitted to Microbial Physiology and Metabolism, a section of the journal Frontiers in Microbiology

RECEIVED 06 June 2022
ACCEPTED 01 July 2022
PUBLISHED 19 July 2022

CITATION
Brault A, Mbuya B and Labbé S (2022) Sib1, Sib2, and Sib3 proteins are required for ferrichrome-mediated cross-feeding interaction between *Schizosaccharomyces pombe* and *Saccharomyces cerevisiae*. *Front. Microbiol.* 13:962853. doi: 10.3389/fmicb.2022.962853

COPYRIGHT
© 2022 Brault, Mbuya and Labbé. This is an open-access article distributed under the terms of the Creative Commons Attribution License (CC BY). The use, distribution or reproduction in other forums is permitted, provided the original author(s) and the copyright owner(s) are credited and that the original publication in this journal is cited, in accordance with accepted academic practice. No use, distribution or reproduction is permitted which does not comply with these terms.

Sib1, Sib2, and Sib3 proteins are required for ferrichrome-mediated cross-feeding interaction between *Schizosaccharomyces pombe* and *Saccharomyces cerevisiae*

Ariane Brault, Berthy Mbuya and Simon Labbé*

Département de Biochimie et de Génomique Fonctionnelle, Faculté de Médecine et des Sciences de la Santé, Université de Sherbrooke, Sherbrooke, QC, Canada

Although *Saccharomyces cerevisiae* is unable to produce siderophores, this fungal organism can assimilate iron bound to the hydroxamate-type siderophore ferrichrome (Fc) produced and secreted by other microbes. Fc can enter *S. cerevisiae* cells *via* Arn1. Unlike *S. cerevisiae*, *Schizosaccharomyces pombe* synthesizes and secretes Fc. The *sib1*$^{+}$ and *sib2*$^{+}$ genes encode, respectively, a Fc synthetase and an ornithine-N^{5}-oxygenase, which are required for Fc production. When both genes were expressed in *S. pombe*, cross-feeding experiments revealed that *S. cerevisiae fet3*Δ *arn1-4*Δ cells expressing Arn1 could grow in the vicinity of *S. pombe* under low-iron conditions. In contrast, deletion of *sib1*$^{+}$ and *sib2*$^{+}$ produced a defect in the ability of *S. pombe* to keep *S. cerevisiae* cells alive when Fc is used as the sole source of iron. Further analysis identified a gene designated *sib3*$^{+}$ that encodes an N^{5}-transacetylase required for Fc production in *S. pombe*. The *sib3*Δ mutant strain exhibited a severe growth defect in iron-poor media, and it was unable to promote Fc-dependent growth of *S. cerevisiae* cells. Microscopic analyses of *S. pombe* cells expressing a functional Sib3-GFP protein revealed that Sib3 was localized throughout the cells, with a proportion of Sib3 being colocalized with Sib1 and Sib2 within the cytosol. Collectively, these results describe the first example of a one-way cross-feeding interaction, with *S. pombe* providing Fc that enables *S. cerevisiae* to grow when Fc is used as the sole source of iron.

KEYWORDS

siderophore, ferrichrome, cross-feeding, fission yeast, budding yeast

Abbreviations: bp, base pair(s); Dip, 2, 2′-dipyridyl; EMM, Edinburgh minimal medium; Fc, ferrichrome; FsC, fusarinine; TAFC, triacetylfusarinine C; GFP, green fluorescent protein; GNAT, GCN5-related N-acetyltransferase; MFS, major facilitator superfamily; NRPS, non-ribosomal peptide synthetase; ORF, open reading frame; PCR, polymerase chain reaction; RND, resistance/nodulated/cell division; RT-PCR, reverse transcription PCR; RT-qPCR, real-time quantitative reverse transcription PCR; SC, synthetic complete medium; SDS, sodium dodecyl sulfate; TLC, thin-layer chromatography; WT, wild-type; YES, yeast extract plus supplements.

Introduction

Eukaryotes require iron for their growth. Iron serves as a redox-active cofactor for numerous cellular enzymes required for essential processes such as DNA synthesis and repair, energy production, amino acid biosynthesis, and lipid metabolism (Puig et al., 2017; Galaris et al., 2019; Philpott et al., 2020). Despite the fact that iron is an abundant metal on Earth, its bioavailability is low at physiological pH because of its oxidative conversion into insoluble ferric hydroxide forms under atmospheric oxygen conditions (Aguiar et al., 2021). To overcome the challenging problem of poor iron bioavailability, all organisms, including fungi, have developed different strategies to acquire this metal ion from different sources. One strategy consists of producing siderophores or utilizing xenosiderophores, which are siderophores produced by other organisms in the same surroundings. Siderophores are low-molecular-mass molecules that specifically bind ferric iron (Haas et al., 2008; Hider and Kong, 2010; Haas, 2014). Once synthesized and secreted by producer cells, siderophores bind to iron in the external environment, and siderophore-iron complexes (holo-siderophores) can be captured by specific siderophore-mediated transport systems. These siderophore-mediated uptake systems are expressed by the producer microbe or an opportunistic microbe that is unable to produce siderophores but is capable of taking up xenosiderophore-bound iron (Miethke and Marahiel, 2007).

Under iron starvation conditions, the fission yeast *Schizosaccharomyces pombe* synthesizes, accumulates, and excretes ferrichrome (Fc), a hydroxamate-type siderophore (Schrettl et al., 2004; Mercier and Labbé, 2010). The first enzymatic step in Fc biosynthesis consists of the N^5 hydroxylation of ornithine by an ornithine-N^5-oxygenase, denoted Sib2 (Schrettl et al., 2004). This initial step generates N^5-hydroxyornithine. The subsequent acetylation of N^5-hydroxyornithine by an unidentified N^5-transacetylase produces N^5-acetyl-N^5-hydroxyornithine. This substrate is then used in combination with three glycine residues to assemble the finished Fc product through the action of the non-ribosomal peptide synthetase (NRPS) Sib1 (Schrettl et al., 2004). In addition to synthesizing Fc, *S. pombe* expresses Str1, which specifically transports Fc across the plasma membrane (Pelletier et al., 2003; Plante and Labbé, 2019). In this context, after its excretion into the surrounding environment, Fc-bound iron can be recovered by *S. pombe* through its cell surface Fc transporter, Str1.

Expression of the *sib1*$^+$, *sib2*$^+$, and *str1*$^+$ genes is regulated at the transcriptional level as a function of iron availability (Pelletier et al., 2003; Mercier and Labbé, 2010; Plante and Labbé, 2019). They are induced under conditions of iron deprivation and are repressed under iron-replete conditions. The iron-responsive transcription factor Fep1 represses *sib1*$^+$, *sib2*$^+$, and *str1*$^+$ gene expression (Pelletier et al., 2002, 2003; Mercier and Labbé, 2010; Plante and Labbé, 2019). In contrast, when the availability of iron is limited, Fep1 is unable to bind its GATA cis-acting elements on chromatin, resulting in the transcription of *sib1*$^+$, *sib2*$^+$, and *str1*$^+$ (Jbel et al., 2009).

Although *Saccharomyces cerevisiae* does not secrete siderophores, it possesses four genes that encode members of a subfamily of the major facilitator superfamily (MFS) of transporters that take up siderophores produced by other microbial species (Moore et al., 2003). These four genes are denoted *ARN1*, *ARN2* (*TAF1*), *ARN3* (*SIT1*), and *ARN4* (*ENB1*) (Lesuisse et al., 1998, 2001; Heymann et al., 1999, 2000a,b; Yun et al., 2000a). The four Arn1-4 transporters exhibit different siderophore specificities. Arn1 exhibits high specificity for Fc-iron, whereas Arn2 mediates triacetylfusarinine C uptake. Ferrioxamine B-iron is the preferred siderophore substrate of Arn3. A common property of Arn1, Arn2, and Arn3 is that all three transmembrane proteins transport hydroxamate-type siderophores. In contrast, Arn4 exhibits uptake activity for bacterial enterobactin, a siderophore of the catecholate class (Yun et al., 2000b; Philpott et al., 2002). The expression of *ARN1-4* allows *S. cerevisiae* to directly transport siderophores into cells under iron-deficient conditions. When siderophores are trapped and bound within the cell wall by Fit1-3 proteins (Protchenko et al., 2001; Philpott et al., 2002), *S. cerevisiae* can use its cell-surface reductases Fre1-3 to catalyze the reduction of iron bound to siderophores, fostering iron release, which in turn can be transported into the cell by the Ftr1-Fet3 permease-oxidase complex (Askwith et al., 1994; De Silva et al., 1995; Stearman et al., 1996; Askwith and Kaplan, 1998; Yun et al., 2000a, 2001).

In microbiology, cross-feeding usually refers to an interaction in which a microbial cell utilizes a metabolite that has been produced and secreted from another cell (Pande and Kost, 2017; D'Souza et al., 2018; Fritts et al., 2021). Four criteria are considered predictive of a cross-feeding interaction. First, the process involves different species forming two genotypically or phenotypically distinct populations. Second, a metabolite is transferred from a producing cell (producer) to a neighboring cell (recipient). Third, the transferred metabolite is assimilated by the recipient. Fourth, the recipient's ability to survive depends on its capacity to assimilate or use the transferred metabolite. There are different types of cross-feeding interactions (Seth and Taga, 2014; Pande and Kost, 2017; D'Souza et al., 2018; Fritts et al., 2021). For simplicity, the number and identity of cells that can participate in producing and/or utilizing a metabolite are often presented in a context in which only two types of microbial cells exchange a metabolite. Using this binary approach, cross-feeding has been classified as follows: (i) unidirectional or one-way cross-feeding, where a donor cell secretes a metabolite without a fitness cost that is utilized by the recipient; (ii) bidirectional or two-way cross-feeding, involving reciprocal exchange of metabolite(s) without fitness costs between two partners; (iii) one partner secretes a costly

metabolite to support the recipient, which in turn supplies the producer with increased concentrations of a metabolic by-product (by-product reciprocity); and (iv) both microbial species carry the fitness cost of metabolite biosynthesis and secretion and benefit from the mutual cross-feeding interaction (also called cooperative cross-feeding) (Pande and Kost, 2017).

As secreted molecules, siderophores have been shown to participate in cross-feeding interactions in which one donor microbial strain produces and releases a siderophore that benefits another recipient microbe under iron-poor conditions (Joshi et al., 2006; Galet et al., 2015; Butaitë et al., 2017; Fritts et al., 2021). Although several examples of bacterial species are involved in siderophore cross-feeding between strains, only a limited number of yeasts exhibit such one-way cross-feeding relationships. In this study, we demonstrate that the introduction of the wild-type *ARN1* allele in *S. cerevisiae fet3*Δ *arn1-4*Δ cells restores their ability to acquire exogenous Fc. The results consistently show that *S. cerevisiae fet3*Δ *arn1-4*Δ cells expressing Arn1 are able to grow in the vicinity of *S. pombe* cells that produce Fc. Furthermore, the Fc-dependent growth of *ARN1*-expressing *S. cerevisiae fet3*Δ *arn1-4*Δ cells is improved in the presence of *S. pombe* donor cells lacking the Fc uptake transporter Str1. Inactivation of the *sib3*$^{+}$ gene, which encodes a predicted N-transacetylase, results in the inability of *S. pombe* cells to produce Fc. *sib3*Δ mutant cells exhibit severe growth defects when inoculate in iron-poor media compared with wild-type cells. Furthermore, *S. pombe sib3*Δ cells fail to promote the growth of *S. cerevisiae fet3*Δ *arn1-4*Δ *ARN1* cells when both strains are point-inoculated in the vicinity of each other. Taken together, these results reveal that *S. pombe* cells capable of producing Fc can engage in a one-way cross-feeding interaction with *S. cerevisiae fet3*Δ *arn1-4*Δ *ARN1* cells that are unable to grow without an external Fc supply.

Materials and methods

Yeast strains and growth conditions

Genotypic descriptions[1] of the *S. pombe* and *S. cerevisiae* strains used in this study are presented in **Table 1**. *S. pombe* strains were grown on yeast extract plus supplement (YES) medium under non-selective growth conditions, as described previously (Sabatinos and Forsburg, 2010). To transform and maintain plasmids in *S. pombe* strains, Edinburgh minimal medium (EMM) lacking a specific ribonucleotide base or particular amino acids was used for ensuring the selection of transformed yeast cells (Moreno et al., 1991). *S. cerevisiae* strains were cultured in YPD medium under non-selective conditions, whereas synthetic dropout (SC) media was used for DNA plasmid transformation, as described previously (Sherman, 2002). For cross-feeding experiments, aliquots of the indicated cultures of *S. pombe* and *S. cerevisiae* strains were spotted in the vicinity of one another on a modified synthetic dextrose minimal (SD) medium containing bacto-yeast nitrogen base (1.7 g/l), which was depleted of copper and iron, as described previously (Beaudoin and Labbé, 2001). This SD^{-Cu-Fe} medium additionally contained ammonium sulfate (5 g/L), dextrose (3%), and 225 mg/L uracil, lysine, adenine, tryptophan, and histidine.

For detection of Fc by TLC, cells were grown in liquid cultures to an OD_{600} of 0.5 and subsequently treated with Dip (100 μM) for 5 h, unless otherwise stated. For *S. cerevisiae* growth assays on solid media, cells were spotted on SC-Leu containing 75 μM Dip or a combination of 75 μM Dip and 2 μM Fc. Growth assays for *S. pombe* strains were performed on solid media similar to that for *S. cerevisiae* cells, except that YES medium containing 0 or 140 μM Dip was used. In the case of pairwise co-culture assays, iron-replete *S. pombe* cells grown to an OD_{600} of 1.0 were subsequently adjusted to 1×10^7 cells/10 μl and then spotted on SD^{-Cu-Fe} medium. In parallel experiments, mid-logarithmic phase cultures of *S. cerevisiae fet3*Δ *arn1-4*Δ cells expressing *ARN1* were diluted (3,000 cells/10 μL) and spotted in the vicinity of *S. pombe* strains. In the case of pairwise liquid co-culture assays, *S. pombe* strains were precultured in the presence of 10 μM $FeCl_3$, whereas *S. cerevisiae* strains were grown in liquid SD^{-Cu-Fe} medium. Subsequently, the indicated *S. pombe* and *S. cerevisiae* strains were mixed in a 1:1 ratio and grown in liquid SD^{-Cu-Fe} medium in the presence of Dip (100 μM) for 18 h. Each pairwise co-culture was examined using Nomarski optics for determining the number of *S. cerevisiae* cells vs. the number of *S. pombe* cells during this period. To monitor the mRNA and protein steady-state levels of Str1 and Sib1-3 in response to changes in iron levels, *S. pombe* cultures were seeded to an OD_{600} of 0.5, grown to the exponential phase (OD_{600} of 1.0) and either left untreated or treated with Dip (250 μM) or $FeCl_3$ (100 μM) for 90 min, as described previously (Mercier et al., 2008).

Plasmids

The *S. cerevisiae ARN1* coding sequence was isolated by PCR and cloned into the *Spe*I-*Xma*I-cut p415GPD vector (Mumberg et al., 1995). The resulting centromeric plasmid was named p415GPD*ARN1*. We amplified the *ARN1* gene without its stop codon, using primers containing *Spe*I

1 We use the standard nomenclature for *S. cerevisiae* and *S. pombe* genes and proteins. *S. cerevisiae* wild-type genes are capitalized and italicized (e.g., *ARN1*). *S. pombe* wild-type genes are designated as three italicized lowercase letters, with a superscripted "+" at the end (e.g., *str1*$^{+}$). *S. cerevisiae* and *S. pombe* proteins are written in plain text with one capital letter, followed by two lowercase letters and a number (e.g., Arn1 and Str1).

TABLE 1 Yeast strains used in this study.

S. pombe strain	Genotype	Source
FY435	*h*$^+$ *his7-366 leu1-32 ura4-Δ18 ade6-M210*	Pelletier et al., 2002
fep1Δ	*h*$^+$ *his7-366 leu1-32 ura4-Δ18 ade6-M210 fep1Δ:ura4*$^+$	Pelletier et al., 2002
AMY58	*h*$^+$ *his7-366 leu1-32 ura4-Δ18 ade6-M210 sib1Δ sib2Δ:KAN*^{r}	Mercier and Labbé, 2010
ABY115	*h*$^+$ *his7-366 leu1-32 ura4-Δ18 ade6-M210 str1Δ:KAN*^{r}	This study
ABY151	*h*$^+$ *his7-366 leu1-32 ura4-Δ18 ade6-M210 sib2Δ:KAN*^{r}	This study
ABY127	*h*$^+$ *his7-366 leu1-32 ura4-Δ18 ade6-M210 sib3Δ:KAN*^{r}	This study
ABY152	*h*$^+$ *his7-366 leu1-32 ura4-Δ18 ade6-M210 sib2Δ:loxP fep1Δ:KAN*^{r}	This study
ABY146	*h*$^+$ *his7-366 leu1-32 ura4-Δ18 ade6-M210 sib3Δ:loxP fep1Δ:KAN*^{r}	This study
ABY147	*h*$^+$ *his7-366 leu1-32 ura4-Δ18 ade6-M210 sib1*$^+$*-GFP:KAN*^{r}	This study
ABY148	*h*$^+$ *his7-366 leu1-32 ura4-Δ18 ade6-M210 sib2*$^+$*-GFP:KAN*^{r}	This study
ABY149	*h*$^+$ *his7-366 leu1-32 ura4-Δ18 ade6-M210 sib3*$^+$*-GFP:KAN*^{r}	This study
ABY150	*h*$^+$ *his7-366 leu1-32 ura4-Δ18 ade6-M210 sib3*$^+$*-Cherry:KAN*^{r}	This study
***S. cerevisiae* strain**	**Genotype**	**Source**
YPH499	*MAT***a** *ura3-52 lys2-801 ade2-101 trp1-63Δ his3-200Δ leu2-1Δ*	Yun et al., 2000a
fet3Δ arn1-4Δ	*MAT***a** *ura3-52 lys2-801 ade2-101 trp1-63Δ his3-200Δ leu2-1Δ fet3Δ:HIS3 arn1Δ:HISG arn2Δ:HISG arn3Δ:HISG arn4Δ:HISG-URA3-HISG*	Yun et al., 2000a

and *Xma*I restriction sites. The resulting PCR product was inserted into the corresponding sites of p415GPD to create p415GPD*ARN1*nostop. The coding region of GFP was amplified by PCR, digested with *Xma*I and *Xho*I, and inserted in-frame with *ARN1* into the corresponding sites of p415GPD*ARN1*nostop, generating the p415*GPDARN1-GFP* construct. The *S. pombe str1*$^+$ gene was isolated by PCR using primers amplifying the *str1*$^+$ locus starting at -966 bp from the initiator codon up to the stop codon of *str1*$^+$. The PCR product was digested with *Kpn*I and *Bam*HI, and subsequently inserted into the corresponding sites of pJK148 (Keeney and Boeke, 1994). The resulting plasmid was denoted pJK-966*str1*$^+$. The integrative pJK-966*str1*$^+$*-GFP* plasmid was constructed as previously described (Plante and Labbé, 2019). To generate the integrative pJK-501*sib3*$^+$ plasmid, a 1,506-bp *Apa*I-*Sac*I-amplified DNA segment containing the *sib3*$^+$ gene starting at position -501 from the start codon up to the stop codon was cloned into the *Apa*I and *Sac*I sites of pJK148. The same *sib3*$^+$ DNA segment was amplified without its stop codon and then cloned into the *Apa*I and *Xma*I sites of pJK148, creating the plasmid pJKsib3nostop. Next, the *GFP*, *Cherry*, or *TAP* coding sequence was inserted into pJKsib3nostop at the *Xma*I and *Sac*I sites, generating three plasmids, denoted pJK*sib3*$^+$*-GFP*, pJK*sib3*$^+$*-Cherry*, and pJK*sib3*$^+$*-TAP*, respectively. For generating the plasmid used for pull-down experiments, the *sib3*$^+$ locus starting at –501 bp from the start codon up to the penultimate codon of the gene was isolated by PCR using primers containing *Apa*I and *Xma*I restriction sites. The PCR-amplified DNA fragment was cloned into the *Apa*I and *Xma*I sites of pSP1 (Cottarel et al., 1993), generating the plasmid pSP1sib3nostop. Subsequently, the coding sequence of NTAP was isolated by PCR, digested with *Xma*I and *Sac*I, and inserted in-frame with *sib3*$^+$ into pSP1sib3nostop, creating the plasmid pSP1sib3-TAP.

The 5′ end of the *sib1*$^+$- *sib2*$^+$ intergenic promoter region containing 597 bp was PCR-amplified using a set of primers that generated *Apa*I and *Pst*I sites at the extremities of the PCR product. The intergenic promoter fragment was cloned into the corresponding sites of pJK148 or pJB1, creating pJK-597prom or pJB1-597prom plasmids. The *sib2*$^+$ coding sequence was amplified without its stop codon and inserted downstream of the intergenic promoter region using *Pst*I and *Xma*I restriction sites. Subsequently, the GFP coding sequence was inserted downstream and in-frame to the *sib2*$^+$ ORF at the *Xma*I and *Sac*I restriction sites, creating pJK-597*sib2*$^+$*-GFP* and pJB1-597*sib2*$^+$*-GFP* plasmids, respectively.

The plasmid pJB1tpsib2-GFP was constructed as follows: an *Apa*I-*Eco*RV PCR-amplified fragment from the *tpx1*$^+$ promoter containing the first 1,500 bp of the 5′-non-coding region was inserted into the *Apa*I and *Eco*RV sites of pJB1, creating pJB1-1500tpx1prom. The *sib2*$^+$ ORF without its stop codon was isolated by PCR using primers containing *Eco*RV and *Xma*I restriction sites. The PCR product was cloned into the corresponding sites of pJB1-1500tpx1prom, creating the plasmid pJB1tpsib2nostop. A DNA sequence encoding GFP was amplified using primers containing the *Xma*I and *Sac*I restriction sites, and the resulting PCR product was digested and inserted into pJB1tpsib2nostop.

For creating strains in which the GFP or Cherry coding sequence was integrated downstream of and in-frame to the 3′ chromosomal regions of *sib1*$^+$, *sib2*$^+$, and *sib3*$^+$ genes, a PCR-based gene fusion strategy using the pFA6a-GFP(S65T)-kanMX6 or pFA6A-Cherry-kanMX6 module was performed as described previously (Bahler et al., 1998). This approach allowed site-specific integration of GFP or Cherry at the chromosomal locus of *sib1*$^+$, *sib2*$^+$, or *sib3*$^+$, fostering the replacement of the wild-type allele with GFP- or Cherry-tagged *sib1*$^+$, *sib2*$^+$, or *sib3*$^+$ alleles.

RNA extraction and analysis by real-time quantitative reverse transcription PCR assays

Total RNA was isolated from the indicated cell cultures using the hot phenol method, as described previously (Chen et al., 2003). Reverse transcription reactions were performed in a 20-μL reaction mixture that contained 1 μg of RNA, 2 μL of random primer mix (60 μM) [including 25 μM oligo(dT) and 35 μM random hexamers], 2 μL of 10 × RT buffer, 1 μL of dNTP mix (10 mM), 0.2 μL of RNase inhibitor (40 U/μL), and 0.2 μL of MMuLV RT (200 U/μL). cDNA synthesis was performed using the following steps: hybridization for 5 min at 25°C, elongation for 60 min at 42°C, and inactivation for 20 min at 65°C. qPCR reactions were performed in a 20-μL reaction mix containing 2 μL of cDNA (1:10 dilution), 300 nM of forward and reverse specific primers, and 10 μL of Supermix qPCR 2X that included SYBR Green, dNTPs, and thermostable DNA polymerase. The reaction was performed on a CFX96 Touch Real-Time PCR System (Bio-Rad) with the following steps: 3 min at 95°C (initial denaturation), 15 s at 95°C, 30 s at 60°C, and 30 s at 72°C. The last three steps were repeated for over 45 cycles. Each target gene (*sib1*$^+$, *sib2*$^+$, or *sib3*$^+$) was analyzed in experiments that included a minimum of three biological replicates, and assays were performed in triplicate. Results were considered valid if the target-specific fluorescent signal showed a C_t value ≤ 37 cycles, and all positive and negative control reactions yielded successful and no amplification, respectively. Fold changes of each transcript (*sib1*$^+$, *sib2*$^+$, or *sib3*$^+$) in wild-type and *fep1*Δ mutant samples were calculated using the ΔΔCt method normalized to *act1*$^+$, the internal control (Livak and Schmittgen, 2001; Schmittgen and Livak, 2008; Protacio et al., 2022). Calculations were performed using the following equation: ΔΔCt = [(Ct gene–Ct ref) in wild-type] vs. [(Ct gene–Ct ref) in *fep1*Δ) under the indicated experimental conditions that were performed as a function of iron availability. In the case of *sib1*$^+$, the primer pair allowed the detection of an amplicon corresponding to the coding region between positions + 810 and + 910 down to the first nucleotide of the initiator codon. For *sib2*$^+$ and *sib3*$^+$, the amplicons corresponded to the coding regions between positions + 205 to + 301 and + 362 to + 451, respectively. To detect the expression of *act1*$^+$, a primer pair was used for amplifying the coding sequence between + 173 and + 280 down to the first base of the ATG codon of *act1*$^+$.

Detection of Fc

A modified Fc extraction method (Moore et al., 2003; Mercier and Labbé, 2010; Plante and Labbé, 2019) was used for analyzing the presence of Fc in *S. cerevisiae* and *S. pombe* strains. Yeast cells were harvested at the exponential growth phase and resuspended in saturated ammonium sulfate solution (300 μL; 571 g/L) containing 1.6 mM $FeCl_3$. After the addition of benzyl alcohol (Sigma-Aldrich, #305197) and glass beads (200 μL) to the resuspended cells, the mixtures were lysed using FastPrep disruption (MP-24 instrument; MP Biomedicals). Cell lysates were mixed with an additional 300 μL of saturated ammonium sulfate solution. After mixing, the samples were centrifuged (13,000 rpm for 10 min at 25°C) and the organic layers (upper fraction) were collected. The latter fraction was diluted with 3 volumes (1.2 mL) of diethyl ether (Acros Organics, #364335000) and mixed by vortexing with water (150 μL). The phases were separated by centrifugation (13,000 rpm for 10 min), and the aqueous layer (lower fraction) was collected, washed with 1 vol of diethyl ether, and lyophilized. Dried samples were resuspended in 3 μL water and spotted on preheated silica gel 60 F_{254} thin-layer chromatography plastic sheets (EMD Millipore). TLC was performed using a solvent containing 80% aqueous methanol. Commercially purified holo-Fc (15 μg) (Sigma-Aldrich, F8014) was used as the positive control for signal detection.

Fluorescence microscopy and protein analysis

Fluorescence and differential interference contrast images (Nomarski) of cells were obtained using a Nikon Eclipse E800 epifluorescence microscope (Nikon, Melville, NY) equipped with a Hamamatsu ORCA-ER digital cooled camera (Hamamatsu, Bridgewater, NJ). The cells were viewed using 1,000 × magnification and the following two filters: 465–495 nm (GFP signal) and 510–560 nm (Cherry signal). Representative fields of cells shown correspond to a minimum of three independent experiments. Furthermore, the cell fields shown represent protein localization in 200 cells tested per condition.

Cell extracts from *S. cerevisiae* were prepared with glass beads using a FastPrep-24 instrument (MP Biomedicals, Solon, OH). Cells were lysed in TMN_{150} buffer containing 50 mM Tris-HCl (pH 7.5), 150 mM NaCl, 5 mM $MgCl_2$, 1% Nonidet P-40, 1 mM phenylmethylsulfonyl fluoride (PMSF), and a complete protease inhibitor cocktail (P8340, Sigma-Aldrich). Cell lysates were incubated with Triton X-100 (1%) for 30 min on ice prior to being resolved on 7% sodium dodecyl sulfate (SDS)-polyacrylamide gels. Arn1-GFP and PGK proteins were detected by immunoblotting with anti-GFP and anti-PGK antibodies, respectively. For *S. pombe* Str1 protein detection, cells were lysed in Thorner buffer [40 mM Tris-HCl (pH 6.8), 8 M urea, 5% SDS, 0.01 mM ethylenediaminetetraacetic acid (EDTA), 1% β-mercaptoethanol and 0.4 mg/mL bromophenol blue] with glass beads using two successive rounds of disruption using the FastPrep-24 instrument. Between each round, cell lysates were incubated for 10 min at 37°C and centrifuged to retrieve the supernatant fraction. After 15 min at 37°C, aliquots of the supernatant fraction were resolved by electrophoresis on 8% SDS-polyacrylamide gels prior to Western blot analysis. To analyze Sib2 and Sib3 protein levels, whole cell extracts were

prepared using a trichloroacetic acid (TCA) extraction method as described previously (Foiani et al., 1994; Ioannoni et al., 2012).

In pull-down experiments, *sib2*Δ *sib3*Δ cells were co-transformed with pSP1sib3-TAP and pJB1tpsib2-GFP or pSP1sib3-TAP and pBPGFP. Cultures were grown in EMM to an OD_{600} of 1.0 in the presence of Dip (50 μM). After washes, aliquots of the cultures were left untreated or treated with Dip (250 μM) or $FeCl_3$ (100 μM) for 90 min. Total cell lysates were prepared by glass bead disruption and subjected to pull-down assays using IgG-Sepharose 6 Fast-Flow beads (GE Healthcare) as described previously (Jacques et al., 2014).

Immunodetection of GFP-tagged proteins (Arn1-GFP, Str1-GFP, Sib2-GFP, and Sib3-GFP), TAP-tagged Sib3, PGK, and α-tubulin was performed using the following primary antibodies: monoclonal anti-GFP antibody B-2 (Santa Cruz Biotechnology), polyclonal anti-mouse IgG antibody (ICN Biomedicals), monoclonal anti-PGK antibody 22C5-D8 (Molecular Probes), and monoclonal anti-α-tubulin antibody B-5-1-2 (Sigma-Aldrich). After incubation with the primary antibodies, the membranes were washed and incubated with the appropriate horse-radish peroxidase-conjugated secondary antibodies (Amersham Biosciences). Proteins were detected using ECL reagents (Amersham Biosciences) and visualized using chemiluminescence.

Results

Expression of Arn1 in *Saccharomyces cerevisiae fet3*Δ *arn1-4*Δ cells restores their ability to acquire ferrichrome

Previous studies have shown that the Arn1 protein in *S. cerevisiae* functions as an Fc transporter (Heymann et al., 2000b; Yun et al., 2000b; Lesuisse et al., 2001). To validate the role of Arn1 in the context of our experimental system, we used an *S. cerevisiae fet3*Δ *arn1-4*Δ mutant strain defective in the uptake of siderophore iron. To this strain, a wild-type *ARN1* allele expressed from a centromeric plasmid was returned by transformation. Similarly, a *GFP*-tagged *ARN1* allele was returned by transformation to determine whether the fusion allele retained its wild-type function. *fet3*Δ *arn1-4*Δ cells expressing an empty plasmid, *ARN1*, or *ARN1-GFP* allele were grown to the mid-logarithmic phase and then incubated in the presence of the iron chelator Dip (100 μM) without Fc supplementation or with Fc supplementation (2 μM) for 5 h. To determine whether the cells accumulated Fc when *ARN1* or *ARN1-GFP* was reintroduced into *fet3*Δ *arn1-4*Δ cells, extracts from the indicated transformed strains were analyzed by thin-layer chromatography (TLC). In Fc-treated *fet3*Δ *arn1-4*Δ cells expressing *ARN1* or *ARN1-GFP*, a positive Fc signal was detected, indicating their ability to assimilate exogenous Fc (**Figure 1A**). In contrast, in the absence of exogenous Fc, the same strains failed to show an Fc signal (**Figure 1A**). Extracts from the *fet3*Δ *arn1-4*Δ mutant strain harboring an empty plasmid were devoid of detectable Fc, irrespective of the absence or presence of exogenous Fc into the medium (**Figure 1A**).

In the case of *fet3*Δ *arn1-4*Δ cells that were transformed with a GFP epitope-tagged *ARN1* allele under the control of the constitutive *GDP* promoter, steady-state protein levels of Arn1-GFP were analyzed by immunoblotting. The results showed that Arn1-GFP was produced under all experimental conditions, including basal, iron-starved, and iron-replete conditions in the presence or absence of Fc (**Figure 1B**). Considering that Arn1 was required for the uptake of exogenous Fc, we next sought to examine its localization when *fet3*Δ *arn1-4*Δ cells expressing *ARN1-GFP* were incubated under low-iron conditions in the presence of exogenous Fc. After 5 h, the Arn1-GFP fluorescence signal was primarily detected at the contour of the cells (**Figure 1C**). When *fet3*Δ *arn1-4*Δ cells expressing *ARN1-GFP* were cultured in Fc-free medium containing Dip (100 μM), analysis of the localization of Arn1-GFP revealed that only a fraction of the fluorescence signal was observed at the periphery of the cells, whereas a significant proportion of the Arn1-GFP signal appeared as fluorescent intracellular structures within the cell (**Figure 1C**). Under basal and iron-replete conditions, fluorescence microscopy revealed that Arn1-GFP signal was mainly detected in the cytosol of the cells, without distinct fluorescence visible at the periphery of the cells (**Figure 1C**).

Consistent with Arn1 functioning as an Fc-iron transporter, the results showed that when *ARN1* and *ARN1-GFP* alleles were returned in *fet3*Δ *arn1-4*Δ cells, their expression restored growth in the presence of exogenous Fc (2 μM) under low-iron conditions (**Figure 1D**). Growth rescue was Fc-specific because utilization of media without Fc supplementation resulted in no detectable growth under iron-limited conditions (Dip, 75 μM) (**Figure 1D**). An isogenic wild-type strain could grow on synthetic complete medium that was left untreated (control) or supplemented with Dip (75 μM) or Dip plus Fc (2 μM) (**Figure 1D**). Collectively, these results showed that Arn1 is required for *S. cerevisiae* growth when cells take up exogenous Fc as the sole source of iron under iron-limited conditions.

Cross-feeding between Fc-producing *Schizosaccharomyces pombe* cells and *Saccharomyces cerevisiae fet3*Δ *arn1-4*Δ cells expressing ARN1

Previous studies have shown that *S. pombe* biosynthesizes, accumulates and secretes Fc, especially under conditions of iron deprivation (Schrettl et al., 2004; Mercier and Labbé, 2010; Plante and Labbé, 2019). Considering that *S. cerevisiae* lacks the ability to synthesize siderophores but can assimilate exogenous siderophores, we examined whether *S. pombe* could support the

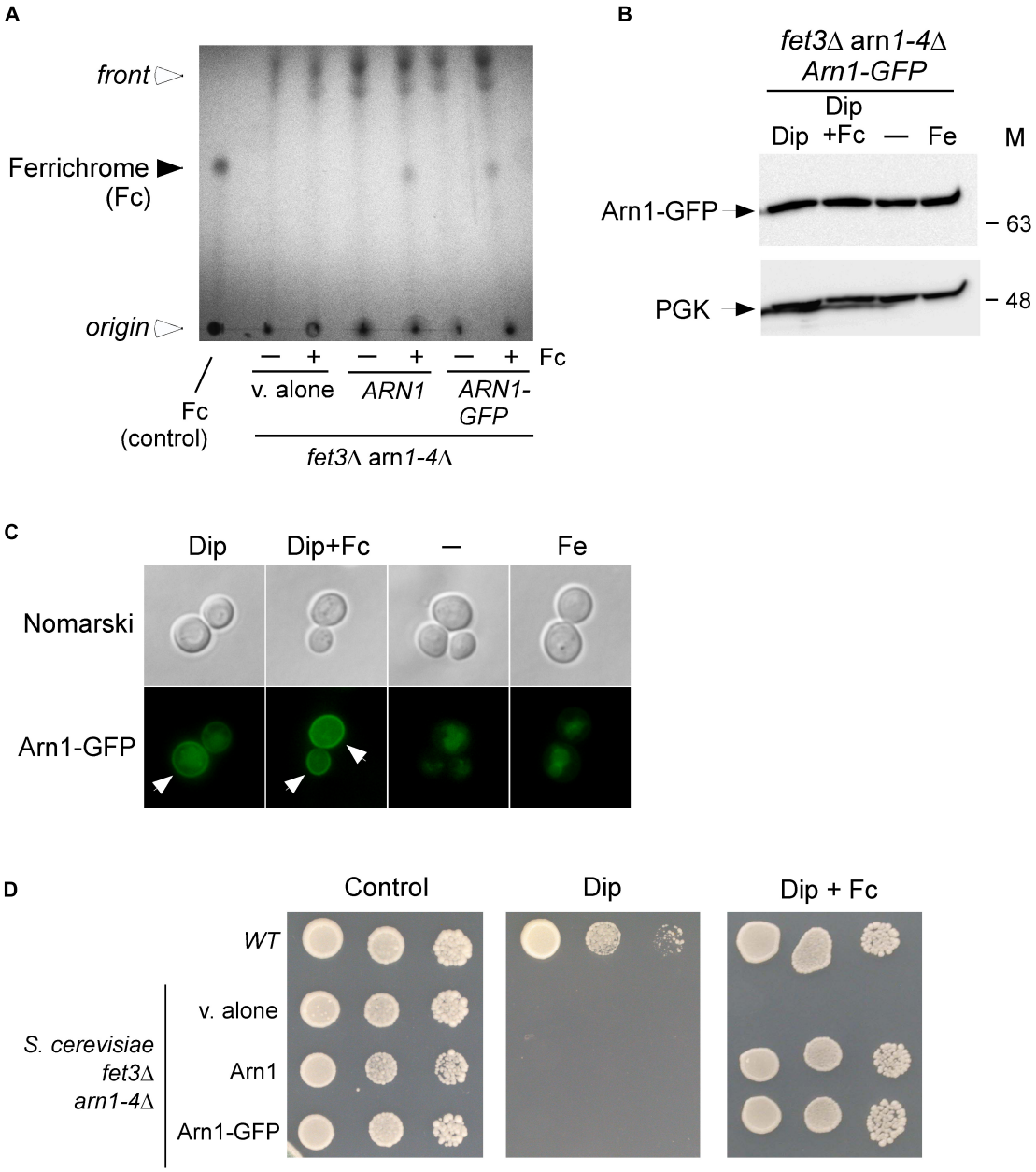

FIGURE 1
Expression of ARN1 in *S. cerevisiae fet3Δ arn1-4Δ* cells complements the Fc acquisition deficiency of cells defective in the uptake of Fc. **(A)** *S. cerevisiae fet3Δ arn1-4Δ* mutant cells expressing an empty plasmid, *ARN1* or *ARN1-GFP* alleles were grown in SC medium to the mid-logarithmic phase. The cells were then incubated in the presence of Dip (100 μM) without Fc supplementation or with Fc supplementation (2 μM) for 5 h. Whole extracts were prepared and total Fc content was analyzed by thin-layer chromatography on silica gel sheets. Commercially purified Fc (15 μg) was run as a reference (control, far left lane). The solid arrowhead indicates the migration position of Fc, whereas the open arrowheads show the position of sample loading and the front of gel migration. **(B)** *S. cerevisiae fet3Δ arn1-4Δ* cells expressing Arn1-GFP were grown to the mid-logarithmic phase and subsequently left untreated (-) or treated with Dip (100 μM), Dip plus Fc (2 μM), or iron (Fe, 100 μM) for 5 h. Whole cell extract preparations were analyzed using immunoblot assays with anti-GFP and anti-PGK antibodies. The positions of the molecular weight standards (in kDa) are indicated on the right side. **(C)** Aliquots of cultures used in *panel B* were analyzed by fluorescence microscopy for visualizing cellular location of Arn1-GFP. Cell morphology was examined using Nomarski optics. White arrows indicate the cell periphery. The results are representative of three independent experiments. **(D)** Aliquots of cultures used in *panel A* were spotted in serial dilutions onto medium without Dip or Fc supplementation (control) or supplemented with Dip or a combination of Dip (75 μM) and Fc (2 μM). An isogenic wild-type (WT) strain was grown under the same conditions used in **(A)** and then spotted at different cellular densities onto the same indicated solid media as a control. All plates were incubated for 4 days at 30°C, and photographed.

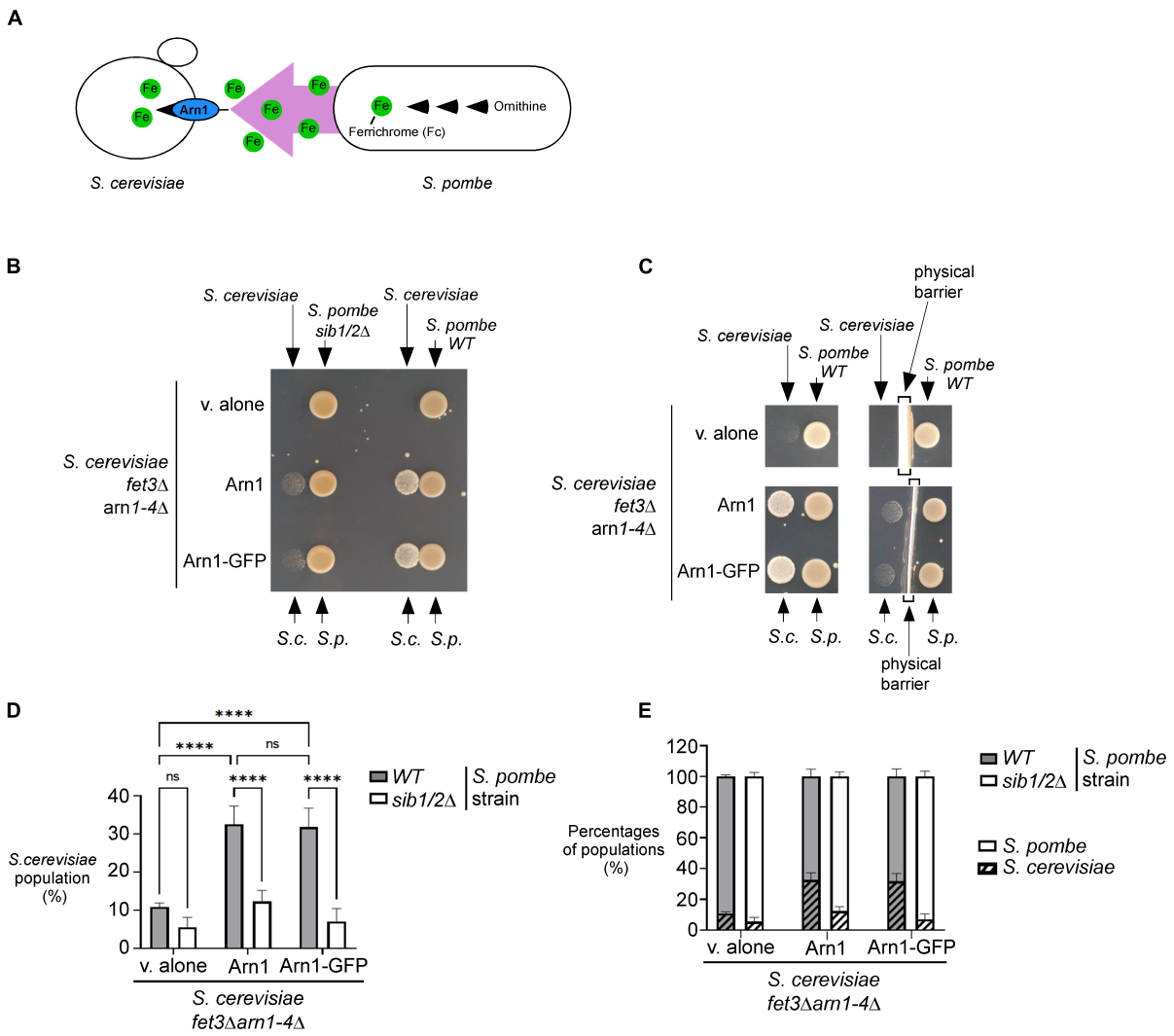

FIGURE 2
S. pombe Fc promotes growth of a *S. cerevisiae fet3Δ arn1-4Δ* mutant in which the *ARN1* gene is returned. **(A)** Schematic representation of a *S. cerevisiae fet3Δ arn1-4Δ* mutant expressing *ARN1* in co-culture with a *S. pombe* strain that was competent to synthesize and excrete Fc-iron. **(B,C)** *S. pombe* wild-type (WT) and *sib1Δ sib2Δ* strains were grown to an OD_{600} of 1.0 in the presence of $FeCl_3$ (10 μM), and half of cells (1×10^7 cells/10 μl) were spotted (right side of each pair of spots) onto SD^{-Cu-Fe} medium. *S. cerevisiae fet3Δ arn1-4Δ* cells harboring an empty vector (v. alone) or expressing *ARN1* or *ARN1-GFP* were grown in SD^{-Cu-Fe} to an OD_{600} of 1.0. Cells were washed, diluted 10,000-fold, and spotted (3,000 cells/10 μL) (left side of each pair of spots) onto SD^{-Cu-Fe} medium in the vicinity of the *S. pombe* strains. In the representative experiment in **(C)** (right side), a physical barrier was installed between point-inoculated *S. cerevisiae* and *S. pombe* strains. S.c., *S. cerevisiae*; S.p., *S. pombe*. **(D,E)** *S. pombe* wild-type (WT) and *sib1Δ sib2Δ* strains were mixed with the indicated plasmid-transformed *S. cerevisiae fet3Δ arn1-4Δ* strain in a 1:1 ratio. Each pairwise co-culture was grown in liquid SD^{-Cu-Fe} medium in the presence of Dip (100 μM) for 18 h. The morphology of yeast cells was examined by Nomarski optics for determining the number of *S. cerevisiae* cells vs. the total number of fungal cells. Representative results are presented for the percentages of *S. cerevisiae* cells with the indicated plasmids in co-culture with *S. pombe* (WT or *sib1Δ sib2Δ*) **(D)**. Comparative results of percentages of each population representing *S. cerevisiae* cells vs. *S. pombe* cells after they were grown together for 18 h **(E)**. A minimum of 300 cells were examined for each pairwise co-culture. The results are representative of three independent experiments. The error bars indicate the standard deviation (± SD; error bars). The asterisks correspond to $p < 0.0001$ (****) (two-way ANOVA with Tuckey's multiple comparisons test against the genotypes of *S. pombe* and *S. cerevisiae* strains), whereas ns stands for not significant.

growth of *S. cerevisiae* through its ability to donate Fc-iron as a sole source of iron (Figure 2A). For testing this possibility, an *S. pombe* wild-type or *sib1Δ sib2Δ* strain was cultured in the presence of $FeCl_3$ (10 μM) and subsequently spotted (1×10^7 cells/10 μl) on a copper- and iron-poor medium, denoted SD^{-Cu-Fe}. The *S. cerevisiae fet3Δ arn1-4Δ* mutant strain that had been transformed with an empty vector, an untagged *ARN1* or GFP-tagged *ARN1* allele was used for cross-feeding assays. *S. cerevisiae* cultures were grown in SD^{-Cu-Fe} medium until the logarithmic phase. At this point, the indicated

cultures were diluted 10,000-fold and point-inoculated in the vicinity of *S. pombe* cells (wild-type and *sib1*Δ *sib2*Δ strains). The results showed that the *S. cerevisiae fet3*Δ *arn1-4*Δ cells expressing *ARN1* and *ARN1-GFP* alleles were able to grow in the vicinity of the wild-type *S. pombe* strain (**Figure 2B**). In contrast, *S. cerevisiae fet3*Δ *arn1-4*Δ cells were unable to grow in the presence of an *S. pombe sib1*Δ *sib2*Δ mutant strain defective in Fc biosynthesis, regardless of the absence or presence of *ARN1* and *ARN1-GFP* alleles (**Figure 2B**). Considering that Fc is a small molecule secreted by the donor *S. pombe*, we tested whether physical separation using a sterile spacer between *S. pombe* and *S. cerevisiae* prevented cross-feeding. Indeed, the presence of a physical barrier that blocked the diffusion of *S. pombe* Fc in the surrounding medium resulted in no significant growth of *S. cerevisiae* cells containing an untagged *ARN1* or GFP-tagged *ARN1* allele (**Figure 2C**). In contrast, *S. cerevisiae fet3*Δ *arn1-4*Δ cells expressing *ARN1* and *ARN1-GFP* alleles grew on plates devoid of a spacer that served as a physical barrier (**Figure 2C**). This result suggests that Fc dispersed in the medium can reach neighboring cells of *S. cerevisiae* that can benefit from the Fc available in their proximal environment.

To further analyze the effects of cross-feeding between the two species of yeast, budding and fission yeast forms were examined using Nomarski optics for comparing the proportion of *S. cerevisiae fet3*Δ *arn1-4*Δ cells with the proportion of *S. pombe* cells (wild-type or *sib1*Δ *sib2*Δ strain) when both yeast species were co-cultured in SD^{-Cu-Fe} liquid medium over 18 h. After mixing the indicated cultures of *S. cerevisiae* and *S. pombe* (wild-type strain) in a 1:1 ratio, microscopic analysis of co-culture aliquots showed that *S. cerevisiae fet3*Δ *arn1-4*Δ cells harboring an empty plasmid exhibited 21.8 and 21.0% less growth compared to *S. cerevisiae fet3*Δ *arn1-4*Δ cells expressing *ARN1* and *ARN1-GFP* alleles, respectively, over a period of 18 h (**Figure 2D**). Interestingly, this difference in their ability to grow was markedly attenuated when *S. cerevisiae fet3*Δ *arn1-4*Δ cells were co-cultured with *S. pombe sib1*Δ *sib2*Δ cells defective in Fc biosynthesis. Over the same period (18 h), when they were co-cultured with *S. pombe sib1*Δ *sib2*Δ cells, *S. cerevisiae fet3*Δ *arn1-4*Δ cells expressing *ARN1* and those expressing *ARN1-GFP* alleles exhibited 20.3 and 24.8% less growth, respectively, compared to when they were grown in the presence of Fc-producing *S. pombe* cells (wild-type) (**Figure 2D**). *ARN1*- or *ARN1-GFP*-expressing *S. cerevisiae* strains were co-cultured with *S. pombe* (wild-type or *sib1*Δ *sib2*Δ) strains. The results showed that growth of *S. cerevisiae* cells was very limited when they were co-cultured with *S. pombe sib1*Δ *sib2*Δ cells because of the lack of Fc production (from *S. pombe*) to fuel the growth of *S. cerevisiae* cells (**Figure 2E**). Taken together, these results indicate that Fc produced by *S. pombe* promotes the growth of *S. cerevisiae fet3*Δ *arn1-4*Δ cells expressing the Fc transporter Arn1, when Fc-bound iron is the sole source of iron.

Fc-dependent growth of *Saccharomyces cerevisiae fet3*Δ *arn1-4*Δ cells expressing Arn1 is improved in the presence of *Schizosaccharomyces pombe* cells lacking Str1

Previous studies have shown that Fc assimilation relies on Str1 in *S. pombe* (Pelletier et al., 2003; Plante and Labbé, 2019). To further validate that *S. pombe* cells require the presence of Str1 for the acquisition of exogenous Fc in the context of the current experimental system, we used a *str1*Δ mutant strain in which an empty vector, $str1^+$ allele, or $str1^+$-*GFP* allele was returned by integration. Proliferating *str1*Δ cells bearing $str1^+$, $str1^+$-*GFP*, or an empty vector were spotted onto YES medium without Dip supplementation (control) or supplemented with a combination of Dip (140 μM) and Fc (2 μM). The cells carrying a disrupted $str1^+$ allele (*str1*Δ containing an empty plasmid) failed to grow under low-iron conditions when exogenous Fc-bound iron was added as the sole source of iron (**Figure 3A**). In contrast, under these conditions, *str1*Δ cells expressing $str1^+$ or $str1^+$-*GFP* allele exhibited robust growth (**Figure 3A**). As the control, the wild-type strain was able to grow on YES medium without Dip supplementation or with Dip (140 μM) and Fc (2 μM) supplementation (**Figure 3A**).

Considering the property of Str1 to take up Fc-iron in *S. pombe*, we reasoned that its inactivation (*str1*Δ) could benefit the growth of *ARN1*-expressing *S. cerevisiae fet3*Δ *arn1-4*Δ cells in co-culture experiments, since *S. pombe str1*Δ donor cells were unable to retrieve the Fc that they produced. To test this possibility, a *str1*Δ strain that had been transformed with an empty vector, an untagged $str1^+$ allele, or GFP-tagged $str1^+$ allele was precultured under iron-replete conditions (10 μM $FeCl_3$) and subsequently spotted on the SD^{-Cu-Fe} medium. *S. cerevisiae fet3*Δ *arn1-4*Δ cells expressing *ARN1* were grown to the logarithmic phase in SD^{-Cu-Fe} liquid medium, diluted, and point-inoculated in the vicinity of *str1*Δ cells. The growth of recipient *S. cerevisiae fet3*Δ *arn1-4*Δ *ARN1* cells was more robust near *S. pombe str1*Δ cells harboring an empty plasmid than near *S. pombe str1*Δ cells expressing functional $str1^+$ and $str1^+$-*GFP* alleles (**Figure 3B**). As the negative control, the recipient *S. cerevisiae fet3*Δ *arn1-4*Δ *ARN1* cells were unable to grow when spotted in the vicinity of *S. pombe sib1*Δ *sib2*Δ cells, which are defective in Fc production (**Figure 3B**).

Additional co-culture liquid assays were performed for verifying that *S. pombe str1*Δ cells were indeed more effective than Str1-expressing cells in promoting cross-feeding of *S. cerevisiae fet3*Δ *arn1-4*Δ *ARN1* cells. Prior to the co-cultures of *S. pombe* and *S. cerevisiae*, *S. pombe* strains were separately grown to an OD_{600} of 1.0 in SD^{-Cu-Fe} medium supplemented with $FeCl_3$ (10 μM), whereas *S. cerevisiae fet3*Δ *arn1-4*Δ *ARN1* cells were separately grown in the same

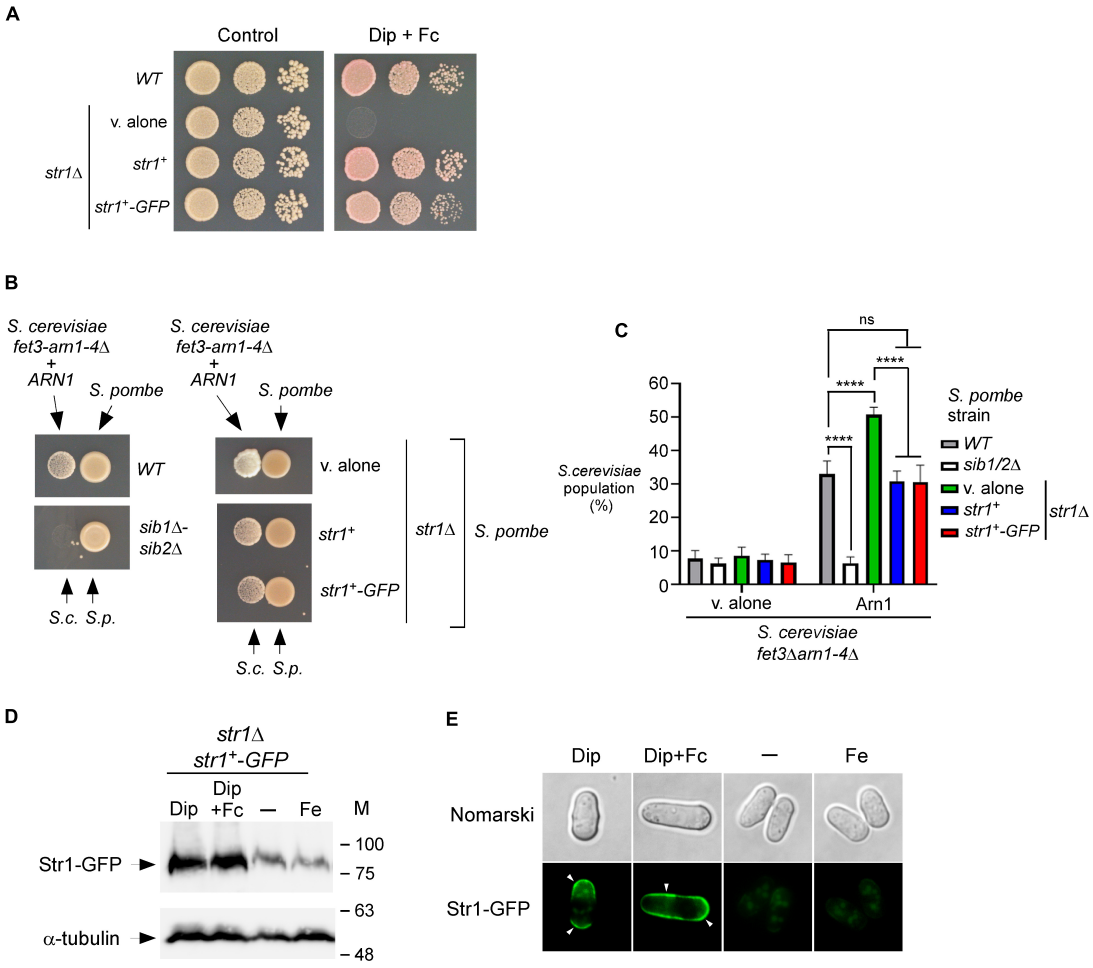

FIGURE 3
str1^{+} gene disruption in *S. pombe* favors Fc-dependent growth of an *S. cerevisiae fet3*Δ *arn1-4*Δ mutant expressing *ARN1*. **(A)** *S. pombe str1*Δ strain containing an empty vector (v. alone) or expressing *str1*$^{+}$ and *str1*$^{+}$*-GFP* alleles were grown to an OD_{600} of 1.0. Cells were spotted in serial dilutions onto YES medium containing Dip (140 μM) and Fc (2 μM) (right side). Cell viability of *S. pombe* wild-type (WT) and *str1*Δ strains was assayed on untreated medium (control, left side). **(B)** *S. pombe* wild-type, *sib1*Δ *sib2*Δ, and *str1*Δ strains were grown to an OD_{600} of 1.0 under iron-replete conditions (10 μM $FeCl_3$). *str1*Δ cells contained an empty vector (v. alone) or expressed either the *str1*$^{+}$ or *str1*$^{+}$*-GFP* allele. At this point, the cells were spotted (1×10^7 cells/10 μl) (right side of each pair of spots) onto SD^{-Cu-Fe} medium. *S. cerevisiae fet3*Δ *arn1-4*Δ cells expressing *ARN1* were grown to an OD_{600} of 1.0. At this stage, the cells were diluted 10,000-fold and spotted (3,000 cells/10 μL) in the vicinity of the *S. pombe* strains (left side of each pair of spots). S.c., *S. cerevisiae*; S.p., *S. pombe*. **(C)** The indicated *S. pombe* strains were mixed with the plasmid-transformed *S. cerevisiae fet3*Δ *arn1-4*Δ strain (harboring an empty plasmid or *ARN1* allele) in a 1:1 ratio. Each pairwise co-culture was grown in liquid SD^{-Cu-Fe} medium in the presence of Dip (100 μM) for 18 h. Morphology of yeast cells was examined by Nomarski optics for determining the number of *S. cerevisiae* cells vs. the total number of fungal cells. Representative results are shown for the percentages of *S. cerevisiae* cells in co-culture with *S. pombe* (WT, *sib1*Δ *sib2*Δ or *str1*Δ containing an empty plasmid, *str1*$^{+}$, or *str1*$^{+}$*-GFP* allele). A minimum of 300 cells were examined for each pairwise co-culture. The results are representative of three independent experiments. Error bars indicate standard deviation (± SD; error bars). The asterisks correspond to $p < 0.0001$ (****) (two-way ANOVA with Tukey's multiple comparisons test against the indicated *S. pombe* and *S. cerevisiae fet3*Δ *arn1-4*Δ *ARN1* strains), whereas ns stands for not significant. **(D)** *str1*Δ cells expressing Str1-GFP were left untreated (-) or treated with $FeCl_3$ (Fe, 100 μM), Dip (100 μM), or Dip plus Fc (2 μM) for 90 min. Aliquots of total cell extract preparations were analyzed using immunoblot assays with anti-GFP and anti-α-tubulin antibodies. The positions of the molecular weight standards (in kDa) are indicated on the right side. **(E)** Fluorescence microscopy was performed on cells incubated from each group of cultures described in **(D)** to visualize cellular location of Str1-GFP. Cell morphology was examined using Nomarski optics. White arrowheads indicate the cell periphery. Results are representative of three independent experiments.

medium without $FeCl_3$ supplementation. Following precultures, *S. pombe* and *S. cerevisiae* strains were diluted, and the co-cultures were initiated at a 1:1 ratio and monitored by microscopic examination. *S. cerevisiae fet3*Δ *arn1-4*Δ *ARN1* cells exhibited 17.8–20.1% more growth when co-cultured with *S. pombe str1*Δ cells compared to wild-type (*str1*$^{+}$) or *str1*Δ cells expressing *str1*$^{+}$ and *str1*$^{+}$*-GFP* alleles (Figure 3C). As the negative control, *S. cerevisiae fet3*Δ *arn1-4*Δ *ARN1* cells exhibited poor growth when co-cultured with *S. pombe sib1*Δ *sib2*Δ cells (Figure 3C). This inability to grow was comparable

to the background growth level of *S. cerevisiae fet3*Δ *arn1-4*Δ cells lacking Arn1, which are defective in taking up Fc produced by prototrophic *S. pombe* strains (**Figure 3C**).

Previous studies in *S. pombe* have shown that transcript levels of *str1*$^{+}$ are induced in response to iron deficiency (Pelletier et al., 2003; Plante and Labbé, 2019). In co-culture experiments, the growth of the recipient *S. cerevisiae fet3*Δ *arn1-4*Δ *ARN1* strain was dependent on Fc production by *S. pombe* cells that secreted Fc into their external environment under low-iron conditions. Using this biological system and immunoblotting assays, we tested whether the protein levels of Str1 were increased when *S. pombe* cells harboring the *str1*$^{+}$*-GFP* allele were grown in SD^{-Cu-Fe} medium in the presence of Dip (100 μM) or a combination of Dip and Fc (2 μM) (**Figure 3D**). In cells expressing *str1*$^{+}$*-GFP* that were left untreated or incubated in the presence of iron (100 μM), the levels of Str1-GFP decreased compared with the protein levels of Str1-GFP observed in Dip-treated cells (**Figure 3D**). Fluorescence microscopy analysis consistently revealed that Str1-GFP was primarily localized at the cell surface when Str1-GFP-expressing *str1*Δ cells were incubated with Dip (100 μM) (**Figure 3E**). When the Dip-treated cells were supplemented with Fc (2 μM), the green fluorescence signal associated with Str1-GFP was stronger at the contour of the cell (**Figure 3E**). In contrast, the Str1-GFP fluorescence signal was dramatically reduced when the cells were left untreated or treated with iron (100 μM) (**Figure 3E**). Under these conditions, Str1-GFP fluorescence was observed as a weakly fluorescent intracellular structure within the cell (**Figure 3E**). Taken together, these results show that *str1*Δ disruption, which abolishes the capacity of *S. pombe* cells to assimilate exogenous Fc, favors the Fc-dependent growth of an *S. cerevisiae fet3*Δ *arn1-4*Δ mutant expressing *ARN1*.

Disruption of sib3^{+} leads to cross-feeding inhibition between *Schizosaccharomyces pombe* and *Saccharomyces cerevisiae fet3*Δ *arn1-4*Δ *ARN1* cells

According to a proposed pathway for Fc biosynthesis, the first enzymatic step consists of the N^5 hydroxylation of ornithine by the ornithine-N^5-oxygenase Sib2 of *S. pombe* to produce N^5-hydroxyornithine (Haas, 2003, 2014; Haas et al., 2008). This product is predicted to be acetylated by an unknown *S. pombe* N^5-transacetylase to yield N^5-acetyl-N^5-hydroxyornithine (Mercier and Labbé, 2010). On the basis of a prediction inferred from sequence similarity with *Aspergillus fumigatus* transacetylase SidL (Blatzer et al., 2011), the *SPBC17G9.06c* gene encoding a putative acetyltransferase, denoted Sib3, has been suggested to participate in Fc biosynthesis (Mercier and Labbé, 2010). However, its biological role in Fc production has not been demonstrated. Previous studies have shown that *S. pombe* cells lacking Sib1 and Sib2 exhibit severe growth defects in iron-poor media (Mercier and Labbé, 2010; Plante and Labbé, 2019). To test whether an *S. pombe* strain with deletion of the *sib3*$^{+}$ gene phenocopied the inability to grow on iron-deficient media associated with Sib1 and Sib2 deletions, we generated a *sib3*Δ mutant strain. *sib3*Δ cells containing an empty vector were spotted onto an iron-poor medium and compared with *sib1*Δ *sib2*Δ cells. As observed for *sib1*Δ *sib2*Δ cells, *sib3*Δ cells containing an empty vector were unable to grow on a medium supplemented with Dip (140 μM), unlike the wild-type cells, which exhibited growth (**Figure 4A**). In the case of *sib3*Δ cells containing an untagged *sib3*$^{+}$ or GFP-tagged *sib3*$^{+}$ allele that had been reintegrated, their ability to grow was restored in the presence of Dip (**Figure 4A**). As controls, the wild-type and mutant strains were equally competent to grow on iron-replete YES medium under non-selective conditions (**Figure 4A**, left panel).

We next investigated whether the loss of Sib3 affected the ability of the *sib3*Δ mutant strain to promote the growth of the *S. cerevisiae fet3*Δ *arn1-4*Δ *ARN1* strain when they were spotted in the vicinity of each other on SD^{-Cu-Fe} medium. Results showed that *S. pombe sib3*Δ cells containing an empty vector failed to support the growth of the *S. cerevisiae fet3*Δ *arn1-4*Δ *ARN1* strain, unlike the wild-type *S. pombe* strain (**Figure 4B**). In contrast, this growth defect of *S. cerevisiae fet3*Δ *arn1-4*Δ *ARN1* cells was reversed when they were point-inoculated near *S. pombe sib3*Δ cells expressing an integrated *sib3*$^{+}$ or *sib3*$^{+}$*-GFP* allele (**Figure 4B**). As a negative control, the reference *S. pombe sib1*Δ *sib2*Δ strain failed to promote the growth of *S. cerevisiae fet3*Δ *arn1-4*Δ cells expressing *ARN1* (**Figure 4B**).

We next assessed whether Sib3 is required for Fc biosynthesis. Extracts from the wild-type, *sib1*Δ *sib2*Δ, *fep1*Δ, and *sib3*Δ strains were analyzed by thin-layer chromatography. In contrast to the wild-type or *sib3*Δ strain expressing an untagged *sib3*$^{+}$ or GFP-tagged *sib3*$^{+}$ allele, the *sib3*Δ mutant harboring an empty vector exhibited no detectable Fc signal (**Figure 4C**). As additional controls, extract preparations from the *sib1*Δ *sib2*Δ mutant strain were devoid of detectable Fc, whereas extracts from the *fep1*Δ mutant exhibited a strong Fc signal because of the lack of complete transcriptional repression of *sib1*$^{+}$ and *sib2*$^{+}$ genes in the absence of Fep1 (**Figures 4C,D**; Mercier and Labbé, 2010; Plante and Labbé, 2019).

On the basis of the finding that Sib3 is required along with Sib1 and Sib2 for Fc biosynthesis, we tested whether *sib3*$^{+}$ mRNA levels were affected in response to changes in iron concentrations or as a function of the presence or absence of Fep1. Using RT-qPCR assays, we monitored *sib1*$^{+}$, *sib2*$^{+}$, and *sib3*$^{+}$ transcript levels in wild-type (*fep1*$^{+}$) and *fep1*Δ cells grown in either the absence or presence of iron or Dip. The gene expression levels of *sib3*$^{+}$ in Dip- or iron-treated cells were not significantly different compared to the basal levels in untreated cells in both *fep1*$^{+}$ and *fep1*Δ strains (**Figure 4D**).

10.3389/fmicb.2022.962853

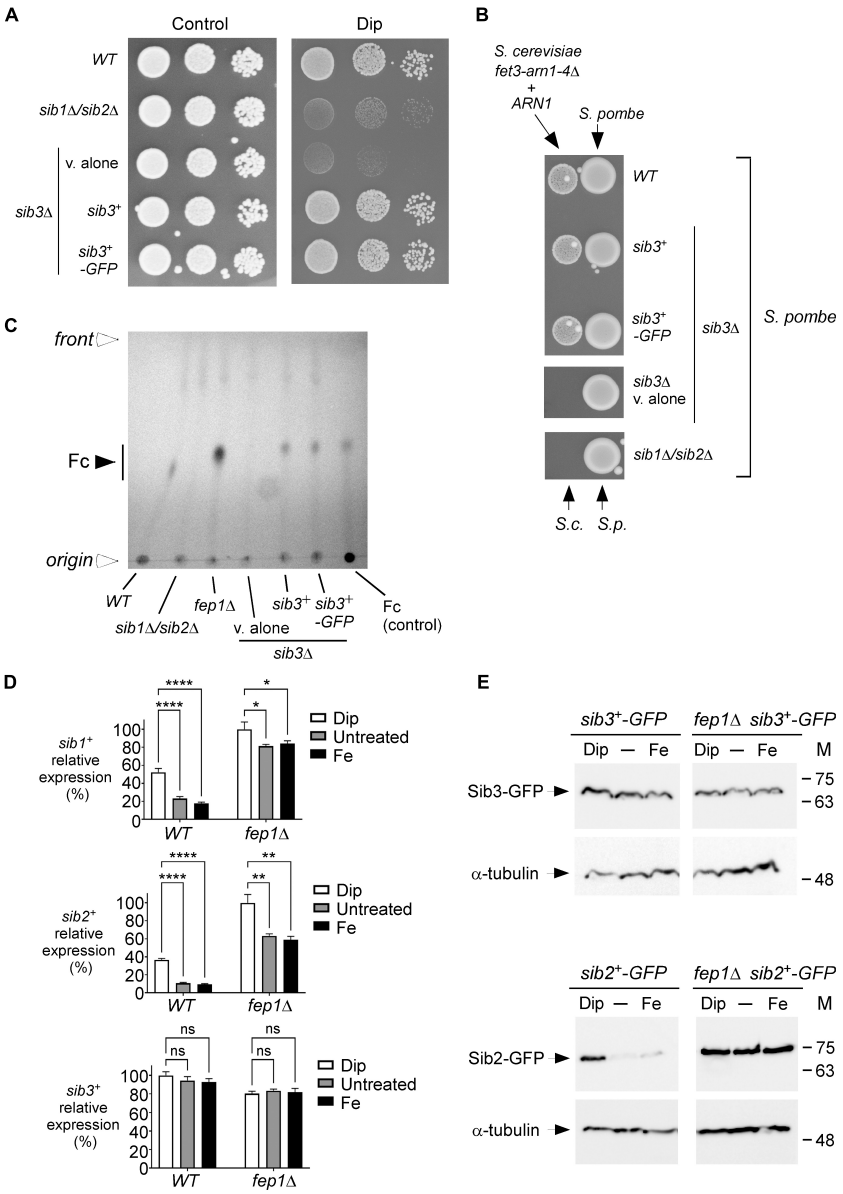

FIGURE 4

S. pombe requires Sib3 to promote Fc-dependent growth of *S. cerevisiae fet3Δ arn1-4Δ* cells expressing ARN1. **(A)** Wild-type, *sib1Δ sib2Δ*, and *sib3Δ* strains were assayed for their ability to grow on YES medium containing 0 μM (control) or 140 μM Dip. In the case of the *sib3Δ* mutant, an empty plasmid (v. alone), *sib3*$^+$, or *sib3*$^+$*-GFP* allele was returned in the strain. Once spotted on the control and iron-starved media, the strains were incubated for 4 days at 30°C, and photographed. **(B)** The indicated *S. pombe* strains described in **(A)** were grown in the presence of iron (10 μM) to an OD_{600} of 1.0. Subsequently, these strains were inoculated (1×10^7 cells/10 μl) (right side of each pair of spots) onto SD^{-Cu-Fe} medium. *S. cerevisiae fet3Δ arn1-4Δ* cells expressing *ARN1* were grown to the mid-logarithmic phase, diluted, and spotted (3,000 cells/10 μL) in the vicinity of *S. pombe* strains (left side of each pair of spots). S.c., *S. cerevisiae*; S.p., *S. pombe*. **(C)** The indicated *S. pombe* strains were grown to an OD_{600} of 0.5 in YES medium and incubated in the presence of Dip (100 μM) for 5 h. Total Fc was extracted and analyzed by TLC on silica gel sheets. Commercially purified Fc (15 μg) (control) was loaded as a reference. Solid arrowhead indicates the migration position of Fc, whereas open arrowheads show the origin of sample loading and front of gel migration. **(D)** Shown are expression profiles of *sib1*$^+$, *sib2*$^+$, and *sib3*$^+$ genes. Wild-type (WT) and *fep1Δ* strains were grown in YES medium and were either left untreated or treated with Dip (250 μM) or $FeCl_3$ (Fe; 100 μM) for 90 min. Total RNA was prepared from culture aliquots, and steady-state mRNA levels of *sib1*$^+$, *sib2*$^+$, and *sib3*$^+$ were analyzed by RT-qPCR assays. Graphic representations of quantification of three independent RT-qPCR assays. Error bars indicate the standard deviation (± SD; error bars). The asterisks correspond to $p < 0.05$ (*), $p < 0.01$ (**), and $p < 0.0001$ (****) (two-way ANOVA with Tukey's multiple comparisons test against the indicated strain grown under low-iron conditions), whereas ns stands for not significant. **(E)** A genetic approach was used for allowing homologous integration of the *GFP* coding sequence at the chromosomal loci of *sib2*$^+$ and *sib3*$^+$, respectively, therefore creating strains containing GFP-tagged *sib2*$^+$ and *sib3*$^+$ alleles. Subsequently, these two strains were used for disrupting the *fep1*$^+$ gene and generating *sib2*$^+$*-GFP fep1Δ* and *sib3*$^+$*-GFP fep1Δ* strains. All four *S. pombe* strains were left untreated (-) or treated with Dip or $FeCl_3$ (Fe), as described in **(D)**. Aliquots of whole cell extract preparations were analyzed by immunoblot assays using anti-GFP and anti-α-tubulin antibodies. The positions of the molecular weight standards (in kDa) are indicated on the right side.

In accordance with previous results obtained using the wild-type strain (Mercier and Labbé, 2010; Plante and Labbé, 2019), *sib1*$^+$ and *sib2*$^+$ transcript levels were induced in the presence of Dip. In contrast, their transcript levels were down regulated under basal and iron-replete conditions (**Figure 4D**). The *sib1*$^+$ and *sib2*$^+$ mRNA levels were repressed 2.9- and 3.9-fold, respectively, under high-iron conditions relative to the corresponding levels under low-iron conditions (**Figure 4D**). To validate the predominant role of Fep1 in iron-mediated repression of *sib1*$^+$ and *sib2*$^+$ transcription, the expression levels of these genes were derepressed in both untreated and iron-treated *fep1*Δ cells (**Figure 4D**). Although the levels of derepression were not as high as that under iron-limiting conditions, they were considerably higher (4.7- and 6.2-fold, respectively) than that observed under the same iron-replete conditions in the wild-type strain (**Figure 4D**).

To ascertain whether the steady-state protein levels of Sib2-GFP and Sib3-GFP were consistent with that of *sib2*$^+$*-GFP* and *sib3*$^+$*-GFP* transcripts, we created strains in which the *GFP* coding sequence was integrated at the chromosomal loci of *sib2*$^+$ and *sib3*$^+$ in the wild-type and *fep1*Δ mutant strains. These strains were grown to the logarithmic phase and left untreated or treated with Dip (250 μM) or $FeCl_3$ (100 μM) for 90 min. Whole cell extracts were prepared and analyzed by immunoblotting. The results showed that Sib3-GFP steady-state levels were constitutively expressed in both the wild-type and *fep1*Δ strains, irrespective of the cellular iron status (**Figure 4E**). In the case of steady-state protein levels of Sib2-GFP, results showed that they were elevated in the presence of Dip but low in untreated or iron-treated wild-type cells. In the case of *fep1*Δ cells expressing *sib2*$^+$*-GFP*, results showed that Sib2-GFP protein levels remained elevated and nearly unchanged under all experimental conditions (**Figure 4E**). Taken together, these results indicate that Sib3 is constitutively expressed and its presence is required for the Fc production, which could be utilized as an iron source by *S. cerevisiae fet3*Δ *arn1-4*Δ *ARN1* cells.

Sib1, Sib2, and Sib3 proteins exhibit a common subcellular localization under low-iron conditions

The finding that Sib1, Sib2, and Sib3 participated in Fc biosynthesis suggested that these proteins share a common subcellular localization when they are active, especially under low-iron conditions. To ascertain the localization of Sib1, Sib2, and Sib3 proteins in *S. pombe*, functional GFP-tagged *sib1*$^+$, *sib2*$^+$, and *sib3*$^+$ alleles were created. In the case of *sib3*$^+$, its GFP- or Cherry-tagged version functionally complemented the growth deficiency of a *sib3*Δ strain on iron-depleted media in a manner indistinguishable from the untagged *sib3*$^+$ allele (**Figures 4A**, **5A**). For *sib1*$^+$ and *sib2*$^+$, two *S. pombe* strains were used in which the *GFP* coding sequence was directly integrated at these chromosomal loci. Cultures of the strains expressing *sib1*$^+$*-GFP* and *sib2*$^+$*-GFP* were grown, and a serial dilution series of each culture was analyzed to test whether they restored growth defects in a medium supplemented with Dip compared to the wild-type strain for which growth was observed (**Figure 5A**). As expected, strains harboring GFP-tagged *sib1*$^+$ and *sib2*$^+$ alleles regained the ability to grow on medium containing Dip (**Figure 5A**). In contrast, the *sib1*Δ *sib2*Δ mutant strain was unable to grow on the medium supplemented with Dip, unlike the wild-type strain (**Figure 5A**).

Next, we examined the cellular localization of GFP-tagged Sib1, Sib2, and Sib3 proteins in cells that had been incubated in the absence or presence of Dip or $FeCl_3$. Under low-iron conditions, fluorescence microscopy showed that Sib1-GFP and Sib2-GFP fluorescent signals were primarily observed throughout the cytoplasm and that they appeared to be largely absent in the nucleus (**Figure 5B**). Consistent with the iron-dependent regulated expression of *sib1*$^+$ and *sib2*$^+$, Sib1-GFP and Sib2-GFP fluorescence signals were lost when the cells were untreated (basal conditions) or treated with high concentrations of iron (100 μM $FeCl_3$) (**Figure 5B**). The green fluorescence signal associated with Sib3-GFP was pancellular; it was detected throughout the cytoplasm and nucleus. Furthermore, the Sib3-GFP-associated fluorescent signal remained unchanged under basal, iron-starved, and iron-replete conditions (**Figure 5B**).

To further examine the cellular localization of fluorescent fusion proteins when co-expressed in cells, experiments were set by integrating functional *sib1*$^+$*-GFP* and *sib3*$^+$*-Cherry* or *sib2*$^+$*-GFP* and *sib3*$^+$*-Cherry* alleles into *sib1*Δ *sib3*Δ, *sib2*Δ *sib3*Δ, or *sib1*Δ *sib2*Δ *sib3*Δ cells. For simplicity, we have presented the results obtained using the *sib1*Δ *sib2*Δ *sib3*Δ triple mutant strain in which the indicated alleles were returned because identical results were observed using the *sib1*Δ *sib3*Δ or *sib2*Δ *sib3*Δ strain prior to the reintroduction of *sib1*$^+$*-GFP* and *sib3*$^+$*-Cherry* or *sib2*$^+$*-GFP* and *sib3*$^+$*-Cherry* alleles. Following the growth of cells under low-iron conditions, fluorescence microscopy analysis showed that co-expression of Sib1-GFP and Sib3-Cherry or Sib2-GFP and Sib3-Cherry exhibited identical patterns of fluorescent signals compared to that observed when each of the fluorescent proteins was expressed separately in iron-starved cells (**Figure 5C**). Sib1-GFP and Sib2-GFP fluorescent proteins were primarily localized in the cytosol, whereas the Sib3-Cherry fluorescent signal displayed a pancellular distribution (**Figure 5C**). Taken together, these results indicate that all three proteins can be found in the cytosol, where they participate in Fc biosynthesis.

Considering that Sib2 and Sib3 represent the first two enzymes of the pathway that are required for Fc biosynthesis, and the observation that they exhibited a common subcellular localization suggested that these proteins could interact with one another. To test whether Sib2 and Sib3 are interacting partners, *S. pombe sib2*Δ *sib3*Δ mutant cells were used

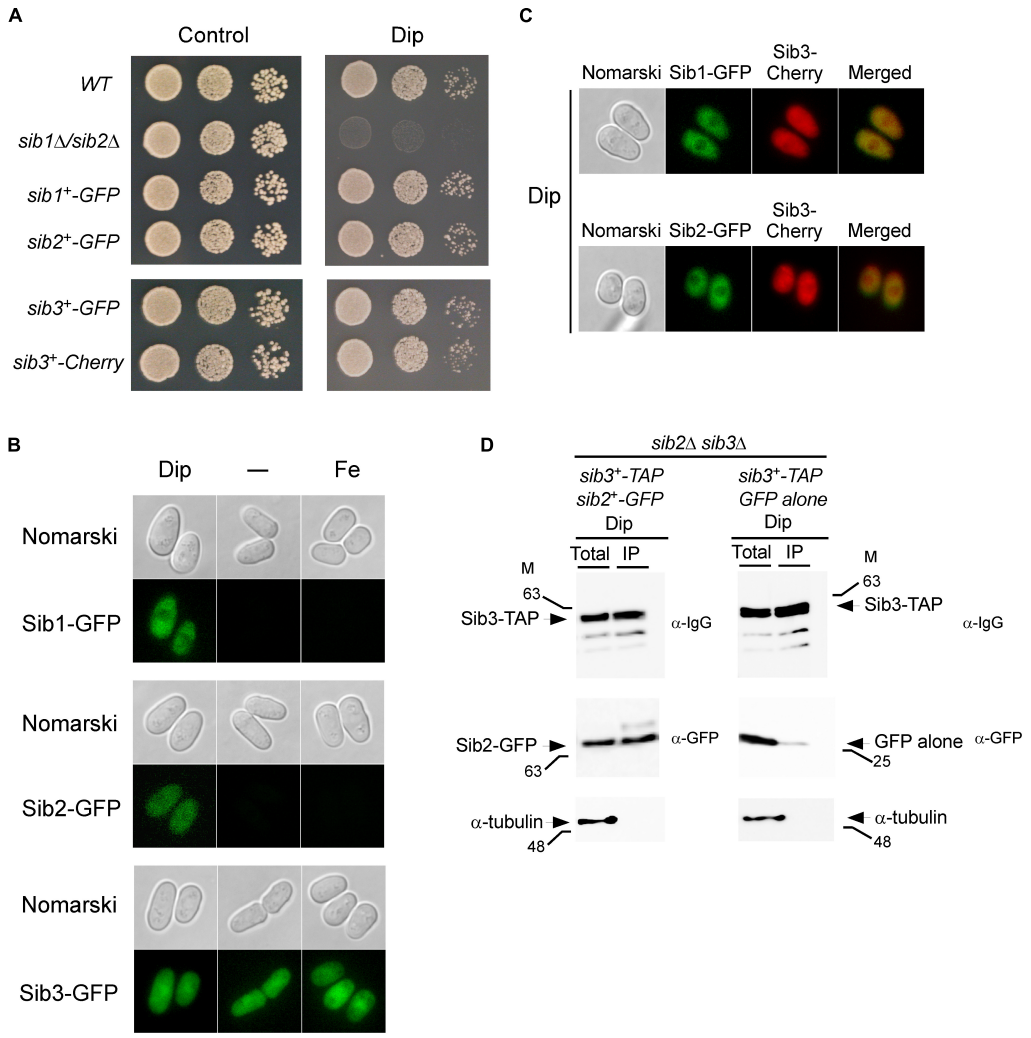

FIGURE 5
Localization of Sib1, Sib2 and Sib3 proteins in *S. pombe*. **(A)** Strains in which the *GFP* coding sequence was directly integrated at the chromosomal locus of *sib1*$^+$, *sib2*$^+$, or *sib3*$^+$ were created and termed *sib1*$^+$-GFP, *sib2*$^+$-GFP, and *sib3*$^+$-GFP strains, respectively. In the case of *sib3*$^+$, an identical approach was performed using the Cherry coding sequence, thereby creating the *sib3*$^+$-Cherry strain. Wild-type (WT), *sib1*Δ *sib2*Δ, *sib1*$^+$-GFP, *sib2*$^+$-GFP, *sib3*$^+$-GFP, and *sib3*$^+$-Cherry strains were grown to the logarithmic phase under non-selective growth conditions and spotted in serial dilutions onto YES medium without Dip (control) or with Dip (140 μM). **(B)** Strains expressing *sib1*$^+$*-GFP*, *sib2*$^+$*-GFP*, and *sib3*$^+$*-GFP* alleles under the control of their own promoters were untreated (-) or treated with Dip (250 μM) or $FeCl_3$ (100 μM) for 90 min. Cells were analyzed by fluorescence microscopy for the presence of GFP-dependent fluorescence signals (*bottom of each pair of panels*). Nomarski optics (*top of each pair of panels*) was used for examining cell morphologies. **(C)** Strains co-expressing Sib3-Cherry in combination with Sib1-GFP or Sib2-GFP were incubated in the presence of Dip (250 μM) for 90 min. Fluorescence signals of Sib3-Cherry co-expressed with Sib1-GFP or Sib2-GFP were observed by fluorescence microscopy (*middle panels*). Merged images of co-expressed fluorescent proteins are shown in the *far right panels*. Cell morphology was examined by Nomarski optics in the *far left panels*. Results of microscopy are representative of five independent experiments. **(D)** *sib2*Δ *sib3*Δ cells co-expressing GFP-tagged Sib2 and TAP-tagged Sib3 or GFP alone and TAP-tagged Sib3 were grown to the mid-logarithmic phase and incubated in the presence of Dip (250 μM) for 90 min. Whole cell extracts (Total) were incubated with IgG-Sepharose beads. The immunoprecipitated fractions (IP) were analyzed by immunoblot assays using anti-mouse IgG (α-IgG), anti-GFP (α-GFP) and anti-α-tubulin antibodies. Aliquots of whole cell extracts (Total) were probed with the same antibodies to ascertain the presence of epitope-tagged proteins prior to incubation with beads. As an additional control, aliquots of total cell lysates and bound fractions were assayed using an anti-α-tubulin antibody. The positions of the molecular weight standards (in kDa) are indicated on the left and right sides of the panels.

for co-expressing *sib3*$^+$*-TAP* and *sib2*$^+$*-GFP* or *sib3*$^+$*-TAP* and *GFP* alleles. *S. pombe* cells were grown in a medium containing Dip (250 μM). Whole-cell extracts were prepared and subsequently incubated in the presence of IgG-Sepharose beads that selectively bound TAP-tagged Sib3. The results showed that Sib3-TAP was retained on the beads and detected in the immunoprecipitated fraction (IP) (Figure 5D). Furthermore, the IP contained Sib2-GFP, which interacted with Sib3-TAP (Figure 5D). Interaction between Sib3-TAP and GFP alone was not observed in pull-down experiments, unlike the

interaction between Sib3-TAP and Sib2-GFP (**Figure 5D**). To assess the specificity of the pull-down experiments, whole-cell extracts (Total) and bound fractions (IP) were analyzed by immunoblotting using an antibody directed against α-tubulin. The results showed that α-tubulin was present in whole cell extracts but not in IPs (**Figure 5D**). Taken together, these results revealed that Sib2-GFP and Sib3-TAP interact with each other to form a protein complex that is co-immunoprecipitated from whole-cell extracts isolated from iron-starved cells.

Discussion

In this study, we established experimental culture conditions in which *S. cerevisiae* cells that are unable to synthesize Fc took advantage of Fc secreted from *S. pombe* cells to survive under iron deficiency. Considering that this exchange of Fc was unidirectional, with donor *S. pombe* cells providing Fc to recipient *S. cerevisiae* cells, the interaction was classified as one-way cross-feeding. Fc serves as an essential metabolite required for the cellular growth of *S. cerevisiae* as a sole source of iron. Although previous studies have reported that siderophores can participate in one-way cross-feeding between different bacterial species (Joshi et al., 2006; Galet et al., 2015; Butaitë et al., 2017; D'Souza et al., 2018), such cross-feeding interactions are much less known between different fungal species. A previous study suggested that Fc secreted by *S. pombe* allows conidial germination of an *Aspergillus nidulans sidA*Δ strain deficient in siderophore synthesis (Schrettl et al., 2004). However, the latter study only used a wild-type *S. pombe* strain without further characterization of the genes and proteins required for establishing one-way cross-feeding between the two yeast species. Another study showed that *Paracoccidiodes lutzii* and *P. brasiliensis* yeasts could donate siderophores to a non-producer *A. nidulans sidA*Δ mutant (Silva-Bailão et al., 2014). In *Paracoccidiodes* yeasts, the identity of cellular components involved in one-way cross-feeding with *A. nidulans sidA*Δ cells remains unknown. Thus, in fungal species, the nature of molecules and mechanisms whereby cross-feeding occurs remain poorly defined.

To identify the *S. pombe* genes required for Fc production, which can affect the survival of a neighboring yeast, we set experimental conditions in which *S. cerevisiae* obligately utilized *S. pombe* Fc to survive. As expected, we found that disruption of the *sib1*$^+$ and *sib2*$^+$ genes of *S. pombe* blocked Fc biosynthesis, thus preventing Fc-dependent growth of *S. cerevisiae* cells. To identify a putative transacetylase involved in Fc biosynthesis, we initially searched the entire set of genetic information of the *S. pombe* database. Analysis of genomic DNA sequences revealed 38 genes that encode known or putative members of the GCN5-related N-acetyltransferase (GNAT) protein family. This family of proteins includes functionally diverse enzymes that catalyze the transfer of an acetyl group from acetyl-CoA to the primary amine of different acceptor substrates. Among them, only one gene (*SPBC17G9.06c*, denoted *sib3*$^+$) contains a pfam10331/AlcB domain, which is typically found in siderophore-biosynthetic transacetylase enzymes (de Lorenzo et al., 1986; Card et al., 2005; Challis, 2005; Blatzer et al., 2011). Enzymes that catalyze the transfer of an acetyl group from acetyl-CoA during the biosynthesis of siderophores include *Bordetella bronchiseptica* AlcB, *E. coli* IucB, *Mycobacterium tuberculosis* Rv1347c, and *Aspergillus fumigatus* SidL (de Lorenzo et al., 1986; Card et al., 2005; Challis, 2005; Blatzer et al., 2011).

Inactivation of N^5-hydroxyornithine acetyl-CoA-N^5-transacetylase SidL (*sidL*Δ) prevents ferricrocin biosynthesis under iron-replete conditions (Blatzer et al., 2011). However, a *sidL*Δ mutant is still able to produce ferricrocin under low-iron conditions, suggesting the existence of a second uncharacterized N^5-hydroxyornithine acetyl-CoA-N^5-transacetylase that is induced to compensate for the loss of SidL (*sidL*Δ) under iron-poor conditions (Blatzer et al., 2011). Deletion of *S. pombe* Sib3 blocked Fc biosynthesis irrespective of cellular iron status. Moreover, an *S. pombe sib3*Δ mutant failed to provide Fc to *S. cerevisiae fet3*Δ *arn1-4*Δ *ARN1* cells when the two yeast species were spotted in close proximity, resulting in growth defects in the case of *S. cerevisiae fet3*Δ *arn1-4*Δ *ARN1* cells. In contrast to *A. fumigatus*, *S. pombe* does not possess a second N^5-hydroxyornithine acetyl-CoA-N^5-transacetylase because inactivation of *sib3*$^+$ (*sib3*Δ) results in a complete inability to produce Fc under both iron-replete and iron-depleted conditions.

In general, the expression of fungal genes encoding siderophore biosynthetic enzymes is transcriptionally repressed in response to high iron concentrations (Haas, 2003, 2014; Haas et al., 2008). In contrast, the transcript levels of these genes are generally induced under iron-starvation conditions. A few exceptions include the *npgA* and *sidL* genes in *A. nidulans* that are constitutively expressed (Oberegger et al., 2003; Blatzer et al., 2011). Similar to *A. nidulans npgA* and *sidL*, *sib3*$^+$ is constitutively expressed in *S. pombe* under basal, iron-starved, and iron-replete conditions. The iron-dependent downregulation of fungal iron-regulated siderophore biosynthetic genes is primarily mediated by iron-regulatory GATA-type transcription factors, including SreA in *A. nidulans* and *A. fumigatus*, URBS1 in *Ustilago maydis*, and Fep1 in *S. pombe* (Haas et al., 2008; Brault et al., 2015; Hortschansky et al., 2017). However, Sib3 being a constitutively expressed gene, the mRNA and protein levels of Sib3 did not vary significantly with respect to either the presence or absence of Fep1, confirming its non-canonical expression profile compared to that of classical iron regulon genes.

The localization of *S. pombe* Sib3 was observed throughout the cells, suggesting that it is localized to both the cytosol and nucleus. In contrast, the Sib1 and Sib2 proteins were primarily cytosolic. Because the common cellular compartment of Sib1, Sib2, and Sib3 is the cytosol, Fc biosynthesis most likely occurs in the cytoplasmic compartment, as it has been

proposed for ferricrocin biosynthesis in *A. fumigatus* (Haas, 2014). For Fc biosynthesis, Sib2 is required for the conversion of ornithine to N^5-hydroxyornithine. The results presented here reveal that Sib2 and Sib3 co-localize in the cytosol and interact with one another. One can envision that the step involving Sib2-dependent conversion of ornithine possibly includes an additional mechanism that favors the simultaneous recruitment of Sib3 to facilitate the next sequential reaction, which consists of the acetylation of N^5-hydroxyornithine. This would favor the first two sequential reactions, allowing efficient accumulation of N^5-acetyl-N^5-hydroxyornithine that needs to be combined with three glycine residues to assemble the finished Fc product through the action of Sib1.

As previously reported in the case of *S. cerevisiae* Arn1 (Kim et al., 2002), our results showed that the protein primarily localizes to the endosomal compartment under basal growth conditions in a Fc-free medium. When *S. cerevisiae* cells are exposed to low concentrations of Fc under low-iron conditions, Arn1 undergoes re-localization from the endosomal compartment to the plasma membrane (Kim et al., 2002, 2005). Our results showed that the localization of *S. pombe* Str1 moved away from an intracellular compartment to occupy the periphery of the cell when cells had been treated with Dip or Dip plus Fc. At this point, however, it is unclear how Str1 re-localized to the cell surface in the presence of Fc under low-iron conditions. In the case of *S. cerevisiae* Arn1, studies have shown that an extracytosolic carboxyl-terminal domain of the protein is required for its cycling between the plasma membrane and endosomal compartments, where uptake of Fc occurs (Kim et al., 2005). At this stage, although the carboxyl-terminal region of Str1 contains conserved amino acid residues with the Fc-responsive extracytosolic loop of Arn1, the identification of a specific Fc receptor domain of Str1 that may control its trafficking will require additional studies.

Following Fc biosynthesis, one can envision the existence of transporter(s) for Fc secretion. Fc secretion is believed to be a necessary step for releasing Fc into the environment before the reuptake of Fc-bound iron by *S. pombe* cells. As shown in this study, the secreted Fc could be recovered and utilized by *S. cerevisiae* cells in the vicinity of *S. pombe* cells. Key cell-surface membrane proteins have been identified for the secretion of enterobactin from *E. coli* cells into the extracellular environment (Wilson et al., 2016). First, enterobactin is exported from the cytosol to the periplasm by EntS, a MFS-type transporter. Subsequently, the efflux of enterobactin across the outer membrane involves the concerted action of a resistance/nodulated/cell division (RND)-class transporter (AcrB, AcrD, or MdtABC) and the protein channel TolC (Horiyama and Nishino, 2014; Wilson et al., 2016). Considering the complexity of the siderophore efflux system in *E. coli*, it is not surprising that little is known regarding siderophore secretion in fungi. In *Aspergillus fumigatus*, fusarinine C (FsC) and triacetylfusarinine C (TAFC) siderophores are produced and secreted into the external environment (Schrettl et al., 2007). Although the proteins involved in their biosynthesis have been identified, the transporters for the secretion of FsC and TAFC have not yet been identified. Further investigation will be necessary to decipher the precise mechanisms by which *S. pombe* secretes Fc into the external milieu.

Data availability statement

The original contributions presented in this study are included in the article/supplementary material, further inquiries can be directed to the corresponding author.

Author contributions

AB, BM, and SL: methodology, validation, formal analysis, investigation, review and editing, and resources. AB and SL: conceptualization, writing—original draft preparation. SL: supervision, project administration, and funding acquisition. All authors have read, reviewed and approved the final version of the manuscript.

Funding

This study was supported by the Natural Sciences and Engineering Research Council of Canada (NSERC, grant #RGPIN-2020/2025-04802) to SL.

Acknowledgments

We are grateful to Dr. Gilles Dupuis for critical reading of the manuscript and for his valuable comments.

Conflict of interest

The authors declare that the research was conducted in the absence of any commercial or financial relationships that could be construed as a potential conflict of interest.

Publisher's note

All claims expressed in this article are solely those of the authors and do not necessarily represent those of their affiliated organizations, or those of the publisher, the editors and the reviewers. Any product that may be evaluated in this article, or claim that may be made by its manufacturer, is not guaranteed or endorsed by the publisher.

References

Aguiar, M., Orasch, T., Misslinger, M., Dietl, A. M., Gsaller, F., and Haas, H. (2021). The siderophore transporters Sit1 and Sit2 are essential for utilization of ferrichrome-, ferrioxamine- and coprogen-type siderophores in *Aspergillus fumigatus*. *J. Fungi.* 7:768. doi: 10.3390/jof7090768

Askwith, C., Eide, D., Van Ho, A., Bernard, P. S., Li, L., Davis-Kaplan, S., et al. (1994). The *FET3* gene of *S. cerevisiae* encodes a multicopper oxidase required for ferrous iron uptake. *Cell* 76, 403–410. doi: 10.1016/0092-8674(94)90346-8

Askwith, C. C., and Kaplan, J. (1998). Site-directed mutagenesis of the yeast multicopper oxidase Fet3p. *J. Biol. Chem.* 273, 22415–22419. doi: 10.1074/jbc.273.35.22415

Bahler, J., Wu, J. Q., Longtine, M. S., Shah, N. G., McKenzie, A. III, Steever, A. B., et al. (1998). Heterologous modules for efficient and versatile PCR-based gene targeting in *Schizosaccharomyces pombe*. *Yeast* 14, 943–951. doi: 10.1002/(SICI)1097-0061(199807)14:10<943::AID-YEA292<3.0.CO;2-Y

Beaudoin, J., and Labbé, S. (2001). The fission yeast copper-sensing transcription factor Cuf1 regulates the copper transporter gene expression through an Ace1/Amt1-like recognition sequence. *J. Biol. Chem.* 276, 15472–15480. doi: 10.1074/jbc.M011256200

Blatzer, M., Schrettl, M., Sarg, B., Lindner, H. H., Pfaller, K., and Haas, H. (2011). SidL, an *Aspergillus fumigatus* transacetylase involved in biosynthesis of the siderophores ferricrocin and hydroxyferricrocin. *Appl. Environ. Microbiol.* 77, 4959–4966. doi: 10.1128/aem.00182-11

Brault, A., Mourer, T., and Labbé, S. (2015). Molecular basis of the regulation of iron homeostasis in fission and filamentous yeasts. *IUBMB Life* 67, 801–815. doi: 10.1002/iub.1441

Butaitë, E., Baumgartner, M., Wyder, S., and Kümmerli, R. (2017). Siderophore cheating and cheating resistance shape competition for iron in soil and freshwater *Pseudomonas* communities. *Nat. Commun.* 8:414. doi: 10.1038/s41467-017-00509-4

Card, G. L., Peterson, N. A., Smith, C. A., Rupp, B., Schick, B. M., and Baker, E. N. (2005). The crystal structure of Rv1347c, a putative antibiotic resistance protein from *Mycobacterium tuberculosis*, reveals a GCN5-related fold and suggests an alternative function in siderophore biosynthesis. *J. Biol. Chem.* 280, 13978–13986. doi: 10.1074/jbc.M413904200

Challis, G. L. (2005). A widely distributed bacterial pathway for siderophore biosynthesis independent of nonribosomal peptide synthetases. *Chembiochem* 6, 601–611. doi: 10.1002/cbic.200400283

Chen, D., Toone, W. M., Mata, J., Lyne, R., Burns, G., Kivinen, K., et al. (2003). Global transcriptional responses of fission yeast to environmental stress. *Mol. Biol. Cell* 14, 214–229. doi: 10.1091/mbc.E02-08-0499

Cottarel, G., Beach, D., and Deuschle, U. (1993). Two new multi-purpose multicopy *Schizosaccharomyces pombe* shuttle vectors, pSP1 and pSP2. *Curr. Genet.* 23, 547–548. doi: 10.1007/BF00312650

de Lorenzo, V., Bindereif, A., Paw, B. H., and Neilands, J. B. (1986). Aerobactin biosynthesis and transport genes of plasmid ColV-K30 in *Escherichia coli K-12*. *J. Bacteriol.* 165, 570–578. doi: 10.1128/jb.165.2.570-578.1986

De Silva, D. M., Askwith, C. C., Eide, D., and Kaplan, J. (1995). The *FET3* gene product required for high affinity iron transport in yeast is a cell surface ferroxidase. *J. Biol. Chem.* 270, 1098–1101. doi: 10.1074/jbc.270.3.1098

D'Souza, G., Shitut, S., Preussger, D., Yousif, G., Waschina, S., and Kost, C. (2018). Ecology and evolution of metabolic cross-feeding interactions in bacteria. *Nat. Prod. Rep.* 35, 455–488. doi: 10.1039/c8np00009c

Foiani, M., Marini, F., Gamba, D., Lucchini, G., and Plevani, P. (1994). The B subunit of the DNA polymerase alpha-primase complex in *Saccharomyces cerevisiae* executes an essential function at the initial stage of DNA replication. *Mol. Cell. Biol.* 14, 923–933. doi: 10.1128/mcb.14.2.923-933.1994

Fritts, R. K., McCully, A. L., and McKinlay, J. B. (2021). Extracellular metabolism sets the table for microbial cross-feeding. *Microbiol. Mol. Biol. Rev.* 85, e135–e120. doi: 10.1128/mmbr.00135-20

Galaris, D., Barbouti, A., and Pantopoulos, K. (2019). Iron homeostasis and oxidative stress: an intimate relationship. *Biochim. Biophys. Acta Mol. Cell Res.* 1866:118535. doi: 10.1016/j.bbamcr.2019.118535

Galet, J., Deveau, A., Hôtel, L., Frey-Klett, P., Leblond, P., and Aigle, B. (2015). Pseudomonas fluorescens pirates both ferrioxamine and ferricoelichelin siderophores from *Streptomyces ambofaciens*. *Appl. Environ. Microbiol.* 81, 3132–3141. doi: 10.1128/aem.03520-14

Haas, H. (2003). Molecular genetics of fungal siderophore biosynthesis and uptake: the role of siderophores in iron uptake and storage. *Appl. Microbiol. Biotechnol.* 62, 316–330. doi: 10.1007/s00253-003-1335-2

Haas, H. (2014). Fungal siderophore metabolism with a focus on *Aspergillus fumigatus*. *Nat. Prod. Rep.* 31, 1266–1276. doi: 10.1039/c4np00071d

Haas, H., Eisendle, M., and Turgeon, B. G. (2008). Siderophores in fungal physiology and virulence. *Annu. Rev. Phytopathol.* 46, 149–187. doi: 10.1146/annurev.phyto.45.062806.094338

Heymann, P., Ernst, J. F., and Winkelmann, G. (1999). Identification of a fungal triacetylfusarinine C siderophore transport gene (TAF1) in *Saccharomyces cerevisiae* as a member of the major facilitator superfamily. *Biometals* 12, 301–306. doi: 10.1023/a:1009252118050

Heymann, P., Ernst, J. F., and Winkelmann, G. (2000a). A gene of the major facilitator superfamily encodes a transporter for enterobactin (Enb1p) in *Saccharomyces cerevisiae*. *Biometals* 13, 65–72. doi: 10.1023/a:1009250017785

Heymann, P., Ernst, J. F., and Winkelmann, G. (2000b). Identification and substrate specificity of a ferrichrome-type siderophore transporter (Arn1p) in *Saccharomyces cerevisiae*. *FEMS Microbiol. Lett.* 186, 221–227. doi: 10.1111/j.1574-6968.2000.tb09108.x

Hider, R. C., and Kong, X. (2010). Chemistry and biology of siderophores. *Nat. Prod. Rep.* 27, 637–657. doi: 10.1039/b906679a

Horiyama, T., and Nishino, K. (2014). AcrB, AcrD, and MdtABC multidrug efflux systems are involved in enterobactin export in *Escherichia coli*. *PLoS One* 9:e108642. doi: 10.1371/journal.pone.0108642

Hortschansky, P., Haas, H., Huber, E. M., Groll, M., and Brakhage, A. A. (2017). The CCAAT-binding complex (CBC) in *Aspergillus* species. *Biochim. Biophys. Acta Gene Regul. Mech.* 1860, 560–570. doi: 10.1016/j.bbagrm.2016.11.008

Ioannoni, R., Beaudoin, J., Lopez-Maury, L., Codlin, S., Bahler, J., and Labbé, S. (2012). Cuf2 is a novel meiosis-specific regulatory factor of meiosis maturation. *PLoS One* 7:e36338. doi: 10.1371/journal.pone.0036338

Jacques, J. F., Mercier, A., Brault, A., Mourer, T., and Labbé, S. (2014). Fra2 is a co-regulator of Fep1 inhibition in response to iron starvation. *PLoS One* 9:e98959. doi: 10.1371/journal.pone.0098959

Jbel, M., Mercier, A., Pelletier, B., Beaudoin, J., and Labbé, S. (2009). Iron activates in vivo DNA binding of *Schizosaccharomyces pombe* transcription factor Fep1 through its amino-terminal region. *Eukaryot. Cell* 8, 649–664. doi: 10.1128/EC.00001-09

Joshi, F., Archana, G., and Desai, A. (2006). Siderophore cross-utilization amongst rhizospheric bacteria and the role of their differential affinities for Fe3+ on growth stimulation under iron-limited conditions. *Curr. Microbiol.* 53, 141–147. doi: 10.1007/s00284-005-0400-8

Keeney, J. B., and Boeke, J. D. (1994). Efficient targeted integration at leu1-32 and ura4-294 in *Schizosaccharomyces pombe*. *Genetics* 136, 849–856. doi: 10.1093/genetics/136.3.849

Kim, Y., Lampert, S. M., and Philpott, C. C. (2005). A receptor domain controls the intracellular sorting of the ferrichrome transporter, ARN1. *EMBO J.* 24, 952–962. doi: 10.1038/sj.emboj.7600579

Kim, Y., Yun, C. W., and Philpott, C. C. (2002). Ferrichrome induces endosome to plasma membrane cycling of the ferrichrome transporter, Arn1p, in *Saccharomyces cerevisiae*. *EMBO J.* 21, 3632–3642. doi: 10.1093/emboj/cdf382

Lesuisse, E., Blaiseau, P. L., Dancis, A., and Camadro, J. M. (2001). Siderophore uptake and use by the yeast *Saccharomyces cerevisiae*. *Microbiology* 147, 289–298. doi: 10.1099/00221287-147-2-289

Lesuisse, E., Simon-Casteras, M., and Labbé, P. (1998). Siderophore-mediated iron uptake in *Saccharomyces cerevisiae*: the *SIT1* gene encodes a ferrioxamine B permease that belongs to the major facilitator superfamily. *Microbiology* 144, 3455–3462. doi: 10.1099/00221287-144-12-3455

Livak, K. J., and Schmittgen, T. D. (2001). Analysis of relative gene expression data using real-time quantitative PCR and the 2(-Delta Delta C(T)) Method. *Methods* 25, 402–408. doi: 10.1006/meth.2001.1262

Mercier, A., and Labbé, S. (2010). Iron-dependent remodeling of fungal metabolic pathways associated with ferrichrome biosynthesis. *Appl. Environ. Microbiol.* 76, 3806–3817. doi: 10.1128/AEM.00659-10

Mercier, A., Watt, S., Bahler, J., and Labbé, S. (2008). Key function for the CCAAT-binding factor Php4 to regulate gene expression in response to iron deficiency in fission yeast. *Eukaryot. Cell* 7, 493–508. doi: 10.1128/EC.00446-07

Miethke, M., and Marahiel, M. A. (2007). Siderophore-based iron acquisition and pathogen control. *Microbiol. Mol. Biol. Rev.* 71, 413–451. doi: 10.1128/mmbr.00012-07

Moore, R. E., Kim, Y., and Philpott, C. C. (2003). The mechanism of ferrichrome transport through Arn1p and its metabolism in *Saccharomyces cerevisiae*. *Proc. Natl. Acad. Sci. USA* 100, 5664–5669. doi: 10.1073/pnas.1030323100

Moreno, S., Klar, A., and Nurse, P. (1991). Molecular genetic analysis of fission yeast Schizosaccharomyces pombe. *Methods Enzymol.* 194, 795–823. doi: 10.1016/0076-6879(91)94059-l

Mumberg, D., Muller, R., and Funk, M. (1995). Yeast vectors for the controlled expression of heterologous proteins in different genetic backgrounds. *Gene* 156, 119–122. doi: 10.1016/0378-1119(95)00037-7

Oberegger, H., Eisendle, M., Schrettl, M., Graessle, S., and Haas, H. (2003). 4'-phosphopantetheinyl transferase-encoding npgA is essential for siderophore biosynthesis in Aspergillus nidulans. *Curr. Genet.* 44, 211–215. doi: 10.1007/s00294-003-0434-z

Pande, S., and Kost, C. (2017). Bacterial unculturability and the formation of intercellular metabolic networks. *Trends Microbiol.* 25, 349–361. doi: 10.1016/j.tim.2017.02.015

Pelletier, B., Beaudoin, J., Mukai, Y., and Labbé, S. (2002). Fep1, an iron sensor regulating iron transporter gene expression in *Schizosaccharomyces pombe*. *J. Biol. Chem.* 277, 22950–22958. doi: 10.1074/jbc.M202682200

Pelletier, B., Beaudoin, J., Philpott, C. C., and Labbé, S. (2003). Fep1 represses expression of the fission yeast *Schizosaccharomyces pombe* siderophore-iron transport system. *Nucleic Acids Res.* 31, 4332–4344.

Philpott, C. C., Patel, S. J., and Protchenko, O. (2020). Management versus miscues in the cytosolic labile iron pool: the varied functions of iron chaperones. *Biochim. Biophys. Acta Mol. Cell Res.* 1867:118830. doi: 10.1016/j.bbamcr.2020.118830

Philpott, C. C., Protchenko, O., Kim, Y. W., Boretsky, Y., and Shakoury-Elizeh, M. (2002). The response to iron deprivation in *Saccharomyces cerevisiae*: expression of siderophore-based systems of iron uptake. *Biochem. Soc. Trans.* 30, 698–702. doi: 10.1042/bst0300698

Plante, S., and Labbé, S. (2019). Spore germination requires ferrichrome biosynthesis and the siderophore transporter Str1 in *Schizosaccharomyces pombe*. *Genetics* 211, 893–911. doi: 10.1534/genetics.118.301843

Protacio, R. U., Mukiza, T. O., Davidson, M. K., and Wahls, W. P. (2022). Molecular mechanisms for environmentally induced and evolutionarily rapid redistribution (plasticity) of meiotic recombination. *Genetics* 220:212. doi: 10.1093/genetics/iyab212

Protchenko, O., Ferea, T., Rashford, J., Tiedeman, J., Brown, P. O., Botstein, D., et al. (2001). Three cell wall mannoproteins facilitate the uptake of iron in *Saccharomyces cerevisiae*. *J. Biol. Chem.* 276, 49244–49250. doi: 10.1074/jbc.M109220200

Puig, S., Ramos-Alonso, L., Romero, A. M., and Martínez-Pastor, M. T. (2017). The elemental role of iron in DNA synthesis and repair. *Metallomics* 9, 1483–1500. doi: 10.1039/c7mt00116a

Sabatinos, S. A., and Forsburg, S. L. (2010). Molecular genetics of *Schizosaccharomyces pombe*. *Methods Enzymol.* 470, 759–795. doi: 10.1016/S0076-6879(10)70032-X

Schmittgen, T. D., and Livak, K. J. (2008). Analyzing real-time PCR data by the comparative C(T) method. *Nat. Protoc.* 3, 1101–1108. doi: 10.1038/nprot.2008.73

Schrettl, M., Bignell, E., Kragl, C., Sabiha, Y., Loss, O., Eisendle, M., et al. (2007). Distinct roles for intra- and extracellular siderophores during *Aspergillus fumigatus* infection. *PLoS Pathog.* 3:1195–1207. doi: 10.1371/journal.ppat.0030128

Schrettl, M., Winkelmann, G., and Haas, H. (2004). Ferrichrome in *Schizosaccharomyces pombe* - an iron transport and iron storage compound. *BioMetals* 17, 647–654. doi: 10.1007/s10534-004-1230-z

Seth, E. C., and Taga, M. E. (2014). Nutrient cross-feeding in the microbial world. *Front. Microbiol.* 5:350. doi: 10.3389/fmicb.2014.00350

Sherman, F. (2002). Getting started with yeast. *Methods Enzymol.* 350, 3–41. doi: 10.1016/s0076-6879(02)50954-x

Silva-Bailão, M. G., Bailão, E. F., Lechner, B. E., Gauthier, G. M., Lindner, H., Bailão, A. M., et al. (2014). Hydroxamate production as a high affinity iron acquisition mechanism in *Paracoccidioides spp*. *PLoS One* 9:e105805. doi: 10.1371/journal.pone.0105805

Stearman, R., Yuan, D. S., Yamaguchi-Iwai, Y., Klausner, R. D., and Dancis, A. (1996). A permease-oxidase complex involved in high-affinity iron uptake in yeast. *Science* 271, 1552–1557. doi: 10.1126/science.271.5255.1552

Wilson, B. R., Bogdan, A. R., Miyazawa, M., Hashimoto, K., and Tsuji, Y. (2016). Siderophores in iron metabolism: from mechanism to therapy potential. *Trends Mol. Med.* 22, 1077–1090. doi: 10.1016/j.molmed.2016.10.005

Yun, C. W., Bauler, M., Moore, R. E., Klebba, P. E., and Philpott, C. C. (2001). The role of the FRE family of plasma membrane reductases in the uptake of siderophore-iron in *Saccharomyces cerevisiae*. *J. Biol. Chem.* 276, 10218–10223. doi: 10.1074/jbc.M010065200

Yun, C. W., Ferea, T., Rashford, J., Ardon, O., Brown, P. O., Botstein, D., et al. (2000a). Desferrioxamine-mediated iron uptake in *Saccharomyces cerevisiae*. Evidence for two pathways of iron uptake. *J. Biol. Chem.* 275, 10709–10715. doi: 10.1074/jbc.275.14.10709

Yun, C. W., Tiedeman, J. S., Moore, R. E., and Philpott, C. C. (2000b). Siderophore-iron uptake in *Saccharomyces cerevisiae*. Identification of ferrichrome and fusarinine transporters. *J. Biol. Chem.* 275, 16354–16359. doi: 10.1074/jbc.M001456200

frontiers | Frontiers in Microbiology

TYPE Original Research
PUBLISHED 04 August 2022
DOI 10.3389/fmicb.2022.956421

Check for updates

OPEN ACCESS

EDITED BY
Pinmei Wang,
Zhejiang University, China

REVIEWED BY
Ang Ren,
Nanjing Agricultural University, China
Atsushi Okazawa,
Osaka Metropolitan University, Japan

*CORRESPONDENCE
Zhuang Li
liz552@126.com
Wei Wang
uniwangwei@163.com

SPECIALTY SECTION
This article was submitted to Microbial Physiology and Metabolism, a section of the journal Frontiers in Microbiology

RECEIVED 30 May 2022
ACCEPTED 18 July 2022
PUBLISHED 04 August 2022

CITATION
Meng L, Zhou R, Lin J, Zang X, Wang Q, Wang P, Wang L, Li Z and Wang W (2022) Transcriptome and metabolome analyses reveal transcription factors regulating ganoderic acid biosynthesis in *Ganoderma lucidum* development. *Front. Microbiol.* 13:956421. doi: 10.3389/fmicb.2022.956421

COPYRIGHT
© 2022 Meng, Zhou, Lin, Zang, Wang, Wang, Wang, Li and Wang. This is an open-access article distributed under the terms of the Creative Commons Attribution License (CC BY). The use, distribution or reproduction in other forums is permitted, provided the original author(s) and the copyright owner(s) are credited and that the original publication in this journal is cited, in accordance with accepted academic practice. No use, distribution or reproduction is permitted which does not comply with these terms.

Transcriptome and metabolome analyses reveal transcription factors regulating ganoderic acid biosynthesis in *Ganoderma lucidum* development

Li Meng, Ruyue Zhou, Jialong Lin, Xizhe Zang, Qingji Wang, Panmeng Wang, Li Wang, Zhuang Li* and Wei Wang*

Shandong Provincial Key Laboratory of Agricultural Microbiology, College of Plant Protection, Shandong Agricultural University, Tai'an, China

Ganoderma lucidum is an important medicinal fungus in Asian countries. Ganoderic acid (GA) is the major variety of bioactive and medicative components in *G. lucidum*. Biosynthesis of secondary metabolites is usually associated with cell differentiation and development. However, the mechanism underlying these phenomena remain unclear. Transcription factors play an essential regulatory role in the signal transduction pathway, owing to the fact that they represent the major link between signal transduction and expression of target genes. In the present study, we performed transcriptome and metabolome analyses to identify transcription factors involved in GA biosynthesis during development of *G. lucidum*. Transcriptome data revealed differentially expressed genes between mycelia and primordia, as well as between mycelia and the fruiting body. Results from gene ontology enrichment analysis and metabolome analyses suggested that GAs and flavonoids biosynthetic process significantly changed during fungal development. The analysis of predicted occurrences of DNA-binding domains revealed a set of 53 potential transcription factor families in *G. lucidum*. Notably, we found homeobox transcription factor and velvet family protein played important role in GA biosynthesis. Combined with previous studies, we provided a model diagram of transcription factors involved in GA biosynthesis during fruiting body formation. Collectively, these results are expected to enhance our understanding into the mechanisms underlying secondary metabolite biosynthesis and development in fungi.

KEYWORDS

development, medicinal fungi, regulatory mechanisms, secondary metabolites, *Ganoderma lucidum*

Introduction

Fungi are remarkable organisms that readily produce a wide range of natural products often called secondary metabolites (Calvo et al., 2002), some of which are beneficial to humankind (Demain and Fang, 2000). *Ganoderma* spp., an important medicinal fungus, has been widely used to improve health and prevent certain diseases in traditional Chinese medicine for thousands of years (Ahmad, 2018), owing to a variety of biomedical efficacies including anti-cancer, anti-tumor, immune modulatory effects. Results from phytochemical studies over the last 40 years have resulted in isolation of 431 secondary metabolites from various *Ganoderma* species. The major secondary compounds isolated from these species include C30 lanostanes, C27 lanostanes, C24, C25 lanostanes, C30 pentacyclic triterpenes, meroterpenoids, and farnesyl hydroquinones, and so on (Baby et al., 2015).

Ganoderic acids (GAs), a triterpenoid produced by *Ganoderma lucidum* that has a range of biological activities, is regulated by interplay between external (environmental) and internal (genetic) factors. Previous studies have shown that expression of GA biosynthetic machinery can be modulated by various external factors, including salicylic acid (Cao et al., 2017), sodium acetate (Meng et al., 2019), and ethylene (Zhang et al., 2017a; Meng et al., 2022), and so on. Additionally, genes encoding 3-hydroxy-3-methylglutaryl CoA reductase (HMGR) (Shang et al., 2008), squalene synthase (SQS) (Zhao et al., 2007), and oxidosqualene cyclase (OSC) (Shang et al., 2010) as well as other important transcription factors reportedly contribute to GA biosynthesis.

Although biosynthesis of natural products has been associated with cell differentiation and development, previously reports have demonstrated that mutants of transcription factors not only affect mycelia morphology, growth rate, hypha branch, primordia and fruiting body formation, but also play a role in biosynthesis of secondary metabolites. Notably, Cary et al. (2017) revealed that homeobox transcription factor gene *hbx1* is required for the development and aflatoxin biosynthesis in *Aspergillus flavus*. Moreover, the MAP kinase Fus3 (AnFus3) interacts with the conserved nuclear transcription factor AnSte12 to initiate sexual development and phosphorylates VeA, which is a major regulatory protein required for sexual development and coordinated secondary metabolite production in *A. nidulans* (Bayram et al., 2012). In *G. lucidum*, APSES transcription factor (GlSwi6) (Zhang et al., 2018; Lian et al., 2022), GATA transcription factor (AreA) (Zhu et al., 2019), Cys2His2 zinc finger protein gene C2H2-type transcription factor (CRZ1) (Li and Zhong, 2020), and Pcc1 transcription factor (PacC) (Wu et al., 2016) were found to play a role in fungal growth, fruiting body development and GA biosynthesis. We previously identified and characterized a transcription factor MADS1, which can regulate GA biosynthesis, and the gene-silencing mutants of MADS1 hinder the formation of the primordia in *G. lucidum* (Meng et al., 2021). Collectively, these studies have provided insights into molecular mechanisms and pathways that link chemical and morphological differentiation processes in fungi.

Although previous reports have shown that most secondary metabolites are produced by organisms that exhibit filamentous growth and have a relatively complex morphology, the mechanism underlying this connection unclear.

In the present study, we performed transcriptome and metabolome analyses to identify genes involved in GA biosynthesis during development of *G. lucidum*. Particularly, we evaluated the effect of transcription factors in GA biosynthesis by quantitatively analyzing GA accumulation, intermediate formation, and gene expression of key regulatory enzymes. This is the first time to investigate the global changes of transcription factors during development of *G. lucidum*. Taken together, our results provide invaluable insights into the connection between secondary metabolism and fruiting body formation in *G. lucidum*, and are expected to guide future studies.

Materials and methods

Fungal strains and culture conditions

A *G. lucidum* strain (accession number: ACCC53264) was provided by Prof. Mingwen Zhao of Nanjing Agricultural University, and preserved at the Agricultural Culture Collection of China. Fungal mycelia were cultured in complete yeast medium (CYM), comprising 1% maltose, 2% glucose, 0.2% yeast extract, 0.2% tryptone, 0.05% $MgSO_4$ $7H_2O$, and 0.46% KH_2PO_4, and maintained at 28°C. Spawn was prepared in polypropylene bags and incubated at growth conditions described in a previous study (Meng et al., 2019). Samples were collected at three stages, namely mycelia, primordia, and fruiting body, then stored in liquid nitrogen.

RNA sequencing and transcriptomic analysis

RNA was isolated from samples (Mycelia, Primordia, and Fruiting body), and detected RNA concentration and purity using previously described methods (Meng et al., 2022). 1.5 μg of total RNA per sample was reverse transcribed to complementary DNA (cDNA). The cDNA was purified and ligated to sequencing adapters, then resolved on an agarose gel. cDNA fragments (300 bp)

were extracted from the gels, purified and enriched by PCR to construct the final cDNA library (Mycelia, Primordia, and Fruiting body). Libraries were generated using the NEBNext® Ultra™ RNA Library Prep Kit for Illumina® (NEB, United States). Clustering of the index-coded samples was performed on a cBot Cluster Generation System using TruSeq PE Cluster Kit v3-cBot-HS (Illumina) according to the manufacturer's instructions. Next, libraries were sequenced on the Illumina Hiseq platform, to generate 150-bp paired-end reads. About 47 M raw reads were generated per sample.

Raw reads (fastq format) were first processed through in-house perl scripts to remove adapters, as well as low-quality reads and those containing poly-N. At the same time, we calculated Q20, Q30, GC-content and sequence duplication level of the clean data. All other downstream analyses were performed on clean, high-quality data. The transcriptome was assembled by mapping the reads to *G. lucidum* reference genome (Project accession number PRJNA71455) (Chen et al., 2012). Transcript abundances were presented as normalized fragments per kb of transcript per million mapped reads. A gene was considered to be significantly differentially expressed if its expression differed between two samples by a fold change > 2 and a p-value < 0.05.

Annotations, to identify gene function, were performed on the following databases: NCBI non-redundant (Nr) protein sequences; NCBI non-redundant nucleotide sequences (Nt); Protein family (Pfam); Clusters of Orthologous Groups of Proteins (KOG/COG); Swiss-Prot (A manually annotated and reviewed protein sequence database); KEGG Ortholog database (KO); and Gene Ontology (GO).

Sample preparation and LC-MS analysis

Samples for LC-MS analysis were prepared as previously reported (Meng et al., 2022). Briefly, 80 mg of each sample was extracted by 1 mL solution of methanol-water (7: 3, v/v). Ultrasonic extraction was performed in an ice-water bath for 30 min, after which extracts were stored overnight at −20°C. The supernatants were then collected, filtered through 0.22 μm polyvinylidene fluoride membranes, and stored at −80°C until subsequent LC-MS analysis. All sample extracts were mixed with 20 μL of 2-chloro-l-phenylalanine (0.3 mg/mL methanol), as an internal standard.

To identify differentially accumulated metabolites cross various periods, we randomly analyzed 18 samples from three independent biological replicates *via* LC-MS as described previously (Meng et al., 2022). Chromatographic separation of samples was performed using an ACQUITY UPLC HSS T3 column (2.1 mm × 100 mm, 1.8 μm) equipped with a binary solvent system (solvent A: 0.1% formic acid in deionized water; solvent B: 0.1% formic acid in acetonitrile). The following gradient elution procedure was used: 0–2 min, 5% B; 2–4 min, 5% B; 4–8 min, 30% B; 8–10 min, 50% B; 10–14 min, 80% B; 14–15 min, 100% B; 15.1 min, 5% B and 16 min, 5% B. The process included a flow rate of 0.35 mL/min, an injection volume of 2 μL, and column temperature maintained at 45°C. Instrument settings were as follows: Ion source: ESI; capillary temperature: 320°C; spray voltages: (+3.8, -3) kV; mass scan range: 100–1200; resolution (full scan): 70000; resolution (HCD MS/MS scans): 17500; sheath gas flow rate (Arb): 35 (positive ion) and 35 (negative ion); aux. gas flow rate (Arb): 8 (positive ion) and 8 (negative ion). Metabolomics data were deposited to the EMBL-EBI MetaboLights database (Haug et al., 2019).

Transcription factors identification

Identification of transcription factors were according to Fungal Transcription Factor Database (FTFD), which was designed for integrating the putative fungal transcription factors and its references. This site provides sequences, taxonomical and phylogomic context of all putative fungal transcription factors. Transcription factor family map and transcription factor matrix will provide overall sketch of all fungal transcription factors. FTFD included 123,899 fungal and Oomycetes transcription factors, 75,064 transcription factors belonging to phylum Ascomycota, and 37,831 transcription factors belonging to the phylum Basidiomycota, and others belonging to Chytridiomycota, Microsporidia, and Peronosporomycota. Blastp was used to find paralogs for all proteins (initial blastp parameters at limit expect value < 1e-5, and matrix was BLOSUM62).

Metabolite identification

Identification of differentially expressed metabolites in the raw data was performed using the UNIFI 1.8.1 software. Baseline filtration, peak identification, peak alignment, peak filling, retention time (RT), and normalization of the raw data were statistically analyzed using QI v2.3 (Waters Corporation, Milford, United States). Metabolite identification was performed based on exact mass to charge ratios (m/z), isotope distributions, fragmentation patterns and database hits (The Human Metabolome Database, Lipidmaps, and METLIN). Additionally, we applied a self-written R package and in-house self-built secondary mass spectrometry database containing 550 metabolites for metabolite identification. Data processing parameters were as follows: precursor tolerance 5 ppm, fragment tolerance 10 ppm, and product ion threshold

5%. Compounds with more than 50% missing values, for each condition, were eliminated while the remaining missing values were replaced by half of the minimum value. Qualitative data were analyzed according to the score of qualitative results. Compounds with a score of more than 36 (a full score of 60) and less than 36 were accepted and deleted, respectively. The maximum total score was 60 points, allocated as follows: 20 points for MS/MS matching, 20 points for MS/MS fragmentation matching, and 20 points for isotopic distribution matching.

Determination of total ganoderic acid and flavonoid contents

Ganoderic acid content and flavonoid contents were measured as described in our previous studies (Meng et al., 2019; Meng et al., 2021).

Analysis of gene function

Functional analyses were performed *via* gene silencing and fungal transformation, using constructs developed as previously described (Meng et al., 2021). Briefly, the fungal RNAi vector pAN7-ura3-dual was used to silence genes encoding homeobox transcription factor and velvet family proteins in *G. lucidum*. The cDNA fragment was digested with *Kpn*I and *Spe*I (Takara) and then inserted into pAN7-ura3-dual at the corresponding restriction sites. This vector was used to transform the *G. lucidum* protoplasts by liposome transformation, with a 1:1 volumetric ratio of liposome to vector. Coincubation was performed for half an hour at 4°C.

Gene expression analysis

Total RNA was extracted from all samples using the RNAiso Plus Kit (Takara, Kusatsu, Japan) according to the manufacturer's instructions. Equal concentrations of the RNA were reverse transcribed to cDNA using the TransStart All-in-One first-strand cDNA synthesis supermix (TransGen Biotech, Beijing, China). The cDNA was then used for quantitative real time PCR (qRT-PCR) using the SYBR Green kit (Bio-Rad, Hercules, United States), performed on a LightCycler 96 SW 1.1 instrument, to analyze the transcription levels of gene-silenced strains. Primer sequences for the target genes are listed in **Table 1**. Expression data for genes in silenced strains were normalized against the internal reference gene 18S rRNA. The relative expression levels were calculated by comparing the cycle threshold (Ct) of each target gene with the corresponding internal reference gene using the $2^{-\Delta\Delta Ct}$ method (Livak and Schmittgen, 2001).

Yeast one-hybrid assays

Yeast one hybrid assays were conducted using the Matchmaker One-hybrid System (Clontech). Briefly, a 100-bp AATT region surrounding the *osc* and *hmgr* promoter sequences was synthesized with *Hind* III and *Xho* I flanking restriction sites, then cloned into pAbAi. Next, *GL25472* cDNA were cloned into the pGADT7 vector for expression in yeast. Plasmids for yeast one-hybrid were co-transformed into yeast Gold strain, then cells harboring the target plasmids cultivated in SD medium lacking leucine containing 200 ng/μL Aureobasidin A (AbA). The primers sequences of the target fragments used are outlined in **Table 1**.

Results

Differential gene expression profiles

We elucidated the relationship between secondary metabolites and fruiting body formation at different developmental stages using transcriptome and metabolome profiling, including mycelia (CYM), primordia (PR-H_2O), and fruiting body (MA-H_2O). Transcriptome data were deposited in the NCBI database, under accession numbers PRJNA 825330 and PRJNA769204. Results revealed 5332 and 4822 differentially expressed genes (DEGs) between CYM and PR-H_2O, MA-H_2O, respectively (**Figures 1A,B** and **Supplementary Tables 1**, **2**). Among them, 3369 DEGs were common between PR-H_2O vs. CYM and MA-H_2O vs. CYM (**Figure 1C**). To test the level of coregulation among differentially expressed genes, we performed cluster analysis of the 3,369 differentially regulated genes (**Figure 1D**), and found that most genes were highly expressed in mycelia but lowly in both primordia and fruiting body except a few genes. Interestingly, genes were differentially expressed between mycelia and primordia, but not between primordia and fruiting body. Results from GO enrichment analysis showed that 3,369 common DEGs were enriched in various terms, namely flavonoid biosynthetic process, regulation of the jasmonic acid mediated signaling pathway, electron transport chain, and secondary metabolite biosynthetic process (**Figure 1E**). Moreover, primordia not only represented a transition from vegetative to reproductive growth, but was also an important turning point during fungal growth and development. GO terms suggested that secondary metabolite biosynthetic process significantly changed during fungal development.

TABLE 1 The primers in this study.

	Forward primer (5′ to 3′)	Reverse primer (5′ to 3′)
SpeI-GL25472-RNAi	ACTGACTAGTCGGTTGTAGGTTTCGTT	ACTGGGTACCGCCCTCAAGATTCGC
RT-GL25472	CCTATTGGTGGCTATCAG	GGTTCGGGGAGGTTGG
NdeI-GL25472-pGADT7	CGAAGACATATG ATGATCGGAGGCCCTG	ACTGAATTC TCATGGCTCCTCCG
HindIII-Hmgr-pABAi	GAGTAAGCTTCTGGTAAGGCGGTGTCCC	TGCTCTCGAGCAGTAGGTGGGATGGATT
HindIII-Osc-pABAi	GAGTAAGCTTCGCTTGCTCAACAACCTC	TGCTCTCGAGGAATGTTGGTTGGGTTAA
SpeI-GL19230-RNAi	CTGACTAGTATCGCCGACCTATTGACC	CTTGGTACCTGCCAGGGAACTTCTTCG
SpeI-GL21819-RNAi	TCTACTAGTGTGGACCTGCCGTTTCTGG	GTTGGTACCCGATCATTCGAGCACCTTG
RT-GL19230	CCACTGCAAATCCATCTTCTCC	GAGGGAACAGGACAGTGGAGTTG
RT-GL21819	TCCAGCATCCTCACCG	ATGGGGCGAAGACACC
RT-HMGR	GTCATCCTCCTATGCCAAAC	GGGCGTAGTCGTAGTCCTTC
RT-SQS	CTGCTTATTCTACCTGGTGCTACG	GGCTTCACGGCGAGTTTGT
RT-OSC	AGGGAGAACCCGAAGCATT	CGTCCACAGCGTCGCATAAC
RT-18S	TATCGAGTTCTGACTGGGTTGT	ATCCGTTGCTGAAAGTTGTAT

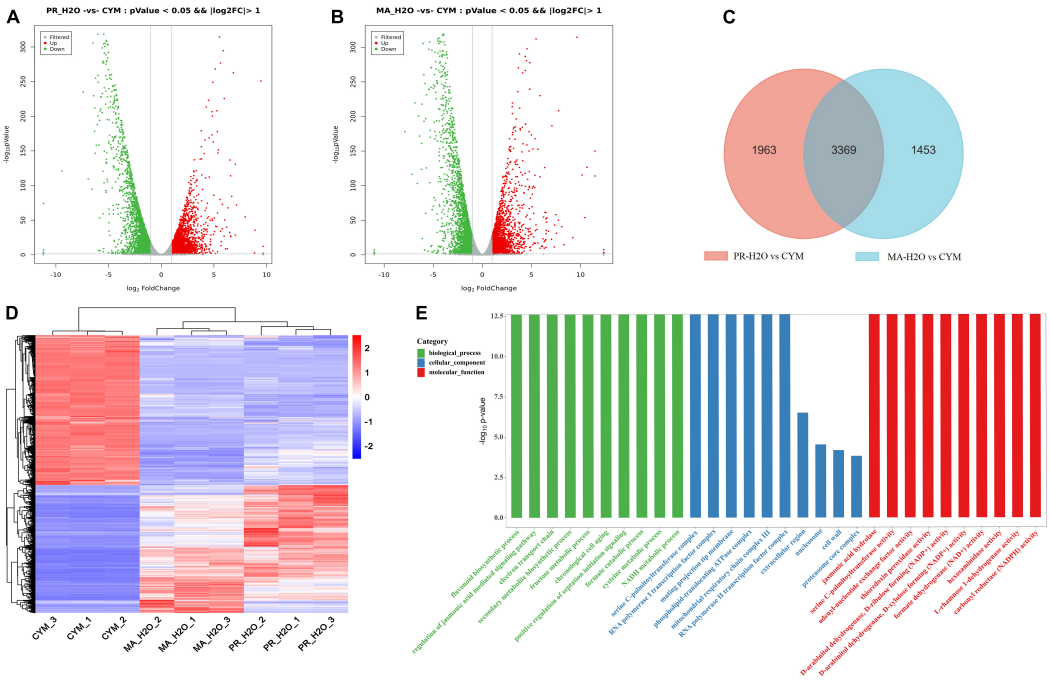

FIGURE 1
The transcriptome analysis in different developmental stages. Panels **(A,B)** are the DEGs in PR-H_2O vs. CYM and MA-H_2O vs. CYM, respectively. Panel **(C)** is Venn diagram of DEGs between (PR-H_2O vs. CYM) and (MA-H_2O vs. CYM). Panels **(D,E)** are the heat map and GO enrichment analysis of common genes. CYM, mycelia; PR-H_2O, primordia; MA-H_2O, fruiting body. There are three replicates in each sample of transcriptome.

Metabolite profiles during development of *Ganoderma lucidum*

Non-targeted metabolomics analysis revealed a total of 16,327 metabolites in mycelia of *G. lucidum*, of which 5,920 were successfully annotated (Figure 2A and Supplementary Table 3). The major metabolites included lipids and lipid-like molecules, organic acids and derivatives, organoheterocyclic compounds, and organic nitrogen compounds. Notably, 24,876 metabolites were detected in the primordia and fruiting body stages, of which 8,245 metabolites were successfully annotated (Figure 2B and Supplementary Table 4). Mycelia, primordia and fruiting body stages resulted in largely similar types of metabolites, with a total of 2003 found to be common among the aforementioned stages (Figure 2C). Notably, there were 32 and 61 compounds annotated as GAs and flavonoids in the primordia and fruiting

body, which were more than those obtained in mycelia (10 and 29 compounds annotated as GAs and flavonoids) (**Figure 2D** and **Supplementary material**). In addition, GA and flavonoid contents in the primordia and fruiting body were higher than those obtained in mycelia (**Figures 2E,F**).

Effect of development on the expression of key ganoderic acid biosynthesis genes

In order to elucidate mechanism underlying the effect of development on triterpenoid biosynthesis, we examined encoding enzymes involved in terpenoid backbone biosynthesis (**Figure 3A**). Results showed that phosphomevalonate kinase (MPK, *GL17808*), acetyl-CoA acetyltransferase (ACAT, *GL26574*), and farnesyl diphosphate synthase (FDPS, *GL25499*, GL22068) genes were significantly upregulated with fruiting body development (**Figure 3B**). Specifically, MPK, ACAT, and 2 FDPSs exhibited a 1.82-fold, 1.97-fold, 7.85-fold, and 10.60-fold upregulation in the fruiting body, respectively. Moreover, squalene monooxygenase (SE, *GL22565*) exhibited a 1.58-fold upregulation in the primordia compared with mycelia, while isopentenyl-diphosphate isomerase (IDI, *GL29704*), squalene synthase (SQS, *GL21690*) and oxidosqualene cyclase (OSC, *GL18675*) exhibited a 1. 06-, 1. 10-, and 1.16-fold upregulation, respectively, in the fruiting body relative to mycelia. Notably, the highest expression for most genes encoding enzymes was recorded during primordia or fruiting body developmental periods (**Figure 3**).

Transcription factors in *Ganoderma lucidum*

Transcription factors regulate gene expression in a cell, thus in many respects, their repertoire determines the cell's life and functionality. To better understand the regulatory mechanisms underlying fungal development and secondary metabolism, we analyzed expression patterns of transcription factors during *G. lucidum* development.

Consequently, we identified a total of 516 homologous protein of transcription factors in *G. lucidum*. Among them, 90 had more than two domains, and belonged to 53 transcription factor families (**Figure 4A** and **Supplementary Table 5**). The highest number of significantly affected genes encoding transcription factors belonged to the C2H2 transcription factor family, followed by Zn2Cys6 and Zf-MYND (**Figure 4B**). A total of 110 differentially expressed transcription factors were recorded across the three stages (**Supplementary Table 6**). Moreover, 67 C2H2, 70 Zn2Cys6, and 50 Zine finger-MYND (Zf-MYND) transcription factors, including 24 DEGs of C2H2, 27 DEGs of Zn2Cys6, and 13 DEGs of Zf-MYND were expressed across the three stages Interestingly, mycelia exhibited the highest transcriptional levels for 15 DEGs of C2H2 (62.5%), and 24 DEGs of Zn2Cys6 (88.9%) transcription factors, while other DEGs expressed in the primordia or fruiting body. The primordia or fruiting body exhibited the highest transcriptional levels for 10 DEGs of Zf-MYND (76.9%) transcription factors. Collectively, these results suggested that these transcription factor homologs might be vital regulators of gene expression and play different roles at different developmental stages of *G. lucidum*.

Homeobox transcription factor regulates the ganoderic acid biosynthesis

Although homeobox transcription factors have been implicated in secondary metabolism in fungi (Cary et al., 2017), their roles in GA biosynthesis in *G. lucidum* are largely unknown. To further identify the relationship between homeobox transcription factors and GA biosynthesis, we annotated 9 homeobox transcription factors from the fungal transcription factor database, including 1 gene (*GL30604*) that was not expressed (**Figure 5A**). To screen the key homeobox transcription factors, we analyzed 1 kb promoter sequences upstream of *hmgr* and *osc* (pHmgr and pOsc) coding region *via* Yeastract database, and compared the *cis*-regulatory elements (CREs) present in pHmgr and pOsc with homeobox protein YOX1 in *S. cerevisiae*. Previous studies have shown that many common CREs in corresponding sites shared by pHmgr and pOsc can be recognized by many transcriptional factors (Guo et al., 2015). In the present study, we found that a homeobox transcription factor GL25472 contained CREs located in the promoter region of *hmgr* and *osc* (**Figure 5B**), and Yeast-one-hybrid results showed that *GL25472* could bind to the promoter regions of *hmgr* and *osc* (**Figure 5C**). Therefore, we selected *GL25472* for further investigations.

To determine whether *GL25472* influences GA biosynthesis in *G. lucidum*, we constructed an RNAi vector targeting the *GL25472* gene. qRT-PCR results revealed silencing efficiencies of 70, 75, and 71% for *GL25472i-38*, *GL25472i-43*, and *GL25472i-50*, respectively (**Figure 5D**). Moreover, *GL25472i-38*, *GL25472i-43*, and *GL25472i-50* silencing constructs mediated a 35.73, 42.33, and 28.91% reduction in GA content of mycelia, respectively, compared to the WT strain (**Figure 5E**). Strains in which the *GL25472* had been silenced also exhibited reduced growth rates (**Figure 5F**). Moreover, silencing of the *GL26472* mediated a significant downregulation of *HMGR*, *SQS*, and *OSC*, key genes involved in GA biosynthesis, relative to WT strain (**Figure 5G**).

10.3389/fmicb.2022.956421

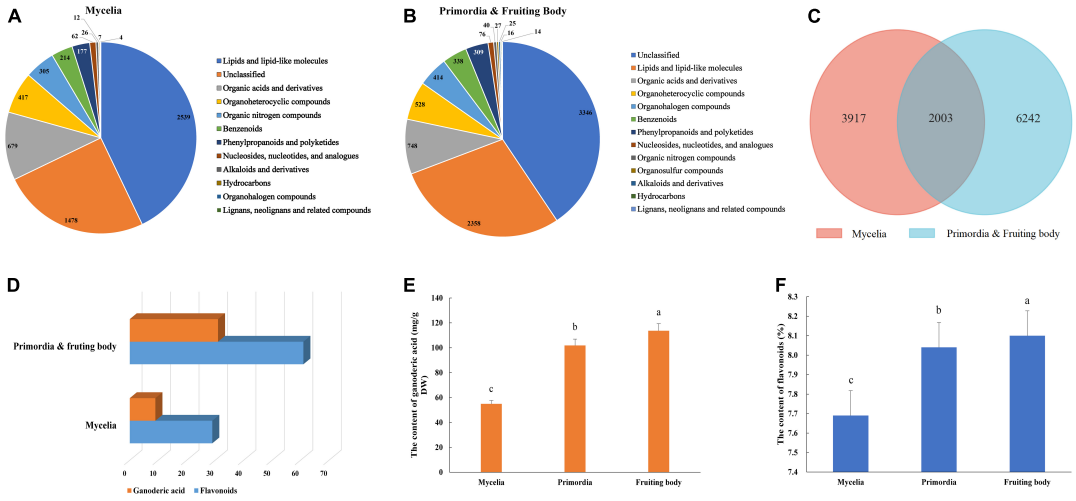

FIGURE 2
Metabolite identification in the development of *G. lucidum*. Panels **(A,B)** are the kinds of metabolites in the Mycelia, and Primordia and Fruiting body. Panel **(C)** the is Venn diagram of common metabolites in the Mycelia and Primordia and Fruiting body. Panels **(D–F)** are the kinds of secondary metabolites, contents of GAs and flavonoids. Means within a column carrying the same letter are not significantly different. Different superscript lowercase letters (a, b, and c) indicate significant differences ($p < 0.05$).

Velvet family regulates the ganoderic acid biosynthesis

Previous studies have shown that the VeA-VelB-LaeA complex can activate secondary metabolism in fungi (Bayram et al., 2008). Therefore, we analyzed expression levels of members of the velvet family and LaeA across different development stages. We annotated three genes encoding velvet family protein, including VeA (*GL19230*), VelB (*GL21819*), and VelC (*GL23472*), and one gene (*GL26103*) encoding LaeA (**Figure 6A**). All velvet family proteins contain a velvet conserved domain, while VeA has a proline glutamic acid serine and threonine (PEST) rich sequence. Additionally, LaeA contains a S-adenosyl methionine-binding site (SAM) and a methyltransferase domain (MTD) in its amino acid sequence. Notably, VeA expression was upregulated during fruiting body development, with the highest level recorded at the fruiting body stage (**Figure 6B**). By contrast, VelB showed relatively high expression at primordia stage, while VelC was lowly expressed at the fruiting body stage. LaeA was down-regulated at both primordia and fruiting body stages.

To further study the function of velvet family proteins, we separately silenced two important key velvet family proteins, namely VeA and VelB, in *G. lucidum via* RNAi (**Figure 6C**). qRT-PCR results revealed a silencing efficiency of > 70%. Results showed that silencing of *VeA* and *VelB* mediated a significant reduction in GA content of mycelia compared to the WT strain (**Figure 6D**). Moreover, *HMGR*, *SQS*, and *OSC*, key genes involved in GA biosynthesis, were markedly down-regulated in *VeA* and *VelB* silencing strains compared to WT (**Figures 6E,F**). Collectively, these results indicated that velvet family proteins play a key role in development and GA biosynthesis in *G. lucidum*.

Discussion

Transcription factors play essential roles in the signal transduction pathway, being the last link between signal flow and target genes expression. Fungi have significantly lower number of experimentally verified transcription factors compared to higher eukaryotes, as reflected in databases such as TRANSFAC (Wingender et al., 1996) and MycoPath. This phenomenon may be attributed to two possible scenarios: either they are really less abundant or they have not yet been identified. In this study, we estimated the potential mechanism underlying regulation of secondary metabolism during development of *G. lucidum*.

The transcriptional regulation process is a complex and dynamic process that is regulated by transcription factors. Expression of developmental transcription factors has also been found to be transiently present. Therefore, we quantified gene expression using previously described datasets (Chen et al., 2012). Although most gene expression models were similar in available transcriptome data, there were also localized distinctions between transcriptome data from different strains and growth status. In this study, transcriptome data revealed differentially expressed genes between mycelia and primordia, as well as between mycelia and the fruiting body. The difference is likely caused by two reasons. On the one hand, the discrepancy of gene expression profile could be due to

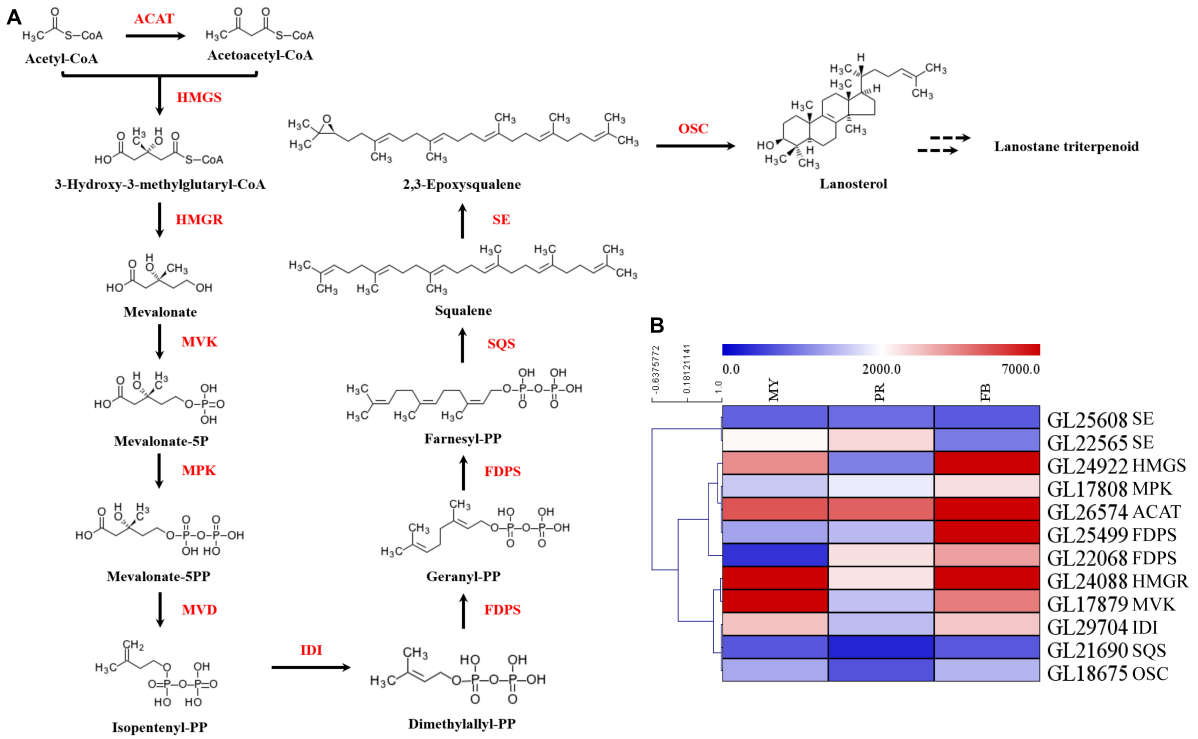

FIGURE 3
The key genes of enzymes in ganoderic acid biosynthesis pathway of *G. lucidum*. Panel **(A)** the terpenoid backbone biosynthesis in *G. lucidum*. Red represents the enzyme, and black represents the metabolites. Panel **(B)** the gene expression levels of enzymes involved in terpenoid backbone biosynthesis. ATAC, acetyl-CoA -acetyltransferase; HMGS, hydroxymethylglutaryl-CoA synthase; HMGR, 3-hydroxy-3-methylglutaryl-coenzyme A reductase; MVK, mevalonate kinase; MPK, phosphomevalonate kinase; MVD, pyrophosphomevalonate decarboxylase; IDI, isopentenyl-diphosphate isomerase; FDPS, farnesyl diphosphate synthase; SQS, squalene synthase; SE, squalene epoxidase; OSC, 2,3-oxidosqualene-lanosterol cyclase. MY, mycelia; PR, primordia; FB, fruiting body.

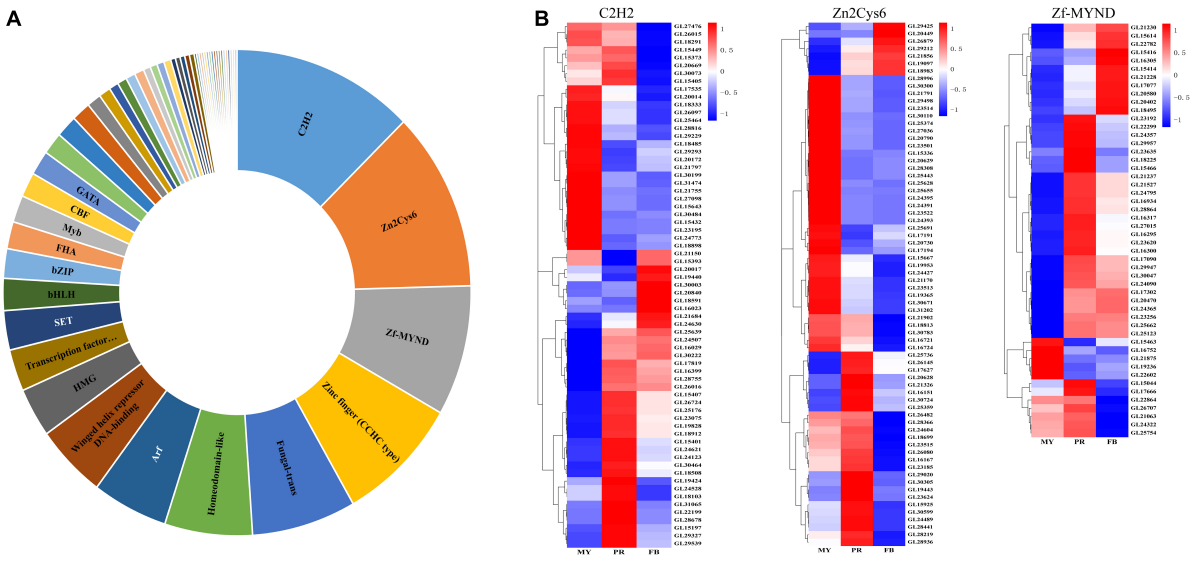

FIGURE 4
The transcription factors in *Ganoderma lucidum*. Panel **(A)** is the transcription factors family in *G. lucidum*. Panel **(B)** is the expression levels of C2H2, Zn2Cys6, and Zf-MYND in the development of *G. lucidum*. MY, mycelia; PR, primordia; FB, fruiting body.

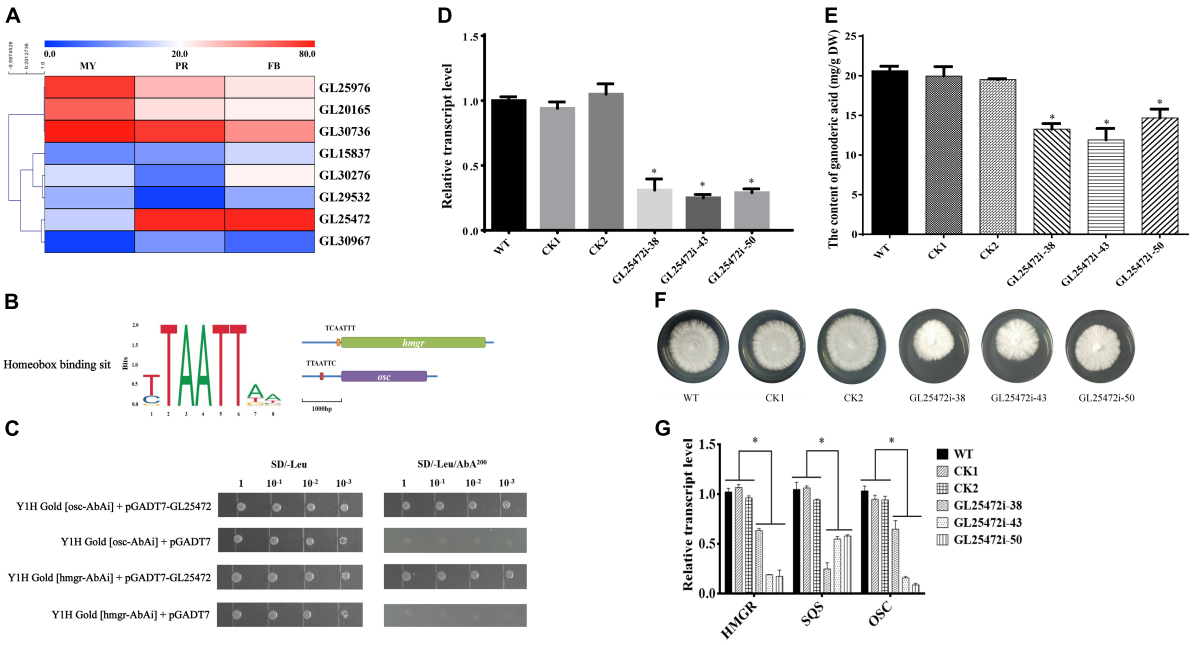

FIGURE 5
The effects of homeobox transcription factors on ganoderic acid biosynthesis in *G. lucidum*. Panel **(A)** is the gene expression level of homeobox transcription factors. MY, mycelia; PR, primordia; FB, fruiting body. Panel **(B)** is the binding sit of homeobox transcription factor. The orange box (TCAATTT) and red box (TTAATTC) were CREs located in the promoter region of hmgr and osc. Panel **(C)** is yeast one-hybrid assay. Panels **(D,E)** are the relative transcript levels and GA contents of gene-silencing strains. Panel **(F)** the mycelial colony. Panel **(G)** the transcript levels of the genes encoding key enzymes. WT (wild-type), CK1 and CK2 (the empty vector controls), *GL25472* (38, 43, 50) were gene-silencing strains. HMGR, 3-hydroxy-3-methylglutaryl-coenzyme A reductase; SQS, squalene synthase; OSC, 2,3-oxidosqualene-lanosterol cyclase. The histograms marked with * represent significant differences; it indicates statistical significance ($p < 0.05$) compared to WT.

differences *Ganoderma* in important aspects of growth and development. On the other hand, it could also be due to the differences between media.

Moreover, metabolome is often thought of as a "readout" of physiological states. Therefore, it is widely used in the study of the growth and development of organisms. Notably, mycelia, primordia and fruiting body stages resulted in largely similar types of metabolites, the major metabolites included lipids and lipid-like molecules, organic acids and derivatives, organoheterocyclic compounds, and organic nitrogen compounds. However, a large diversity of metabolites between mycelia and primordia/fruiting body were also significantly different. There were 3,917 specific metabolites in mycelia, and 6,242 specific metabolites in primordia and fruiting body stages. Previous report has revealed that fungal lipids are involved in organism development as well as regulatory machinery for secondary metabolism (Tugizimana et al., 2019). In this regard, linolenic -, oleic -, nonanoic - and decanoic acids have been shown to participate in the regulation of spore development and mycotoxin production in *Aspergillus* spp., and *Fusarium verticillioides* (Christensen and Kolomiets, 2011). Concerning secondary metabolites during developmental stages, ten out of the thirty-two GAs in the primordia/fruiting body stages were same with those in mycelia stage. Twenty-two GAs were unique in primordia/fruiting body, such as Ganoderenic acid B, Ganoderenic acid A, and so on, and the flavonoids greatly varied between mycelia and primordia/fruiting body (**Supplementary material**). These results implied that secondary metabolite patterns were altered as development progresses. The mechanism for this association may be multifaceted. One speculation might be perhaps that the variation in development resulted in diversity of metabolites. Another speculation might be perhaps that the various metabolites had an impact on the fungal development.

This is the first time a direct link has been shown between fruiting body development and GA biosynthesis in *G. lucidum* (**Figure 7**). In this study, we found that the homeobox transcription factor and velvet family protein played an important role in regulating the GA biosynthesis in during *G. lucidum* development. We previously identified and characterized a transcription factor *MADS1*, which can regulate GA biosynthesis, and the gene-silencing mutants of *MADS1* hinder the formation of the primordia in *G. lucidum* (Meng et al., 2021). Previous studies have shown that strains in which the Cys2His2 zinc finger protein gene C2H2 has been inactivated are arrested at the aggregate stage (Ohm et al., 2011). Results of the present study revealed that C2H2 transcription factors were upregulated in mycelia than in

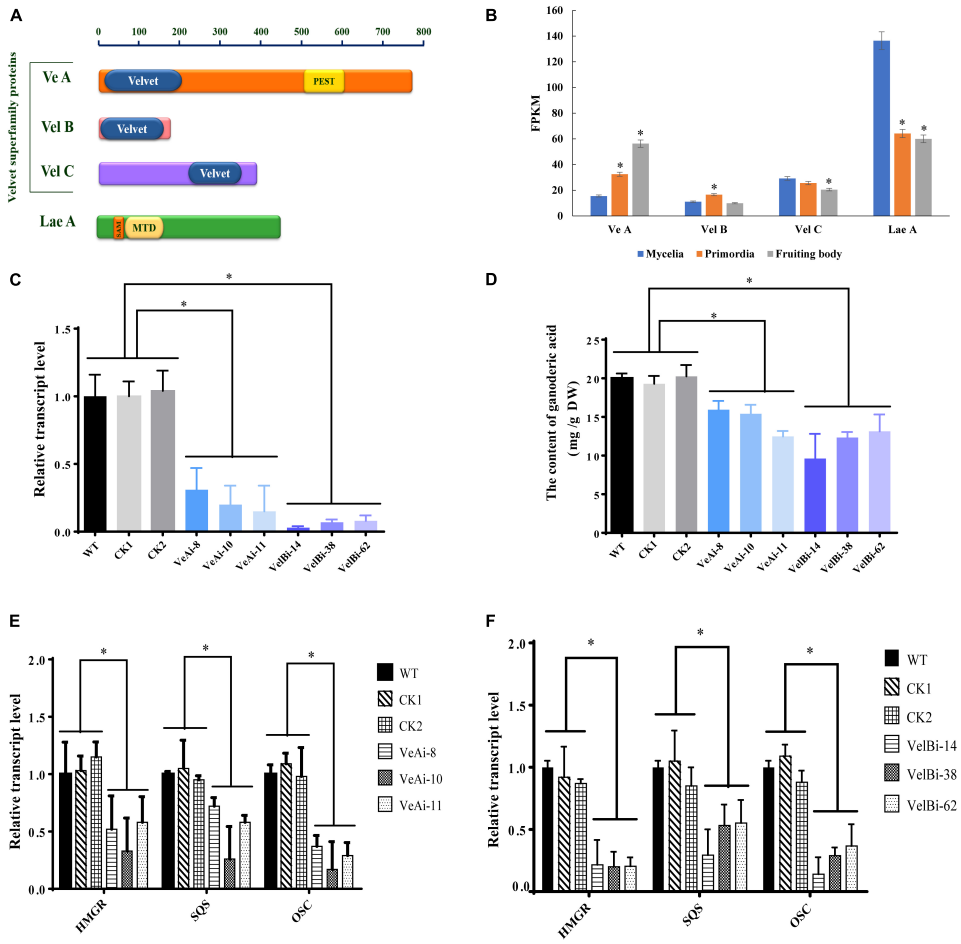

FIGURE 6
The effects of velvet family on ganoderic acid biosynthesis in *G. lucidum*. Panel **(A)** is predicted conserved domains. Panel **(B)** the gene expression level in development of *G. lucidum*. FPKM, Fragments Per Kilobase Million. Panels **(C,D)** are the gene expression levels and GA contents of VeA and VelB. Panels **(E,F)** are the transcript levels of the genes encoding key enzymes. WT (wild-type), CK1 and CK2 (the empty vector controls), VeAi (8, 10, 11) and VelBi (14, 38, 62) were gene-silencing strains. HMGR, 3-hydroxy-3-methylglutaryl-coenzyme A reductase; SQS, squalene synthase; OSC, 2,3-oxidosqualene-lanosterol cyclase. The histograms marked with * represent significant differences; it indicates statistical significance ($p < 0.05$) compared to WT.

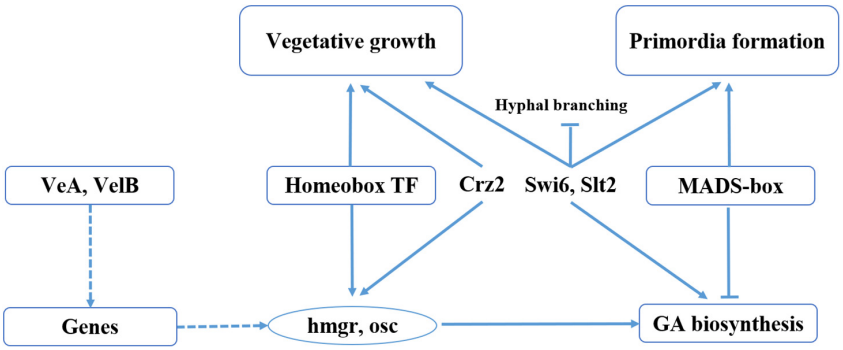

FIGURE 7
Model of regulation of fruiting body development and GA biosynthesis in *G. lucidum*. Solid lines represent the determined regulatory effect, dotted lines represent the regulatory effect of an unknown regulatory mechanism, arrows represent the facilitated effect, and short lines represent inhibition.

both primordia and fruiting body, a phenomenon that may contribute to mycelia aggregation. Studies have also shown that C2H2 transcription factors, such as *glcrz2*, play an important role in secondary metabolism (Li and Zhong, 2020). Notably, knocking out *glcrz2* resulted in marked attenuation of both mycelia growth and GA synthesis, and this was accompanied by a decline in GA production even with Ca^{2+} treatment. In addition, Zhang et al. (2018) found that silencing *GlSwi6* reduced fungal growth and increased hyphal branching, and the *GlSwi6*-silenced strains did not exhibit primordium or fruiting body formation. Moreover, the GA level of the *GlSwi6*-silenced strains decreased approximately 25% compared with those of the WT strain. The similar phenotypic characteristics were found in knockdown of *GlSlt2* (Zhang et al., 2017b). These results showed that *GlSwi6* and *GlSlt2* were involved in fungal growth, development and GA biosynthesis in *G. lucidum*.

Furthermore, there are several no defined InterPro Term in the Fungal Transcription Factor Database, such as the heat shock factor. Previous studies have demonstrated that heat stress modulates heat shock protein expression, thereby affecting GA biosynthesis and hyphal branching of *G. lucidum via* Cytosolic Ca^{2+}. However, the identified transcription factors might be less than the actual number in *G. lucidum*, due to lack the defined InterPro. The large array of transcription factors annotated in the present study warrant further research attention. There is also need to investigate many aspects, such as the function of transcription factors, gene interactions, and transcriptional regulatory networks, among others.

Conclusion

In summary, transcription factors act as an important link between secondary metabolites biosynthesis and fungal development. In the present study, we found that genes were differentially expressed between mycelia and primordia. GO terms of the DEGs revealed that secondary metabolite biosynthetic process significantly changed during fungal development. A set of 53 potential transcription factor families was annotated in *G. lucidum*. Notably, we found homeobox transcription factor and velvet family protein played important role in GA biosynthesis. Combined with previous studies, we provided a model diagram of transcription factors involved in GA biosynthesis during fruiting body formation. Taken together, these findings are expected to significantly improve our understanding of secondary metabolites biosynthesis and development in fungi.

Data availability statement

The datasets presented in this study can be found in online repositories. The names of the repository/repositories and accession number(s) can be found in the article/**Supplementary material**.

Author contributions

LM: conceptualization, funding acquisition, and writing – original draft. RZ: methodology. XZ: investigation. JL: formal analysis. QW: visualization. PW: software. LW: project administration. ZL: supervision. WW: writing – review and editing. All authors contributed to the article and approved the submitted version.

Funding

This work was financially supported by the National Natural Science Foundation of China (grant number 32002107) and the Mushroom Technology System of Shandong Province (grant number SDAIT-07-06).

Acknowledgments

We thank the Shanghai LuMing biological technology Co., Ltd., (Shanghai, China) for providing metabolomics services.

Conflict of interest

The authors declare that the research was conducted in the absence of any commercial or financial relationships that could be construed as a potential conflict of interest.

Publisher's note

All claims expressed in this article are solely those of the authors and do not necessarily represent those of their affiliated organizations, or those of the publisher, the editors and the reviewers. Any product that may be evaluated in this article, or claim that may be made by its manufacturer, is not guaranteed or endorsed by the publisher.

Supplementary material

The Supplementary Material for this article can be found online at: https://www.frontiersin.org/articles/10.3389/fmicb.2022.956421/full#supplementary-material

References

Ahmad, M. F. (2018). *Ganoderma lucidum*: Persuasive biologically active constituents and their health endorsement. *Biomed. Pharmacother.* 107, 507–519. doi: 10.1016/j.biopha.2018.08.036

Baby, S., Johnson, A. J., and Govindan, B. (2015). Secondary metabolites from *Ganoderma*. *Phytochemistry* 114, 66–101.

Bayram, Ö, Bayram, ÖS., Ahmed, Y. L., Maruyama, J., Valerius, O., Rizzoli, S. O., et al. (2012). The *Aspergillus nidulans* MAPK module AnSte11-Ste50-Ste7-Fus3 controls development and secondary metabolism. *PLoS Genet.* 8:e1002816. doi: 10.1371/journal.pgen.1002816

Bayram, Ö, Krappmann, S., Ni, M., Bik, J. W., Helmstaedt, K., Valerius, O., et al. (2008). VelB/VeA/LaeA complex coordinates light signal with fungal development and secondary metabolism. *Science* 320, 1504–1506. doi: 10.1126/science.1155888

Calvo, A. M., Wilaon, R. A., Bok, J. W., and Keller, N. P. (2002). Relationship between secondary metabolism and fungal development. *Microbiol. Mol. Biol. Rev.* 66, 447–459.

Cao, P. F., Wu, C., Dang, Z., Shi, L., Jiang, A., Ren, A., et al. (2017). Effects of exogenous salicylic acid on ganoderic acid biosynthesis and the expression of key genes in the ganoderic acid biosynthesis pathway in the lingzhi or reishi medicinal mushroom, *Ganoderma lucidum* (*Agaricomycetes*). *Int. J. Med. Mushrooms* 19, 65–73. doi: 10.1615/IntJMedMushrooms.v19.i1.70

Cary, J. W., Harris-Coward, P., Scharfenstein, L., Mack, B. M., Chan, P., Wei, Q., et al. (2017). The *Aspergillus flavus* homeobox gene, hbx1, is required for development and aflatoxin production. *Toxins* 9:315. doi: 10.3390/toxins9100315

Chen, S., Xu, J., Liu, C., Zhu, Y., Nelson, D. R., Zhou, S., et al. (2012). Genome sequence of the model medicinal mushroom *Ganoderma lucidum*. *Nat. Commun.* 3:913.

Christensen, S. A., and Kolomiets, M. V. (2011). The lipid language of plant-fungal interactions. *Fungal Genet. Biol.* 48, 4–14. doi: 10.1016/j.fgb.2010.05.005

Demain, A. L., and Fang, A. (2000). "The natural functions of secondary metabolites," in *History of modern biotechnology i. advances in biochemical engineering/biotechnology*, Vol. 69, ed. A. Fiechter (Berlin: Springer).

Guo, D., Yi, H., Li, H., Liu, C., Yang, Z., and Peng, S. (2015). Molecular characterization of HbCZF1, a *Hevea brasiliensis* CCCH-type zinc finger protein that regulates hmg1. *Plant Cell Rep.* 34, 1569–1578. doi: 10.1007/s00299-015-1809-6

Haug, K., Cochrane, K., Nainala, V. C., Williams, M., Chang, J., Jayaseelan, K. V., et al. (2019). MetaboLights: A resource evolving in response to the needs of its scientific community. *Nucleic Acids Res.* 48, D440–D444. doi: 10.1093/nar/gkz1019

Li, H., and Zhong, J. (2020). Role of calcineurin-responsive transcription factor CRZ1 in ganoderic acid biosynthesis by *Ganoderma lucidum*. *Process Biochem.* 95, 166–173.

Lian, L., Shi, L., Zhu, J., Liu, R., Shi, L., Ren, A., et al. (2022). GlSwi6 positively regulates cellulase and xylanase activities through intracellular Ca2+ signaling in *Ganoderma lucidum*. *J. Fungi* 8:187. doi: 10.3390/jof8020187

Livak, K. J., and Schmittgen, T. D. (2001). Analysis of relative gene expression data using real-time quantitative PCR and the 2-ΔΔCt method. *Methods* 25, 402–408.

Meng, L., Bai, X., Zhang, S., Zhang, M., Zhou, S., Mukhtar, I., et al. (2019). Enhanced ganoderic acids accumulation and transcriptional responses of biosynthetic genes in *Ganoderma lucidum* fruiting bodies by elicitation supplementation. *Int. J. Mol. Sci.* 20:2830. doi: 10.3390/ijms20112830

Meng, L., Zhang, S., Chen, B., Bai, X., Li, Y., Yang, J., et al. (2021). The MADS-box transcription factor GlMADS1 regulates secondary metabolism in *Ganoderma lucidum*. *Mycologia* 113, 12–19. doi: 10.1080/00275514.2020.1810515

Meng, L., Zhou, R., Lin, J., Wang, Q., Wang, P., Wang, W., et al. (2022). Integrated transcriptomics and nontargeted metabolomics analysis reveal key metabolic pathways in *Ganoderma lucidum* in response to ethylene. *J. Fungi* 8:456. doi: 10.3390/jof8050456

Ohm, R. A., de Jong, J. F., de Bekker, C., Wösten, H. A. B., and Lugones, L. G. (2011). Transcription factor genes of *Schizophyllum* commune involved in regulation of mushroom formation. *Mol. Microbiol.* 81, 1433–1445. doi: 10.1111/j.1365-2958.2011.07776.x

Shang, C., Shi, L., Ren, A., Qin, L., and Zhao, M. (2010). Molecular cloning, characterization, and differential expression of a lanosterol synthase gene from *Ganoderma lucidum*. *Biosci. Biotechnol. Biochem.* 74, 974–978. doi: 10.1271/bbb.90833

Shang, C., Zhu, F., Li, N., Ou-Yang, X., Shi, L., Zhao, M., et al. (2008). Cloning and characterization of a gene encoding HMG-CoA reductase from *Ganoderma lucidum* and its functional identification in yeast. *Biosci. Biotechnol. Biochem.* 72, 1333–1339. doi: 10.1271/bbb.80011

Tugizimana, F., Djami-Tchatchou, A. T., Fahrmann, J. F., Steenkamp, P. A., Piater, L. A., and Dubery, I. A. (2019). Time-resolved decoding of metabolic signatures of in vitro growth of the hemibiotrophic pathogen *Colletotrichum sublineolum*. *Sci. Rep.* 9:3290. doi: 10.1038/s41598-019-38692-7

Wingender, E., Dietze, P., Karas, H., and Knüppel, R. (1996). TRANSFAC: A database on transcription factors and their DNA binding sites. *Nucleic Acids Res.* 24, 238–241.

Wu, F., Zhang, G., Ren, A., Dang, Z., Shi, L., Jiang, A., et al. (2016). The pH-responsive transcription factor PacC regulates mycelial growth, fruiting body development, and ganoderic acid biosynthesis in *Ganoderma lucidum*. *Mycologia* 108, 1104–1113. doi: 10.3852/16-079

Zhang, G., Ren, A., Shi, L., Zhu, J., Jiang, A., Shi, D., et al. (2018). Functional analysis of an APSES transcription factor (GlSwi6) involved in fungal growth, fruiting body development and ganoderic-acid biosynthesis in *Ganoderma lucidum*. *Microbiol. Res.* 207, 280–288. doi: 10.1016/j.micres.2017.12.015

Zhang, G., Ren, A., Wu, F., Yu, H., Shi, L., and Zhao, M. (2017a). Ethylene promotes mycelial growth and ganoderic acid biosynthesis in *Ganoderma lucidum*. *Biotechnol. Lett.* 39, 269–275. doi: 10.1007/s10529-016-2238-5

Zhang, G., Sun, Z., Ren, A., Shi, L., Shi, D., Li, X., et al. (2017b). The mitogen-activated protein kinase GlSlt2 regulates fungal growth, fruiting body development, cell wall integrity, oxidative stress and ganoderic acid biosynthesis in *Ganoderma lucidum*. *Fungal Genet. Biol.* 104, 6–15. doi: 10.1016/j.fgb.2017.04.004

Zhao, M., Liang, W., Zhang, D., Wang, N., Wang, C., and Pan, Y. (2007). Cloning and characterization of squalene synthase (SQS) gene from *Ganoderma lucidum*. *J. Microbiol. Biotechnol.* 17, 1106–1112.

Zhu, J., Sun, Z., Shi, D., Song, S., Lian, L., Shi, L., et al. (2019). Dual functions of AreA, a GATA transcription factor, on influencing ganoderic acid biosynthesis in *Ganoderma lucidum*. *Environ. Microbiol.* 21, 4166–4179. doi: 10.1111/1462-2920.14769

frontiers | Frontiers in Microbiology

TYPE Original Research
PUBLISHED 04 August 2022
DOI 10.3389/fmicb.2022.969499

Check for updates

OPEN ACCESS

EDITED BY
Pinmei Wang,
Zhejiang University,
China

REVIEWED BY
Ishrat,
Sciences and Technology Islamabad,
Pakistan
Weaam Ebrahim,
Mansoura University,
Egypt

*CORRESPONDENCE
Dan Shu
shudan@cib.ac.cn
Hong Tan
abath@cib.ac.cn

SPECIALTY SECTION
This article was submitted to Microbial Physiology and Metabolism, a section of the journal Frontiers in Microbiology

RECEIVED 15 June 2022
ACCEPTED 07 July 2022
PUBLISHED 04 August 2022

CITATION
Wei Z, Shu D, Sun Q, Chen D-b, Li Z-m, Luo D, Yang J and Tan H (2022) The BcLAE1 is involved in the regulation of ABA biosynthesis in *Botrytis cinerea* TB-31. *Front. Microbiol.* 13:969499. doi: 10.3389/fmicb.2022.969499

COPYRIGHT
© 2022 Wei, Shu, Sun, Chen, Li, Luo, Yang and Tan. This is an open-access article distributed under the terms of the Creative Commons Attribution License (CC BY). The use, distribution or reproduction in other forums is permitted, provided the original author(s) and the copyright owner(s) are credited and that the original publication in this journal is cited, in accordance with accepted academic practice. No use, distribution or reproduction is permitted which does not comply with these terms.

The BcLAE1 is involved in the regulation of ABA biosynthesis in *Botrytis cinerea* TB-31

Zhao Wei[1,2,3], Dan Shu[1]*, Qun Sun[2], Dong-bo Chen[1,3], Zhe-min Li[1], Di Luo[1], Jie Yang[1] and Hong Tan[1]*

[1]CAS Key Laboratory of Environmental and Applied Microbiology, Environmental Microbiology Key Laboratory of Sichuan Province, Chengdu Institute of Biology, Chinese Academy of Sciences, Chengdu, China, [2]Key Laboratory of Bio-Resources and Eco-Environment Ministry of the Education, College of Life Sciences, Sichuan University, Chengdu, China, [3]University of the Chinese Academy of Sciences, Beijing, China

Abscisic acid (ABA), as a classic plant hormone, is a key factor in balancing the metabolism of endogenous plant hormones, and plays an important role in regulating the activation of mammalian innate immune cells and glucose homeostasis. Currently, *Botrytis cinerea* has been used for fermentation to produce ABA. However, the mechanism of the regulation of ABA biosynthesis in *B. cinerea* is still not fully understood. The putative methyltransferase LaeA/LAE1 is a global regulator involved in the biosynthesis of a variety of secondary metabolites in filamentous fungi. In this study, we demonstrated that BcLAE1 plays an important role in the regulation of ABA biosynthesis in *B. cinerea* TB-31 by knockout experiment. The deletion of *Bclae1* caused a 95% reduction in ABA yields, accompanied by a decrease of the transcriptional level of the ABA synthesis gene cluster *Bcaba1-4*. Further RNA-seq analysis indicated that deletion of *Bclae1* also affected the expression level of key enzymes of BOA and BOT in secondary metabolism, and accompanied by clustering regulatory features. Meanwhile, we found that BcLAE1 is involved in epigenetic regulation as a methyltransferase, with enhanced H3K9me3 modification and attenuated H3K4me2 modification in Δ*Bclae1* mutant, and this may be a strategy for BcLAE1 to regulate ABA synthesis.

KEYWORDS

***Botrytis cinerea*, abscisic acid, LAE1, secondary metabolism, gene regulation**

Introduction

Botrytis cinerea is a notorious phytopathogenic ascomycete that causes gray mold disease in more than 200 host plant species and significantly damages large amounts of crops around the world every year (Dean et al., 2012; Fillinger and Elad, 2016). Although *B. cinerea* is a plant pathogen, this fungus produces several economically important compounds. The *B. cinerea* T4 and B05.10 genome sequences predicted 43 genes probably encoding key enzymes (KEs) for secondary metabolite (SM) biosynthesis, including 21 polyketide synthases (PKS), 1 chalcone synthase, 6 sesquiterpene cyclases (STC), 9

non-ribosomal peptide synthases (NRPS), 2 dimethylallyl tryptophan synthases (DMATS), and 5 diterpene cyclases (DTC; Amselem et al., 2011). It indicated that *B. cinerea* has the potential to produce them.

The classical phytohormone ABA, often referred to as the "stress hormone," plays important roles in enhancing the tolerance abilities of plants to various kinds of abiotic or biotic stresses. The most common effect of ABA's action is inhibition of growth and germination. It also regulates a number of processes such as seed ripening and dormancy, root growth, leaf aging, the transition from vegetative to generative growth，the activation of innate immune cells, and glucose homeostasis in mammals (Sakthivel et al., 2016). Thus, ABA has its broad application prospects in agriculture and medicine. Marumo et al. (1982) first reported that *B. cinerea* could synthesize ABA in 1982. Since then, other ABA-producing *B. cinerea* strains have also been confirmed and this plant pathogenic fungus has been studied as a model system for ABA production (Shi et al., 2017). Several *B. cinerea* strains have been particularly used for the fermentative overproduction of ABA at the industrial scale. In our laboratory, the *B. cinerea* wild-type strain TBC-6 (Tan et al., 1998) was isolated from wheat stems and leaves in southwest China. Strain improvements were performed on TBC-6, generating a series of *B. cinerea* mutants with different yields of ABA (Gong et al., 2014), such as TB-31, TB-3-H8, and TBC-A, which were used for biosynthesis regulation research and industrial production of ABA (Ding et al., 2016).

The putative methyltransferase LaeA/LAE1 has been demonstrated to be involved in regulating the biosynthesis of secondary metabolites (SMs) in most filamentous fungi (Bok and Keller, 2004). As a global regulator, studies have shown that LAE1 ortholog was characterized in *Penicillium chrysogenum*, *Fusarium fujikuroi*, and *Cochliobolus heterostrophus*, and their general function was found to be conserved in ascomycetes (Niehaus et al., 2018). LAE1 has the ability to activate biosynthesis potential, and its overexpression is considered to be an effective strategy to activate silent biosynthesis pathway and promote the discovery of new SMs in fungi. For example, a series of sorbicillinoids, including two new sorbitins, were found by overexpressing *lae1* in *Penicillium dipodomyis* (Yu et al., 2019). The overexpression of *lae1* upregulated the expression of chaetoglobosin biosynthetic gene cluster in *Chaetomium globosum*, which led to the discovery of a new cytochalasin (Jiang et al., 2016). In *B. cinerea* B05.10, LAE1 forms a trimeric protein complex with VEL1 and VEL2, which is very important in executing biological functions on morphogenesis under light control and the coordination of secondary metabolism. Studies have shown that BcVEL1 and BcLAE1 are required for the formation of oxalic acid (OA), tolerance to oxidative stress, and full virulence to infected plants. Meanwhile, BcVEL1 and BcLAE1 have strong effects on the expression of SM-related genes, including participation in phytotoxin biosynthesis. 16 SM key enzymes were differentially expressed in Δ*Bcvel1* and Δ*Bclae1* mutants compared with wild type (Schumacher et al., 2015).

LAE1 contains a hypothetical S-adenosine methyl-9-dependent (SAM) domain, which is similar to arginine methyltransferase. The truncation experiment showed that the N-terminal SAM-binding domain of LAE1 is necessary and has the function of nuclear localization (Bayram and Braus, 2012). Tudzynski et al. constructed mutants carrying a mutated *lae1* copy of the SAM domain in *Fusarium fujikura*, and found that the mutated gene copy $lae1^{SAM}$ did not appear to be functional in contrast to wild type (Niehaus et al., 2018). Since no gibberellin acid (GA) gene expression and only very low product levels were detectable in the *lae1SAM-complemented* strain, indicating that the SAM domain is essential for the full activity of LAE1 in *F. fujikura*. The substrate for LAE1 methylation has not yet been determined, but there are more and more indications that LAE1 is involved in chromatin modification. For example, in *Aspergillus nidulans*, H4K12 acetylation of active gene clusters requires LAE1 to play a full role, most efficiently translating the acetylation signal into the noted increased transcriptional levels (Soukup et al., 2012). At the same time, in *Aspergillus luchuensis* mut. Kawachii, LaeA regulates citric acid production by regulating the expression of a putative citrate exporter-encoding gene *cexA via* changing methylation levels of the histones H3K4 and H3K9 (Kadooka et al., 2020). In addition, it has also been proved that LAE1 is resistant to the establishment of some gene cluster heterochromatin regions. Under the background of Δ*lae1*, the sterigmatocystin (ST) production level of wild type (WT) has been partially restored by knockout heterochromatin 1 (Hep1) or H3K9 methyltransferase ClrD (Reyes-Dominguez et al., 2010).

So far, the effect of LAE1 deletion or overexpression on ABA synthesis is unknown. In this work, we investigated the importance of the global regulator BcLAE1 on ABA biosynthesis in the high ABA-producing strain *B. cinerea* TB-31 and further presented its regulatory role in secondary metabolism and development. Meanwhile, we found that BcLAE1 is involved in the regulation of chromatin modification *B. cinerea* TB-31, which may be an important way of its function.

Materials and methods

Strains, plasmids, and ATMT

The ABA-hyperproducing *B. cinerea* mutant TB-31 was generated from multiple rounds of mutagenesis and screening initiated from TBC-6. Binary vectors pCBh1, pCBg1, and pCBsilent1 used in this study were constructed by our laboratory (Ding et al., 2015). *Escherichia coli* strain DH5α was used as the host for transformation and genetic manipulation of plasmid DNA; 50 μg/ml kanamycin (Amresco,Solon, United States) was used to select positive colonies on LB agar plates. *B. cinerea* strains were grown on potato dextrose agar (PDA) slants at 25 C for 7 days. After conidia maturation, *Agrobacterium tumefaciens* EHA105-mediated transformation (ATMT) was performed, as described by Rolland et al. (2003),

with some modifications. The recombinant plasmid was transfected into *A.tumefaciens* EHA105, 28 C, 220 rpm for 6 h to OD_{600} = 0.35–0.45. 100 µl conidia and 100 µl bacteria were mixed and spread on solid medium 3 with nitrocellulose membrane for 2 days. The membrane was then transferred to PDA solid medium for 3 days. 50 µg/ml hygromycin B (Sigma, St. Louis, United States) and 100 µg/ml glufosinate ammonium (Sigma) were used to select transformants on solid PDA plates. Further selection of gene overexpression transformants was performed by regenerating single conidia of the transformants on PDA plates supplemented with corresponding antibiotics.

RNA and DNA extraction

The mycelium of the *B. cinerea* mutants and their control strain TB-31 cultured for 6 days were collected and washed with demineralized water, dried with filter paper, quenched in liquid nitrogen immediately, and ground into powder. Total RNA extraction was performed with E.Z.N.A. TM Fungal RNA Miniprep Kit (OMEGA, Cat # R6840-01) following the manufacturers' instructions and on membrane DNaseI digestion was performed with E.Z.N.A. RNase-Free DNase I Set (OMEGA, Cat # E1091) for further DNA removal. The integrity and concentration of the extracted RNAs were quantified by NanoDrop spectrophotometer (Thermo Fisher Scientific, Waltham, MA, United States). Fungal genomic DNA was prepared according to E.Z.N.A.TM Fungal DNA Mini Kit (OMEGA, Cat # D3390-01).

Construction of BcLAE1 transformants

A list of all primers used to prepare transformants and RT-qPCR is shown in Supplementary Table 1.

The knockout transformants were constructed using a double-combined PCR method to construct the *Bclae1* gene knockout fragment (Yu et al., 2004), and the upstream fragment (582 bp) and downstream fragment (672 bp) of *Bclae1* ORF were amplified with primer pairs *Lae1*-5-F1/−R1 and *Lae1-3*-F1/−R1, respectively. The hygromycin expression cassette fragment (*PoliC::hph*) was then amplified using the primer pair Hph-F1/Hph-R1. The knockout cassette was obtained by overlapping PCR with primer pair *Lae1*-5-F1/*Lae1*-3-R1, and then transformed into TB-31 protoplasts. The protoplasts were produced as previously described (Choquer et al., 2008). The construction of silencing transformants，complement transformants, and overexpression transformants was carried out by ATMT transformation method to transfer target vectors into corresponding strains. Transformants were selected on PDA containing hygromycin (50 µg/ml) or glyphosate (100 µg/ml) and purified by three rounds of subculture on PDA containing the same antibiotic selection.

Extracellular ABA quantification

Single conidia of the *B. cinerea* transformants and the control strain were grown for 6–12 days on solid PDA 24-well plates at 25 C with 1.5 ml of PDA solid medium per well. The extracellular ABA that was secreted into the PDA medium was extracted with acetone, and the ABA contents of these extracted samples were measured with high-performance liquid chromatography (HPLC) using a commercial S-(+)-ABA (98% w/w, Lomon Bio Technology Co., Ltd., Sichuan, China) as the standard sample. The ABA standard curve was prepared by external standard method to detect samples. The Agilent 1,200 Pure Liquid Chromatography system (An Agilent 1,260 Infinity Quaternary Pump VL with An Agilent 1,260 Infinity Standard Autosampler and an Agilent 1,260 Infinity Variable Wavelength Detector) was used with a Luna® 5 µm C18(2) LC Column (Phenomenex, Cat # 00G-4,252-E0). The acetone-extracted samples were diluted to the same volume, and the ABA counts of these samples were determined based on their absorption at 254 nm (Supplementary Figure 1). All measurements were performed independently in triplicate.

Quantitative RT-PCR

Quantitative reverse transcription-PCR (qRT-PCR) was performed to determine the relative expression levels of selected transcripts. The total RNA samples were utilized for gDNA-free cDNA synthesis with the ReverTra Ace-α-® kit (Cat # FSK-101, TOYOBO, Japan). The synthesized cDNA was used as the template for PCR amplification of the selected genes with their corresponding primer pairs (Supplementary Table 1). The *B. cinerea* tubulin gene (BC1G_05600) was used to correct for sample-to-sample variation in the amount of RNA (Dulermo et al., 2010). Amplification was carried out by the CFX96 Real-Time PCR Detection System (BioRad, United States), using the TransStart Green qPCR SuperMix UDG (Transgen, China). The relative abundances of selected transcripts were calculated by the $2^{-\Delta\Delta Ct}$ method from the mean of three independent determinations of the threshold cycle (Schmittgen and Livak, 2008).

Histone extraction and analysis

We modified the procedures for the extraction of histone described by Sidoli et al. (2016). Strains were grown on PDA plates at 25°C for 6 days. Mycelium was collected and ground into small tissues with Dounce homogenizer and resuspended in 50 ml of ice-cold NIB buffer (15 mm Tris-HCl [PH 8.5], 60 mm KCl, 15 mm NaCl, 5 mm MgCl2, 1 mm CaCl2, 250 mm sucrose, 1 mm PMSF, 1 ug/ml leupeptin, and 1 ug/ml pepstatin). The nuclear fraction was pellet by centrifugation (8,500 rpm), washed in the same buffer, and again recovered by centrifugation. Resuspend the nuclear fraction in ice-cold

0.4 M H2SO4 at a volume of 1:5. Shake at 4°C for 6 h, centrifuge the suspension (10,000 rpm) for 6 min, and transfer the supernatant to a new tube. Add cooled 100% TCA to the supernatant at a ratio of 1:3 (to obtain an optimal concentration of 33% TCA), invert the tube several times to mix, and incubate on ice overnight. After centrifugation again at 12,000 rpm for 30 min, precipitated histones were washed in ice-cold acetone twice and dried at room temperature. The purified histones were suspended in 100μl H2O and subjected to SDS-polyacrylamide gel electrophoresis and western blotting using antibodies against Histone H3 (catalog no.17168-1-AP; Proteintech), H3K4me (catalog no. 39498; Active Motif), H3K4me2 (catalog no.39141; Active Motif), H3K4me3 (catalog no.39060; Active Motif), H3K27me3 (catalog no. 39055; Active Motif), H3K14ac (catalog no. 39599; Active Motif), H3K9me (catalog no. 39887; Active Motif), H3K9me2 (catalog no. 39239; Active Motif), and H3K9me3 (catalog no. 39062; Active Motif).

RNA-Seq

Undifferentiated hyphae of *B. cinerea* TB-31 and Δ*Bclae1* transformant were identified, and the hyphae were harvested after dark cultivation on potato dextrose agar (PDA) plates at 25°C for 6 days. Total RNA was extracted using E.Z.N.A.TM Fungal RNA Miniprep Kit according to the manufacturer's protocol. RNA quality was assessed on an Agilent 2,100 Bioanalyzer (Agilent Technologies, Palo Alto, CA, United States) and checked using RNase-free agarose gel electrophoresis. After total RNA was extracted, eukaryotic mRNA was enriched by Oligo(dT) beads. After total RNA was extracted, prokaryotic mRNA was enriched by removing rRNA by Ribo-ZeroTM Magnetic Kit (Epicentre, Madison, WI, United States). Then, the enriched mRNA was fragmented into short fragments using fragmentation buffer and reversly transcribed into cDNA by using NEBNext Ultra RNA Library Prep Kit for Illumina (NEB #7530, New England Biolabs, Ipswich, MA, United States). The purified double-stranded cDNA fragments were end repaired, a base was added, and ligated to Illumina sequencing adapters. The ligation reaction was purified with the AMPure XP Beads (1.0X). Ligated fragments were subjected to size selection by agarose gel electrophoresis and poly merase chain reaction (PCR) amplified. The resulting cDNA library was sequenced using Illumina Novaseq 6,000 by Gene Denovo Biotechnology Co. (Guangzhou, China).

Statistical analysis

Data were expressed as the mean ± SD. Histograms were generated using GraphPad Prism software, and *t*-tests for qPCR experiments were performed using Excel. Differences in ABA production of strains for different cultivation days were compared using SPSS v.16.0 (SPSS Inc., Chicago, IL, United States).

Results

Identification of the LAE1 ortholog in *Botrytis cinerea* TB-31

BcLAE1 was identified in the *B. cinerea* TB-31 genome database by SnapGene software analyses using the sequence of *B. cinerea* B05.10 LAE1 as query. The unique putative homolog of LAE1 showed a methyltransferase domain (100% identity). Like LAE1 in the *B. cinerea* B05.10, the open reading frame (ORF) of *Bclae1* in the *B. cinerea* TB-31 comprises 1,572 bp and encodes a protein of 327 aa (Schumacher et al., 2015). Meanwhile, the ORF is interrupted by six introns (181, 65, 73, 57, 64, and 148 bp). The only difference is that four bases "TACT" are deleted at the end of the 3′UTR (Supplementary Figure 2).

BcLAE1 is required for ABA production in *Botrytis cinerea* TB-31

In order to study whether BcLAE1 will affect ABA synthesis, we previously constructed silencing strains of *Bclae1* gene based on the binary vector pCBSilent1 of gene silencing in the ATMT system. We randomly selected 8 *Bclae1* silencing transformants and cultured them for 7 days to determine ABA production. The results showed that the silencing of *Bclae1* gene reduced the production of ABA in different degrees (Figure 1A). To further identify the function of BcLAE1, we constructed the knockout transformant, the conserved domain was replaced by hygromycin expression cassette, and diagnostic PCR and qRT-PCR was used to confirm the deletion of *Bclae1* gene in Δ*Bclae1* transformant (Supplementary Figure 2). Then, the ABA yield of Δ*Bclae1* transformant and *B. cinerea* TB-31 was detected for 6–12 days, the results demonstrated that Δ*Bclae1* transformant hardly produced ABA, and its yield decreased by 95% compared with TB-31 at 12 days, indicating that BcLAE1 was essential for ABA synthesis (Figure 1B). After that, we focused on the expression patterns of the ABA biosynthesis gene cluster and positive regulator in *B. cinerea* strain: two hypothetical P450 monooxygenase coding genes (*Bcaba1* and *Bcaba2*; Takino et al., 2019), hypothetical FPP catalysis gene (*Bcaba3*; Shu et al., 2018), presumptive short-chain dehydrogenase/reducase coding genes (*Bcaba4*; Takino et al., 2019), and putative pathway-specific transcription factors (*BcabaR1*; Wang et al., 2018). The RNA of control strain TB-31 and Δ*Bclae1* transformant grown on PDA plates for 6 days were extracted and transformed into cDNA for RT-qPCR experiment. It was found that the expression level of *Bcaba1-4* gene in ABA biosynthesis gene cluster was significantly decreased except for pathway-specific transcription factors *BcabaR1* (Figure 1C).

To understand whether BcLAE1 supplementation can restore the ABA yield difference between Δ*Bclae1* and TB-31, the complement vector pCBg1-*Bclae1* was constructed and transferred into the Δ*Bclae1* transformant. Three BcLAE1 complement strains (Δ*Bclae1*-C) were randomly selected for

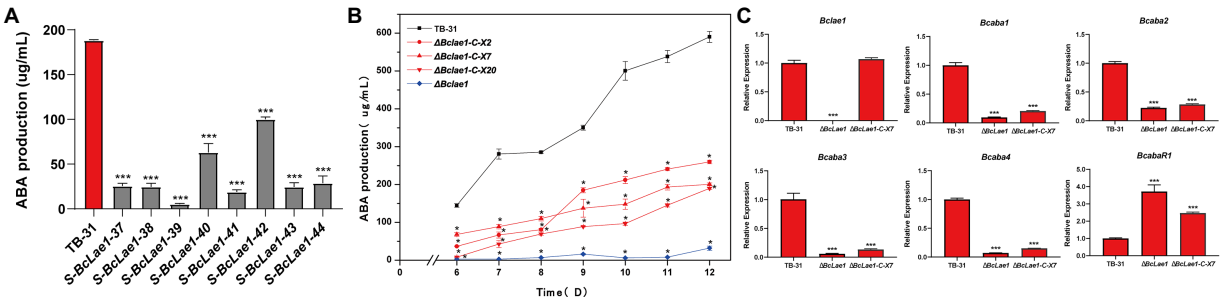

FIGURE 1
Deletion of *Bclae1* affects ABA synthesis. **(A)** Eight *Bclae1* gene silencing strains were randomly selected to grow on PDA. Samples for the quantitative determination of ABA production were collected at day 7. The error bars indicate the standard errors of the mean (SEM) for three replicate cultures (n=3). Asterisks indicate significant differences in ABA production between selected silencing mutants and TB-31 (p<0.001). **(B)** The Δ*Bclae1* mutant and three randomly selected Δ*Bclae1*-C mutants (Δ*Bclae1*-C-X2, Δ*Bclae1*-C-X7, Δ*Bclae1*-C-X20) were grown on PDA. Samples for the quantitative determination of ABA production were collected at 6–12days. The error bars indicate the standard errors of the mean for three replicate cultures (n=3). Asterisks indicate significant differences in ABA production between selected mutants and TB-31 (p<0.05). **(C)** RT-qPCR examining the transcriptional levels of ABA gene cluster, *BcabaR1* and *Bclae1* in Δ*Bclae1* mutant, Δ*Bclae1*-C-X7, and TB-31. The relative transcriptional levels of selected genes were obtained after normalization to the constitutive tubulin reference gene (BC1G_05600) at 6days. The relative values for selected genes transcription at 6days in TB-31 were arbitrarily assigned as 100%. Shown are means and SEM, n=3 independent biological replicates. ***p<0.001 versus the same genes of the TB-31 group.

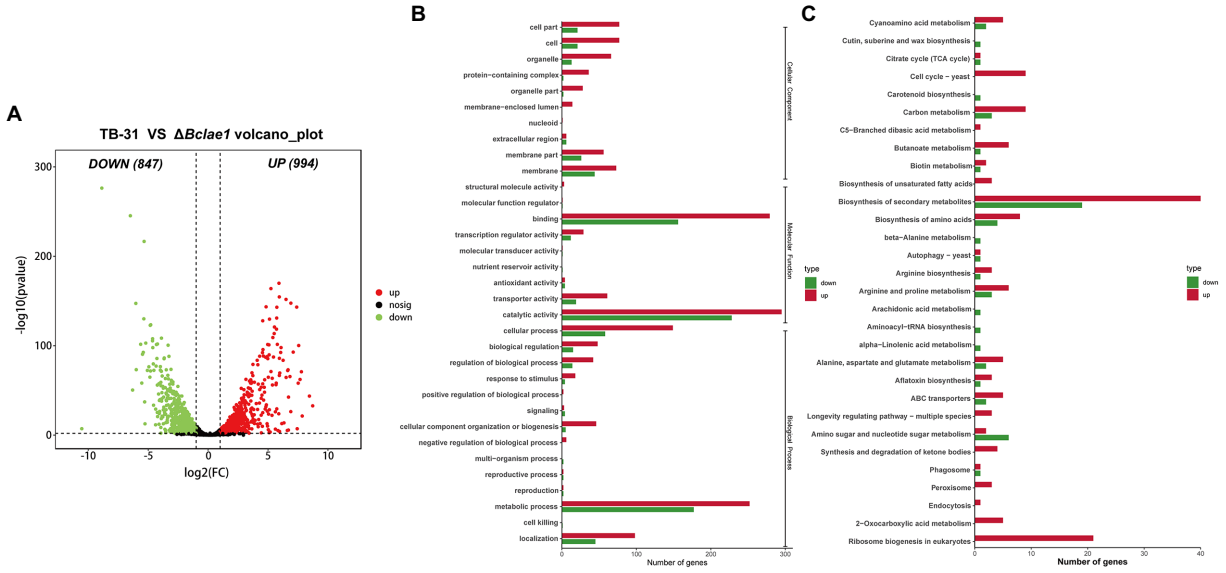

FIGURE 2
Genome-wide regulation of *Bclae1* deletion in *B. cinerea* TB-31. **(A)** The number of differentially expressed genes between TB-31 and Δ*Bclae1* mutant on day 6 of PDA culture. The criteria for the selection of DEGs were a log2 |fold change|≥1, value of p <0.05, and RPKM of at least one sample larger than 1. **(B,C)** Counts of differentially expressed genes significantly enriched to GO function classes and KEGG pathways, respectively.

6–12 days of yield determination (Figure 2C). The results showed that the ABA yield was partially restored by *Bclae1* gene complementation, but it did not reach the level of the control strain TB-31. We selected complement transformant Δ*Bclae1*-C-X7 for RT-qPCR analysis. Although the expression level of *lae1* in Δ*Bclae1*-C-X7 was similar to that of control strain TB-31, the gene cluster *Bcaba1-4* was only slightly upregulated, and the expression level of *BcabaR1* was still in a high expression state. The expression pattern of *Bcaba1-4* was not significantly improved following the ectopic complementation of *Bclae1* gene (Figure 1C).

Identification of differentially expressed genes between TB-31 and Δ*Bclae1*

In order to understand the impact of *Bclae1* deletion on the gene expression profiles, comparative transcriptome analysis was

performed to identify the differentially expressed genes (DEGs) between the TB-31 and Δ*Bclae1* transformant by RNA-seq experiment. The undifferentiated mycelium spots were cultured on PDA solid medium for 6 days. Three biologically duplicated total RNA were extracted and marked respectively, and then, RNA-seq was performed. Based on the results of differential analysis, the differentially expressed genes (DEGs) were identified between the transformants using the threshold log2 |fold change| ≥ 1, value of $p < 0.05$, and RPKM value of at least one sample larger than 1. And there were a total of 1841 differentially expressed genes, of which 994 genes were upregulated and 847 genes were downregulated (Figure 2A). To determine the main biological functions of the DEGs, we performed GO and KEGG database analysis and annotation definition on the DEGs set to reveal the biological process affected by *Bclae1* deletion. The results demonstrated that compared with TB-31, the DEGs of Δ*Bclae1* transformant were significantly labeled as membrane-related in the cell components of GO database, which accounted for a larger proportion of the total differential genes. In molecular function and cell process, it is annotated as cofactor binding, oxidoreductase activity, catalytic activity, hydrolase activity, ribosome biogenesis, etc. (Figure 2B). In addition, the deletion of *Bclae1* had an obvious effect on the biosynthesis of secondary metabolites, ribosomal biogenesis, biosynthesis of amino acids, carbon metabolism, and other KEGG enrichment pathways (Figure 2C). We focus on significant transcriptional changes in metabolic networks related to carbon source transport and utilization and acetyl coenzyme A (acetyl-CoA) and ABA biosynthesis.

The effect of *Bclae1* deletion on ABA synthesis pathway

The ABA synthesis pathway of *B. cinerea* is mainly divided into six stages, namely the transport and utilization of glucose, the synthesis of pyruvate, the synthesis of acetyl-CoA, the synthesis of isopentenyl pyrophosphate (IPP), the synthesis of farnesate pyrophosphate (FPP), and finally to ABA. As heterotrophs, glucose in cytoplasm is transported from outside the cells, and PDA medium contains a large amount of glucose, so we first analyzed the transcriptional level of sugar transporters and permeases. The results showed that the transcriptional levels of five putative sugar transporters and permeases increased significantly, namely BC1G_08389 (FC of 1.42), BC1G_11623 (FC of 3.55), BC1G_05673 (FC of 3.12), BC1G_12189 (FC of 3.01), and BC1G_05489 (FC of 1.79; Baruffini et al., 2006). Moreover, the transcriptional level of some β-glucosidases was also increased, such as BC1G_10877 (FC of 1.66), BC1G_11255 (FC of 2.1), BC1G_02551 (FC of 2.22), which indicated that the utilization efficiency of Δ*Bclae1* transformant to carbon source was enhanced compared with TB-31 (Supplementary Table 2.1).

The central metabolite acetyl-CoA is the link between the primary metabolic pathway and the secondary metabolic pathway, and is also the precursor of the synthesis of ABA in *B. cinerea*. The ultimate source of ABA is acetyl-CoA in the *B. cinerea* cytosol. Therefore, the genes involved in the biosynthesis and transportation of acetyl-CoA were analyzed. Pyruvate is an important node in the synthesis of glucose to acetyl-CoA. Glucose enters cells to generate pyruvate *via* glycolysis and pentose phosphate pathway (PPP). Except for the decreased transcriptional level of fructose-bisphosphate aldolase (FBA), the transcriptional levels of other rate-limiting enzymes in the glycolysis pathway did not change much. Meanwhile, there was little difference in the transcriptional levels of key genes in PPP, which indicated that the deletion of *Bclae1* has not greatly affected the carbon flux from glucose to pyruvate.

Cell cytosol pyruvate can be transformed into acetyl-CoA by two different pathways, the first being pyruvate dehydrogenase bypass (PDH bypass), it converts pyruvate to acetyl-CoA in cells (Shiba et al., 2007). And another pathway is that PDH catalyzes pyruvate decarboxylation and releases acetyl-CoA into mitochondrial matrix to participate in the tricarboxylic acid (TCA) cycle (Guest et al., 1989). In contrast, there was no significant difference in the transcriptional levels of genes encoding different components of PDH between TB-31 and Δ*Bclae1* transformant, but the transcriptional level of acetyl-CoA synthetase was elevated, which is conducive to increasing the content of acetyl-CoA in the cytosol. In most fungi, acetyl-CoA can also be produced by β-oxidation of fatty acids in mitochondria and peroxisomes. The transcriptional level of the 21 genes involved in the β-oxidation of mitochondria and peroxisomes had little change except that the Enoyl-CoA hydratase increased slightly, so the content of acetyl-CoA was no significant change by the β-oxidation of fatty acids. Since the TCA cycle is the main metabolic pathway to mitochondrial consumption of acetyl-CoA, we also analyzed the key genes in the TCA cycle. The data showed that the transcriptional level of citrate synthase increased, but pyruvate was the main donor of oxaloacetate in mitochondria, and the decreased transcriptional level of pyruvate carboxylase reduced the ability of pyruvate to produce oxaloacetate, which may affect the synthesis of citrate. At the same time, in the glyoxylic acid cycle (GYC), the transcriptional level of isocitrate lyase decreased, thus reducing the ability of isocitrate to synthesize glyoxylic acid and succinate, which may interfere with glyoxylate consumption of acetyl-CoA to synthesize apple acid. These changes may impede the fluidity of the TCA cycle, resulting in impaired acetyl-CoA utilization in the TCA cycle. In addition, acetyl-CoA in the cytoplasm is also the precursor of cellular lipids (such as fatty acids; Camões et al., 2015). Compared with TB-31, the transcriptional levels of genes encoding fatty acid synthesis-related enzymes, such as fungi-type fatty acid synthase and [acyl-carrier-protein] S-malonyltransferase, were not significantly altered in Δ*Bclae1* transformant. Carnitine/acetylcarnitine shuttle system is very important for the intracellular transport of acetyl-CoA between mitochondria, peroxisomes, and cytoplasm (Strijbis et al., 2010; Lee et al., 2011). We analyzed three possible carnitine O-acetyltransferases and found that the transcriptional

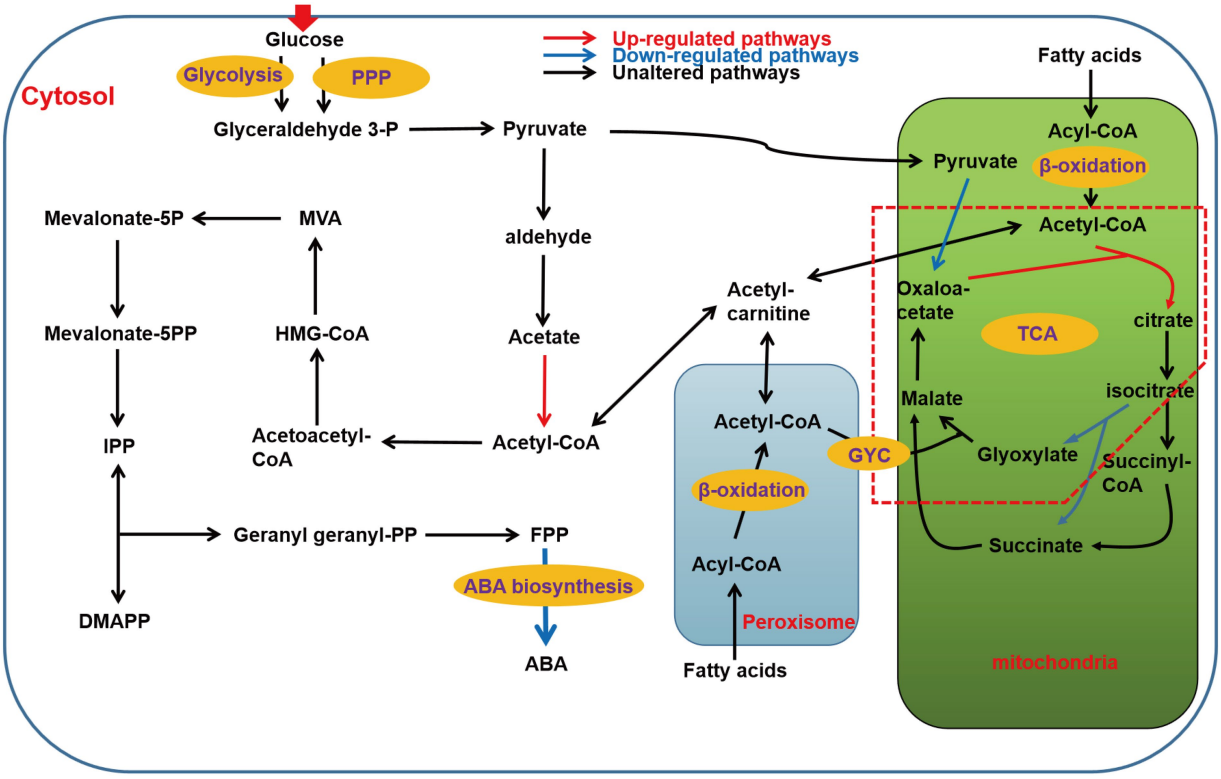

FIGURE 3
Schematic of metabolic pathways associated with ABA production affected by *Bclae1* deletion. The red arrows indicate upregulated pathways, blue arrows indicate downregulated pathways, and black arrows indicate pathways that were not observably regulated. The red dashed box annotates the GYC pathway (log2 |fold change|≥1, value of $p<0.05$ and RPKM of at least one sample larger than 1).

level also did not change significantly (Supplementary Table 2.2). In conclusion, the accumulation of cytosol acetyl-CoA was not greatly affected by the deletion of the *Bclae1* gene.

In *B. cinerea*, acetyl-CoA can synthesize IPP and dimethylallyl-diphosphate (DMAPP) through the MVA pathway (Oritani and Kiyota, 2003), which are precursors for terpenoid backbone biosynthesis. This is followed by the biosynthesis of FPP, which is a direct precursor for the biosynthesis of ABA from IPP (Dewick, 2002). RNA-Seq analysis showed that there were no significant changes in the transcriptional level of all enzymes from acetyl-CoA to FPP. However, the transcriptional level of ABA synthetic gene cluster changed greatly, in which the FPKM average of BC1G_07529 (*Bcaba4*) gene decreased from 139 to 20, the FPKM average of BC1G_07530 (*Bcaba2*) gene decreased from 666 to 278, the FPKM average of BC1G_07531 (*Bcaba1*) gene decreased from 1743 to 290, and the FPKM average of BC1G_07534 (*Bcaba3*) gene decreased from 504 to 53, which indicated that the deletion of *Bclae1* was mainly aimed at the decrease of transcriptional level of ABA synthetic gene cluster (Supplementary Table 2.3). Since Bcaba1-4 plays an important role in the final synthesis of FPP to ABA, combined with the above RT-qPCR data, we believe that this may be the key factor of decreased ABA production in the Δ*Bclae1* transformant (Figure 3).

Transcriptional level of KEs in secondary metabolism is affected

The KEGG pathway enrichment results showed that BcLAE1 has a significant regulatory effect on secondary metabolism; so in addition to ABA synthesis, we also analyzed differentially expressed genes for 43 key enzymes of secondary metabolism in transcriptome data (Supplementary Table 2.4). KEs with FPKM less than 1 were eliminated, and the transcriptional level of 6 KEs was obviously changed (value of $p<0.05$). The expression level of the sesquiterpene synthase gene *BcSTC3* was upregulated (FC of 1.1). Although the corresponding compound has not been discovered, a new sesquiterpene structure associated with eremophil-9-ene was found in the presence of chemical induction of copper sulfate with the increased expression of *BcSTC3* and *BcSTC4* gene (Pinedo et al., 2016). The expression level of another sesquiterpene cyclase *BcSTC1*/*Bcbot2* gene was significantly decreased (FC of-4.6). *Bcbot2* is a key gene for the synthesis of sesquiterpenoid botrydial (BOT), which induces hypersensitivity and uses host defense mechanisms to generate necrotic cells (Simon et al., 2013). We also analyzed the BOT synthetic gene cluster and found that not only the *Bcbot2* gene but also the other four genes (*Bcbot1-5*) were significantly downregulated. At the same time, the expression level of *BcPKS13*, a putative synthesis gene of polyketide derivative

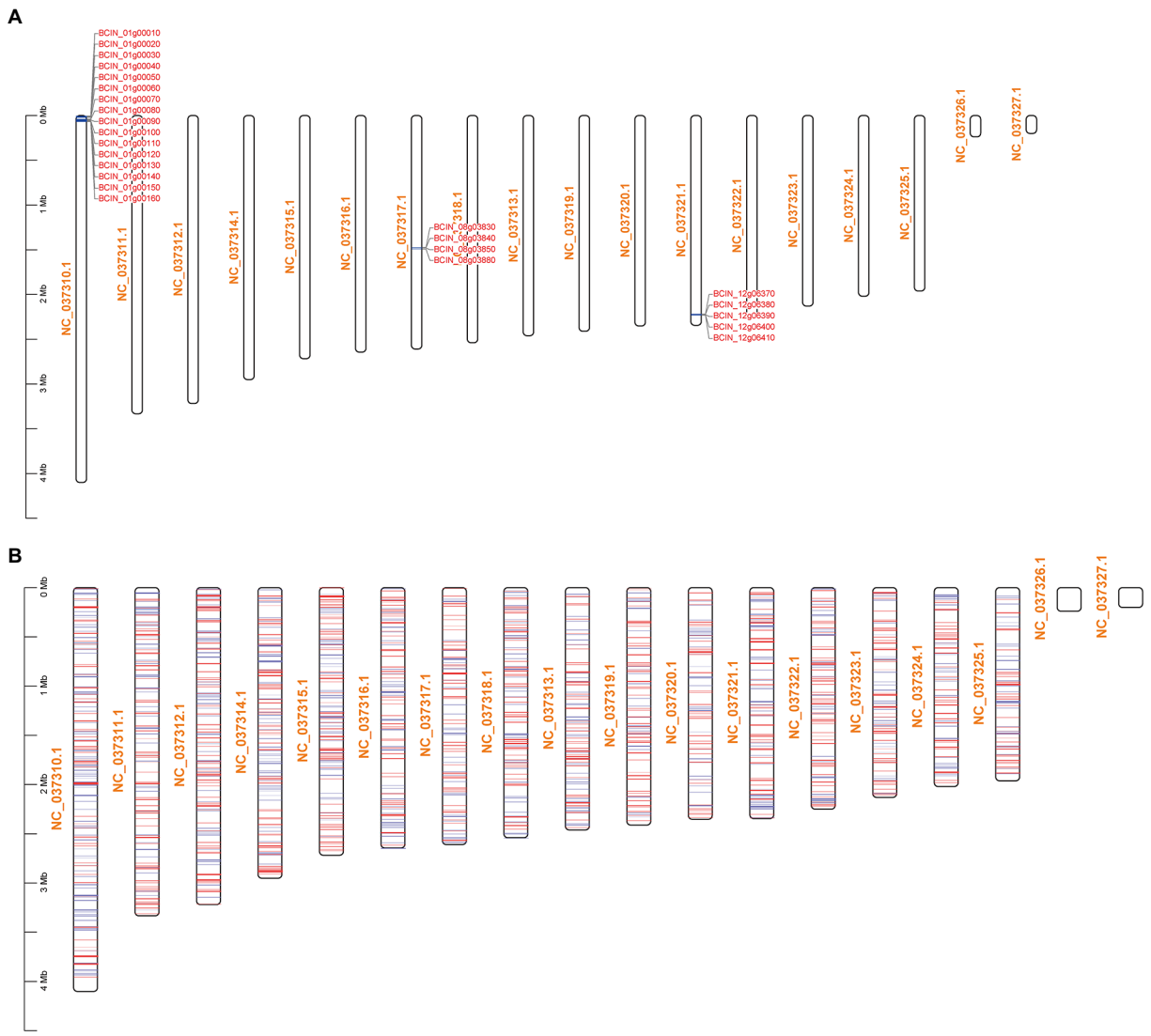

FIGURE 4
Schematic of DEGs mapping across chromosomes. NC_037310.1-NC_037327.1 are the numbers of the 16 chromosomes of *B. cinerea*. **(A)** BCIN_01g00010-BCIN_01g00160 are BOA synthetic gene cluster, BCIN_08g03830-BCIN_08g03880 are ABA synthetic gene cluster, and BCIN_12g06370-BCIN_12g06410 are BOT synthetic gene cluster. **(B)** The mapping of all DEGs on chromosomes, the red line represents genes with upregulated transcription level, and the blue line represents genes with downregulated transcription level.

1,8-Dihydroxynaphthalene (DHN)-melanin (Schumacher, 2016), was also downregulated (FC of-1.2). The transcriptional levels of the other two differential polyketide synthase (PKS) genes, *BcPKS19* (FC of-1.2) and *BcPKS8* (FC of-2), were downregulated like the non-ribosomal peptide synthase gene *BcNRPS5* (FC of-1.2), but their corresponding compounds have yet to be identified. Meanwhile, we also found that the transcriptional levels of most botcinic acid (BOA; Porquier et al., 2019) synthesis genes were significantly downregulated (value of $p < 0.05$), including *Bcboa3-5* genes in BOA gene cluster A and *Bcboa10, 12, 16, 17* genes in BOA gene cluster B. Moreover, the FPKM of key genes *BcPKS6* and *BcPKS9* and other genes in the cluster also decreased, suggesting that BcLAE1 is involved in the regulation of the transcriptional level of the whole cluster. It was obviously that BcLAE1 affects the expression of SM-related gene expression in *B. cinerea* TB-31, and shows a preference for the whole cluster regulation. After that, we mapped the ABA gene cluster, the BOT gene cluster, the BOA gene cluster, and all the differential genes to the chromosomes of *B. cinerea,* respectively (Figure 4). It was found that some of the differential expression genes caused by *Bclae1* deletion showed aggregation.

To confirm the expression pattern of Δ*Bclae1* transformant genes in the RNA-Seq, we selected *Bcbot1*, *Bcbot2*, *Bcbot3*, *Bcboa3*, *BcPKS13*, *Bccit3*, *Bcfas1*, *Bcfas2*, *BcACS*, *BcFBA*, *BcICL*, *BcMLS*, *BcNRPS5*, *BcPKS19*, *BcPYC*, BC1G_05489, and BC1G_11623 genes to design primers, and used the isolated RNA for RT-qPCR verification (Supplementary Figure 3). The results indicated that the selected genes basically conformed to the expression pattern predicted by the RNA-Seq.

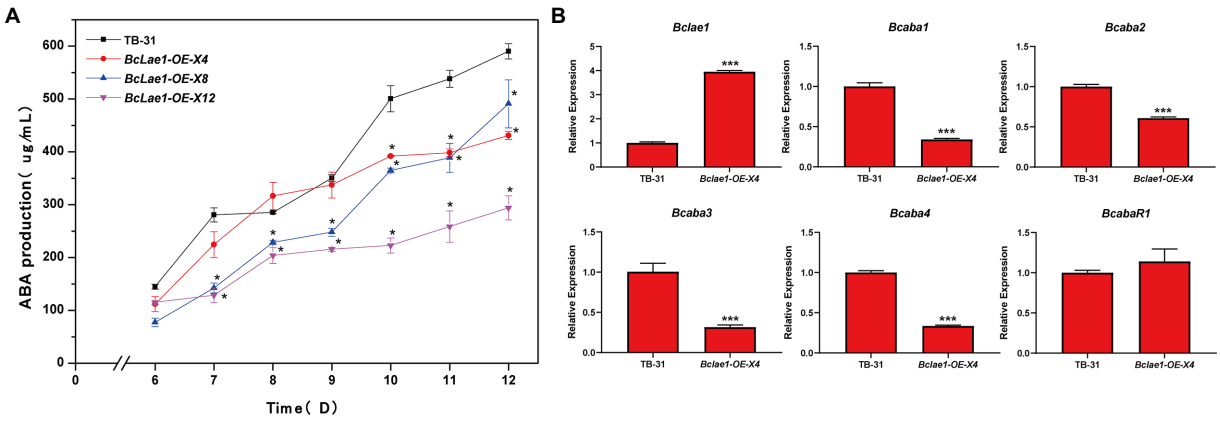

FIGURE 5
Overexpression of *Bclae1* reduced ABA synthesis in *B. cinerea* TB-31. **(A)** The TB-31 and 3 randomly selected *Bclae1*-OE mutants (*Bclae1*-OE-X4, *Bclae1*-OE-X8, *Bclae1*-OE-X12) were grown on PDA. Samples for the quantitative determination of ABA production were collected at 6–12days. The error bars indicate the standard errors of the mean for three replicate cultures (n=3). Asterisks indicate significant differences in ABA production between selected mutants and TB-31 (p<0.05). **(B)** RT-qPCR examining the transcriptional levels of ABA gene cluster, *BcabaR1* and *Bclae1* in *Bclae1*-OE-X4 and TB-31. The relative transcriptional levels of selected genes were obtained after normalization to the constitutive tubulin reference gene (BC1G_05600) at 6days. The relative values for selected genes transcription at 6days in TB-31 were arbitrarily assigned as 100%. Shown are means and SEM, n=3 independent biological replicates. ***p<0.001 versus the same genes of the TB-31 group.

Overexpression of *Bclae1* did not increase ABA production in *Botrytis cinerea* TB-31

Based on the data of silence strains and knockout strain, it was found that the deletion of *Bclae1* gene reduced the yield of ABA. Considering that BcLAE1 has a significant effect on the synthesis of secondary metabolites, we further analyzed the effect of constitutive expression of *Bclae1* on ABA production in *B. cinerea* TB-31. We constructed the overexpression transformant *Bclae1*-OE by using the overexpression vector pCBh1 with hygromycin resistance gene. The obtained 12 overexpression transformants were cultured for 7 days for ABA production detection, and it was found that the ABA production of all transformants decreased compared with TB-31 transferred into pCBh1 empty vector (Supplementary Figure 4). Considering whether the ABA yield would recover at the later stage of strain culture, three *Bclae1*-OE transformants were randomly selected for 6–12 days ABA yield determination. The results showed that even if the three *Bclae1*-OE transformants were cultured for 12 days, ABA production was still reduced (Figure 5A). Transcriptional levels of ABA synthesis gene cluster and pathway-specific transcription factor were detected in *Bclae1*-OE-X4 transformant. The results showed that the expression of the *Bclae1* gene was significantly increased compared with the control strain TB-31, while the expression of *Bcaba1-4* gene was decreased, and there was no significant difference in the expression of *BcabaR1* (Figure 5B). This indicates that overexpression of *Bclae1* is not beneficial for ABA synthesis in *B. cinerea* TB-31.

The SAM domain of BcLAE1 is involved in ABA biosynthesis in *Botrytis cinerea* TB-31

Since LAE1 can also act as a putative methyltransferase to affect chromatin modification changes to regulate secondary metabolic synthesis, to illuminate whether BcLAE1 plays a role as a methyltransferase in ABA synthesis, we studied the conserved sites of the BcLAE1 SAM domain. We selected six functionally characterized LaeA/ LAE1 orthologs from ascomycetes for comparison with BcLAE1, namely *Aspergillus fumigatus* LaeA (Dagenais et al., 2010), *Aspergillus nidulans* LaeA (Khan et al., 2020), *Cochliobolus heterostrophus* LAE1 (Wu et al., 2012), *Fusarium fujikuroi* LAE1 (Wiemann et al., 2010), *Penicillium chrysogenum* LaeA (Kosalková et al., 2009), and *Trichoderma reesei* LAE1 (Karimi-Aghcheh et al., 2013; Figure 6A). The methyltransferase domain was demonstrated and three conserved glycine residues G^{90}, G^{92}, and G^{94} were marked. Then, the three glycine were replaced by alanine to construct the complement vector pCBg1-*Bclae1*^{G90,92,94A}. The vector was transferred into Δ*Bclae1* transformant and the ABA yield of the Δ*Bclae1*-C^{SAM} transformant was measured from 6 to 12 days; the results showed that B*clae1*^{G90,92,94A} gene did not restore the yield of ABA, and the production data were basically consistent with the Δ*Bclae1* transformant (Figure 6B). We further analyzed the expression of B*clae1*^{G90,92,94A} in Δ*Bclae1*-C^{SAM} transformants by RT-qPCR validation, and found that the expression levels of *Bclae1*^{G90,92,94A} in the transformant was close to that of *Bclae1* in TB-31. At the same time, we examined the expression of ABA synthesis gene clusters and pathway-specific transcription factors, and the results were similar to the Δ*Bclae1* transformant (Figure 6C). These data suggested that the SAM domain of

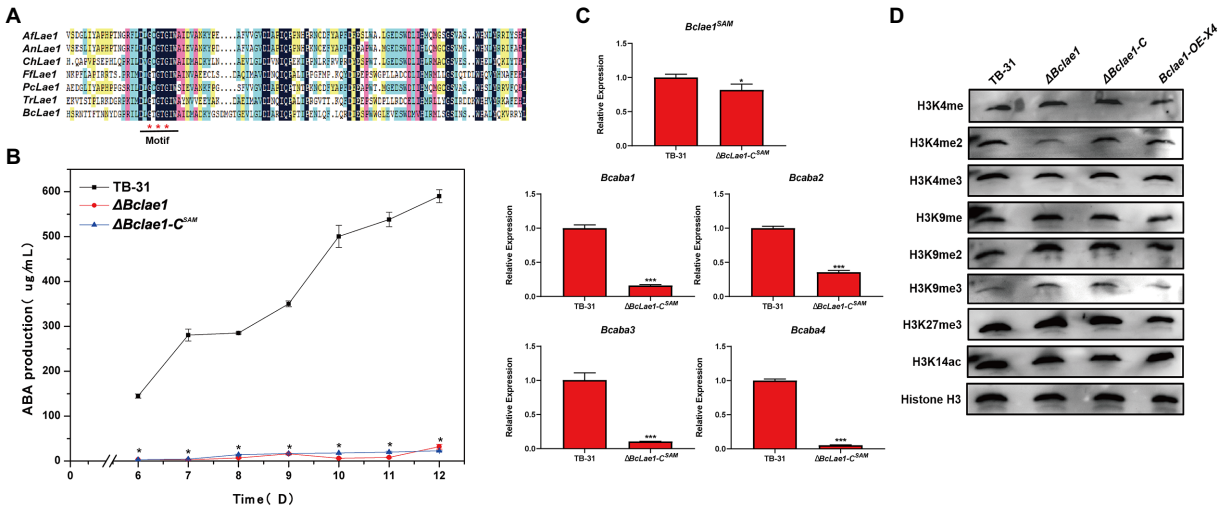

FIGURE 6
The SAM domain of BcLAE1 is essential for its full activity. **(A)** Multiple sequence alignment of the LaeA/ LAE1 SAM domain from *Aspergillus fumigatus* LaeA, *Aspergillus nidulans* LaeA, *Cochliobolus heterostrophus* LAE1, *Fusarium fujikuroi* LAE1, *Cochliobolus heterostrophus* LAE1, *Trichoderma reesei* LAE1, and *B. cinerea* LAE1. Black, pink, blue, and yellow represent 100%, greater than 75%, greater than 50%, and greater than 30% homology levels, respectively. The red * marked the glycine that was replaced for alanine. **(B)** The TB-31, Δ*Bclae1* mutant, and Δ*Bclae1*-C^{SAM} mutant were grown on PDA. Samples for the quantitative determination of ABA production were collected at 6–12days. The error bars indicate the standard errors of the mean for three replicate cultures (n=3). Asterisks indicate significant differences in ABA production between selected mutants and TB-31 (p<0.05). **(C)** RT-qPCR examining the transcriptional levels of ABA gene cluster and *Bclae1* in Δ*Bclae1*-C^{SAM} and TB-31. The relative transcriptional levels of selected genes were obtained after normalization to the constitutive tubulin reference gene (BC1G_05600) at 6days. The relative values for selected genes transcription at 6days in TB-31 were arbitrarily assigned as 100%. Shown are means and SEM, n=3 independent biological replicates. *p<0.05/***p<0.001 versus the same genes of the TB-31 group. **(D)** Western blots for H3K4me1/2/3, H3K9me1/2/3, H3K27me3, and H3K14ac global status in the histone extracts isolated from the 6days cultures of the TB-31, Δ*Bclae1*, Δ*Bclae1*-C (X7), and *Bclae1*-OE-X4 mutants. Anti-H3 was used as a loading control.

BcLAE1 plays important roles in ABA biosynthesis in *B. cinerea* TB-31.

The deletion of *Bclae1* affects H3K9me3 and H3K4me2 modification

The above experiments suggest that BcLAE1 may play the role of methyltransferase. Although the substrate of LAE1 methylation is not clear, more and more indirect evidence suggests that LAE1 may affect expression of SMs gene clusters through the apparent genetic modification of chromatin structure. For example, HstD/AoHst4 may be involved in epigenetic regulation caused by laeA gene expression to coordinate fungal development and secondary metabolism (Kawauchi et al., 2013).

In order to study the possible effect of BcLAE1 on histone modification, we extracted histone of TB-31, Δ*Bclae1*, Δ*Bclae1*-C, and *Bclae1*-OE-X4 transformants; then, the modification levels of H3K4me1/2/3, H3K9me1/2/3, H3K27me3, and H3K14ac were analyzed by Western blot (WB). The results showed that there was no significant change in *Bclae1*-OE-X4 transformant compared with TB-31. The modification levels of H3K4me, H3K4me3, H3K9me2, H3K9me2, H3K27me3, and H3K14ac in Δ*Bclae1* were also not significantly affected, but the level of H3K4me2 was decreased and the level of H3K9me3 was increased, suggesting that BcLAE1 was involved in chromatin modification regulation (Figure 6D). The Δ*Bclae1*-C transformant partially recovered the level of H3K4me2, but did not completely reduce the accumulation of H3K9me3. As heterochromatin is important for maintaining genome integrity, it is characterized by histone H3K9 methylation and tail hypoacetylation (Steinhauf et al., 2014). In other words, the loss of *Bclae1* may lead to changes in the heterochromatin landscape in the genomic region that regulate fungal development and secondary metabolism.

Deleting *Bclae1* changes the strain development and differentiation program

LAE1 is involved in the growth, morphology and reproductive development of fungi (Bayram and Braus, 2012), the TB-31, Δ*Bclae1*, Δ*Bclae1*-C, and *Bclae1*-OE-X4 transformants were cultivated to track the morphology of hyphal, colony growth. When cultured to the 6th day, the Δ*Bclae1* transformant showed excessive aerial hyphal formation, which gave the colony as "marshmallow" appearance. At the same time, the hyphal color of the Δ*Bclae1* transformant did not show gray, but turned white. The Δ*Bclae1*-C transformant made their mycelium morphology and color close to TB-31, which indicated that BcLAE1 was indeed involved in the regulation of mycelial development. Furthermore, the colony diameter of *Bclae1*-OE transformant became smaller than that of TB-31 (Figure 7A). Although the morphology of

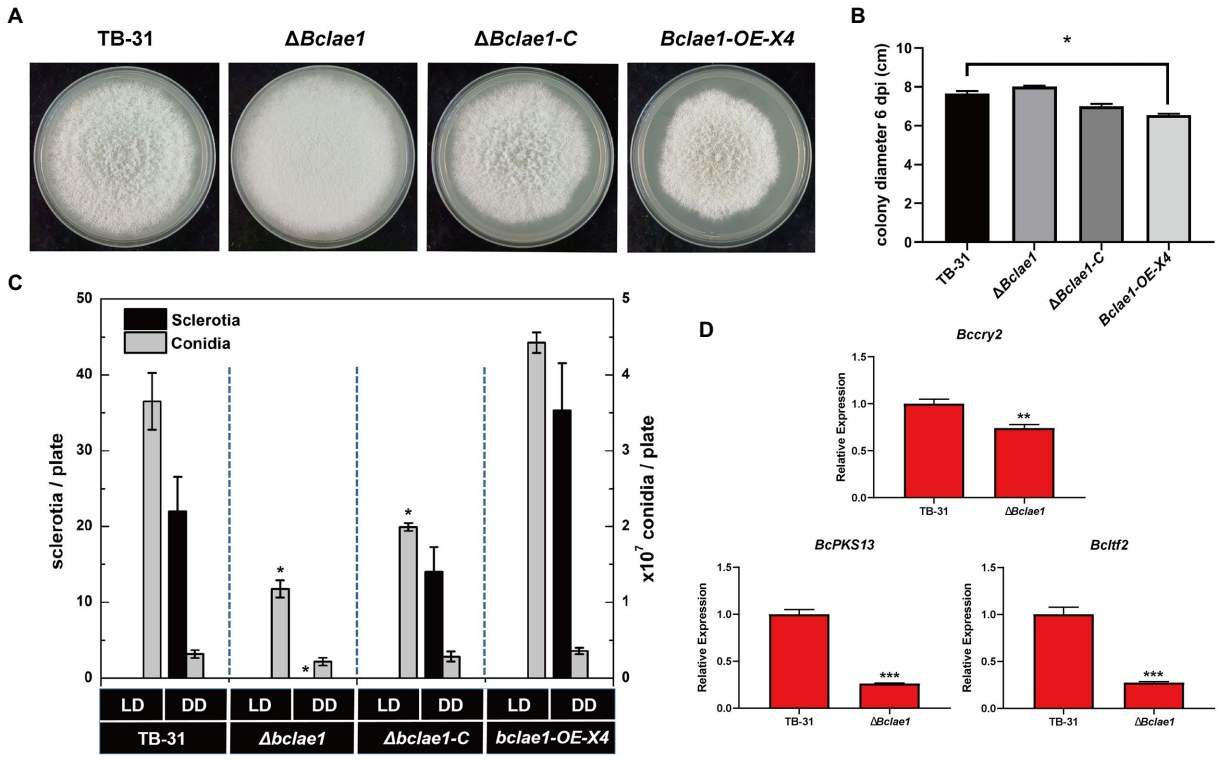

FIGURE 7
Deleting *Bclae1* changes the growth, morphology, and reproductive development. **(A)** The TB-31, Δ*Bclae1*, Δ*Bclae1*-C (X7), and *Bclae1*-OE-X4 mutants were photographed after 6days of PDA growth under DD culture conditions, and the colony diameters were calculated **(B)**. Shown are means and SEM, $n=3$ independent biological replicates. *$p<0.05$ versus the colony diameter of the TB-31 group. **(C)** Under DD or LD conditions, TB-31, Δ*Bclae1*, Δ*Bclae1*-C (X7), and *Bclae1*-OE-X4 mutants were counted for sclerotia and conidia numbers after 14days of PDA growth. Shown are means and SEM, $n=3$ independent biological replicates. *$p<0.05$ versus the TB-31 group. **(D)** RT-qPCR examining the transcriptional levels of *Bccry2*, *BcPKS13*, and *Bcltf2* in TB-31 and Δ*Bclae1*. Shown are means and SEM, $n=3$ independent biological replicates. **$p<0.01$/***$p<0.001$ versus the same genes of the TB-31 group.

hyphae did not change, the growth rate was slowed down (Figure 7B). The transcriptome data (Supplementary Table 2.5) revealed that the gene transcriptional levels of the putative UV-light-sensing cryptochrome *Bccry2* (Cohrs and Schumacher, 2017) were upregulated in Δ*Bclae1* compared to TB-31. The gene transcriptional levels of the key melanin synthesis enzyme *BcPKS13* and the conidial regulator *Bcltf2* (Cohrs et al., 2016) were downregulated in Δ*Bclae1* (value of $p<0.05$). RT-qPCR analysis indicated that the expression levels of *BcPKS13* and *Bcltf2* were consistent with the RNA-Seq except for *Bccry2* (Figure 7D).

We also detected the growth of conidia and sclerotia under different light conditions. Conidia, as the source of inoculation for host infection, are mainly produced under light conditions. As the female parent of sexual reproduction, the sclerotia is mainly produced in the absence of light. Since it takes longer for sclerotia to form than conidia, the number of conidia and sclerotia of transformants was detected after 2 weeks of culture. Under continuous darkness (DD) and 12-h light and 12-h dark (LD) photoperiod, the Δ*Bclae1* transformant did not form sclerotia under DD photoperiod, but only a small number of conidia formed (Figure 7C). However, the *Bclae1*-OE-X4 transformant formed more sclerotinia and conidia than control strain TB-31. Due to the lack of sclerotia formation, the Δ*Bclae1* transformant was female sterile. At the same time, under the condition of LD photoperiod, the number of conidia decreased a lot compared with the control strain TB-31. The Δ*Bclae1*-C transformant made up for the lack of sclerotia formation function and increased the conidia production compared with the Δ*Bclae1* transformant. Overall, LAE1 is critical to the differentiation program under light control.

Discussion

Botrytis cinerea, as a filamentous ascomycete, is the pathogen that causes gray mold infection in more than 1,000 plants (Dean et al., 2012). Therefore, most of the studies on *B. cinerea* are mainly related to virulence factors. For example, BcReg1 in *B. cinerea* is involved in regulating the production of plant toxins (Michielse et al., 2011). Reboledo et al. (2020) studied genome-wide transcriptional profiling of *B. cinerea* during different infection stages. In addition, the two secondary metabolites BOT and BOA produced by *B. cinerea* are also the focus of research (Dalmais et al., 2011; Malmierca et al., 2016). In addition to phytotoxins,

B. cinerea can also secrete a variety of secondary metabolites, one of the most famous secondary metabolites is ABA. LAE1/LaeA is a secondary metabolic regulator, and its deletion or overexpression affects the expression patterns of multiple SM genes. Studies have shown that LaeA regulates penicillin production in *P. chrysogenum* (Kosalková et al., 2009). In addition, overexpression of *laeA* orthologs also resulted in higher production of trichothecenes in *F. Graminearum* (Kim et al., 2013), aflatoxin in *Aspergillus flavus* (Kale et al., 2008), T-toxin in *C. heterostrophus* (Wu et al., 2012), and pigments in *Monascus pilosus* (Lee et al., 2013). Up to now, there has been no report on the effect of LAE1 on the synthesis of ABA in *B. cinerea*. In this study, *B. cinerea* TB-31 with high ABA yield was used to observe the effect of *Bclae1* deletion on ABA production, and the differential genes in ABA synthesis pathway were screened by RNA-seq data. It was found that BcLAE1 significantly affected the expression of ABA synthesis gene cluster. At the same time, BcLAE1 plays its own methyltransferase function and participates in the regulation of histone modification, which may also be a way for BcLAE1 to regulate ABA synthesis.

In order to study the effect of BcLAE1 on ABA synthesis, we first constructed *Bclae1* silencing strain. Yield assays confirmed that *Bclae1* silencing resulted in decreased ABA synthesis. Then, we constructed the *Bclae1* knockout mutant, after 6–12 days of cultivation, it was found that the deletion of *lae1* seriously disrupted the ABA synthesis ability, accompanied by a decrease of the transcriptional level of the ABA synthesis gene cluster *Bcaba1-4*. In a previous study, we found a novel Cys2His2 transcription factor (TF), BcabaR1, which is a positive regulator of ABA biosynthesis in *B. cinerea*. BcabaR1 regulates the transcriptional levels of ABA synthase genes by binding specifically to the promoter region of *Bcaba1-4* genes (Wang et al., 2018). In this study, the transcriptional level of *BcabaR1* gene in Δ*Bclae1* was upregulated compared with TB-31, which did not drive the transcriptional level of the entire ABA gene cluster to increase, indicating that there are other unknown regulatory ways of ABA synthesis.

In some fungi such as *Fusarium fujikuroi*, although the deletion of *lae1* gene led to a sharp decrease in the expression of SM genes, the overexpression of *lae1* gene also led to the increase of some SM genes expression, which led to the improvement of product level (Niehaus et al., 2018). Therefore, the overexpression of *laeA/ lae1* has also been successfully used to activate some gene clusters. LAE1, as the main focus of fungal strain improvement, we also overexpressed *Bclae1* in TB-31. However, the yield of ABA decreased after overexpression of *Bclae1*. The transcriptional level of the ABA gene cluster was downregulated in *Bclae1*-OE-X4 transformant, indicating that the overexpression of *Bclae1* is not beneficial to the biosynthesis of ABA in *B. cinerea* TB-31. We speculate that the reason for this phenomenon is that the regulation triggered by LAE1 is global, which is affected by many unknown factors, such as growth and development. LAE1 does not regulate specific secondary metabolism, and the yield of a single secondary metabolism is not positively correlated with the expression level of *lae1*. Although overexpression of *lae1* resulted in the overproduction of some secondary metabolites, it did not lead to increased expression levels of all KEs in secondary metabolism (Kim et al., 2013; Niehaus et al., 2018). At the same time, the product changes caused by lae1 overexpression are different in different strains, so how LAE1 increases the production of a specific secondary metabolite needs to be studied.

To further understand how the effect of *Bclae1* deletion on ABA synthesis, we compared RNA-seq data to analyze the differentially expressed genes in ABA synthesis pathway. The Δ*Bclae1* transformant has significantly improved the transport and utilization efficiency of glucose, which is definitely favorable for the synthesis of acetyl-CoA. However, the transcriptional levels of genes involved in pyruvate synthesis, acetyl-CoA synthesis, IPP synthesis, and FPP synthesis did not change significantly, and only the expression level of *Bcaba1-4* in the ABA synthesis gene cluster was severely downregulated. Therefore, we believed that this was the direct cause of the decreased ABA synthesis in the Δ*Bclae1* transformant.

In addition to the secondary metabolite ABA, we also paid attention to the expression of the other 43 key enzymes in the secondary metabolism. The transcriptional levels of six key enzyme genes were changed, which were *BcSTC1/Bcbot2* (FC of-4.6), *BcSTC3* (FC of 1.1), *BcPKS13* (FC of-1.2), *BcPKS19* (FC of-1.2), *BcPKS8* (FC of-2), and *BcNRPS5* (FC of-1.2). The corresponding compounds of the BcSTC3, BcPKS19, BcPKS8, and BcNRPS5 have yet to be identified. *Bcbot2* is the key gene for the synthesis of the virulence factor botrydial (BOT). We found that the entire BOT synthesis gene cluster, including *Bcbot2*, was downregulated at the transcriptional level like the ABA synthesis gene cluster. This downregulation even affected *Bcbot6* and *Bcbot7* (Porquier et al., 2016), which are 10 kb away from the BOT gene cluster. Bcbot6 is a positive regulatory transcription factor of the BOT gene cluster, and Bcbot7 is predicted to be a dehydrogenase that may be involved in the transformation of BOT to dihydrobotrydial. Studies have shown that *Bcbot1-Bcbot5* genes and the newly discovered *Bcbot7* gene are all dependent on the regulation of BcBot6, but the deletion of *Bclae1* down-regulates all *Bcbot1-7* genes, suggesting that LAE1-induced clustering regulation may have a higher priority in secondary metabolic regulation than transcription factors. In another virulence factor bocinic acid (BOA) gene cluster, the FPKM of the entire BOA gene cluster including *BcPKS6* and *BcPKS9* was decreased. When the expression level of BOT and BOA clusters was downregulated, the virulence of *B. cinerea* was inevitably affected. This is consistent with the phenomenon in *B. cinerea* B05.10, where deletion of *lae1* directly impairs infectivity (Schumacher et al., 2015). In addition, this also reflects that although the key SM genes affected by BcLAE1 are located at different chromosomal locations, it tends to regulate the whole cluster and have no significant influence on the outside of the cluster region, while *BcabaR1* does not have the same expression pattern as *Bcaba1-4*, probably it is not in the ABA gene cluster or not connected to the cluster. This form of regulation is similar to the regulation of *Aspergillus nidulans* on the ST gene cluster; Chip experiment showed that the LaeA-mediated

heterochromatin state reversal was limited to the cluster region, and the sequence outside the cluster remained heterochromatin under all metabolic conditions (Reyes-Dominguez et al., 2010). Therefore, we hypothesized that BcLAE1 might play the role of methyltransferase, because the way LAE1 regulates secondary metabolism by chromatin modification is conducive to the easy acquisition and coordinated regulation of gene clusters.

So far, no methylation substrate of LAE1 has been found. Patananan et al. (2013) used [3H] AdoMet in *Aspergillus nidulans* to observe the automethylation of LaeA only on methionine residues, but there was more and more evidence that LAE1 was involved in histone modification. In *Penicillium oxalicum*, PoTup1 recruited methyltransferase PoLaeA to modify the chromatin structure of the upstream region of the cellulose decomposition gene, thereby promoting the binding of transcription mechanisms to activate the corresponding cellulose gene expression (Zhang et al., 2022). In *Trichoderma reesei*, LAE1 induces gene expression by changing the H3K4me3 marks (Karimi-Aghcheh et al., 2013). Therefore, we mutated the SAM domain of BcLAE1, but the yield of ABA was not significantly increased in Δ*Bclae1*-C^{SAM} transformant compared with the Δ*Bclae1* transformant, suggesting that the SAM domain of BcLAE1 was very important to its function. In subsequent WB validation experiments, the deletion of *Bclae1* increased the level of H3K9me3 modification and decreased the level of H3K4me2 modification, confirming that BcLAE1 is involved in chromatin landscape regulation. Meantime, the histone modification marks did not change significantly in the *Bclae1*-OE-X4 transformant. The level of H3K4me2 was recovered in Δ*Bclae1*-C transformant, while the level of H3K9me3 modification did not change significantly.

At the same time, we observed differences in growth, morphology, and reproductive development of different *Bclae1* transformants. With the reduced expression of melanin key synthetic genes, the mycelium of the Δ*Bclae1* transformant appeared white compared with that of TB-31. Analysis of related pigment genes revealed increased transcriptional level of the putative UV-light-sensing cryptochrome *Bccry2* and decreased transcriptional level of the conidial positive regulator *Bcltf2*, which would result in reduced conidia, reduced melanin, and excess aerial hyphae. This coincides with the phenotypic characteristics of the Δ*Bclae1* transformant. However, RT-qPCR data showed that the expression level of *Bccry2* was not increased, indicating that Bccry2 was not the main factor causing this phenotype. Of course, studies have shown that the deletion of *Bcatf1* would also result in impaired conidial production, abnormal growth, and thick layers of aerial hyphae (Temme et al., 2012), but its expression level had not changed significantly. Meanwhile, under DD and LD photoperiods, the Δ*Bclae1* transformant lacked sclerotia formation in addition to the reduced number of conidia, so it was female sterile. The Δ*Bclae1*-C transformant not only had mycelial morphology and color close to TB-31, but also compensated for the functional defect of sclerotia formation and increased conidia production compared with the Δ*Bclae1* transformant. A recent study by Hou et al. (2020) found that H3K4me2/3 controlled the pathogenic development and virulence of *B. cinerea*, affecting spore germination, infection pad (IC) formation, appressorium formation, and stress adaptation. An interesting phenomenon is that in Δ*Bclae1* transformant, H3K4me2 modification is decreased, mycelium morphology is changed, and sporulation ability is significantly decreased. And in Δ*Bclae1*-C transformant, H3K4me2 modification was restored, the morphology of mycelium was close to TB-31, and the sporulation ability was recovered. However, the level of H3K9me3 modification was increased in the Δ*Bclae1* transformant but not significantly decreased in the Δ*Bclae1*-C transformant, and ABA production was also not fully restored.

We conjectured that ectopic complementation of BcLAE1 affected the regulation of histone modification and did not completely reverse the formation of heterochromatin, thus affecting the expression of SM clusters, which may be one of the reasons for the incomplete recovery of ABA production in Δ*Bclae1-C* transformant. As the ectopic expression of SM activators may lead to the separation of SM gene expression from the usual signaling pathway, such as the addition of an additional transcription regulator aflR outside the *A.nidulans* ST gene cluster restores ST production in Δ*laeA* transformant (Bok et al., 2006). Brahag et al. constructed multiple ectopically integrated inverters using the hypothesized activation gene *apdR*, successfully activating silenced clusters (aspyridinone) under unknown natural expression conditions (Bergmann et al., 2007). At the same time, another possibility cannot be ruled out, that the ectopic expression of *Bclae1* may affect its connection with its interaction partners, thereby interfering with the cooperative regulation of secondary metabolic networks, such as linking with BcVEL1 and BcVEL2 to form a heterotrimeric complex, or interacting with the homologous protein of the chromosome segregation protein Spc105 (Zhi et al., 2019), etc. Of course, studies have shown that ectopic *laeA* complementation in *Aspergillus fumigatus* restored NRPS gene expression levels (Perrin et al., 2007). Therefore, in view of the specificity of LAE1 protein, we will continue to explore how it regulates histone modification.

In conclusion, we found that BcLAE1 is essential for ABA biosynthesis in *B. cinerea* TB-31, and its deletion leads to the downregulation of the overall expression level of ABA synthesis gene cluster, while this aggregated regulation is widely distributed on chromosomes. In addition, BcLAE1 is involved in histone modification regulation, which affects the changes of H3K4me2 and H3K9me3 modification markers, which may also be one of the reasons affecting ABA and other secondary metabolisms synthesis. The regulatory pattern of LAE1 targeting secondary metabolic gene clusters found in this study is instructive for the subsequent mining of LAE1 targets. Our future work will compare the ABA yield of *Bclae1 in situ* complementation and ectopic complementation, and understand whether the difference of *Bclae1* insertion position has an effect on the location preference of cluster gene regulation from the point of view of chromatin modification.

Data availability statement

The data presented in the study are deposited in the Science Data Bank (Science DB) repository, accession number 10.57760/sciencedb.01984. This data can be found here: http://doi.org/10.57760/sciencedb.01984.

Author contributions

ZW designed and performed the experiments and prepared the original draft. ZW and DS designed the manuscript. ZW and D-bC analyzed the data. All authors contributed to the article and approved the submitted version.

Funding

This research received financial support from the National Natural Science Foundation of China (32070059). We acknowledge funding from the Open Research Fund of Key Laboratory of Environmental and Applied Microbiology, Chengdu Institute of Biology, Chinese Academy of Sciences (KLEAMCAS201901).

Conflict of interest

The authors declare that the research was conducted in the absence of any commercial or financial relationships that could be construed as a potential conflict of interest.

Publisher's note

All claims expressed in this article are solely those of the authors and do not necessarily represent those of their affiliated organizations, or those of the publisher, the editors and the reviewers. Any product that may be evaluated in this article, or claim that may be made by its manufacturer, is not guaranteed or endorsed by the publisher.

Supplementary material

The Supplementary material for this article can be found online at: https://www.frontiersin.org/articles/10.3389/fmicb.2022.969499/full#supplementary-material

References

Amselem, J., Cuomo, C. A., van Kan, J. A., Viaud, M., Benito, E. P., Couloux, A., et al. (2011). Genomic analysis of the necrotrophic fungal pathogens Sclerotinia sclerotiorum and Botrytis cinerea. *PLoS Genet.* 7:e1002230. doi: 10.1371/journal.pgen.1002230

Baruffini, E., Goffrini, P., Donnini, C., and Lodi, T. (2006). Galactose transport in Kluyveromyces lactis: major role of the glucose permease Hgt1. *FEMS Yeast Res.* 6, 1235–1242. doi: 10.1111/j.1567-1364.2006.00107.x

Bayram, O., and Braus, G. H. (2012). Coordination of secondary metabolism and development in fungi: the velvet family of regulatory proteins. *FEMS Microbiol. Rev.* 36, 1–24. doi: 10.1111/j.1574-6976.2011.00285.x

Bergmann, S., Schümann, J., Scherlach, K., Lange, C., Brakhage, A. A., and Hertweck, C. (2007). Genomics-driven discovery of PKS-NRPS hybrid metabolites from Aspergillus nidulans. *Nat. Chem. Biol.* 3, 213–217. doi: 10.1038/nchembio869

Bok, J. W., and Keller, N. P. (2004). LaeA, a regulator of secondary metabolism in Aspergillus spp. *Eukaryot. Cell* 3, 527–535. doi: 10.1128/ec.3.2.527-535.2004

Bok, J. W., Noordermeer, D., Kale, S. P., and Keller, N. P. (2006). Secondary metabolic gene cluster silencing in Aspergillus nidulans. *Mol. Microbiol.* 61, 1636–1645. doi: 10.1111/j.1365-2958.2006.05330.x

Camões, F., Islinger, M., Guimarães, S. C., Kilaru, S., Schuster, M., Godinho, L. F., et al. (2015). New insights into the peroxisomal protein inventory: acyl-CoA oxidases and-dehydrogenases are an ancient feature of peroxisomes. *Biochim. Biophys. Acta* 1853, 111–125. doi: 10.1016/j.bbamcr.2014.10.005

Choquer, M., Robin, G., Le Pêcheur, P., Giraud, C., Levis, C., and Viaud, M. (2008). Ku70 or Ku80 deficiencies in the fungus Botrytis cinerea facilitate targeting of genes that are hard to knock out in a wild-type context. *FEMS Microbiol. Lett.* 289, 225–232. doi: 10.1111/j.1574-6968.2008.01388.x

Cohrs, K. C., and Schumacher, J. (2017). The two Cryptochrome/Photolyase family proteins fulfill distinct roles in DNA Photorepair and regulation of Conidiation in the gray Mold fungus Botrytis cinerea. *Appl. Environ. Microbiol.* 83:17. doi: 10.1128/aem.00812-17

Cohrs, K. C., Simon, A., Viaud, M., and Schumacher, J. (2016). Light governs asexual differentiation in the grey mould fungus Botrytis cinerea *via* the putative transcription factor BcLTF2. *Environ. Microbiol.* 18, 4068–4086. doi: 10.1111/1462-2920.13431

Dagenais, T. R., Giles, S. S., Aimanianda, V., Latgé, J. P., Hull, C. M., and Keller, N. P. (2010). Aspergillus fumigatus LaeA-mediated phagocytosis is associated with a decreased hydrophobin layer. *Infect. Immun.* 78, 823–829. doi: 10.1128/iai.00980-09

Dalmais, B., Schumacher, J., Moraga, J., Pascal, L. E. P., Tudzynski, B., Collado, I. G., et al. (2011). The Botrytis cinerea phytotoxin botcinic acid requires two polyketide synthases for production and has a redundant role in virulence with botrydial. *Mol. Plant Pathol.* 12, 564–579. doi: 10.1111/j.1364-3703.2010.00692.x

Dean, R., Van Kan, J. A., Pretorius, Z. A., Hammond-Kosack, K. E., Di Pietro, A., Spanu, P. D., et al. (2012). The top 10 fungal pathogens in molecular plant pathology. *Mol. Plant Pathol.* 13, 414–430. doi: 10.1111/j.1364-3703.2011.00783.x

Dewick, P. M. (2002). The biosynthesis of C5-C25 terpenoid compounds. *Nat. Prod. Rep.* 19, 181–222. doi: 10.1039/b002685i

Ding, Z. T., Zhang, Z., Luo, D., Zhou, J. Y., Zhong, J., Yang, J., et al. (2015). Gene overexpression and RNA silencing tools for the genetic manipulation of the S-(+)-Abscisic acid producing Ascomycete Botrytis cinerea. *Int. J. Mol. Sci.* 16, 10301–10323. doi: 10.3390/ijms160510301

Ding, Z. T., Zhang, Z., Zhong, J., Luo, D., Zhou, J. Y., Yang, J., et al. (2016). Comparative transcriptome analysis between an evolved abscisic acid-overproducing mutant Botrytis cinerea TBC-A and its ancestral strain Botrytis cinerea TBC-6. *Sci. Rep.* 6:12. doi: 10.1038/srep37487

Dulermo, T., Rascle, C., Billon-Grand, G., Gout, E., Bligny, R., and Cotton, P. (2010). Novel insights into mannitol metabolism in the fungal plant pathogen Botrytis cinerea. *Biochem. J.* 427, 323–332. doi: 10.1042/bj20091813

Fillinger, S., and Elad, Y. (2016). *Botrytis – the Fungus, the Pathogen and Its Management in Agricultural Systems*. United States: Springer International Publishing.

Gong, T., Shu, D., Zhao, M., Zhong, J., Deng, H. Y., and Tan, H. (2014). Isolation of genes related to abscisic acid production in Botrytis cinerea TB-3-H8 by cDNA-AFLP. *J. Basic Microbiol.* 54, 204–214. doi: 10.1002/jobm.201200311

Guest, J. R., Angier, S. J., and Russell, G. C. (1989). Structure, expression, and protein engineering of the pyruvate dehydrogenase complex of *E. coli*. *Ann. N. Y. Acad. Sci.* 573, 76–99. doi: 10.1111/j.1749-6632.1989.tb14988.x

Hou, J., Feng, H. Q., Chang, H. W., Liu, Y., Li, G. H., Yang, S., et al. (2020). The H3K4 demethylase Jar1 orchestrates ROS production and expression of pathogenesis-related genes to facilitate Botrytis cinerea virulence. *New Phytol.* 225, 930–947. doi: 10.1111/nph.16200

Jiang, T., Wang, M., Li, L., Si, J., Song, B., Zhou, C., et al. (2016). Overexpression of the global regulator LaeA in Chaetomium globosum leads to the biosynthesis of Chaetoglobosin Z. *J. Nat. Prod.* 79, 2487–2494. doi: 10.1021/acs.jnatprod.6b00333

Kadooka, C., Nakamura, E., Mori, K., Okutsu, K., Yoshizaki, Y., Takamine, K., et al. (2020). LaeA controls citric acid production through regulation of the citrate exporter-encoding cexA gene in Aspergillus luchuensis Mut. Kawachii. *Appl. Environ. Microbiol.* 86:19. doi: 10.1128/aem.01950-19

Kale, S. P., Milde, L., Trapp, M. K., Frisvad, J. C., Keller, N. P., and Bok, J. W. (2008). Requirement of LaeA for secondary metabolism and sclerotial production in Aspergillus flavus. *Fungal Genet. Biol.* 45, 1422–1429. doi: 10.1016/j.fgb.2008.06.009

Karimi-Aghcheh, R., Bok, J. W., Phatale, P. A., Smith, K. M., Baker, S. E., Lichius, A., et al. (2013). Functional analyses of Trichoderma reesei LAE1 reveal conserved and contrasting roles of this regulator. *G three* 3, 369–378. doi: 10.1534/g3.112.005140

Kawauchi, M., Nishiura, M., and Iwashita, K. (2013). Fungus-specific sirtuin HstD coordinates secondary metabolism and development through control of LaeA. *Eukaryot. Cell* 12, 1087–1096. doi: 10.1128/ec.00003-13

Khan, I., Xie, W. L., Yu, Y. C., Sheng, H., Xu, Y., Wang, J. Q., et al. (2020). Heteroexpression of Aspergillus nidulans laeA in marine-derived Fungi triggers Upregulation of secondary metabolite biosynthetic genes. *Mar. Drugs* 18:652. doi: 10.3390/md18120652

Kim, H. K., Lee, S., Jo, S. M., McCormick, S. P., Butchko, R. A., Proctor, R. H., et al. (2013). Functional roles of FgLaeA in controlling secondary metabolism, sexual development, and virulence in Fusarium graminearum. *PLoS One* 8:e68441. doi: 10.1371/journal.pone.0068441

Kosalková, K., García-Estrada, C., Ullán, R. V., Godio, R. P., Feltrer, R., Teijeira, F., et al. (2009). The global regulator LaeA controls penicillin biosynthesis, pigmentation and sporulation, but not roquefortine C synthesis in Penicillium chrysogenum. *Biochimie* 91, 214–225. doi: 10.1016/j.biochi.2008.09.004

Lee, K., Kerner, J., and Hoppel, C. L. (2011). Mitochondrial carnitine palmitoyltransferase 1a (CPT1a) is part of an outer membrane fatty acid transfer complex. *J. Biol. Chem.* 286, 25655–25662. doi: 10.1074/jbc.M111.228692

Lee, S. S., Lee, J. H., and Lee, I. (2013). Strain improvement by overexpression of the laeA gene in Monascus pilosus for the production of monascus-fermented rice. *J. Microbiol. Biotechnol.* 23, 959–965. doi: 10.4014/jmb.1303.03026

Malmierca, M. G., Izquierdo-Bueno, I., McCormick, S. P., Cardoza, R. E., Alexander, N. J., Barua, J., et al. (2016). Trichothecenes and aspinolides produced by Trichoderma arundinaceum regulate expression of Botrytis cinerea genes involved in virulence and growth. *Environ. Microbiol.* 18, 3991–4004. doi: 10.1111/1462-2920.13410

Marumo, S., Katayama, M., Komori, E., Ozaki, Y., Natsume, M., and Kondo, S. (1982). Microbial production of Abscisic acid by Botrytis cinerea. *Agric. Biol. Chem.* 46, 1967–1968. doi: 10.1271/bbb1961.46.1967

Michielse, C. B., Becker, M., Heller, J., Moraga, J., Collado, I. G., and Tudzynski, P. (2011). The Botrytis cinerea Reg1 protein, a putative transcriptional regulator, is required for pathogenicity, conidiogenesis, and the production of secondary metabolites. *Mol. Plant-Microbe Interact.* 24, 1074–1085. doi: 10.1094/mpmi-01-11-0007

Niehaus, E. M., Rindermann, L., Janevska, S., Münsterkötter, M., Güldener, U., and Tudzynski, B. (2018). Analysis of the global regulator Lae1 uncovers a connection between Lae1 and the histone acetyltransferase HAT1 in Fusarium fujikuroi. *Appl. Microbiol. Biotechnol.* 102, 279–295. doi: 10.1007/s00253-017-8590-0

Oritani, T., and Kiyota, H. (2003). Biosynthesis and metabolism of abscisic acid and related compounds. *Nat. Prod. Rep.* 20, 414–425. doi: 10.1039/b109859b

Patananan, A. N., Palmer, J. M., Garvey, G. S., Keller, N. P., and Clarke, S. G. (2013). A novel automethylation reaction in the Aspergillus nidulans LaeA protein generates S-methylmethionine. *J. Biol. Chem.* 288, 14032–14045. doi: 10.1074/jbc.M113.465765

Perrin, R. M., Fedorova, N. D., Bok, J. W., Cramer, R. A., Wortman, J. R., Kim, H. S., et al. (2007). Transcriptional regulation of chemical diversity in Aspergillus fumigatus by LaeA. *PLoS Pathog.* 3:e50. doi: 10.1371/journal.ppat.0030050

Pinedo, C., Moraga, J., Barua, J., González-Rodríguez, V. E., Aleu, J., Durán-Patrón, R., et al. (2016). Chemically induced cryptic Sesquiterpenoids and expression of Sesquiterpene Cyclases in Botrytis cinerea revealed new Sporogenic (+)-4-Epieremophil-9-en-11-ols. *ACS Chem. Biol.* 11, 1391–1400. doi: 10.1021/acschembio.5b00931

Porquier, A., Moraga, J., Morgant, G., Dalmais, B., Simon, A., Sghyer, H., et al. (2019). Botcinic acid biosynthesis in Botrytis cinerea relies on a subtelomeric gene cluster surrounded by relics of transposons and is regulated by the Zn(2)Cys(6) transcription factor BcBoa13. *Curr. Genet.* 65, 965–980. doi: 10.1007/s00294-019-00952-4

Porquier, A., Morgant, G., Moraga, J., Dalmais, B., Luyten, I., Simon, A., et al. (2016). The botrydial biosynthetic gene cluster of Botrytis cinerea displays a bipartite genomic structure and is positively regulated by the putative Zn(II)(2) Cys(6) transcription factor BcBot6. *Fungal Genet. Biol.* 96, 33–46. doi: 10.1016/j.fgb.2016.10.003

Reboledo, G., Agorio, A., Vignale, L., Batista-García, R. A., and Ponce De León, I. (2020). Botrytis cinerea Transcriptome during the infection process of the bryophyte Physcomitrium patens and angiosperms. *J. Fungi.* 7:11. doi: 10.3390/jof7010011

Reyes-Dominguez, Y., Bok, J. W., Berger, H., Shwab, E. K., Basheer, A., Gallmetzer, A., et al. (2010). Heterochromatic marks are associated with the repression of secondary metabolism clusters in Aspergillus nidulans. *Mol. Microbiol.* 76, 1376–1386. doi: 10.1111/j.1365-2958.2010.07051.x

Rolland, S., Jobic, C., Fèvre, M., and Bruel, C. (2003). Agrobacterium-mediated transformation of Botrytis cinerea, simple purification of monokaryotic transformants and rapid conidia-based identification of the transfer-DNA host genomic DNA flanking sequences. *Curr. Genet.* 44, 164–171. doi: 10.1007/s00294-003-0438-8

Sakthivel, P., Sharma, N., Klahn, P., Gereke, M., and Bruder, D. (2016). Abscisic acid: A Phytohormone and mammalian cytokine as novel Pharmacon with potential for future development into clinical applications. *Curr. Med. Chem.* 23, 1549–1570. doi: 10.2174/0929867323666160405113129

Schmittgen, T. D., and Livak, K. J. (2008). Analyzing real-time PCR data by the comparative C(T) method. *Nat. Protoc.* 3, 1101–1108. doi: 10.1038/nprot.2008.73

Schumacher, J. (2016). DHN melanin biosynthesis in the plant pathogenic fungus Botrytis cinerea is based on two developmentally regulated key enzyme (PKS)-encoding genes. *Mol. Microbiol.* 99, 729–748. doi: 10.1111/mmi.13262

Schumacher, J., Simon, A., Cohrs, K. C., Traeger, S., Porquier, A., Dalmais, B., et al. (2015). The VELVET complex in the gray Mold fungus Botrytis cinerea: impact of BcLAE1 on differentiation, secondary metabolism, and virulence. *Mol. Plant-Microbe Interact.* 28, 659–674. doi: 10.1094/mpmi-12-14-0411-r

Shi, T. Q., Peng, H., Zeng, S. Y., Ji, R. Y., Shi, K., Huang, H., et al. (2017). Microbial production of plant hormones: opportunities and challenges. *Bioengineered* 8, 124–128. doi: 10.1080/21655979.2016.1212138

Shiba, Y., Paradise, E. M., Kirby, J., Ro, D. K., and Keasling, J. D. (2007). Engineering of the pyruvate dehydrogenase bypass in *Saccharomyces cerevisiae* for high-level production of isoprenoids. *Metab. Eng.* 9, 160–168. doi: 10.1016/j.ymben.2006.10.005

Shu, D., Tan, H., Zhou, J., Luo, D., Yang, J., Ding, Z. T., et al. (2018). New sesquiterpene cyclase BcABA3 useful for synthesizing 2Z, 4E-alpha-ionylideneehane or abscisic acid, preferably D-abscisic acid, comprises amino acid sequence. CHN Patent No CN108753744B. Beijing, China: China National Intellectual Property Administration.

Sidoli, S., Bhanu, N. V., Karch, K. R., Wang, X., and Garcia, B. A. (2016). Complete workflow for analysis of histone post-translational modifications using bottom-up mass spectrometry: From histone extraction to data analysis. *J Vis Exp.* 111:112. doi: 10.3791/54112

Simon, A., Dalmais, B., Morgant, G., and Viaud, M. (2013). Screening of a Botrytis cinerea one-hybrid library reveals a Cys2His2 transcription factor involved in the regulation of secondary metabolism gene clusters. *Fungal Genet. Biol.* 52, 9–19. doi: 10.1016/j.fgb.2013.01.006

Soukup, A. A., Chiang, Y. M., Bok, J. W., Reyes-Dominguez, Y., Oakley, B. R., Wang, C. C., et al. (2012). Overexpression of the Aspergillus nidulans histone 4 acetyltransferase EsaA increases activation of secondary metabolite production. *Mol. Microbiol.* 86, 314–330. doi: 10.1111/j.1365-2958.2012.08195.x

Steinhauf, D., Rodriguez, A., Vlachakis, D., Virgo, G., Maksimov, V., Kristell, C., et al. (2014). Silencing Motifs in the Clr2 Protein from Fission Yeast, Schizosaccharomyces pombe. *PLoS One* 9:e86948. doi: 10.1371/journal.pone.0086948

Strijbis, K., van Roermund, C. W., van den Burg, J., van den Berg, M., Hardy, G. P., Wanders, R. J., et al. (2010). Contributions of carnitine acetyltransferases to intracellular acetyl unit transport in *Candida albicans*. *J. Biol. Chem.* 285, 24335–24346. doi: 10.1074/jbc.M109.094250

Takino, J., Kozaki, T., Ozaki, T., Liu, C., Minami, A., and Oikawa, H. (2019). Elucidation of biosynthetic pathway of a plant hormone abscisic acid in phytopathogenic fungi. *Biosci. Biotechnol. Biochem.* 83, 1642–1649. doi: 10.1080/09168451.2019.1618700

Tan, H., Ge, G., Zhidong, L. I., Shulin, P., Baoliang, L., Amp, L. D., et al. (1998). High yield ABA producing strain obtained by UV irradiation of protoplasts. *Chin. J. Appl. Environmen. Biol.*

Temme, N., Oeser, B., Massaroli, M., Heller, J., Simon, A., Collado, I. G., et al. (2012). BcAtf1, a global regulator, controls various differentiation processes and phytotoxin production in Botrytis cinerea. *Mol. Plant Pathol.* 13, 704–718. doi: 10.1111/j.1364-3703.2011.00778.x

Wang, Y., Zhou, J., Zhong, J., Luo, D., Li, Z., Yang, J., et al. (2018). Cys(2)his(2) zinc finger transcription factor BcabaR1 positively regulates Abscisic acid production in Botrytis cinerea. *Appl. Environ. Microbiol.* 84:18. doi: 10.1128/aem.00920-18

Wiemann, P., Brown, D. W., Kleigrewe, K., Bok, J. W., Keller, N. P., Humpf, H. U., et al. (2010). FfVel1 and FfLae1, components of a velvet-like complex in Fusarium fujikuroi, affect differentiation, secondary metabolism and virulence. *Mol. Microbiol.* 77, 972–994. doi: 10.1111/j.1365-2958.2010.07263.x

Wu, D., Oide, S., Zhang, N., Choi, M. Y., and Turgeon, B. G. (2012). ChLae1 and ChVel1 regulate T-toxin production, virulence, oxidative stress response, and development of the maize pathogen Cochliobolus heterostrophus. *PLoS Pathog.* 8:e1002542. doi: 10.1371/journal.ppat.1002542

Yu, J. H., Hamari, Z., Han, K. H., Seo, J. A., Reyes-Domínguez, Y., and Scazzocchio, C. (2004). Double-joint PCR: a PCR-based molecular tool for gene manipulations in filamentous fungi. *Fungal Genet. Biol.* 41, 973–981. doi: 10.1016/j.fgb.2004.08.001

Yu, J., Han, H., Zhang, X. Y., Ma, C. T., Sun, C. X., Che, Q., et al. (2019). Discovery of two new Sorbicillinoids by overexpression of the global regulator LaeA in a marine-derived fungus Penicillium dipodomyis YJ-11. *Mar. Drugs* 17:12. doi: 10.3390/md17080446

Zhang, X., Hu, Y., Liu, G., Liu, M., Li, Z., Zhao, J., et al. (2022). The complex Tup1-Cyc8 bridges transcription factor ClrB and putative histone methyltransferase LaeA to activate the expression of cellulolytic genes. *Mol. Microbiol.* 117, 1002–1022. doi: 10.1111/mmi.14885

Zhi, Q. Q., He, L., Li, J. Y., Li, J., Wang, Z. L., He, G. Y., et al. (2019). The kinetochore protein Spc105, a novel interaction partner of LaeA, regulates development and secondary metabolism in Aspergillus flavus. *Front. Microbiol.* 10:1881. doi: 10.3389/fmicb.2019.01881

frontiers | Frontiers in Microbiology

TYPE Original Research
PUBLISHED 21 September 2022
DOI 10.3389/fmicb.2022.1004454

Check for updates

OPEN ACCESS

EDITED BY
Pinmei Wang,
Zhejiang University, China

REVIEWED BY
Lukasz Stepien,
Institute of Plant Genetics, Polish Academy of Sciences, Poland
Asadollah Ahmadikhah,
Shahid Beheshti University, Iran
Hojjat Asadollahpour Nanaei,
Northwest A&F University, China

*CORRESPONDENCE
Ling Wang
wangling03@caas.cn
Shaoqing Tang
tangshaoqing@caas.cn
Peisong Hu
peisonghu@126.com

†These authors have contributed equally to this work

SPECIALTY SECTION
This article was submitted to Microbial Physiology and Metabolism, a section of the journal Frontiers in Microbiology

RECEIVED 27 July 2022
ACCEPTED 26 August 2022
PUBLISHED 21 September 2022

CITATION
Wang L, Liu Q, Ge S, Liang W, Liao W, Li W, Jiao G, Wei X, Shao G, Xie L, Sheng Z, Hu S, Tang S and Hu P (2022) Genomic footprints related with adaptation and fumonisins production in *Fusarium proliferatum*. *Front. Microbiol.* 13:1004454. doi: 10.3389/fmicb.2022.1004454

COPYRIGHT
© 2022 Wang, Liu, Ge, Liang, Liao, Li, Jiao, Wei, Shao, Xie, Sheng, Hu, Tang and Hu. This is an open-access article distributed under the terms of the Creative Commons Attribution License (CC BY). The use, distribution or reproduction in other forums is permitted, provided the original author(s) and the copyright owner(s) are credited and that the original publication in this journal is cited, in accordance with accepted academic practice. No use, distribution or reproduction is permitted which does not comply with these terms.

Genomic footprints related with adaptation and fumonisins production in *Fusarium proliferatum*

Ling Wang*†, Qing Liu†, Shuailing Ge, Wenhao Liang, Weiyang Liao, Wen Li, Guiai Jiao, Xiangjin Wei, Gaoneng Shao, Lihong Xie, Zhonghua Sheng, Shikai Hu, Shaoqing Tang* and Peisong Hu*

State Key Laboratory of Rice Biology, China National Center for Rice Improvement, China National Rice Research Institute, Hangzhou, China

Fusarium proliferatum is the principal etiological agent of rice spikelet rot disease (RSRD) in China, causing yield losses and fumonisins contamination in rice. The intraspecific variability and evolution pattern of the pathogen is poorly understood. Here, we performed whole-genome resequencing of 67 *F. proliferatum* strains collected from major rice-growing regions in China. Population structure indicated that eastern population of *F. proliferatum* located in Yangtze River with the high genetic diversity and recombinant mode that was predicted as the putative center of origin. Southern population and northeast population were likely been introduced into local populations through gene flow, and genetic differentiation between them might be shaped by rice-driven domestication. A total of 121 distinct genomic loci implicated 85 candidate genes were suggestively associated with variation of fumonisin B1 (FB1) production by genome-wide association study (GWAS). We subsequently tested the function of five candidate genes (*gabap*, *chsD*, *palA*, *hxk1,* and *isw2*) mapped in our association study by FB1 quantification of deletion strains, and mutants showed the impact on FB1 production as compared to the wide-type strain. Together, this is the first study to provide insights into the evolution and adaptation in natural populations of *F. proliferatum* on rice, as well as the complex genetic architecture for fumonisins biosynthesis.

KEYWORDS

***Fusarium proliferatum*, rice spikelet rot disease, fumonisins, genome resequencing, genetic variation, genome-wide association study**

Introduction

Rice spikelet rot disease (RSRD), also called pecky rice or kernel spotting, is one of the fastest spreading diseases in China, particularly along the middle and lower reaches of the Yangtze River (Huang et al., 2011a). It was categorized as a minor disease that occurred only sporadically before 2006. After that, RSRD epidemics became more frequent and serious due to the extensive cultivation of *japonica* varieties and *indica-japonica* hybrids (Wang L. et al., 2022). *Fusarium proliferatum* (teleomorph: *Gibberella fujikuroi*) is the most predominant pathogenic fungus associated with RSRD (Huang et al., 2011b; Wang et al., 2021). Rice is highly susceptible to *F. proliferatum* during the flowering stage (Sun et al., 2019a). After spore germination, the fungal hyphae enter glumes through the anthers at the pollen-filling stage, proceed to colonize pistils and endosperms, and finally infect the whole floral tissues (Sun et al., 2019b). The initial lesions of spikelet rot symptom are reddish-brown or rust-red on rice spikelets at the flowering and milking stage, eventually become blackish-brown during the ripening stage. High precipitation, relative humidity, and warm temperature during anthesis in rice favor the development of RSRD. The percentage of diseased panicles can reach up to 80% under the severe situation of the epidemic (Li et al., 2015). To date, RSRD has been estimated to occur in one third of rice-growing regions in China, resulting in yield losses of 5–30% (Wang L. et al., 2022). How and why the disease emerged in rice is still a matter of speculation. Examination of the spatial and temporal dynamics of disease progression that is prerequisite to develop risk assessments and provide the effective management approaches.

F. proliferatum is well known for its pathogenicity to a wide range of cereals, such as wheat, rice, barley, maize, rye and oats. Moreover, the pathogen is notorious for producing multiple mycotoxins, including fumonisins, moniliformin, fusaric acid, fusarin C, and beauvericin (Studt et al., 2012). Fumonisins are associated with multiple human and animal diseases, as they are potent inhibitors of sphingolipid metabolism in eukaryotes (Braun and Wink, 2018). Fumonisins induce equine leukoencephalomalacia in horses, pulmonary edema in pigs, as well as liver and kidney toxicities in rats (Riley and Merrill, 2019). Epidemiological evidences indicated a causal relationship between high levels of fumonisins exposure and neural tube defects and esophageal cancer in human beings (Yu et al., 2021). A widespread survey of fumonisins contamination on a global scale in the post-harvest grain foods ranged from 39% in Europe to 95% in North and South America (Lee and Ryu, 2017). Fumonisins comprise a group of 28 analog, which can be separated into four main groups, fumonisin A, B, C, and P (Braun and Wink, 2018). Fumonisin B (FB) analogs include FB1, FB2, and FB3, with FB1 being the most prevalent component and usually being found at the highest levels (Kamle et al., 2019). International Agency for Research on Cancer (IARC) classified FB1 as a class 2B possible carcinogen for human (International Agency for Research on Cancer [IARC], 1993). The European Union had set maximum limits for fumonisins in food and feedstuffs intended for human consumption (European Commission [EC], 2006). In order to prevent the reproduction and contamination of *F. proliferatum* as efficiently as possible, the control methods should be implemented in dependence on the fungi growth, reproduction, infection and mycotoxins formation in the agricultural fields.

Currently, it is known that the activation of biosynthesis pathways of secondary metabolites (SMs) not only depends on pathway-specific regulators, but also on global transcriptional complexes, signal transduction regulation, and transcriptional and epigenetic manipulation (Brakhage, 2013; Keller, 2019). Fumonisins are a family of polyketide synthases (PKS) derived SMs, consisting of a linear 20-carbon aminopolyhydroxyalkyl chain backbone. The 42-kb long cluster of fumonisin biosynthetic genes (*FUM*) had been well characterized in *Fusarium verticillioides* (Brown et al., 2007; Proctor et al., 2013). *FUM* genes are usually silent or expressed at very low levels under non-inducing conditions. Several external triggers, such as nutritional input (Kim and Woloshuk, 2008), light regulation (Wiemann et al., 2010), ambient pH (Flaherty et al., 2003), and water activity (Cendoya et al., 2018), had been characterized to be involved in fumonisins production. It is therefore necessary to decipher the key molecular players regulating the biosynthesis of fumonisins, as well as the interplay between the lifestyle of toxigenic fungi and genetic constitution.

To date, no reports have been elucidated about the biology and genetics of *F. proliferatum* population from rice. In this study, we reported the genome sequences of 67 *F. proliferatum* strains collected from major rice-growing regions in China, in order to characterize its genetic diversity and population structure, and dissect the genetic determinants involved in fumonisins biosynthesis. The findings of this study provided a genome-wide perspective on the population of *F. proliferatum* and clarified their genetic relationships with fumonisins production.

Materials and methods

Fungal strains and growth conditions

The *F. proliferatum* strains were isolated from naturally infected spikelets of rice at different geographical locations in China (**Figure 1** and **Table 1**). The monoconidial culture was grown on potato dextrose agar (PDA, 20% potato extract, 2% dextrose, 1.5% agar) and minimal media [MM: 1% (w/v) carbon source, 50 ml of a 20 × salt solution (120 g/l $NaNO_3$, 10.4 g/l KCl, 30 g/l KH_2PO_4, and 10.4 g/l $MgSO_4$), and 1 ml of 5 × trace elements (22.0 g/l $ZnSO_4$, 11 g/l boric acid, 5 g/l $MnCl_2$, 5 g/l $FeSO_4$, 1.6 g/l $CoCl_2$, 1.6 g/l $CuSO_4$, 1.1 g/l $(NH_4)_2MoO_4$, and

50 g/l EDTA), pH 6.5] at 28°C. The test of the evaluation of different carbon sources included the adding to the MM of glucose, sucrose, fructose, maltose and galactose. PDA media supplemented with H_2O_2 (3 mM), sodium dodecyl sulfonate (SDS, 0.025%) and calcofluor white (CW, 50 μg/mL) were used for stress response assays. Conidia were obtained in YEPD liquid media (0.5% yeast extract, 1% peptone and 2% glucose) and stored into 20% glycerol at −80°C for long term storage. Species identification was performed based on colony morphology and PCR amplification as previously described (Mulè et al., 2004). Mating-type (MAT) idiomorph was determined by blasting the known MAT gene sequences (Steenkamp et al., 2000). The chitin content was measured by percentage of N-acetylglucosamine (GlcNAc) relative to the dry mycelial weight (Kong et al., 2012).

Determination of fumonisin B1 production and fungal biomass

To investigate FB1 content, *F. proliferatum* strains were inoculated on cracked rice kernels or defined liquid (DL, 10 mM glutamine, 22 mM KH_2PO_4, 2.5 mM $MgSO_4$, 85 mM NaCl, 117 mM sucrose, pH 5.9) media as described with some modification (Shim and Woloshuk, 1999). FB1 production was quantified by high-performance liquid chromatography–tandem mass spectrometry (HPLC–MS/MS) (Li et al., 2012). Briefly, samples were extracted with acetonitrile: water (1:1, v/v) and separated on HPLC (Thermo Fisher Scientific Waltham, MA, United States) equipped with Zorbax Extend-C18 column (100 mm × 2.1 mm, 3.5 μm). Methanol–water–formic acid (75:25:0.2, v/v/v) was used as the mobile phases at flow rate of 0.2 mL/min. The settings were used for MS/MS detection equipped with electrospray ionization (ESI) mode as follows: capillary voltage, 3,500 V; source temperature, 120°C; desolvation temperature, 350°C; and flow rate of desolvation gas, 600 L/h. Ergosterol content was measured as quantitative assessment of fungal growth with HPLC as described previously (Kim and Woloshuk, 2008). Samples were extracted overnight in chloroform: methanol (2:1, v/v). After centrifugation, the supernatants were filtered and injected into HPLC system with Eclipse XDB-C18 column (4.6 mm × 250 mm, 5 μm) and UV detector (Agilent Technologies, Inc., Santa Clara, CA, United States) set to monitor at 282 nm using 100% methanol as the mobile phases at a flow rate of 1.0 mL/min. Finally, FB1 content per fungal biomass was evaluated by the ratio of FB1 production and ergosterol content.

Genome resequencing and variant calling

Genomic DNA of *F. proliferatum* was extracted from the mycelium using DNeasy Plant Mini Kit (Qiagen, Hilden, Germany) following the manufacturer's instructions. Paired-end (PE) libraries with insert fragment around 350 bp were constructed and sequenced by Illumina Hiseq4000 platform. Library construction and sequencing were performed at the Beijing Novogene Bioinformatics Technology Co., Ltd., Beijing, China. Raw sequences were pre-processed by the removal of sequencing adapters and low-quality reads by Fastq-mcf with default parameters. Filtered sequencing reads were aligned to the reference genome of *F. proliferatum* strain Fp9 (GenBank accession no. WKFO00000000) using BWA v0.7.8 (Li and Durbin, 2010), and *de novo* genome assembly of the reference strain was previously performed (Wang L. et al., 2022). Spurious reads were filtered with SAMtools v0.1.19 (Li, 2011). Local realignment, duplicate marking and base quality recalibration were further processed using Picard v1.88.[1] Variant calling for single nucleotide polymorphism (SNPs) and insertions and deletions (Indels) were calculated and identified by GATK v3.6.0 (McKenna et al., 2010) with default parameters. HaplotypeCaller and GenotypeGVCFs, followed by hard filtering with VariantFiltration (generic filter recommendations of GATK plus DP > 200.0, DP < 10.0). All the SNPs retrieved from sequencing reads were mapped to the reference genomes and functionally annotated with SnpEff program (Cingolani et al., 2012).

The genes of *F. proliferatum* strain Fp9 were originally identified through homology searches of *F. proliferatum* strain ET1 sequence (GenBank accession no. FJOF00000000). The SNPs were categorized as occurring in exonic regions (overlapping with a coding exon), intronic regions (overlapping with an intron), splicing sites (within 2 bp of a splicing junction) or intergenic regions. Based on the putative effects of SNPs, the genes were classified as follows, "non-functional genes" with loss of the function, "modified genes" with change of one or few amino acid sequences without major disruption of protein function, "conserved genes" with only change of nucleotide but no change of amino composition, and "highly conserved genes" with no variant in nucleotide sequence. Multigene families were chosen to analyze variants of SNPs. Among them, putative carbohydrate-active enzymes (CAZymes) were identified and classified with the CAZyme database.[2] Cytochrome P450 monooxygenases (CYPs) were predicted with the fungal cytochrome P450 database.[3] The homologs of known pathogen-host interaction (PHI-base) genes were predicted using the PHI database.[4] Secreted proteins with N-terminal signal peptides were predicted by SignalP 5.0 (Almagro et al., 2019). Membrane transporters were predicted by Phobius[5] and TMHMM (Krogh et al., 2001), and

1 https://github.com/broadinstitute/picard
2 http://www.cazy.org/
3 http://drnelson.uthsc.edu/cytochromeP450.html
4 http://www.phi-base.org/
5 https://phobius.sbc.su.se/

FIGURE 1
Map of China showing the location (dots) where *Fusarium proliferatum* strains were collected.

classified based on the fungal transcription factor database.[6] The annotation of biosynthesis genes of secondary-metabolite (SM) were performed using antiSMURF 4.0 with the Hidden Markov Model (Blin et al., 2017).

Phylogenetic analysis and population structure

Differences of pairwise SNPs were used to calculate the genetic distances among strains of *F. proliferatum*. The phylogenetic tree was constructed by neighbor-joining method using MEGA 7.0 program (Kumar et al., 2016) based on the genetic differences of strains with 1,000 bootstrap replicates. According to the geographical origin of the strains, three groups including nine strains (G7, X4, X7, X8, V4, V6, V8, V10, and S1Fv), ten strains (A1, A2, A3, E3, E7, N4, N5, J8, J10, and S8Fp) and six strains (C10, K5, U7, S3, S5, and S9) were defined as northeast population, eastern population, and southern population, respectively. Nucleotide diversity (π) within populations, as well as genetic differentiation (fixation index, F_{ST}) and gene flow (Nm) between populations were calculated by VCFtools v.0.1.14 (Danecek et al., 2011) with a 50-kb slide window. Population structure was performed using STRUCTURE v.2.3.4 (Pritchard et al., 2000) with the admixture model for the most likely number of clusters (K) ranging from 2 to 5. The length of burn-in period and the number of Monte Carlo Markov Chain (MCMC) replications after burn-in were set to 50,000 and 100,000, respectively.

Genome-wide association study

FB1 production of *F. proliferatum* strains were used as a phenotype for the association analysis. The genome-wide association study (GWAS) was performed by linear regression analysis using PLINK v1.90 (Purcell et al., 2007) with the following parameters: minor allele frequency (>0.05), proportion of missing genotypes (<0.05) and the Hardy-Weinberg equilibrium ($> 1e^{-5}$). *P*-value of each site was estimated and graphically displayed using Haploview v3.2 (Barrett et al., 2005). Raw *p*-values were adjusted for multiple testing with Benjamini-Hochberg correction to control false discovery rate. Sequences for predicted genes at associated loci were retrieved from the reference genome of *F. proliferatum*. Genes with *Q*-value (adjusted *p*-value < 0.05) as cut-off were considered for significance. The regional plots were generated

6 http://ftfd.snu.ac.kr/

TABLE 1 Fumonisin FB1 production and variant calling statistics of *Fusarium proliferatum*.

Strains	Geographic origin	FB1 content	MAT type	SRA ID	Reads depth (X)	Genome coverage (%)	SNPs	Indels	Exonic variants	Intronic variants	Non-genic variants	Splice site variant	Variant density (/kb)
A1	Hangzhou, Zhejiang	1.7	1–1	SRS4609098	55.7	99.68	80,361	7	46,721	4,084	28,412	1,144	2.07
A2	Hangzhou, Zhejiang	1.7	1–1	SRS4609317	58.3	99.63	80,766	2	46,492	4,145	28,991	1,138	2.08
A3	Hangzhou, Zhejiang	1.4	1–2	SRS4609316	56.4	99.59	68,620	2	39,838	3,515	24,279	988	1.77
B3	Hefei, Anhui	34.9	1–2	SRS4609184	51.9	99.57	82,013	4	47,211	4,133	29,503	1,166	2.11
B8	Hefei, Anhui	235.9	1–1	SRS4609783	61.0	99.68	93,966	3	52,177	4,824	35,635	1,330	2.42
B9	Hefei, Anhui	4034.9	1–1	SRS4610521	67.0	99.61	65,091	2	37,444	3,377	23,376	894	1.68
C10	Nanning, Guangxi	162.1	1–2	SRS4610514	58.6	99.54	127,726	13	69,651	6,654	49,604	1,817	3.29
D2	Zhengzhou, Henan	13.0	1–1	SRS4610558	51.6	99.62	110,117	8	60,030	5,762	42,736	1,589	2.84
D3	Zhengzhou, Henan	4411.0	1–2	SRS4610571	52.0	99.59	108,308	10	59,104	5,576	42,082	1,546	2.79
E3	Chongming, Shanghai	51.5	1–2	SRS4610652	54.0	99.54	37,244	2	22,217	1,957	12,516	554	0.96
E7	Chongming, Shanghai	22.2	1–2	SRS4610661	56.0	99.64	67,654	2	38,662	3,523	24,475	994	1.74
F5	Wuhan, Hubei	0.7	1–1	SRS4610679	55.7	99.63	83,632	50	37,809	4,637	40,101	1,085	2.16
G7	Shenyang, Liaoning	2185.6	1–1	SRS4614286	51.4	99.64	110,239	9	60,349	5,740	42,271	1,879	2.84
H10	Hanzhou, Shanxi	25.2	1–1	SRS4616162	67.4	99.67	95,493	7	53,246	4,866	36,017	1,364	2.46
H2	Hanzhou, Shanxi	32.6	1–1	SRS4614328	60.4	99.68	86,419	3	48,727	4,409	32,054	1,229	2.23
H3	Hanzhou, Shanxi	0.5	1–1	SRS4614441	88.5	99.64	62,395	2	36,904	3,189	21,412	890	1.61
H9	Hanzhou, Shanxi	0.5	1–1	SRS4614451	57.2	99.63	73,988	18	33,884	4,051	35,087	966	1.91
I10	Nanchang, Jiangxi	3.6	1–1	SRS4730442	50.9	99.59	67,914	2	39,671	3,488	23,797	958	1.75
I4	Nanchang, Jiangxi	0.2	1–1	SRS4619648	55.4	99.63	111,259	17	61,031	5,733	42,888	1,607	2.87
I5	Nanchang, Jiangxi	5.8	1–2	SRS4620145	55.3	99.59	66,579	1	38,833	3,381	23,443	922	1.72
J10	Fuzhou, Fujian	0.7	1–2	SRS4730550	55.9	99.65	44,342	0	27,216	2,262	14,211	653	1.14
J8	Fuzhou, Fujian	2.0	1–1	SRS4730448	53.2	99.69	109,903	15	59,785	5,709	42,832	1,577	2.83
K5	Chendou, Sichuan	2124.7	1–2	SRS4730552	52.5	99.68	110,246	9	60,196	5,710	42,802	1,538	2.84
K9	Chendou, Sichuan	3641.9	1–1	SRS4730720	54.3	99.62	97,947	6	54,838	5,061	36,635	1,413	2.53
L7	Yixing, Jiangsu	4.2	1–1	SRS4733465	55.2	99.58	80,588	38	36,898	4,446	38,185	1,059	2.08
M1	Xiangyang, Hubei	477.8	1–2	SRS4733467	57.4	99.69	39,527	0	24,975	1,990	12,008	554	1.02
M2	Xiangyang, Hubei	2.5	1–1	SRS4733602	58.9	99.63	111,342	16	60,834	5,743	43,157	1,608	2.87
M5	Xiangyang, Hubei	1.2	1–2	SRS4733641	53.9	99.71	111,362	9	62,009	5,750	42,009	1,594	2.87
M7	Xiangyang, Hubei	850.0	1–2	SRS4733714	51.9	99.72	81,808	41	37,087	4,430	39,204	1,087	2.11

(Continued)

10.3389/fmicb.2022.1004454

TABLE 1 (Continued)

Strains	Geographic origin	FB1 content	MAT type	SRA ID	Reads depth (X)	Genome coverage (%)	SNPs	Indels	Exonic variants	Intronic variants	Non-genic variants	Splice site variant	Variant density (/kb)
M9	Xiangyang, Hubei	5905.0	1–2	SRS4733719	67.8	99.62	88,648	5	50,112	4,480	32,848	1,208	2.29
N4	Taizhou, Jiangsu	19.2	1–2	SRS4733770	67.6	99.63	6,712	0	3,219	175	3,226	92	0.17
N5	Taizhou, Jiangsu	5900.3	1–1	SRS4733771	51.1	99.61	16,341	0	10,587	836	4,707	211	0.42
O4	Chaohu, Anhui	873.9	1–2	SRS4733779	54.3	99.56	59,881	1	35,220	3,087	20,735	839	1.54
O5	Chaohu, Anhui	268.4	1–2	SRS4734220	52.3	99.65	98,841	7	55,162	5,055	37,255	1,369	2.55
O7	Chaohu, Anhui	4103.6	1–2	SRS4734283	56.9	99.68	30,610	2	19,207	1,604	9,351	448	0.79
P3	Guangzhou, Guangdong	48.0	1–2	SRS4734256	59.0	99.71	80,842	38	36,395	4,360	39,013	1,074	2.09
P6	Guangzhou, Guangdong	7.0	1–1	SRS4735031	74.3	99.68	96,245	8	53,634	4,857	36,376	1,378	2.48
P7	Guangzhou, Guangdong	2.0	1–1	SRS4735067	54.5	99.66	110,521	14	60,390	5,702	42,839	1,590	2.85
R10	Tai'an, Shandong	699.8	1–1	SRS4738028	50.9	99.73	112,108	13	61,274	5,836	43,390	1,608	2.89
R7	Tai'an, Shandong	542.4	1–2	SRS4735418	53.3	99.63	111,504	13	61,557	5,779	42,598	1,570	2.88
R8	Tai'an, Shandong	6.8	1–1	SRS4735417	54.2	99.71	113,036	10	62,095	5,870	43,432	1,639	2.91
S1	Baoshan, Yunnan	2.8	1–1	SRS4738030	51.0	99.69	83,204	43	37,735	4,602	39,790	1,077	2.17
S3	Baoshan, Yunnan	3001.7	1–2	SRS4740220	65.3	99.58	107,949	13	59,683	5,547	41,207	1,512	2.78
S5	Baoshan, Yunnan	2161.2	1–2	SRS4743831	67.5	99.54	108,594	19	60,050	5,577	41,462	1,505	2.80
S9	Baoshan, Yunnan	2554.5	1–2	SRS4743887	58.7	99.59	109,702	8	60,845	5,675	41,627	1,555	2.83
T3	Yongchuan, Chongqing	0.6	1–1	SRS4748998	56.3	99.61	112,509	12	61,654	5,874	43,357	1,624	2.90
T7	Yongchuan, Chongqing	5.0	1–1	SRS4749290	71.5	99.65	101,781	5	57,462	5,180	37,700	1,439	2.62
T8	Yongchuan, Chongqing	229.3	1–2	SRS4749292	54.5	99.59	111,741	12	61,388	5,726	43,036	1,591	2.88
T9	Yongchuan, Chongqing	3.7	1–1	SRS4749298	56.6	99.67	112,645	9	61,989	5,834	43,187	1,635	2.90
U7	Kaili, Guizhou	3059.6	1–2	SRS4749303	51.1	99.68	109,952	15	60,642	5,664	42,101	1,545	2.84

(Continued)

10.3389/fmicb.2022.1004454

TABLE 1 (Continued)

Strains	Geographic origin	FB1 content	MAT type	SRA ID	Reads depth (X)	Genome coverage (%)	SNPs	Indels	Exonic variants	Intronic variants	Non-genic variants	Splice site variant	Variant density (/kb)
U8	Kaili, Guizhou	2799.4	1–1	SRS4749553	51.4	99.61	83,413	44	37,736	4,583	40,012	1,082	2.15
V10	Ha'erbing, Heilongjiang	1016.9	1–1	SRS4751061	55.3	99.66	115,168	12	62,995	6,001	44,503	1,669	2.97
V4	Ha'erbing, Heilongjiang	2.9	1–1	SRS4749363	53.9	99.73	108,827	9	60,445	5,612	41,211	1,559	2.81
V6	Ha'erbing, Heilongjiang	1.7	1–1	SRS4749565	50.9	99.59	106,965	3	59,018	5,501	40,906	1,540	2.76
V8	Ha'erbing, Heilongjiang	1.3	1–1	SRS4749564	65.0	99.62	110,936	10	60,978	5,712	42,647	1,599	2.86
W1	Jinan, Shandong	290.9	1–2	SRS4751062	60.7	99.57	11,299	0	6,298	384	4,461	156	0.29
W3	Jinan, Shandong	27.0	1–1	SRS4751209	78.1	99.62	118,235	15	64,315	6,190	46,012	1,718	3.05
W5	Jinan, Shandong	10.3	1–1	SRS4751211	68.5	99.59	85,669	60	38,748	4,733	41,082	1,106	2.21
X4	Tonghua, Jilin	1076.4	1–1	SRS4751212	55.1	99.54	112,319	14	61,668	5,828	43,197	1,626	2.90
X7	Tonghua, Jilin	3.9	1–1	SRS4751219	60.1	99.61	113,963	9	62,820	5,952	43,537	1,654	2.94
X8	Tonghua, Jilin	0.2	1–1	SRS4751488	61.3	99.58	114,379	12	62,647	5,962	44,127	1,643	2.95
S1Fp	Jingzhou, Hubei	0.4	1–1	SRS4740097	70.5	99.57	36,470	3	16,936	1,971	17,061	502	0.94
S2Fp	Xuancheng, Anhui	77.7	1–1	SRS4739228	58.2	99.61	84,499	56	38,166	4,657	40,578	1,098	2.18
S8Fp	Yongkang, Zhejiang	688.7	1–2	SRS4744290	67.8	99.54	84,324	69	38,027	4,580	40,618	1,099	2.18
S10Fp	Changsha, Hunan	6.6	1–1	SRS4748962	62.2	99.73	107,408	11	59,893	5,484	40,530	1,501	2.77
S11Fp	Nanyang, Henan	1.1	1–2	SRS4748961	66.8	99.65	52,033	3	30,502	2,717	18,107	707	1.34
S1Fv	Ha'erbing, Heilongjiang	37.4	1–1	SRS4738501	53.0	99.58	112,345	8	61,380	5,781	43,562	1,622	2.90

10.3389/fmicb.2022.1004454

using the *asplot* function in the R package "gap" (Zhao, 2007). The functional annotations were performed on the annotated genes with Trinotate pipeline (Haas et al., 2013).

Gene deletion and complementation

Deletion mutants of target genes were constructed by homologous recombination. For each gene, upstream and downstream flanking sequences were amplified with the primer pairs 5F/5R and 3F/3R, then cloned into the pFGL821 vector with hygromycin resistance cassette (*hph*). The deletion cassettes were transformed into protoplasts of wild-type strain Fp9 using the polyethylene glycol (PEG) method as previously described (Sun et al., 2019a). Positive transformants were screened with 100 μg/ml hygromycin B (Calbiochem, LaJolla, CA, United States) as selection marker, and verified using PCR with the primer pairs P1/P2 and P3/P4 to confirm gene replacement events. The single copy mutants were checked by the real-time genomic PCR analysis as described before (Wang G. et al., 2022). For complementation assays, the target gene with its full-length promoter region was amplified with primer pairs P5/P6 and co-transformed with *Xho*I-digested plasmid pDL2 into yeast strain XK1-25. The fusion constructs rescued from Trp^+ yeast transformants were confirmed by sequencing and transformed into the respective knockout mutant as described (Yin et al., 2020). Transformants of complementation were screened with 100 μg/ml geneticin (Sigma, St. Louis, MO, United States) and were identified using primer pairs P5/P6. Primers used for fragments amplification were listed in **Supplementary Table 1**.

RNA extraction and relative gene expression analysis

Total RNA was isolated from mycelia of *F. proliferatum* using Trizol reagent (Invitrogen, Carlsbad, CA, United States). RNA quantity was measured on the NanoDrop 2000 spectrophotometer (Thermo Fischer Scientific, Waltham, United States). The cDNA was carried out with the ReverTraAce qPCR RT Master Mix with gDNA Remover Kit (Toyobo, Osaka, Japan) following the manufacture's protocol. Quantitative real-time reverse transcription PCR (qRT-PCR) was performed in a volume of 20 μl containing 100 ng template cDNA, 10 μl THUNDERBIRD SYBR qPCR Mix (Toyobo, Japan), and 200 nM forward and reverse primers. Reactions were performed on ABI 7300 Real-Time System (Applied Biosystems, Foster City, CA, United States). The β-tubulin encoding gene (*TUB2*) was used as the internal control. Relative transcript level of each gene was calculated by the $2^{-\Delta\Delta Ct}$ method (Livak and Schmittgen, 2001). qRT-PCR assays were repeated with three biological replicates. Primers utilized for qRT-PCR were shown in **Supplementary Table 1**.

Virulence assay and infectious growth

To assay virulence, conidia were harvested from 5-day-old YEPD cultures and re-suspended to 3.0×10^5 conidia per ml in sterile distilled water. Rice spikelets of cultivar Xiushui 134 were inoculated with conidial suspension and examined disease symptoms as previously described (Sun et al., 2019b). Typical symptoms of spikelets were observed at 14 days post-inoculation. For assaying infectious growth, glumes of rice were collected from inoculated spikelets at 24 h post-inoculation and photographed under scanning electron microscope. All the infection assays were repeated at least three times.

Statistical analysis

The data were presented as means and standard deviations with three biological replicates. Statistical analysis was performed using Student's *t*-test implemented in the SAS software package (SAS Institute). The level of $p < 0.05$ was considered statistically significant.

Results

Genome sequencing and variation discovery

The entire collection of 67 *F. proliferatum* strains covered the regions with frequent outbreaks of RSRD (**Figure 1** and **Table 1**). To investigate the genomic variability of 67 strains, we carried out the whole-genome resequencing using Illumina platform. Sequencing data was submitted to NCBI Short Read Archive (SRA) under the BioProject PRJNA517364 (**Table 1**). Approximately 500 million PE reads of the 67 sequenced strains were aligned to the reference genome of strain Fp9. The effective mapped read depth ranged from 50- to 100-fold coverage, and the average genome coverage was 99.63%. A total of 5,908,467 SNPs and 883 Indels were observed at non-redundant polymorphic sites (**Table 1**). Out of these, 3,206,711 variants were located in exonic regions, 307,113 in intronic regions, 2,311,110 in non-genic regions, and 85,426 in splice sites. The average of SNP density was 2.3 per kb in the whole genome of *F. proliferatum*. A little more than half of the SNPs (59.45%) were located in coding domains, with the number of synonymous SNPs amounting to 114,185 vs. 53,401 of that of non-synonymous SNPs (**Supplementary Figure 1A**). Genes were classified based on functional annotation of variants, and the majority (81.8%) of

them were regarded as "modified genes" with non-synonymous effects (**Supplementary Figure 1B**). The "modified genes" were overrepresented in categories of CAZymes, CYPs, PHI-base, secreted proteins, membrane transporters and SM-encoding genes (**Supplementary Figure 2**).

Population genetic structure

Phylogenetic tree in radial pattern was constructed based on the genome-wide SNPs of *F. proliferatum* strains using the neighbor-joining method, which indicated that the strains were genetically independent of each other and not congruent with geographical distribution of the strains (**Figure 2A**). With minor exceptions, the phylogenetic relationship of strains based on genome-wide SNPs was inconsistent with the characteristics revealed by SNPs variations of *FUM* gene cluster (R = 0.007, p = 0.957) (**Figure 2B**). We investigated the genetic structure of three geographical populations. The eastern population of *F. proliferatum* exhibited the highest heterogeneity as indicated by nucleotide diversity (π = 0.213%) relative to that of southern population (π = 0.064%) and northeastern population (π = 0.047%). The eastern population showed low levels of genetic differentiation and moderate levels of gene flow against southern population (F_{ST} = 0.171, Nm = 0.962) and northeastern population (F_{ST} = 0.178, Nm = 0.908), respectively (**Table 2**). Genetic differentiation between northeastern and southern populations was fairly high (F_{ST} = 0.334) due to restricted gene flow (Nm = 0.248). Structure analysis indicated that *F. proliferatum* population was optimally partitioned with two ancestral components (equivalent to K = 2) (**Figure 3**). The genetic admixture at the individual level (K ranging from 3 to 5) revealed the significant signature of within-species introgression in recent evolutionary history. The sexual reproduction of the ascomycetes is determined by MAT loci, and an intact MAT1 locus contains one of the two idiomorphs typical for a heterothallic bipolar mating system. We observed that the frequency (59.7%) of MAT1-1 idiomorph predominated over that of MAT1-2 idiomorph within *F. proliferatum* population (**Table 1**). Two idiomorphs at the MAT1 locus were identified in the eastern and southern populations, supporting the expectation of footprints of sexual development. Conversely, only single MAT1-1 idiomorph was found in the northeastern population, showing the probability of clonal reproduction during the process of population establishment.

Genetic elements associated with fumonisins production

FB1 amounts of 67 strains of *F. proliferatum* were determined with rice kernels, ranging from 6.0 to 390,790.9 mg/kg with a mean amount of 46,187.2 mg/kg. Ergosterol was used as an indicator of the fungal biomass. There was the notable difference for relative ratios of FB1 production and ergosterol content among the strains of *F. proliferatum* (**Table 1**). GWAS was performed to investigate genetic variants associated with phenotypic variation of FB1 production. A total of 121 SNPs was found to be significantly associated with variation of FB1 content per unit of fungal biomass (**Figure 4** and **Supplementary Table 2**). The identified associations were located in 85 candidate genes, and the majority (56.5%) of them were implicated the exon regions. The top 35 candidate genes significantly associated with FB1 production were depicted in **Table 3**. Functional enrichment analysis with GO term indicated that the genic SNPs were significantly associated with oxidation-reduction processes (GO:0016705, GO:0016491), transmembrane transport (GO:0055085), carbohydrate metabolism (GO:0005975), amine metabolism (GO:0009308), lipid metabolic process (GO:0006629) and chitin biosynthetic process (GO:0006031). Subsequently, we selected five associations in coding regions of genes with FB1 production to validate their functions in the reference strain Fp9.

Examination of possible genetic elements from genome-wide association study

The γ-aminobutyric acid (GABA) shunt is a bypass of tricarboxylic acid (TCA) cycle. A strongest association (11:704266) of the gene encoding GABA permease (GABAP) was found to be involved in FB1 production (**Table 3**). Compared with wide type, the growth morphology of deletion mutant Δ*gabap* appeared unaffected in MM media (**Figure 5A**). While GABA was supplied as the sole nitrogen source rather than nitrate, the vegetative growth of the mutant Δ*gabap* was retarded as expected. The mutant Δ*gabap* produced only 34.7% as much FB1 amount as that of wild type (**Figure 5B**). The addition of glutamate, the precursor to GABA, had no impact on the growth and sporulation, but down-regulated gene expression of TCA cycle in the mutant Δ*gabap* (**Figure 5C**). The transcriptional levels of *FUM1* encoding polyketide synthase responsible for fumonisin biosynthesis and nitrogen metabolite activator *AreA* virtually declined in Δ*gabap* (**Figure 5D**).

Chitin is an essential component of cell wall in filamentous fungi. A SNP (8:1551092) located in the chitin synthase gene (*chsD*) was detected to be correlated with FB1 production (**Table 3**). Deletion of *chsD* gene led to reduction, but not significant, of FB1 production by 16.7% (**Figure 6A**). Compared to wild type, the mutant Δ*chsD* displayed a decrease of 56.7% in chitin content (**Figure 6B**) and an increase of sensitivity to cell wall stressing agents (**Figure 6C**). Moreover, pathogenicity assays showed that Δ*chsD* mutant lost virulence on rice (**Figure 6D**). Perhaps not surprisingly, *chsD* was necessary for cell wall sensitivity and pathogenicity in *F. proliferatum*.

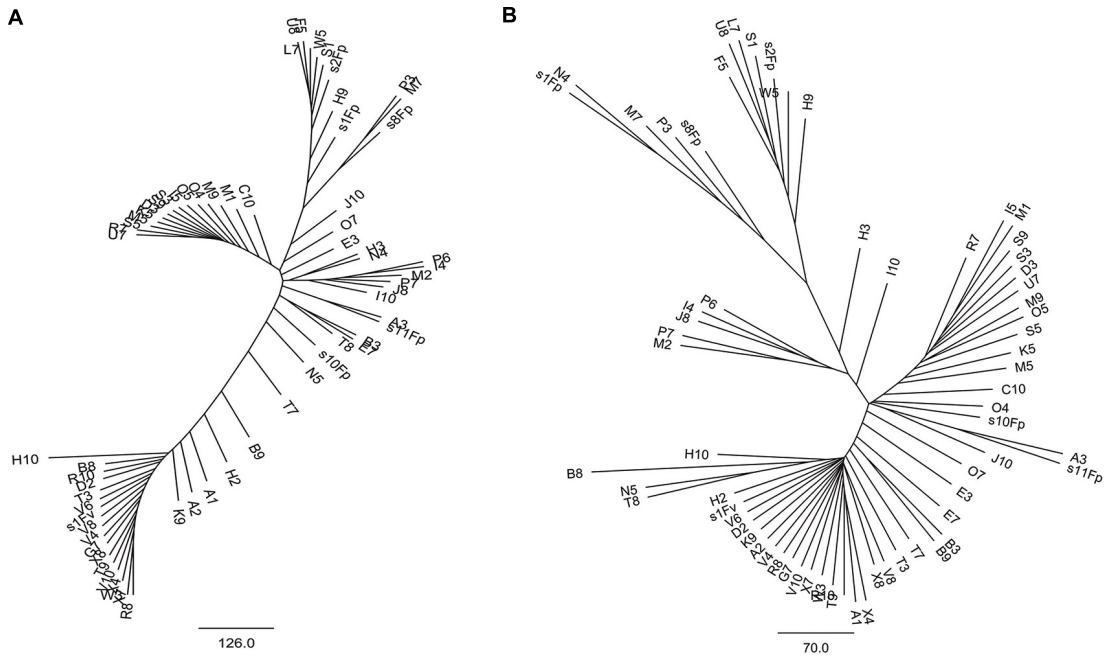

FIGURE 2
Radial neighbor-joining phylogenetic tree of genetic diversity within *Fusarium proliferatum*. **(A)** Genomic phylogeny determined based on SNP differences using whole-genome alignments of 67 strains to the reference strain Fp9. **(B)** Genomic phylogeny constructed based on SNP differences using *FUM*-cluster alignments of 67 strains to the reference strain Fp9. Branch lengths were proportional to the number of segregating sites that differentiated each pair of strains.

TABLE 2 Pairwise comparisons of gene flow (*Nm*, above diagonal) and genetic differentiation (F_{ST}, below diagonal) of *Fusarium proliferatum* populations.

	Northeast population	Eastern population	Southern population
Northeastern population		0.908	0.248
Eastern population	0.178		0.962
Southern population	0.334	0.171	

PAL signal transduction pathway is known to adapt fungi to sense and respond the changes in the external pH (Peñalva et al., 2008). The pathway relies on the endosomal sorting complex required for transport (ESCRT) complex assembled by PalA and PalB on the endosome membrane, which mediates cytoplasmic proteolysis of transcription factor PacC that activates or represses transcription of acidic- or alkaline-pH responsive genes (Lucena-Agell et al., 2015). We found an associated SNP (1:491549) that was located in the gene encoding PalA (**Table 3**). FB_1 amount of disruption mutant Δ*palA* was similar to that of wild type under acidic-inducing conditions, but drastically increased under alkaline-repressing conditions (**Figures 7A,B**). The transcriptional level of *FUM1* gene was positively correlated with FB1 accumulation (**Figure 7C**). Accordingly, we concluded that PalA might be involved in FB1 biosynthesis in pH-dependent manner.

Hexokinases (HXK) are known to be involved in carbon catabolism and glucose sensing in fungi (Santangelo, 2006). We found a significant association (6:1695154) of the gene encoding hexokinase1 (HXK1) with FB1 production (**Supplementary Table 2**). Gene disruption showed that Δ*hxk1* was unable to grow in MM media with fructose as the sole carbon source, and its morphological growth was repaired when glucose was provided (**Figure 8A**). The transcriptional levels of *FBP1* encoding fructose-1,6-biophosphatase and *ICL1* encoding isocitrate lyase in gluconeogenesis were elevated in mutant Δ*hxk1* relative to wild type, while *PFK1* encoding phosphofructokinase in the glycolytic pathway performed the reverse reaction (**Figure 8B**). The deletion of HXK1 exhibited obvious reduction in the expression of *FUM* genes and FB1 production (**Figures 8C,D**). One could simply speculate that the activity of HXK1 was more likely to be responsible for FB1 production *via* sugar metabolism.

The initiation switch (ISWI) is a subfamily of ATP-dependent chromatin remodeling complexes. It can alter

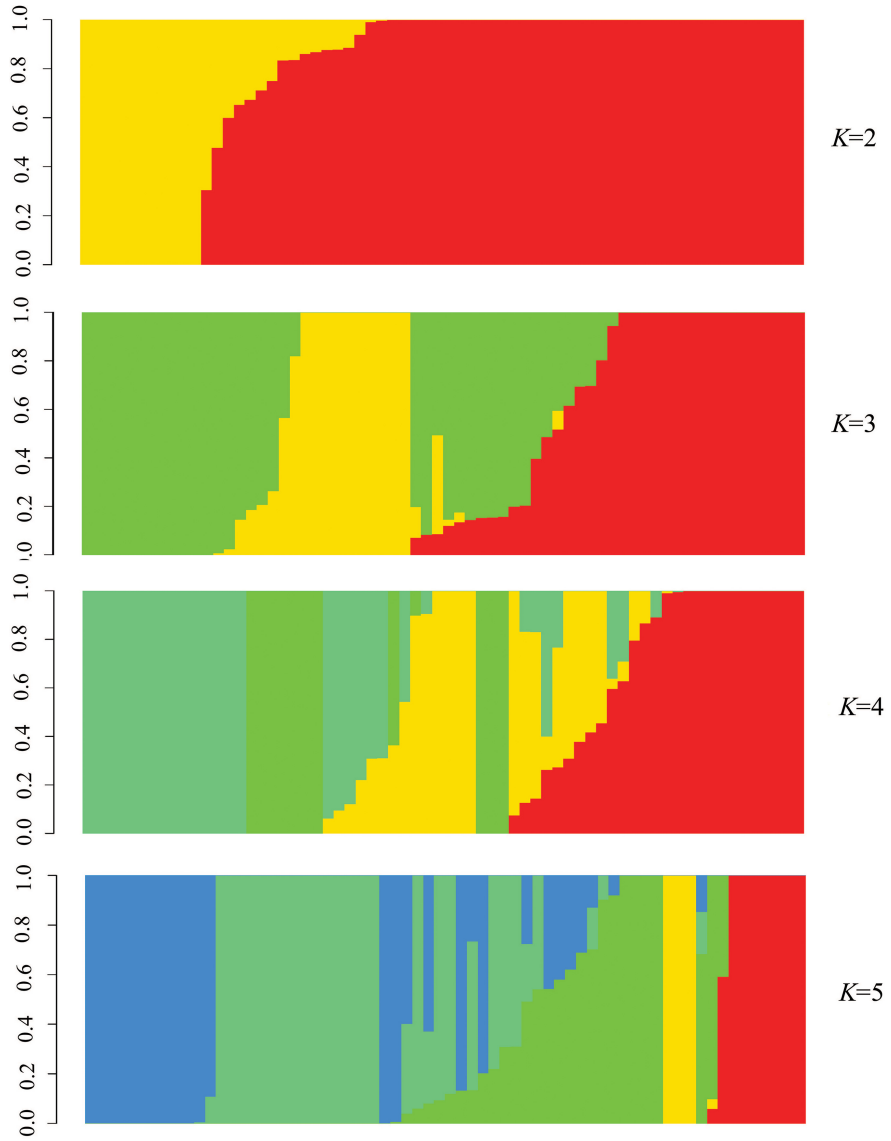

FIGURE 3
Population structure of *Fusarium proliferatum* strains. Each strain was represented by a vertical bar. Each color represented one ancestral population, and the length of each colored segment in vertical bar represented the proportion contributed by ancestral populations.

nucleosome positioning, catalyze chromatin assembly, and lead to chromosome condensation (Clapier and Cairns, 2012). Of particular interest was the serendipitous observation that a SNP (5:763640) located in the gene encoding ISWI catalytic subunit (ISW2) that was associated with FB1 production (**Table 3**). Although ISW2 was not required for hyphal growth and pathogenicity, the deletion mutant Δ*isw2* was substantially impaired in FB1 production. Unlike wild type, the lack of ISW2 exhibited down-regulation of the expression levels of SMs cluster genes responsible for fumonisins, fusarubin and bikaverin under nitrogen-starved conditions (**Figure 9A**), as well as that of the cluster genes responsible for fusarin C and fusaric acid under nitrogen-sufficient conditions (**Figure 9B**).

Discussion

In the last decade, RSRD has been one of the most widespread diseases in China, causing severe reduction in rice yield and grains contamination by producing toxic metabolites that are hazardous to humans and livestocks. More importantly, the application of fungicides was not fully operative in controlling accumulation of mycotoxins. Few technologies and approaches are available to prevent fumonisins contamination.

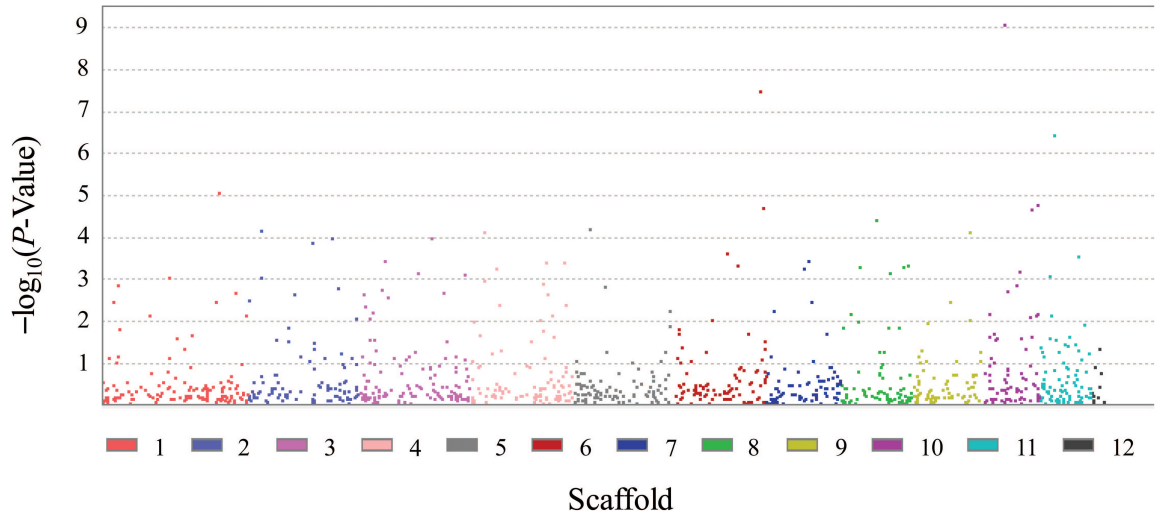

FIGURE 4
Genomic polymorphisms associated with FB1 production amongst 67 strains of *Fusarium proliferatum*.

Given its economic and public health impacts, an efficient way is to gain the perspective of population biology of *F. proliferatum* before the control is implemented. To the best of our knowledge, this was the first report of the genomic features of *F. proliferatum* population obtained from the major rice-growing region in China (**Figure 1** and **Table 1**). These findings provided new insights into its epidemiologic characteristics and evolutionary processes of this fungus. Such information could contribute to future prospects in designing disease management for RSRD.

The contemporary patterns of pathogen composition and population structure were shaped by historical evolutionary processes over time and space. However, the early history of *F. proliferatum* on cultivated rice, especially the impact of rice domestication on pathogen population, remains still unknown. Here, high level of genetic variation and recombinant mode were found in eastern population of *F. proliferatum* located in the middle and lower valley of the Yangtze River in China, where traditional varieties of *indica* and *japonica* rice were domesticated and co-cultivated with a long history. A hypothetical but straightforward scenario was that the eastern population might be the origin center from where *F. proliferatum* migrate toward the rest of regions, whereas the southern and northeastern populations were the founder populations that may undergo genetic bottlenecks or recent population introduction. There was evidence of gene flow between eastern population and southern or northeastern populations (**Table 2**), probably as a consequence of human activities like trade and transportation of *F. proliferatum*–contaminated rice seeds.

Intriguingly, southern and northeast populations of *F. proliferatum* showed geographically habitat preferences at the regional scale. Northeast population was represented in areas where *japonica* varieties were cultivated. Conversely, southern population was prevalent in regions where *indica* varieties were grown. The geographical populations of *F. proliferatum* followed the unique evolutionary trajectory, which suggested the signature of rice domestication as the major driving force for population divergence. In *Microbotryum* fungi, species-specific genes corresponded to putative adaptations responding to host-mediated selection (Badouin et al., 2017). Such epidemiological implications, probably accompanied by the host specialization, exemplified that the deployment of resistance cultivars must keep up with co-evolutionary "arm races." By introducing the genes, such as major resistance genes and defense-responsive or defense-related genes specific for one subspecies into the other subspecies, *F. proliferatum* might confront selection pressures imposed by host resistance that it has never met before.

Sexual reproduction plays the fundamental roles in maintaining the genetic diversity and enhancing the adaptation to environments in fungi. Nonetheless, the stage of teleomorph of *F. proliferatum* has not been well described. One reason for the widespread spread of *F. proliferatum* was its ability to produce vast numbers of mitotically derived asexual spores, namely conidia. Our results supported that heterothallism was likely to occur frequently in the eastern and southern populations demonstrated by existence of two MAT idiomorphs (**Table 1**). The opposite mating types were needed for the perithecium formation of *F. proliferatum*. Epidemic of RSRD was possibly aggravated by the ability of the pathogen to spread through airborne ascospores. The phenomenon of *F. proliferatum* strains containing both MAT idiomorphs over large regions was congruent

TABLE 3 Top 35 candidate genes significantly associated with FB1 production in *Fusarium proliferatum*.

SNP ID	-log$_{10}P$	Location	Gene ontology	Annotation
10:978249	9.07	Intron	GO:0055085; GO:0022857	Nicotinamide mononucleotide permease
6:3814483	7.49	Extron	NONE	Unknown protein
11:704266	6.43	Extron	GO:0055085; GO:0022857; GO:0016020	GABA permease
1:5104401	5.08	Intron	GO:0006355; GO:0000981; GO:0008270	Unknown protein
10:2416760	4.77	Extron	GO:0000160; GO:0007165; GO:0016310; GO:0055085; GO:0000155; GO:0022857; GO:0016772; GO:0016021	Hypothetical protein
10:2185626	4.67	Intron	GO:0000160; GO:0007165; GO:0016310; GO:0055085; GO:0000155; GO:0022857; GO:0016772; GO:0016021	Hypothetical protein
8:1551092	4.43	Extron	GO:0004100; GO:0016758	Chitin synthase D
5:763640	4.20	Extron	NONE	ISWI protein
4:649480	4.13	Extron	NONE	Hypothetical protein
3:3181193	4.00	Extron	NONE	DUF domain protein
2:2827389	3.88	Extron	NONE	Hypothetical protein
6:2347812	3.63	Extron	GO:0006637; GO:0047617	Acyl-CoA thiolesterase
3:1088369	3.45	Extron	GO:0016020	Stomatin family protein
4:3363019	3.42	Extron	GO:0004497; GO:0020037; GO:0016705; GO:0005506	Cytochrome P450
6:2821397	3.33	Extron	NONE	Hypothetical protein
8:845338	3.28	Extron	NONE	Hypothetical protein
8:2772117	3.28	Extron	GO:0050660; GO:0071949; GO:0016491	6-hydroxy-d-nicotine oxidase
7:1643803	3.24	Extron	NONE	Nucleolar complex-associated protein
10:1657227	3.18	Extron	GO:0005975; GO:0055085; GO:0004553; GO:0022857	Beta-glucosidase
8:2182492	3.16	Extron	GO:0007165	Unknown protein
11:467792	3.07	Extron	NONE	Unknown protein
4:633741	2.98	Extron	GO:0003824	Enoyl-CoA hydratase
4:3219957	2.88	Extron	GO:0005515	MFS transporter
1:639420	2.85	Extron	GO:0055085; GO:0022857; GO:0016020; GO:0016021	Unknown protein
2:3915482	2.77	Extron	GO:0020037; GO:0005506; GO:0016705; GO:0004497; GO:0051536; GO:0051537; GO:0016491	Cytochrome P450
3:962262	2.76	Extron	GO:0055085; GO:0005524; GO:0140359; GO:0042626; GO:0016020; GO:0016021	ABC1 transport protein
10:1076521	2.70	Intron	GO:0005975; GO:0003824	Transaldolase B
3:3700605	2.68	Extron	GO:0003723; GO:0003676	KRR1 protein
4:3403391	2.65	Extron	NONE	Beta transducin-like protein
3:224842	2.64	Extron	GO:0016787	Unknown protein
2:35602	2.52	Extron	GO:0008652; GO:0004072	Aspartate kinase
1:491549	2.45	Extron	GO:0071985; GO:0005515	palA protein
9:1619685	2.45	Extron	GO:0006351; GO:0003677; GO:0003899; GO:0008270	DNA-directed RNA polymerase I
4:1336420	2.40	Extron	GO:0005515	Anaphase control protein
4:4196263	2.38	Extron	NONE	Unknown protein

to the previous observations of that collected from durum wheat and garlic bulb (Palacios et al., 2015; Gálvez et al., 2017). The evidences implied that there was probability that *F. proliferatum* propagate asexually by conidia and sexually by ascospores allowing both selfing and outcrossing. The strains with strong competition exhibit dominance in geographical areas, which enhanced its potentiality to respond to disease management, e.g., fungicides modes,

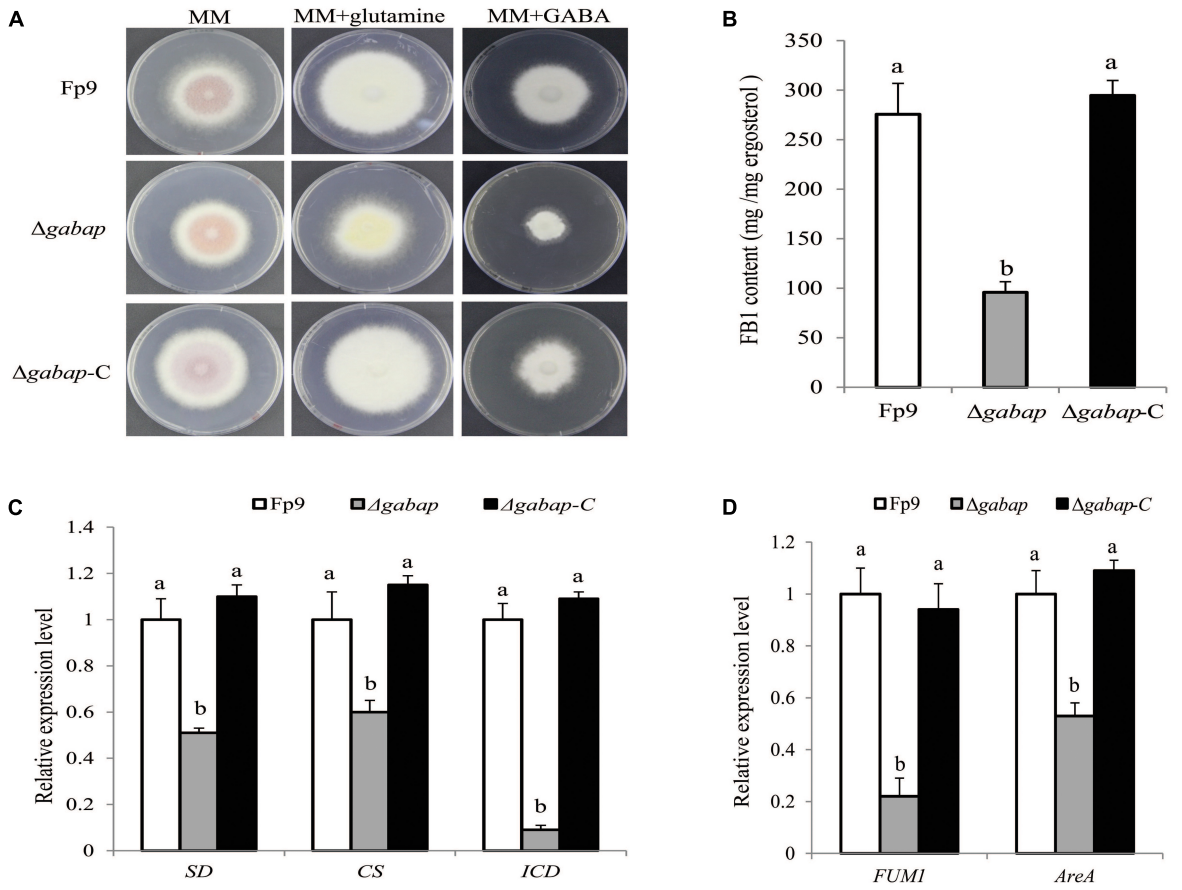

FIGURE 5
Impact of GABAP on the TCA cycle and FB1 production. **(A)** Five-day-old colony of Δ*gabap* mutant grown on minimal media (MM) containing 30 mM glutamine or GABA as the sole nitrogen source. **(B)** FB1 production of Δ*gabap* cultured with 15-day-old rice kernels. **(C)** The expression levels of *SD* encoding succinate dehydrogenase, *CS* encoding citrate synthase and *ICD* encoding isocitric dehydrogenase of Δ*gabap* grown in YEPD media for 72 h before switching to DL cultures for 3 h. Its relative expression level in wild-type strain Fp9 was arbitrarily set to 1. Different letters on bars indicated a significant difference ($p < 0.05$) with three biological replicates. **(D)** The expression levels of *FUM1* and *AreA* genes of Δ*gabap* grown in YEPD media for 72 h before switching to DL cultures for 48 h. Its relative expression level in wild-type strain Fp9 was arbitrarily set to 1.

resistant cultivars, agronomic practices, or even the climate change. In addition, a single clonal lineage of mating type MAT1-1 was detected in northeast population (**Table 1**). From the practical standpoint, the finding highlighted the need for persistent vigilance of northeast population, to prevent the invasion of MAT1-2 idiomorph that might initiate sexual component to the rice-*F. proliferatum* pathosystem.

On a broader scale, the genome-wide level of polymorphism in *F. proliferatum* was 2.3 variants per kb (**Table 1**), which was similar to that in wheat powdery mildew *Blumeria graminis* (1.4–2.0 SNPs/kb) (Wicker et al., 2013), larger than blackleg *Leptosphaeria maculans* (0.5 SNPs/kb) (Zander et al., 2013), but much lower than poplar rust *Melampsora larici-populina* (6 SNPs/kb) (Persoons et al., 2014). Naturally, plant pathogens with higher diversity have relative advantages of the ecological fitness. Combining effects of natural selection, sexual recombination and genome-wide polymorphism, *F. proliferatum* was considered as the high-adaptive pathogen with the ability to occupy ecological niches or infect broad range of hosts during fungal population expansion. In this regard, continued surveillance of pathogen will be critical for evaluation of resistant cultivars. Resistance breeding can benefit from the inclusion of representative strains of *F. proliferatum* rather than a single strain when screening resistance varieties to RSRD.

There was the remarkable difference in capability of fumonisins biosynthesis among *F. proliferatum* strains from rice (**Table 1**). Similar phenotypic differences were observed among *F. proliferatum* strains from asparagus (von Bargen et al., 2009), pineapple (Stêpieñ et al., 2013), pea (Waśkiewicz et al., 2013), and garlic (Gálvez et al., 2017). It has been proved that the regulatory networks for fungal

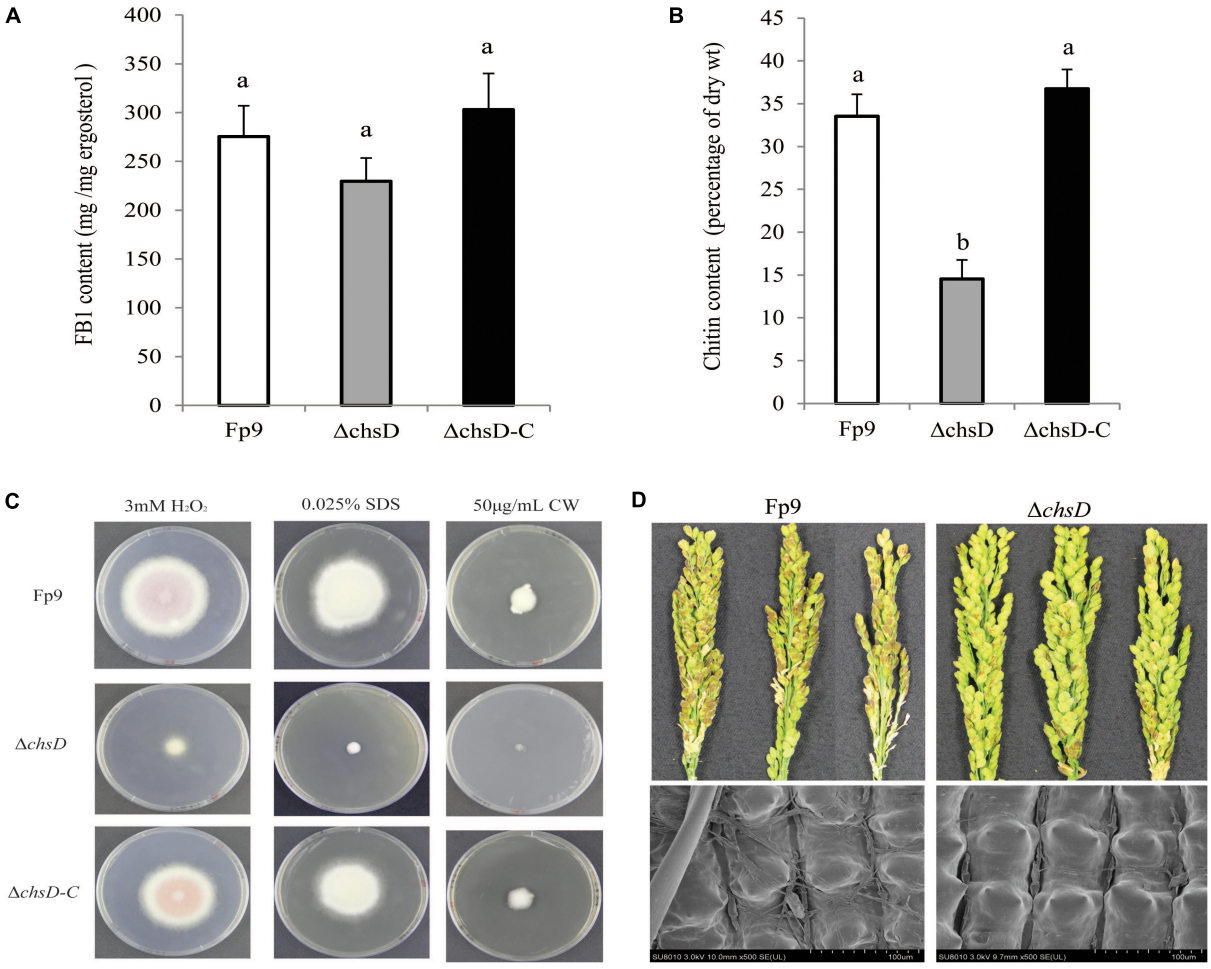

FIGURE 6
Defects of Δ*chsD* mutant in response to cell wall stress and virulence. **(A)** FB1 production of Δ*chsD* mutant cultured with 15-day-old rice kernels. **(B)** Chitin content of vegetative hyphae of Δ*chsD* harvested from 5-day-old PDA cultures. Different letters on bars indicated a significant difference ($p < 0.05$) with three biological replicates. **(C)** Sensitivity to cell wall perturbing agents of Δ*chsD* on PDA media with 3 mM H_2O_2, 0.025% SDS and 50 μg/mL calcofluor white (CW) for 5 days, respectively. **(D)** Disease severity of infected spikelets (upper) and mycelial growth on the outer surface of infected glumes (lower) inoculated with Δ*chsD* strain. Scale bars = 100 μm.

SMs are modulated by hierarchical interconnection with diverse cellular processes from cluster-specific pathways to global transcriptional complexes (Macheleidt et al., 2016). Biogenesis of fumonisins at the levels of pathway steps and their regulation remains a challenging task. There is a knowledge gap in the genetic diversity and fumonisins production capacity of *F. proliferatum*. Several attempts have been made to decipher certain interested genes located outside *FUM* gene cluster, it is not sufficient to elucidate the unexplored biomolecules responsible for fumonisins formation. This work aimed to depict the regulation factors involved in fumonisins production in *F. proliferatum* using GWAS based on whole-genome resequencing. Currently, GWAS is a preferable method for detection of the genetic determinants associated with phenotypic variation for fungal pathogens at species level, such as cold tolerance in *Clonostachys rosea* (Broberg et al., 2018), virulence in *Zymoseptoria tritici* (Hartmann et al., 2017), as well as aggressiveness, deoxynivalenol (DON) production and azole sensitivity in *Fusarium graminearum* (Talas et al., 2016). As far as we know, this is the first study to apply GWAS to link polymorphism in the genome to functional variability associated with fumonisins production among natural populations of *F. proliferatum* strains.

We identified that oxidation-reduction processes (GO:0016705, GO:0016491) were connected with fumonisins biosynthesis in *F. proliferatum* (**Table 3**). Similarly, the activation roles of cellular redox stress were previously found on aflatoxin biosynthesis in *Aspergillus flavus* (Fountain et al., 2019) and trichothecene production in *F. graminearum* (Montibus et al., 2013). The majority of oxidation, reduction

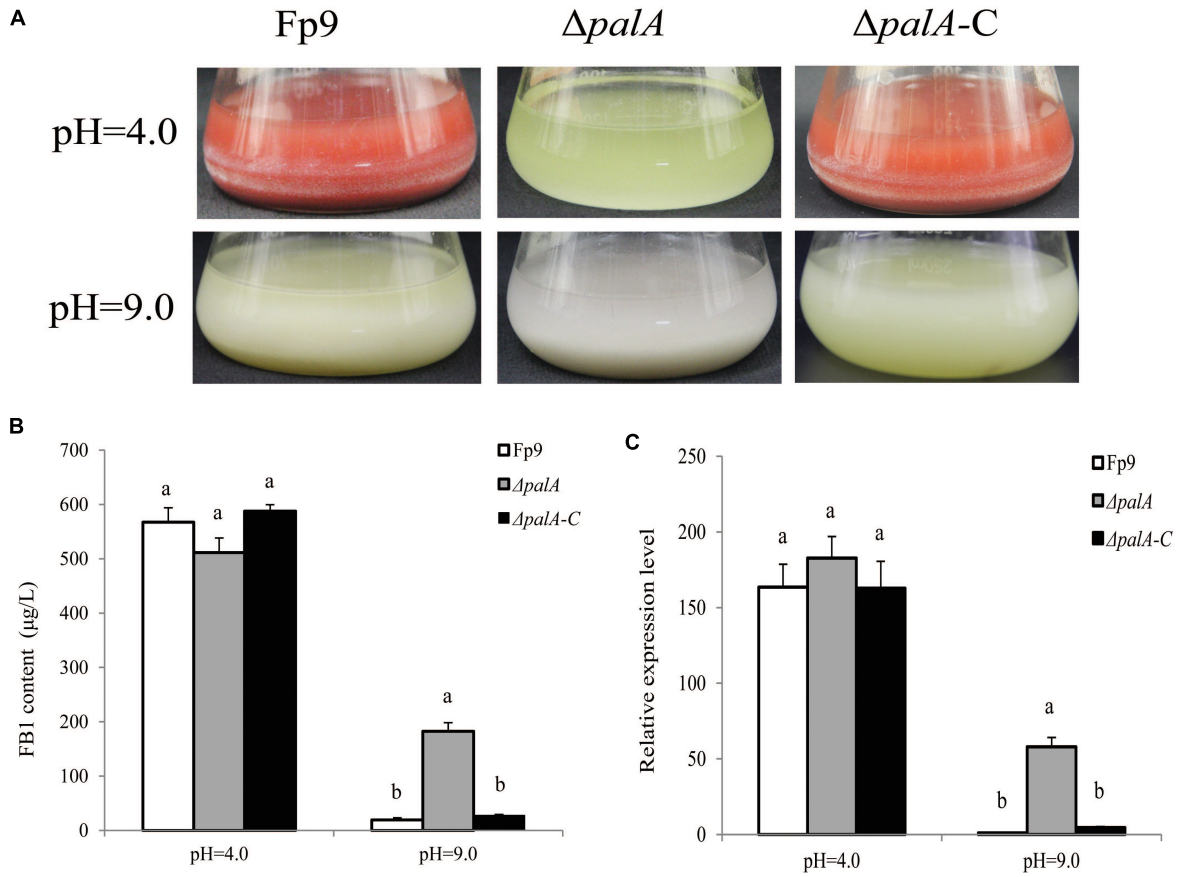

FIGURE 7
FB1 production activated by PalA in pH-dependent manner. **(A)** Seven-day-old DL cultures of Δ*palA* mutant. **(B)** FB1 production of Δ*palA* grown in YEPD media for 72 h before switching to DL cultures for 7 days at pH = 4.0 and pH = 9.0, respectively. Different letters on bars indicated a significant difference ($p < 0.05$) with three biological replicates. **(C)** The expression levels of *FUM1* gene of Δ*palA* grown in YEPD media for 72 h before switching to DL cultures for 48 h at pH = 4.0 and pH = 9.0, respectively.

and hydrolysis reactions are performed by CYPs. CYPs enzymes have unique ability to catalyze regio-, chemo-, and stereospecific conversions of lipophilic compounds to hydrophilic derivatives by introducing an oxygen atom. Three members from CYPs (FPRO_06718, FPRO_05147, FPRO_05649) were identified to be related with fumonisins production (**Supplementary Table 2**). Several CYPs participating in SMs biosynthesis pathways had been characterized in other fungi. Among 26 genes located in aflatoxin biosynthesis gene cluster, *aflG*, *aflQ*, *aflU,* and *aflV* encoded CYPs in *A. flavus* (Yu et al., 2004). In *F. graminearum*, three CYPs (*TRI1*, *TRI4,* and *TRI11*) were responsible for trichothecene biosynthesis, and three CYPs encoded ergosterol biosynthetic enzymes (Shin et al., 2017). In *Verticillium dahliae*, *VdCYP1* had a pronounced effect on 14 kinds of fungal metabolites that likely contributed to pathogenic process (Zhang D. D. et al., 2016). Therefore, it was conceivable that the catalytic regulation of fungal CYPs was essential for cell viability and secondary metabolism.

Transmembrane transport (GO:0055085) was found to be involved in fumonisins production (**Table 3**). Transporters are responsible for nutrient uptake, metabolite extrusion, multidrug resistance and signal exchange. ATP-binding cassette (ABC) transporters are a superfamily of proteins that use the energy from ATP hydrolysis to transport substances across the cell membrane. Our results showed that fumonisins production was affected by an ABC transport (FPRO_03446) (**Supplementary Table 2**). This seemed to be the case for *Bacillus cereus* as well because ABC transporters were involved in the biosynthesis of metabolites, such as toxins, antibiotics and siderophores (Gacek-Matthews et al., 2020), but the underlying mechanisms remain unclear. Peptide transporters belonging to the major facilitator superfamily (MFS) transporters use the proton-motive force to translocate di- and tripeptides. Internalized peptides are rapidly hydrolyzed and the resulting amino acids are used for protein synthesis or alternative sources of nitrogen and carbon. We found that a peptide transporter (FPRO_13944) was associated

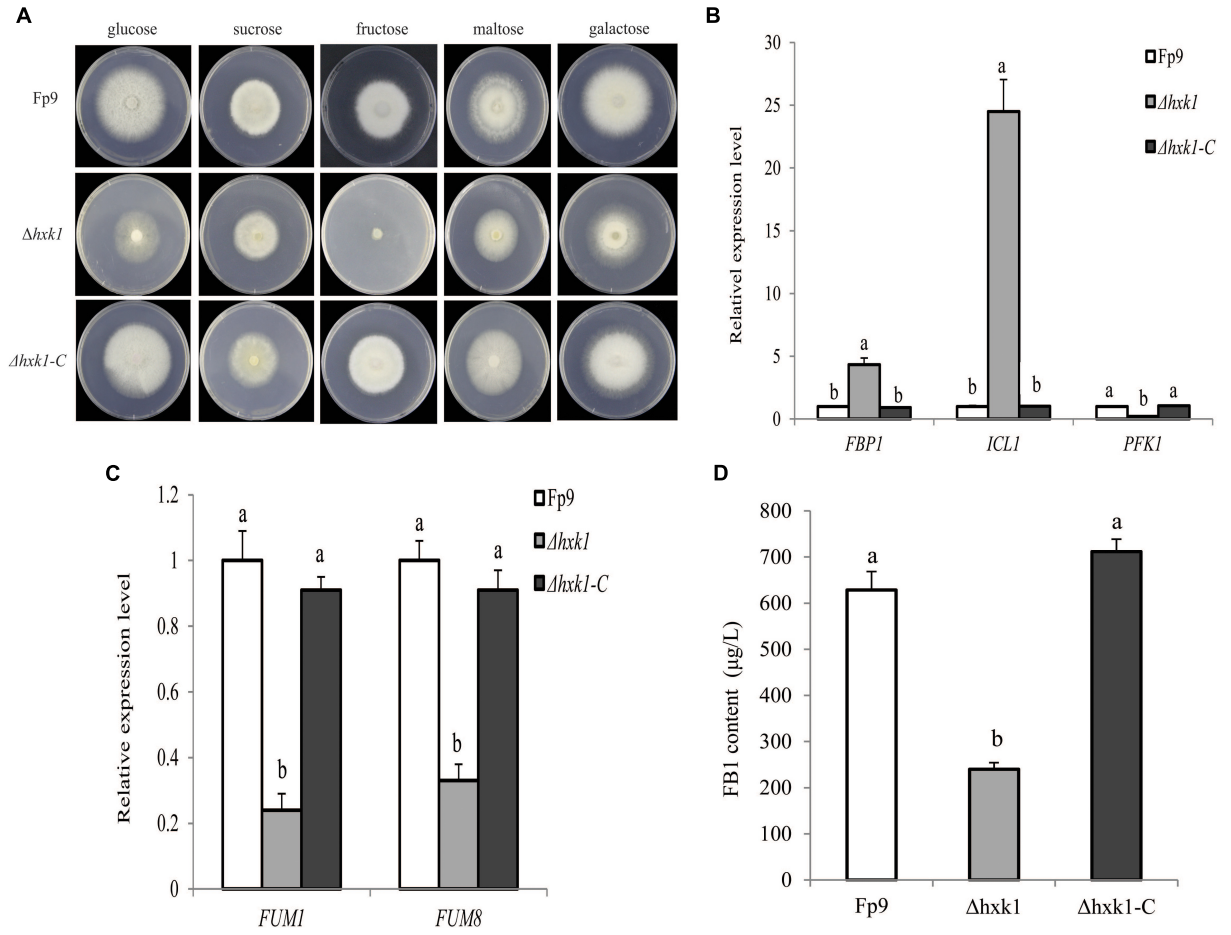

FIGURE 8
Defects of Δ*hxk1* mutant in fructose assimilation and FB1 production. **(A)** Five-day-old colonies of Δ*hxk1* mutant grown on minimal media (MM) containing glucose, sucrose, fructose, maltose and galactose as the sole carbon source at 55 mM concentration, respectively. **(B)** The expression levels of *FBP1* encoding fructose-1,6-biophosphatas, *ICL1* encoding isocitrate lyase and *PFK1* encoding phosphofructokinase of Δ*hxk1* grown in YEPD media for 72 h before switching to DL cultures for 3 h. Its relative expression level in wild-type strain Fp9 was arbitrarily set to 1. Different letters on bars indicated a significant difference ($p < 0.05$) with three biological replicates. **(C)** The expression levels of *FUM1* and *FUM8* encoding aminotransferase of Δ*hxk1* grown in YEPD media for 72 h before switching to DL cultures for 48 h, respectively. Its relative expression level in wild-type strain Fp9 was arbitrarily set to 1. **(D)** FB1 production of Δ*hxk1* grown in YEPD media for 72 h before switching to DL cultures for 7 days.

with fumonisins biosynthesis (**Supplementary Table 2**). In *F. graminearum*, deletion of peptide transporters (FgPTR2A, FgPTR2C, and FgPTR2D) resulted in a sharp increase in DON and zearalenone and a decrease in fusarielin H. The three mycotoxins fell under the regulation of nitrogen regulator AreA because that the transportation activity of peptide transporters was influenced by the quality of the nitrogen source (Droce et al., 2017). Further studies are required to understand the exact nature of how the peptide transporters modulate the genetic regulatory network underlying the SM biosynthesis.

Carbohydrate metabolic process (GO:0005975) was shown the association with fumonisins production in *F. proliferatum* (**Table 3**). The sources of carbon available were reported to play a critical role in induction of SM biosynthesis, such as fumonisins biosynthesis in *F. verticillioides* (Malapi-Wight et al., 2013), aflatoxin production in *A. flavus* (Fasoyin et al., 2018), ochratoxin A biosynthesis in *Aspergillus ochraceus* (Wang et al., 2020). Glucose is the preferred carbon source for the filamentous fungi. Several genes encoding enzymes (e.g., xylanases, cellulases, and arabinases) required for the use of alternative carbon sources, such as lignocellulose, are repressed by carbon catabolite repression (CCR) when glucose is present. From the GWAS, three significant SNPs were located in genes encoding β-glucosidase (FPRO_14041, FPRO_03671, FPRO_15192) (**Supplementary Table 2**). β-glucosidase mainly hydrolyze β-glucosidic bonds to release glucose from the non-reducing end of β-glucoologosaccharides or glucosides. This effect was mediated in part by sucrose non-fermenting (SNF1) kinase that was regarded as

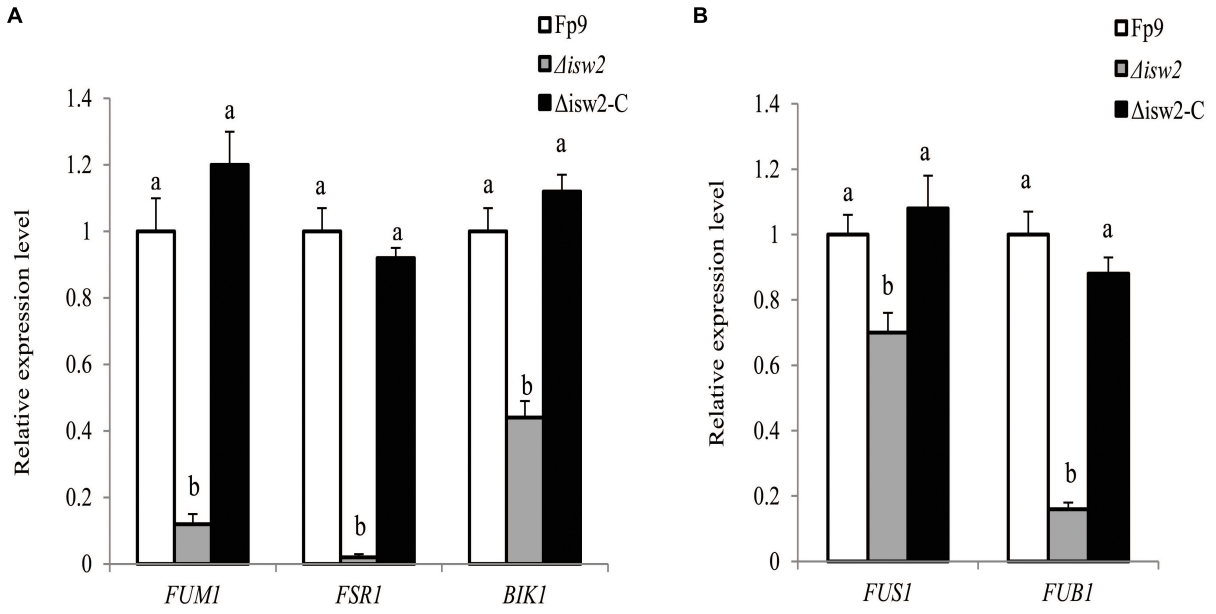

FIGURE 9
ISW2 affected the expression of SM biosynthetic gene clusters. **(A)** Expression of *FUM1* encoding fumonisin cluster-polyketide synthase, *FSR1* encoding fusarubin cluster-polyketide synthase, and *BIK1* encoding bikaverin cluster-polyketide synthase of Δ*isw2* mutant grown in YEPD media for 72 h before switching to DL cultures for 48 h with 6 mM glutamine as the sole nitrogen source. Its relative expression level in wild-type strain Fp9 was arbitrarily set to 1. Different letters on bars indicated a significant difference ($p < 0.05$) with three biological replicates. **(B)** Expression of *FUS1* encoding fusarin C cluster-polyketide synthase, *FUB1* encoding fusaric acid cluster-polyketide synthase of Δ*isw2* grown in YEPD media for 72 h before switching to DL cultures for 48 h with 60 mM glutamine as the sole nitrogen source. Its relative expression level in wild-type strain Fp9 was arbitrarily set to 1.

an important regulator in cellulose degradation and sterigmatocystin biosynthesis in *Podospora anserina* (Li et al., 2020). Several fungal and bacterial β-glucosidases had the abilities to hydrolyze the *Fusarium* mycotoxins, such as DON, nivalenol and HT-2 toxin (Michlmayr et al., 2015). Thus, this would be reasonable that fungi have evolved mechanisms to balance the operation of substrate feeding (enzyme production) and secondary metabolism during life cycle.

Amine metabolic process (GO:0009308) was found to exert influences on fumonisins biosynthesis (**Supplementary Table 2**). Nitrogen status directly affected the ability of filamentous fungi to biosynthesize SMs (Tudzynski, 2014). Biogenic amines are low molecular weight organic nitrogen compounds in living cells. Amine oxidases catalyze the oxidative deamination of amine substrates to their corresponding aldehydes, including aliphatic and aromatic monoamines, diamines, tertiary amines, polyamines, and amino acids. Amine oxidases were known to be involved in primary amine metabolism, but the effects of amine oxidases on SMs production is rare. Two genes encoding amine oxidase (FPRO_13752, FPRO_06592) were identified to be related to fumonisins production in *F. proliferatum* (**Supplementary Table 2**). Amine oxidases of *Aspergillus niger* and *Cochliobolus victoriae* were capable of enzymatic conversion of fumonisins and victorin into deaminated and detoxified counterparts, respectively (Garnham et al., 2020; Kessler et al., 2020), which demonstrated relaxed substrate specificity of amine oxidases in mycotoxins biosynthesis.

The *gabap* gene encoding GABA permease was found to be significantly associated with FB1 production (**Figure 5B**). The *gabap* mutant failed to synthesize FB1 and inactivated the expression of *FUM1* gene responsible for fumonisin biosynthesis. There were several indications for the connectivity between GABA shunt and the regulation of FB1 production. GABA metabolism had been previously described to link MFS transporters that pumped out DON mycotoxin in *F. graminearum* (Wang et al., 2018). The addition of GABA-inducible agmatine promoted the production of starting substrate for DON biosynthesis in *Fusarium asiaticum* (Suzuki et al., 2013). Deletion of *gabap* impaired GABA utilization in *F. proliferatum*, which was partially regulated by the global nitrogen regulator AreA. The mutant Δ*gabap* showed downregulation of the key enzymes of the TCA cycle. Thus, we proposed that GABA as a nitrogen source positively regulated FB1 accumulation in *F. proliferatum*.

We identified a correlation between *chsD* gene encoding chitin synthase and FB1 production (**Figure 6A**). Disruption of

chsD resulted in reduced accumulation of chitin and enhanced sensitivity against cell wall perturbing agents. In addition, our study found that chitin synthase played an important role in pathogenicity in *F. proliferatum* as previous studies on *Magnaporthe oryzae* (Kong et al., 2012) and *Botrytis cinerea* (Cui et al., 2013). The reduced FB1 production in the Δ*chsD* deletion mutant further verified the involvement of chitin synthase in aggressiveness since FB1 played an important role in the infection of *F. proliferatum* in rice tissue (Sun et al., 2019a). The effect of *chsD* gene on FB1 production in *F. proliferatum* was similar to that on DON production in *F. graminearum* (Liu et al., 2016). Our results demonstrated that essentiality of chitin biosynthesis in vegetative growth, virulence and FB1 production in *F. proliferatum*, which allow the development of novel inhibitory agents in the control of this pathogen by targeting the chitin synthase.

Fungal microorganisms must be able to sense and respond to ambient pH for mycelial growth, host colonization and toxin production. The ambient pH signaling pathway in filamentous fungi was medicated by six Pal proteins (PalA, PalB, PalC, PalF, PalH, and PalI) and transcription factor PacC (Peñalva et al., 2008). It was clear from previous studies that PacC was a key factor for biosynthesis of various SMs, such as ochratoxin A in *A. ochraceus* (Barda et al., 2020), fumonisins in *F. verticillioides* (Flaherty et al., 2003), dipicolinic acid in *Beauveria bassiana* (Luo et al., 2017), patulin in *Penicillium expansum* (Chen et al., 2018). The activation of PacC by proteolysis required interactions of with PalA and PalB in an alkaline pH dependent manner. In the present study, the *palA* gene was involved in the association of FB1 production (**Figure 7B**). Genetic disruption of *palA* rendered enhanced FB1 accumulation under external pH alkalinization in *F. proliferatum*. To further characterize the mechanism of the environmental pH-sensing complex on fumonisins, studies are underway to dissect this intriguing phenomenon.

Our findings suggested a relationship between *hxk1* gene encoding hexokinase and FB1 biosynthesis in *F. proliferatum* (**Figure 8D**). The deletion mutant of *hxk1* failed to grow on fructose and down-regulated the expression level of glycolytic genes. More importantly, Δ*hxk1* produced a dramatically low level of FB1, indicating that *hxk1* was involved in FB1 biosynthesis in *F. proliferatum*. Pyruvate, the end-product of glycolysis, was controlled by hexokinase as the main substrate of acetyl-CoA for the biosynthesis of many SMs (Gao et al., 2016), including fumonisins, aflatoxin, trichothecene, DON, and penicillin. HXK1 had been shown to regulate DON production in *F. graminearum* (Zhang L. et al., 2016) and FB1 production in *F. verticillioides* (Kim et al., 2011). Our observations demonstrated that HXK1 was required for FB1 biosynthesis by establishing genetic link between primary and secondary metabolism in *F. proliferatum*.

ISWI catalytic subunit (ISW2) belonging to a subfamily of chromatin remodeling complexes was associated with FB1 production (**Figure 9A**). Perhaps the more striking observation was that the effects of ISW2 on biosynthesis of multiple SMs were regulated by nitrogen availability in *F. proliferatum*. The concept of ISW2 triggering SMs biosynthesis in filamentous fungi was almost without precedent. The chromatin remodeling complex RSC1 had been well characterized in *Saccharomyces cerevisiae*, which was required for TOR protein kinase (Yu et al., 2015). TOR signaling pathway is a central regulatory hub that connects nitrogen availability with fungal development and metabolic processes (Dobrenel et al., 2016). Therefore, it was quite likely that ISW2 played an indirect role for secondary metabolism by establishing the genetic link between nutrient-signaling regulation and SMs production.

As noted above, five candidate genes (*gabap*, *chsD*, *palA*, *hxk1,* and *isw2*) from the GWAS that were all required for FB1 production, possibly reflecting pleiotropic effects in coordinating the processes of fumonisins biosynthesis. It was very likely that, in such cases, SM production of filamentous fungi was controlled by a complex regulatory and biosynthesis pathways in a manner related to fungal development or in response to abiotic and biotic stressors. However, it was worthy to note that some associations were poorly annotated with unknown contributions to SM production. Further research should be intensified to identify and validate the physiological functions of the genetic components. The top hit from our association analysis will serve as excellent targets for genetic and biochemical efforts to detoxify or decontaminate mycotoxins of *F. proliferatum*.

Conclusion

In this study, we firstly characterized the intraspecific genomic variation of *F. proliferatum* populations from rice in China, to highlight rapid evolution shaped by high genetic diversity and sexual recombination, and elucidate selection pressures imposed by host domestication on population structure. These findings provided the evidences that the host-specific selection left signatures of genetic differentiation in *F. proliferatum* populations. Additionally, this work indicated the capability of association mapping to pinpoint genetic determinants involved in fumonisins formation in *F. proliferatum*. The regulatory factors related with secondary metabolism need to be validated for their potential functions. The sustainability of resistant cultivars and fungicides used to control RSRD should be geared toward information on the population characteristics of *F. proliferatum*, which contribute to monitor the influx of pathogen with novel adaptations, as well as discover pharmaceutical chemicals to impact positively on food safety and security.

Data availability statement

The datasets presented in this study can be found in online repositories. The names of the repository/repositories and accession number(s) can be found at: https://www.ncbi.nlm.nih.gov/bioproject/?term=PRJNA517364.

Author contributions

LW, ST, and PH contributed to the idea and design of the research. LW, GJ, XW, GS, and LX collected the strains. LW, SG, WHL, WYL, and WL conducted the experiments. QL was responsible for the whole-genome sequencing and analysis work. ZS and SH collected the data and performed statistics. LW wrote the first draft of the manuscript. ST and PH performed the revision and editing of the final manuscript. All authors contributed to revisions of the manuscript, read, and approved the submitted version.

Funding

This work was supported by the National Natural Science Foundation of China (32188102 and 31800133), the Zhejiang Provincial Natural Science Foundation of China (LQ18C140005), the Key Research and Development Program of Zhejiang Province (2021C02063, 2021C02056, and 2022C02011), the Science and Technology Major Project of Anhui Province (202203c08020006), and the Agricultural Sciences and Technologies Innovation Program of Chinese Academy of Agricultural Sciences (CAAS-ZDRW202001).

Conflict of interest

The authors declare that the research was conducted in the absence of any commercial or financial relationships that could be construed as a potential conflict of interest.

Publisher's note

All claims expressed in this article are solely those of the authors and do not necessarily represent those of their affiliated organizations, or those of the publisher, the editors and the reviewers. Any product that may be evaluated in this article, or claim that may be made by its manufacturer, is not guaranteed or endorsed by the publisher.

Supplementary material

The Supplementary Material for this article can be found online at: https://www.frontiersin.org/articles/10.3389/fmicb.2022.1004454/full#supplementary-material

References

Almagro, A. J. J., Tsirigos, K. D., Sønderby, C. K., Petersen, T. N., Winther, O., Brunak, S., et al. (2019). SignalP 5.0 improves signal peptide predictions using deep neural networks. *Nat. Biotechnol.* 37, 420–423. doi: 10.1038/s41587-019-0036-z

Badouin, H., Gladieux, P., Gouzy, J., Siguenza, S., Aguileta, G., Snirc, A., et al. (2017). Widespread selective sweeps throughout the genome of model plant pathogenic fungi and identification of effector candidates. *Mol. Ecol.* 26, 2041–2062. doi: 10.1111/mec.13976

Barda, O., Maor, U., Sadhasivam, S., Bi, Y., Zakin, V., Prusky, D., et al. (2020). The pH-responsive transcription factor PacC governs pathogenicity and ochratoxin A biosynthesis in *Aspergillus carbonarius*. *Front. Microbiol.* 11:210. doi: 10.3389/fmicb.2020.00210

Barrett, J. C., Fry, B., Maller, J., and Daly, M. J. (2005). Haploview: analysis and visualization of LD and haplotype maps. *Bioinformatics* 21, 263–265. doi: 10.1093/bioinformatics/bth457

Blin, K., Wolf, T., Chevrette, M. G., Lu, X., Schwalen, C. J., Kautsar, S. A., et al. (2017). antiSMASH 4.0—improvements in chemistry prediction and gene cluster boundary identification. *Nucleic Acids Res.* 45, W36–W41. doi: 10.1093/nar/gkx319

Brakhage, A. A. (2013). Regulation of fungal secondary metabolism. *Nat. Rev. Microbiol.* 11, 21–32. doi: 10.1038/nrmicro2916

Braun, M. S., and Wink, M. (2018). Exposure, occurrence, and chemistry of fumonisins and their cryptic derivatives. *Compr. Rev. Food Sci. Food Saf.* 17, 769–791. doi: 10.1111/1541-4337.12334

Broberg, M., Dubey, M., Sun, M. H., Ihrmark, K., Schroers, H., Li, S., et al. (2018). Out in the cold: Identification of genomic regions associated with cold tolerance in the biocontrol fungus *Clonostachys rosea* through genome-wide association mapping. *Front. Microbiol.* 9:2844. doi: 10.3389/fmicb.2018.02844

Brown, D. W., Butchko, R. A. E., Busman, M., and Proctor, R. H. (2007). The *Fusarium verticillioides FUM* gene cluster encodes a $Zn(II)_2Cys_6$ protein that affects *FUM* gene expression and fumonisin production. *Eukaryot. Cell* 6, 1210–1218. doi: 10.1128/EC.00400-06

Cendoya, E., Monge, M. D. P., Chiacchiera, S. M., Farnochi, M. C., and Ramirez, M. L. (2018). Influence of water activity and temperature on growth and fumonisin production by *Fusarium proliferatum* strains on irradiated wheat grains. *Int. J. Food Microbiol.* 266, 158–166. doi: 10.1016/j.ijfoodmicro.2017.12.001

Chen, Y., Li, B., Xu, X., Zhang, Z., and Tian, S. (2018). The pH-responsive PacC transcription factor plays pivotal roles in virulence and patulin biosynthesis in *Penicillium expansum*. *Environ. Microbiol.* 20, 4063–4078. doi: 10.1111/1462-2920.14453

Cingolani, P., Platts, A., Wang, L. L., Coon, M., Nguyen, T., Wang, L., et al. (2012). A program for annotating and predicting the effects of single nucleotide polymorphisms, SnpEff: SNPs in the genome of Drosophila melanogaster strain w1118; iso-2; iso-3. *Fly* 6, 80–92. doi: 10.4161/fly.19695

Clapier, C. R., and Cairns, B. R. (2012). Regulation of ISWI involves inhibitory modules antagonized by nucleosomal epitopes. *Nature* 492, 280–284. doi: 10.1038/nature11625

Cui, Z., Wang, Y., Lei, N., Wang, K., and Zhu, T. (2013). *Botrytis cinerea* chitin synthase BcChsVI is required for normal growth and pathogenicity. *Curr. Genet.* 59, 119–128. doi: 10.1007/s00294-013-0393-y

Danecek, P., Auton, A., Abecasis, G., Albers, C. A., Banks, E., DePristo, M. A., et al. (2011). The variant call format and VCFtools. *Bioinformatics* 27, 2156–2158. doi: 10.1093/bioinformatics/btr330

Dobrenel, T., Caldana, C., Hanson, J., Robaglia, C., Vincentz, M., Veit, B., et al. (2016). TOR Signaling and Nutrient Sensing. *Annu. Rev. Plant Biol.* 67, 261–285. doi: 10.1146/annurev-arplant-043014-114648

Droce, A., Sørensen, J. L., Sondergaard, T. E., Rasmussen, J. J., Lysøe, E., and Giese, H. (2017). PTR2 peptide transporters in *Fusarium graminearum* influence secondary metabolite production and sexual development. *Fungal Biol.* 121, 515–527. doi: 10.1016/j.funbio.2017.02.003

European Commission [EC] (2006). Commission Recommendation of 17 August 2006 on the presence of deoxynivalenol, zearalenone, ochratoxin A, T-2 and HT-2 and fumonisins in products intended for animal feeding. *Off. J. Eur. Union* 229, 7–9.

Fasoyin, O. E., Wang, B., Qiu, M., Han, X., Chung, K. R., and Wang, S. (2018). Carbon catabolite repression gene *creA* regulates morphology, aflatoxin biosynthesis and virulence in *Aspergillus flavus*. *Fungal Genet. Biol.* 115, 41–51. doi: 10.1016/j.fgb.2018.04.008

Flaherty, J. E., Pirttila, A. M., Bluhm, B. H., and Woloshuk, C. P. (2003). PAC1, a pH-regulatory gene from *Fusarium verticillioides*. *Appl. Environ. Microbiol.* 69, 5222–5227. doi: 10.1128/AEM.69.9.5222-5227.2003

Fountain, J. C., Yang, L., Pandey, M. K., Bajaj, P., Alexander, D., Chen, S., et al. (2019). Carbohydrate, glutathione, and polyamine metabolism are central to *Aspergillus flavus* oxidative stress responses over time. *BMC Microbiol.* 19:209. doi: 10.1186/s12866-019-1580-x

Gacek-Matthews, A., Chromiková, Z., Sulyok, M., Lücking, G., Barák, I., and Ehling-Schulz, M. (2020). Beyond toxin transport: novel role of ABC transporter for enzymatic machinery of cereulide NRPS assembly line. *mBio* 11:e01577-20. doi: 10.1128/mBio.01577-20

Gálvez, L., Urbaniak, M., Waśkiewicz, A., Stępień, L., and Palmero, D. (2017). *Fusarium proliferatum* - causal agent of garlic bulb rot in Spain: genetic variability and mycotoxin production. *Food Microbiol.* 67, 41–48. doi: 10.1016/j.fm.2017.05.006

Gao, T., Chen, J., and Shi, Z. (2016). *Fusarium graminearum* pyruvate dehydrogenase kinase 1 (FgPDK1) is critical for conidiation, mycelium growth, and pathogenicity. *PLoS One* 2016:e0158077. doi: 10.1371/journal.pone.0158077

Garnham, C. P., Butler, S. G., Telmer, P. G., Black, F. E., Renaud, J. B., and Sumarah, M. W. (2020). Identification and characterization of an *Aspergillus niger* amine oxidase that detoxifies intact fumonisins. *J. Agric. Food Chem.* 68, 13779–13790. doi: 10.1021/acs.jafc.0c04504

Haas, B. J., Papanicolaou, A., Yassour, M., Grabherr, M., Blood, P. D., Bowden, J., et al. (2013). De novo transcript sequence reconstruction from RNA-seq using the Trinity platform for reference generation and analysis. *Nat. Protoc.* 8, 1494–1512. doi: 10.1038/nprot.2013.084

Hartmann, F. E., Sánchez-Vallet, A., McDonald, B. A., and Croll, D. (2017). A fungal wheat pathogen evolved host specialization by extensive chromosomal rearrangements. *ISME J.* 11, 1189–1204. doi: 10.1038/ismej.2016.196

Huang, S. W., Wang, L., Liu, L. M., Tang, S. Q., Zhu, D. F., and Savary, S. (2011a). Rice spikelet rot disease in China: 2. Pathogenicity tests, assessment of the importance of the disease, and preliminary evaluation of control options. *Crop Prot.* 30, 10–17. doi: 10.1016/j.cropro.2010.06.008

Huang, S. W., Wang, L., Liu, L. M., Tang, S. Q., Zhu, D. F., and Savary, S. (2011b). Rice spikelet rot disease in China: 1. Characterization of fungi associated with the disease. *Crop Prot.* 30, 1–9. doi: 10.1016/j.cropro.2010.07.010

International Agency for Research on Cancer [IARC] (1993). *Some Naturally Occurring Substances: Food Items and Constituents, Heterocyclic Aromatic Amines And Mycotoxins, IARC Monographs on the Evaluation of Carcinogenic Risks to Humans*. Lyon: IARC, doi: 10.1016/0278-6915(89)90053-7

Kamle, M., Mahato, D. K., Devi, S., Lee, K. E., Kang, S. G., and Kumar, P. (2019). Fumonisins: impact on agriculture, food, and human health and their management strategies. *Toxins* 11:328. doi: 10.3390/toxins11060328

Keller, N. P. (2019). Fungal secondary metabolism: regulation, function and drug discovery. *Nat. Rev. Microbiol.* 17, 167–180. doi: 10.1038/s41579-018-0121-1

Kessler, S. C., Zhang, X. H., McDonald, M. C., Gilchrist, C. L. M., Lin, Z., Rightmyer, A., et al. (2020). Victorin, the host-selective cyclic peptide toxin from the oat pathogen *Cochliobolus victoriae*, is ribosomally encoded. *Proc. Natl. Acad. Sci. U.S.A.* 117, 24243–24250. doi: 10.1073/pnas.2010573117

Kim, H., Smith, J. E., Ridenour, J. B., Woloshuk, C. P., and Bluhm, B. H. (2011). HXK1 regulates carbon catabolism, sporulation, fumonisin B(1) production and pathogenesis in *Fusarium verticillioides*. *Microbiology* 157, 2658–2669. doi: 10.1099/mic.0.052506-0

Kim, H., and Woloshuk, C. P. (2008). Role of *AREA*, a regulator of nitrogen metabolism, during colonization of maize kernels and fumonisin biosynthesis in *Fusarium verticillioides*. *Fungal Genet. Biol.* 45, 947–953. doi: 10.1016/j.fgb.2008.03.007

Kong, L. A., Yang, J., Li, G. T., Qi, L. L., Zhang, Y. J., Wang, C. F., et al. (2012). Different chitin synthase genes are required for various developmental and plant infection processes in the rice blast fungus *Magnaporthe oryzae*. *PLoS Pathog.* 8:e1002526. doi: 10.1371/journal.ppat.1002526

Krogh, A., Larsson, B., von Heijne, H. G., and Sonnhammer, E. L. (2001). Predicting transmembrane protein topology with a hidden Markov model: application to complete genomes. *J. Mol. Biol.* 305, 567–580. doi: 10.1006/jmbi.2000.4315

Kumar, S., Stecher, G., and Tamura, K. (2016). MEGA7: molecular evolutionary genetics analysis version 7.0 for bigger datasets. *Mol. Biol. Evol.* 33, 1870–1874. doi: 10.1093/molbev/msw054

Lee, H. J., and Ryu, D. (2017). Worldwide occurrence of mycotoxins in cereals and cereal-derived food products: public health perspectives of their co-occurrence. *J. Agric. Food Chem.* 65, 7034–7051. doi: 10.1021/acs.jafc.6b04847

Li, C., Wu, Y. L., Yang, T., and Huang-Fu, W. G. (2012). Rapid determination of fumonisins B1 and B2 in corn by liquid chromatography-tandem mass spectrometry with ultrasonic extraction. *J. Chromatogr. Sci.* 50, 57–63. doi: 10.1093/chromsci/bmr009

Li, H. (2011). A statistical framework for SNP calling, mutation discovery, association mapping and population genetical parameter estimation from sequencing data. *Bioinformatics* 27, 2987–2993. doi: 10.1093/bioinformatics/btr509

Li, H., and Durbin, R. (2010). Fast and accurate long-read alignment with Burrows–Wheeler transform. *Bioinformatics* 26, 589–595. doi: 10.1093/bioinformatics/btp698

Li, L., Liu, L. M., Wang, G. R., Wang, A. J., Wang, L., Sun, L., et al. (2015). Research progress of spikelet rot disease and bacterial panicle blight of rice. *Chin. J. Rice Sci.* 29, 215–222. doi: 10.3969/j.issn.1001-7216.2015.02.014

Li, Y. J., Yan, P. F., Lu, X. J., Qiu, Y. L., Liang, S., Liu, G., et al. (2020). Involvement of *PaSNF1* in fungal development, sterigmatocystin biosynthesis, and lignocellulosic degradation in the filamentous fungus *Podospora anserina*. *Front. Microbiol.* 11:1038. doi: 10.3389/fmicb.2020.01038

Liu, Z. Y.,, X. P., Liu, X., Fu, C. Y., Han, X. Y., Yin, Y. N., et al. (2016). The chitin synthase FgChs2 and other FgChss co-regulate vegetative development and virulence in *F. graminearum*. *Sci. Rep.* 6:34975. doi: 10.1038/srep34975

Livak, K. J., and Schmittgen, T. D. (2001). Analysis of relative gene expression data using real-time quantitative PCR and the 2(T) (-Delta Delta C) method. *Methods* 25, 402–408. doi: 10.1006/meth.2001.1262

Lucena-Agell, D., Galindo, A., Arst, H. N. Jr., and Peñalva, M. A. (2015). *Aspergillus nidulans* ambient pH signaling does not require endocytosis. *Eukaryot. Cell* 14, 545–553. doi: 10.1128/EC.00031-15

Luo, Z., Ren, H., Mousa, J. J., Rangel, D. E., Zhang, Y., Bruner, S. D., et al. (2017). The PacC transcription factor regulates secondary metabolite production and stress response, but has only minor effects on virulence in the insect pathogenic fungus *Beauveria bassiana*. *Environ. Microbiol.* 19, 788–802. doi: 10.1111/1462-2920.13648

Macheleidt, J., Mattern, D. J., Fischer, J., Netzker, T., Weber, J., Schroeckh, V., et al. (2016). Regulation and role of fungal secondary metabolites. *Annu. Rev. Genet.* 50, 371–392. doi: 10.1146/annurev-genet-120215-035203

Malapi-Wight, M., Smith, J., Campbell, J., Bluhm, B. H., and Shim, W. B. (2013). Sda1, a Cys(2)-His(2) zinc finger transcription factor, is involved in polyol metabolism and fumonisin B-1 production in *Fusarium verticillioides*. *PLoS One* 8:e67656. doi: 10.1371/journal.pone.0067656

McKenna, A., Hanna, M., Banks, E., Sivachenko, A., Cibulskis, K., Kernytsky, A., et al. (2010). The genome analysis Toolkit: a MapReduce framework for analyzing next-generation DNA sequencing data. *Genome. Res.* 20, 1297–1303. doi: 10.1101/gr.107524.110

Michlmayr, H., Varga, E., Malachova, A., Nguyen, N. T., Lorenz, C., Haltrich, D., et al. (2015). Versatile family 3 glycoside hydrolase from bifidobacterium adolescentis hydrolyzes β-glucosides of the *Fusarium* mycotoxins deoxynivalenol, nivalenol, and HT-2 Toxin in cereal matrices. *Appl. Environ. Microbiol.* 81, 4885–4893. doi: 10.1128/AEM.01061-15

Montibus, M., Ducos, C., Bonnin-Verdal, M., Bormann, J., Ponts, N., Richard-Forget, F., et al. (2013). The bZIP transcription factor Fgap1 mediates oxidative stress response and trichothecene biosynthesis but not virulence in *Fusarium graminearum*. *PLoS One* 8:e83377. doi: 10.1371/journal.pone.0083377

Mulè, G., Susca, A., Stea, G., and Moretti, A. (2004). A species-specific PCR assay based on the calmodulin partial gene for identification of *Fusarium verticillioides*,

F. proliferatum and *F. subglutinans*. *Eur. J. Plant Pathol.* 110, 495–502. doi: 10.1023/b:ejpp.0000032389.84048.71

Palacios, S. A., Susca, A., Haidukowski, M., Stea, G., Cendoya, E., Ramírez, M. L., et al. (2015). Genetic variability and fumonisin production by *Fusarium proliferatum* isolated from durum wheat grains in Argentina. *Int. J. Food Microbiol.* 201, 35–41. doi: 10.1016/j.ijfoodmicro.2015.02.011

Peñalva, M. A., Tilburn, J., Bignell, E., and Arst, H. N. Jr. (2008). Ambient pH gene regulation in fungi: making connections. *Trends Microbiol.* 16, 291–300. doi: 10.1016/j.tim.2008.03.006

Persoons, A., Morin, E., Delaruelle, C., Payen, T., Halkett, F., Frey, P., et al. (2014). Patterns of genomic variation in the poplar rust fungus *Melampsora larici-populina* identify pathogenesis-related factors. *Front. Plant Sci.* 5:450. doi: 10.3389/fpls.2014.00450

Pritchard, J. K., Stephens, M., and Donnelly, P. (2000). Inference of population structure using multilocus genotype data. *Genetics* 155, 945–959. doi: 10.1093/genetics/155.2.945

Proctor, R. H., Hove, F. V., Susca, A., Stea, G., Busman, M., van der Lee, T., et al. (2013). Birth, death and horizontal transfer of the fumonisin biosynthetic gene cluster during the evolutionary diversification of *Fusarium*. *Mol. Microbiol.* 90, 290–306. doi: 10.1111/mmi.12362

Purcell, S., Neale, B., Todd-Brown, K., Thomas, L., Ferreira, M. A. R., Bender, D., et al. (2007). PLINK: a tool set for whole-genome association and population-based linkage analyses. *Am. J. Hum. Genet.* 81, 559–575. doi: 10.1086/519795

Riley, R. T., and Merrill, A. H. Jr. (2019). Ceramide synthase inhibition by fumonisins: a perfect storm of perturbed sphingolipid metabolism, signaling, and disease. *J. Lipid Res.* 60, 1183–1189. doi: 10.1194/jlr.S093815

Santangelo, G. M. (2006). Glucose signaling in *Saccharomyces cerevisiae*. *Microbiol. Mol. Biol. Rev.* 70, 253–282. doi: 10.1128/MMBR.70.1.253-282.2006

Shim, W. B., and Woloshuk, C. P. (1999). Nitrogen repression of fumonisin B1 biosynthesis in *Gibberella fujikuroi*. *FEMS Microbiol. Lett.* 177, 109–116. doi: 10.1111/j.1574-6968.1999.tb13720.x

Shin, J. Y., Bui, D. C., Lee, Y., Nam, H., Jung, S., Fang, M., et al. (2017). Functional characterization of cytochrome P450 monooxygenases in the cereal head blight fungus *Fusarium graminearum*. *Environ. Microbiol.* 19, 2053–2067. doi: 10.1111/1462-2920.13730

Steenkamp, E. T., Wingfield, B. D., Coutinho, T. A., Zeller, K. A., Wingfield, M. J., Marasas, W. F. O., et al. (2000). PCR-based identification of *MAT-1* and *MAT-2* in the *Gibberella fujikuroi* species complex. *Appl. Environ. Microbiol.* 66, 4378–4382. doi: 10.1128/AEM.66.10.4378-4382.2000

Stêpień, Ł, Koczyk, G., and Waśkiewicz, A. (2013). Diversity of *Fusarium* species and mycotoxins contaminating pineapple. *J. Appl. Genet.* 54, 367–380. doi: 10.1007/s13353-013-0146-0

Studt, L., Troncoso, C., Gong, F., Hedden, P., Toomajian, C., Leslie, J. F., et al. (2012). Segregation of secondary metabolite biosynthesis in hybrids of *Fusarium fujikuroi* and *Fusarium proliferatum*. *Fungal Genet. Biol.* 49, 566–577. doi: 10.1016/j.fgb.2012.05.005

Sun, L., Chen, X., Gao, J., Zhao, Y., Liu, L. M., Hou, Y. X., et al. (2019a). Effects of disruption of five *FUM* genes on fumonisin biosynthesis and pathogenicity in *Fusarium proliferatum*. *Toxins* 11:327. doi: 10.3390/toxins11060327

Sun, L., Wang, L., Liu, L. M., Hou, Y. X., Xu, Y. H., Liang, M. Q., et al. (2019b). Infection and colonization of pathogenic fungus *Fusarium proliferatum* in rice spikelet rot disease. *Rice Sci.* 26, 60–68. doi: 10.1016/j.rsci.2018.08.005

Suzuki, T., Kim, Y. K., Yoshioka, H., and Iwahashi, Y. (2013). Regulation of metabolic products and gene expression in *Fusarium asiaticum* by agmatine addition. *Mycotoxin Res.* 29, 103–111. doi: 10.1007/s12550-013-0158-y

Talas, F., Kalih, R., Miedaner, T., and McDonald, B. A. (2016). Genome-wide association study identifies novel candidate genes for aggressiveness, deoxynivalenol production, and azole sensitivity in natural field populations of *Fusarium graminearum*. *Mol. Plant Microbe Interact.* 29, 417–430. doi: 10.1094/MPMI-09-15-0218-R

Tudzynski, B. (2014). Nitrogen regulation of fungal secondary metabolism in fungi. *Front. Microbiol.* 5:656. doi: 10.3389/fmicb.2014.00656

von Bargen, S., Martinez, O., Schadock, I., Eisold, A. M., Gossmann, M., and Büttner, C. (2009). Genetic variability of phytopathogenic *Fusarium proliferatum* associated with crown rot in *Asparagus officinalis*. *J. Phytopathol.* 157, 446–456. doi: 10.1111/j.1439-0434.2008.01525.x

Wang, G., Li, Y., Yang, B., Li, E., Wu, W., Si, P., et al. (2022). *AwAreA* regulates morphological development, ochratoxin A production, and fungal pathogenicity of food spoilage fungus *Aspergillus westerdijkiae* revealed by an efficient gene targeting system. *Front. Microbiol.* 13:857726. doi: 10.3389/fmicb.2022.857726

Wang, L., Ge, S., Liang, W., Liao, W., Li, W., Jiao, G., et al. (2022). Genome-wide characterization reveals variation potentially involved in pathogenicity and mycotoxins biosynthesis of *Fusarium proliferatum* causing spikelet rot disease in rice. *Toxins* 14:568. doi: 10.3390/toxins14080568

Wang, G., Wang, Y. L., Yang, B. L., Zhang, C. X., Zhang, H. Y., Xing, F. G., et al. (2020). Carbon catabolite repression gene *AoCreA* regulates morphological development and ochratoxin A biosynthesis responding to carbon sources in *Aspergillus ochraceus*. *Toxins* 12:697. doi: 10.3390/toxins12110697

Wang, L., Ge, S. L., Zhao, K. H., and Huang, S. W. (2021). First report of *Fusarium incarnatum* causing spikelet rot on rice in China. *Plant Dis.* 105:3306. doi: 10.1094/PDIS-12-20-2660-PDN

Wang, Q. H., Chen, D. P., Wu, M. C., Zhu, J. D., Jiang, C., Xu, J. R., et al. (2018). MFS transporters and GABA metabolism are involved in the self-defense against DON in *Fusarium graminearum*. *Front. Plant Sci.* 9:438. doi: 10.3389/fpls.2018.00438

Waśkiewicz, A., Stêpień, Ł, Wilman, K., and Kachlicki, P. (2013). Diversity of pea-associated *F. proliferatum* and *F. verticillioides* populations revealed by *FUM1* sequence analysis and fumonisin biosynthesis. *Toxins* 5, 488–503. doi: 10.3390/toxins5030488

Wicker, T., Oberhaensli, S., Parlange, F., Buchmann, J. P., Shatalina, M., Roffler, S., et al. (2013). The wheat powdery mildew genome shows the unique evolution of an obligate biotroph. *Nat. Genet.* 45, 1092–1096. doi: 10.1038/ng.2704

Wiemann, P., Brown, D. W., Kleigrewe, K., Bok, J. W., Keller, N. P., Humpf, H., et al. (2010). *FfVel1* and *FfLae1*, components of a velvet-like complex in *Fusarium fujikuroi*, affect differentiation, secondary metabolism and virulence. *Mol. Microbiol.* 77, 972–994. doi: 10.1111/j.1365-2958.2010.07263.x

Yin, J. R., Hao, C. F., Niu, G., Wang, W., Wang, G. H., Xiang, P., et al. (2020). FgPal1 regulates morphogenesis and pathogenesis in *Fusarium graminearum*. *Environ. Microbiol.* 22, 5373–5386. doi: 10.1111/1462-2920.15266

Yu, F. F., Imamura, Y., Ueno, M., Suzuki, S. W., Ohsumi, Y., Yukawa, M., et al. (2015). The yeast chromatin remodeler Rsc1-RSC complex is required for transcriptional activation of autophagy-related genes and inhibition of the TORC1 pathway in response to nitrogen starvation. *Biochem. Biophys. Res. Commun.* 464, 1248–1253. doi: 10.1016/j.bbrc.2015.07.114

Yu, J., Chang, P. K., Ehrlich, K. C., Cary, J. W., Bhatnagar, D., Cleveland, T. E., et al. (2004). Clustered pathway genes in aflatoxin biosynthesis. *Appl. Environ. Microbiol.* 70, 1253–1262. doi: 10.1128/AEM.70.3.1253-1262.2004

Yu, S., Jia, B. X., Liu, N., Yu, D. Z., Zhang, S., and Wu, A. B. (2021). Fumonisin B1 triggers carcinogenesis via HDAC/PI3K/Akt signaling pathway in human esophageal epithelial cells. *Sci. Total Environ.* 787:147405. doi: 10.1016/j.scitotenv.2021.147405

Zander, M., Patel, D. A., Wouw, A. V., Lai, K., Lorenc, M. T., Campbell, E., et al. (2013). Identifying genetic diversity of avirulence genes in *Leptosphaeria maculans* using whole genome sequencing. *Funct. Integr. Genomics* 13, 295–308. doi: 10.1007/s10142-013-0324-5

Zhang, D. D., Wang, X. Y., Chen, J. Y., Kong, Z. Q., Gui, Y. J., Li, N. Y., et al. (2016). Identification and characterization of a pathogenicity-related gene *VdCYP1* from *Verticillium dahliae*. *Sci. Rep.* 6:27979. doi: 10.1038/srep27979

Zhang, L., Li, B., Zhang, Y., Jia, X., and Zhou, M. (2016). Hexokinase plays a critical role in deoxynivalenol (DON) production and fungal development in *Fusarium graminearum*. *Mol. Plant Pathol.* 17, 16–28. doi: 10.1111/mpp.12258

Zhao, J. H. (2007). Gap: genetic analysis package. *J. Stat. Softw.* 23, 1–18. doi: 10.18637/jss.v023.i08

frontiers | Frontiers in Microbiology

TYPE Original Research
PUBLISHED 13 October 2022
DOI 10.3389/fmicb.2022.1025983

Check for updates

OPEN ACCESS

EDITED BY
Pinmei Wang,
Zhejiang University,
China

REVIEWED BY
Ishrat Khan
Federal Urdu University of Arts,
Sciences and Technology, Pakistan
Han Xiao,
Shanghai Jiao Tong University, China

*CORRESPONDENCE
Na Li
nli@kust.edu.cn
Jun-Wei Xu
xjuwei@163.com;
jwxu@kust.edu.cn

SPECIALTY SECTION
This article was submitted to
Microbial Physiology and Metabolism,
a section of the journal
Frontiers in Microbiology

RECEIVED 23 August 2022
ACCEPTED 20 September 2022
PUBLISHED 13 October 2022

CITATION
Luo Q, Li N and Xu J-W (2022) A methyltransferase LaeA regulates ganoderic acid biosynthesis in *Ganoderma lingzhi*. *Front. Microbiol.* 13:1025983.
doi: 10.3389/fmicb.2022.1025983

COPYRIGHT
© 2022 Luo, Li and Xu. This is an open-access article distributed under the terms of the Creative Commons Attribution License (CC BY). The use, distribution or reproduction in other forums is permitted, provided the original author(s) and the copyright owner(s) are credited and that the original publication in this journal is cited, in accordance with accepted academic practice. No use, distribution or reproduction is permitted which does not comply with these terms.

A methyltransferase LaeA regulates ganoderic acid biosynthesis in *Ganoderma lingzhi*

Qin Luo[1], Na Li[2]* and Jun-Wei Xu[1]*

[1]Faculty of Life Science and Technology, Kunming University of Science and Technology, Kunming, China, [2]Faculty of Science, Kunming University of Science and Technology, Kunming, China

The methyltransferase LaeA is a global regulator involved in the biosynthesis of secondary metabolites by ascomycete fungi. However, little is known of its regulatory role in basidiomycete fungi. In this study, the *laeA* gene was identified in the basidiomycete *Ganoderma lingzhi* and its function in regulating the biosynthesis of anti-tumor ganoderic acids was evaluated. A *laeA* deletion (ΔlaeA) *Ganoderma* strain exhibited significantly reduced concentration of ganoderic acids. qRT-PCR analysis further revealed that the transcription levels of genes involved in the biosynthesis of ganoderic acids were drastically lower in the ΔlaeA strain. Moreover, deletion of *laeA* resulted in decreased accumulation of intermediates and abundances of asexual spores in liquid static culture of *G. lingzhi*. In contrast, constitutive overexpression of *laeA* resulted in increased concentration of ganoderic acids. These results demonstrate an essential role of LaeA in the regulation of ganoderic acid biosynthesis in *Ganoderma*.

KEYWORDS

ganoderma, ganoderic acids, regulator LaeA, biosynthesis, secondary metabolite

Introduction

Ganoderm lingzhi is a well-known medicinal fungus that has been used to improves health and prevent human diseases for over 2000 years (Bishop et al., 2015; Hsu and Cheng, 2018). Ganoderic acids (GAs) are lanosterol-type triterpenoids produced by *Ganoderma* that possess multiple bioactivities including anti-cancer, anti-inflammatory, antioxidant, and anti-HIV activities (Xu et al., 2010b; Ahmad et al., 2022). Moreover, different types of GAs exhibit distinct bioactivities. For example, ganoderic acid T (GA-T) induces apoptosis of lung cancer cells (Tang et al., 2006), and ganoderic acid Me (GA-Me) inhibits lung cancer metastasis (Chen et al., 2008).

GAs are synthesized from the triterpene squalene, and the early biosynthetic steps are common for both GA and ergosterol pathways, including the sequential conversion of squalene to 2, 3-oxidosqualene, and lanosterol (Shi et al., 2010; Xu and Zhong, 2015). The downstream biosynthetic steps after lanosterol formation include several oxidation, reduction, and acetylation reactions (Xu et al., 2010a; Chen et al., 2012; Sun et al., 2021).

During GA biosynthesis, squalene synthase (SQS) catalyzes the first step specific to triterpene synthesis, while lanosterol synthase (LS) is responsible for the formation of the lanostane skeletons of GAs (Figure 1).

Interest in regulating GA biosynthesis by *Ganoderma* has increased in recent years, due to their important pharmacological activities and commercial value. Environmental factors like heat stress, pH, and nitrogen sources all affect GA biosynthesis in *Ganoderma* (Zhao et al., 2011; Wu et al., 2016; Zhang et al., 2016). Further, signaling molecules like reactive oxygen species (ROS), cyclic adenosine monophosphate (cAMP), nitric oxide (NO), and Ca^{2+} participate in *Ganoderma* GA biosynthesis (Xu and Zhong, 2012; You et al., 2017; Ren et al., 2019; Liu et al., 2021). Moreover, the transcription factors AreA, PacC, and MADS1 are involved in regulating GA biosynthesis (Wu et al., 2016; Zhu et al., 2019; Meng et al., 2021). Besides, promoting sporulation was favorable to the biosynthesis of ganoderic acids in *G. lucidum* (Sun et al., 2021). Previous studies have indicated that the regulation of GA biosynthesis comprises a complex regulatory system. Further investigation of this system is needed to improve our understanding of GA biosynthesis regulation in *Ganoderma*.

The methyltransferase LaeA (loss of aflR expression-A) has been demonstrated to be involved in regulating the biosynthesis of numerous secondary metabolites in ascomycete fungi like *Aspergillus nidulans*, *Fusarium fujikuroi*, *Penicillium chrysogenum*, and *Trichoderma longibrachiatum* (Bok and Keller, 2004; Kosalkova et al., 2009; Wiemann et al., 2010; Shi et al., 2020). However, the function of LaeA has never been reported in other basidiomycete fungi, with the exception of *Coprinopsis cinerea*, in which the knockout of *laeA* improved coprinoferrin production (Tsunematsu et al., 2019). A LaeA ortholog has been identified in *Ganoderma* (Chen et al., 2012). However, it is currently unclear if and how LaeA influences GA biosynthesis in *Ganoderma*.

Here, we show that LaeA positively regulates GA biosynthesis in the basidiomycete *Ganoderma* for the first time. Targeted deletion of *laeA* significantly reduced GA production. Moreover, the expression of GA biosynthetic genes, accumulation of intermediates, and the abundance of asexual spores also decreased in the Δ*laeA Ganoderma*. Further analysis revealed that constitutive overexpression of *laeA* increased the production of GAs in *Ganoderma*.

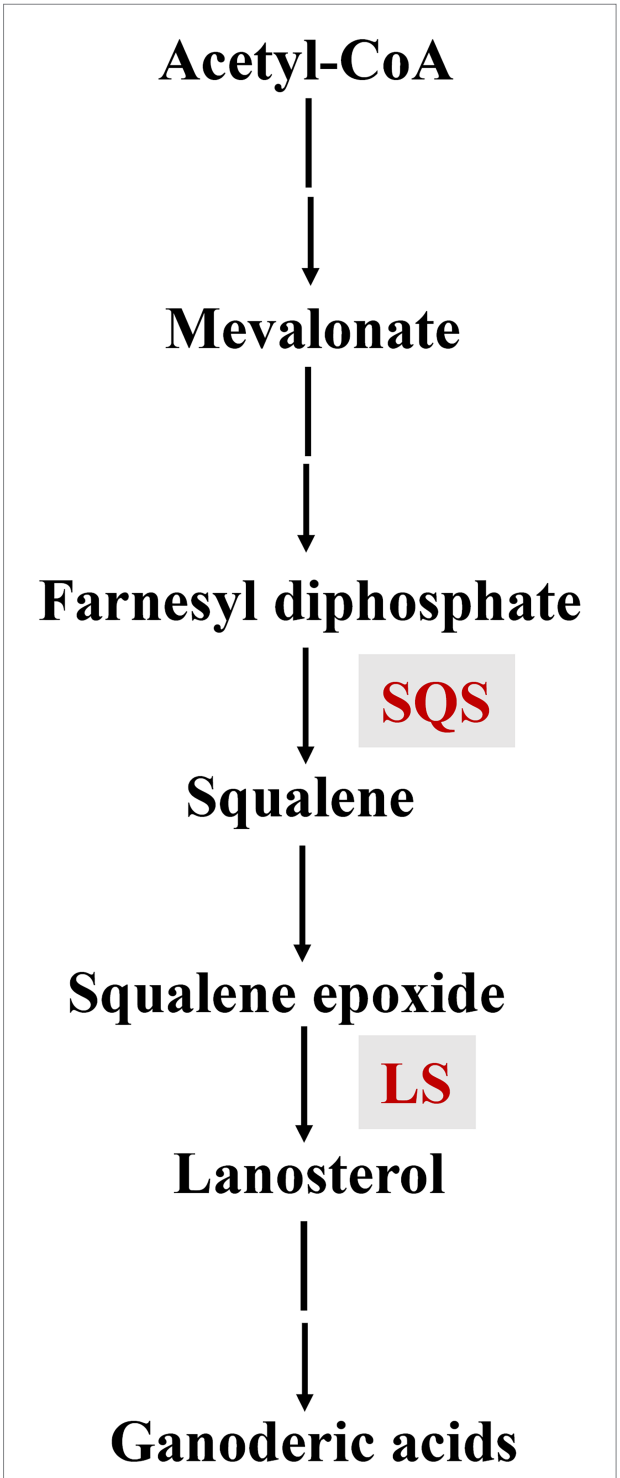

FIGURE 1
The biosynthetic pathway of ganoderic acids.

Materials and methods

Strains and culture conditions

The strains *G. lingzhi* pJW-EXP-intron-opCas9 (Tu et al., 2021) and *G. lingzhi* CGMCC 5.616-1 (Sun et al., 2021) were maintained in our laboratory and used in this study. These strains were routinely maintained on potato dextrose agar and incubated at 30°C. The genotypes of the used *Ganoderma* strains are given in Supplementary Table S1. *Escherichia coli* JM109 was used for plasmid construction and cloning. Pre-culturing and liquid static fermentation of *G. lingzhi* mycelia were conducted as previously described (Xu et al., 2010a, 2012a). The fermentation medium for liquid static culture consisted of the following components (g/l): lactose, 35; $KH_2PO_4{\cdot}H_2O$, 1; $MgSO_4{\cdot}7H_2O$, 0.5; peptone, 5; yeast extract, 5; and vitamin B1, 0.05. Asexual spores formed after 3 days of cultivation in liquid static condition.

In vitro transcription of *laeA* sgRNAs and construction of the pJW-EXP-LaeA plasmid

Two sgRNA cassettes (Supplementary Data S1), including two *laeA* targeting sequences and a sgRNA sequence, were generated with a T7 promoter. The sequences were synthesized by Shanghai Sangon Led., Corp. (Shanghai, China). The two sgRNA cassettes were transcribed *in vitro* using a HiScribe™ T7 High Yield RNA Kit (NEB, Beijing, China) and purified using the RNA Clean and Concentration™ – 25 Kit (Zymo Research, Beijing, China).

The *laeA* sequence was amplified from *G. lingzhi* genomic DNA using the primers gpd-LaeA-F: 5′-ttcatccccctctcaac ATGGCCATCGAATACGCCCG-3′ and ter-LaeA-R: 5′-ctctctgac ccgctcat CTACAGGCGGCGCGCGT-3′. The amplified PCR product was fused with the plasmid pJW-EXP (Yu et al., 2014) that was digested with *Nhe*I using the ClonExpress MutiS one-step cloning kit (Vazyme, Nanjing, China) to produce the PJW-EXP-LaeA plasmid.

Genetic transformation of *Ganoderma lingzhi* protoplasts and identification of transformants

PEG-mediated genetic transformation of *G. lingzhi* protoplasts was conducted as previously described (Xu and Zhong, 2015). Following the genetic transformation of the plasmid pJW-EXP-LaeA into the wild-type strain (monokaryotic CGMCC 5.616–1), LaeA transformants were screened on CYM selective plates containing 2 mg/l carboxin (Fei et al., 2019). Selective transformants were analyzed by PCR amplification of the fusion fragment containing the glyceraldehyde-3-phosphate dehydrogenase gene (*gpd*) promoter and *laeA* using the primers gpd-F: 5′-CGAGTGACGCAGGTGGTGAC-3′ and ter-R: 5′-GCAGTCGCACAATCTAGCCCT-3′. To screen the Δ*laeA* mutants, transformants were picked from CYM selective plates containing 250 mg/l hygromycin B after genetic transformation of *G. lingzhi* (the pJW-EXP-intron-opCas9 strain) protoplasts with the pJW-EXP-ophph plasmid (Tu et al., 2021) and the transcribed sgRNAs that targeted *laeA*. *laeA* was amplified from the genomic DNA of the control and mutant strains and then sequenced to confirm the gene deletion.

Determination of mycelial growth, asexual spore numbers, GA contents, and the accumulation of squalene and lanosterol

Mycelial dry weight were measured using the gravimetric method. Briefly, mycelia were scraped from the surface of the liquid static culture and washed three times with distilled water. Mycelia were scraped from the surface of the liquid static culture and inoculated into H_2O. The number of asexual spores (Xu et al., 2012b) was determined with a hemacytometer and expressed as the number of asexual spores per 1 cm^2 (Zhang and Zhong, 2010; Sun et al., 2021). Total GAs and individual GAs, in addition to squalene and lanosterol, were extracted from *G. lingzhi* and determined using previously described methods (Zhou et al., 2014; Xu et al., 2019) and are shown in the Supplementary Data S2.

Nucleic acid isolation

Ganoderma lingzhi mycelia were collected by filtration, washed with distilled water, frozen, and ground with liquid nitrogen. Genomic DNA was then extracted using the cetyltrimethylammonium bromide method (Saghai-Maroof et al., 1984), and RNA was extracted using TRIzol (Invitrogen, Carlsbad, CA, USA) according to the manufacturer's protocol.

Quantitative real time-PCR (qRT-PCR) analysis

Following RNA isolation, 1 μg of total RNA was treated with DNase I (Fermentas, Canada) and reverse-transcribed using the PrimeScript™ RT reagent kit (Takara, China). The transcription levels of the squalene synthase gene (*sqs*), lanosterol synthase gene (*ls*), *laeA*, and *gl25098* were then determined with the cDNA pools by qRT-PCR, as previously described (Zhang et al., 2017). The qRT-PCR primers used for amplification of *sqs*, *ls,* and *gl25098* were also previously described (Sun et al., 2021). In addition, the primers used to amplify *laeA* included: qRT-LaeA-F: 5′-CCCACTCCGATCATTACCTCTC-3′ and qRT-LaeA-R: 5′-GGTTTAGCCCGTTTTGTCTTTC-3′. The transcription levels of target genes were normalized to the levels of the internal reference, the 18S-rRNA gene. Gene expression from the control strain was defined as 1.0, and the transcription levels of genes from other strains were expressed as fold changes in comparison to control strain expression. Relative expression levels were calculated using the $2^{\Delta\Delta Ct}$ method.

Sequence analysis

Amino acid sequence alignments were performed using Clustal W (Thompson et al., 2002). Phylogenetic tree was constructed with MEGA 7.0 using the neighbor-joining method with 1,000 bootstraps (Kumar et al., 2016).

Statistical analysis

Data are presented as averages for three biological replicates, and the error bars indicate standard deviations from three replicates. Statistical analysis were performed using student's t-test. Differences with value of $p < 0.05$ were considered statistically significant.

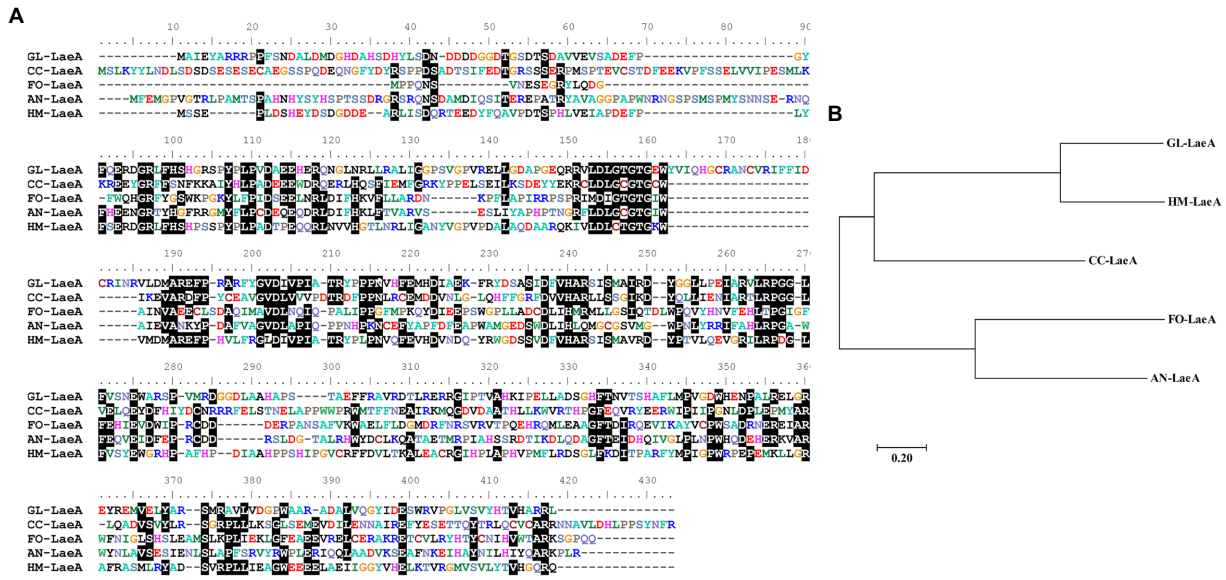

FIGURE 2
(A) Multiple alignment of amino acid sequences of GL-LaeA (*G. lingzhi*) and homologous proteins including CC-LaeA (*C. cinerea*, CC1G_00498), FO-LaeA (*F. oxysporum*, RKL38237.1), AN-LaeA (*A. nidulans*, C8VQG9.1), and HM-LaeA (*H. marmoreus*, RDB17513.1). Alignments were generated using ClustalW. **(B)** Phylogenetic reconstruction of amino acid sequences of LaeA from different strains. The tree was constructed using the neighbor-joining method with complete gap deletion in MEGA version 6.0.

Results

Identification of a *laeA* ortholog in *Ganoderma lingzhi*

To identify *laeA* ortholog encoded by *G. lingzhi*, its genome was queried using the LaeA amino acid sequence of *Hypsizygus marmoreus* (RDB17513). The protein encoding gene gl27879 that is hereafter referred to as LaeA was identified with 44% to RDB17543 and with a corresponding E value of <1.00E−80. *G. lingzhi laeA* is 1,379-bp long and has an open reading frame of 1,125-bp that encodes a protein of 375 amino acids. The amino acid residues in the 115–295 region of *G. lingzhi* LaeA encode an S-adenosylmethionine-dependent methyltransferase domain (Kadooka et al., 2020). Protein BLAST analysis revealed that *G. lingzhi* LaeA shares sequence identity with LaeA from *H. marmoreus, C. cinerea*, *Fusarium oxysporum*, and *A. nidulans*, (Figure 2A). Further, phylogenetic analysis indicated that *G. lingzhi* LaeA is more closely related to LaeA from basidiomycetes than to homologs in ascomycetes (Figure 2B).

Deletion of *Ganoderma lingzhi laeA*

To delete the *laeA* of *G. lingzhi*, two *in vitro*-transcribed sgRNAs and the pJW-EXP-ophph plasmid were combined and transformed into *G. lingzhi* pJW-EXP-intron-opCas9 protoplasts using a PEG-mediated method (Liu et al., 2020; Tu et al., 2021). Numerous colonies were present on the selective CYM plates containing 250 mg/l hygromycin B (Figure 3A). Putative transformants were chosen from the selective CYM plates after three rounds of growth on nonselective CYM plates (Figure 3B). No evident morphological differences were observed when comparing the transformants and control strains (data not shown). The transformants were subsequently characterized by genomic PCR. Amplification of a clear band for *laeA* (950 bp) was observed in the control strain and transformants 1 and 2, while amplification of an approximately 250 bp band was observed for the transformant 3 (Figure 3C). Further, a > 1,000 bp amplicon was identified in transformant 4, indicating the presence of an insertion mutant. Sequence analysis of the PCR products indicated that the sequence between LaeA-sgRNA1 and LaeA-sgRNA2 was deleted, as expected in transformant 3 (Figure 3D). Thus, *laeA* was successfully deleted from *G. lingzhi.*

Deletion of *laeA* reduced GA concentration by *Ganoderma lingzhi*

To analyze the effects of *laeA* deletion on GA production by *G. lingzhi*, the kinetics of mycelial growth, total GA concentration, and the concentrations of GA-T and GA-Me were determined in liquid static culture conditions. Mycelial growth and accumulation of GA exhibited similar trends in the control and Δ*laeA* strain (Figure 4). The maximum dry cell weights in the control and Δ*laeA* strains were 8.13 and 6.95 g/l on day 12, respectively (Figure 4A). Thus, the Δ*laeA* strain exhibited a decrease in biomass accumulation by 15%. GA-T and GA-Me are the major

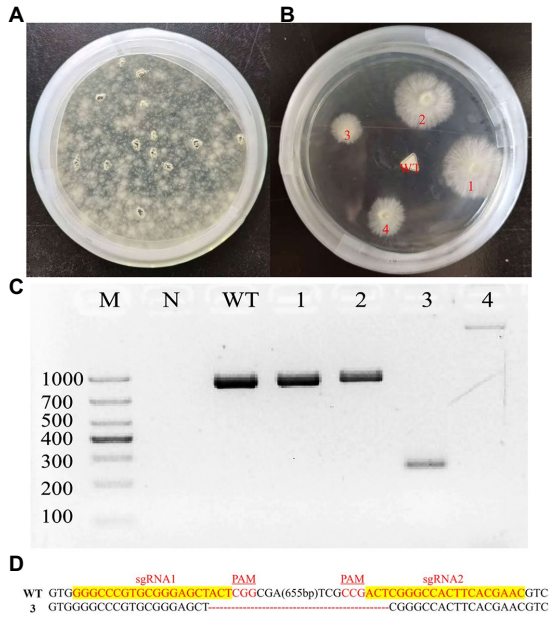

FIGURE 3
Deletion of *laeA* in *G. lingzhi*. **(A)** Screening and **(B)** re-selection of hygromycine resistant transformants after sgRNA1 and sgRNA2 targeted the *laeA* were delivered into the Cas9 strain. **(C)** Determination of *laeA* deletion in *G. lingzhi* transformants by genomic PCR. **(D)** TA-cloning of *laeA* deletions in selected transformant 3. The sgRNA-guiding sequences are highlighted in yellow. WT, wild-type strain; 3, the *laeA* deletion strain.

GA components of *G. lingzhi* mycelia (Xu et al., 2019). Temporal analysis of total GAs, GA-T, and GA-Me in both the control and Δ*laeA* strains is shown in Figures 4B–D. GA concentrations significantly increased and reached maximum values at day 9, followed by a slight decrease until the end of the fermentation. The maximum concentrations of total GAs, GA-T, and GA-Me in the Δ*laeA* strain were 2.46 mg, 277 μg, and 115 μg per 100 mg dry weight on day 9, 12 and 12, respectively, representing decreases of 67, 60, and 49% compared to values on day 9 for the control strain, respectively.

Effects of *laeA* deletion on accumulation of intermediates and expression of GA biosynthesis genes

Squalene and lanosterol are key intermediates in GA biosynthesis, and their accumulations were consequently determined in the control and Δ*laeA* strains. The concentrations of squalene and lanosterol increased until day 9 and day 6 (Figures 5A,B), respectively, and then decreased thereafter in both strains. The maximum squalene concentration observed in the Δ*laeA* strain was 0.5 μg/100 mg DW, representing a 0.51–time decrease in concentration compared to the control strain. The maximum lanosterol concentration in the Δ*laeA* strain was 4.5 μg/100 mg DW, representing a 67% decrease compared to the control strain. Thus, less intermediates accumulated in the Δ*laeA* strain compared to the control strain. The transcription levels of *sqs* in the Δ*laeA* strain were 62, 18, and 30% those of the control strain on days 6, 9, and 12, respectively (Figure 5C). *ls* transcription levels in the Δ*laeA* strain decreased to 46, 62, and 38% of the levels of the control strain on days 6, 9, and 12, respectively (Figure 5D).

Deletion of *laeA* decreased asexual spore abundances in *Ganoderma lingzhi*

The numbers of asexual spores were measured in both strains under liquid static culture condition. Temporal trends of asexual spore numbers were similar in the control (pJW-EXP-intron-opCas9 strain) and Δ*laeA* strains, wherein asexual spore numbers increased during fermentation and reached maximum values on day 12 (Figure 6A). The Δ*laeA* strain produced 1.72×10^7 asexual spores per cm^2 on day 12, representing 81% of that produced by the control strain. The transcription levels of the asexual sporulation specific gene *gl25098* (Sun et al., 2021) were also examined in the control and Δ*laeA* strains. The transcription levels of *gl25098* in the Δ*laeA* strain were 20, 47, and 3% of the levels in the control strain on days 6, 9, and 12, respectively (Figure 6B).

LaeA overexpression in *Ganoderma lingzhi*

The plasmid pJW-Exp-LaeA (Figure 7A) was transformed into *G. lingzhi* (wild-type strain) protoplasts. Transformants were selected on CYM plates containing 2 mg/l carboxin after three rounds of growth on nonselective CYM plates (Figure 7B). The obtained transformants were confirmed with genomic PCR. Amplification yielded a clear band for the fused *gpd* promoter and the *laeA* fragment (1,670 bp) in the positive control and transformants 1, 2, 3, and 5 (Figure 7C). qRT-PCR analysis was then conducted to compare the transcription level of *laeA* in the mycelia of the wild type (WT) and the transformant 1 strains. *laeA* was overexpressed in transformant 1 under liquid static culture conditions. Further, the transcription levels of *laeA* in transformant 1 were 5.0-, 4.1-, and 5.5-fold higher than those of the WT strain on days 3, 6, and 9, respectively (Figure 7D).

LaeA overexpression increased GA concentration in *Ganoderma lingzhi*

The temporal trends of mycelial growth, concentrations of GA-Me and GA-T, and the abundances of asexual spores were evaluated in the *laeA* overexpressing and WT strains. Mycelial growth exhibited similar trends in both strains, with the maximum dry weights in the WT and *laeA* overexpressing strains being 9.31 and 9.75 g/l, respectively, under liquid static culture conditions

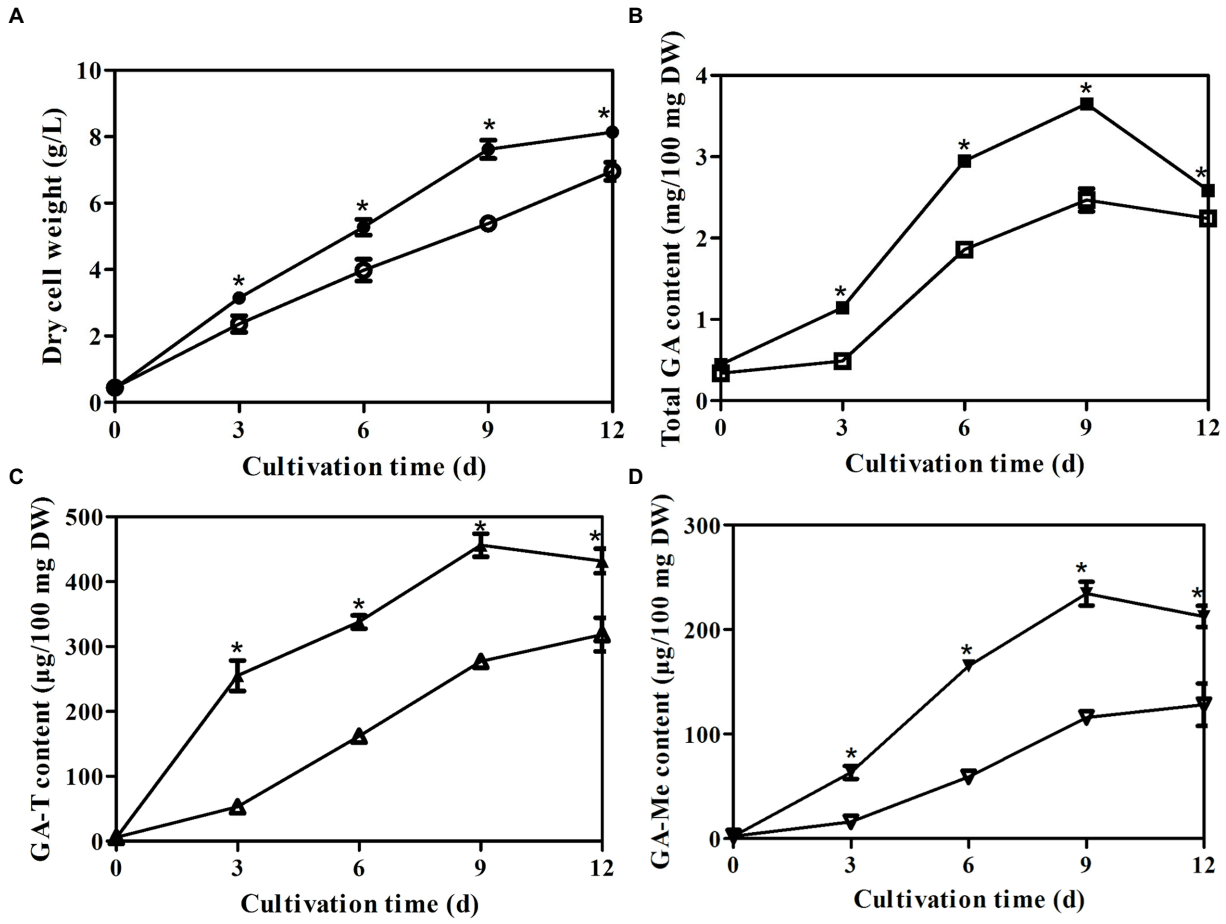

FIGURE 4
Temporal profiles of **(A)** mycelial growth **(A)** and **(B)** concentrations of total GAs, **(C)** GA-T and **(D)** GA-Me in liquid static culture of control (filled) and Δ*laeA* (open) strains.*a significantly different value compared to the control strain.

(Figure 8A). Similar GA concentrations and asexual spore abundances were also observed for both strains (Figures 8B-D and Supplementary Figure S1). GA-T and GA-Me concentrations reached maximum levels on day 9 and declined on day 12, whereas the numbers of asexual spores increased during fermentation and reached maximum values at the end of fermentation. The maximum GA-T and GA-Me concentrations were 497 and 234 μg/100 mg DW in the *laeA* overexpressing strain, respectively, representing 1.25- and 1.20-fold higher values in the WT strain, respectively. In addition, the *laeA* overexpressing strain produced 2.70×10^7 asexual spores per cm^2 on day 12, representing a 25% higher abundance than the WT strain.

Discussion

Here, the involvement of LaeA in GA biosynthesis regulation was investigated by gene deletion and overexpression experiments. Deletion of *laeA* led to reduced GA concentration, whereas overexpression of *laeA* led to increased GA concentration. These results indicated that LaeA is a positive regulator of GA biosynthesis in *Ganoderma*. Previous studies have shown that LaeA plays an important role in regulating some secondary metabolites in ascomycetes. For example, LaeA is a positive regulator of the biosynthesis of helvolic acid (Tsunematsu et al., 2019), penicillin (Kosalkova et al., 2009), bikaverin (Wiemann et al., 2010) and mycotoxins (Estiarte et al., 2016) in *Aspergillus fumigatus*, *P. chrysogenum*, *F. fujikuroi*, and *Alternaria alternata* CBS 116.329 strain, respectively. LaeA also negatively regulates the biosynthesis of the virulence factor dothistromin (Chettri and Bradshaw, 2016) and the mycotoxin alternariol (Estiarte et al., 2016) in *Dothistroma septosporum* and *A. alternata* ATCC 66981 strain, respectively. Tsunematsu et al. recently reported that the deletion of *laeA* resulted in increased production of the siderophore coprinoferrin in the basidiomycete *C. cinerea* (Tsunematsu et al., 2019). Thus, the identification and characterization of different *laeA* will facilitate a broader understanding of GA biosynthesis regulation in *Ganoderma*.

sqs and *ls* transcription levels were drastically decreased in the Δ*laeA* strain, suggesting LaeA regulated expression of GA biosynthesis genes. Similarly, deletion of *laeA* was shown to reduce

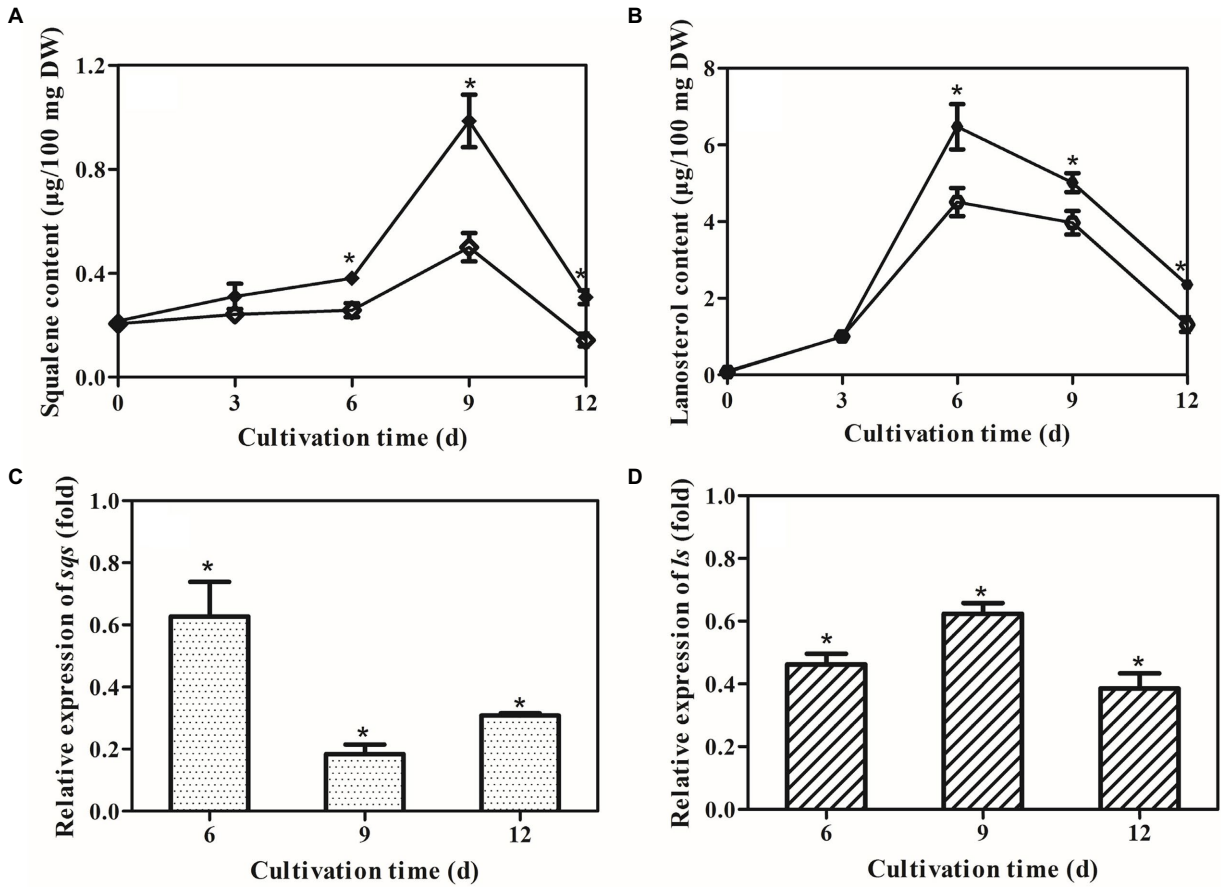

FIGURE 5
Effects of *laeA* deletion on intermediate accumulation and gene expression levels of *sqs* and *ls*. Accumulation of **(A)** squalene and **(B)** lanosterol in the control (filled) and Δ*laeA* (open) strains. Transcriptional levels of **(C)** *sqs* and **(D)** *ls* in the control and Δ*laeA* strains. Expression of genes in the control strain is defined as 1.0, and the expression levels in the Δ*laeA* strain are shown as fold changes compared to the reference.

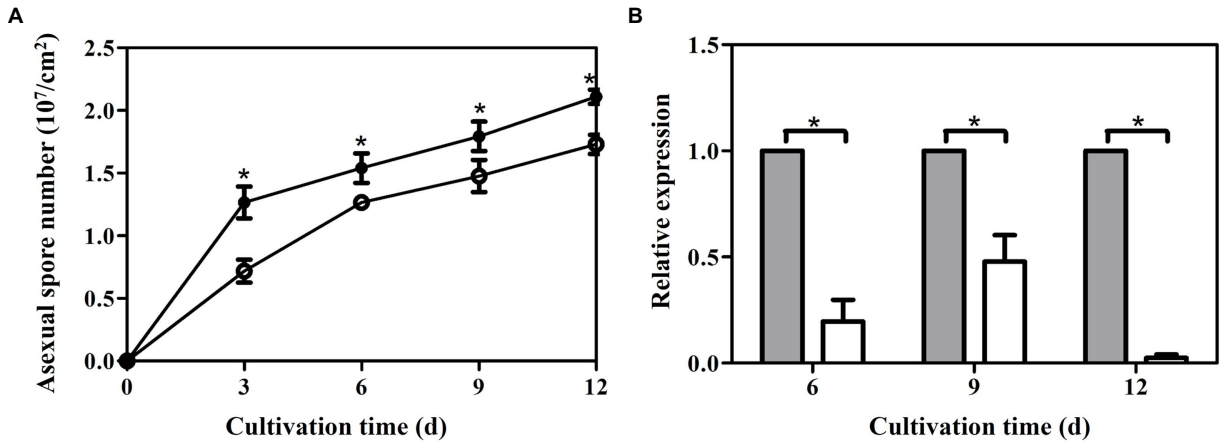

FIGURE 6
Temporal profiles of asexual spore numbers **(A)** and **(B)** transcription levels of *gl25098* during liquid static culture of the control (filled) and Δ*laeA* (open) strains. *, significant difference compared to the control value. The transcription levels of genes in the control strain are defined as 1.0, and the transcription levels of genes in the Δ*laeA* strain are expressed as fold changes relative to the control references.

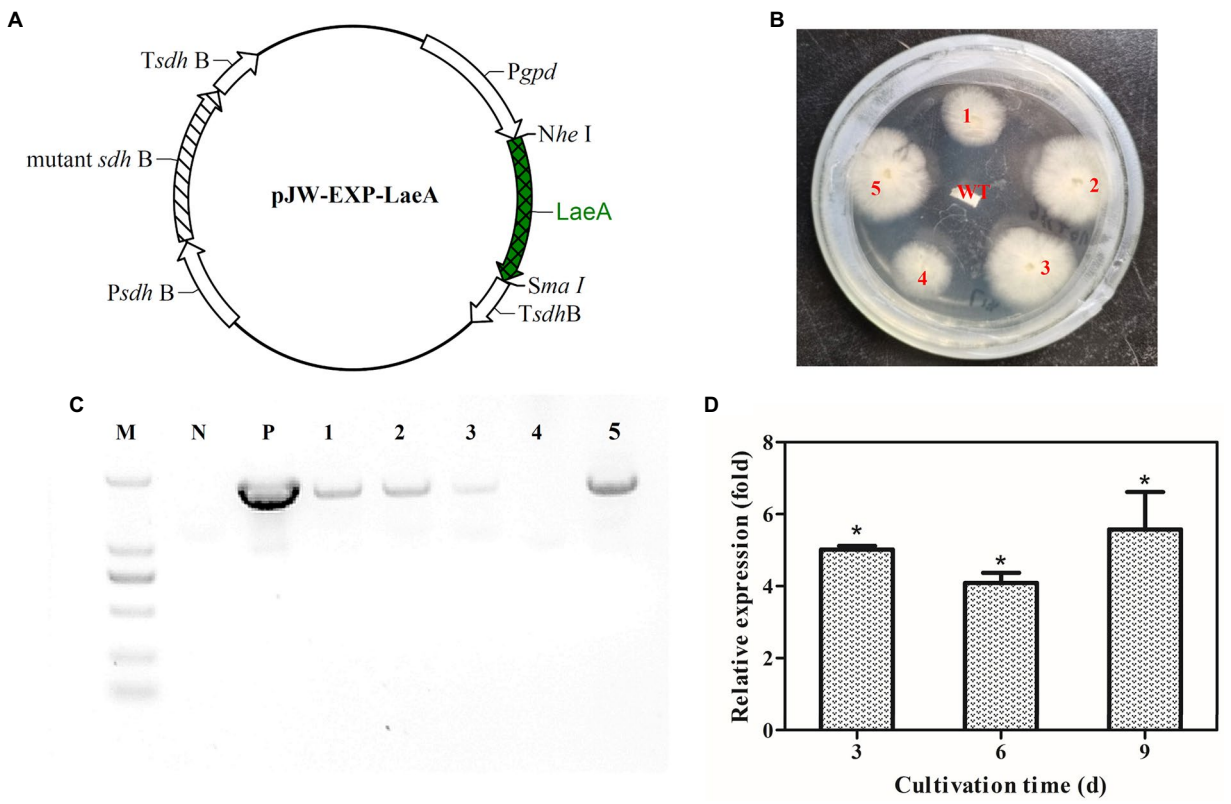

FIGURE 7
(A) Plasmid pJW-EXP-LaeA used for transformation of *G. lingzhi* protoplasts and identification of *laeA* overexpressing strains. **(B)** Selection of *laeA* transformants on selective CYM plates. **(C)** Amplification patterns obtained with primers for the fusion *gpd* promoter-*laeA* fragment in genomic DNA isolated from different strains. **(D)** Relative transcriptional levels of *laeA* in the WT and *laeA* transformant strains. M, DNA marker; P, positive control; WT, wild-type strain.

the expression of the biosynthetic genes of sterigmatocystin (Bok and Keller, 2004) and bikaverin (Butchko et al., 2012) in *A. nidulans* and *Fusarium verticillioides*, respectively. It was hypothesized that LaeA could regulate the expression of genes involved in secondary metabolism by modifying fungal chromatin structure (Jain and Keller, 2013; Sarikaya-Bayram et al., 2015). However, the regulatory mechanism of GA biosynthesis by LaeA remains unclear and requires further investigation. The concentrations of the intermediates squalene and lanosterol were lower in the Δ*laeA* strain compared to the control strain, consistent with decreased production of GA. Decreased transcription levels of *sqs* and *ls* may lead to lower accumulations of squalene and lanosterol in the Δ*laeA* strains (Zhou et al., 2014; Zhang et al., 2017). The results from this study indicated that the decreased concentration of GAs in the Δ*laeA* strain could be attributed to the down-regulated expression of biosynthesis genes and decreased precursor concentrations. These results are consistent with previous observation of *Vitreoscilla* hemoglobin gene overexpression (Li et al., 2016a) and nitrogen limitation (Li et al., 2016b) in *G. lucidum*.

The Δ*laeA* strain accumulates fewer asexual spores than the control strain, and the numbers of asexual spores were higher in the *laeA* overexpressing strain than in the WT strain. qRT-PCR indicated that the expression levels of asexual sporulation-specific genes were lower in the Δ*laeA* strain. Thus, these results suggest that LaeA may be involved in the regulation of asexual sporulation in *Ganoderma*. Decreased asexual sporulation in *Aspergillus flavus* (Kale et al., 2008), *Alternaria alternate* (Takao et al., 2016), and *T. longibrachiatum* (Shi et al., 2020) *laeA* deletion strains had been previously documented. The influence of LaeA on asexual sporulation may be related to the expression of velvet family proteins in fungi (Jain and Keller, 2013; Aghcheh et al., 2014; Sarikaya-Bayram et al., 2015). Previous studies have shown that asexual spores accumulate higher levels of GAs than mycelia in liquid static culture of *G. lucidum* (Zhang and Zhong, 2010; Sun et al., 2021). The results of this study suggest that the decreased GA concentration in the Δ*laeA* strain may be at least partially related to decreased accumulation of asexual spores.

Conclusion

In this study, the function of LaeA was investigated by gene deletion and overexpression in *G. lingzhi*. The results suggested that LaeA plays an important role in GA biosynthesis by regulating the expression of biosynthetic genes and asexual sporulation. These new insights help improve our understanding of the regulatory mechanisms of GA biosynthesis in *Ganoderma*.

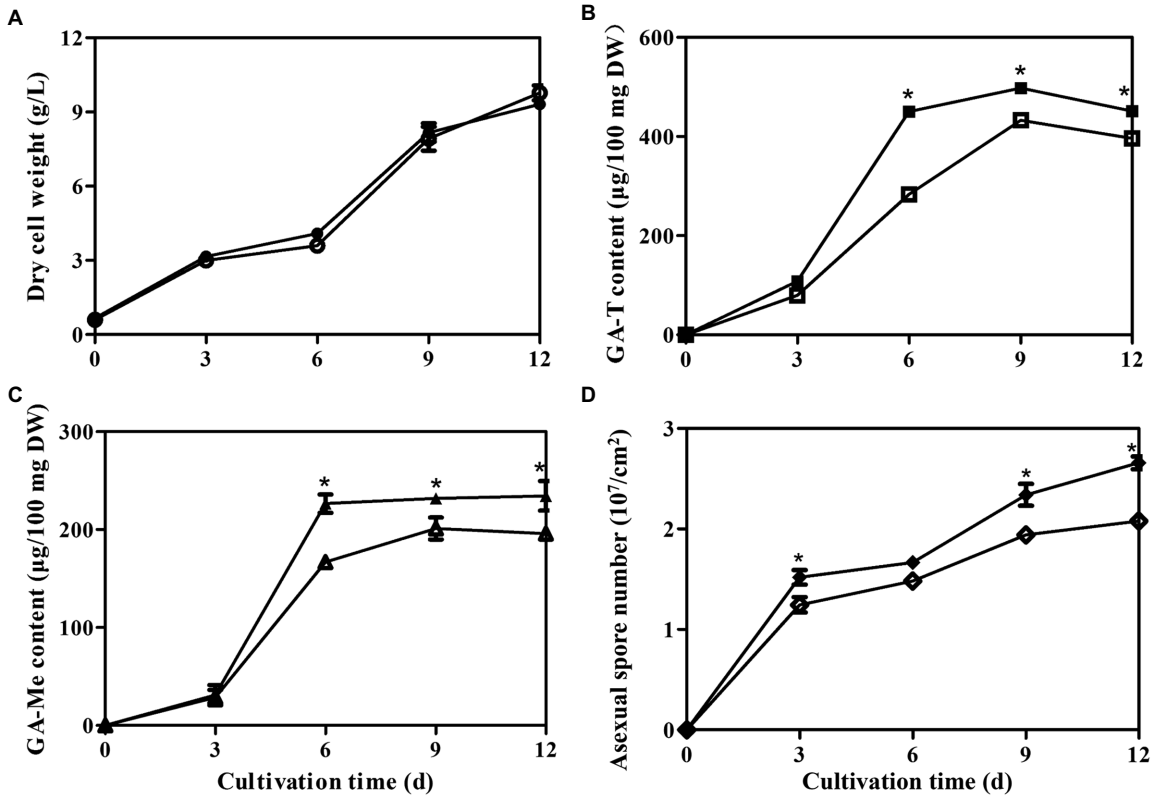

FIGURE 8
Temporal profiles of **(A)** mycelial growth, **(B)** Concentrations of GA-T and **(C)** GA-Me, and **(D)** asexual spore numbers in liquid static culture of wild-type *G. lingzhi* (open) and *laeA* overexpressing strains (filled).* significantly difference in values compared to the wild-type *G. lingzhi*.

Data availability statement

The original contributions presented in the study are included in the article/Supplementary material, further inquiries can be directed to the corresponding authors.

Author contributions

QL and NL: methodology, validation, investigation and writing—original draft preparation. J-WX: supervision, project administration, funding acquisition and writing—review and editing. All authors contributed to the article and approved the submitted version.

Funding

This work was financially supported by the National Natural Science Foundation of China (No. 81860668) and the Yunnan Applied Basic Research Project (No. 2018FB065). J-WX also thanks to the Yunnan 10,000 Talents Plan-Young and Elite Talents Project.

Conflict of interest

The authors declare that the research was conducted in the absence of any commercial or financial relationships that could be construed as a potential conflict of interest.

Publisher's note

All claims expressed in this article are solely those of the authors and do not necessarily represent those of their affiliated organizations, or those of the publisher, the editors and the reviewers. Any product that may be evaluated in this article, or claim that may be made by its manufacturer, is not guaranteed or endorsed by the publisher.

Supplementary material

The supplementary material for this article can be found online at: https://www.frontiersin.org/articles/10.3389/fmicb.2022.1025983/full#supplementary-material.

References

Aghcheh, R. K., Nemeth, Z., Atanasova, L., Fekete, E., Paholcsek, M., Sandor, E., et al. (2014). The VELVET a orthologue VEL1 of *Trichoderma reesei* regulates fungal development and is essential for cellulase gene expression. *PLoS One* 9, e112799. doi: 10.1371/journal.pone.0112799

Ahmad, M. F., Wahab, S., Ahmad, F. A., Ashraf, S. A., Abullais, S. S., and Saad, H. H. (2022). *Ganoderma lucidum*: a potential pleiotropic approach of ganoderic acids in health reinforcement and factors influencing their production. *Fungal Biol. Rev.* 39, 100–125. doi: 10.1016/j.fbr.2021.12.003

Bishop, K. S., Kao, C. H. J., Xu, Y., Glucina, M. P., Paterson, R. R. M., and Ferguson, L. R. (2015). From 2000 years of *Ganoderma lucidum* to recent developments in nutraceuticals. *Phytochemistry* 114, 56–65. doi: 10.1016/j.phytochem.2015.02.015

Bok, J. W., and Keller, N. P. (2004). LaeA, a regulator of secondary metabolism in *aspergillus* spp. *Eukaryot. Cell* 3, 527–535. doi: 10.1128/ec.3.2.527-535.2004

Butchko, R. A. E., Brown, D. W., Busman, M., Tudzynski, B., and Wiemann, P. (2012). Lae1 regulates expression of multiple secondary metabolite gene clusters in *fusarium verticillioides*. *Fungal Genet. Biol.* 49, 602–612. doi: 10.1016/j.fgb.2012.06.003

Chen, N. H., Liu, J. W., and Zhong, J. J. (2008). Ganoderic acid me inhibits tumor invasion through down-regulating matrix metalloproteinases 2/9 gene expression. *J. Pharmacol. Sci.* 108, 212–216. doi: 10.1254/jphs.SC0080019

Chen, S. L., Xu, J., Liu, C., Zhu, Y. J., Nelson, D. R., Zhou, S. G., et al. (2012). Genome sequence of the model medicinal mushroom *Ganoderma lucidum*. *Nat. Commun.* 3:913. doi: 10.1038/ncomms1923

Chettri, P., and Bradshaw, R. E. (2016). LaeA negatively regulates dothistromin production in the pine needle pathogen *Dothistroma septosporum*. *Fungal Genet. Biol.* 97, 24–32. doi: 10.1016/j.fgb.2016.11.001

Estiarte, N., Lawrence, C. B., Sanchis, V., Ramos, A. J., and Crespo-Sempere, A. (2016). LaeA and VeA are involved in growth morphology, asexual development, and mycotoxin production in *Alternaria alternata*. *Int. J. Food Microbiol.* 238, 153–164. doi: 10.1016/j.ijfoodmicro.2016.09.003

Fei, Y., Li, N., Zhang, D. H., and Xu, J. W. (2019). Increased production of ganoderic acids by overexpression of homologous farnesyl diphosphate synthase and kinetic modeling of ganoderic acid production in *Ganoderma lucidum*. *Microb. Cell Factories* 18:115. doi: 10.1186/s12934-019-1164-3

Hsu, K.-D., and Cheng, K.-C. (2018). From nutraceutical to clinical trial: frontiers in *Ganoderma* development. *Appl. Microbiol. Biotechnol.* 102, 9037–9051. doi: 10.1007/s00253-018-9326-5

Jain, S., and Keller, N. (2013). Insights to fungal biology through LaeA sleuthing. *Fungal Biol. Rev.* 27, 51–59. doi: 10.1016/j.fbr.2013.05.004

Kadooka, C., Nakamura, E., Mori, K., Okutsu, K., Yoshizaki, Y., Takamine, K., et al. (2020). LaeA controls citric acid production through regulation of the citrate exporter-encoding cexA gene in *aspergillus luchuensis* Mut. Kawachii. *Appl. Environ. Microbiol.* 86, e01950–19. doi: 10.1128/aem.01950-19

Kale, S. P., Milde, L., Trapp, M. K., Frisvad, J. C., Keller, N. P., and Bok, J. W. (2008). Requirement of LaeA for secondary metabolism and sclerotial production in *aspergillus flavus*. *Fungal Genet. Biol.* 45, 1422–1429. doi: 10.1016/j.fgb.2008.06.009

Kosalkova, K., Garcia-Estrada, C., Ullan, R. V., Godio, R. P., Feltrer, R., Teijeira, F., et al. (2009). The global regulator LaeA controls penicillin biosynthesis, pigmentation and sporulation, but not roquefortine C synthesis in *Penicillium chrysogenum*. *Biochimie* 91, 214–225. doi: 10.1016/j.biochi.2008.09.004

Kumar, S., Stecher, G., and Tamura, K. (2016). MEGA7: molecular evolutionary genetics analysis version 7.0 for bigger datasets. *Mol. Biol. Evol.* 33, 1870–1874. doi: 10.1093/molbev/msw054

Li, H. J., He, Y. L., Zhang, D. H., Yue, T. H., Jiang, L. X., Li, N., et al. (2016a). Enhancement of ganoderic acid production by constitutively expressing *Vitreoscilla* hemoglobin gene in *Ganoderma lucidum*. *J. Biotechnol.* 227, 35–40. doi: 10.1016/j.jbiotec.2016.04.017

Li, H. J., Zhang, D. H., Han, L. L., Yu, X. Y., Zhao, P., Li, T., et al. (2016b). Further improvement in ganoderic acid production in static liquid culture of *Ganoderma lucidum* by integrating nitrogen limitation and calcium ion addition. *Bioprocess Biosyst. Eng.* 39, 75–80. doi: 10.1007/s00449-015-1491-7

Liu, K., Sun, B., You, H., Tu, J. L., Yu, X. Y., Zhao, P., et al. (2020). Dual sgRNA-directed gene deletion in basidiomycete *Ganoderma lucidum* using the CRISPR/Cas9 system. *Microb. Biotechnol.* 13, 386–396. doi: 10.1111/1751-7915.13534

Liu, R., Zhu, T., Yang, T., Yang, Z. Y., Ren, A., Shi, L., et al. (2021). Nitric oxide regulates ganoderic acid biosynthesis by the S-nitrosylation of aconitase under heat stress in *Ganoderma lucidum*. *Environ. Microbiol.* 23, 682–695. doi: 10.1111/1462-2920.15109

Meng, L., Zhang, S. Y., Chen, B. Z., Bai, X. R., Li, Y. F., Yang, J., et al. (2021). The MADS-box transcription factor GlMADS1 regulates secondary metabolism in *Ganoderma lucidum*. *Mycologia* 113, 12–19. doi: 10.1080/00275514.2020.1810515

Ren, A., Shi, L., Zhu, J., Yu, H. S., Jiang, A. L., Zheng, H. H., et al. (2019). Shedding light on the mechanisms underlying the environmental regulation of secondary metabolite ganoderic acid in *Ganoderma lucidum* using physiological and genetic methods. *Fungal Genet. Biol.* 128, 43–48. doi: 10.1016/j.fgb.2019.03.009

Saghai-Maroof, M. A., Soliman, K. M., Jorgensen, R. A., and Allard, R. W. (1984). Ribosomal DNA spacer-length polymorphisms in barley Mendelian inheritance, chromosomal location, and population dynamics. *Proc. Natl. Acad. Sci. U.S.A.* 81, 8104–8108.

Sarikaya-Bayram, O., Palmer, J. M., Keller, N., Braus, G. H., and Bayram, O. (2015). One Juliet and four Romeos: VeA and its methyltransferases. *Front. Microbiol.* 6, 1. doi: 10.3389/fmicb.2015.00001

Shi, J.-C., Shi, W.-L., Zhou, Y.-R., Chen, X.-L., Zhang, Y.-Z., Zhang, X., et al. (2020). The putative methyltransferase TlLAE1 is involved in the regulation of peptaibols production in the biocontrol fungus *Trichoderma longibrachiatum* SMF2. *Front. Microbiol.* 11, 1267. doi: 10.3389/fmicb.2020.01267

Shi, L. A., Ren, A., Mu, D. S., and Zhao, M. W. (2010). Current progress in the study on biosynthesis and regulation of ganoderic acids. *Appl. Microbiol. Biotechnol.* 88, 1243–1251. doi: 10.1007/s00253-010-2871-1

Sun, B., You, H., and Xu, J. W. (2021). Enhancement of ganoderic acid production by promoting sporulation in a liquid static culture of *Ganoderma species*. *J. Biotechnol.* 328, 72–77. doi: 10.1016/j.jbiotec.2021.01.014

Takao, K., Akagi, Y., Tsuge, T., Harimoto, Y., Yamamoto, M., and Kodama, M. (2016). The global regulator LaeA controls biosynthesis of host-specific toxins, pathogenicity and development of *Alternaria alternata* pathotypes. *J. Gen. Plant Pathol.* 82, 121–131. doi: 10.1007/s10327-016-0656-9

Tang, W., Liu, H. W., Zhao, W. M., Wei, D. Z., and Zhong, J. J. (2006). Ganoderic acid T from *Ganoderma lucidum* mycelia induces mitochondria mediated apoptosis in lung cancer cells. *Life Sci.* 80, 205–211. doi: 10.1016/j.lfs.2006.09.001

Thompson, J. D., Gibson, T. J., and Higgins, D. G. (2002). Multiple sequence alignment using ClustalW and ClustalX. *Curr. Protoc. Bioinform.* 2, 2.3.1–2.3.22. doi: 10.1002/0471250953.bi0203s00

Tsunematsu, Y., Takanishi, J., Asai, S., Masuya, T., Nakazawa, T., and Watanabe, K. (2019). Genomic mushroom hunting decrypts coprinoferrin, a siderophore secondary metabolite vital to fungal cell development. *Org. Lett.* 21, 7582–7586. doi: 10.1021/acs.orglett.9b02861

Tu, J. L., Bai, X. Y., Xu, Y. L., Li, N., and Xu, J. W. (2021). Targeted gene insertion and replacement in the basidiomycete *Ganoderma lucidum* by inactivation of nonhomologous end joining using CRISPR/Cas9. *Appl. Environ. Microbiol.* 87:e0151021. doi: 10.1128/aem.01510-21

Wiemann, P., Brown, D. W., Kleigrewe, K., Bok, J. W., Keller, N. P., Humpf, H. U., et al. (2010). FfVel1 and FfLae1, components of a velvet-like complex in *fusarium fujikuroi*, affect differentiation, secondary metabolism and virulence. *Mol. Microbiol.* 77, 972–994. doi: 10.1111/j.1365-2958.2010.07263.x

Wu, F. L., Zhang, G., Ren, A., Dang, Z. H., Shi, L., Jiang, A. L., et al. (2016). The pH-responsive transcription factor PacC regulates mycelial growth, fruiting body development, and ganoderic acid biosynthesis in *Ganoderma lucidum*. *Mycologia* 108, 1104–1113. doi: 10.3852/16-079

Xu, J. W., Xu, N., and Zhong, J. J. (2012a). Enhancement of ganoderic acid accumulation by overexpression of an N-terminally truncated 3-hydroxy-3-methylglutaryl coenzyme a reductase gene in the basidiomycete *Ganoderma lucidum*. *Appl. Environ. Microbiol.* 78, 7968–7976. doi: 10.1128/aem.01263-12

Xu, J. W., Xu, Y. N., and Zhong, J. J. (2010a). Production of individual ganoderic acids and expression of biosynthetic genes in liquid static and shaking cultures of *Ganoderma lucidum*. *Appl. Microbiol. Biotechnol.* 85, 941–948. doi: 10.1007/s00253-009-2106-5

Xu, J. W., Yue, T. H., Yu, X. Y., Zhao, P., Li, T., and Li, N. (2019). Enhanced production of individual ganoderic acids by integrating *Vitreoscilla* haemoglobin expression and calcium ion induction in liquid static cultures of *Ganoderma lingzhi*. *Microb. Biotechnol.* 12, 1180–1187. doi: 10.1111/1751-7915.13381

Xu, J. W., Zhao, W., Xu, Y. N., and Zhong, J. J. (2012b). Isolation and analysis of differentially expressed genes during asexual sporulation in liquid static culture of *Ganoderma lucidum* by suppression subtractive hybridization. *Mol. Biol. Rep.* 39, 3603–3610. doi: 10.1007/s11033-011-1134-2

Xu, J. W., Zhao, W., and Zhong, J. J. (2010b). Biotechnological production and application of ganoderic acids. *Appl. Microbiol. Biotechnol.* 87, 457–466. doi: 10.1007/s00253-010-2576-5

Xu, J. W., and Zhong, J. J. (2015). Genetic engineering of *Ganoderma lucidum* for the efficient production of ganoderic acids. *Bioengineered* 6, 357–360. doi: 10.1080/21655979.2015.1119341

Xu, Y. N., and Zhong, J. J. (2012). Impacts of calcium signal transduction on the fermentation production of antitumor ganoderic acids by medicinal mushroom *Ganoderma lucidum*. *Biotechnol. Adv.* 30, 1301–1308. doi: 10.1016/j.biotechadv.2011.10.001

You, B. J., Tien, N., Lee, M. H., Bao, B. Y., Wu, Y. S., Hu, T. C., et al. (2017). Induction of apoptosis and ganoderic acid biosynthesis by cAMP signaling in *Ganoderma lucidum*. *Sci. Rep.* 7:318. doi: 10.1038/s41598-017-00281-x

Yu, X. Y., Ji, S. L., He, Y. L., Ren, M. F., and Xu, J. W. (2014). Development of an expression plasmid and its use in genetic manipulation of *Lingzhi* or *Reishi* medicinal mushroom, *Ganoderma lucidum* (higher basidiomycetes). *Int. J. Med. Mushrooms* 16, 161–168. doi: 10.1615/IntJMedMushr.v16.i2.60

Zhang, D. H., Li, N., Yu, X. Y., Zhao, P., Li, T., and Xu, J. W. (2017). Overexpression of the homologous lanosterol synthase gene in ganoderic acid biosynthesis in *Ganoderma lingzhi*. *Phytochemistry* 134, 46–53. doi: 10.1016/j.phytochem.2016.11.006

Zhang, W. X., and Zhong, J. J. (2010). Effect of oxygen concentration in gas phase on sporulation and individual ganoderic acids accumulation in liquid static culture of *Ganoderma lucidum*. *J. Biosci. Bioeng.* 109, 37–40. doi: 10.1016/j.jbiosc.2009.06.024

Zhang, X., Ren, A., Li, M. J., Cao, P. F., Chen, T. X., Zhang, G., et al. (2016). Heat stress modulates mycelium growth, heat shock protein expression, ganoderic acid biosynthesis, and hyphal branching of *Ganoderma lucidum* via cytosolic Ca^{2+}. *Appl. Environ. Microbiol.* 82, 4112–4125. doi: 10.1128/aem.01036-16

Zhao, W., Xu, J. W., and Zhong, J. J. (2011). Enhanced production of ganoderic acids in static liquid culture of *Ganoderma lucidum* under nitrogen-limiting conditions. *Bioresour. Technol.* 102, 8185–8190. doi: 10.1016/j.biortech.2011.06.043

Zhou, J. S., Ji, S. L., Ren, M. F., He, Y. L., Jing, X. R., and Xu, J. W. (2014). Enhanced accumulation of individual ganoderic acids in a submerged culture of *Ganoderma lucidum* by the overexpression of squalene synthase gene. *Biochem. Eng. J.* 90, 178–183. doi: 10.1016/j.bej.2014.06.008

Zhu, J., Sun, Z. H., Shi, D. K., Song, S. Q., Lian, L. D., Shi, L., et al. (2019). Dual functions of AreA, a GATA transcription factor, on influencing ganoderic acid biosynthesis in *Ganoderma lucidum*. *Environ. Microbiol.* 21, 4166–4179. doi: 10.1111/1462-2920.14769

frontiers | Frontiers in Microbiology

TYPE Original Research
PUBLISHED 26 October 2022
DOI 10.3389/fmicb.2022.972294

Check for updates

OPEN ACCESS

EDITED BY
Pinmei Wang,
Zhejiang University, China

REVIEWED BY
Zhaogeng Lu,
Yangzhou University, China
Jingwen Zhou,
Jiangnan University, China
Robert Coppock,
University of Alberta, Canada

*CORRESPONDENCE
Yili Liang
liangyili6@csu.edu.cn

†These authors have contributed equally to this work

SPECIALTY SECTION
This article was submitted to Microbial Physiology and Metabolism, a section of the journal Frontiers in Microbiology

RECEIVED 18 June 2022
ACCEPTED 06 October 2022
PUBLISHED 26 October 2022

CITATION
Wu X, Zou K, Liu X, Fu S, Zhang S, Duan Z, Zhou J and Liang Y (2022) The novel distribution of intracellular and extracellular flavonoids produced by *Aspergillus* sp. Gbtc 2, an endophytic fungus from *Ginkgo biloba* root.
Front. Microbiol. 13:972294.
doi: 10.3389/fmicb.2022.972294

COPYRIGHT
© 2022 Wu, Zou, Liu, Fu, Zhang, Duan, Zhou and Liang. This is an open-access article distributed under the terms of the Creative Commons Attribution License (CC BY). The use, distribution or reproduction in other forums is permitted, provided the original author(s) and the copyright owner(s) are credited and that the original publication in this journal is cited, in accordance with accepted academic practice. No use, distribution or reproduction is permitted which does not comply with these terms.

The novel distribution of intracellular and extracellular flavonoids produced by *Aspergillus* sp. Gbtc 2, an endophytic fungus from *Ginkgo biloba* root

Xinhong Wu[1,2†], Kai Zou[3†], Xueduan Liu[1,2], Shaodong Fu[1,2], Shuangfei Zhang[1,2], Zhenchun Duan[1,2], Jin Zhou[1,2] and Yili Liang[1,2*]

[1]School of Minerals Processing and Bioengineering, Central South University, Changsha, China, [2]Key Laboratory of Biometallurgy, Ministry of Education, Changsha, Hunan, China, [3]College of Advanced Materials Engineering, Jiaxing Nanhu University, Jiaxing, Zhejiang, China

Here, we reported a *Ginkgo* endophyte, *Aspergillus* sp. Gbtc 2, isolated from the root tissue. Its flavonoid biosynthesis pathway was reconstructed, the effect of phenylalanine on the production of flavonoids was explored, and the flavonoid metabolites were identified with the high-resolution Liquid chromatography–mass spectrometry (LC–MS). Some essential genes were annotated to form the upstream of the complete biosynthesis pathway, indicating that *Aspergillus* sp. Gbtc 2 has the ability to synthesize the C6–C3–C6 flavonoid monomers. HPLC results showed that adding an appropriate amount of phenylalanine could promote the production of flavonoids by *Aspergillus* Gbtc 2. LC–MS results depicted a significant difference in many flavonoids between intracellularly and extracellularly. Most of the flavonoids gathered in the cell contained glycosylation groups, while almost all components with multiple hydroxyls showed much higher concentrations extracellularly than intracellularly; they likely have different biological functions. A variety of these substances can be mapped back to the pathway pattern of flavonoid biosynthesis and prove the ability of flavonoid production once again. This study expanded the information on flavonoid biosynthesis in *Aspergillus* and provided a solid theoretical basis for developing the fungi into genetically engineered strains undertaking flavonoid industrialized production.

KEYWORDS

***Ginkgo biloba*, endophytic fungi, pathway, Liquid chromatography–tandem mass spectrometry, flavonoids**

Introduction

As a necessary traditional medicine, *Ginkgo* flavonoids can be used to treat cardiovascular and cerebrovascular disease, Alzheimer's disease, and other diseases (Eliana et al., 2013; Qian et al., 2016). However, the flavonoid content in *Ginkgo* extract is extremely low, which is challenging to meet the growing market demand (Isah, 2015). Due to the long-term co-evolution, plants and endophytic fungi may share some functional enzymes in the metabolic process (Teimoori-Boghsani et al., 2019; Wang H. et al., 2022). Endophytic fungi have been shown to indirectly or directly synthesize some intermediates of host plants (Jia et al., 2016; Ferreira et al., 2021), participating in plant signal pathways and assisting plants in completing physiological and biochemical processes (Shymanovich et al., 2015).

The taxol production provides a new direction for producing flavonoids by endophytic fungi (Cheng et al., 2018). In addition, endophytic fungi act as activators of plant host and synthesize active substances. A typical example is that *Aspergillus niger* could stimulate the rapid accumulation of taxol in the suspension cells of *Taxus* (Wang et al., 2001). In recent years, some studies on the metabolites of endophytic fungi in *Ginkgo biloba* have illustrated that *Penicillium* and *Mucor Circinelloides* SN2017 can produce flavonoids with anticancer and antioxidant activities (Trisuwan et al., 2010; Yuan et al., 2014; Ferreira et al., 2021). Moreover, in *Aspergillus niger* 13/5, substrate 7-hydroxyflavanone was transformed into 7-hydroxyflavone by dehydrogenase at C-2 and C-3 positions with a biotransformation rate up to 98% (Edyta and Tomasz, 2012). A variety of endophytic fungi also are isolated from *Ginkgo* and confirmed to have the ability to produce flavonoids (Qiu et al., 2010). It is reported that the flavonoid accumulation in suspension cells of *Ginkgo* can be induced by the abscisic acid (ABA) from fungal endophytes ((Hao et al., 2010)), which pushed us not to ignore the potential effect of endophytes in flavonoid synthesis and coevolution.

The flavonoid biosynthesis in plants mainly originates from the metabolic pathway of phenylalanine (Kazuki et al., 2013; Deng et al., 2021). Phenylalanine is catalyzed by phenylalanine ammonia-lyase (PLA) key enzymes to produce cinnamic acid, coumaroyl acid, and caffeoyl acid, and then, they are further catalyzed by 4-coumaric acid CoA ligase (4CL) enzymes to produce a variety of phenylalanine deamination derivatives, including cinnamoyl-CoA, p-coumaroyl-CoA, caffeoyl-CoA, and feruloyl-CoA. The upstream of this pathway mainly forms the basic C6-C3-C6 skeleton of flavonoids, which was transformed into a variety of chalcones by the chalcone synthase (CHS; Wang et al., 2020). Further, chalcones are condensed by chalcone isomerase (CHI) to form the parent structure of flavonoids. With flavone synthase (FNS), isoflavone synthase (IFS), flavonol synthase (FLS), and flavanone-3-hydroxylase (F3H), they are transformed into flavones, isoflavones, flavonols, and dihydroflavonols, respectively, (Xiaojia et al., 2017). In another branch of the pathway, dihydroflavonols are catalyzed by dihydroflavanol-4 reductase (DFR) to produce colorless anthocyanins, which are then catalyzed by anthocyanin synthase (ANS) and colorless anthocyanin reductase (LAR) to produce anthocyanins and flavones, respectively (Xie et al., 2003). Endophytic fungi and host plants symbiotically form a mutually beneficial relationship. In general, 4CL, CHS, CHI, and DFR were key functional enzymes for flavonoid biosynthesis in plants and endophytic fungi (Petit et al., 2007; Dao et al., 2011; Kaltenbach et al., 2018). At present, the biosynthetic pathway of flavonoids in plants has been clearly studied (Sajid et al., 2021). However, compared with higher host plants, endophytic fungi have the problem that some functional enzyme genes cannot be expressed. Therefore, the biosynthetic pathway of flavonoids in endophytic fungi was not necessarily the same as that in plants. The target product was still obtained by skipping the relevant enzymes in a certain pathway during flavonoid biosynthesis (Zang et al., 2019). In addition, the flavonoid biosynthesis pathway in plants becomes more complex due to the influence of various environmental factors, and this process may synthesize many by-products that are difficult to be controlled artificially (Pandey et al., 2016; Marsafari et al., 2020). Endophytic fungi are microorganisms, which have an advantage in reconstituting the biosynthetic pathway of flavonoids *in vitro* and controlling the reaction conditions accurately (Sajid et al., 2021). Moreover, microbial fermentation can form large-scale production in a short time, which is more suitable for industrial applications.

Extracting flavonoids directly from wild *Ginkgo* has the problems of long growth cycle, low extraction efficiency, high extraction cost, and non-renewable resources (Jiang et al., 2005). In this study, wild *Ginkgo* roots were sampled to isolate endophytes. Based on genomic analysis and metabolites identification, the flavonoid biosynthesis pathway of *Aspergillus* sp. Gbtc 2 was predicted and reconstructed. The intracellular and extracellular flavonoid products of *Aspergillus* sp. Gbtc 2 were detected and analyzed by Liquid Chromatography–Tandem Mass Spectrometry (LC–MS). At the same time, the effect of a certain amount of phenylalanine on the flavonoid synthesis of *Aspergillus* sp. Gbtc 2 was explored. Therefore, if *Ginkgo* flavonoids' microbial source is reliable, it is expected to produce *Ginkgo* flavonoids through *Aspergillus* sp. Gbtc 2 fermentation. This method can significantly increase the yield of *Ginkgo* flavonoids and protect the resources of *Ginkgo*, so as to provide a theoretical basis for the subsequent industrialization of flavonoid synthesis by genetic engineering fungi.

Materials and methods

Endophytes isolation and genome extraction

The endophytic fungus was isolated from the root tissue of wild *Ginkgo biloba*, which grew in Linyi City, Shandong Province, China. The detailed location was 34°36′34″ N, 118°12′8″ E with an altitude of 40 m. On October 13, 2019, the

healthy wild *Ginkgo* tree with the largest DBH (0.64 m) in this area was chosen to collect the root materials. Evenly located around the tree, three locations were selected to collect the samples. Several root tissues of 2 cm diameter were cut off from the part of the tree, which was 1.5 m horizontally away for the trunk and 1 m deep underground. Then mixed to make a composite sample, which was used for endophyte isolation after strict surface disinfection. The specific surface disinfection methods were as follows: a. the rhizosphere soil and other attachments were completely removed by the brush and thoroughly washed with water; b. the samples were rinsed successively with 70% ethanol for 2 min, 5.25% sodium hypochlorite for 4 min, and sterile distilled water for 5 times; and c. the last eluent was used as a blank control for the verification experiment of thorough surface disinfection. Endophytic fungus was cultured on the Potato Dextrose Agar (PDA) medium at 25°C for 7–10 days. Hexadecyl Trimethyl Ammonium Bromide (CTAB) was chosen to extract the genomic DNA. Approximate 200 mg of fungal mycelia were homogenized and pestled with liquid nitrogen, successively followed by DNA extraction and purification as per the manufacturer's recommendations. The concentration and purity were determined on a NanoDrop ND-1000 spectrophotometer (NanoDrop Technologies, Wilmington, United States). 1% (*w*/*v*) TAE-agarose gel stained with Elution Buffer (EB) was also used to detect DNA quality (Lei et al., 2021). A total of two DNA samples were extracted, one for BGISEQ-500 sequencing and the other for Pacbio Sequel sequencing. The 18S rRNA sequences of fungi and the similar sequences aligned with them in Genebank were analyzed by ClustalW (Juárez-Hernández et al., 2021). The method was neighbor-joining (NJ), the model was Kimura 2-parameter model, and the phylogenetic tree was constructed with MEGA X (Kumar et al., 2018). Bootstrap support was shown for cases in which the value was greater than 50% based on 1,000 replications.

Library construction and sequencing

The pair-ended sequencing library was built as follows: (a) 1 μg DNA samples were fragmented in Covaris M220 focused ultrasonicator (Covaris, Inc.); (b) magnetic beads were used to screen DNA fragments with the size of 200 ~ 400 bp; (c) Qbit 2.0 was used to quantify the genomic libraries after screening and purification; (d) the DNA end was repaired with adding base A at the 3′ end; (e) the adapter sequence was stably connected to the DNA at a specific temperature; (f) DNA was further purified by magnetic beads, and then dissolved in EB; and (g) the fragment size of the library was confirmed by Agilent 2,100 Bioanalyzer instrument. To obtain more accurate genomes, another 20 μg DNA extracts were subjected to DNA interruption, terminal repair, linker sequence connection, fragment purification, primer hybridization, and polymerase binding, and finally determined as the library for single-molecule sequencing. Pair-ended sequencing was completed on the BGISEQ-500 platform (BGI, Shenzhen, China), and single-molecule sequencing was completed on the Pacbio Sequel platform.

Genome assembly and functional annotation

Clean data were obtained by removing the adapter, ploy-N, and low-quality reads from raw data. The genomic assembly was accomplished in Canu (v1.9) using the single-molecule sequencing data (Koren et al., 2017), and then corrected with the pair-ended clean reads in NextPolish (v1.0.5; Hu et al., 2020). After that, BUSCO (V4.1.2) was employed to evaluate the assembly quality (Simão et al., 2015). GeneMark-ES (v4.48_3.60_lic) was run to predict the gene composition (Sayers et al., 2022), and the obtained CDS sequences were functionally annotated according to the universal database resources. The diamond (v2.0.4) program was used to do blasting against the NR database (Buchfink et al., 2015). KAAS system was used for annotation and pathway mapping (Moriya et al., 2007), with the default e-value 1E-6. The COG classification of all predicted amino acid sequences was analyzed in the eggnog-mapper (Huerta-Cepas et al., 2017, 2019). Subsequently, the metabolic pathway was reconstructed in iPath3 (Darzi et al., 2018).

Liquid chromatography–tandem mass spectrometry sample preparation

The LC–MS samples were prepared by Potato Dextrose Broth (PDB) liquid culture method. The mycelium and spores were scraped from the surface of the medium by a sterile blade and suspended in a centrifuge tube. 10 μl suspension (~ 10^6 cells/ml) was inoculated into 500 ml sterile PDB. After inoculation, all liquid media were placed in a shaking incubator at 140 rpm at 25°C for 14 days. Four biological replicates were set up in this experiment, one of which was used to prepare QC samples. The blank control group was set synchronously to filter the bottom noise during LC–MS detection. Three biological repetitions were filtered with sterile gauze and the mycelium was separated from the culture medium. The mycelium and culture medium were put into BLK-FD-0.5 Vacuum Freeze Dryer (Jiangsu Bolike Refrigeration Technology, Changzhou, Jiangsu) for freeze-drying. The freeze-dried samples were ground at −4°C for 15 min by a grinding instrument with a power set to 30 Hz. Then, the sample was collected in a centrifuge tube and added 100 ml of 70% methanol. The QC sample was a mixture of mycelium and culture medium and followed the same experimental treatment. The blank control was directly freeze-dried from the blank medium, and the follow-up operation was the same as the three biological replicates. All the samples added with methanol were extracted overnight at 4°C, during which they were whirled three times. 1.0 ml of mycelium extract

(intracellular metabolites), culture medium extract (extracellular metabolites), blank sample extract, and QC extract were put into the centrifuge tube. The sample was centrifuged for 15 min at 10000 × *g* within 4°C temperature control. The supernatant was filtered through a 0.22 μm membrane before LC–MS analysis. In this experiment, substances in mycelium were defined as intracellular flavonoid metabolites, while substances secreted into culture medium were defined as extracellular flavonoid metabolites.

Liquid chromatography–tandem mass spectrometry conditions

Chromatographic separation was carried out on Shim-pack UFLC SHIMADZU CBM30A liquid chromatographic system (Shimadzu, Duisburg, Germany) equipped with a Water ACQUITY UPLC HSS T3 C18 column (1.8 μm, 2.1 mm * 100 mm) at 35°C. A flow rate of 0.4 ml/min was chosen to use while 0.04% acetic water (A) and Acetonitrile (B) with 0.04% acetic acid comprised the mobile phase. Gradient elution program was optimized as follows: 0 ~ 11.0 min, 5% → 95% B; 11.0 ~ 12.0 min, 95% → 95% B; 12.0 ~ 12.1 min, 95% → 5% B; 12.1 ~ 15.0 min, and 5% → 5% B. The injection volume was 5 μl. MS was carried out on an Applied Biosystems 4,500 QTRAP system (AB SCIEX Technologies, United States), equipped with electrospray ionization (ESI) and UHPLC system to scan 100 to 1,500 molecular weight parent ions at 550°C. Other MS parameters were set as follows: MS voltage: 5,500 V; curtain gas (CUR): 25 psi; collision-activated dissociation (CAD): high; declustering potential (DP) and collision energy (CE): specific optimization (Chen et al., 2013).

Liquid chromatography–tandem mass spectrometry quality control and flavonoid identification

The raw data output from LC–MS was pretreated by Analyst 1.6.1 (AB SCIEX Technologies, United States; Chen et al., 2009), including peak recognition, alignment, calibration of the internal standard, filtering, and normalization to total area. Analyst 1.6.1 (AB SCIEX Technologies, United States) was also used to visualize the target components in a two-stage mass-to-charge ratio map as recommended. The repeatability of metabolite extraction and instrument detection can be judged by analyzing the overlap of mass spectrometry total ion chromatograms (TIC diagram). Based on the local MWDB database (Wuhan Metware Biotechnology Co., Ltd., Wuhan, Hubei) and metabolic public databases, like MassBank (Horai et al., 2010), KNAPSAcK (Sur et al., 2022), HMDB (Wishart et al., 2018), METLIN (Domingo-Almenara et al., 2018), and so on, the components were identified based on fragment ion information.

HPLC sample preparation

Hundred ml sterile PDB liquid medium was set as the blank control group. The samples with 0.0 mg/ml, 1.0 g/l, 2.0 g/l, 5.0 g/l, and 10.0 g/l exogenous phenylalanine were set as the experimental group. Three replicates were set in the blank control and experimental groups. In this experiment, the total flavonoids in the whole fermentation broth were determined, and the mycelium and culture medium were not separated. The methods of inoculation, culture, freeze-drying, and extraction were the same as described in "Liquid chromatography–tandem mass spectrometry sample preparation".

Accurately weigh 10 mg quercetin, 20 mg kaempferol, and 10 mg isorhamnetin, and three standards were mixed. The standard stock solution was obtained by using 25 ml of methanol at constant volume. The standard stock solution was diluted to 2×, 5×, 10×, 25×, and 50× to prepare the standard curve. After determination by HPLC, the peak areas (X) of quercetin, kaempferol, and isorhamnetin were substituted into the standard curve formula to obtain the corresponding flavone concentrations, which were expressed in Q, K, and I respectively, so as to calculate the flavone content of each sample. The formula was as follows: C = 2.51Q + 2.64 K + 2.39I.

The supernatant was filtered through a 0.22 μm membrane before HPLC analysis. Analysis was carried out using an LC-20AT liquid chromatographic system (Shimadzu, Japan). HPLC separations were accomplished on a 5.0 um, 150 mm * 6.0 mm Shimadzu ODS C18 column (Shimadzu, Japan) at 35°C. A flow rate of 1.0 ml/min was chosen to use while 0.04% acetic water (A) and Acetonitrile (B) with 0.04% acetic acid comprised the mobile phase. The optimized gradient elution program was the same as described in "Liquid chromatography–tandem mass spectrometry sample preparation". The injection volume was 10 μl. A wavelength of 360 nm was selected for quantification.

Results

Strain identification

After the last elution solution was coated on the culture medium, the growth of sterile colony showed that the surface was completely disinfected. The endophytic fungus was isolated from the root of *Ginkgo* and named *Aspergillus* sp. Gbtc 2. According to the BLASTN result of the 18S rRNA region, Gbtc 2 is the most similar to *Aspergillus flavus* (98%). The phylogenetic tree was built in Figure 1 based on 34 18S rRNA sequences (the accession numbers of 33 reference sequences were shown in Supplementary Table S1) by the neighbor-joining (NJ) method in MEGA X. Combined with phylogenetic analysis and sequence homology, the strain Gbtc 2 was identified as *Aspergillus flavus*. However, through KEGG and NR database annotation, no gene related to aflatoxins synthesis was found in *Aspergillus* sp. Gbtc 2.

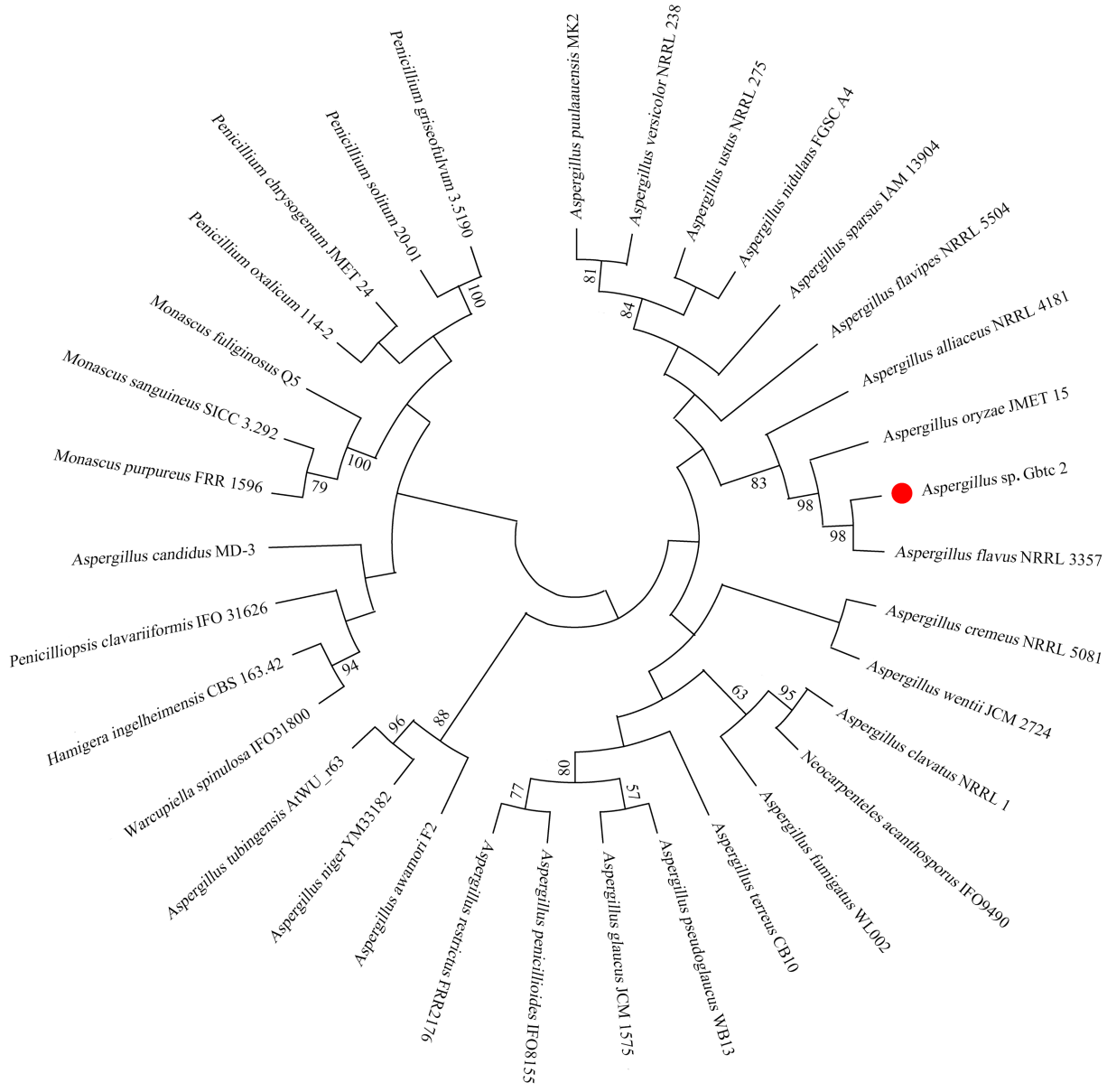

FIGURE 1
Molecular phylogenetic analysis of fungal isolates. The numbers at the nodes indicate the levels of bootstrap support based on Kimura distance and the neighbor-joining method. Bootstrap support was shown for cases in which the value was greater than 50% based on 1,000 replications.

Sequencing, assembly, and functional annotation

As the detailed information listed in Table 1, a total of 34,022,048 clean reads (BGISEQ-500, PE150) were obtained to include 5,097,121,946 clean bases for Gbtc 2, and its Q20 was 96.58%. Considering that fungi generally have a larger genome than bacteria, the introduction of the Single Molecule, Real-Time (SMRT) Sequencing technology was necessary to improve the assembly quality. Here, next polished with the pair-ended PE150 reads, the Pacbio Sequel output was assembled into the high-quality draft genome of Gbtc 2 (16 contigs). Gbtc 2 had a genome of 37,929,866 bp with an N50 of 4,075,796 bp. The G + C content was 47.45%, similar to the strains in the GeneBank database. On the other hand, the protein sequences of the model strain homologous to Gbtc 2 were selected for BUSCO evaluation, and the accession numbers were XP_043133698.1 (*Aspergillus chevalieri*), XP_041140511.1 (*Aspergillus flavus* NRRL3357), XP_748963.1 (*Aspergillus fumigatus* Af293), XP_041544984.1 (*Aspergillus luchuensis*), XP_001821344.1 (*Aspergillus oryzae* RIB40), and XP_041556067.1 (*Aspergillus puulaauensis*), respectively. The BUSCO held 74.5% integrity assessment, indicating that the genome assembly results were acceptable (Supplementary Figure S1).

TABLE 1 The statistics of gene assembly and function annotation.

Attributes	Characteristic
Clean reads	34,022,048
Clean base	5,097,121,946
Q20(%)	96.58
Scaffolds	16
N50	4,075,796
Total base	37,929,866
GC content (%)	47.45
CDS	13,307
rRNA genes	68
tRNA genes	290
Genes assigned to KEGG	3,902
Genes assigned to NR	13,216
Genes assigned to COG/KOG	10,739
All[1]	3,899
At least one[2]	13,216
Percentage[3] (%)	99.32

A total of 13,307 CDSs, as well as 68 rRNA and 290 tRNA genes, were predicted in the genome. Of these, 3,902 CDSs were successfully annotated in KEGG database, while 10,739 sequences in COG/KOG database and 13,216 sequences in NR database. Commonly, the NR database depicted the highest annotation rate. The global annotation rate of this fungus reached 99.32% (Table 1).

The datasets presented in this study can be viewed in online repositories. The names of the repository/repositories and accession number can be found at: https://www.ncbi.nlm.nih.gov/bioproject/PRJNA870667.

Reconstruction of Gbtc 2 flavonoid metabolic pathway

The anabolism of flavonoids generally exists in most plants. It was the primary way for plants to resist excessive ultraviolet radiation and oxidative damage (Sun et al., 2020). At the same time, flavonoids also have a particular ability to resist diseases and pests (Erb and Kliebenstein, 2020; Singh et al., 2021). Here, we reconstructed the flavonoid biosynthetic pathway of Gbtc 2 according to the model of flavonoids in plants, although it may not be suitable for endophytic fungi. As shown in Figure 2, Gbtc 2 has almost the complete upstream of flavonoid synthesis to form the basic C6–C3–C6 flavonoid monomer. In the KEGG database, the coding genes corresponding to PAL, 4CL, and CHS were annotated. Under the catalysis of CHS, cinnamoyl-CoA, p-coumaroyl-CoA, caffeoyl-CoA, and feruloyl-CoA were converted to pinocembrin chalcone, naringenin chalcone, eriodictyol chalcone, and homoeriodictyol chalcone, respectively. Since no gene related to TAL was annotated in the sequencing results, it is indicated that Gbtc 2 may have the ability to synthesize chalcone from phenylalanine. Secondly, when comparing the sequences of unknown functions in the NR database, multiple downstream functional enzyme genes were found to be related to the synthesis and derivation of flavonoids, such as *CHI*, *F3H*, colorless anthocyanin oxygenase gene (*LDOX*), and flavonoid-3′-monooxygenase gene (*F3′M*) (Enzyme genes with gene_ID involved in flavonoid metabolism pathway in *Aspergillus* sp. Gbtc 2 were listed in Supplementary Table S2). Of them, CHI was responsible for converting various chalcone into flavonoid monomers, such as pinocembrin, liquiritigenin, butin, and naringenin, while F3H catalyzes these flavonoid monomers into dihydroflavonols. Notably, the genes encoding flavonoid 3′-monooxygenase (F3′M) have been successfully annotated in the assembly (Figure 2), which will lead to frequent synergistic transformations between flavonoid compounds, such as from kaempferol to quercetin. In conclusion, Gbtc 2 can be considered to have the potential to synthesize flavonoids independently, which points out the direction for metabolic detection and identification.

Analysis of flavonoid metabolites

After filtering the blank control signal, there were relatively many kinds of metabolites in the sample. The positive ion and negative ion modes reflected the reliability of sample preparation and LC–MS detection (Supplementary Figure S2A). In the multi-peak diagram of MRM metabolite detection in multi-reaction monitoring mode, the samples seen in positive ion and negative ion modes are displayed, and the peaks of different colors represent different metabolites (Supplementary Figure S2B). A total of 71 flavonoids were identified based on the local and public databases, including 13 flavones, 4 isoflavones, 18 flavonols, 8 flavanones, 14 C-glycosyl flavonoids, 12 anthocyanins, and 2 procyanidins. Table 2 shows the top 30 substances in the signal intensity of flavonoids in Gbtc 2 mycelium and culture medium under the same conditions. The signal intensity of other flavonoids is listed in Supplementary Table S3. According to the descending order of total signal intensity, cyanin, afzelechin, dihydromyricetin, kaempferol 3-O-glucoside, di-O-methylquercetin, genistein, trifolin, and 4′-hydroxy-5,7-dimethoxyflavanone had higher total signal intensity. While components with weaker signal strength may be affected by detection conditions, there is no doubt that elements with higher signal strength really exist.

The identification results of metabolites were added to the flavonoid metabolic pathway in "Reconstruction of Gbtc 2 flavonoid metabolic pathway" for joint mapping. As shown in Figures 2, a total of 13 metabolites were mapped into the existing flavonoid synthesis pathway, including dihydromyricetin, dihydrokaempferol, taxifolin, quercetin, myricetin, and afzelechin, etc. These metabolites play essential roles in flavonoid synthesis, proving that the existing plant-based flavonoid biosynthesis model may also be applicable to Gbtc 2.

In addition, the relative concentrations of different flavonoids were quite different in intracellular and extracellular. Based on the

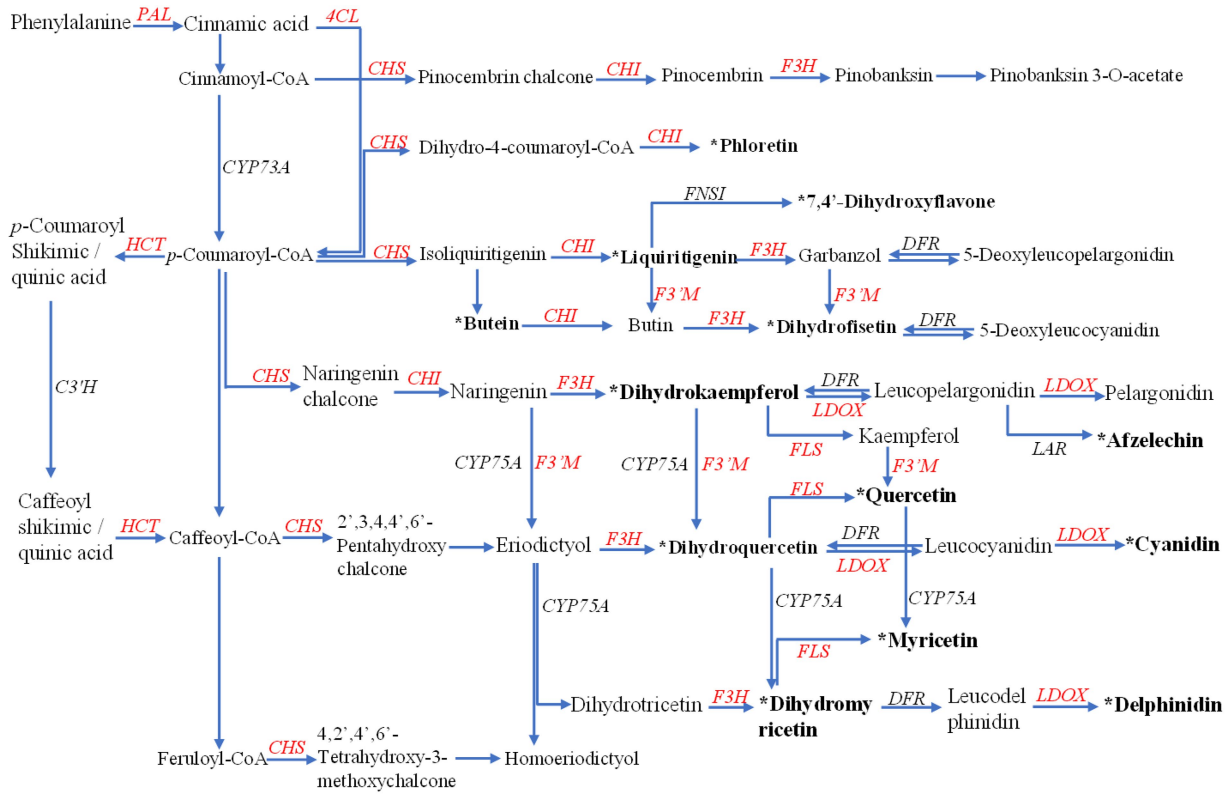

FIGURE 2
The remodeling of the flavonoid metabolism pathway in *Aspergillus* sp. Gbtc 2. The enzymes annotated in Gbtc 2's genome are marked in red, including phenylalanine ammonia-lyase (PAL), shikimate O-hydroxycinnamoyltransferase (HTC), 4-coumarate: CoA ligase (4CL), chalcone synthase (CHS), chalcone isomerase (CHI), flavanone 3-hydroxylase (F3H), flavonoid 3'-monooxygenase (F3'M), flavonol synthase (FLS), and leucoanthocyanidin dioxygenase (LDOX); while the unannotated in black, including trans-cinnamate 4-monooxygenase (CYP73A), 5-O-(4-coumaroyl)-D-quinate 3'-monooxygenase (C3'H), flavonoid 3',5'-hydroxylase (CYP75A), flavone synthase I (FNS I), dihydroflavonol 4-reductase (DFR), and leucoanthocyanidin reductase (LAR). The flavonoids identified in the metabolites of Gbtc 2 are shown in bold black text with an asterisk.

logarithm of the ratio (log_2FC) of metabolites' intracellular and extracellular ion signal intensity, 20 metabolites with the highest difference in intracellular and extracellular concentrations are shown in Figure 3. The results showed that genistein, orobol, baicalein, quercetin, apigenin O-malonylhexoside, rhamnetin, taxifolin, and other metabolites were much higher extracellularly than intracellularly. Meanwhile, astragalin, trifolin, cynaroside, liquiritigenin, chrysoeriol-7-O-rutinoside, isovitexin, phloretin, kaempferol-3-O-rhamnoside, kaempferin, spiraeoside, and other metabolites mainly accumulated intracellularly. Moreover, most of the flavonoids gathered intracellular contain glycosylation groups, such as astragalin, trifolin, cynaroside, kaempferol, etc., while almost all metabolites with much higher concentration extracellular than intracellular were flavonoid monomers with multiple hydroxyls.

Effects of phenylalanine on total flavonoids

According to the relationship between peak area (X) and concentration (Q, K, I) of quercetin, kaempferol, and isorhamnetin, the standard curve was $Q = 2.5072 \times 10^{-7} \times X + 2.9841 \times 10^{-4}$ ($R^2 = 0.9981$), $K = 1.9469 \times 10^{-7} \times X + 3.1478 \times 10^{-4}$ ($R^2 = 0.9987$) and $I = 1.2007 \times 10^{-7} \times X + 3.2847 \times 10^{-4}$ ($R^2 = 0.9989$). The concentrations of quercetin, kaempferol, and isorhamnetin in samples were determined by HPLC to calculate the concentration of total flavonoids in each sample (Supplementary Figure S3). Since isorhamnetin was not detected in all samples, it was not counted in Supplementary Table S4.

PDB medium was widely used to culture fungi. In this experiment, Gbtc 2 was screened out on PDA medium, and Gbtc 2 was verified to grow well on the PDB medium. Since the main component of PDB medium contains higher plant potato, the flavonoid content compounds in the blank PDB medium were tested to compare the flavonoid content in the fermentation broth cultured with Gbtc 2. It was verified that Gbtc 2 indeed has the ability to produce flavonoids. However, we did not choose *Ginkgo biloba* as the experimental materials, because *Ginkgo biloba* tissue also contains a large number of other active substances, and its components are more complex than PDB medium. In addition, *Ginkgo biloba* tissue also contains some toxic substances, such as ginkgolic acid, which are very likely to have adverse effects on the growth of Gbtc 2.

10.3389/fmicb.2022.972294

TABLE 2 The qualitative and relative quantitative table of flavonoids.

Rt (min)	Mr (Da)	Ionization mode	Compounds	Class	Culture medium	Mycelium
2.26	611	Protonated	Cyanin	F	1.51E+06	2.26E+05
3.29	274.084	[M–H]–	Afzelechin	D	1.14E+06	1.74E+05
3.36	320.053	[M–H]–	Dihydromyricetin	B	4.34E+05	1.28E+05
4.03	448.101	[M–H]–	Kaempferol 3-O-glucoside	B	9.00E+00	5.22E+05
5.76	330.1	[M–H]–	Di-O-methylquercetin	B	5.03E+04	4.45E+05
5.45	270.053	[M + H]+	Genistein	C	4.47E+05	9.00E+00
3.86	448.101	[M–H]–	Trifolin	B	9.00E+00	4.44E+05
6.58	300.1	[M–H]–	4′-Hydroxy-5,7-dimethoxyflavanone	D	6.68E+04	3.63E+05
3.05	474.1	[M–H]–	Pelargonidin O-acetylhexoside	F	1.92E+05	6.32E+04
3.7	448.101	[M–H]–	Cynaroside	A	9.00E+00	2.47E+05
4.83	286.048	[M + H]+	Orobol	C	2.11E+05	9.00E+00
3.05	948.1	[M + H]+	C-hexosyl-luteolin O-feruloyl-hexosyl-hexoside	E	1.36E+05	4.98E+04
2.94	756.1	[M + H]+	6-C-hexosyl-apigenin O-hexosyl-O-hexoside	E	1.15E+05	3.07E+04
4.43	288.063	[M–H]–	Dihydrokaempferol	B	9.47E+04	1.88E+03
4.87	256.074	[M–H]–	Liquiritigenin	D	9.00E+00	9.50E+04
2.87	548.1	[M–H]–	Peonidin O-malonylhexoside	F	4.12E+04	4.48E+04
6.84	402.132	[M + H]+	Nobiletin	A	2.13E+04	6.42E+04
3.93	608.4	[M + H]+	Chrysoeriol 7-O-rutinoside	A	9.00E+00	8.28E+04
3.99	610.19	[M–H]–	Hesperidin	D	4.54E+03	7.82E+04
3.61	432.1056	[M–H]–	Isovitexin	E	9.00E+00	8.11E+04
2.9	303.24	Protonated	Delphinidin	F	4.69E+04	3.16E+04
2.45	449.1	Protonated	Cyanidin 3-O-glucoside	F	3.60E+04	2.74E+04
7.32	372.121	[M + H]+	Tangeretin	A	1.75E+04	4.58E+04
4.09	610.19	[M + H]+	Neohesperidin	D	1.46E+04	4.81E+04
3.7	594.159	[M–H]–	Biorobin	B	6.63E+03	5.28E+04
4.39	318.038	[M + H]+	Myricetin	B	4.83E+04	1.18E+03
5.34	274.084	[M–H]–	Phloretin	D	9.00E+00	4.70E+04
4.37	270.053	[M–H]–	2′-Hydroxydaidzein	C	3.11E+04	1.18E+04
5.8	270.053	[M–H]–	Baicalein	A	4.21E+04	9.00E+00
3.51	610.153	[M + H]+	Rutin	B	3.37E+03	3.77E+04

A. Flavone; B. Flavonol; C. Isoflavone; D. Flavanones; E. Flavone C-glycosides; F. Anthocyanins.

In PDB blank medium (CK), quercetin accounted for the vast majority of total flavonoids, while kaempferol and isorhamnetin were almost absent (Supplementary Figure S4), and the contents of quercetin, kaempferol, and total flavonoids were 16.2672, 0.0121, and 40.8627 μg/ml, respectively. However, after inoculation with Gbtc 2, the contents of quercetin, kaempferol, and total flavonoids were significantly increased (Supplementary Figure S5), and the contents of quercetin, kaempferol, and total flavonoids were 68.1733, 10.6600, and 199.2575 μg/ml, respectively. At the same time, the addition of phenylalanine in PDB was 1.0 and 2.0 g/l, which greatly promoted the production of quercetin, thus increasing the yield of flavonoids. When the amount of phenylalanine was 2.0 g/l, the contents of quercetin, kaempferol, and total flavonoids reached the highest, 176.6467, 15.4267, and 484.1095 μg/ml, respectively. It shows that Gbtc 2 can make good use of phenylalanine to accumulate a large amount of coumaric acid, so as to metabolize and produce more flavonoids. However, when the amount of exogenous phenylalanine was 5.0 and 10.0 g/l, the content of total flavonoids in the fermentation broth was not significantly different from that of the total flavonoids without exogenous phenylalanine, and even its content was lower than that of the control group without phenylalanine. The experimental results show that adding a certain concentration of phenylalanine can promote the flavonoid yield of Gbtc 2, but adding excessive phenylalanine may inhibit the production of flavonoids by Gbtc 2 (Figure 4).

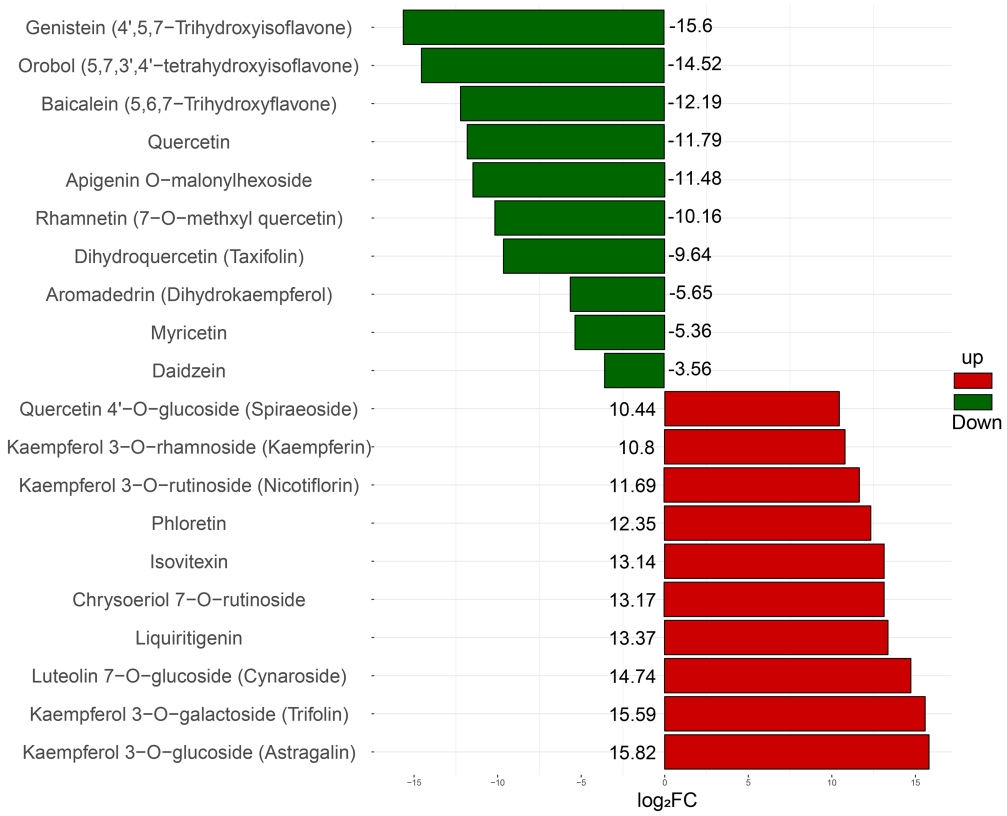

FIGURE 3
The relative concentration difference of intracellular and extracellular flavonoid metabolites. FC represents the ratio of the ion signal intensity of intracellular flavonoid metabolites to the ion signal intensity of extracellular flavonoid metabolites. The up-regulated metabolites were relatively large amounts of intracellular aggregation, while the downregulated metabolites were relatively large amounts of extracellular aggregation.

Discussion

Gbtc 2 and *ginkgo* root may share the secondary metabolic pathways of flavonoids

For a long time, the symbiosis and evolution of endophytic fungi and plant hosts have established a special relationship closely related to the production of active metabolites in plants (Toghueo, 2020). The *Ginkgo* host has a complete MEP pathway to synthesize IPP and DMAPP, while the IDI gene was only identified in the multiple isolates, indicating that these endophytic fungi may play a key role in regulating the mutual transformation of these two components (Liu et al., 2022). If the MEP pathway of *Ginkgo* comes from an endosymbiotic prokaryote as widely accepted, the MVK gene involved in the original MVA pathway of *Ginkgo* may have a non-highly-homologous replaceable copy, or it may be compensated by endophytes due to a long-term symbiotic relationship, like *Cellulomonas* sp. Gbtc_1 (Zou et al., 2021). Endophytic fungi were the production source of many known or unknown new bioactive metabolites (Queiroz and Santana, 2020; Aftab et al., 2021; Bezerra et al., 2021). In the study of *Aspergillus oryzae*, a complete phenylalanine flavonoid metabolic pathway with *CHS*-like genes as the core was found, and the functional enzymes in the pathway were also verified (Juvvadi et al., 2005). Moreover, information exchanged between *Ginkgo* and endophytes may be carried out through LTR-RT genetic elements. *Streptomyces* sp. Gbtc 1 was also shown to contain genes for key functional enzymes in synthesis pathway of natural products and local secondary metabolites similar to *Ginkgo* host (Zou et al., 2021). *Mucor circinelloides* DF20 has been reported to promote biosynthesis and accumulation of tanshinone in *Salvia miltiorrhiza* (Chen et al., 2021). The ability of Gbtc 2 to promote host flavonoid synthesis was inferred after comparing the Gbtc 2 genome to the published *Ginkgo* genome. Furthermore, potential functional complementarity, substitution, and genetic evolution exist between Gbtc 2 and host *Ginkgo*.

So far, few bacteria have been observed to possess PAL, 4CL, and CHS, which reflects that it was difficult for bacteria to produce chalcone directly (Moore et al., 2002). Gbtc 2 has the potential to produce chalcones because it carries these three genes at the same time. *CHI* homologous genes commonly exist in some fungi, myxomycetes, and γ-proteus. But microbes with *CHI* genes generally lack the upstream *CHS* homolog (Gensheimer and Mushegian, 2004), and our results supplement the lack of information in this regard. Endophytic fungi can produce new

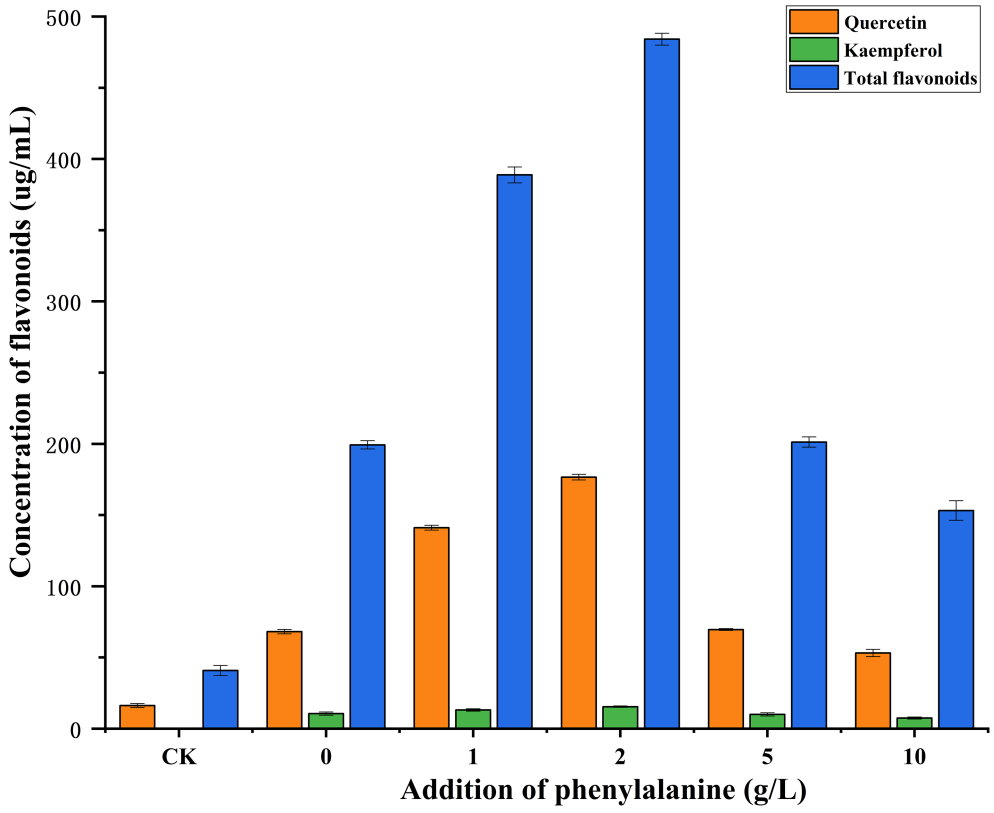

FIGURE 4
Comparison of flavonoid content between phenylalanine added/non-phenylalanine added treatment and PDB blank control group. CK stands for PDB blank control group; 0, 1, 2, 5, and 10 represent the amount of phenylalanine.

flavonols or metabolize glycosyl flavonoids into glycosyl flavonoid aglycones (Yan et al., 2013), and further participate in the flavonoid metabolism of plant hosts (Yuan et al., 2014). In this study, Gbtc 2 may derive downstream flavonoids by adding hydroxyl groups. Considering that most flavonoids, lignin, lignans, and hydroxycinnamic acid are synthesized from the same substrate (Zou et al., 2019), Gbtc 2 and *Ginkgo* host may be involved in the regulation of substance flow at the same time.

Comparison of intracellular and extracellular differences in flavonoid production of Gbtc 2

Endophytic fungi are closely related to the ability of plants to produce flavonoids. Most of the functional enzymes related to flavonoid synthesis exist in fungi, including PAL, CHS, CHI, F3H, DFR, ANS, LAR, etc. (Xie et al., 2003; Li et al., 2012; Cheng et al., 2018). Traces of *Aspergillus oryzae* phenylpropane-flavonoid metabolic pathway indicated the ability to synthesize flavonoid substances (Juvvadi et al., 2005; Mohanta, 2020). Combined with the second-generation and third-generation sequencing techniques, the relatively complete genome of Gbtc 2 was constructed, and the entire flavonoid synthesis pathway was predicted. HPLC/LC–MS detection and metabolite database analysis showed that flavonoids in Gbtc 2 metabolites were diverse and abundant (Bampali et al., 2021). As a prerequisite for the synthesis of flavonoids, the addition of phenylalanine in the medium can promote the production of flavonoids by Gbtc 2 (Liu et al., 2022; Wang S. et al., 2022). A total of 71 flavonoids were identified, and the properties and structures of each flavonoid had certain uniqueness. The flavonoids identified also have more applications in the industrial field, such as quercetin can be used as a feed additive for the animal husbandry industry. This was one of the few reports of *Aspergillus* fungi to produce flavonoids.

From previous studies on endophytic fungi of *Ginkgo*, few researchers classified the fermentation broth of endophytic fungi into intracellular and extracellular metabolites for analysis. In this study, metabolites of Gbtc 2 mycelium and culture medium were detected and identified separately. LC–MS results showed that various flavonoid metabolites could be directly mapped to the metabolic process, which strongly proved that Gbtc 2 could synthesize flavonoids. In this experiment, the types and concentrations of Gbtc 2 intracellular and extracellular metabolites were different to some extent. Most flavonoid metabolites gathered intracellularly have glycosylation groups, such as astragalin,

trifolin, and cynaroside. However, almost all flavonoid monomers gathered extracellularly contain multiple hydroxyl groups. At present, no relevant reports have discussed the distribution rules of different types of flavonoid derivatives intracellularly and extracellularly, which can provide a certain reference for subsequent studies.

Studies have shown that hydroxylation and glycosylation often significantly improve or promote the solubility, storage, and stability of flavonoids (Xiao et al., 2009). Polyhydroxy can reduce the hydrophobicity of flavonoids, thus hindering the interaction in biofilm (Saleh et al., 2020), so that the polyhydroxy flavonoids produced by Gbtc 2 can better enter the culture medium through the cell membrane (Chunjian et al., 2014). Glycosylation of flavonoids will increase their chemical stability and solubility intracellularly, enabling them to enter the active membrane transport system that recognizes glycosylated compounds but does not recognize their aglycones (Xiao et al., 2014). Furthermore, Glycosylation and hydroxylation of isoflavones have been reported to be associated with protein binding and quenching. Hydroxylation increases binding affinity while glycosylation decreases binding affinity (Jinyao and Fenglian, 2008). It was speculated that glycosylation and hydroxylation play a key role in distinguishing functional specificity and suggest that glycosylated flavonoids and hydroxylated flavonoids may have different usages.

Gbtc 2 has the potential to become a flavonoid producing engineering strain

Flavonoids are the main source of medicine, cosmetics, and food additives. The availability of flavonoids in plants is affected by seasonal or regional variations and is limited by the low abundance of single compounds in complex mixtures (Zhao et al., 2019). Traditional extraction methods and excessive exploitation have led to the exhaustion of plant resources and environmental pollution. It is difficult to entirely rely on chemical synthesis to generate the complex structure of flavonoids, so they were inefficient and cost-effective (Liu et al., 2021). In recent years, reports on the production of paclitaxel by endophytic fungi have shown that endophytic fungi can produce active substances similar to host plants, which provides a new way for the development and production of medicinal components of *Ginkgo* (Stierle et al., 1993; Ajikumar et al., 2010). With the maturity of synthetic biology and multi-omics, engineering cells to produce natural plant products has achieved great success (Ranganathan and Mahalingam, 2019). Due to the transparent metabolic background and strong genetic operability, microbial cells, such as *Escherichia coli*, *Saccharomyces cerevisiae*, and *Corynebacterium glutamicum*, had been widely used as chassis cells to produce natural plant products (Galanie et al., 2015; Bian et al., 2017; Luo et al., 2019). A direct import of a large number of exogenous genetic fragments into chassis cells usually has a low success rate and the possibility of synthesis of flavonoids. If endophytes were screened from the host tissue, they were highly likely to have some functional genes for the synthesis of flavonoids similar to the host during the long-term co-symbiosis (Zou et al., 2019). Meanwhile, endophytes were also possible to have high expression and high activity of plant functional enzymes and the most suitable reaction environment. The specific metabolic pathways of microorganisms have stringent regulatory mechanisms (Wusheng, 2015). Endophytic fungi, which are eukaryotic cells, may be easier to achieve similar expression regulation with plants than endophytic bacteria.

It is reported that *Arabidopsis thaliana* contains GTPase sequences from Cyanobacteria and α-Proteobacteria through endosymbiotic gene transfer (EGT), which is one of the genetic exchanges between plants and endophytes (I N and M Nengah et al., 2014). The results showed that Gbtc 2 possesses several key functional enzyme genes (*4CL* and *CHS*) and a local flavonoid synthesis pathway similar to the *Ginkgo* host. Gbtc 2 has the potential to be developed as an engineering fungus for flavonoid synthesis. Therefore, if the chassis cell itself has some flavonoid metabolic pathways, it is an ideal choice for flavonoid production. Microbial secondary metabolic pathways usually exist in the form of gene clusters on chromosomes, which is helpful for pathway analysis and modification (Kwon et al., 2021). Moreover, the three *DFR*s cloned from *Ginkgo* showed a unique substrate bias by heterologous expression, in which *GbDFR1* and *GbDFR3* showed a tendency to dihydroquercetin substrate, while *GbDFR2* showed a propensity to convert dihydrokaempferol into leucopelargonidin (Cheng et al., 2018). In this study, while analyzing the genome and metabolites of Gbtc 2 from *Ginkgo* root, we also searched for ideal chassis cells that could synthesize flavonoids, providing theoretical basis for the construction of genetically engineered strains producing flavonoids in the future.

Conclusion

In this study, the flavonoid synthesis pathway of endophytic fungus Gbtc 2 in *Ginkgo* was re-analyzed and reconstructed based on genomic and metabolic analysis, and the secondary flavonoid metabolites were detected by HPLC/LC–MS. The functional enzymes expressed by these genes constitute an almost complete upstream of flavonoid synthesis, which proves that Gbtc 2 has the ability to synthesize basic C6–C3–C6 flavonoid monomers. Gbtc 2 contains key genes or local secondary metabolite synthesis pathways similar to the *Ginkgo* host. Gbtc 2 promoted the production of flavonoids by adding the appropriate amount of phenylalanine. The relative concentrations of intracellular and extracellular flavonoids are pretty different. Most of the flavonoid substances gathered intracellularly possess glycosylated groups, while the components with much higher concentration extracellularly than intracellularly are almost flavonoid monomers with multiple hydroxyls. The reason may be that binding and quenching of proteins are related to glycosylation and hydroxylation, thus fulfilling different biological functions

intracellularly and extracellularly. Furthermore, a variety of substances were targeted to the flavonoid synthesis pathway, demonstrating the flavonoid production capacity of Gbtc 2. This study provides a solid basis to the development of genetically engineered fungi to synthesize flavonoids.

Data availability statement

The datasets presented in this study can be found in online repositories. The names of the repository/repositories and accession number(s) can be found in the article/Supplementary material.

Author contributions

XW, KZ, XL, and YL conceived and designed the work. KZ, SF, SZ, and XW performed the experiments. XW and KZ wrote and revised the manuscript and contributed equally to this study. ZD revised the manuscript. All authors contributed to the article and approved the submitted version.

Funding

This work was supported by the following grants: Chinese National Science and Technology Support Program (2013BAC09B00), National Natural Science Foundation of China (302001124 and 31570113), and Graduate Research and Innovation Project (1053320170629) in Central South University, China.

Conflict of interest

The authors declare that the research was conducted in the absence of any commercial or financial relationships that could be construed as a potential conflict of interest.

Publisher's note

All claims expressed in this article are solely those of the authors and do not necessarily represent those of their affiliated organizations, or those of the publisher, the editors and the reviewers. Any product that may be evaluated in this article, or claim that may be made by its manufacturer, is not guaranteed or endorsed by the publisher.

Supplementary material

The Supplementary material for this article can be found online at: https://www.frontiersin.org/articles/10.3389/fmicb.2022.972294/full#supplementary-material

References

Aftab, U. M., Akter, S., et al. (2021). A plant endophyte *Staphylococcus hominis* strain MBL_AB63 produces a novel lantibiotic, homicorcin and a position one variant. *Sci. Rep.* 11, 1–12. doi: 10.1038/s41598-021-90613-9

Ajikumar, P. K., Xiao, W., et al. (2010). Isoprenoid pathway optimization for Taxol precursor overproduction in *Escherichia coli*. *Science* 330, 70–74. doi: 10.1126/science.1191652

Bampali, E., Germer, S., Bauer, R., and Kulić, Ž. (2021). HPLC-UV/HRMS methods for the unambiguous detection of adulterations of *Ginkgo biloba* leaves with Sophora japonica fruits on an extract level. *Pharm. Biol.* 59, 438–443. doi: 10.1080/13880209.2021.1910717

Bezerra, V. H. S., Cardoso, S. L., Fonseca-Bazzo, Y., Silveira, D., Magalhães, P. O., and Souza, P. M. (2021). Protease produced by endophytic fungi: a systematic review. *Molecules* 26. doi: 10.3390/molecules26227062

Bian, G., Yuan, Y., Tao, H., Shi, X., Zhong, X., Han, Y., et al. (2017). Production of taxadiene by engineering of mevalonate pathway in *Escherichia coli* and endophytic fungus *Alternaria alternata* TPF6. *Biotechnol. J.* 12. doi: 10.1002/biot.201600697

Buchfink, B., Xie, C., and Huson, D. H. (2015). Fast and sensitive protein alignment using DIAMOND. *Nat. Methods* 12, 59–60. doi: 10.1038/nmeth.3176

Chen, W., Gong, L., Guo, Z., Wang, W., Zhang, H., Liu, X., et al. (2013). A novel integrated method for large-scale detection, identification, and quantification of widely targeted metabolites: application in the study of Rice metabolomics. *Mol. Plant* 6, 1769–1780. doi: 10.1093/mp/sst080

Chen, H., Qi, Y., He, X., Xu, L., Zhang, W., Lv, X., et al. (2021). Endophytic fungus *Mucor circinelloides* DF20 promote tanshinone biosynthesis and accumulation in *salvia miltiorrhiza* root. *Plant Sci.* 307:110898. doi: 10.1016/j.plantsci.2021.110898

Chen, Y., Zhang, R., Song, Y., He, J., Sun, J., Bai, J., et al. (2009). RRLC-MS/MS-based metabonomics combined with in-depth analysis of metabolic correlation network: finding potential biomarkers for breast cancer. *Analyst* 134, 2003–2011. doi: 10.1039/b907243h

Cheng, H., Li, L., Cheng, S., Cao, F., Xu, F., Yuan, H., et al. (2018). Molecular cloning and characterization of three genes encoding dihydroflavonol-4-reductase from *Ginkgo biloba* in anthocyanin biosynthetic pathway. *PLoS One* 8:7. doi: 10.1371/journal.pone.0072017

Chunjian, Z., Chunying, L., Shuaihua, L., and Lei, Y. (2014). The Galloyl Catechins contributing to Main antioxidant capacity of tea made from *Camellia sinensis* in China. *Sci. World J.* 2014:863984. doi: 10.1155/2014/863984

Dao, T. T. H., Linthorst, H. J. M., and Verpoorte, R. (2011). Chalcone synthase and its functions in plant resistance. *Phytochem. Rev.* 10, 397–412. doi: 10.1007/s11101-011-9211-7

Darzi, Y., Letunic, I., Bork, P., and Yamada, T. (2018). iPath3.0: interactive pathways explorer v3. *Nucleic Acids Res.* 46, W510–W513. doi: 10.1093/nar/gky299

Deng, Y., Huang, H., Lei, F., Fu, S., Zou, K., Zhang, S., et al. (2021). Endophytic bacterial communities of *Ginkgo biloba* leaves during leaf developmental period. *Front. Microbiol.* 12. doi: 10.3389/fmicb.2021.698703

Domingo-Almenara, X., Montenegro-Burke, J. R., Ivanisevic, J., Thomas, A., Sidibé, J., Teav, T., et al. (2018). XCMS-MRM and METLIN-MRM: a cloud library and public resource for targeted analysis of small molecules. *Nat. Methods* 15, 681–684. doi: 10.1038/s41592-018-0110-3

Edyta, K., and Tomasz, J. (2012). Microbial transformations of 7-Hydroxyflavanone. *Sci. World J.* 2012. doi: 10.1100/2012/254929

Eliana, P., Lillian, B., and Isabel, C. F. R. F. (2013). Chemical characterization of *Ginkgo biloba* L. and antioxidant properties of its extracts and dietary supplements. *Ind. Crops Prod.* 51, 244–248. doi: 10.1016/j.indcrop.2013.09.011

Erb, M., and Kliebenstein, D. J. (2020). Plant secondary metabolites as defenses, regulators, and primary metabolites: the blurred functional trichotomy. *Plant Physiol.* 184, 39–52. doi: 10.1104/pp.20.00433

Ferreira, M. C., de Carvalho, C. R., Bahia, M., Barreto, D. L. C., Azevedo, R. N., Cota, B. B., et al. (2021). Plant-associated fungi: methods for taxonomy, diversity, and bioactive secondary metabolite bioprospecting. *Methods Mol. Biol.* 2232, 85–112. doi: 10.1007/978-1-0716-1040-4_9

Galanie, S., Thodey, K., Trenchard, I. J., Filsinger Interrante, M., and Smolke, C. D. (2015). Complete biosynthesis of opioids in yeast. *Science* 349, 1095–1100. doi: 10.1126/science.aac9373

Gensheimer, M., and Mushegian, A. (2004). Chalcone isomerase family and fold: no longer unique to plants. *Protein Sci.* 13, 540–544. doi: 10.1110/ps.03395404

Hao, G. P., du, X., Zhao, F., and Ji, H. (2010). Fungal endophytes-induced abscisic acid is required for flavonoid accumulation in suspension cells of *Ginkgo biloba*. *Biotechnol. Lett.* 32, 305–314. doi: 10.1007/s10529-009-0139-6

Horai, H., Arita, M., Kanaya, S., Nihei, Y., Ikeda, T., Suwa, K., et al. (2010). MassBank: a public repository for sharing mass spectral data for life sciences. *J. Mass Spectrom.* 45, 703–714. doi: 10.1002/jms.1777

Hu, J., Fan, J., Sun, Z., and Liu, S. (2020). NextPolish: a fast and efficient genome polishing tool for long-read assembly. *Bioinformatics* 36, 2253–2255. doi: 10.1093/bioinformatics/btz891

Huerta-Cepas, J., Forslund, K., Coelho, L. P., Szklarczyk, D., Jensen, L. J., von Mering, C., et al. (2017). Fast genome-wide functional annotation through Orthology assignment by eggNOG-mapper. *Mol. Biol. Evol.* 34, 2115–2122. doi: 10.1093/molbev/msx148

Huerta-Cepas, J., Szklarczyk, D., Heller, D., Hernández-Plaza, A., Forslund, S. K., Cook, H., et al. (2019). eggNOG 5.0: a hierarchical, functionally and phylogenetically annotated orthology resource based on 5090 organisms and 2502 viruses. *Nucleic Acids Res.* 47, D309–D314. doi: 10.1093/nar/gky1085

Isah, T. (2015). Rethinking *Ginkgo biloba* L.: medicinal uses and conservation. *Pharmacogn. Rev.* 9, 140–148. doi: 10.4103/0973-7847.162137

Jia, M., Chen, L., Xin, H. L., Zheng, C. J., Rahman, K., Han, T., et al. (2016). A friendly relationship between endophytic fungi and medicinal plants: a systematic review. *Front. Microbiol.* 7. doi: 10.3389/fmicb.2016.00906

Jiang, H. X., Wood, K. V., and Morgan, J. A. (2005). Metabolic engineering of the phenylpropanoid pathway in *Saccharomyces cerevisiae*. *Appl. Environ. Microbiol.* 71, 2962–2969. doi: 10.1128/AEM.71.6.2962-2969.2005

Jinyao, Z., and Fenglian, R. (2008). Influence of hydroxylation and glycosylation in ring a of soybean isoflavones on interaction with BSA. *Spectrochim. Acta A Mol. Biomol. Spectrosc.* 72, 682–685. doi: 10.1016/j.saa.2008.10.058

Juárez-Hernández, J., Castillo-Hernández, D., Pérez-Parada, C., Nava-Galicia, S., Cuervo-Parra, J. A., Surian-Cruz, E., et al. (2021). Isolation of fungi from a textile industry effluent and the screening of their potential to degrade industrial dyes. *J. Fungi* 7, 1–17. doi: 10.3390/jof7100805

Juvvadi, P. R., Seshime, Y., and Kitamoto, K. (2005). Genomics reveals traces of fungal phenylpropanoid-flavonoid metabolic pathway in the filamentous fungus *aspergillus oryzae*. *J. Microbiol.* 6, 475–486.

Kaltenbach, M., Burke, J. R., Dindo, M., Pabis, A., Munsberg, F. S., Rabin, A., et al. (2018). Evolution of chalcone isomerase from a noncatalytic ancestor. *Nat. Chem. Biol.* 14, 548–555. doi: 10.1038/s41589-018-0042-3

Kazuki, S., Keiko, Y., Ryo, N., Yasuhiro, H., Mami, Y., Takayuki, T., et al. (2013). The flavonoid biosynthetic pathway in *Arabidopsis*: structural and genetic diversity. *Plant Physiol. Biochem.* 72, 21–34. doi: 10.1016/j.plaphy.2013.02.001

Koren, S., Walenz, B. P., Berlin, K., Miller, J. R., Bergman, N. H., and Phillippy, A. M. (2017). Canu: scalable and accurate long-read assembly via adaptive k -mer weighting and repeat separation. *Genome Res.* 27, 722–736. doi: 10.1101/gr.215087.116

Kumar, S., Stecher, G., Li, M., Knyaz, C., and Tamura, K. (2018). MEGA X: molecular evolutionary genetics analysis across computing platforms. *Mol. Biol. Evol.* 35, 1547–1549. doi: 10.1093/molbev/msy096

Kwon, M. J., Steiniger, C., Cairns, T. C., Wisecaver, J. H., Lind, A. L., Pohl, C., et al. (2021). Beyond the biosynthetic gene cluster paradigm: genome-wide Coexpression networks connect clustered and Unclustered transcription factors to secondary metabolic pathways. *Microbiology Spectrum* 9, e00898–e00821. doi: 10.1128/Spectrum.00898-21

Lei, F., Liu, X., Huang, H., Fu, S., Zou, K., Zhang, S., et al. (2021). The *Macleaya cordata* symbiont: revealing the effects of plant niches and alkaloids on the bacterial community. *Front. Microbiol.* 12. doi: 10.3389/fmicb.2021.681210

Li, H., Qiu, J., Chen, F., Lv, X., Fu, C., Zhao, D., et al. (2012). Molecular characterization and expression analysis of dihydroflavonol 4-reductase (DFR) gene in *Saussurea medusa*. *Mol. Biol. Rep.* 39, 2991–2999. doi: 10.1007/s11033-011-1061-2

Liu, H., Wang, X., Wang, G., Cui, P., Wu, S., Ai, C., et al. (2021). The nearly complete genome of *Ginkgo biloba* illuminates gymnosperm evolution. *Nature Plants* 7, 748–756. doi: 10.1038/s41477-021-00933-x

Liu, Y. X., Xin, H. W., Zhang, Y., Che, F., Shen, N., and Cui, Y. (2022). Leaves, seeds and exocarp of *Ginkgo biloba* L. (Ginkgoaceae): a comprehensive review of traditional uses, phytochemistry, pharmacology, resource utilization and toxicity. *J. Ethnopharmacol.* 298:115645. doi: 10.1016/j.jep.2022.115645

Luo, X., Reiter, M. A., d'Espaux, L., Wong, J., Denby, C. M., Lechner, A., et al. (2019). Complete biosynthesis of cannabinoids and their unnatural analogues in yeast. *Nature* 567, 123–126. doi: 10.1038/s41586-019-0978-9

Marsafari, M., Samizadeh, H., Rabiei, B., Mehrabi, A. A., Koffas, M., and Xu, P. (2020). Biotechnological production of flavonoids: An update on plant metabolic engineering, microbial host selection, and genetically encoded biosensors. *Biotechnol. J.* 15:1900432. doi: 10.1002/biot.201900432

Mohanta, T. K. (2020). Fungi contain genes associated with flavonoid biosynthesis pathway. *J. Funct. Foods* 68:103910. doi: 10.1016/j.jff.2020.103910

Moore, B. S., Hertweck, C., Hopke, J. N., Izumikawa, M., Kalaitzis, J. A., Nilsen, G., et al. (2002). Plant-like biosynthetic pathways in bacteria: from benzoic acid to chalcone. *J. Nat. Prod.* 65, 1956–1962. doi: 10.1021/np020230m

Moriya, Y., Itoh, M., Okuda, S., Yoshizawa, A. C., and Kanehisa, M. (2007). KAAS: an automatic genome annotation and pathway reconstruction server. *Nucleic Acids Res.* 35S, W182–W185. doi: 10.1093/nar/gkm321

Nengah, S. I., Masatsugu, D., Saki, Y., Chak Han, I., Woo Young, B., and Ohniwa, R. L. (2014). Evidence for lateral gene transfer (LGT) in the evolution of eubacteria-derived small GTPases in plant organelles. *Front. Plant Sci.* 5. doi: 10.3389/fpls.2014.00678

Pandey, R. P., Parajuli, P., Koffas, M. A. G., and Sohng, J. K. (2016). Microbial production of natural and non-natural flavonoids: pathway engineering, directed evolution and systems/synthetic biology. *Biotechnol. Adv.* 34, 634–662. doi: 10.1016/j.biotechadv.2016.02.012

Petit, P., Granier, T., d'Estaintot, B. L., Manigand, C., Bathany, K., Schmitter, J. M., et al. (2007). Crystal structure of grape Dihydroflavonol 4-reductase, a key enzyme in flavonoid biosynthesis. *J. Mol. Biol.* 368, 1345–1357. doi: 10.1016/j.jmb.2007.02.088

Qian, Y., Kang, J., Luo, Y. K., Zhao, J. J., He, J., and Geng, K. (2016). A Bilobalide-producing endophytic fungus, Pestalotiopsis uvicola from medicinal plant *Ginkgo biloba*. *Current Microbiol* 73, 280–286. doi: 10.1007/s00284-016-1060-6

Qiu, M., Xie, R. S., Shi, Y., Zhang, H., and Chen, H. M. (2010). Isolation and identification of two flavonoid-producing endophytic fungi from *Ginkgo biloba* L. *Ann. Microbiol.* 60, 143–150. doi: 10.1007/s13213-010-0016-5

Queiroz, C. B. D., and Santana, M. F. (2020). Prediction of the secretomes of endophytic and nonendophytic fungi reveals similarities in host plant infection and colonization strategies. *Mycologia* 112, 491–503. doi: 10.1080/00275514.2020.1716566

Ranganathan, N., and Mahalingam, G. (2019). Secondary metabolite as therapeutic agent from endophytic fungi *Alternaria* longipes strain VITN14G of mangrove plant *Avicennia officinalis*. *J. Cell. Biochem.* 120, 4021–4031. doi: 10.1002/jcb.27686

Sajid, M., Channakesavula, C. N., Stone, S. R., and Kaur, P. (2021). Synthetic biology towards improved flavonoid pharmacokinetics. *Biomol. Ther.* 11. doi: 10.3390/biom11050754

Saleh, A., Leonardo, P. D. S., Maria, B., and Alisdair, R. F. (2020). The style and substance of plant flavonoid decoration; towards defining both structure and function. *Phytochemistry* 174. doi: 10.1016/j.phytochem.2020.112347

Sayers, E. W., Bolton, E. E., Brister, J. R., Canese, K., Chan, J., Comeau, D. C., et al. (2022). Database resources of the national center for biotechnology information. *Nucleic Acids Res.* 50, D20–D26. doi: 10.1093/nar/gkab1112

Shymanovich, T., Saari, S., Lovin, M. E., Jarmusch, A. K., Jarmusch, S. A., Musso, A. M., et al. (2015). Alkaloid variation among epichloid endophytes of sleepygrass (*Achnatherum robustum*) and consequences for resistance to insect herbivores. *J. Chem. Ecol.* 41, 93–104. doi: 10.1007/s10886-014-0534-x

Simão, F. A., Waterhouse, R. M., Ioannidis, P., Kriventseva, E. V., and Zdobnov, E. M. (2015). BUSCO: assessing genome assembly and annotation completeness with single-copy orthologs. *Bioinformatics* 31, 3210–3212. doi: 10.1093/bioinformatics/btv351

Singh, S., Kaur, I., and Kariyat, R. (2021). The multifunctional roles of polyphenols in plant-herbivore interactions. *Int. J. Mol. Sci.* 22. doi: 10.3390/ijms22031442

Stierle, A., Strobel, G., and Stierle, D. (1993). Taxol and Taxane production by *Taxomyces andreanae*, an endophytic fungus of Pacific yew. *Science* 260, 214–216. doi: 10.1126/science.8097061

Sun, W. J., Ma, Z. T., and Liu, M. (2020). Cytochrome P450 family: genome-wide identification provides insights into the rutin synthesis pathway in Tartary buckwheat and the improvement of agricultural product quality. *Int. J. Biol. Macromol.* 164, 4032–4045. doi: 10.1016/j.ijbiomac.2020.09.008

Sur, G., Ryu, S. Y., Kim, J. W., and Lim, H. (2022). A deep reinforcement learning-based scheme for solving multiple Knapsack problems. *Appl. Sci.* 12:3068. doi: 10.3390/app12063068

Teimoori-Boghsani, Y., Ganjeali, A., Cernava, T., Muller, H., Asili, J., and Berg, G. (2019). Endophytic fungi of native *Salvia abrotanoides* plants reveal high taxonomic diversity and unique profiles of secondary metabolites. *Front. Microbiol.* 10. doi: 10.3389/fmicb.2019.03013

Toghueo, R. M. K. (2020). Endophytes from Gingko biloba: the current status. *Phytochem. Rev.* 19, 743–759. doi: 10.1007/s11101-020-09679-4

Trisuwan, K., Rukachaisirikul, V., Sukpondma, Y., Phongpaichit, S., Preedanon, S., and Sakayaroj, J. (2010). Furo[3,2-h]isochroman, furo[3,2-h]isoquinoline, isochroman, phenol, pyranone, and pyrone derivatives from the sea fan-derived fungus *Penicillium* sp PSU-F40. *Tetrahedron* 66, 4484–4489. doi: 10.1016/j.tet.2010.04.073

Wang, H., Guo, Y., Luo, Z., Gao, L., Li, R., Zhang, Y., et al. (2022). Recent advances in *Alternaria* Phytotoxins: a review of their occurrence, structure, bioactivity, and biosynthesis. *Journal of Fungi* 8. doi: 10.3390/jof8020168

Wang, J., Liu, S., Song, Z. Q., Xu, T. C., Liu, C. S., Hou, Y. G., et al. (2020). Naturally occurring flavonoids and Isoflavonoids and their microbial transformation: a review. *Molecules* 25. doi: 10.3390/molecules25215112

Wang, S., Liu, Z., Wang, X., Liu, R., and Zou, L. (2022). Mushrooms do produce flavonoids: metabolite profiling and transcriptome analysis of flavonoid synthesis in the medicinal mushroom *Sanghuangporus baumii*. *Journal of fungi* 8. doi: 10.3390/jof8060582

Wang, C., Wu, J., and Mei, X. (2001). Enhancement of Taxol production and excretion in *Taxus chinensis* cell culture by fungal elicitation and medium renewal. *Appl. Microbiol. Biotechnol.* 55, 404–410. doi: 10.1007/s002530000567

Wishart, D. S., Feunang, Y. D., Marcu, A., Guo, A. C., Liang, K., Vázquez-Fresno, R., et al. (2018). HMDB 4.0: the human metabolome database for 2018. *Nucleic Acids Res.* 46, D608–D617. doi: 10.1093/nar/gkx1089

Wusheng, L. (2015). Plant synthetic biology. *Trends Plant Sci.* 20, 309–317. doi: 10.1016/j.tplants.2015.02.004

Xiao, J., Cao, H., Wang, Y., Zhao, J., and Wei, X. (2009). Glycosylation of dietary flavonoids decreases the affinities for plasma protein. *J. Agric. Food Chem.* 57, 6642–6648. doi: 10.1021/jf901456u

Xiao, J., Muzashvili, T. S., and Georgiev, M. I. (2014). Advances in the biotechnological glycosylation of valuable flavonoids. *Biotechnol. Adv.* 32, 1145–1156. doi: 10.1016/j.biotechadv.2014.04.006

Xiaojia, S., Guoan, S., Shaokang, D., Richard, A. D., and Yongzhen, P. (2017). Characterization of *UGT*716A1 as a multi-substrate UDP:flavonoid glucosyltransferase gene in *Ginkgo biloba*. *Front. Plant Sci.* 8. doi: 10.3389/fpls.2017.02085

Xie, D. Y., Sharma, S. B., Paiva, N. L., Ferreira, D., and Dixon, R. A. (2003). Role of Anthocyanidin reductase, encoded by *BANYULS* in plant flavonoid biosynthesis. *Science* 299, 396–399. doi: 10.1126/science.1078540

Yan, T., Guo, Z. K., Jiang, R., Wei, W., Wang, T., Guo, Y., et al. (2013). New flavonol and diterpenoids from the endophytic fungus *aspergillus* sp. YXf3. *Planta Med.* 79, 348–352. doi: 10.1055/s-0032-1328260

Yuan, T., Severine, A., Didier, B., Caroline, K., Francois, H., Joelle, D., et al. (2014). The fungal leaf endophyte *Paraconiothyrium variabile* specifically metabolizes the host-plant metabolome for its own benefit. *Phytochemistry* 108, 95–101. doi: 10.1016/j.phytochem.2014.09.021

Yuan, Y., Tian, J., Xiao, J., Shao, Q., and Gao, J. M. (2014). Bioactive metabolites isolated from *Penicillium* sp. YY-20, the endophytic fungus from *Ginkgo biloba*. *Nat. Prod. Res.* 28, 278–281. doi: 10.1080/14786419.2013.850686

Zang, Y., Zha, J., Wu, X., Zheng, Z., Ouyang, J., and Koffas, M. A. G. (2019). In *vitro* Naringenin biosynthesis from *p*-Coumaric acid using recombinant enzymes. *J. Agric. Food Chem.* 67, 13430–13436. doi: 10.1021/acs.jafc.9b00413

Zhao, Y., Fan, G., Yin, P. P., Sun, S., Li, N., Hong, X., et al. (2019). Resequencing 545 ginkgo genomes across the world reveals the evolutionary history of the living fossil. *Nat. Commun.* 10, 4201–4210. doi: 10.1038/s41467-019-12133-5

Zou, K., Liu, X., Hu, Q., Zhang, D., Fu, S., Zhang, S., et al. (2021). Root endophytes and *Ginkgo biloba* are likely to share and compensate secondary metabolic processes, and potentially exchange genetic information by LTR-RTs. *Front. Plant Sci.* 12. doi: 10.3389/fpls.2021.704985

Zou, K., Liu, X., Zhang, D., Yang, Q., Fu, S., Meng, D., et al. (2019). Flavonoid biosynthesis is likely more susceptible to elevation and tree age than other branch pathways involved in Phenylpropanoid biosynthesis in *ginkgo* leaves. *Front. Plant Sci.* 10. doi: 10.3389/fpls.2019.00983

frontiers | Frontiers in Microbiology

TYPE Original Research
PUBLISHED 24 November 2022
DOI 10.3389/fmicb.2022.1052377

Check for updates

OPEN ACCESS

EDITED BY
Wenbing Yin,
Institute of Microbiology (CAS), China

REVIEWED BY
Han Xiao,
Shanghai Jiao Tong University, China
Chenyang Huang,
Institute of Agricultural Resources and Regional Planning (CAAS), China

*CORRESPONDENCE
Shilin Chen
slchen@icmm.ac.cn
Junshan Ruan
ruanjunshan@163.com

†These authors have contributed equally to this work

SPECIALTY SECTION
This article was submitted to Microbial Physiology and Metabolism, a section of the journal Frontiers in Microbiology

RECEIVED 23 September 2022
ACCEPTED 31 October 2022
PUBLISHED 24 November 2022

CITATION
Xu X, Zhu F, Zhu Y, Li Y, Zhou H, Chen S and Ruan J (2022) Transcriptome profiling of transcription factors in *Ganoderma lucidum* in response to methyl jasmonate.
Front. Microbiol. 13:1052377.
doi: 10.3389/fmicb.2022.1052377

COPYRIGHT
© 2022 Xu, Zhu, Zhu, Li, Zhou, Chen and Ruan. This is an open-access article distributed under the terms of the Creative Commons Attribution License (CC BY). The use, distribution or reproduction in other forums is permitted, provided the original author(s) and the copyright owner(s) are credited and that the original publication in this journal is cited, in accordance with accepted academic practice. No use, distribution or reproduction is permitted which does not comply with these terms.

Transcriptome profiling of transcription factors in *Ganoderma lucidum* in response to methyl jasmonate

Xiaolan Xu[1], Fengli Zhu[2], Yuxuan Zhu[2], Yujie Li[2], Hao Zhou[2], Shilin Chen[3,4*†] and Junshan Ruan[5*†]

[1]College of Animal Sciences (College of Bee Science), Fujian Agriculture and Forestry University, Fuzhou, China, [2]College of Food Science, Fujian Agriculture and Forestry University, Fuzhou, China, [3]Institute of Chinese Materia Medica, China Academy of Chinese Medical Sciences, Beijing, China, [4]Institute of Herbgenomics, Chengdu University of Traditional Chinese Medicine, Chengdu, China, [5]Fujian Provincial Hospital, Fuzhou, China

Ganoderma lucidum is a traditional Chinese medicine and its major active ingredients are ganoderma triterpenoids (GTs). To screen for transcription factors (TFs) that involved in the biosynthetic pathway of GTs in *G. lucidum*, the chemical composition in mycelia, primordium and fruiting body were analyzed, and the transcriptomes of mycelia induced by methyl jasmonate (MeJA) were analyzed. In addition, the expression level data of MeJA-responsive TFs in mycelia, primordia and fruiting body were downloaded from the database, and the correlation analysis was carried out between their expression profiles and the content of total triterpenoids. The results showed that a total of 89 components were identified, and the content of total triterpenoids was the highest in primordium, followed by fruiting body and mycelia. There were 103 differentially expressed TFs that response to MeJA-induction including 95 upregulated and 8 downregulated genes. These TFs were classified into 22 families including C2H2 (15), TFII-related (12), HTH (9), fungal (8), bZIP (6), HMG (5), DADS (2), etc. Correlation analysis showed that the expression level of GL23559 (MADS), GL26472 (HTH), and GL31187 (HMG) showed a positive correlation with the GTs content, respectively. While the expression level of GL25628 (fungal) and GL26980 (PHD) showed a negative correlation with the GTs content, respectively. Furthermore, the over expression of the *Glmhr1* gene (GL25628) in *Pichia pastoris* GS115 indicated that it might be a negative regulator of GT biosynthesis through decreasing the production of lanosterol. This study provided useful information for a better understanding of the regulation of TFs involved in GT biosynthesis and fungal growth in *G. lucidum*.

KEYWORDS

***Ganoderma lucidum*, ganoderma triterpenoid, UPLC/Q-TOF-MS/MS, methyl jasmonate, *Glmhr*, transcription factors**

Introduction

Ganoderma lucidum, also named "Lingzhi," has been used as a traditional Chinese medicine with the effects of improving health and promoting longevity for thousands of years in China. The chemical constituents of *G. lucidum* are very complex, including triterpenoids, polysaccharides, nucleosides, furan derivatives, sterols, alkaloids and polypeptides (Ren et al., 2010; Li et al., 2013; Xie et al., 2020; Dong et al., 2021). Among them, triterpenoids are one of the most important bioactive components, exhibiting antitumor, apoptotic, antiviral and immune-modulatory pharmaceutical activities (Chi et al., 2018; Liang et al., 2019; Shao et al., 2021; Chen et al., 2022a). Ganoderma triterpenoids (GTs) are derived from lanosterol, which is the intermediate of triterpenoids and synthesized by lanosterol synthase (LSS) through the mevalonate (MVA) pathway. Currently, approximately 150 GTs have been identified in *G. lucidum*, such as ganoderic acids, methyl ganoderate, lucidenic acid, and ganolucidic acid (Chen et al., 2012; Xie et al., 2020).

Triterpenoids concentration in aerial mycelia is minimal, but it may be raised by liquid fermentation, which is influenced by the growth conditions and medium used. To improve the production of GT, a few biotic and abiotic elicitors had been used to enhance the GT production, such as ozone gas, nitric oxide, ozone gas, methyl jasmonate (MeJA), and salicylic acid (SA) (Ren et al., 2010; Shi et al., 2015; Sudheer et al., 2016; Gu et al., 2017; Liu et al., 2018). JA and its derivatives MeJA, which have been used widely as important elicitors, are effective in inducing the production of secondary metabolites in many plant and fungal species (Wang et al., 2014; Ali et al., 2015; Kim et al., 2017; Zhou et al., 2019; Lin et al., 2020; Chen et al., 2022b). In *G. lucidum,* MeJA also has been confirmed as an effective elicitor for the induction of GT via an ROS signaling pathway (Shi et al., 2015). Except for the induction of secondary metabolites, the MeJA induction also affects plant and fungal stress resistance, growth development, external morphology and other physiological processes (Aranega-Bou et al., 2014).

Secondary metabolites are all biosynthesized through metabolic pathways, which are controlled by a complex regulatory network that regulated by transcription regulators. Many transcription factors (TFs), which participate in JA- and MeJA-induced secondary metabolite biosynthesis, could upregulate or downregulate the expression of genes involved in metabolism biosynthesis (Wang et al., 2014; Ali et al., 2015; Kim et al., 2017; Zhou et al., 2019; Lin et al., 2020; Chen et al., 2022b). A few genome-wide transcriptome analyses have revealed that JA and MeJA could extensively regulate TFs to enhance the production of secondary metabolites including terpene, taxol, nicotine, and flavonoid. These MeJA-responsive TFs include the ORCA, ERF, MYC, WRKY, bHLH, MYB, and bZIP families (Tsubasa and Takashi, 2011; Yu et al., 2012; Afrin et al., 2015; Lin et al., 2020; Chen et al., 2022b). For example, the bHLH TFs positively regulated the terpenoid indole alkaloid biosynthesis in *Catharanthus roseus* and the nicotine biosynthesis in *Nicotiana benthamiana* (Suttipanta et al., 2011; Zhang et al., 2011). The identification of MeJA-responsive TFs by transcriptome analysis is an effective method to screen for candidate genes involved in metabolism biosynthesis pathway and provide useful information to elucidate the transcriptional regulation of a particular biosynthetic pathway.

The functions of many TFs in plants and fungi have been verified. *G. lucidum* was found to have approximately 600 TFs in the whole genome (Chen et al., 2012), but until now, a few TFs, such as *GlPacC*, *GlSwi6*, *GlSkn7*, and *CRZ1*, have been reported (Liu et al., 2013; Wu et al., 2016; Wang et al., 2018; Zhang et al., 2018; Hu et al., 2019; Li and Zhong, 2020). These TFs were involved in the growth process of *G. lucidum*, and their silencing resulted in the changes of the content of ganoderma acids (Liu et al., 2013; Wang et al., 2018; Zhang et al., 2018). In *G. lucidum*, the function of a large number of TFs is still unclear. Consequently, the understanding of the transcriptional regulation in this fungus is limited. In this study, the chemical components in different growth phases and the transcriptome profile *G. lucidum* were analyzed to screen TFs that possibly be involved in the synthesis of triterpenoids. Furthermore, the over expression of *Glmhr1* (GL25628), a GAL4-like TF, in *Pichia pastoris* GS115 revealed that it was negative correlation with GTs yield in *G. lucidum*. This study provided information about the roles of TFs in the GTs biosynthesis and fungal growth.

Materials and methods

Chemical analysis

The primordia and fruiting body (fruiting body formation stage) of *G. lucidum* G203 were collected from Jianning, Fujian province in China. Aerial mycelia were collected by culturing on potato dextrose agar (PDA) plates with glass paper at 28°C for 10 days. All the samples were ultrasonic extracted using the method as described in "Chinese pharmacopoeia 2020." Samples (2 g) were extracted with ethanol (50 ml) by ultrasonic method with the parameters of 140 W and 42 kHz for 45 min. The extracts were filtered and adjusted to 100 ml using ethanol. The ethanol extracts of samples were used for the detection of total triterpenoids and chemical composition. To create a standard curve for determining the content of total triterpenoids, 0.0, 0.2, 0.3, 0.4, 0.5, and 0.6 ml of oleanolic acid (0.2 mg/ml) were added 5% vanillin-glacial acetic acid solution (0.2 ml) and perchloric acid (0.8 ml), respectively. The mixtures were heated in the 70°C water bath for 15 min, and then reacted with ethyl acetate solution (4 ml). The absorbance of the samples were measured at 560 nm and the standard curve obtained is $y = 8.6735\ x - 0.0073$ ($R^2 = 0.9993$).

The extracts of samples were filtered through 0.22 μm filter membrane for constituent analysis. Analyses were carried out on a Waters UPLC system using an ACQUITY UPLC HSS T3 column (2.1 × 100 mm, 1.7 μm) at a flow rate of 0.3 mL/min. The mobile phases A and B consisted of 0.1% formic acid in water and acetonitrile, respectively. The mobile phase gradient program was as follows: 0–1 min, 100% A; 1–35 min, 100% A–50% A; 35–50 min, 50% A–20% A; 50–55 min, 20% A–0% A; 55–57 min, 0% A, 57.1–60 min, 100% A. The on-line UV spectra were scanned from 200 to 400 nm.

The mass spectra were acquired in both positive and negative ion modes by using a Waters definition accurate mass quadrupole time-of-flight (Q-TOF) Xevo G2-XS mass spectrometer (Waters, Milford, MA, USA) equipped with an ESI source. The optimized operating parameters were as follows: mass range, m/z 50–1,500; the flow rate of drying gas (N_2), 800 L/h; drying gas temperature, 400°C; cone gas flow, 100 L/h; source temperature, 120°C; capillary voltage, 2.5 kV; cone voltage, 40 V; In MSe mode, the energies for collision induced dissociation (CID) were 6 V for the precursor ion at low energy mode and 20–60 V for fragmentation information at high energy mode. An external reference (Lock-Spray TM) consisting of a 0.2 ng/mL solution of Leucine enkephalin was used in both positive (m/z 556.2771 $[M + H]^+$) and negative mode (m/z 554.2615 $[M–H]^-$), infused at a flow of 5 μL/min. All the data was acquired using Mass Lynx TM 4.1 software (Waters, Milford, MA, USA).

Strains culture and methyl jasmonate treatment

The monokaryotic *G. lucidum* strain G.260125-1, whose whole-genome had been sequenced, was used for transcriptome analysis. The mycelia of *G. lucidum* strain G.260125-1 were treated with MeJA according to the previously reported method (Shi et al., 2015). After the strain was cultured on PDA plates at 28°C for 7 days, the mycelia were cultured in potato-dextrose broth with MeJA at final concentrations of 0, 50, 100, 150, 200, and 300 μM at 28°C and 150 rpm for 7 days in a shock incubator. The mycelia treated with equal volume of solvent without MeJA were used as control. Thereafter, the biomass and the contents of total triterpenoids were determined. Each treatment and all determinations were carried out in triplicate.

Transcriptome analysis

Total RNA was extracted from mycelia that treated with MeJA at final concentrations of 0, 200, and 300 μM using Trizol reagent (Invitrogen, Carlsbad, CA, USA) according to the manufacturer's protocol. RNA quantity and quality were evaluated with a NanoDrop 2000 spectrophotometer (Thermo Fisher Scientific, MA, USA) and an Agilent 2100 Bioanalyzer (Agilent Technologies, Santa Clara, CA). The samples whose RNA Integrity Number (RIN) values were greater than 8.5 were used for further experiment. And mRNA was isolated from total RNA using poly- (T) oligo- linked magnetic beads. All isolated mRNA was sheared into short fragments (150–200 nt) by adding fragmentation buffer and used for first strand cDNA synthesis with random primers. The second strand cDNA were synthesized and purified with a QIAquick PCR Purification Kit (Qiagen, Dusseldorf, Germany). After the purified cDNAs were end repaired and acetylated at their 3′ ends, the pair-end adapters were connected. At last, the cDNA libraries were verified using an Agilent 2100 Bioanalyzer and ABI StepOnePlus Real-time PCR system and sequenced using an Illumina HiSeqTM 4000 (Illumina Inc., Delaware, USA). All the raw data have been submitted to the NCBI database (Accession No: PRJNA865720).

Raw data in fasta format were processed using Perl scripts, and clean data were obtained by removing adapter sequences, reads containing more than 10% "N" rate and low-quality reads. The clean reads were mapped to the genome sequence of *G. lucidum* G.260125-1 (Accession No: AGAX00000000.1) using Bowtie2 software. The genes that were quantitatively analyzed using RSEM and Noiseq software were used to screen the differentially expressed genes (DEGs) between different treatment groups according to the fragments per kilobase of transcript sequence per millions base pairs sequenced (FPKM) method. The genes with $|\log2FC| \geq 1$ and probability value >0.8 were considered as DEGs.

Verification of quantitative real-time PCR

Total RNA was extracted using Magnetic bead Method Universal RNA Extraction Kit (Thermo Fisher Scientific, MA, USA) according the manufacturer' procedure. Residual genomic DNA was removed, and 500 ng of RNA without genomic DNA was reverse-transcribed for quantitative real-time PCR (qRT-pCR) according the manufacturer's procedure (Takara Bio, Kyoto, Japan). The gene transcription levels of different treatment groups were quantified by qRT-PCR. The primer sequences are shown in **Table 1**. The reaction procedure was performed on CFX 384 Real-Time System C1000 Touch Thermal Cycler (BioRad, California, USA) using a two-step method as follows: 95°C for 30 s, 40 cycles of 95°C for 5 s, and 60°C for 30 s. Transcript level of genes was calculated according to the $2^{-\Delta\Delta CT}$ method and *G. lucidum* glyceraldehyde-3-phosphate dehydrogenase (*GL-GPD*) gene transcripts were used as an internal control.

TABLE 1 Primer sequences used for qRT-PCR analysis.

Primers	Sequences (F)	Sequences (R)
GPD	GATGAAGGACTGGCGTGGT	CCGTTGAGGCTGGGAATGAC
GL22438	GGAAAGGGGAAAGGTGTC	CGTTGGCGAGGGAGAAG
GL29539	CCCTTACGAGGTGTCCG	GCGACTGGTCCATCTGC
GL22204	TACAAGACCATCCTCAAC	GCTCTCCTTCTTCTGATAT
GL25456	TATCTGCTATCGTCCATT	CCCTTGACTTGATCTATG
GL25655	GTCTTCGCCTCTATATCC	AGATACTTCAGGACTCAAG
GL31187	CTCCACCCAGAACCCAAG	GGATTGAAGACATAGAACTGTAGT
GL20710	AATCTTCAGCAGCAGGTC	TTGGTGTTGACTTGTCTGT
GL19576	AATCGGCTCTATCCTTGG	GTAGGCATAACAGTCACC
GL24137	TCCAAGTGGCGTCAAGGT	TCATCGTCTTCTTCATCGTCTTCA

Over expression of *Glmhr1* gene

The over expression of *Glmhr1* gene (GL25628) in *P. pastoris* GS115 were performed according to the method that described in previous study (Ren et al., 2012). RNA was isolated and reverse transcription was carried out using the PrimeScript RT Master Mix kit (Takara Bio, Kyoto, Japan). *Glmhr* cDNA was amplified from *G. lucidum* using the forward primer 5′-GAATTCATGGCCGAGGAGCGGAAACCCT-3′ and the reverse primer 5′-GCGGCCGCCTAGCCCAACA AGACTTGAAA-3′. Purified PCR product was connected with T vector (Takara Bio, Kyoto, Japan) and the plasmid was transformed into the competent *Escherichia coli* DH 5α cells. The positive colony was verified by PCR and sequencing.

The verified *Glmhr* cDNA fragment was digested with *Xho*I and *Not*I enzymes, and the digested fragment was ligated into the *Xho*I/*Not*I-digested pPIC9k to construct the recombinant plasmid pPIC/Glmhr1, which was then transformed into the competent *E. coli DH* 5α cells. The positive colony was verified by PCR and sequencing. The plasmid pPIC/Glmhr1 was digested by *Sal*I, and then purified by agarose gel electrophoresis. The linearized plasmids were transformed into the competent *P. pastoris* GS115 cells by electroporation under 1,500 V. The positive colony were selected according to the method that described in previous study (Buensanteai et al., 2010), and then verified by PCR using the primers 5′-GCAAATGGCATTCTGACATCC-3′ and 5′-GACTGGTTCCAATTGACAAGC-3′. And the positive strain was named as GS115/Glmhr1.

The strain GS115/Glmhr1 was grown in 50 ml of BMGY medium for about 20 h at 30°C and 200 rpm. When the OD600 nm reached at about 4.0–8.0, cells were centrifuged and then resuspended and inoculated in 100 ml of BMMY medium. The yeasts were cultured for 5 days and 100% methanol was added every 24 h to the final concentration of 0.5%. After 5 days culture, the cells were collected and the expression of recombinant proteins was analyzed by western blot, and the contents of lanosterol and ergosterol were determined.

In vitro lanosterol and ergosterol content determination assay

Yeast strains GS115/Glmhr1 and GS115 cultures were centrifuged at 7,000 g for 10 min and resuspended twice in sterile distilled water to remove culture media. The yeasts were freeze-dried and treated with 10% KOH-methanol solution in 90°C water bath for 2 h, then equal volume of n-hexane was added. The n-hexane extracts were used to determine the contents of lanosterol and ergosterol. Analyses were carried out on an Agilent HPLC system using an Eclipse Pluse C18 (2.1 × 50 mm, 1.8 μm). The mobile phases A (95%, v/v) was 0.1% acetic acid in water and B (5%, v/v) was methanol. The flow rate was 0.2 mL/min, and the detection wavelength was 210 nm.

Statistics analysis

The correlation analysis between the contents of total triterpenoids and the expression profiles of TFs were carried out using SPSS version 20.0 (SPSS Inc., Chicago, IL, USA). The data mean ± standard error is calculated based on the results of three technical replicates using SPSS version 20.0 (SPSS Inc., Chicago, IL, USA). Experimental data was analyzed by One-way ANOVA followed by a *post-hoc* Tukey test, and $P < 0.05$ was considered statistically significant.

Results

Chemical analysis of *Ganoderma lucidum*

The content of total triterpenoids was the highest in primordia (15.77 mg/g) followed by fruiting body (13.52 mg/g) and aerial mycelia (6.44 mg/g), which is consistent with our previous study (Chen et al., 2012). The chemical composition

in different periods were further analyzed by UPLC/Q-TOF-MS/MS. As shown in Figure 1, a total of 89 components were detected in mycelia, primordium and fruiting body, including triterpenoids, organic acids, alkaloids, fatty acids and flavonoids, among which triterpenoids were the most important components (Table 2). Most of the components were found both at the positive and negative poles, and some were detected only at the positive pole or at the negative

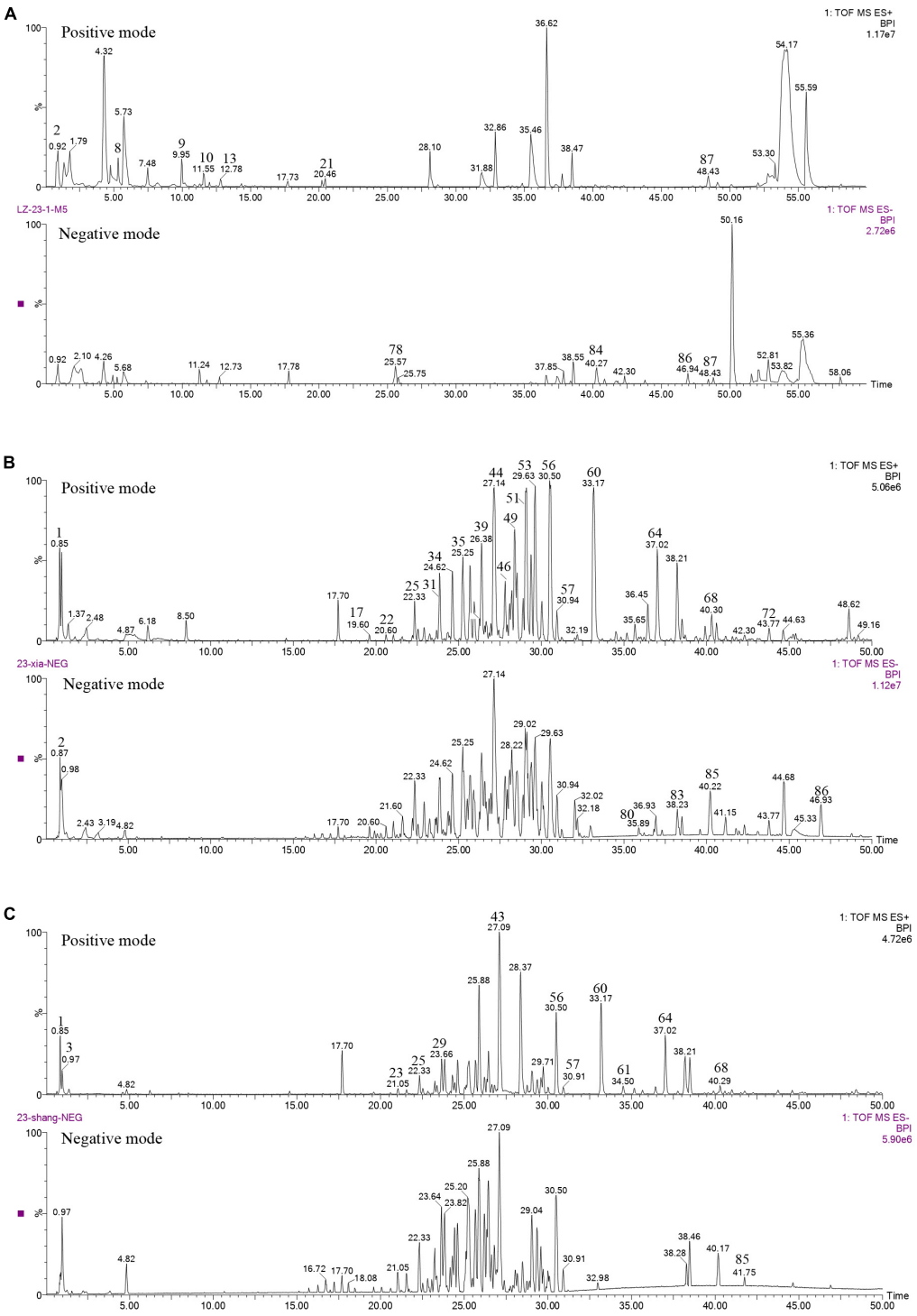

FIGURE 1
Chemical analysis of *G. lucidum* in different growth periods. **(A)** Aerial mycelia, **(B)** primordium, **(C)** fruiting body.

TABLE 2 Chemical analysis of *G. lucidum* in different growth periods.

NO.	tR (min)	Identification	Source	Selected ion	Elemental composition	NO.	tR (min)	Identification	Source	Selected ion	Elemental composition
1	0.85	5-Methylcytidine	M, P, F	$[M + H]^+$	C10H15N3O5	46	27.76	Resinacein G#	P, F	$[M + H]^+$	C30H40O8
2	0.87	Gluconic acid	M, P, F	$[M-H]^-$	C6H12O7	47	28.05	Lucideric acid A#	P, F	$[M + H]^+$	C27H38O6
3	0.97	Sucrose	P, F	$[M + HCOO]^-$	C12H22O11	48	28.19	Ganoleucoin E#	P, F	$[M + H]^+$	C27H38O6
4	1.22	Malic acid	P, F	$[M-H]^-$	C4H6O5	49	28.49	Ganoderenic acid D#	P, F	$[M + H]^+$	C30H40O7
5	2.20	Citric acid	P	$[M-H]^-$	C6H8O7	50	28.85	Lucidenic acid F#	P, F	$[M + H]^+$	C27H36O6
6	3.83	Uridine	M, P, F	$[M-H]^-$	C9H12N2O6	51	29.04	Gibbosic acid L#	P, F	$[M + H]^+$	C30H40O6
7	5.07	Histidylprolinamide	P	$[M + H]^+$	C11H17N5O2	52	29.35	Lucidenic acid D#	P, F	$[M + H]^+$	C29H38O8
8	5.37	Phenylalanine	M, P	$[M + H]^+$	C9H11NO2	53	29.63	Ganoderic acid E#	P, F	$[M + H]^+$	C30H40O7
9	9.95	hexahydro-7-hydroxy-3-[(1R) –1–methylpropyl]-Pyrrolo[1,2-a]pyrazine-1,4-dione	M	$[M + H]^+$	C11H18N2O3	54	29.99	Ganolucidic acid D#	P, F	$[M + H]^+$	C30H44O6
10	11.55	L-Leu-L-Phe	M	$[M + H]^+$	C14H16N2O3	55	30.13	Ganodernoid D#	F	$[M + H]^+$	C32H40O9
11	11.67	Riboflavin	P, F	$[M + H]^+$	C17H20N4O6	56	30.50	Ganoderic acid F#	P, F	$[M + H]^+$	C32H42O9
12	11.99	Cyclo(pro-leu)	M	$[M + H]^+$	C11H18N2O2	57	30.94	Ganoderic acid LM2#	P, F	$[M + H]^+$	C30H42O7
13	12.78	cyclo(L-IIe-L-Pro)	M	$[M + H]^+$	C11H18N2O2	58	31.27	12β-Acetoxy-3,7,11,15,23-pentaoxolanosta-8,20-dien-26-oic acid#	P, F	$[M + H]^+$	C32H40O9
14	14.33	cyclo(L-Phe-L-Pro)	M	$[M + H]^+$	C14H16N2O2	59	32.27	Ganoderiol D#	P, F	$[M + H]^+$	C30H48O5
15	15.87	Oregonensin A	F	$[M-H]^-$	C16H16O6	60	33.17	Phytosphingosine	P, F	$[M + H]^+$	C18H39NO3
16	16.99	Hesperidin	P	$[M + H]^+$	C28H34O15	61	34.51	Ganoderitriol M#	P, F	$[M + H]^+$	C30H50O4
17	19.0	12-Hydroxyganoderic acid C2#	P, F	$[M + H]^+$	C30H46O8	62	35.29	C19-Phytosphingosine	M, P, F	$[M + H]^+$	C19H41NO3
18	19.91	Applanatumol S	F	$[M-H]^-$	C16H20O6	63	36.04	Ganolucidic acid E#	P	$[M + H]^+$	C30H44O5
19	20.06	Sebacic acid#	P, F	$[M-H]^-$	C10H18O4	64	37.02	C20-Phytosphingosine	P, F	$[M + H]^+$	C20H43NO3
20	20.20	α-Solanine	M	$[M + H]^+$	C45H73NO15	65	37.17	C20-Phytosphingosine	P, F	$[M + H]^+$	C20H43NO3
21	20.46	Chaconine	M	$[M + H]^+$	C45H73NO14	66	39.72	24,25-epoxy-26,27-dihydryoxy-Lanosta-7,9(11)-dien-3-one#	F	$[M + H]^+$	C30H46O4
22	20.60	Ganoderic acid L#	P, F	$[M + Na]^+$	C30H46O8	67	40.17	Linolenic acid	M	$[M + H]^+$	C18H30O2
23	21.05	Ganoderic acid AP#	P	$[M + H]^+$	C30H42O9	68	40.30	2-Amino-1,3-docosanediol	P, F	$[M + H]^+$	C22H47NO2
24	21.60	(3β,7β,25R)-3,7,20,24-tetrahydroxy-11,15,23-trioxo-Lanost-8-en-26-oic acid#	P	$[M + H]^+$	C30H44O9	69	41.13	Ganodermaside D	F	$[M + H]^+$	C28H40O2
25	22.33	Ganoderic acid G#	P, F	$[M + H]^+$	C30H44O8	70	41.78	9-Hydroxy-(10E,12Z,15Z)-octadecatrienoic acid#	M, P, F	$[M + H]^+$	C18H30O3

(Continued)

10.3389/fmicb.2022.1052377

TABLE 2 (Continued)

NO.	tR (min)	Identification	Source	Selected ion	Elemental composition	NO.	tR (min)	Identification	Source	Selected ion	Elemental composition
26	22.53	Ganoderic acid C6[#]	P, F	$[M + H]^+$	C30H42O8	71	41.91	Ganoderiol E[#]	F	$[M + Na]^+$	C30H48O4
27	22.89	3β,7β,15α,24-tetrahydroxy-11,23-dioxo-5α-lanosta-8,20E-dien-26-oic acid[#]	P, F	$[M + H]^+$	C30H44O8	72	43.79	Ganoderic acid DM[#]	P, F	$[M + H]^+$	C30H44O4
28	23.24	Ganoderenic acid C[#]	P, F	$[M + H]^+$	C30H44O7	73	45.15	Ganodermanondiol[#]	P	$[M + H]^+$	C30H48O3
29	23.66	Ganoderic acid H[#]	P, F	$[M + H]^+$	C32H44O9	74	47.34	Demethylincisterol A3	M	$[M + H]^+$	C21H32O3
30	23.80	Ganoderic acid C2[#]	P, F	$[2M + H]^+$	C30H46O7	75	48.46	9(11)-Dehydroergosterol	M	$[M + H]^+$	C28H42O
31	24.17	Ganoderic acid J[#]	P	$[M + H]^+$	C30H42O7	76	23.06	Lucidenic acid M[#]	P	$[M-H]^-$	C27H42O6
32	24.29	Lucidenic Acid R[#]	P, F	$[M + H]^+$	C32H44O10	77	24.40	Lucidenic acid N[#]	P, F	$[M-H]^-$	C27H40O6
33	24.47	Ganolucidate F[#]	P, F	$[M + H]^+$	C30H46O6	78	25.57	Pinellic acid	M	$[M-H]^-$	C18H34O5
34	24.62	Resinacein H[#]	P, F	$[M + H]^+$	C30H42O8	79	29.77	12-Acetoxy-3-hydroxy-7,11,15-trioxolanost-8,16,24-trien-26-oic acid[#]	P	$[M-H]^-$	C32H42O8
35	25.25	7β,15α,20-Trihydroxy-3,11,23-trioxo-5α-lanosta-8-en-26-oic Acid[#]	P, F	$[M + H]^+$	C30H44O8	80	35.89	Elfvingic acid B[#]	F	$[M-H]^-$	C30H40O8
36	25.65	Ganoderic acid B[#]	P, F	$[M + H]^+$	C30H44O7	81	36.89	7-Oxoganoderic acid Z[#]	F	$[M + HCOO]^-$	C30H46O4
37	25.94	Ganoderic acid D[#]	P, F	$[M + H]^+$	C30H42O7	82	37.30	Ganoderic Acid ZXYL[#]	F	$[M-H]^-$	C30H46O5
38	26.19	Ganoderenic acid K[#]	P, F	$[M + H]^+$	C32H44O9	83	38.23	Ganomycin I	F	$[M-H]^-$	C21H26O4
39	26.38	Ganoderic acid C[#]	P, F	$[M + H]^+$	C32H42O7	84	40.27	13 hydroxyoctadecadieno?ic acid	M, P, F	$[M-H]^-$	C18H32O3
40	26.46	Spiroganocalitone D[#]	P, F	$[M + H]^+$	C32H44O8	85	41.75	(11α)-11,26,27-trihydroxy-lanosta-8,24-diene-3,7-dione[#]	P	$[M-H]^-$	C30H46O5
41	26.63	Ganoderic acid V1[#]	P, F	$[M + H]^+$	C30H42O7	86	46.93	2-Hydroxy-hexadecanoic acid	M, P, F	$[M-H]^-$	C16H32O3
42	26.79	(7β,12β,20Z)-12-(Acetyloxy)-7-hydroxy-3,11,15,23-tetraoxolanosta-8,20(22)-dien-26-oic acid[#]	P	$[M + H]^+$	C32H42O9	87	48.43	Ganoderic acid T[#]	M	$[M-H]^-$	C36H52O8
43	27.11	12β-Acetoxyganoderic Acid θ[#]	P	$[M + H]^+$	C32H44O9	88	48.79	Palmitoleic acid	M	$[M-H]^-$	C16H30O2
44	27.14	Ganoderic acid A[#]	P, F	$[M-H_2O + H]^+$	C30H44O7	89	51.57	2-Hydroxy-octadecanoic acid	M, P, F	$[M-H]^-$	C18H36O3
45	27.39	Ganolucidic acid A[#]	P, F	$[M + H]^+$	C30H44O6						

M, mycelia; P, primordium; F, fruiting body. [#]GT.

10.3389/fmicb.2022.1052377

pole (**Supplementary Table 1**). Only Ganoderic acid T was detected out in the mycelia, while there were 45 and 48 triterpenoids in the primordium and fruiting body, respectively. Of these triterpenoids, 37 were identified in both primordium and fruiting body, and contents of many triterpenoids in the primordia were higher than that in fruiting body formation.

Methyl jasmonate–induced biomass and ganoderma triterpenoids production of the mycelia

The mycelia were treated with MeJA at final concentrations of 50, 100, 150, 200, and 300 μM, the fugal biomass (dry weight, DW) and the contents of total triterpenoids were shown in **Figure 2**. The biomass of mycelia with different concentration of MeJA treatment were 2.13, 2.09, 2.32, 6.26, and 4.87-fold greater than that of the control (**Figure 2A**), and total triterpenoids contents were 1.09, 1.23, 1.38, 2.17, and 1.93-fold higher (**Figure 2B**). The results showed that the biomass and the contents of total triterpenoids could be significantly increased through the induction of MeJA, and both peaked at 200 μM. Based on the change of biomass and the contents of total triterpenoids, the mycelia treated with MeJA at final concentrations of 0, 200, and 300 μM were used for transcriptome analysis.

Identification of putative transcription factors involved in ganoderma triterpenoid synthesis

Three groups of RNA samples were used for the Illumina sequencing to obtain totals of 134577592, 133451088, and 132872034 clean reads. As a result, a total of 1,316 and 2,448 DEGs were identified in 200 μM treatment group and 300 μM treatment group, respectively (**Supplementary Table 2**). To validate the reliability of the RNA-Seq data, the expression level of 9 TFs was randomly selected for qRT-PCR assays (**Figure 3**). The results showed that the expression levels detected by qRT-PCR assay matched well with the RNA-Seq data, and the qRT-PCR data confirmed the reliability of the results in the RNA-Seq analysis.

In the genome of *G. lucidum*, there are approximately 600 TFs, 103 of which were significantly differentially expressed in response to MeJA elicitation (**Supplementary Table 3**). These differently expressed TFs (DETs) are involved the fungal growth, secondary metabolism and stress responses, including C2H2 (18), TFII-related (15), HTH (12), fungal (9), bZIP (6), HMG (6), etc (**Figure 4A**). Among them, there were 39 DETs that detected in both 200 μM group and 300 μM treatment group. And the expression level of 25 DETs in 200 μM was higher than that in 300 μM, which was consistent with the change trend of the contents of triterpenoids and mycelia biomass after MeJA treatment. Besides, 8 TFs were down-regulated after MeJA induction.

Our group had reported the transcriptome of *G. lucidum* at different growth stages including mycelia, primordium and fruiting body (fruiting body formation stage) (Chen et al., 2012). The gene expression levels of 103 DETs in different periods were evaluated to more precisely screen the TFs that possibly be involved in the GT synthesis (**Figure 4B** and **Supplementary Table 3**). Overall, 19 TFs were highly expressed in mycelia (relative expression level > 100), 25 TFs in primordia and 15 TFs in fruiting body. Among them, 9 TFs (GL28195, GL30199, GL28074, GL22646, GL23680, GL23585, GL31314, GL23559, and GL31381) were highly expressed in mycelia, primordia and fruiting body periods, especially GL28195 (bZIP) and GL30199 (C2H2). Additionally, GL25628 (fungal) was especially highly expressed in mycelia, while GL26472 (HSF) was highly expressed in primordia and fruiting body.

Correlation analysis revealed that the expression profiles of 35 MeJA-responsive TFs were positively correlated with the contents of total triterpenoid during development [correlation coefficient (r) > 0.85] and 5 were negatively correlated with the contents of total triterpenoid ($r < -0.85$), suggesting they might be involved in triterpenoid biosynthesis (**Supplementary Table 3**). On the basis of the expression profiles of these 40 TFs, GL23559 (MADS), GL26472 (HTH), and GL31187 (HMG) were most likely to positively regulate GTs biosynthesis, while GL25628 (fungal) and GL26980 (PHD) were most likely to be negative regulators. Among them, *Glmhr1* (GL25628) was a candidate TF for regulating the expression of *FPS*, which is one of the important genes for lanosterol production through MVA pathway (Xu et al., 2020).

The effect of *Glmhr1* on the lanosterol and ergosterol content

A 1,732 bp DNA product of *Glmhr1* (GL25628) gene was obtained and ligated into the pPIC9k vector to construct the recombinant plasmid pPIC9k/Glmhr1, which was verified by *Xho*I and *Not*I digestion (**Figure 5A**). The linearized plasmid pPIC9k/Glmhr1 was transformed into *P. pastoris* GS115 to obtain recombinant strain GS115/Glmhr. Positive transformants were selected on MD plates and verified by PCR amplification. Western blotting revealed that the molecular weight of expressed Glmhr1 in recombinant strain GS115/Glmhr1 was about 74 kDa, which was consistent with the theoretical molecular weight (**Figure 5B**). In addition, the contents of lanosterol and ergosterol in GS115 were 261.5 mg/g DCW (dry cell weight) and 195.4 mg/g, respectively. While those in GS115/Glmhr1 were 163.7 and 194.7 mg/g, respectively (**Figure 5C**). The lanosterol content in GS115/Glmhr1 was significantly less than that of GS115, but there was no difference

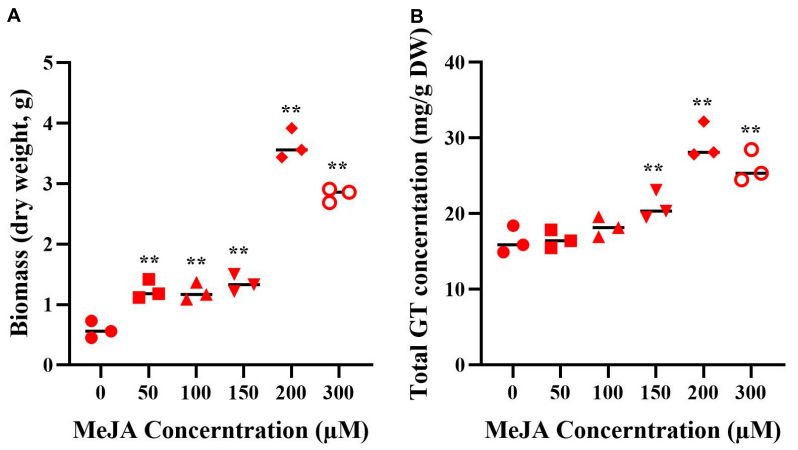

FIGURE 2
The biomass **(A)** and GT content **(B)** of *G. lucidum* in response to MeJA treatment. One-way analysis of variance (ANOVA) followed by a post-hoc Tukey test. **Means extremely significant difference between treatment and control, p-value < 0.01.

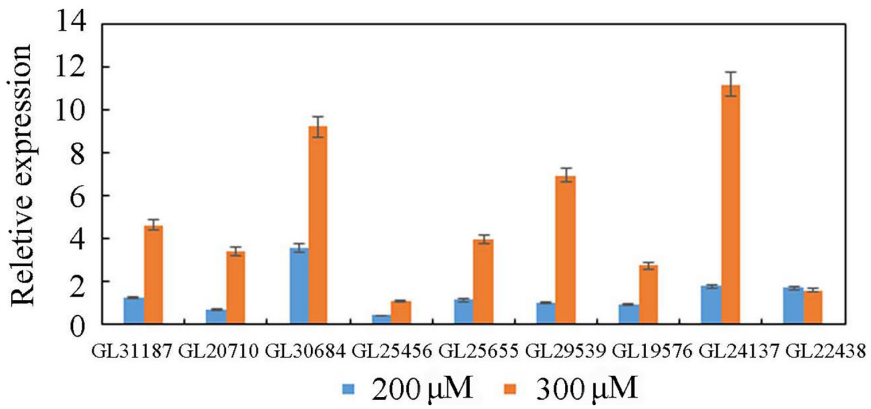

FIGURE 3
Quantitative real-time PCR analysis of TFs.

in ergosterol content between them suggesting that *Glmhr1* has a negative regulation effect on lanosterol production.

Discussion

G. lucidum contains significant amounts of triterpenoids, which are bioactive compounds with antitumor and immune-modulatory properties. At present, more than 150 triterpenoids have been discovered in *G. lucidum*. Forty-eight and 40 triterpenoids were identified in the fruiting body of strain G203 and CICC 14022, respectively, but only a few were detected in both strains, such as Ganoderic acid A, D, F, G, H, and L, indicating that the GT composition varied depending on the growth stage and place of origin (Xie et al., 2020). In this study primordium and fruiting body have similar triterpene composition, but the contents of many components in primordium were higher than that in fruiting body. The amount and contents of triterpenes in aerial mycelia were lower than those in primordia and fruiting body, which is consistent with our previous study (Chen et al., 2012). Triterpenoids are important bioactive components and biosynthesized through the MVA pathway in *G. lucidum*. Some known genes associated with the MVA pathway had been reported to be upregulated in responsive to MeJA, including hydroxy-3-methylglutaryl-coenzyme A synthase (*HMGS*), hydroxy-3-methylglutaryl-coenzyme A reductase (*HMGR*), mevalonate-5-pyrophosphate decarboxylase (*MVD*), farnesyl pyrophosphate synthase (*FPS*), squalene synthase (*SQS*), and oxidosqualene cyclase (*OSC*) (Ren et al., 2010). Meanwhile, the yield of ganoderic acids was 45.3% higher than the untreated control sample after 254 μM of methyl jasmonate treatment (Ren et al., 2010). In this study, the content of total GTs reached the highest value at 200 μM, which was 2.17

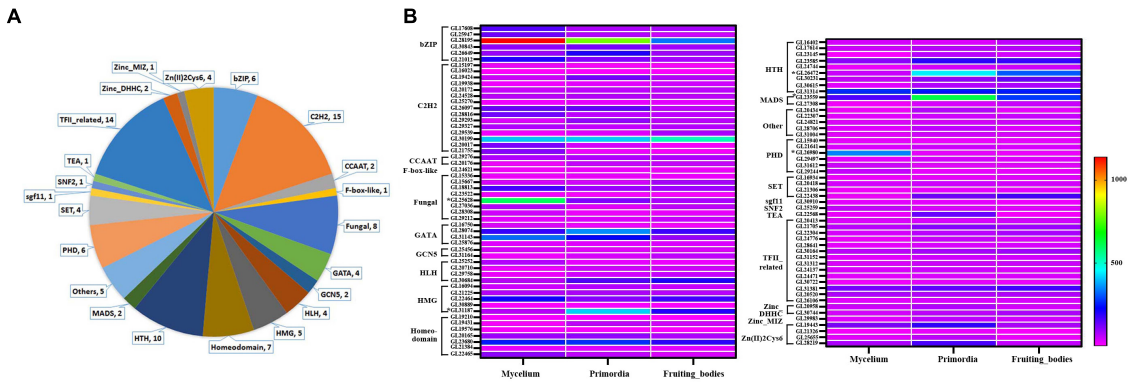

FIGURE 4
Classes analysis of differently expressed TFs and their expression level in mycelia, primordium and fruiting body. **(A)** Classes analysis; **(B)** expression level.

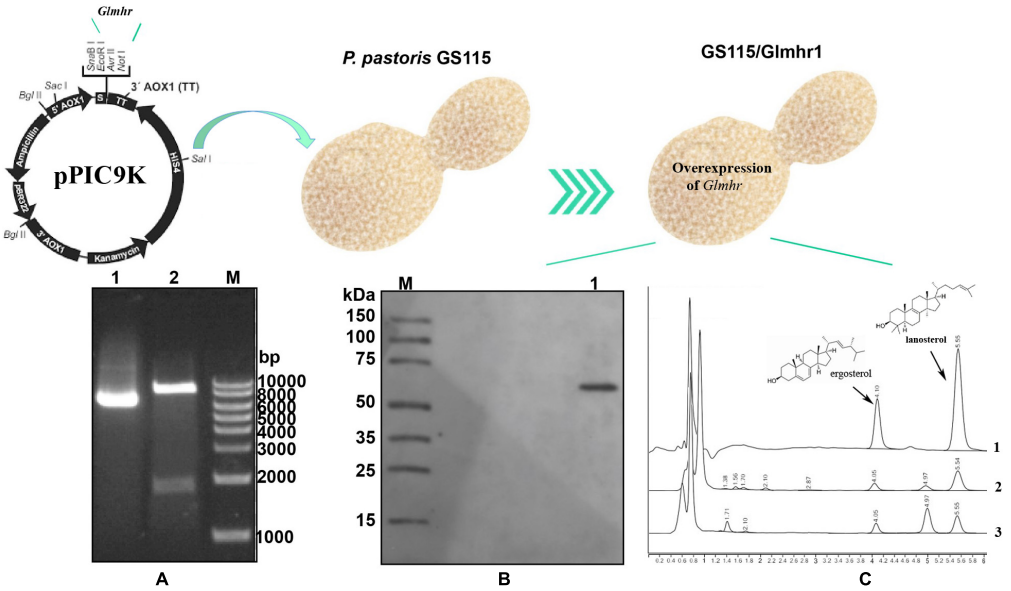

FIGURE 5
Over expression of Glmhr1 gene. **(A)** Verification of the recombinant plasmid pPIC9k/Glmhr1. M: Maker; 1: plasmid pPIC9k/Glmhr1; 2: *Xho*I/*Not*I- digested plasmid pPIC9k/Glmhr1. **(B)** Western blotting analysis. M: Maker; 1: positive colony. **(C)** Determination of the content of lanosterol and ergosterol. 1: standard; 2: strain GS115; 3: strain GS115/Glmhr1.

times higher than that of the control group, also indicating that MeJA could increase the production of GT.

There have been some reports on the induction of the content of total triterpenoids using MeJA and other elicitors, only a few genes have been further described (Chuang et al., 2009; Zhang et al., 2010; Zhang and Zhong, 2013; Da et al., 2015; Sudheer et al., 2016; Feng et al., 2017; Gu et al., 2017). In *G. lucidum*, ozone gas and nitric oxide (NO) also had been reported to increase the content of GTs (Sudheer et al., 2016; Gu et al., 2017), and the transcriptome analysis of nitric oxide response had been reported. Besides, NO might decrease Acon activity by S-nitrosylation at Cys-594 to regulate GA biosynthesis under heat stress condition in *G. lucidum*. Previous research have described the mechanism by which elicitors the biosynthesis of triterpenoids, but few TFs were described in detail. Additionally, cDNA-AFLP was used to screen differentially expressed transcripts (TDFs) of the MeJA-treated mycelia of *G. lucidum* and to gain insights into the regulatory mechanisms of GA biosynthesis in response to MeJA. Only 90 TDFs were annotated with known functions through BLASTX searching of the GenBank database (Ren et al., 2013a). As previous reported, there were a total of 16,113 genes in the *G. lucidum* genome (Chen et al., 2012). The above studies have

provided limited information about the function of TFs involved in the regulation of GTs biosynthesis.

Many TFs in plants have been extensively studied for their roles in secondary metabolites biosynthesis, such as, JA- or MeJA-responsive AP2/ERF, C2H2, MYC, MYB, HLH, and WRKY TFs and their functions have been described to improve both the production of metabolites and biomass, as well as upregulated the expression of genes (Tsubasa and Takashi, 2011; Zhang et al., 2011; Yu et al., 2012). However, TFs in fungi are more reported for their roles in the growth and development than in secondary metabolites biosynthesis, resulting in a limited understanding of the transcriptional regulation of filamentous fungi. In *G. lucidum*, *GlPacC* (GL370073) silencing inhibits the growth rate of mycelium, the development of the fruiting body and the synthesis of ganoderma acids (Wu et al., 2016). *Swi6*, which belongs to the APSES family, is a TF unique to fungi. Study have shown that the silencing mutant of *GlSwi6* (GL18755) in *G. lucidum* reduced the growth rate of mycelium, increased mycelium branches, inhibited the formation of fruiting body, and reduced the content of ganoderma acid (Zhang et al., 2018). Additionally, *GlSkn7*, is a highly conserved stress-responsive TF, whose silencing resulted in hypersensitivity to oxidative stress and the increase of the content of GAs (Wang et al., 2018). These transcription factors involved in mycelial growth are also involved in triterpenoids synthesis. In this study, 40 TFs were found to be correlated with the contents of triterpenoids (**Supplementary Table 3**), suggesting that they might be involved in the regulation of GTs biosynthesis.

Eight negatively regulated TFs were screened by MeJA treatment, and *Glmhr1* was proved to negatively regulate lanosterol synthesis. *Glmhr1* contained a fungal_ TF_ MHR domain functional domain, which is present in the fungal zinc cluster transcription factors that contain a GAL4-like C6 zinc binuclear cluster DNA-binding domain. In our previous study, *Glmhr1* was screened by yeast one-hybrid library system and considered to be a candidate TF for regulating the expression of *FPS*, which is the important gene involved in lanosterol biosynthesis (Xu et al., 2020). Some GAL4-like transcription factors, like GAL4 and STB5, has been extensively studied for their regulatory role in the metabolic process. *Gal4* is a transcriptional activator of genes associated with galactose metabolism. Yeast Gal4 recognizes and binds promoter UAS through its N-terminal DNA-binding domain, and initiates RNA polymerase II complex assembly and transcription by interacting with transcription factors through its C-terminal activation domain. *SUT2*, a Gal4-like gene in *Pichia pastoris*, whose overexpression could increase ergosterolcontent in cells (Yang et al., 2020). While, *STB5* is a negative regulator of azole resistance in *Candida glabrata*. Its overexpression resulted in the repressed azole resistance, and its deletion caused a modest increase in resistance (Noble et al., 2013). In this study, the overexpression of *Glmhr1* resulted in the decrease of lanosterol content, indicating that it may affect triterpene content of *G. lucidum* by decreasing the production of lanosterol. But how does *Glmhr1* regulate the lanosterol biosynthesis need further study.

HMG-box TFs were reported to play a great important role in fungal growth development. There are total of 20 HMG-box TFs in the genome, and 5 genes could be elicited by MeJA. Among them, GL31187 was highly expressed in primordia and fruiting body, especially in primordia. GL31187 was identified as *NHP6B* that was small and abundant chromatin proteins without sequence specificity for DNA binding (Stillman, 2010). In yeast, Nhp6A/B proteins, whose deletion mutant (nhp6DD mutant) is temperature sensitive for growth, were required for the activation of RNA polymerase II and the promotion of RNA polymerase III transcription (Costigan et al., 1994; Stillman, 2010). Several other fungal HMG-box TFs such as *pcc1*, *exp, hom1*, and *hom2* played an imprtant role in fruiting body formation and spore production (Ohm et al., 2011; Ait et al., 2013).

MADS-box TFs were also involved in the regulation of hyphal growth and sexual development. In the *G. lucidum* genome, both 2 MADS-box TFs were upregulated in response to MeJA treatment. Among them, GL23559 was highly expressed during the three growth periods, especially in the primordia, indicating its participation in all the growth periods. It was identified as a MADS-box TF homologous to TF *Mcm1* in *S. cerevisiae*, which regulated the expression of genes related to arginine metabolism, G2-specificd transcription and mating-type switching (Messenguy and Dubois, 1993; Wu et al., 1998). *Mcm1* homologous have also been characterized in the *Beauveria bassiana* and *Fusarium graminearum* (Yang et al., 2015; Zhao et al., 2019), which also involved in fungal development. Mcm1 homologous TF *SrfA* is required for pore differentiation through regulation of the expression of spore-specific genes involved in late events of spore maturation. And the *mcm1* gene deletion mutant resulted in increased hyphal branching, reduced biomass, and reduced hyphal compartment length during vegetative growth. The mutant strain was unable to produce a fruiting body or ascospores and microconidium during sexual development (Nolting and Pöggeler, 2006; Zhou et al., 2011; Qu et al., 2014).

In addition, there were some other MJ-responsive transcription factors that were also involved in fungal growth. Current researches revealed that bZIP TFs play an important role in response to biotic and abiotic stresses, regulation of growth and development, and biosynthesis of secondary metabolites (Balázs et al., 2010; Gai et al., 2022). There are 12 bZIP TFs in the genome, and 6 of them were upregulated in response to MeJA treatment. Among them, GL28195 was expressed in the mycelia, the primordia and the fruiting body at high level, indicating its participation in all the growth processes. In addition, GL26649 was identified as *Aft1*, which is a homolog to the gene isolated from *Saccharomyces cerevisiae*

and *Schizosaccharomyces pombe*. *Aft1* plays a central role in iron homeostasis and interacts with an iron-responsive element (FeRE), affect the osmotic stress response (OSA), and also is necessary for sexual development in entry into the stationary phase (Berthelet et al., 2010; Miao et al., 2011). What's more, GL30843 was predicted to contain a YAP domain similar to *S. cerevisiae YAP1*, which is required for tolerance of oxidative and osmotic stress (Gruhlke et al., 2017). The yapA deletion mutant exhibited delays in the rate of growth, germination, and conidiation. The same regulatory function in stress tolerance had been characterized in *Epichloe festucae* and *Aspergillus fumigatus* (Lessing et al., 2007; Cartwright and Scott, 2013). These bZIP genes properly played an important role in the growth period of *G. lucidum*.

The C2H2 TFs are one of the most ubiquitous transcription factor families in eukaryotes (Ren et al., 2013b; Yuan et al., 2018). In fungi, C2H2 TFs are involved in cell differentiation, mycelia growth, asexual reproduction and oxidative stress signaling pathways (Messenguy and Dubois, 1993; Jin et al., 2014; Malapi-Wight et al., 2014; Yao et al., 2016). In the *G. lucidum* genome, there are 79 C2H2 TFs. Among them, the C2H2 TF *PacC* (GL30073), the deletion of which would inhibit the growth of mycelia and the spore production (Wu et al., 2016), was not detected in this study. While its expression level in the mycelia, the primordia and the fruiting body was not high, indicating that some genes with low expression level are also indispensable in the growth period. In this study, 14 C_2H_2 DETs were upregulated and 1 downregulated in response to MeJA. GL26097, identified as *Sfp1* that has been reported as a stress- and nutrient-sensitive TF that regulates ribosomal protein gene expression in yeast (Marion et al., 2004). Deletion of the *Sfp1* gene resulted in slow cell growth and cell adhesion, indicating that *Sfp1* is required for normal fungal growth (Albert et al., 2018).

Conclusion

In *G. lucidum*, the composition of triterpenes is different in different stages, and MeJA could induce an increase in triterpene concentration and biomass of mycelia. Transcriptome sequencing was used to analyze TFs in response to MeJA-induction, and a total of 103 DETs were identified. Furthermore, corresponding expression levels of these TFs in mycelia, primordia and fruiting body were analyzed. The results revealed that most of MeJA-responsive TFs extensive participation in the period of GTs biosynthesis and growth development. Furthermore, *Glmhr1* was verified to have a negative regulatory effect through decreasing the production of lanosterol.

Data availability statement

The datasets presented in this study can be found in online repositories. The names of the repository/repositories and accession number(s) can be found in the article/**Supplementary material**.

Author contributions

XX, SC, and JR conceived and designed the experiments. FZ, YL, and YZ performed the experiments. XX and FZ analyzed the data. FZ and HZ contributed to the reagents, materials, and analysis tools. XX wrote the manuscript. SC and JR revised the manuscript. All authors contributed to the article and approved the submitted version.

Funding

This research was funded by the Natural Science Foundation of the Fujian Province (No. 2020J01131023); National Natural Science Foundation of China (No. 81503189); and Special Funds for Science and Technology Innovation in Fujian Agriculture and Forestry University (No. KFA20065A).

Conflict of interest

The authors declare that the research was conducted in the absence of any commercial or financial relationships that could be construed as a potential conflict of interest.

Publisher's note

All claims expressed in this article are solely those of the authors and do not necessarily represent those of their affiliated organizations, or those of the publisher, the editors and the reviewers. Any product that may be evaluated in this article, or claim that may be made by its manufacturer, is not guaranteed or endorsed by the publisher.

Supplementary material

The Supplementary Material for this article can be found online at: https://www.frontiersin.org/articles/10.3389/fmicb.2022.1052377/full#supplementary-material

References

Afrin, S., Huang, J. J., and Luo, Z. Y. (2015). JA-mediated transcriptional regulation of secondary metabolism in medicinal plants. *Sci. Bull. 60, 1062–1072.* doi: 10.1007/s11434-015-0813-0

Ait, B. J., Coppin, E., Brun, S., Peraza-Reyes, L., Martin, T., Dixelius, C., et al. (2013). Network of HMG-box transcription factors regulates sexual cycle in the fungus *Podospora anserina*. *PLoS Genet.* 9:e1003642. doi: 10.1371/journal.pgen.1003642

Albert, B., Tomassetti, S., Gloor, Y., Dilg, D., Mattarocci, S., and Kubik, S. (2018). Sfp1 regulates transcriptional networks driving cell growth and division through multiple promoter binding modes. *Genes Dev.* 33, 288–293. doi: 10.1101/420794

Ali, M., Abbasi, B. H., and Ali, G. S. (2015). Elicitation of antioxidant secondary metabolites with jasmonates and gibberellic acid in cell suspension cultures of *Artemisia absinthium* L. *Plant Cell Tissue Organ. Cult.* 120, 1099–1106. doi: 10.1007/s11240-014-0666-2

Aranega-Bou, P., de la O Leyva, M, Finiti, I., García-Agustín, P., and González-Bosch, C. (2014). Priming of plant resistance by natural compounds. Hexanoic acid as a model. *Front. Plant Sci.* 5:488. doi: 10.3389/fpls.2014.00488

Balázs, A., Pócsi, I., Hamari, Z., Leiter, É, Emri, T., Miskei, M., et al. (2010). AtfA bZIP-type transcription factor regulates oxidative and osmotic stress responses in *Aspergillus nidulans*. *Mol. Genet. Genom.* 283, 289–303. doi: 10.1007/s00438-010-0513-z

Berthelet, S., Usher, J., Shulist, K., Hamza, A., Maltez, N., Johnston, A., et al. (2010). Functional genomics analysis of the *Saccharomyces cerevisiae* iron responsive transcription factor Aft1 reveals iron-independent functions. *Genetics* 185, 1111–1128. doi: 10.1534/genetics.110.117531

Buensanteai, N., Mukherjee, P. K., Horwitz, B. A., Cheng, C., Dangott, L. J., and Kenerley, C. M. (2010). Expression and purification of biologically active *Trichoderma virens* proteinaceous elicitor Sm1 in *Pichia pastoris*. *Protein Expr. Purif.* 72, 131–138. doi: 10.1016/j.pep.2010.03.006

Cartwright, G. M., and Scott, B. (2013). Redox regulation of an AP-1-like transcription factor, YapA, in the fungal symbiont *Epichloe festucae*. *Eukaryot Cell* 12, 1335–1348. doi: 10.1128/EC.00129-13

Chen, S., Li, Z., Zhang, S., Zhou, Y., Xiao, X., Cui, P., Xu, B., Zhao, Q., Kong, S., Dai, Y. (2022a). Emerging biotechnology applications in natural product and synthetic pharmaceutical analyses. *Acta Pharm. Sin. B* 12, 4075–4097. doi: 10.1016/j.apsb.2022.08.025

Chen, C., Liu, Fu, Zhang, K., Niu, X., Zhao, H., Liu, Q., et al. (2022b). MeJA-responsive bHLH transcription factor LjbHLH7 regulates cyanogenic glucoside biosynthesis in *Lotus japonicus*. *J. Exp. Bot.* 73, 2650–2665. doi: 10.1093/jxb/erac026

Chen, S., Xu, J., Liu, C., Zhu, Y., Nelson, D. R., and Zhou, S. (2012). Genome sequence of the model medicinal mushroom *Ganoderma lucidum*. *Nat. Commun.* 3, 913–913. doi: 10.1038/ncomms1923

Chi, B., Wang, S., Bi, S., Qin, W., Wu, D., Luo, Z., et al. (2018). Effects of ganoderic acid A on lipopolysaccharide-induced proinflammatory cytokine release from primary mouse microglia cultures. *Exp. Ther. Med.* 15, 847–853. doi: 10.3892/etm.2017.5472

Chuang, H. W., Wang, I. W., Lin, S. Y., and Chang, Y. L. (2009). Transcriptome analysis of cadmium response in *Ganoderma lucidum*. *FEMS Microbiol. Lett.* 293, 205–213. doi: 10.1111/j.1574-6968.2009.01533.x

Costigan, C., Kolodrubetz, D., and Snyder, M. (1994).). NHP6A and NHP6B, which encode HMG1-like proteins, are candidates for downstream components of the yeast SLT2 mitogen-activated protein kinase pathway. *Mol. Cell Biol.* 14, 2391–2403. doi: 10.1128/MCB.14.4.2391

Da, J., Cheng, C. R., Yao, S., Long, H. L., Wang, Y. H., Khan, I. A., et al. (2015). A reproducible analytical system based on the multi-component analysis of triterpene acids in *Ganoderma lucidum*. *Phytochemistry* 114, 146–154. doi: 10.1016/j.phytochem.2014.08.007

Dong, Z., Dong, G., Lai, F., Wu, H., and Zhan, Q. (2021). Purification and comparative study of bioactivities of a natural selenized polysaccharide from *Ganoderma Lucidum* mycelia. *Int. J. Biol. Macromol.* 190, 101–112. doi: 10.1016/j.ijbiomac.2021.08.189

Feng, J., Zhang, J. S., Feng, N., Yan, M. Q., Yang, Y., Jia, W., et al. (2017). A novel *Ganoderma lucidum* G0119 fermentation strategy for enhanced triterpenes production by statistical process optimization and addition of oleic acid. *Eng. Life Sci.* 17, 430–439. doi: 10.1002/elsc.201600071

Gai, Y., Li, L., Liu, B., Ma, H., Chen, Y., Zheng, F., et al. (2022). Distinct and essential roles of bZIP transcription factors in the stress response and pathogenesis in *Alternaria alternata*. *Microbiol. Res.* 256:126915. doi: 10.1016/j.micres.2021.126915

Gruhlke, M. C. H., Schlembach, I., Leontiev, R., Uebachs, A., Gollwitzer, P. U. G., Weiss, A., et al. (2017). Yap1p, the central regulator of the S. cerevisiae oxidative stress response, is activated by allicin, a natural oxidant and defence substance of garlic. *Free Radic. Biol. Med.* 108, 793–802. doi: 10.1016/j.freeradbiomed.2017.05.004

Gu, L., Zhong, X., Lian, D., Zheng, Y., Wang, H., and Liu, X. (2017). Triterpenoid Biosynthesis and the Transcriptional Response Elicited by Nitric Oxide in Submerged Fermenting *Ganoderma lucidum*. *Process Biochem.* 60, 19–26. doi: 10.1016/j.procbio.2017.05.029

Hu, Y., Lian, L., Xia, J., Hu, S., Xu, W., Zhu, J., et al. (2019). Influence of *PacC* on the environmental stress adaptability and cell wall components of *Ganoderma lucidum*. *Microbiol. Res.* 230:126348. doi: 10.1016/j.micres.2019.126348

Jin, W. B., Wiemann, P., Garvey, G. S., Fang, Y. L., Haas, B., Wortman, J., et al. (2014). Illumina identification of RsrA, a conserved C2H2 transcription factor coordinating the NapA mediated oxidative stress signaling pathway in Aspergillus. *BMC Genomics* 15:1011. doi: 10.1186/1471-2164-15-1011

Kim, M. J., Chiu, Y. C., Kim, N. K., Park, H. M., Lee, C. H., Juvik, J. A., et al. (2017). Cultivar-Specific Changes in Primary and Secondary Metabolites in *Pak Choi* (Brassica Rapa, Chinensis Group) by Methyl Jasmonate. *Int. J. Mol. Sci.* 18:1004. doi: 10.3390/ijms18051004

Lessing, F., Kniemeyer, O., Wozniok, W., Loeffler, J., Kurzai, O., Haertl, A., et al. (2007). The *Aspergillus fumigatus* transcriptional regulator AfYap1 represents the major regulator for defense against reactive oxygen intermediates but is dispensable for pathogenicity in an intranasal mouse infection model. *Eukaryotic Cell* 6:2290. doi: 10.1128/EC.00267-07

Li, H., and Zhong, J. J. (2020). Role of calcineurin-responsive transcription factor CRZ1 in ganoderic acid biosynthesis by *Ganoderma lucidum*. *Process Biochem.* 95, 166–173. doi: 10.1016/j.procbio.2020.05.027

Li, P., Deng, Y. P., Wei, X. X., and Xu, J. H. (2013). Triterpenoids from *Ganoderma lucidum* and their cytotoxic activities. *Nat. Prod. Res.* 27, 17–22. doi: 10.1080/14786419.2011.652961

Liang, C., Tian, D., Liu, Y., Li, H., Zhu, J., Li, M., et al. (2019). Review of the molecular mechanisms of *Ganoderma lucidum* triterpenoids: Ganoderic acids A, C2, D, F, DM, X and Y. *Eur. J. Med. Chem.* 174, 130–141. doi: 10.1016/j.ejmech.2019.04.039

Lin, T., Du, J., Zheng, X., Zhou, P., and Lu, X. (2020). Comparative transcriptome analysis of MeJA-responsive AP2/ERF transcription factors involved in notoginsenosides biosynthesis. *3 Biotech* 10:290. doi: 10.1007/s13205-020-02246-w

Liu, N., Fan, F., Qiu, D., and Jiang, L. (2013). The transcription cofactor FgSwi6 plays a role in growth and development, carbendazim sensitivity, cellulose utilization, lithium tolerance, deoxynivalenol production and virulence in the filamentous fungus *Fusarium graminearum*. *Fungal Genet. Biol.* 58-59, 42–52. doi: 10.1016/j.fgb.2013.08.010

Liu, R., Cao, P., Ren, A., Wang, S., Yang, T., Zhu, T., et al. (2018). SA inhibits complex III activity to generate reactive oxygen species and thereby induces GA overproduction in *Ganoderma lucidum*. *Redox Biol.* 16, 388–400. doi: 10.1016/j.redox.2018.03.018

Malapi-Wight, M., Kim, J. E., and Shim, W. B. (2014). The N-terminus region of the putative C2H2 transcription factor Ada1 harbors a species-specific activation motif that regulates asexual reproduction in *Fusarium verticillioides*. *Fungal Genet. Biol.* 62, 25–33. doi: 10.1016/j.fgb.2013.10.008

Marion, R. M., Regev, A., Segal, E., Barash, Y., Koller, D., Friedman, N., et al. (2004). Sfp1 Is a Stress- and Nutrient-Sensitive Regulator of Ribosomal Protein Gene Expression. *Proc. Natl. Acad. Sci. U S A.* 101, 14315–14322. doi: 10.1073/pnas.0405353101

Messenguy, F., and Dubois, E. (1993). Genetic evidence for a role for MCM1 in the regulation of arginine metabolism in *Saccharomyces cerevisiae*. *Mol. Cell. Biol.* 13, 2586–2592. doi: 10.1128/MCB.13.4.2586

Miao, R., Holmes-Hampton, G. P., and Lindahl, P. A. (2011). Biophysical investigation of the iron in Aft1-1 (up) and Gal-YAH1 *Saccharomyces cerevisiae*. *Biochemistry* 50, 2660–2671. doi: 10.1021/bi102015s

Noble, J. A., Tsai, H. F., Suffis, S. D., Su, Q., Myers, T. G., and Bennett, J. E. (2013). *STB5* is a negative regulator of azole resistance in *Candida glabrata*. Antimicrob. Agents Chemother. 57, 959–967. doi: 10.1128/aac.01278-12

Nolting, N., and Pöggeler, S. (2006). A MADS box protein interacts with a mating-type protein and is required for fruiting body development in the homothallic ascomycete *Sordaria macrospora*. *Eukaryotic Cell* 5, 1043–1056. doi: 10.1128/EC.00086-06

Ohm, R. A., de Jong, J. F., de Bekker, C., Wosten, H. A., and Lugones, L. G. (2011). Transcription factor genes of *Schizophyllum commune* involved in regulation of mushroom formation. *Mol. Microbiol.* 81, 1433–1445. doi: 10.1111/j.1365-2958.2011.07776.x

Qu, X., Yu, B., Liu, J., Zhang, X., Li, G., Zhang, D., et al. (2014). MADS-box transcription factor SsMADS is involved in regulating growth and virulence in *Sclerotinia sclerotiorum*. *Int. J. Mol. Sci.* 15, 8049–8062. doi: 10.3390/ijms15058049

Ren, A., Li, M. J., Shi, L., Mu, D. S., Jiang, A. L., Han, Q., et al. (2013a). Profiling and quantifying differential gene transcription provide insights into ganoderic acid biosynthesis in *Ganoderma lucidum* in response to methyl jasmonate. *PLoS One* 8:e65027. doi: 10.1371/journal.pone.0065027

Ren, A., Ouyang, X., Shi, L., Jiang, A. L., Mu, D. S., Li, M. J., et al. (2013b). Molecular characterization and expression analysis of GlHMGS, a gene encoding hydroxymethylglutaryl-CoA synthase from *Ganoderma lucidum* (Ling-zhi) in ganoderic acid biosynthesis pathway. *World J. Microbiol. Biotechnol.* 29, 523–531. doi: 10.1007/s11274-012-1206-z

Ren, A., Qin, L., Shi, L., Dong, X., Mu, D. S., Li, Y. X., et al. (2010). Methyl jasmonate induces ganoderic acid biosynthesis in the basidiomycetous fungus *Ganoderma lucidum*. *Bioresour. Technol.* 101, 6785–6790. doi: 10.1016/j.biortech.2010.03.118

Ren, X., Kong, Q., Wang, H., Yu, T., Zhou, W., and Zheng, X. (2012). Biocontrol of fungal decay of citrus fruit by *Pichia pastoris* recombinant strains expressing cecropin A. *Food Chem.* 131, 796–801. doi: 10.1016/j.foodchem.2011.09.046

Shao, C. S., Feng, N., Zhou, S., Zheng, X. X., Wang, P., Zhang, J. S., et al. (2021). Ganoderic acid T improves the radiosensitivity of HeLa cells via converting apoptosis to necroptosis. *Toxicol. Res.* 10, 531–541. doi: 10.1093/toxres/tfab030

Shi, L., Gong, L., Zhang, X., Ren, A., Gao, T., and Zhao, M. (2015). The regulation of methyl jasmonate on hyphal branching and GA biosynthesis in *Ganoderma lucidum* partly via ROS generated by NADPH oxidase. *Fungal Genet. Biol.* 81, 201–211. doi: 10.1016/j.fgb.2014.12.002

Stillman, D. J. (2010). Nhp6: A small but powerful effector of chromatin structure in *Saccharomyces cerevisiae*. *Biochim. Biophys. Acta* 1799, 175–180. doi: 10.1016/j.bbagrm.2009.11.010

Sudheer, S., Yeoh, W. K., Manickam, S., and Ali, A. (2016). Effect of ozone gas as an elicitor to enhance the bioactive compounds in *Ganoderma lucidum*. *Postharvest Biol. Technol.* 117, 81–88. doi: 10.1016/j.postharvbio.2016.01.014

Suttipanta, N., Pattanaik, S., Kulshrestha, M., Patra, B., Singh, S. K., and Yuan, L. (2011). The transcription factor CrWRKY1 positively regulates the terpenoid indole alkaloid biosynthesis in *Catharanthus roseus*. *Plant Physiol.* 157, 2081–2093. doi: 10.1104/pp.111.181834

Tsubasa, S., and Takashi, H. (2011). Tobacco MYC2 regulates jasmonate-inducible nicotine biosynthesis genes directly and by way of the *NIC2*-locus *ERF* genes. *Plant Cell Physiol.* 52, 1117–1130. doi: 10.1093/pcp/pcr063

Wang, S., Guo, L. P., Xie, T., Yang, J., Tang, J. F., Li, X., et al. (2014). Different secondary metabolic responses to MeJA treatment in shikonin-proficient and shikonin-deficient cell lines from *Arnebia euchroma* (Royle) Johnst. *Plant Cell Tissue Organ. Cult.* 119, 587–598. doi: 10.1007/s11240-014-0558-5

Wang, S., Shi, L., Hu, Y., Liu, R., Ren, A., Zhu, J., et al. (2018). Roles of the *Skn7* response regulator in stress resistance, cell wall integrity and GA biosynthesis in *Ganoderma lucidum*. *Fungal Genet. Biol.* 114, 12–23. doi: 10.1016/j.fgb.2018.03.002

Wu, C., Weiss, K., Yang, C., Harris, M. A., Tye, B. K., Newlon, C. S., et al. (1998). Mcm1 regulates donor preference controlled by the recombination enhancer in Saccharomyces mating-type switching. *Genes Dev.* 12, 1726–1737. doi: 10.1101/gad.12.11.1726

Wu, F. L., Zhang, G., Ren, A., Dang, Z. H., Shi, L., Jiang, A. L., et al. (2016). The pH-responsive transcription factor *PacC* regulates mycelial growth, fruiting body development, and ganoderic acid biosynthesis in *Ganoderma lucidum*. *Mycologia* 108, 1104–1113. doi: 10.3852/16-079

Xie, C., Yan, S., Zhang, Z., Gong, W., Zuohua, Z., and Yingjun, Z. (2020). Mapping the metabolic signatures of fermentation broth, mycelium, fruiting body and spores powder from *Ganoderma lucidum* by untargeted metabolomics. *LWT* 129:109494. doi: 10.1016/j.lwt.2020.109494

Xu, X. L., Lai, R. C., Chen, T. Q., Shi, L. C., and Chen, S. L. (2020). Construction of yeast one-hybrid library and screening of transcription factors regulating *FPS* expression in *Ganoderma lucidum*. *Chin. Tradit. Herb. Drugs* 51, 3770–3776. doi: 10.19540/j.cnki.cjcmm.20190730.102

Yang, C., Liu, H., Li, G., Liu, M., Yun, Y., Wang, C., et al. (2015). The MADS-box transcription factor *FgMcm1* regulates cell identity and fungal development in *Fusarium graminearum*. *Environ. Microbiol.* 17, 2762–2776. doi: 10.1111/1462-2920.12747

Yang, Y., Zheng, Y., Wang, P., Li, X., Zhan, C., Linhardt, R. J., et al. (2020). Characterization and application of a putative transcription factor (SUT2) in *Pichia pastoris*. *Mol. Genet. Genomics* 295, 1295–1304. doi: 10.1007/s00438-020-01697-3

Yao, G., Li, Z., Wu, R., Qin, Y., Liu, G., and Qu, Y. (2016). Penicillium oxalicum PoFlbC regulates fungal asexual development and is important for cellulase gene expression. *Fungal Genet. Biol.* 86, 91–102. doi: 10.1016/j.fgb.2015.12.012

Yu, Z., Li, J., Yang, C., Hu, W., Wang, L., and Chen, X. (2012). The jasmonate-responsive AP2/ERF transcription factors AaERF1 and AaERF2 positively regulate artemisinin biosynthesis in *Artemisia annua* L. *Mol. Plant* 5, 353–365. doi: 10.1093/mp/ssr087

Yuan, S., Li, X., Li, R., Wang, L., Zhang, C., Chen, L., et al. (2018). Genome-Wide Identification and Classification of Soybean C2H2 Zinc Finger Proteins and Their Expression Analysis in Legume-Rhizobium Symbiosis. *Front. Microbiol.* 9:126. doi: 10.3389/fmicb.2018.00126

Zhang, G., Ren, A., Shi, L., Zhu, J., Jiang, A., Shi, D., et al. (2018). Functional analysis of an APSES transcription factor (GlSwi6) involved in fungal growth, fruiting body development and ganoderic-acid biosynthesis in *Ganoderma lucidum*. *Microbiol. Res.* 207, 280–288. doi: 0.1016/j.micres.2017.12.015

Zhang, H., Hedhili, S., Montiel, G., Zhang, Y., Chatel, G., Pré, M., et al. (2011). The basic helix-loop-helix transcription factor CrMYC2 controls the jasmonate-responsive expression of the ORCA genes that regulate alkaloid biosynthesis in *Catharanthus roseus*. *Plant J.* 67, 61–71. doi: 10.1111/j.1365-313X.2011.04575.x

Zhang, W. X., Tang, Y. J., and Zhong, J. J. (2010). Impact of oxygen level in gaseous phase on gene transcription and ganoderic acid biosynthesis in liquid static cultures of *Ganoderma lucidum*. *Bioprocess Biosyst. Eng.* 33, 683–690. doi: 10.1007/s00449-009-0379-9

Zhang, W. X., and Zhong, J. J. (2013). Oxygen limitation improves ganoderic acid biosynthesis in submerged cultivation of *Ganoderma lucidum*. *Bioprocess Biosyst. Eng.* 18, 972–980. doi: 10.1007/s12257-013-0148-0

Zhao, X., Yang, X., Lu, Z., Wang, H., He, Z., Zhou, G., et al. (2019). MADS-box transcription factor Mcm1 controls cell cycle, fungal development, cell integrity and virulence in the filamentous insect pathogenic fungus *Beauveria bassiana*. *Environ. Microbiol.* 21, 3392–3416. doi: 10.1111/1462-2920.14629

Zhou, C., Li, X., Zhou, Z., Li, C., and Zhang, Y. (2019). Comparative Transcriptome Analysis Identifies Genes Involved in Diosgenin Biosynthesis in *Trigonella foenum-graecum* L. *Molecules* 24:140. doi: 10.3390/molecules24010140

Zhou, X., Liu, W., Wang, C., Xu, Q., Wang, Y., Ding, S., et al. (2011). A MADS-box transcription factor MoMcm1 is required for male fertility, microconidium production and virulence in *Magnaporthe oryzae*. *Mol. Microbiol.* 80, 33–53.

frontiers | Frontiers in Microbiology

TYPE Review
PUBLISHED 20 December 2022
DOI 10.3389/fmicb.2022.1070110

Check for updates

OPEN ACCESS

EDITED BY
Wenbing Yin,
Chinese Academy of Sciences, China

REVIEWED BY
Jiangtao Gao,
Fujian Agriculture and Forestry University, China
Kang Zhou,
Guizhou University, China

*CORRESPONDENCE
Huaxiang Deng
denghxiang@163.com
Yujie Cai
yjcai@jiangnan.edu.cn

SPECIALTY SECTION
This article was submitted to Microbial Physiology and Metabolism, a section of the journal Frontiers in Microbiology

RECEIVED 14 October 2022
ACCEPTED 21 November 2022
PUBLISHED 20 December 2022

CITATION
Deng H, Liang X, Liu J, Zheng X, Fan T-P and Cai Y (2022) Advances and perspectives on perylenequinone biosynthesis.
Front. Microbiol. 13:1070110.
doi: 10.3389/fmicb.2022.1070110

COPYRIGHT
© 2022 Deng, Liang, Liu, Zheng, Fan and Cai. This is an open-access article distributed under the terms of the Creative Commons Attribution License (CC BY). The use, distribution or reproduction in other forums is permitted, provided the original author(s) and the copyright owner(s) are credited and that the original publication in this journal is cited, in accordance with accepted academic practice. No use, distribution or reproduction is permitted which does not comply with these terms.

Advances and perspectives on perylenequinone biosynthesis

Huaxiang Deng[1,2]*, Xinxin Liang[2], Jinbin Liu[3], Xiaohui Zheng[4], Tai-Ping Fan[5] and Yujie Cai[2]*

[1]Center for Synthetic Biochemistry, Shenzhen Institute of Synthetic Biology, Shenzhen Institute of Advanced Technology, Chinese Academy of Sciences, Shenzhen, China, [2]The Key Laboratory of Industrial Biotechnology, Ministry of Education, School of Biotechnology, Jiangnan University, Wuxi, Jiangsu, China, [3]School of Marine and Bioengineering, Yancheng Institute of Technology, Yancheng, Jiangsu, China, [4]College of Life Sciences, Northwest University, Xi'an, Shanxi, China, [5]Department of Pharmacology, University of Cambridge, Cambridge, United Kingdom

Under illumination, the fungal secondary metabolites, perylenequinones (PQs) react with molecular oxygen to generate reactive oxygen species (ROS), which, in excess can damage cellular macromolecules and trigger apoptosis. Based on this property, PQs have been widely used as photosensitizers and applied in pharmaceuticals, which has stimulated research into the discovery of new PQs and the elucidation of their biosynthetic pathways. The PQs-associated literature covering from April 1967 to September 2022 is reviewed in three sections: (1) the sources, structural diversity, and biological activities of microbial PQs; (2) elucidation of PQ biosynthetic pathways, associated genes, and mechanisms of regulation; and (3) advances in pathway engineering and future potential strategies to modify cellular metabolism and improve PQ production.

KEYWORDS

perylenequinones, pathway deciphering, metabolite orchestration, metabolite platform, automatic engineering, high throughput tools

Introduction

Perylenequinones (PQs) comprise a basic 4, 9-dihydroxy-3, 10-PQ structure (Supplementary Figure S1; Daub et al., 2013). They can be substituted in position 2, by two methoxy groups, in positions 1 and 12 by a six-or seven-membered ring, or by two 2-hydroxy-or 2-acyloxy-propyl side chains, and in positions 6 and 7 by a methylenedioxy group, or by two methoxy groups (Daub et al., 2013). These PQs have been divided into four classes based on the substitutional groups (Geris et al., 2022). The PQs progresses of class A, C and D have been reviewed previously (Falk, 1999; Barnes et al., 2001; Miskovsky, 2002; Dumas et al., 2004; Saw et al., 2008; Geris et al., 2022). Therefore, this review is focused on the class B perylenequinones.

In the presence of light, PQs are photoactivated and catalyze the formation of reactive oxygen species (ROS) from singlet oxygen. Excessive ROS can disrupt the balance of cellular redox status and cause oxidative stress, thereby causing oxidative damage to cellular macromolecules, resulting in the inhibition of metabolism and cellular apoptosis in pathogenic microorganisms and cancer cells (Qi et al., 2019; Wang et al., 2019).

Consequently, PQs have been widely applied as photosensitizers in the medical, food, cosmetic, agricultural, and material fields (Table 1; Gao et al., 2012; Zheng et al., 2018).

The high demand for PQs has stimulated research into improving their production and purity, such as sequencing of the potential PQ biosynthesis gene clusters (BGCs), which have served as sequence libraries for improving and diversifying PQ biosynthesis of the full range of PQs, and has improved PQ yields in many instances (Blin et al., 2017). However, no systematic review of PQs is available. To fill this gap, this comprehensive review covers progress in PQ research in three sections: (1) the sources, structural diversity, and biological activity of microbial PQs, (2) elucidation of PQ biosynthetic pathways, associated genes and mechanisms of regulation, and (3) advances in pathway engineering and future potential to modify cellular metabolism and improve PQ production.

Microbial perylenequinones, structural diversity and bioactivity

The five cycle structures (Supplementary Figure S1) contribute to the specific PQs bioactivities against diverse fungi, bacteria, and cancer cells (Kobayashi et al., 1989b). The subtle structure might endow particular bioactivities of PQs (Diwu and Lown, 1990; Surup et al., 2018). The above phenomenon inspires scientists to exploit the corresponding microorganisms and functions of diverse PQs.

Phaeosphaerins

As cytotoxic PQs, phaeosphaerins can be photoactivated to generate ROS, which accumulates in the lysosomes of human tumor cells and induces apoptosis of these cells. Phaeosphaerins A-F **(1–5)** have been isolated from *Phaeosphaeria* sp. (Supplementary Figure S2; Li et al., 2012).

Calphostin and derivatives

Calphostin A, B, C, D, and I (**6–10**; Supplementary Figure S3) have inhibitory activity against protein kinase C (PKC), and Calphostin C is the strongest inhibitor (Kobayashi et al., 1989b). Calphostin C induces cell apoptosis, both *via* the dual leucine zipper-bearing kinase and c-Jun N-terminal kinase (JNK) signaling pathways (Robitaille et al., 2008) and by inducing endoplasmic reticulum stress (Kaul and Maltese, 2009). Calphostin C also inhibits the expression of *Chlamydophila pneumoniae*-associated intracellular adhesion molecule-1 and blocks NF-kappaB translocation (Vielma et al., 2003a,b). These potentially useful biological activities have stimulated extensive research aimed at identifying alternative sources of Calphostins and improving their biosynthetic efficiency. For instance, Calphostins were first isolated from *Cladosporium cladosporioides* culture medium, during screening for protein kinase C (PKC) inhibitors (Iida et al., 1989; Kobayashi et al., 1989a), and other *Cladosporium* species can also produce calphostin derivatives. In addition, *C. cucumwinum* from etiolated cucumber seedlings produces Cladochrome A (**12**; Overeem et al., 1967) and *C. cladosporioides* can biosynthesize diverse PQs after epigenetic modifier treatment, including Cladochromes A **(12)**, B **(13)**, D **(14)**, E **(15)**, *F* **(16)**, G **(17)**, and calphostin B (Williams et al., 2008). *Phaeosphaeria* sp. also produces (+)-calphostin D (Li et al., 2012). The homologous PQs to calphostin, phleichrome **(18)** and isophleichrome **(19)** have been isolated and characterized from the plant pathogens *C. phlei* and *C. herbarum* (Yoshihara et al., 1975; Robeson and Jalal, 1992). Isophleichrome is also produced by *C. cucumwinum* in low yield (Arnone et al., 1989). These phleichromes are stronger inhibitors of HIV-1 and PKC than calphostin, and have antimicrobial, and antitumor activities based on their photodynamic properties (So et al., 2018).

TABLE 1 Functions and original strains of diverse perylenequinones.

Chemicals	Functions*	Strains	References
Phaeosphaerins A-F	Potentially kill human tumor cells	*Phaeosphaeria* sp.	Li et al. (2012)
Calphostin and the derivatives	Induce cell apoptosis; exhibit the activity against Protein kinase C and HIV; display antimicrobial and antitumor activity	*Cladosporium* species; *Phaeosphaeria* sp.	Kaul and Maltese (2009), Li et al. (2012), and So et al. (2018)
Cercosporin and the derivatives	Exhibit antileishmanial activity and cytotoxicity for diverse cells, including glioblastoma multiforme, breast adenocarcinoma, and pig kidney epithelial cells; Biosynthesize medical chemicals	*Cercospora* species; *Scolecotrichum graminis* Fucke; *Septoria pistaciarum*; *Colletotrichum fioriniae*	Tabuchi et al. (1991), Tabuchi et al. (1994), Kumarihamy et al. (2012), de Jonge et al. (2018), Grigalavicius et al. (2019), and Mastrangelopoulou et al. (2019)
Elsinochrome and the derivatives	Exhibits the cytotoxicity to cell L929 and KB3.1; inhibit growth of diverse microorganisms, such as *Staphylococcus aureus*	*Parastagonospora nodorum*; *Stagonospora convolvuli* LA39; *Shiraia* sp.	Boss et al. (2007), Cai et al. (2011), and Surup et al. (2018)
Hypocrellins and the derivatives	Cure skin diseases, rheumatoid arthritis, gastric diseases; induce apoptosis of diverse cancer cells; display the inhibition activity of SARS-CoV-2	*Hypocrella bambuase*; *Shiraia bambusicola*; *Penicillium chrysogenum*; *Phaeosphaeria* sp.	Diwu and Lown (1990), Li et al. (2012, 2021), and Meng et al. (2011)

Cercosporin and derivatives

Cercosporin **(20)** is another well-known photoactivated PQ toxin from diverse *Cercospora* species (Supplementary Figure S3). These phytopathogens cause leaf spot and blight diseases on diverse crop species (Daub, 1981; Daub and Ehrenshaft, 2000). Cercosporin also has antileishmanial activity and cytotoxicity for glioblastoma, breast adenocarcinoma, and human tumor cell lines (Kumarihamy et al., 2012; Grigalavicius et al., 2019; Mastrangelopoulou et al., 2019). Photoactivation of cercosporin has applications in the biosynthesis of medicinal compounds. For instance, the cercosporin-photocatalyzed sp^3(C-H) activation reaction can be used to synthesize pyrrolo[3,4-c]quinolones, which are the backbone structures of various bioactive compounds, such as "A Disintegrin and Metalloproteinase with Thrombospondin Motif" (ADAMTS) inhibitors (Li et al., 2019). The cercosporin-photocatalyzed oxidation reaction can be also employed to synthesize different kynurenine derivatives and the relevant peptides, which present the neuroprotective bioactivity (Yuan et al., 2022). The great pharmacological value of cercosporin and its derivatives has stimulated their isolation from diverse microorganisms. *Cercospora kikuchii* was the first reported cercosporin producer (Kuyama and Tamura, 1957) and at least 24 other *Cercospora* species can produce cercosporin (Assante et al., 1977). Various derivatives of cercosporin with modified functional groups have been also isolated, such as (+)-isocercosporin **(21)** from *Cercospora kikuchii*, and (+)-Isocercosporin and acetylisocercosporin **(22)** from the plant pathogen *Scolecotrichum graminis* Fuckel (Tabuchi et al., 1994). *Septoria pistaciarum* produces (+)-Cercosporin, (+)-14-O-Acetylcercosporin and (+)-di-O-Acetylcercosporin (Kumarihamy et al., 2012). In a study characterizing the cercosporin toxin biosynthesis (CTB) gene cluster in the phytopathogenic genus *Cercospora*, de Jonge et al. also found that treatment of *Colletotrichum fioriniae* with trichostatin A stimulates the production of a cercosporin-associated PQ (de Jonge et al., 2018), thus indicating that *Cercospora* has the potential to produce cercosporin-associated PQs.

Elsinochrome and derivatives

Elsinochrome A is another well-known photoactivated PQs toxin from the phytopathogenic *Elsinoe* species (Supplementary Figure S3; Weiss et al., 1957). Similarly to Cercosporin, Elsinochrome A is cytotoxic to the mouse fibroblast cell line L929 and human HeLa cell line KB3.1 (Surup et al., 2018). Elsinochrome A also has antimicrobial activity against *Bacillus subtilis*, *Mucor hiemalis*, and *Staphylococcus aureus* (Surup et al., 2018). Further research on Elsinochrome-producing microorganisms resulted in the isolation of Elsinochromes A, B, C, and D **(23–26)** from other *Elsinoe* species (Batterham and Weiss, 1963; Lousberg et al., 1969, 1970). Other microorganisms can also produce Elsinochrome, for example, Elsinochrome C is produced by *Parastagonospora nodorum* (Chooi et al., 2017). The mycobiont fungal strain of the lichen *Graphis elongata* biosynthesizes Elsinochrome A (Fazio et al., 2018). *Hypomyces* sp., a parasitic mushroom fungus, produces hypomycin A **(27)** and B **(28)**, with structures closely related to the elsinochromes (Liu et al., 2001; Zhang et al., 2001). It is noted that *Stagonospora convolvuli* LA39 can produce both elsinochrome A and cercosporin (Boss et al., 2007). *Shiraia* sp. SUPER-H168 produces a PQ complex of elsinochrome and hypocrellin (Cai et al., 2011), thus indicating that diverse microorganisms contain the PQ biosynthetic gene clusters (de Jonge et al., 2018).

Hypocrellin and derivatives

As an effective defense compound against disease, hypocrellin has been used for centuries in traditional Chinese medicine, to effectively treat skin diseases, rheumatoid arthritis, and gastric diseases (Diwu and Lown, 1990). Hypocrellin A **(29)** and B **(30)** present excellent antimicrobial and antileishmanial activities (Ma et al., 2004) and can induce apoptosis of diverse cancer cells, such as hepatocellular carcinoma (Wang et al., 2019), human lung adenocarcinoma A549 cells (Qi et al., 2019), and squamous carcinoma A431 cells (Niu et al., 2020). Hypocrellin can also protect human ACE2 cells against infection by SARS-CoV-2 by blocking the receptor-binding domain of the SARS-CoV-2S protein, thereby inhibiting the entry of the virus into human cells (Li et al., 2021). Given its potential as a SARS-CoV-2 entry inhibitor, hypocrellin and its derivatives have been isolated from diverse microorganisms (Supplementary Figure S3) to improve the supply of hypocrellin, which was first isolated from the stroma of *Hypocrella bambuase,* growing on bamboo shoots (Chen et al., 1981). *Shiraia bambusicola,* another bamboo parasitic fungus, is also able to biosynthesize hypocrellins (Liu, 1985), as are *Penicillium chrysogenum* and *Phaeosphaeria* sp. (Meng et al., 2011; Li et al., 2012) and the engineered *Aspergillus* species (Hu et al., 2019).

Elucidating the perylenequinone biosynthetic pathway

The widespread applications of PQs have prompted considerable research efforts to elucidate and exploit their biosynthetic pathways for industrial production (de Jonge et al., 2018; Hu et al., 2019). Initially, bioinformatic methods, such as genome walking and genome evolutionary analysis were used to screen for potential PQ gene clusters (Chooi et al., 2017; de Jonge et al., 2018; Deng et al., 2020b). Then these candidate PQs biosynthetic genes were verified by gene disruption and chemical structure comparison between wild-type strains and mutants (Deng et al., 2017a; Hu et al., 2019). *In-vitro* enzymatic assays were used to confirm the gene functions by heterologous expression of the relevant genes in suitable hosts, enzymatic conversion of substrates

and, determination of structural differences among substrates, intermediates, and products (Newman and Townsend, 2016).

PQ pathway discovery by gene cluster conservation analysis

Genes for PQ biosynthesis are arranged as biosynthetic gene clusters (BGCs; Blin et al., 2017), comprising three modules: i.e., the polyketide synthase (PKS), which synthesizes the core PQ structure; phenol coupling enzymes, which dimerize the core structure; and tailoring enzymes, which modify the functional groups and generate the diversity of PQ structures (Müller et al., 2019; Figures 1A, 2). This collinear BGC structure has facilitated the discovery of new PQs by homology analysis. For example, the elsinochrome BGC from *Elsinoë fawcettii* and the phleichrome BGC from *C. phlei* have been identified through homology analysis of the cercosporin and hypocrellin BGCs, respectively (Ebert et al., 2019; Hu et al., 2019).

The PKS enzymes in different PQ biosynthetic pathways are characterized by high sequence homology and structural conservation. Therefore, using PKS as a screening template is an effective approach to discover potential new PQ BGCs. For example, our group has elucidated and confirmed the hypocrellin pathway in *S. bambusicola*, based on homology analysis of the cercosporin and elsinochrome PKSs (Deng et al., 2017a). A genome evolutionary method has been developed to mine PQ BGCs through PKS homology analysis, based on the collinearity of BGCs (de Jonge et al., 2018), which has been used to discover that the cercosporin BGC has undergone multiple duplications and horizontal transfers across a wide range of plant pathogenic fungi. Three cercosporin BGCs were found in the *Cercospora beticola* genome, two of which shared the major cercosporin-associated genes. A "phylogenetic roadmap" of the putative evolutionary history of polyketide synthase (PKS) was also created (de Jonge et al., 2018), which showed that four duplications and three transfers of the cercosporin PKS had occurred from diverse *Dothideomycetes* and *Glomerellales* species. The identity of the proposed cercosporin PKS remains to be confirmed by gene knockout and chemical characterization of its substrate selectivity/products.

Confirmation of perylenequinone-associated genes through gene disruption

Knockout of a PQ biosynthesis gene may decrease or eliminate the related enzymatic function (Liu et al., 2022). Phenotypical and metabolic differences between wild-type strains and mutants can aid in the elucidation of gene functions, for example, the pentacyclic core structure of PQs confers a variety of colors (Hu et al., 2019; Liu et al., 2022). Wild-type strains are mostly red, whereas mutants exhibit various other colors, owing to the accumulation of biosynthetic intermediates (Newman and Townsend, 2016). This aspect has greatly facilitated the discovery of the specific functions of the essential PQ biosynthetic genes.

Gene knockout by conventional homologous recombination

The split-marker approach is a common genetic manipulation to verify the functions of PQ-associated genes (Figure 1B; You et al., 2009). Based on the lengths of homologous donors fused with selective markers (Figure 1B), the gene targeting efficiency of split-marker technology can be up to 50%. In addition, this approach can also decrease ectopic integration and enhance the corresponding genetic modification. Split marker methods have generated diverse mutants of genes in the PQ pathway (Chen et al., 2007; You et al., 2009; Newman and Townsend, 2016), resulting in metabolite differences between wild-type and mutant strains. For example, the PKS and its transcription factor (TF) in the elsinochrome pathway have been disrupted by the split marker method (Chung and Liao, 2008; Liao and Chung, 2008). The relevant mutants lose the elsinochrome production ability, and the adjacent genes in these mutants show absent or diminished transcription. Deletion of a MAP kinase homolog gene (*CZK3*) also suppresses cercosporin production in the relevant mutant (Shim and Dunkle, 2003). The red pigment around the mycelia of wild-type *Cercospora zeae-maydis* was abolished, resulting in the colorless ΔCZK3 mutant (Shim and Dunkle, 2003). The other eight genes in the cercosporin pathway have also been individually deleted (Chen et al., 2007). Phenotypic analysis has indicated that mycelia of the cercosporin toxin biosynthesis (ΔCTB1) mutant lacks any color pigments, whereas the ΔCTB2, ΔCTB3c, and ΔCTB7 mutants are a yellow-brown color, and ΔCTB5 and ΔCTB6 mutants are a dark orange-red color (Newman and Townsend, 2016). Nor-toralactone, toralactone and naphthoquinone have been produced by the ΔCTB3c mutant, suggesting that CTB3c's functions include the opening cycle, decarboxylation, and hydroxylation (Newman and Townsend, 2016). The ΔCTB6 mutant produces cercoquinone A, which lacks the O-methyl group of the wild-type quinone compound, thus suggesting that CTB6 is involved in the reduction reaction (Newman and Townsend, 2016). In contrast, the ΔCTB1, ΔCTB2, and ΔCTB7 mutants produce no major metabolites and the ΔCTB5 mutant produces cercoquinone B. No cercosporin is detected in the ΔCTB9 mutant and the following *in-vitro* assay further reveals that CTB9 catalyzes the methylenedioxy bridges of cercosporin (Liu et al., 2022).

Gene knockout by CRISPR

Compared with conventional gene knockout tools, the clustered regularly interspaced short palindromic repeats (CRISPR) system is simple, inexpensive and high-throughput (Deng et al., 2020a), and has been widely used for genetic modification of diverse organisms (Deng et al., 2017b). The Cas9 nuclease and sgRNA are two critical elements in the CRISPR system. The complex of Cas9 and sgRNA triggers specific double-strand breaks, induces cellular repair pathways, and modifies the target genes (Sander and Joung, 2014; Figure 1C). Our group has recently constructed a CRISPR

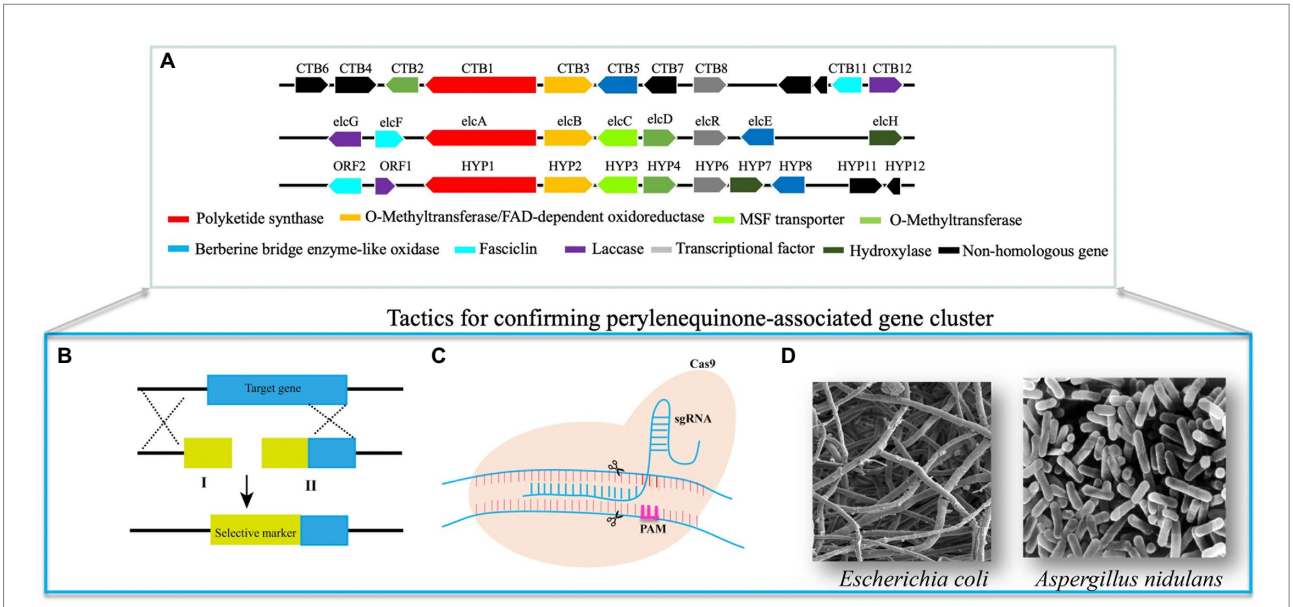

FIGURE 1
Methods for confirming perylenequinone-associated genes and pathways. **(A)** Homologous PQs-associated biosynthetic gene clusters. **(B)** For this split-marker approach, we need to synthesize two nucleotides fragment I and II. Fragments I comprise a partial selective marker and a sequence homologous to 5′ target locus; fragments II contain a partial selective marker and a sequence homologous to 3′ target locus. Thus, 5′ and 3′ homologous arms facilitate relevant homologous recombination of target genes and mutants can be screened on antibiotic regeneration plates due to the overlapping sequences of the selective marker of two fragments. **(C)** The CRISPR system contains two crucial elements, including Cas9 nuclease and sgRNA. The complex of these two elements precisely triggers double-strand breaks, induces cellular repair pathways, and results in relevant gene modification. **(D)** Verification of crucial PQs-associated genes by expressing them in the tractable microorganisms and then following chemical comparisons.

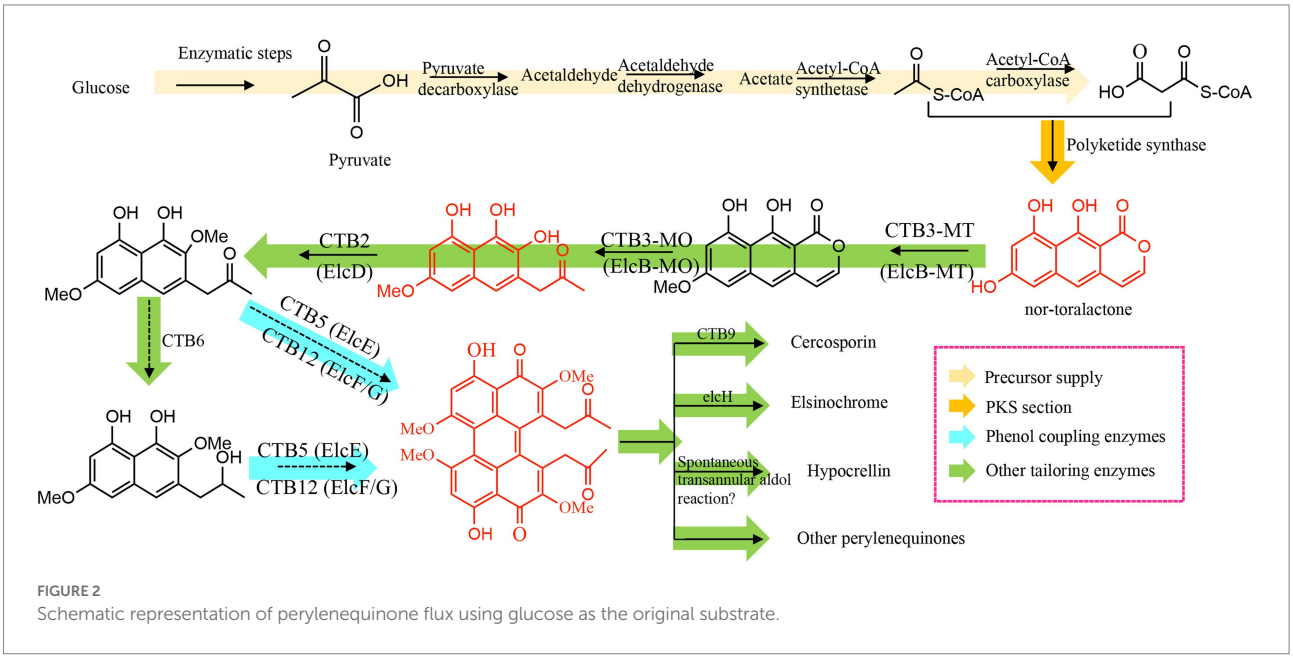

FIGURE 2
Schematic representation of perylenequinone flux using glucose as the original substrate.

system in *S. bambusicola* and generated several mutants (Deng et al., 2017a,c, 2018), including mutants of TF, polyketide synthase, monooxygenase, and a major facilitator superfamily transporter, all of which decrease hypocrellin production. Compared with the red wild-type *S. bambusicola*, transcription factor and polyketide synthase mutants are colorless, whereas mutants of monooxygenase and major facilitator superfamily transporter are brown. None of these mutants could produce hypocrellin. Relative expression experiments have not detected transcription of adjacent genes (Deng et al., 2017a, 2020b), or

the presence of their corresponding intermediates (Deng et al., 2018). These findings remain to be confirmed by heterologous expression of these enzymes and substrate selectivity/product characterization.

Confirmation of PQ-linked gene functions by heterologous expression in host microorganisms

Sometimes, gene disruption mutants can generate no, or ambiguous metabolites, thus hampering the confirmation of their functions. To avoid this situation, the corresponding enzymes can be heterologously expressed in optimized host systems, such as *Escherichia coli* and *Aspergillus* species, and their products can be characterized (Figure 1D).

Escherichia coli has several advantages as a host for gene expression, such as rapid growth rate, high protein expression levels, and well-constructed genetic tools, which has made it the expression system of choice for PQ genetic studies. However, polyketide synthases, the first enzyme in PQ biosynthesis, comprise 2,000–3,000 amino acids, with starter unit acyltransferase (SAT), β-ketoacyl synthase (KS), malonyl acyltransferase (MAT), product template (PT), dual-tandem acyl-carrier protein (ACP_2), and thioesterase (TE) domains (Herbst et al., 2018). These large, multi-domain enzymes cannot be expressed efficiently in *E. coli*, so the Udwary-Merski algorithm (UMA) was designed to predict the locations of individual domains and the linker regions between them (Udwary et al., 2002). This allows the domain structure of the gene to be deconstructed, and individual domains can be expressed in *E. coli*, then purified (Crawford et al., 2008); followed by combining the various domains with substrates and analyzing the PQ products. When the PKS gene was subjected to this analysis, the tri-domain SAT-KS-MAT was expressed in soluble form, but not KS-MAT (Crawford et al., 2008; Herbst et al., 2018), thus indicating that the tri-domain SAT-KS-MAT can assemble as a substrate loading/condensation complex, yielding a heptaketide. Through the same approach, the PT domain is involved in the C4-C9 and C2-C11 cyclizations by this heptaketide (Newman et al., 2014), and the TE domain has been identified to contribute to pyrone formation (O13-C1 cyclization) and nor-toralactone release (Newman et al., 2012).

Unfortunately, codon usage bias and species differences often result in insoluble, or unstable proteins when the bacterial *E. coli* expression system is used for fungal enzyme expression, thus restricting the utility of the deconstruction approach. However, these problems can often be avoided by using fungal expression systems, such as *Aspergillus* (Pahirulzaman et al., 2012; Chiang et al., 2013), which has facilitated the complete elucidation of the PQ biosynthetic pathway. For example, the *Cppks1* gene from *C. phlei* has been expressed in *Cryphonectria parasitica*, thereby facilitating the elucidation of the biosynthetic pathway of the red phleichrome pigment (So et al., 2015). Engineered filamentous fungi such as *Penicillium crustosum* and *Aspergillus* species were successfully transformed and enabled to produce nor-toralactone (Chooi et al., 2017; Hu et al., 2019; Kindinger et al., 2019).

The availability of the PQ precursor nor-toralactone has enabled the verification of other PQ pathway genes (Figure 2); for example, the O-methyltransferase domain of the di-domain enzyme CTB3 O-methylates nor-toralactone (Newman and Townsend, 2016). The monooxygenase domain of CTB3 catalyzes the opening cycle, decarboxylation, and hydroxylation (Newman and Townsend, 2016); similarly, the di-domain protein in the elsinochrome pathway has similar functions (Hu et al., 2019). Engineered *A. nidulans* with elcA and elcB-MT transformed nor-toralactone to toralactone, suggesting the O-methylation function of elcB-MT. Co-expression of elcA and elcB can also convert toralactone to three different products, including one with a molecular mass consistent with cercoquinone A and D (Newman and Townsend, 2016). This finding indicates that elcB is involved in O-methylation, the opening cycle, decarboxylation, and hydroxylation.

It appears that an FAD-linked oxidase is involved in dimerizing the phenolic precursor to the corresponding PQ. However, a laccase-like multicopper oxidase (ElcG) can also catalyze dimerization by combining with a berberine bridge enzyme-like oxidase (ElcE; Hu et al., 2019). The FAD-dependent CTB5 from *Cercospora nicotianae* and Cz_CTB12 from *Cercospora zeae-maydis* appear to synergistically catalyze the dimerization reaction. In addition, a multicopper oxidase has been identified, which can biosynthesize the atropisomer (*P*)-viriditoxin by dimerizing two regionally-selective semiviriditoxin molecules (Hu et al., 2019). A fungal laccase was determined to regionally dimerize the phenol coupling precursor to the (*R*)-semi-vioxanthin, combined with an auxiliary protein (Furtges et al., 2019). Overall, oxidases, particularly multicopper oxidase, perform a crucial function in PQ biosynthesis by dimerizing two phenol precursors.

The subsequent functional group modification of these dimer intermediates results in the wide diversity of PQs, for example, a flavin-dependent monooxygenase (ElcH) can transform hypocrellin into elsinochrome (Hu et al., 2019). In the absence of this flavin-dependent monooxygenase, an engineered *A. nidulans* generated hypocrellin through an intramolecular aldol reaction. A FAD-dependent monooxygenase, CTB7, has been proposed to catalyze the formation of the dioxepine ring of cercosporin (Chung and Liao, 2008); when the CTB7 gene was transferred into *Cercospora zeina*, it enabled cercosporin production (Swart et al., 2017), confirming the involvement of CTB7 in dioxepine ring formation. However, recent reports suggest that CTB9 and CTB10 also contribute to methylenedioxy bridge formation (de Jonge et al., 2018), which was confirmed by the crystal structures of CTB9 with various substrates and the subsequent site-directed mutagenesis study (Liu et al., 2022).

Practical approaches to activate or stimulate the perylenequinone pathways of natural PQ-producing fungi

Gene-cluster-conservation analysis has revealed that many filamentous fungi contain one or more PQ BGCs (de Jonge et al., 2018). However, many of these BCGs are silent or are barely expressed, so these fungi may be potential sources of new or existing PQs. To exploit these potential PQs resources, novel physical, chemical and genetic approaches have been established.

Strategies for modulating regulatory mechanisms of PQs biosynthesis

The regulation system of PQs biosynthesis is extremely complex and employs different modulation levels, including pathway-associated regulators, epigenetic regulators, and global regulators (Macheleidt et al., 2016). This section describes the corresponding regulatory mechanisms and strategies for PQs biosynthesis on basis of these regulatory systems.

Modulating transcription factors

PQ-associated transcription factors (TFs) are often distributed in the PQ biosynthesis gene clusters (BGCs) and are of the Zn_2Cys_6 zinc finger protein type (Figure 3A). They appear to coordinate gene expression in the PQ BGCs and regulate PQ production, so engineering these TFs has great potential for increasing PQ production efficiency. For example, bioinformatics analysis has indicated that the genome of wild-type *Parastagonospora nodorum* contains the elsinochrome BGC, but no elsinochrome production has been detected from this strain. Overexpressing the transcriptional regulator, elcR, has enabled transformants to generate elsinochrome by up-regulating elsinochrome-associated gene transcription (Chooi et al., 2017). Overexpressing elcR also enables elsinochrome production in transformants of *A. nidulans* (Hu et al., 2019), and enhancing gene expression of the hypocrellin-associated TF gene significantly increased hypocrellin production in the engineered *S. bambusicola* (Deng et al., 2020b).

Coordinating epigenetic regulators

Histone proteins act as scaffolds for nucleosome generation. Modifying these epigenetic regulators by genetic manipulation or chemical inhibitors (Figure 3B) can remodel chromatin cascades. Therein, these modifications trigger DNA methylation or acetylation, which stimulates PQ production by regulating gene expression in the PQ BGCs (Pfannenstiel and Keller, 2019). For example, treatment with suberoylanilide hydroxamic acid (Vorinostat, a histone deacetylase inhibitor) stimulates *C. cladosporioides* to produce several PQs, including cladochrome F and calphostin B (Williams et al., 2008). Trichostatin A (histone deacetylase inhibitor) stimulates *Colletotrichum fioriniae* to produce a PQ similar to cercosporin (de Jonge et al., 2018). 5-Azacytidine (DNA methylation inhibitor) down-regulates the light-response transcriptional factors (LaeA and VeA) involved in regulating hypocrellin biosynthesis in *S. bambusicola*, thus inhibiting gene transcription of the hypocrellin BGCs and markedly decreasing hypocrellin production (Ma et al., 2018).

Modulating environmental-response global signaling

Diverse environmental stimuli can also influence PQ production through global regulators (Figure 3), including AreA, CreA, PacC, and velvet complex, which can respond to changes in nitrogen sources, carbon sources, pH, and light, respectively. Unlike PQ-pathway TFs, these global regulators are not located in the PQ BGCs (You et al., 2008).

Among these environmental signals, light is the most influential factor for PQ biosynthesis. Therefore, light or dark signals have been widely used to modulate PQ production. Therein, the velvet complex (VeA and VelB) and laeA regulators respond to these light signals. In dthe arkness, VeA translocates to the nucleus and forms a heterodimer of VeA and VelB; and the constitutive orientation of LaeA promotes this velvet complex formation (Bayram et al., 2008). Therefore, different light conditions can influence velvet-related activities, such as secondary metabolic pathways. For example, switching between light and dark conditions enhances transcriptional levels of ROS-associated genes, thereby stimulating *S. bambusicola* to produce hypocrellin A (Sun et al., 2018), whereas *Cercospora nicotianae* forms cercosporin only under light conditions (You et al., 2008). Red light up-regulates the expression of genes for hypocrellin A and transmembrane transport, increasing hypocrellin production in the mycelia of *S. bambusicola* (Ma et al., 2019). Light stimulates mycelial growth of *Shiraia* sp. SUPER-H168, but suppresses hypocrellin biosynthesis. In contrast, darkness increases hypocrellin biosynthesis (Gao et al., 2018a).

AreA is a central regulator of nitrogen metabolism and consequently regulates PQ production. For instance, different nitrogen sources resulted in different levels of cercosporin production (You et al., 2008). Bioinformatics analysis has indicated that the promoter regions of cercosporin biosynthesis genes comprise one or more hypothetical GATA motifs, bounded by AreA (Chen et al., 2007), thus indicating that the genes in cercosporin BGCs are coordinated by AreA. Similarly, CreA stimulates PQ production by regulating carbon metabolism. Although PQ biosynthetic gene promoters contain no CreA binding sites (Chen et al., 2007), different carbon sources result in different levels of cercosporin production. Moreover, several PQ biosynthetic genes contain the PacC binding motif, indicating that cercosporin production could be influenced by pH (You et al., 2008).

Regulation of PQ-associated genes from central metabolic pathways

The initial PQ precursor, acetyl-CoA is obtained from pyruvate through three enzymic steps (Figure 2). Acetyl-CoA

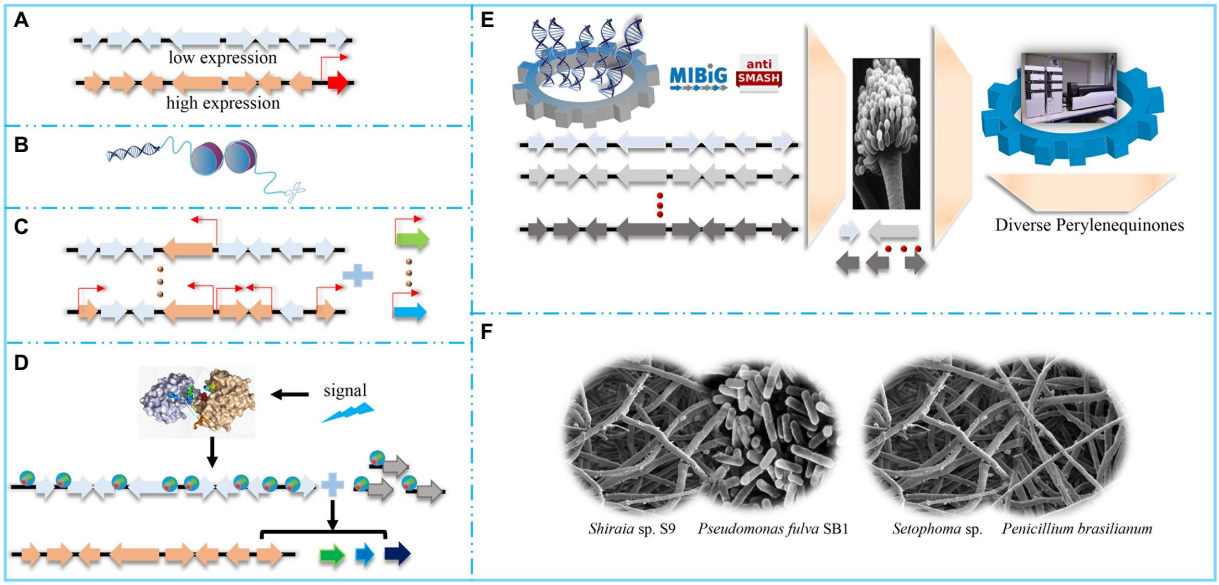

FIGURE 3
Diverse strategies to activate or broaden perylenequinone pools. **(A)** Activate the perylenequinone pathway by overexpressing pathway-specificity transcriptional factors. **(B)** Activate the perylenequinone pathway by engineering epigenetic regulators. **(C)** Enhance the perylenequinone pathway by increasing the central pathway. **(D)** Enhance the perylenequinone pathway by signal pathways. Environmental, chemical and physical signals trigger relevant global regulators, which regulate perylenequinone-linked genes by activating these genes. **(E)** Construct a diverse perylenequinone platform in tractable *Aspergillus* species. **(F)** Improve the perylenequinone pathway by microorganism co-culture, including bacteria-fungi co-cultures and fungi-fungi co-cultures.

carboxylase (ACC) transforms acetyl-CoA to malonyl-CoA, the extension unit for PQ biosynthesis; then PQ is biosynthesized by the central polyketide pathway (Figure 2). Therefore, modulating precursor supply gene expression and the main polyketide pathway increases PQ production (Figures 2, 3C). For example, ACC overexpression increases the acetyl-CoA substrate pool and stimulates polyketide production in various strains, such as *Streptomyces albus* (Lu et al., 2016), *Saccharomyces cerevisiae* (Wattanachaisaereekul et al., 2008), and *Aspergillus species* (Hasan et al., 2018). This suggests that increasing the polyketide precursor pool may be a feasible and generally applicable way to up-regulate production of targeted metabolites. Similarly, overexpressing two amylases can up-regulate the expression levels of carbon catabolic genes (such as *acc* and *pdc*) and hypocrellin pathway genes, resulting in three-fold higher hypocrellin yields in the engineered strains (Gao et al., 2018b). Regulating the genes from the central PQ pathway is another strategy to increase metabolite production. For instance, overexpressing a di-domain protein and a hydroxylase increases hypocrellin production three-and two-fold, respectively (Li et al., 2019). Overexpressing multicopper oxidase promotes the corresponding dimerization reaction and enhances the expression of hypocrellin-associated genes; hypocrellin production in the engineered transformants increases 5-fold compared with wild-type *S. bambusicola* (Deng et al., 2016b). The CRISPR-mediated transcriptional activation system can stimulate multigene activation in *A. nidulans* and should facilitate PQ production by improving related multi-gene expression (Roux et al., 2020).

Strategies to coordinate endogenous signal-response pathways

Microorganism rapidly responds to the dynamic environmental signals for the continuous PQs formations through real-time signal pathways (Keller, 2019). Therefore, comprehending the transient signal translations and the relevant PQs regulatory mechanisms can facilitate PQs biosynthesis. Namely, PQs production might be improved by rationally engineering these signal pathways.

Modulation of the mitogen-activated protein kinase (MAPK) pathway

The MAPK signaling pathway is highly conserved in filamentous fungi and responds to signals from environmental stimuli (You et al., 2008). These signals are delivered by small GTPases to MAPK *via* phosphorylation reaction, thereby inducing translocation of MAPK to the nucleus, where it triggers specific TFs (Macheleidt et al., 2016). Notably, these processes coordinate with each other, suggesting that a crosstalk interaction exists, and may regulate PQ production. For example, the expression level of a MAPK-homologous protein in *Cercospora*

zeae-maydis increases during cercosporin production, and a deletion mutant has decreased expression levels of cercosporin-related genes, thus inhibiting cercosporin biosynthesis. However, the MAPK complementation strain shows restoration of cercosporin production (Shim and Dunkle, 2003).

Regulating the calcium/calmodulin signal pathway

Calcium is a common cellular signal that regulates diverse physiological activities because intracellular calcium homeostasis is critical for PQ biosynthesis. Calcium homeostasis is modulated *via* several effectors (such as the calcium-binding protein, calmodulin) *via* one or more G proteins. Activating the G protein-dependent receptor of protein kinase A promotes the phosphorylation of RCS (regulator of calmodulin signaling) and its attachment to calmodulin, thereby modulating the intracellular Ca^{2+} concentrations and metabolite production. These processes involve crosstalk between the calcium/calmodulin signaling pathway and the MAPK pathway. Therefore, regulating these genes *via* genetic modification, Ca^{2+} addition, or Ca^{2+} complexation can influence PQ production. For example, pharmacological inhibitors block the Ca^{2+} channels, cause calcium ion disorder and inhibit cercosporin production in *Cercospora nicotianae* (Chung et al., 2003). Chemical Ca^{2+} inhibitors that down-regulate PQ biosynthetic gene expression also inhibit hypocrellin biosynthesis in *Shiraia* sp. Slf14 (Liu et al., 2018), whereas Ca^{2+} addition up-regulates PQ biosynthetic genes. For example, Ca^{2+} addition up-regulates the expression of cercosporin biosynthetic genes, including CRG1, CTB8, and CTB1, increasing cercosporin production (You et al., 2008). Similarly, Ca^{2+} addition increases hypocrellin production by up-regulating transcription of genes encoding Ca^{2+} ion sensors and increasing hypocrellin biosynthesis (Liu et al., 2018). Ca^{2+} addition could also ameliorate the repressive influence of inhibitors on gene expression and facilitate hypocrellin production (Liu et al., 2018).

Modulation of the endogenous ROS/oxidative stress-response systems

Oxygen is catalyzed to singlet oxygen and other ROS by the photoactivated PQs. Excessive ROS causes the disorder in cellular redox homeostasis and triggers oxidative stresses, which induce metabolic stagnation and cellular apoptosis (Montibus et al., 2015). However, *S. bambusicola* retains normal morphology and metabolic activity, even under high levels of oxidative stress and elevated hypocrellin production, indicating that these filamentous fungi have a very strong oxidative stress-response system, which protects these strains against the above ROS stresses (Deng et al., 2016a). Therefore, scientists have constructed the chassis for the continuous PQs biosynthesis by rationally engineering oxidative stress-response and regulation systems (Montibus et al., 2015). These processes mainly comprise two sections: (1) convert the toxic ROS to nontoxic compounds *via* global regulators; (2) deliver PQs out of the cells and reduce the ROS stress source by transporters.

AP1 is a well-known global regulator in the antioxidant system. High oxidative stress oxidizes the cysteine domains of the AP1, thereby forming disulfide bonds and activating AP1. The activated AP1 binds to nucleotide binding sites (5'-TTAGTCA-3') of other stress-response genes and strengthens these gene expressions. Subsequently, superoxide radicals are converted into less harmful hydrogen peroxide, then to water, which ensures continuous PQs biosynthesis (Keller, 2015). For instance, AP1 overexpression enables cellular redox homeostasis and increases 6-fold hypocrellin productions by up-regulating expressions of genes, such as superoxide dismutase and catalase (Deng et al., 2020b). Similar to AP1, crg1 also improves the expression of genes, which are involved in the cercosporin biosynthesis and the resistance to cercosporin toxicity (Chung et al., 2003).

Transporter engineering is another promising approach to export the biosynthesized PQs from producer cells, reduce oxidative stress, and facilitate the high yielding PQ production (Chen et al., 2007; Newman and Townsend, 2016). Therein, ATP hydrolysis enables ATP-binding cassette (ABC) transporters to deliver small molecules and macromolecules by concentration gradients, whereas major facilitator superfamily (MSF) transporters can transfer small molecules by chemiosmotic ion differences (Keller, 2015). Therefore, ABC and MSF transporters can remove toxic molecules from filamentous fungi, thus enabling high PQs production and protecting the producer organisms against PQ toxicity. For instance, overexpression of ABC and MSF transporters increases about 5-and 4-fold hypocrellin production, respectively (Deng et al., 2020b). Photoactivated-cercosporin metabolites increase the expression of ABC and MSF transporters, and overexpression of these transporters enables the normally PQ-sensitive *Neurospora crassa* to maintain normal morphology during photoactivated-cercosporin treatment (Beseli et al., 2015). Upregulation of a uracil transporter and a zinc transporter has been also determined to stimulate the PQs biosynthesis (Deng et al., 2017c).

Construction of a diverse PQ platform in the tractable *Aspergillus* species

Genes from the PQ pathway are highly homologous, and other non-conserved genes may be useful for modifying PQ functional groups and generating new combinations thereof (de Jonge et al., 2018; Ebert et al., 2019). Modifying genes for functional group modification should be an effective strategy to construct a diverse PQ platform. For example, *Cryphonectria parasitica* can generate various complex pigments through the polyketide pathway, and transformants with *Cppks1* also produced a non-natural phleichrome (So et al., 2015). Recently, our group has constructed an efficient CRISPR system (Deng et al., 2017a),

which can be used to integrate or replace functional group modification genes to generate novel PQs.

Reconstructing PQ BGCs in tractable filamentous fungi is another feasible approach to generate novel PQs (Figure 3E) because these strains have been engineered as auxotroph. Thus, transforming plasmids (containing the corresponding prototrophic genes) into these mutants can facilitate the growth of positive strains on selective media (Chiang et al., 2013). In addition, PQ biosynthesis genes are colinear in the PQ BGCs (Blin et al., 2017), containing nucleotides larger than 30 kb (Hu et al., 2019). These longer sequences require efficient methods to express partial or whole pathways; therefore, a fungal artificial chromosome (FAC) approach has been designed to randomly transfer the relevant genomic regions (up to 300 kb), thereby facilitating the transfer of the intact PQ BGCs into the expression plasmids (Tsunematsu et al., 2013; Bok et al., 2015). These plasmids contain bacterial and filamentous fungal replication origins, which ensure successful pathway construction in *E. coli* and target metabolite expression in *Aspergillus* species. After expression in *Aspergillus* species, high throughput detection tools are essential to confirm the presence of the target products. Liquid chromatography/mass spectrometry (LC/MS) was previously the method of choice to analyze *Aspergillus* metabolomics. Molecular networking and in-silico MS/MS fragmentation tools have further emerged as efficient methods to exploit complex metabolite profiles and the relevant PQ derivatives in filamentous fungi (Allard et al., 2016). The recently developed Global Natural Products Social Molecular Networking (GNPS; Wang et al., 2016) is an open-access data analysis tool, offering diverse raw, or assigned MS/MS libraries, which facilitates continuous dereplication and reliable product confirmation. In addition, a metabolomics-scoring strategy has been established to determine the FAC-encoded metabolites of different *Aspergillus* species, based on GNPS (Clevenger et al., 2017). For instance, the elsinochrome pathway in *Aspergillus nidulans* has been deconstructed and the target metabolites have been detected; engineering *Aspergillus nidulans* with a flavin-linked monooxygenase generates elsinochrome, whereas the transformants without this monooxygenase produce hypocrellin (Hu et al., 2019). Given the substantial homology between the elsinochrome and cercosporin BGCs, ElcE and ElcG have been used as reference genes, and two oxidases, i.e., FAD-dependent CTB5 from *Cercospora nicotianae* and Cz_CTB12 from *Cercospora zeae-maydis,* have been identified. Through the gene swap principle, ElcE and ElcG of *A. nidulans* have been replaced with CTB5 and Cz-CTB12, and the modified transformants generates the PQ core ring structure (Hu et al., 2019). These findings indicate the possibility of generating diverse PQ structures by reconstructing the pathways in *Aspergillus* species.

A droplet microfluidic platform has been developed in *Aspergillus* species *via* complex digital microfluidic/channel-based droplet chips (Gach et al., 2016). Similarly, liquid-handling robots can largely eliminate repetitive sample handling and facilitate very large-scale automated biochemical experiments; for example, liquid-handling robots have achieved 100% genomic editing frequency in *Aspergillus* (Kuivanen et al., 2019). These two systems offer the possibility to reconstruct the PQ pathway in *Aspergillus* species in a fully automated manner.

Other approaches to stimulate endogenous perylenequinone biosynthesis

Except for endogenously genetic regulation, other methods, such as physical and chemical strategies can also stimulate PQs biosynthesis by increasing expressions of genes that are involved in hypocrellin biosynthesis, secretion, and auto-resistance (Sage and Shikazono, 2017; Sun et al., 2017).

Irradiation

Irradiation causes extensive ionization of DNA, which results in multiple-site damage, such as DNA lesions, abasic sites, or double-strand breaks (Sage and Shikazono, 2017), which can trigger variations in fungal morphology and secondary metabolites. Subsequent high-throughput screening can isolate candidate mutants with higher PQ production, or enable the production of PQs with structural changes. Therefore, irradiation is a common method to promote or modify PQ biosynthetic pathways. For example, gamma irradiation of wild-type *S. bambusicola* spore causes 80% lethality and a 35% positive mutant frequency, which increases hypocrellin production 4-fold (Liu et al., 2016). Low-intensity ultrasound also increases cell membrane permeability, antioxidant enzyme activity, and gene expression of the hypocrellin BGC (Sun et al., 2017). Therein, the up-regulation of hypocrellin biosynthesis, secretion, and auto-resistance increased the hypocrellin yield by 1.8-fold (Sun et al., 2017).

Chemical elicitors

Chemical elicitors are environmental signals which can trigger PQ gene expression, thereby stimulating PQ biosynthesis. For example, the surfactant, Triton-X 100, triggers hypocrellin production, whereas SDS and Tween 40 do not (Cai et al., 2011). Transcriptomic analysis has indicated that Triton-X 100 up-regulates the expression of genes encoding membrane permeability, hypocrellin secretion, and hypocrellin biosynthesis (Lei et al., 2017); i.e., Triton-X 100 triggers hypocrellin production in mycelia and enhances transfer to the medium. The rare-earth element, lanthanum also stimulated hypocrellin production in *S. bambusicola* by enhancing PQ-associated gene expression (Lu et al., 2019). Microbial elicitors can improve membrane permeability and enhance PQ-associated gene expression; therefore, they provide another means of facilitating PQ biosynthesis and transportation. For example, two diketopiperazines from *Epichloe typhina* have been found to

facilitate phleichrome production in *C. phlei* (So et al., 2015). An elicitor from *Aspergillus niger* also enhances hypocrellin production by increasing the production of signaling molecules, including salicylic acid and nitric oxide (Du et al., 2015; Ma et al., 2021).

Co-culture with other organisms

Microbial communities are widespread in nature and relationships among the different species in the community comprise symbiosis, antagonism, and competition, which are mainly mediated by secondary metabolites. Therefore, microorganism co-culture is evolving as an efficient approach to increase the diversity of secondary metabolites in general, particularly for PQs (Figure 3F; Bertrand et al., 2014). Microorganism co-culture involves bacteria-bacteria, bacteria-fungi, and fungi-fungi co-culture. Co-culture facilitates the expression of enzymes that produces metabolite precursors and may also stimulate epigenetic modification of the target host; therefore, co-culture is an effective strategy to stimulate PQ biosynthesis. For example, co-culture of the ΔCTB2 and ΔCTB3 mutants does not generate any cercosporin, whereas red cercosporin is produced from co-culture of the ΔCTB1 and ΔCTB2 mutants (Chen et al., 2007); co-culture compensates for pathway deficiencies in the single mutants and produces an intact PQ pathway. Similarly, neither of the ΔCTB1 and ΔCTB3c mutants was able to produce cercosporin; however, a co-culture of these mutants does produce cercosporin (Chung and Liao, 2008). Similarly, stemphyperylenol and derivatives can be produced by co-culturing *Setophoma* sp. with *Penicillium brasilianum* (Bazioli et al., 2020). Co-culture with *Pseudomonas fulva* SB1 facilitates hypocrellin and elsinochrome production in *Shiraia* sp. S9 (Ma et al., 2019); co-culture stimulates the expression of genes, thereby contributing to PQ biosynthesis and secretion. In addition, *Pseudomonas fulva* SB1 facilitates transient ATP release from *Shiraia* sp. S9 (Li et al., 2021). The extracellular ATP can function as a damage-associated-molecular pattern (DAMP) and this DAMP signal is associated with interactions between bacteria and fungi. Moreover, extracellular ATP is associated with Ca^{2+} signaling and ROS generation, which trigger fungal conidiation and PQ biosynthesis (Li et al., 2021). Endophytic bacteria, including *Bacillus velezensis* B04 and *Lysinibacillus* sp. B15, stimulate cercosporin biosynthesis (Zhou et al., 2021).

Drug resistance screening

The photo-activated ROS by PQs can trigger diverse cellular apoptosis. These candidate PQs can also circumvent the multidrug-resistance resistance of pathogenic organisms. Therefore, the chemicals with antimicrobial activities could be used as an efficient strategy to screen novel PQs from fungal extractions. For example, an extract of *Phialocephala fortinii* growth medium could reverse azole resistance in *C. albicans* (Xie et al., 2016). The active component of the extract is phialocephalarin B, which up-regulates the expression of drug-delivery genes, thereby resulting in the reversal of azole resistance (Xie et al., 2016).

Conclusions and perspectives

As excellent photosensitizers, various PQs have been applied in the medical, food, agricultural, and manufacturing fields. These extensive application prospects have stimulated the development of new and improved technologies for the discovery of new PQs and the elucidation of PQ biosynthetic pathways. Evolving sequencing tools have identified many PQ biosynthetic gene clusters (BGCs) in fungal genomes. Bioinformatics software such as AntiSMASH and the MIBiG repository facilitates the discovery of diverse PQs, based on their highly conserved BCGs. Gene editing technologies, particularly the automated CRISPR system, facilitate the automated high-throughput capability to elucidate and confirm these BGCs. Enzymatic conversion experiments are an essential confirmatory test for PQ genes or pathways. The data obtained from the above techniques have enabled higher PQ yields, titers, and productivity. Modifying only one gene decreases the need for complex genetic mutagenesis for the reassembly of entire PQ pathways and the improvement of PQ production. Regulation of signaling pathways is essential to balance the complex cellular metabolic flux and biosynthetic precursor supply and optimize PQ production. These coordination approaches are complex and difficult to implement in many fungal PQ strains, particularly wild-type organisms. However, reconstructing the PQ biosynthetic pathway in tractable *Aspergillus* species is a feasible and efficient strategy to obtain a high PQ yield. These evolving technologies in tractable *Aspergillus* species should enable the automation of PQ de-and re-construction. These methods involve four stages: (1) the computer-aided design stage can elucidate or associate new PQ pathways, (2) the construction stage can assemble target PQ pathways in tractable *Aspergillus* species, (3) the evaluation stage can determine metabolic bottlenecks and blockages, and (4) the optimization stage can fine-tune the PQ biosynthetic pathways and precursor supply from central metabolism, and facilitates the production of the desired products.

Author contributions

HD and YC designed this review. HD wrote this review. XL and JL draw the figures and tables. XZ and T-PF helped to revise the manuscript. All authors reviewed, contributed to the manuscript, and approved the submitted version.

Funding

This work was supported financially by the Natural Sciences Foundation of China (32201203), the Natural Sciences Foundation of Guangdong Province (2021A1515110263), and the Natural Sciences Foundation of Jiangsu Province (BK20210471).

Conflict of interest

The authors declare that the research was conducted in the absence of any commercial or financial relationships that could be construed as a potential conflict of interest.

Publisher's note

All claims expressed in this article are solely those of the authors and do not necessarily represent those of their affiliated organizations, or those of the publisher, the editors and the reviewers. Any product that may be evaluated in this article, or claim that may be made by its manufacturer, is not guaranteed or endorsed by the publisher.

Supplementary material

The Supplementary material for this article can be found online at: https://www.frontiersin.org/articles/10.3389/fmicb.2022.1070110/full#supplementary-material

References

Allard, P.-M., Péresse, T., Bisson, J., Gindro, K., Marcourt, L., Pham, V. C., et al. (2016). Integration of molecular networking and in-silico MS/MS fragmentation for natural products dereplication. *Anal. Chem.* 88, 3317–3323. doi: 10.1021/acs.analchem.5b04804

Arnone, A., Assante, G., Merlini, L., and Nasini, G. (1989). Structure and stereochemistry of cladochrome D and E, novel perylenequinone pigments from *Cladosporium* cladosporioides. *Gazz. Chimica Ital.* 119, 557–559.

Assante, G., Locci, R., Camarda, L., Merlini, L., and Nasini, G. (1977). Screening of the genus *Cercospora* for secondary metabolites. *Phytochemistry* 16, 243–247. doi: 10.1016/S0031-9422(00)86794-1

Barnes, J., Anderson, L. A., and Phillipson, J. D. (2001). St John's wort (*Hypericum perforatum* L.): a review of its chemistry, pharmacology and clinical properties. *J. Pharm. Pharmacol.* 53, 583–600. doi: 10.1211/0022357011775910

Batterham, T. J., and Weiss, U. (1963). *Structure of Elsinochrome A, Proceedings of the Chemical Society of London (N)*, London: Royal society of chemistry, 89.

Bayram, O., Krappmann, S., Ni, M., Bok, J. W., Helmstaedt, K., Valerius, O., et al. (2008). VelB/VeA/LaeA complex coordinates light signal with fungal development and secondary metabolism. *Science* 320, 1504–1506. doi: 10.1126/science.1155888

Bazioli, J. M., Fill, T. P., Rocha, M. C., Malavazi, I., Filho, E. R., and de Medeiros, L. S. (2020). Perylenequinones production induced by co-culturing *Setophoma* sp. and *Penicillium brasilianum*. *Phytochem Lett* 40, 76–83. doi: 10.1016/j.phytol.2020.09.013

Bertrand, S., Bohni, N., Schnee, S., Schumpp, O., Gindro, K., and Wolfender, J. L. (2014). Metabolite induction via microorganism co-culture: a potential way to enhance chemical diversity for drug discovery. *Biotechnol. Adv.* 32, 1180–1204. doi: 10.1016/j.biotechadv.2014.03.001

Beseli, A., Amnuaykanjanasin, A., Herrero, S., Thomas, E., and Daub, M. E. (2015). Membrane transporters in self resistance of *Cercospora nicotianae* to the photoactivated toxin cercosporin. *Curr. Genet.* 61, 601–620. doi: 10.1007/s00294-015-0486-x

Blin, K., Wolf, T., Chevrette, M. G., Lu, X., Schwalen, C. J., Kautsar, S. A., et al. (2017). antiSMASH 4.0—improvements in chemistry prediction and gene cluster boundary identification. *Nucleic Acids Res.* 45, W36–W41. doi: 10.1093/nar/gkx319

Bok, J. W., Ye, R., Clevenger, K. D., Mead, D., Wagner, M., Krerowicz, A., et al. (2015). Fungal artificial chromosomes for mining of the fungal secondary metabolome. *BMC Genomics* 16:343. doi: 10.1186/s12864-015-1561-x

Boss, D., Maurhofer, M., Schlapfer, E., and Defago, G. (2007). Elsinochrome A production by the bindweed biocontrol fungus *Stagonospora convolvuli* LA39 does not pose a risk to the environment or the consumer of treated crops. *FEMS Microbiol. Ecol.* 59, 194–205. doi: 10.1111/j.1574-6941.2006.00207.x

Cai, Y., Liao, X., Liang, X., Ding, Y., Sun, J., and Zhang, D. (2011). Induction of hypocrellin production by triton X-100 under submerged fermentation with *Shiraia* sp. SUPER-H168. *New Biotechnol.* 28, 588–592. doi: 10.1016/j.nbt.2011.02.001

Chen, W. S., Chen, Y. T., Wan, X. Y., Friedrichs, E., Puff, H., and Breitmaier, E. (1981). Structure of hypocrellin and its photooxidation product peroxyhypocrellin. *Liebigs Annalen Der Chemie* 10, 1880–1885.

Chen, H. Q., Lee, M. H., Daub, M. E., and Chung, K. R. (2007). Molecular analysis of the cercosporin biosynthetic gene cluster in *Cercospora nicotianae*. *Mol. Microbiol.* 64, 755–770. doi: 10.1111/j.1365-2958.2007.05689.x

Chiang, Y. M., Oakley, C. E., Ahuja, M., Entwistle, R., Schultz, A., Chang, S. L., et al. (2013). An efficient system for heterologous expression of secondary metabolite genes in *Aspergillus nidulans*. *J. Am. Chem. Soc.* 135, 7720–7731. doi: 10.1021/ja401945a

Chooi, Y. H., Zhang, G., Hu, J., Muria-Gonzalez, M. J., Tran, P. N., Pettitt, A., et al. (2017). Functional genomics-guided discovery of a light-activated phytotoxin in the wheat pathogen *Parastagonospora nodorum* via pathway activation. *Environ. Microbiol.* 19, 1975–1986. doi: 10.1111/1462-2920.13711

Chung, K. R., Daub, M. E., Kuchler, K., and Schuller, C. (2003). The CRG1 gene required for resistance to the singlet oxygen-generating cercosporin toxin in *Cercospora nicotianae* encodes a putative fungal transcription factor. *Biochem. Biophys. Res. Commun.* 302, 302–310. doi: 10.1016/S0006-291X(03)00171-2

Chung, K.-R., and Liao, H.-L. (2008). Determination of a transcriptional regulator-like gene involved in biosynthesis of elsinochrome phytotoxin by the citrus scab fungus, *Elsinoe fawcettii*. *Microbiology* 154, 3556–3566. doi: 10.1099/mic.0.2008/019414-0

Clevenger, K. D., Bok, J. W., Ye, R., Miley, G. P., Verdan, M. H., Velk, T., et al. (2017). A scalable platform to identify fungal secondary metabolites and their gene clusters. *Nat. Chem. Biol.* 13, 895–901. doi: 10.1038/nchembio.2408

Crawford, J. M., Thomas, P. M., Scheerer, J. R., Vagstad, A. L., Kelleher, N. L., and Townsend, C. A. (2008). Deconstruction of iterative multidomain polyketide synthase function. *Science* 320, 243–246. doi: 10.1126/science.1154711

Daub, M. E. (1981). Cercosporin, a photosensitizing toxin from *Cercospora* species. *Phytopathology* 71:213.

Daub, M. E., and Ehrenshaft, M. (2000). The photoactivated *Cercospora* toxin cercosporin: contributions to plant disease and fundamental biology. *Annu. Rev. Phytopathol.* 38:461. doi: 10.1146/annurev.phyto.38.1.461

Daub, M. E., Herrero, S., and Chung, K. R. (2013). Reactive oxygen species in plant pathogenesis: the role of perylenequinone photosensitizers. *Antioxid. Redox Signal.* 19, 970–989. doi: 10.1089/ars.2012.5080

de Jonge, R., Ebert, M. K., Huitt-Roehl, C. R., Pal, P., Suttle, J. C., Spanner, R. E., et al. (2018). Gene cluster conservation provides insight into cercosporin biosynthesis and extends production to the genus colletotrichum. *Proc. Natl. Acad. Sci. U. S. A.* 115, E5459–E5466. doi: 10.1073/pnas.1712798115

Deng, H., Bai, Y., Fan, T.-P., Zheng, X., and Cai, Y. (2020a). Advanced strategy for metabolite exploration in filamentous fungi. *Crit. Rev. Biotechnol.* 40, 1–19. doi: 10.1080/07388551.2019.1709798

Deng, H., Chen, J., Gao, R., Liao, X., and Cai, Y. (2016a). Adaptive responses to oxidative stress in the filamentous fungal *Shiraia bambusicola*. *Molecules* 21:1118. doi: 10.3390/molecules21091118

Deng, H., Gao, R., Chen, J., Liao, X., and Cai, Y. (2016b). An efficient polyethylene glycol-mediated transformation system of lentiviral vector in *Shiraia bambusicola*. *Process Biochem.* 51, 1357–1362. doi: 10.1016/j.procbio.2016.07.013

Deng, H., Gao, R., Liao, X., and Cai, Y. (2017a). Genome editing in *Shiraia bambusicola* using CRISPR-Cas9 system. *J. Biotechnol.* 259, 228–234. doi: 10.1016/j.jbiotec.2017.06.1204

Deng, H., Gao, R., Liao, X., and Cai, Y. (2017b). CRISPR system in filamentous fungi: current achievements and future directions. *Gene* 627, 212–221. doi: 10.1016/j.gene.2017.06.019

Deng, H., Gao, R., Liao, X., and Cai, Y. (2017c). Characterization of a major facilitator superfamily transporter in *Shiraia bambusicola*. *Res. Microbiol.* 168, 664–672. doi: 10.1016/j.resmic.2017.05.002

Deng, H., Gao, R., Liao, X., and Cai, Y. (2018). Characterisation of a monooxygenase in *Shiraia bambusicola*. *Microbiology* 164, 1180–1188. doi: 10.1099/mic.0.000694

Deng, H., Liang, W., Fan, T.-P., Zheng, X., and Cai, Y. (2020b). Modular engineering of *Shiraia bambusicola* for hypocrellin production through an efficient CRISPR system. *Int. J. Biol. Macromol.* 165, 796–803. doi: 10.1016/j.ijbiomac.2020.09.208

Diwu, Z. J., and Lown, J. W. (1990). Hypocrellins and their use in photosensitization. *Photochem. Photobiol.* 52, 609–616. doi: 10.1111/j.1751-1097.1990.tb01807.x

Du, W., Liang, J., Han, Y., Yu, J., and Liang, Z. (2015). Nitric oxide mediates hypocrellin accumulation induced by fungal elicitor in submerged cultures of *Shiraia bambusicola*. *Biotechnol. Lett.* 37, 153–159. doi: 10.1007/s10529-014-1665-4

Dumas, S., Leprêtre, J.-C., Lepellec, A., Darmanyan, A., and Jardon, P. (2004). Reactivity of the photo excited forms of hypericin, hypocrellin A, hypocrellin B and methylated hypericin towards molecular oxygen: the role of charge transfer interaction. *J Photochem Photobiol A Chem* 163, 297–306. doi: 10.1016/S1010-6030(03)00343-5

Ebert, M. K., Spanner, R. E., de Jonge, R., Smith, D. J., Holthusen, J., Secor, G. A., et al. (2019). Gene cluster conservation identifies melanin and perylenequinone biosynthesis pathways in multiple plant pathogenic fungi. *Environ. Microbiol.* 21, 913–927. doi: 10.1111/1462-2920.14475

Falk, H. (1999). From the photosensitizer Hypericin to the photoreceptor stentorin-the chemistry of phenanthroperylene Quinones. *Angew. Chem. Int. Ed. Engl.* 38, 3116–3136. doi: 10.1002/(SICI)1521-3773(19991102)38:21<3116::AID-ANIE3116>3.0.CO;2-S

Fazio, A. T., Adler, M. T., Parnmen, S., Lücking, R., and Maier, M. S. J. M. P. (2018). Production of the bioactive pigment elsinochrome A by a cultured mycobiont strain of the lichen *Graphis elongata*. *Mycol. Prog* 17, 479–487. doi: 10.1007/s11557-017-1374-1

Furtges, L., Obermaier, S., Thiele, W., Foegen, S., and Muller, M. (2019). Diversity in fungal intermolecular phenol coupling of polyketides - Regioselective laccase-based systems. *Chembiochem* 20, 1928–1932. doi: 10.1002/cbic.201900041

Gach, P. C., Shih, S. C. C., Sustarich, J., Keasling, J. D., Hillson, N. J., Adams, P. D., et al. (2016). A droplet microfluidic platform for automating genetic engineering. *ACS Synth. Biol.* 5, 426–433. doi: 10.1021/acssynbio.6b00011

Gao, L., Fei, J., Zhao, J., Li, H., Cui, Y., and Li, J. (2012). Hypocrellin-loaded gold Nanocages with high two-photon efficiency for Photothermal/photodynamic cancer therapy in vitro. *ACS Nano* 6, 8030–8040. doi: 10.1021/nn302634m

Gao, R., Xu, Z., Deng, H., Guan, Z., Liao, X., Zhao, Y., et al. (2018a). Influences of light on growth, reproduction and hypocrellin production by *Shiraia* sp. SUPER-H168. *Arch. Microbiol.* 200, 1217–1225. doi: 10.1007/s00203-018-1529-8

Gao, R., Xu, Z., Deng, H., Guan, Z., Liao, X., Zhao, Y., et al. (2018b). Enhanced hypocrellin production of *Shiraia* sp. SUPER-H168 by overexpression of alpha-amylase gene. *PLoS One* 13:e0196519. doi: 10.1371/journal.pone.0196519

Geris, R., Pinho, M. A., Boffo, E. F., and Simpson, T. J. (2022). Naturally occurring partially reduced perylenequinones from fungi. *J. Nat. Prod.* 85, 2236–2250. doi: 10.1021/acs.jnatprod.2c00368

Grigalavicius, M., Mastrangelopoulou, M., Berg, K., Arous, D., Ménard, M., Raabe-Henriksen, T., et al. (2019). Proton-dynamic therapy following photosensitiser activation by accelerated protons demonstrated through fluorescence and singlet oxygen production. *Nat. Commun.* 10:3986. doi: 10.1038/s41467-019-12042-7

Hasan, H., Abd Rahim, M. H., Campbell, L., Carter, D., Abbas, A., and Montoya, A. (2018). Overexpression of acetyl-CoA carboxylase in *Aspergillus* terreus to increase lovastatin production. *New Biotechnol.* 44, 64–71. doi: 10.1016/j.nbt.2018.04.008

Herbst, D. A., Huitt-Roehl, C. R., Jakob, R. P., Kravetz, J. M., Storm, P. A., Alley, J. R., et al. (2018). The structural organization of substrate loading in iterative polyketide synthases. *Nat. Chem. Biol.* 14, 474–479. doi: 10.1038/s41589-018-0026-3

Hu, J., Li, H., and Chooi, Y.-H. (2019). A fungal dirigent protein controls the stereoselectivity of multicopper oxidase-catalyzed phenol coupling in viriditoxin biosynthesis. *J. Am. Chem. Soc.* 141, 8068–8072. doi: 10.1021/jacs.9b03354

Hu, J., Sarrami, F., Li, H., Zhang, G., Stubbs, K. A., Lacey, E., et al. (2019). Heterologous biosynthesis of elsinochrome A sheds light on the formation of the photosensitive perylenequinone system. *Chem. Sci.* 10, 1457–1465. doi: 10.1039/C8SC02870B

Iida, T., Kobayashi, E., Yoshida, M., and Sano, H. (1989). Calphostins, novel and specific inhibitors of protein kinase C. II. Chemical structures. *J. Antibiot.* 42, 1475–1481. doi: 10.7164/antibiotics.42.1475

Kaul, A., and Maltese, W. A. (2009). Killing of cancer cells by the photoactivatable protein kinase C inhibitor, calphostin C, involves induction of endoplasmic reticulum stress. *Neoplasia* 11, 823–834. doi: 10.1593/neo.09388

Keller, N. P. (2015). Translating biosynthetic gene clusters into fungal armor and weaponry. *Nat. Chem. Biol.* 11, 671–677. doi: 10.1038/nchembio.1897

Keller, N. P. (2019). Fungal secondary metabolism: regulation, function and drug discovery. *Nat. Rev. Microbiol.* 17, 167–180. doi: 10.1038/s41579-018-0121-1

Kindinger, F., Nies, J., Becker, A., Zhu, T., and Li, S.-M. (2019). Genomic locus of a *Penicillium crustosum* pigment as integration site for secondary metabolite gene expression. *ACS Chem. Biol.* 14, 1227–1234. doi: 10.1021/acschembio.9b00164

Kobayashi, E., Ando, K., Nakano, H., Iida, T., Ohno, H., Morimoto, M., et al. (1989b). Calphostins (UCN-1028), novel and specific inhibitors of protein kinase C. I: fermentation, isolation, physico-chemical properties and biological activities. *J. Antibiot* 42, 1470–1474. doi: 10.7164/antibiotics.42.1470

Kobayashi, E., Ando, K., Nakano, H., and Tamaoki, T. (1989a). UCN-1028A, a novel and specific inhibitor of protein kinase C, from *Cladosporium*. *J. Antibiot. (Tokyo)* 42, 153–155. doi: 10.7164/antibiotics.42.153

Kuivanen, J., Korja, V., Holmstrom, S., and Richard, P. (2019). Development of microtiter plate scale CRISPR/Cas9 transformation method for *Aspergillus* Niger based on in vitro assembled ribonucleoprotein complexes. *Fungal Biol Biotechnol* 6:3. doi: 10.1186/s40694-019-0066-9

Kumarihamy, M., Khan, S. I., Jacob, M., Tekwani, B. L., Duke, S. O., Ferreira, D., et al. (2012). Antiprotozoal and antimicrobial compounds from the plant pathogen *Septoria pistaciarum*. *J. Nat. Prod.* 75, 883–889. doi: 10.1021/np200940b

Kuyama, S., and Tamura, T. (1957). Cercosporin. A pigment of cercosporina kikuchii matsumoto et. tomoyasu. I. Cultivation of fungus, isolation and purification of pigment. *J. Am. Chem. Soc* 79, 5725–5726.

Lei, X. Y., Zhang, M. Y., Ma, Y. J., and Wang, J. W. (2017). Transcriptomic responses involved in enhanced production of hypocrellin A by addition of triton X-100 in submerged cultures of *Shiraia bambusicola*. *J. Ind. Microbiol. Biot.* 44, 1415–1429. doi: 10.1007/s10295-017-1965-5

Li, J., Bao, W., Zhang, Y., and Rao, Y. (2019). Cercosporin-photocatalyzed sp3 (C–H) activation for the synthesis of pyrrolo[3,4-c]quinolones. *Org. Biomol. Chem.* 17, 8958–8962. doi: 10.1039/C9OB01946D

Li, G., Wang, H., Zhu, R., Sun, L., Wang, L., Li, M., et al. (2012). Phaeosphaerins A-F, cytotoxic perylenequinones from an endolichenic fungus, *Phaeosphaeria* sp. *J Nat Prod* 75, 142–147. doi: 10.1021/np200614h

Li, Y.-T., Yang, C., Wu, Y., Lv, J.-J., Feng, X., Tian, X., et al. (2021). Axial chiral Binaphthoquinone and Perylenequinones from the stromata of Hypocrella bambusae are SARS-CoV-2 entry inhibitors. *J. Nat. Prod.* 84, 436–443. doi: 10.1021/acs.jnatprod.0c01136

Li, D., Zhao, N., Guo, B. J., Lin, X., Chen, S. L., and Yan, S. Z. (2019). Gentic overexpression increases production of hypocrellin A in *Shiraia bambusicola* S4201. *J. Microbiol.* 57, 154–162. doi: 10.1007/s12275-019-8259-8

Li, X. P., Zhou, L. L., Guo, Y. H., and Wang, J. W. (2021). The signaling role of extracellular ATP in co-culture of *Shiraia* sp. S9 and Pseudomonas fulva SB1 for enhancing hypocrellin A production. *Microb. Cell Factories* 20:144. doi: 10.1186/s12934-021-01637-9

Liao, H. L., and Chung, K. R. (2008). Genetic dissection defines the roles of elsinochrome Phytotoxin for fungal pathogenesis and conidiation of the citrus pathogen *Elsinoe fawcettii*. *Mol Plant Microbe Interact* 21, 469–479. doi: 10.1094/MPMI-21-4-0469

Liu, J. Y. (1985). The photophysics of hypocrellin Aintramolecular hydrogen transfer and excited aciditybasicity. *Kexue Tongbao* 30, 1077–1080.

Liu, B., Bao, J., Zhang, Z., Yan, R., Wang, Y., Yang, H., et al. (2018). Enhanced production of perylenequinones in the endophytic fungus *Shiraia* sp. Slf14 by calcium/calmodulin signal transduction. *Appl. Microbiol. Biotechnol.* 102, 153–163. doi: 10.1007/s00253-017-8602-0

Liu, X.-Y., Shen, X.-Y., Fan, L., Gao, J., and Hou, C.-L. (2016). High-efficiency biosynthesis of hypocrellin A in *Shiraia* sp. using gamma-ray mutagenesis. *Appl. Microbiol. Biot.* 100, 4875–4883. doi: 10.1007/s00253-015-7222-9

Liu, W. Z., Shen, Y. X., Liu, X. F., Chen, Y. T., and Xie, J. L. (2001). A new perylenequinone from *Hypomyces* sp. *Chin. Chem. Lett.* 12, 431–432.

Liu, X., Yuan, Z., Su, H., Hou, X., Deng, Z., Xu, H., et al. (2022). Molecular basis of the unusual seven-membered methylenedioxy bridge formation catalyzed by Fe(II)/α-KG-dependent oxygenase CTB9. *ACS Catal.* 12, 3689–3699. doi: 10.1021/acscatal.1c04627

Lousberg, R. J., Salemink, C. A., and Weiss, U. (1970). Pigments of *Elsinoe* species. Part V. the structure of elsinochrome D. *J. Chem. Soc. C Organic* 16, 2159–2162.

Lousberg, R. J., Salemink, C. A., Weiss, U., and Batterha, T. J. (1969). Pigments of *Elsinoe* species. Part II. Structure of elsinochromes A, B, and C. *J. Chem. Soc. C Organic* 9, 1219–1227.

Lu, C., Ma, Y., and Wang, J. (2019). Lanthanum elicitation on hypocrellin A production in mycelium cultures of *Shiraia bambusicola* is mediated by ROS generation. *J. Rare Earths* 37, 895–902. doi: 10.1016/j.jre.2018.10.010

Lu, C., Zhang, X., Jiang, M., and Bai, L. (2016). Enhanced salinomycin production by adjusting the supply of polyketide extender units in Streptomyces albus. *Metab. Eng.* 35, 129–137. doi: 10.1016/j.ymben.2016.02.012

Ma, G., Khan, S. I., Jacob, M. R., Tekwani, B. L., Li, Z., Pasco, D. S., et al. (2004). Antimicrobial and Antileishmanial activities of Hypocrellins A and B. *Antimicrob Agents Ch* 48, 4450–4452. doi: 10.1128/AAC.48.11.4450-4452.2004

Ma, Y. J., Li, X. P., Wang, Y., and Wang, J. W. (2021). Nitric oxide donor sodium nitroprusside-induced transcriptional changes and hypocrellin biosynthesis of *Shiraia* sp. S9. *Microb. Cell Factories* 20:92. doi: 10.1186/s12934-021-01581-8

Ma, Y. J., Lu, C. S., and Wang, J. W. (2018). Effects of 5-Azacytidine on growth and hypocrellin production of *Shiraia bambusicola*. *Front. Microbiol.* 9:2508. doi: 10.3389/fmicb.2018.02508

Ma, Y. J., Sun, C. X., and Wang, J. W. (2019). Enhanced production of hypocrellin A in submerged cultures of *Shiraia bambusicola* by red light. *Photochem. Photobiol.* 95, 812–822. doi: 10.1111/php.13038

Ma, Y. J., Zheng, L. P., and Wang, J. W. J. M. C. F. (2019). Inducing perylenequinone production from a bambusicolous fungus *Shiraia* sp. S9 through co-culture with a fruiting body-associated bacterium Pseudomonas fulva SB1. *Microb. Cell Factories* 18:121. doi: 10.1186/s12934-019-1170-5

Macheleidt, J., Mattern, D. J., Fischer, J., Netzker, T., Weber, J., Schroeckh, V., et al. (2016). Regulation and role of fungal secondary metabolites. *Annu. Rev. Genet.* 50, 371–392. doi: 10.1146/annurev-genet-120215-035203

Mastrangelopoulou, M., Grigalavicius, M., Berg, K., Ménard, M., and Theodossiou, T. A. (2019). Cytotoxic and photocytotoxic effects of Cercosporin on human tumor cell lines. *Photochem. Photobiol.* 95, 387–396. doi: 10.1111/php.12997

Meng, L., Sun, P., Tang, H., Li, L., Draeger, S., Schulz, B., et al. (2011). Endophytic fungus *Penicillium chrysogenum*, a new source of hypocrellins. *Biochem. Syst. Ecol.* 39, 163–165. doi: 10.1016/j.bse.2011.02.003

Miskovsky, P. (2002). Hypericin - A new antiviral and antitumor photosensitizer: mechanism of action and interaction with biological macromolecules. *Curr. Drug Targets* 3, 55–84. doi: 10.2174/1389450023348091

Montibus, M., Pinson-Gadais, L., Richard-Forget, F., Barreau, C., and Ponts, N. (2015). Coupling of transcriptional response to oxidative stress and secondary metabolism regulation in filamentous fungi. *Crit. Rev. Microbiol.* 41, 295–308. doi: 10.3109/1040841X.2013.829416

Müller, M., Obermaier, S., Thiele, W., and Fürtges, L. (2019). Enantioselective phenol coupling by laccases in the biosynthesis of fungal dimeric naphthopyrones. *Angew. Chem.* 58, 9125–9128. doi: 10.1002/anie.201903759

Newman, A. G., and Townsend, C. A. (2016). Molecular characterization of the cercosporin biosynthetic pathway in the fungal plant pathogen *Cercospora nicotianae*. *J. Am. Chem. Soc.* 138, 4219–4228. doi: 10.1021/jacs.6b00633

Newman, A. G., Vagstad, A. L., Belecki, K., Scheerer, J. R., and Townsend, C. A. (2012). Analysis of the cercosporin polyketide synthase CTB1 reveals a new fungal thioesterase function. *Chem. Commun.* 48, 11772–11774. doi: 10.1039/c2cc36010a

Newman, A. G., Vagstad, A. L., Storm, P. A., and Townsend, C. A. (2014). Systematic domain swaps of iterative, nonreducing polyketide synthases provide a mechanistic understanding and rationale for catalytic reprogramming. *J. Am. Chem. Soc.* 136, 7348–7362. doi: 10.1021/ja5007299

Niu, T., Tian, Y., Wang, G., Guo, G., Tong, Y., and Shi, Y. (2020). Inhibition of ROS-NF-κB-dependent autophagy enhances Hypocrellin A united LED red light-induced apoptosis in squamous carcinoma A431 cells. *Cell. Signal.* 69:109550. doi: 10.1016/j.cellsig.2020.109550

Overeem, J. C., Sijpesteijn, A. K., and Fuchs, A. (1967). The formation of perylenequinones in etiolated cucumber seedlings infected with *Cladosporium cucumerinum*. *Phytochemistry* 6, 99–105. doi: 10.1016/0031-9422(67)85013-1

Pahirulzaman, K. A. K., Williams, K., and Lazarus, C. M. (2012). "Chapter twelve - a toolkit for heterologous expression of metabolic pathways in *Aspergillus* oryzae" in *Methods in Enzymology*. ed. D. A. Hopwood (Elsevier, Academic Press), 241–260.

Pfannenstiel, B. T., and Keller, N. P. (2019). On top of biosynthetic gene clusters: how epigenetic machinery influences secondary metabolism in fungi. *Biotechnol. Adv.* 37:107345. doi: 10.1016/j.biotechadv.2019.02.001

Qi, S., Guo, L., Yan, S., Lee, R. J., Yu, S., and Chen, S. (2019). Hypocrellin A-based photodynamic action induces apoptosis in A549 cells through ROS-mediated mitochondrial signaling pathway. *Acta Pharm. Sin. B* 9, 279–293. doi: 10.1016/j.apsb.2018.12.004

Robeson, D. J., and Jalal, M. A. F. (1992). Formation of Ent-isophleichrome by *Cladosporium herbarum* isolated from sugar beet. *Biosci. Biotechnol. Biochem.* 56, 949–952. doi: 10.1271/bbb.56.949

Robitaille, K., Daviau, A., Lachance, G., Couture, J. P., and Blouin, R. (2008). Calphostin C-induced apoptosis is mediated by a tissue transglutaminase-dependent mechanism involving the DLK/JNK signaling pathway. *Cell Death Differ.* 15, 1522–1531. doi: 10.1038/cdd.2008.77

Roux, I., Woodcraft, C., Hu, J., Wolters, R., Gilchrist, C. L. M., and Chooi, Y. H. (2020). CRISPR-mediated activation of biosynthetic gene clusters for bioactive molecule discovery in filamentous fungi. *ACS Synth. Biol.* 9, 1843–1854. doi: 10.1021/acssynbio.0c00197

Sage, E., and Shikazono, N. (2017). Radiation-induced clustered DNA lesions: repair and mutagenesis. *Free Radical Bio Med* 107, 125–135. doi: 10.1016/j.freeradbiomed.2016.12.008

Sander, J. D., and Joung, J. K. (2014). CRISPR-Cas systems for editing, regulating and targeting genomes. *Nat. Biotechnol.* 32, 347–355. doi: 10.1038/nbt.2842

Saw, C. L. L., Heng, P. W. S., and Olivo, M. (2008). Potentiation of the photodynamic action of hypericin. *J. Environ. Pathol. Toxicol. Oncol.* 27, 23–33. doi: 10.1615/JEnvironPatholToxicolOncol.v27.i1.30

Shim, W. B., and Dunkle, L. D. (2003). CZK3, a MAP kinase homolog in *Cercospora* zeae-maydis, regulates cercosporin biosynthesis, fungal development, and pathogenesis. *Mol Plant Microbe Interact* 16, 760–768. doi: 10.1094/MPMI.2003.16.9.760

So, K.-K., Chun, J., and Kim, D.-H. (2018). Antimicrobial and antitumor photodynamic effects of Phleichrome from the Phytopathogenic fungus *Cladosporium* phlei. *Mycobiology* 46, 448–451. doi: 10.1080/12298093.2018.1551599

So, K. K., Chung, Y. J., Kim, J. M., Kim, B. T., Park, S. M., and Kim, D. H. (2015). Identification of a polyketide synthase gene in the synthesis of phleichrome of the phytopathogenic fungus *Cladosporium* phlei. *Mol. Cells* 38, 1105–1110. doi: 10.14348/molcells.2015.0208

So, K. K., Jo, I. S., Chae, M. S., Kim, J. M., Chung, H. J., Yang, M. S., et al. (2015). Improved production of phleichrome from the phytopathogenic fungus *Cladosporium* phlei using synthetic inducers and photodynamic ROS production by phleichrome. *J. Biosci. Bioeng.* 119, 289–296. doi: 10.1016/j.jbiosc.2014.08.011

Sun, C. X., Ma, Y. J., and Wang, J. W. (2017). Enhanced production of hypocrellin A by ultrasound stimulation in submerged cultures of *Shiraia bambusicola*. *Ultrason. Sonochem.* 38, 214–224. doi: 10.1016/j.ultsonch.2017.03.020

Sun, C. X., Ma, Y. J., and Wang, J. W. (2018). Improved hypocrellin A production in *Shiraia bambusicola* by light-dark shift. *J Photochem. Photobiol. B Biology* 182, 100–107. doi: 10.1016/j.jphotobiol.2018.04.004

Surup, F., Pommerehne, K., Schroers, H.-J., and Stadler, M. (2018). Elsinopirins A–D, Decalin polyketides from the ascomycete Elsinoë pyri. *Biomolecules* 8:8. doi: 10.3390/biom8010008

Swart, V., Crampton, B. G., Ridenour, J. B., Bluhm, B. H., Olivier, N. A., Meyer, J. J. M., et al. (2017). Complementation of CTB7 in the maize pathogen *Cercospora* zeina overcomes the lack of in vitro cercosporin production. *Mol Plant Microbe Interact* 30, 710–724. doi: 10.1094/MPMI-03-17-0054-R

Tabuchi, H., Tajimi, A., and Ichihara, A. (1991). (+)-Isocercosporin, A phytotoxic compound isolated from Scolecotrichum graminis Fuckel (Organic Chemistry). *Agric. Biol. Chem.* 55, 2675–2676. doi: 10.1080/00021369.1991.10870997

Tabuchi, H., Tajimi, A., and Ichihara, A. (1994). Phytotoxic metabolites isolated from *Scolecotrichum graminis* Fuckel. *Biosci. Biotech. Bioch.* 58, 1956–1959. doi: 10.1271/bbb.58.1956

Tsunematsu, Y., Ishikawa, N., Wakana, D., Goda, Y., Noguchi, H., Moriya, H., et al. (2013). Distinct mechanisms for spiro-carbon formation reveal biosynthetic pathway crosstalk. *Nat. Chem. Biol.* 9, 818–825. doi: 10.1038/nchembio.1366

Udwary, D. W., Merski, M., and Townsend, C. A. (2002). A method for prediction of the locations of linker regions within large multifunctional proteins, and application to a type I polyketide synthase. *J. Mol. Biol.* 323, 585–598. doi: 10.1016/S0022-2836(02)00972-5

Vielma, S. A., Krings, G., and Lopes-Virella, M. F. (2003a). *Chlamydophila pneumoniae* induces ICAM-1 expression in human aortic endothelial cells via protein kinase C–dependent activation of nuclear factor-κB. *Circ. Res.* 92, 1130–1137. doi: 10.1161/01.RES.0000074001.46892.1C

Vielma, S. A., Krings, G., and Lopes-Virella, M. F. (2003b). *Chlamydophila pneumoniae* induces ICAM-1 expression in human aortic endothelial cells via protein kinase C-dependent activation of nuclear factor-kappaB. *Circ. Res.* 92, 1130–1137. doi: 10.1161/01.RES.0000074001.46892.1C

Wang, M., Carver, J. J., Phelan, V. V., Sanchez, L. M., Garg, N., Peng, Y., et al. (2016). Sharing and community curation of mass spectrometry data with global natural products social molecular networking. *Nat. Biotechnol.* 34, 828–837. doi: 10.1038/nbt.3597

Wang, L., Wang, J., Cao, Y., Li, W., Wang, Y., Xu, J., et al. (2019). Molecular evidence for better efficacy of hypocrellin A and oleanolic acid combination in suppression of HCC growth. *Eur. J. Pharmacol.* 842, 281–290. doi: 10.1016/j.ejphar.2018.10.042

Wattanachaisaereekul, S., Lantz, A. E., Nielsen, M. L., and Nielsen, J. (2008). Production of the polyketide 6-MSA in yeast engineered for increased malonyl-CoA supply. *Metab. Eng.* 10, 246–254. doi: 10.1016/j.ymben.2008.04.005

Weiss, U., Flon, H., and Burger, W. C. (1957). The photodynamic pigment of some species of Elsinoë and Sphaceloma. *Arch. Biochem. Biophys.* 69, 311–319. doi: 10.1016/0003-9861(57)90497-6

Williams, R. B., Henrikson, J. C., Hoover, A. R., Lee, A. E., and Cichewicz, R. H. (2008). Epigenetic remodeling of the fungal secondary metabolome. *Org. Biomol. Chem.* 6, 1895–1897. doi: 10.1039/b804701d

Xie, F., Chang, W., Zhang, M., Li, Y., Li, W., Shi, H., et al. (2016). Quinone derivatives isolated from the endolichenic fungus *Phialocephala fortinii* are Mdr1 modulators that combat azole resistance in *Candida albicans*. *Sci Rep.* 6:33687. doi: 10.1038/srep33687

Yoshihara, T., Shimanuki, T., Araki, T., and Sakamura, S. (1975). Phleichrome, a new phytotoxic compound produced by *Cladosporium* phlei. *Agric. Biol. Chem.* 39, 1683–1684. doi: 10.1080/00021369.1975.10861841

You, B. J., Lee, M. H., and Chung, K. R. (2008). Production of cercosporin toxin by the phytopathogenic *Cercospora* fungi is affected by diverse environmental signals. *Can. J. Microbiol.* 54, 259–269. doi: 10.1139/W08-002

You, B.-J., Lee, M.-H., and Chung, K.-R. (2009). Gene-specific disruption in the filamentous fungus *Cercospora nicotianae* using a split-marker approach. *Arch. Microbiol.* 191, 615–622. doi: 10.1007/s00203-009-0489-4

Yuan, Z., Lu, L., Liu, M., Liu, X., Liu, C., Yin, D., et al. (2022). Natural product cercosporin as a bioinspired photocatalyst for the synthesis of peptides containing kynurenine via an energy transfer mechanism. *Green Chem.* 24, 3277–3283. doi: 10.1039/D2GC00116K

Zhang, H. Y., Liu, W., Liu, W. Z., and Xie, J. L. (2001). Photosensitization of hypomycin B - A novel perylenequinonoid pigment with only one intramolecular hydrogen bond. *Photochem. Photobiol.* 74, 191–195. doi: 10.1562/0031-8655(2001)074<0191:POHBAN>2.0.CO;2

Zheng, X., Ge, J., Wu, J., Liu, W., Guo, L., Jia, Q., et al. (2018). Biodegradable hypocrellin derivative nanovesicle as a near-infrared light-driven theranostic for dually photoactive cancer imaging and therapy. *Biomaterials* 185, 133–141. doi: 10.1016/j.biomaterials.2018.09.021

Zhou, T., Yu, S., Hu, Y., Zhang, Y., Song, Y., Chu, J., et al. (2021). Enhanced cercosporin production by co-culturing *Cercospora* sp. JNU001 with leaf-spot-disease-related endophytic bacteria. *Microb. Cell Factories* 20:100. doi: 10.1186/s12934-021-01587-2

frontiers | Frontiers in Microbiology

TYPE Original Research
PUBLISHED 26 January 2023
DOI 10.3389/fmicb.2022.1085000

Check for updates

OPEN ACCESS

EDITED BY
Harsh Mathur,
Teagasc Food Research Centre, Teagasc, Ireland

REVIEWED BY
Pinkuan Zhu,
East China Normal University, China
Duc-Cuong Bui,
University of Texas Medical Branch at Galveston, United States
Ang Ren,
Nanjing Agricultural University, China

*CORRESPONDENCE
Dan Shu
✉ shudan@cib.ac.cn
Hong Tan
✉ abath@cib.ac.cn

SPECIALTY SECTION
This article was submitted to Microbial Physiology and Metabolism, a section of the journal Frontiers in Microbiology

RECEIVED 31 October 2022
ACCEPTED 23 December 2022
PUBLISHED 26 January 2023

CITATION
Chen D, Shu D, Wei Z, Luo D, Yang J, Li Z and Tan H (2023) Combined transcriptome and proteome analysis of Bcfrp1 involved in regulating the biosynthesis of abscisic acid and growth in *Botrytis cinerea* TB-31. *Front. Microbiol.* 13:1085000. doi: 10.3389/fmicb.2022.1085000

COPYRIGHT
© 2023 Chen, Shu, Wei, Luo, Yang, Li and Tan. This is an open-access article distributed under the terms of the Creative Commons Attribution License (CC BY). The use, distribution or reproduction in other forums is permitted, provided the original author(s) and the copyright owner(s) are credited and that the original publication in this journal is cited, in accordance with accepted academic practice. No use, distribution or reproduction is permitted which does not comply with these terms.

Combined transcriptome and proteome analysis of Bcfrp1 involved in regulating the biosynthesis of abscisic acid and growth in *Botrytis cinerea* TB-31

Dongbo Chen[1,2], Dan Shu[1]*, Zhao Wei[1,2], Di Luo[1], Jie Yang[1], Zhemin Li[1] and Hong Tan[1]*

[1]CAS Key Laboratory of Environmental and Applied Microbiology, Environmental Microbiology Key Laboratory of Sichuan Province, Chengdu Institute of Biology, Chinese Academy of Sciences, Chengdu, China, [2]Chengdu Institute of Biology, China Academy of Sciences (CAS), University of the Chinese Academy of Sciences, Chengdu, China

Introduction: Abscisic acid (ABA) is an important sesquiterpene compound that regulates the stress resistance of plants. *Botrytis cinerea* can synthesize ABA via the mevalonic acid pathway. To identify the functional genes that are involved in the biosynthesis of ABA, we performed insertion mutagenesis into *B. cinerea* TB-31.

Methods: We obtained the ABA-reduced mutant E154 by insertion mutagenesis, and we identified the insertion site was located upstream of the gene *bcfrp1* by Thermal asymmetric interlaced PCR. We performed a detailed phenotypic characterization of the *bcfrp1* knockout and complementation mutants in TB-31. Furthermore, transcriptome and proteome analyses were conducted to explore how *bcfrp1* affects the level of the ABA biosynthesis.

Results: The *bcfrp1* gene encodes an F-box protein. The phenotypic results confirmed the positive contribution of *bcfrp1* to the biosynthesis of ABA and growth. Between TB-31 and ΔBcfrp1, we obtained 4,128 and 1,073 differentially expressed genes and proteins, respectively. The impaired ABA biosynthesis in the ΔBcfrp1 mutants was primarily affected by the different levels of expression of the ABA biosynthetic gene cluster and the genes involved in the mevalonic acid pathway. In addition, we further characterized the differentially expressed genes and proteins that participated in the growth, secondary metabolism, and signal transduction in *B. cinerea* based on the transcriptome and proteome data.

Discussion: This research based on the transcriptome and proteome analyses to display the changes after the deletion of *bcfrp1* in *B. cinerea* TB-31, will help us to explore the molecular mechanism of ABA biosynthesis in *B. cinerea*.

KEYWORDS

***bcfrp1*, *Botrytis cinerea*, abscisic acid, carbon metabolism, transcriptome, proteome**

1. Introduction

Abscisic acid (ABA) is a sesquiterpene "stress hormone," which has been shown to be synthesized not only in plants, but also in cyanobacteria, fungi, sponge, human cells amongst others (Gill and Patranabis, 2021). The most common functions of ABA are involved in controlling seed maturation and germination, increasing the tolerance of plants for various kinds of stresses caused by abiotic or biotic factors (Alazem and Lin, 2017). In addition, ABA has also demonstrated its important functions in other organisms (Sakthivel et al., 2016). It plays important roles in regulating the activation of innate immune cells and glucose homeostasis in mammals (Gietler et al., 2020). Interestingly ABA also seems to exist as a communication signal between different species (Lievens et al., 2017). There are reports of some mutualistic host-microbe and host-pathogen interactions dependence on ABA (Lievens et al., 2017; Hewage et al., 2020). For these reasons, it is very important to understand the biosynthesis and regulation mechanism of ABA in non-plant organisms. It will be very interesting to elucidate the biological significant of ABA as a 'universal molecule'.

Phytopathogenic fungi, such as *Botrytis cinerea* has been shown to produce ABA. Marumo et al., first reported that the gray mold fungus *B. cinerea* could synthesize ABA in 1982 (Marumo et al., 1982). After that, other *B. cinerea* strains have been confirmed and considered to be ABA-producing strains (De Simone et al., 2020). Twenty years ago, our research group isolated a wild type strain *Botrytis cinerea* TBC-6 from the stems and leaves of wheat in southwest China. Mutant strains TB-31(with ABA productivity of 0.55 g/L) and TB-3-H8 (with an ABA productivity of 1.4 g/L) were generated after multiple rounds of mutagenesis and screening of TBC-6 (Gong et al., 2014; Wang et al., 2018). Further strain improvement generated the TBC-A strain with an ABA productivity of 2.0 g/L, which has been utilized to reduce the cost of ABA in industrial applications (Gong et al., 2014; Ding et al., 2015). However, little is known about in the molecular mechanisms underlying fungal ABA biosynthesis before these strains can be used in an industrial setting for biotechnological ABA production (Ding et al., 2016).

^{18}O-, ^{2}H-, and ^{13}C-labeling experiments were performed to study the ABA biosynthetic pathway of *B. cinerea*, and a pathway different from plants has been postulated: isopentenyl pyrophosphate (IPP), which is synthesized from the mevalonic acid (MVA) pathway, is converted to C_{15} compound farnesyldiphosphate (FPP). Additionally, after a series of reactions of cyclization, isomerization, desaturation and hydroxylation from FPP, ABA is synthesized (Nambara and Marion-Poll, 2005; Siewers et al., 2006). But there was no genetic information to support this hypothesis, and it was not until 2004 that genes involved in ABA synthesis were discovered. The gene knockout experiments revealed the *bcaba1-4* gene cluster, in which *bcaba1*, *2*, *4* genes were presumed to be responsible for the hydroxylation of carbon atoms C-4′, C-1′ and the oxidation of C-4′ of ABA in *B. cinerea*, respectively (Siewers et al., 2004, 2006).

In order to further understand the synthesis and regulatory mechanisms of ABA, we had carried out systematic research in the previous work. First, Ding et al. (2016) performed a comparative transcriptome analysis to identify the differentially expressed genes which may potentially contribute to the very different phenotypic outcomes of ABA production of the industrial strain TBC-A and the wild-type strain TBC-6. The results of comparative transcriptome analysis helps us understand the crucial genes and metabolic pathways related to ABA biosynthesis, including genes involved in the MVA pathway and the biosynthesis of FPP, which further confirmed that the ABA synthesis pathway of fungi is different from that of plants (Ding et al., 2016). Second, the genes that are required for ABA production and regulation were identified based on the transcriptome data, such as *bcaba3*, *bcabaR1*, and *bclaeA*. In our previous study, the targeted disruption of Bcaba3 showed the loss of ABA synthesis in TB-31, and enabled the detection of 2Z,4E-α-ionylideneethane (data not published). Shu et al. (2018) found that Bcaba3 can catalyze the substrate FPP into 2Z,4E-α-ionylideneethane through the enzyme catalysis experiments, which is consistent with the report of Takino et al. (2018). Wang et al. (2018) reported a Cys_2His_2 Zinc finger transcription factor BcabaR1 which positively regulates the levels of transcription of *bcaba1-4*, by interacting with conserved sequence regions of the ABA gene clusters promoters. Wei et al. (2022) found the global regulator BcLaeA, as 'a putative methyltransferase', also participates in regulating the biosynthesis of ABA in TB-31 (Wei et al., 2022). Third, in order to find some new unknown genes that may be involved in ABA synthesis, we also performed insertional mutagenesis in *B. cinerea* TB-31 by *Agrobacterium tumefaciens*-mediated transformation (ATMT; Chen et al., 2011), which is a useful approach that enables the identification of functional genes.

Plasmid insertion induction is a common method for identifying new genes or discovering new functions of the known gene (Miesel et al., 2003). Duyvesteijn et al. (2005) obtained a pathogenic deletion mutant from *Fusarium oxysporum* f. sp. *lycopersici* by random insertion, and identified that the insertion site occurred in a gene encoding an F-box protein and named Frp1 (Duyvesteijn et al., 2005). It was reported that F-box protein (FBP) is part of SCFs (Skp1-cullin-F-box protein ligase) complexes and linked to the Skp1 protein through the F-box (Gabriel et al., 2021). Of course, F-box proteins function as non-SCF complexes, too (Sadat et al., 2021; Wu et al., 2022). Each eukaryote contains a considerable amount of F-box proteins, and each protein may correspond to a substrate. Lots of fungal F-box protein were revealed, which have been shown to be involved in stress response, catabolite repression, and to be a novel virulence factor that shapes immunogenicity and such (De Assis et al., 2018; Masso-Silva et al., 2018; Sharma et al., 2021). However, there are few reports about the effects of F-box protein on secondary metabolic synthesis in fungi.

In this research, we report an ABA deficient mutant *B. cinerea* E154 from an ATMT-mediated random mutation, and the F-box protein Bcfrp1 was identified which was responsible for the

phenotype of E154. It has not been reported that ubiquitin-related proteins are involved in the regulation of ABA synthesis in *B. cinerea*. The role of Bcfrp1 in ABA biosynthesis and the growth of *B. cinerea* was investigated. A stringent comparative transcriptome and proteome analysis was performed to identify differentially expressed genes participating in the metabolic pathways related to ABA biosynthesis and other pathways in *B. cinerea*. This study could help us to predict and screen genes related to the effect of *bcfrp1* on ABA biosynthesis in *B. cinerea* based on the transcriptome and proteome.

2. Materials and methods

2.1. Strains, plasmids, and culture conditions

Escherichia coli DH5α and *Agrobacterium tumefaciens* EHA105 were used to construct vectors and transform plasmid DNA. *E. coli* and *A. tumefaciens* strains were grown on Luria-Bertani (LB) media. The plasmid pBHt2 enables the selection of hygromycin-resistant (*hph*) transformants. The ABA-producing strain *B. cinerea* TB-31 was transformed with pBHt2 to create insertional mutants by ATMT (Rolland et al., 2003). *B. cinerea* TB-31 was used as a control for this study to generate gene knockout and complementary mutants of *bcfrp1*. *B. cinerea* strains grow on potato glucose agar (PDA) media at 26°C for 7 days, followed by the collection of spores and resuspended to 1×10^6 conidia·mL^{-1}. The PDA plates with 50 μg·mL^{-1} hygromycin B or 100 μg·mL^{-1} glufosinate-ammonium, were purchased from Solar Biotech, to screen the *B. cinerea* transformants.

2.2. Construction of the deletion and complementation mutants of *bcfrp1*

We generated knockout and complementary mutants of *bcfrp1* to explore whether this gene affected the synthesis of ABA in *B. cinerea* TB-31. Lists of all the primers used to prepare these constructs are shown in Supplementary Table S1. The *bcfrp1* gene knockout vector was constructed using the double-joint PCR method (Yu et al., 2004). The genomic DNA of *B. cinerea* TB-31 was extracted by the E.Z.N.A. Fungal DNA Mini kit (Omega, D3390-01, United States). With the DNA of TB-31 as the template, we amplified the 5′ fragment (552 bp) and 3′ fragment (613 bp) of the open reading frame (ORF) of *bcfrp1* by the primer pairs *bcfrp1*-5′F/-R and *bcfrp1*-3′F/-R, respectively. The *hph* fragment was amplified using primer pairs *hph*-F/-R. With the primer pair *bcfrp1*-5′F/3′-R to amplify the gene knockout cassette by overlapping PCR (Supplementary Figure S2A). The gene knockout cassettes were transformed into fungal protoplasts as described by Choquer et al. (2008). Transformants were selected on PDA containing hygromycin (50 μg·mL^{-1}), and three generations were purified on PDA with hygromycin. Transformants were verified by PCR using the primers *bcfrp1*-out-5′F/*hph*-in-R, *hph*-in-F/*bcfrp1*-out-R, *hph*-F/-R, *bcfrp1*-detcet-F/-R which were shown in Supplementary Table S1, and driven by real-time quantitative reverse transcription PCR (qRT-PCR) using the primers qRT-*bcfrp1*-F/-R.

To further confirm that the differences in production of ABA between ΔBcfrp1 and TB-31 were caused by the loss of *bcfrp1*, we constructed the complementary vector pCBg1-*bcfrp1* and then transformed it into a ΔBcfrp1 mutant (Supplementary Figure S2A). We amplified *bcfrp1* cDNA from *B. cinerea* TB-31 using the primers *bcfrp1*-cds-F/−R, and cloned into the *Sca*I and *Xba*I digested sites in pCBg1 to generate pCBg1-*bcfrp1*. The vector, pCBg1-*bcfrp1*, was utilized for ATMT of the conidia of ΔBcfrp1. Transformants were selected on PDA that contained hygromycin (50 μg·mL^{-1}) and glyphosate (100 μg·mL^{-1}), and three generations were purified on PDA with hygromycin and glyphosate. The transformants were verified by PCR using the primers *bcfrp1*-detcet-F/-R, *hph*-F/-R, Bar-in-F/-R, and qRT-PCR using the primers qRT-*bcfrp1*-F/-R.

2.3. Phenotypic analysis of the deletion and complementation mutants of *bcfrp1*

To detect the extracellular ABA in TB-31 and the ΔBcfrp1 and ΔBcfrp1-C mutants, these strains were inoculated on PDA media for 6–12 days at 26°C. The detection of ABA yield was performed by high-performance liquid chromatography (HPLC) as described by Ding et al. (2015). The biomass was quantified by collecting the mycelia of the three strains from 50 ml of PDB after 72, 96 and 120 h. The mycelia were filtered and weighed after drying at 100°C for 60 min (Ding et al., 2016). The colony diameters of the TB-31 and mutant strains were analyzed on agar plates. Briefly, each strain was separately inoculated on Czapek–Dox agar (CDA) media with different sugar carbon sources: 2% D-glucose, 2% sucrose, 2% lactose, or 2% maltose, respectively, for 6 days at 26°C. Each strain was analyzed in triplicate.

2.4. Transcriptome sequencing and analysis

After culturing on PDA in the dark for 6 days at 26°C, the mycelia of the *B. cinerea* TB-31 and ΔBcfrp1 were harvested and stored at −80°C. The total RNA was extracted using TRIzol according to the manufacturer's instructions (Invitrogen, Carlsbad, CA, United States). After the quality and concentration of RNA were tested and qualified, the RNA library was sequenced by Gene Denovo Biotechnology Co., Ltd. (Guangzhou, China) with the Illumina NovaSeq 6,000 (San Diego, CA, United States; Modi et al., 2021). The raw data that were obtained were filtered and mapped to the genome of model microorganism *B. cinerea* B05.10 (NCBI, ASM14353v4) using HISAT2.2.4 (Kim et al., 2015). The genes obtained were quantified using RNA-seq by expectation maximization (RSEM; Li and Dewey, 2011), and their levels of

expression were normalized using Fragments Per Kilobase of transcript per Million mapped reads (FPKM) as described by Li and Dewey (2011). The differential expression analysis was analyzed between TB-31 and ΔBcfrp1 by DESeq2 (Love et al., 2014). The differentially expressed genes (DEGs) were filtered based on fold change ≥2 and false discovery rate (FDR) ≤0.05 (FPKM > 1). The gene functions were annotated against the cluster of orthologs/eukaryotic clusters of orthologs (COG/KOG), Gene Ontology (GO) and Kyoto Encyclopedia of Genes and Genomes (KEGG) database as described by Fang et al. (2021).

2.5. Proteome analysis

Consistent with the samples analyzed by transcriptome sequencing, the samples for proteome analysis were also harvested after 6 days of culture on PDA. The total protein of TB-31 and ΔBcfrp1 was extracted and measured with BCA (Bicinchoninic acid) method as described by Jia et al. (2022). The proteins were digested into peptide fractions and performed with the method of data-independent acquisition (DIA) as described by Jia et al. (2022). DIA raw data were performed by Spectronaut X (Biognosys AG, Schlieren, Switzerland) as described by Long (Long et al., 2020). All the selected precursors passing the filters were employed to quantify. The differentially expressed proteins (DEPs) were filtered based on fold change ≥1.5 and $p < 0.05$ after subjecting them to Student's *t*-test. The protein function were annotated against COG/KOG, GO and KEGG database with $p \leq 0.05$ as described by Wei et al. (2022).

2.6. Correlation analysis of genes and proteins

We have uploaded the Transcriptome and Proteome data in the ScienceDB (https://www.scidb.cn/detail?dataSetId=bf230977945c4b4785ec355293b23d79). First, the differentially expressed genes and proteins were identified between TB-31 and ΔBcfrp1. A significant DEG was screened with fold change ≥2 and FDR <0.05, and a significant DEP was screened with fold change >1.5 and $p < 0.05$, respectively. Second, the correlation analysis between genes and proteins were analyzed as described by Dou et al. (2022). The Venn diagram was used to count the genes/proteins and the differential genes/differential proteins, respectively. The correlation analysis between genes and proteins were carried out by R language (version 3.5.1). In addition, the nine-quadrant map shows the functional enrichment with the GO and KEGG pathway analysis of mRNAs and proteins.

2.7. qRT-PCR analysis

All the mycelial RNA was extracted using TRIzol according to the manufacturer's instructions (Invitrogen, Carlsbad, CA, United States). The quality and concentration of RNA was detected as described by Wang et al. (2018). cDNA was synthesized by the TaKaRa reverse transcriptase kit (TaKaRa, Dalian, China). The qRT-PCR was conducted using the AceQ qPCR SYBR Green master mix kit (Nanjing Vazyme Biotech Co., Ltd., Nanjing, China). The qRT-PCR primers in this study are shown in Supplementary Table S1. The reactions were conducted in a CFX96 real-time PCR detection system (Bio-Rad, Hercules, CA, United States). Each transcript was analyzed using three PCR repetitions in parallel. The tubulin gene (Bcin02g00900) served as an internal control (Dulermo et al., 2010). The fold change in the mRNA was analyzed by $2^{-\Delta\Delta Ct}$ method.

3. Results

3.1. Identification ABA-deficient mutant named E154

Botrytis cinerea TB-31 was transformed with pBHt2, which is a commonly used binary vector for ATMT in filamentous fungi, to create ABA-deficient mutants by insertional mutagenesis. This plasmid enables the selection of hygromycin-resistant (*hph*) transformants. The ATMT resulted in 217 hygromycin-resistant transformants that were grown for 8 days on PDA media and tested for their production of ABA using HPLC. Among the positive transformants, one mutant designated E154 exhibited a reduction of approximately 40% in the yield of ABA compared with the parental strain TB-31 when cultured on PDA agar for 6 days (Supplementary Figure S1A). However, the E154 mutant had a similar colony morphology when compared with TB-31 (Supplementary Figure S1B).

Thermal asymmetric interlaced PCR (TAIL-PCR) was carried out to isolate the portion of the genome that is close to either the right or left boundary of the T-DNA integration event as described from rice blast (*Magnaporthe oryzae*; Chen et al., 2011). In this study, we found that T-DNA was integrated in TB-31 at 1806 bp upstream of the predicted start codon of BC_5_05922 (Supplementary Figure S1C; Supplementary Table S2). A reverse transcription (RT)-PCR assay showed that the level of transcription of BC_5_05922 decreased significantly in the E154 mutant (Supplementary Figure S1D). The full-length DNA and cDNA were also isolated for BC_5_05922 from TB-31, and the complementary assay showed that the reduction of ABA could be complemented in *trans* by integrating a functional copy of the BC_5_05922 cDNA into the E154 strain using the vector pCBg1 (Supplementary Figure S1A). In addition, it showed that the translated protein of BC_5_05922 had 100% amino acid identity with Bcfrp1 (BCIN_11g00230) of *B. cinerea* B05.10 using the BLASTP algorithm from NCBI. These findings suggested that T-DNA integration upstream of the *bcfrp1* gene may be linked to the E154 phenotype.

3.2. *bcfrp1* is required for the biosynthesis of ABA in *Botrytis cinerea* TB-31

To confirm that *bcfrp1* is required for the biosynthesis of ABA by *B. cinerea* TB-31, we knocked out the *bcfrp1* gene and replaced the endogenous *bcfrp1* ORF with the *hph* gene. Moreover, we performed qRT-PCR and diagnostic PCR assays to confirm the *bcfrp1* gene was disrupted in the ΔBcfrp1 mutant (Supplementary Figure S2B). The productivity of ΔBcfrp1 for ABA decreased significantly by approximately 97% compared with TB-31 on PDA for 12 days (Figure 1A). To further confirm that the differences in the amount of ABA produced between TB-31 and ΔBcfrp1 was due to the loss of *bcfrp1*, we constructed the complementation vector pCBg1-*bcfrp1* and then transformed it into the mutant ΔBcfrp1 to generate the complementary mutant ΔBcfrp1-C (Supplementary Figure S2C). The amount of ABA produced by ΔBcfrp1-C returned to 85% of that of the control, TB-31, when cultured on a PDA plate for 12 days (Figure 1A).

Furthermore, the qRT-PCR trial verified that *bcfrp1* was disabled by deleting in the mutant ΔBcfrp1. The levels of transcription of *bcfrp1* in ΔBcfrp1-C were restored to approximately 57% of that produced by TB-31 when grown on a PDA plate for 6 days (Figure 1B). To investigate whether *bcfrp1* was involved in the regulation of ABA gene clusters, we conducted qRT-PCR to analyze the levels of transcription of *bcaba1-4* among the *B. cinerea* strains (Figures 1C–F). The levels of transcription of the *bcaba1-4* in ΔBcfrp1 were decreased to 75, 26, 60 and 40% of TB-31, respectively (Figures 1C–F). Each level of gene expression increased when ABA performance was re-established in ΔBcfrp1-C, which suggests that the deletion of *bcfrp1* affects the

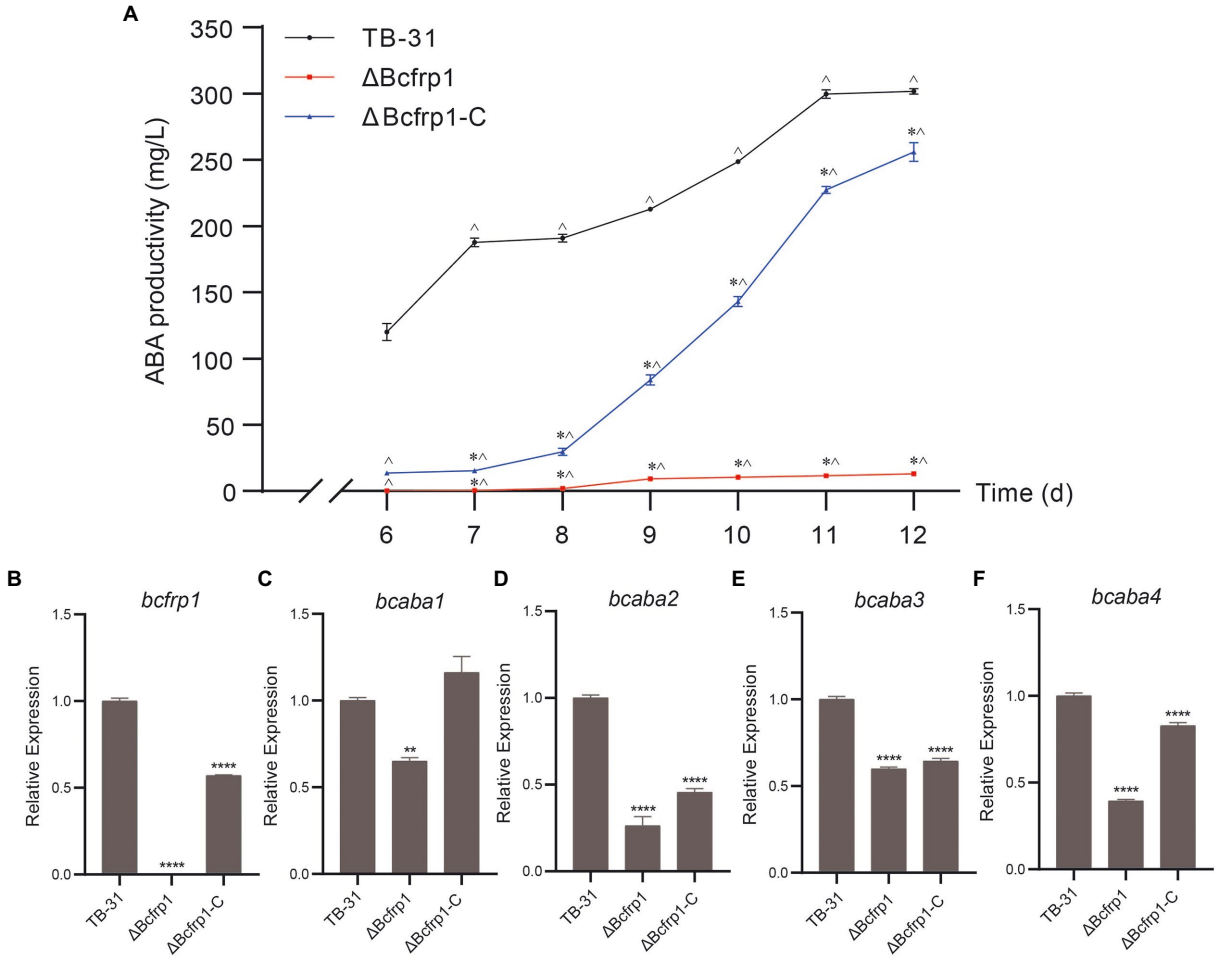

FIGURE 1
Bcfrp1 is required for ABA yield in *Botrytis cinerea* TB-31. **(A)** ABA production of *B. cinerea* TB-31, ΔBcfrp1 and ΔBcfrp1-C mutant strains which were cultured on PDA plates at 26°C. Samples to test for ABA production were collected at seven time points (6, 7, 8, 9, 10, 11 and 12days). The error bars indicate the standard errors of the means ± SEM; n=3 replicate cultures. *, p<0.05 versus the 6-day group; ^, p<0.05 versus the TB-31 groups at the same time. **(B–F)** qRT-PCR examining the transcription levels of *bcfrp1*, *bcaba1-4* in mutant ΔBcfrp1, ΔBcfrp1-C and the parental strain, TB-31. Relative transcription levels of *bcfrp1*, *bcaba1-4* were generated after normalization to the constitutive tubulin reference gene *tubA* for 6days. The relative values for *bcfrp1*, *bcaba1-4* transcription for 6days in TB-31 were arbitrarily assigned a value of 1. Shown are means ± SEM; n=3 replicate cultures. **, p<0.01 versus the transcription level of the TB-31 group; ****, p<0.001 versus the transcription level of the TB-31 group.

transcription of *bcaba1-4*. Combining with the previous data of insertional mutagenesis confirmed that *bcfrp1* is required for the biosynthesis of ABA in TB-31.

3.3. Bcfrp1 disrupts the normal growth of *Botrytis cinerea* TB-31

We compared the morphology and radial growth of *B. cinerea* TB-31, ΔBcfrp1, and ΔBcfrp1-C cultured on PDA. The growth rate of hyphae in ΔBcfrp1 mutant slowed down and no matter how long it takes to cultivate, the hyphae of ΔBcfrp1 could not be extended to the whole plate like TB-31. The hyphae of ΔBcfrp1 also became lighter and had sporadic whiteness. The mycelial layer of ΔBcfrp1 became thinner, with the decrease in the number of conidia compared with those of TB-31. Simultaneously, the introduction of the *bcfrp1* cDNA into ΔBcfrp1 restored the wild-type morphology and growth phenotypes, confirming that this mutant had been complemented (Figures 2A,B). The results showed that *bcfrp1* was positive for the hyphal growth of TB-31. Moreover, we compared the biomass of three strains grown on PDB media. The biomass of ΔBcfrp1 mutant decreased to 56.5% of TB-31 after 120 h of culture on PDB, while the biomass of ΔBcfrp1-C mutant was close to that of the parental strain TB-31 on PDB media (Figure 2C). These results suggested that *bcfrp1* was important for maintaining the normal growth of TB-31.

In addition, we compared the colony diameters of TB-31, ΔBcfrp1, and ΔBcfrp1-C on CDA media for 6 days with several carbon sources (Figure 2D). As shown in Figure 2E, the colony diameter of the ΔBcfrp1 mutant cultured on CDA with 2% D-glucose, 2% maltose, and 2% lactose as carbon sources was 1.5, 1.5 and 3.5 cm, respectively. Moreover, ΔBcfrp1 could not grow on CDA plates that contained sucrose. Moreover, the colony size of ΔBcfrp1 in different carbon sources could be recovered to varying degrees through complementation with *bcfrp1*.

3.4. The transcriptomics and proteomics analysis of *Botrytis cinerea* TB-31 and ΔBcfrp1

To further analyze the dynamic changes in the levels of expression of genes and proteins after the deletion of the *bcfrp1* gene in *B. cinerea* TB-31, mycelial samples of TB-31 and ΔBcfrp1 were collected after cultivation on PDA media for 6 days and subjected to transcriptome and proteome analyses, respectively.

High-throughput RNA sequencing (RNA-seq) generated more than 30 million clean reads for each sample, and three biological replicates were performed for each group. As a result, 12,303 genes were detected in the library, and there are 11,707 genes in the whole genome. The other 596 genes are newly predicted genes. In total, 4,128 (2,661 upregulated and 1,647 downregulated) were identified as DEGs ($\log_2$ratio > 1) in TB-31 (as the control) vs. ΔBcfrp1 (Figure 3A). 15 genes were randomly selected for qRT-PCR analysis to verify RNA-seq data (Figure 3B), and the gene expression levels measured by the two methods were linearly correlated (rpearson = 0.8376).

To examine the proteins altered by *bcfrp1*, proteomic profiles were analyzed between TB-31 and ΔBcfrp1 with three biological replicates. In total, 45,527 peptides and 5,645 proteins were identified in the proteomes of TB-31 and ΔBcfrp1. A Pearson correlation analysis was highly repeatable and reliable (Pearson > 0.97) among the three biological replicates (Figure 3C). A total of 1,073 DEPs ($\log_2$ratio > 0.58) were observed. A total of 446 proteins were downregulated, and 627 proteins were upregulated in the mutant group compared with the TB-31 group ($p < 0.05$; Figure 3A).

3.5. Correlation analysis of transcriptome and proteome

The transcriptome and proteome data were performed with a global correlation analysis. In Figure 4A, a total of 5,615 proteins matched the transcripts, including 1,067 which were DEPs, 2,101 which were DEGs, and 552 were shared as both DEPs and DEGs. In Figure 4B, the nine-quadrant diagram shows that there are 941 NDEGs/NDEPs in quadrant 5. The 268 and 98 candidate proteins were DEGs which differentially transcribed in quadrant 1 and quadrant 9, respectively. The 81 and 86 candidate proteins were DEPs which were not differentially transcribed in quadrant 4 and quadrant 6, respectively. The 12 and 10 candidate proteins had the opposite patterns of expression from their transcripts in quadrant 1 and quadrant 9, respectively. In addition, the 103 and 32 candidate proteins showed the same expression patterns as the transcripts in the quadrants 3 and 7, respectively.

We performed pathway enrichment using the KEGG to explore the possible pathways which may be affected by *bcfrp1*. The results showed that the most DEGs/DEPs were enriched in Metabolic pathways (368 DEGs/ 215 DEPs), and the Biosynthesis of secondary metabolites (153 DEGs/ 97DEPs), and Biosynthesis of amino acids (36 DEGs/ 23 DEPs; Figure 4C). As shown in Figures 4D,E, the DEG/DEP pairs in quadrant 3 and 7 were mainly enriched in the pathways of Metabolic, Secondary metabolites, and Starch and sucrose metabolism.

To screen out the pathways that may play important roles with *bcfrp1*, we performed a pathway enrichment analysis based on the KEGG database. The results showed that the most DEGs/DEPs were involved in metabolic pathways (ko01100, 368 DEGs/ 215 DEPs), followed by the biosynthesis of secondary metabolites (ko01110, 153 DEGs/ 97DEPs), and biosynthesis of amino acids (ko01230, 36 DEGs/ 23 DEPs; Figure 4C). As shown in Figures 4D,E, the DEG/DEP pairs in quadrant 3 and 7 were mainly enriched in the metabolic pathways (ko01100), biosynthesis of secondary metabolites (ko01110), starch and sucrose metabolism (ko00500).

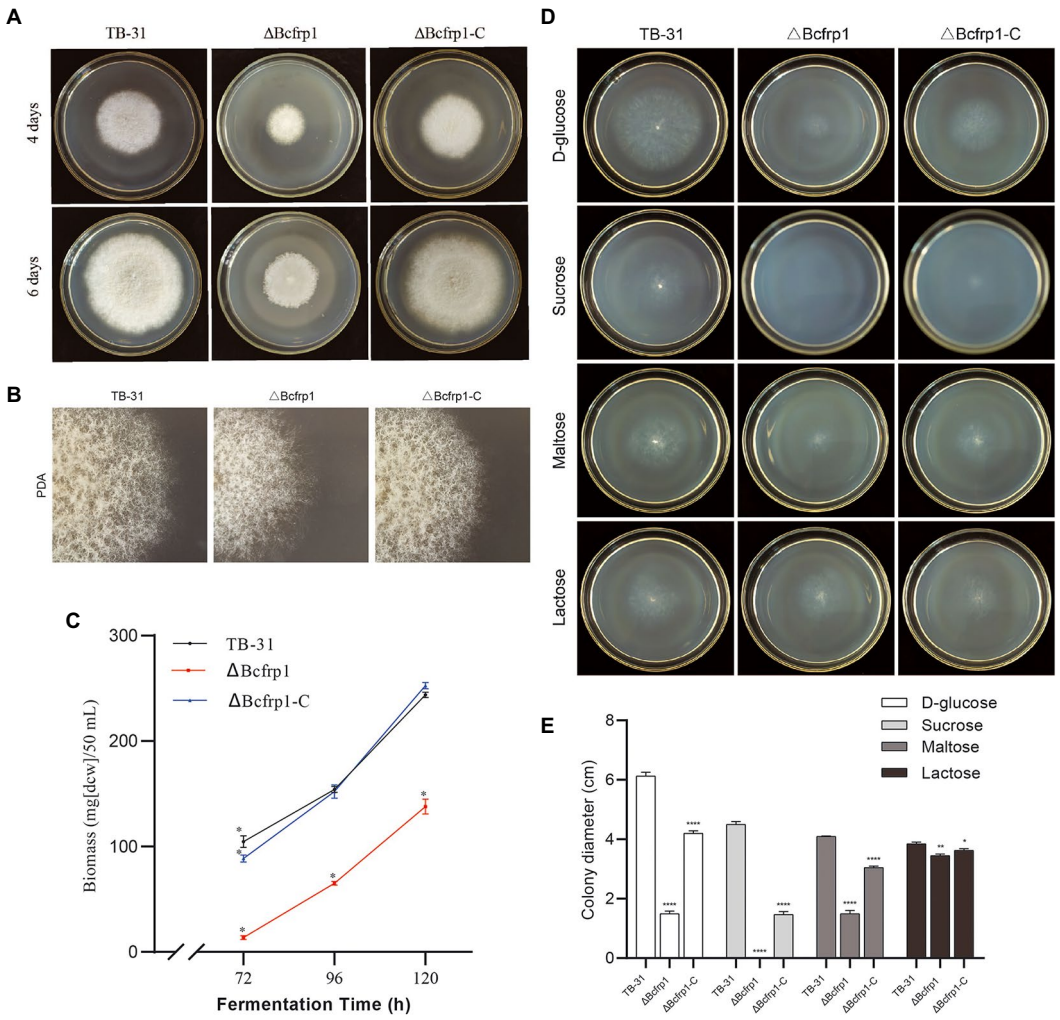

FIGURE 2
The biomass and colony morphology of *B. cinerea* TB-31, ΔBcfrp1 and ΔBcfrp1-C. **(A)** The morphology of TB-31, ΔBcfrp1 and ΔBcfrp1-C on PDA media for 4days and 6days. **(B)** The morphology of TB-31, ΔBcfrp1 and ΔBcfrp1-C on PDA media for 4days and 6days. All images were captured at 3X magnification. **(C)** Biomass of TB-31, ΔBcfrp1 and ΔBcfrp1-C on PDB media at 26°C at 180rpm on an orbital shaker. The mycelia were collected at three time points (72, 96, and 120h). Shown are means ± SEM; n=3 replicate cultures. *, p<0.05 versus the biomass of the TB-31 group. **(D)** The colony morphology of TB-31, ΔBcfrp1 and ΔBcfrp1-C on CDA media with 2% D-glucose, 2% Sucrose, 2% Maltose, and 2% Lactose plates and cultured at 26°C for 6days. **(E)** Colony diameters of the TB-31, ΔBcfrp1 and ΔBcfrp1-C strains on CDA media with 2% D-glucose, 2% Sucrose, 2% Maltose, and 2% Lactose cultured at 26°C for 6days. Shown is means ± SEM; n=3 replicate cultures. *, p<0.05 versus colony sizes of the TB-31 group; **, p<0.01 versus the transcription level of the TB-31 group; ****, p<0.001 versus the transcription level of the TB-31 group.

3.6. DEGs and DEPs involved in putative sugar transport and degradation

We found the DEGs and DEPs involved in putative sugar transport and degradation were significantly changed for expression between *B. cinerea* TB-31 and ΔBcfrp1 (Figure 5; Supplementary Table S3).

Monosaccharide (glucose) and disaccharide (maltose, sucrose and lactose), as nutrients of fungi, can be transported to fungal cells through sugar transporters. Several genes that encode sugar transporters, including three major facilitator superfamily (MFS) sugar transporters (Bchex3, Bchex5, and Bchex6), a glucose transporter rco-3, a glucose/galactose transporter gluP, and a fructose proton symporter (BcFrt1) were upregulated at both the transcription and translation levels in ΔBcfrp1 compared with TB-31 ($p < 0.05$), while a gene that encoded an MFS sugar transporter (Bchex1) was upregulated at the translation level. In addition, a gene that encoded a protein similar to a sucrose transporter Sut1 was downregulated at both the transcription and translation levels, and two genes that encoded the maltose transporters MAL11 and MAL61 were downregulated at the transcription levels.

The transcriptome and proteome analysis also revealed that the genes that encoded two α-amylase enzymes (Bcin02g01420 and Bcin04g06250), two α-glucosidase enzymes (Bcin14g00650 and Bcin12g03390), glycoamylase (Bcgs1), and four glycoside

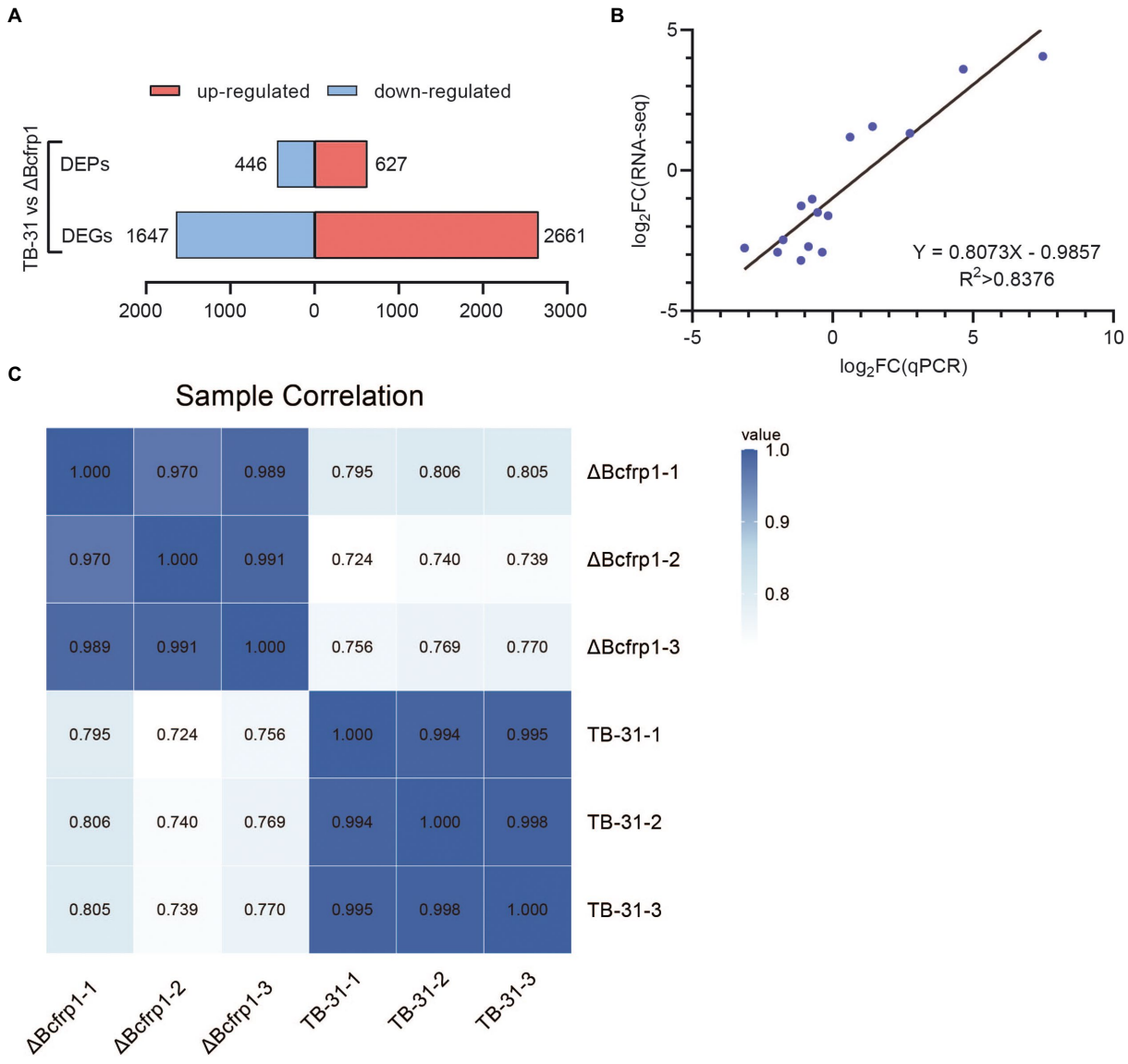

FIGURE 3
The transcriptomics and proteomics analysis of *B. cinerea* TB-31 and ΔBcfrp1. **(A)** Histogram of differential gene and protein expression among different groups. **(B)** Regression analysis of gene expression levels determined by RNA-seq and RT-qPCR ($p<0.05$), rpearson=0.8376. **(C)** The protein sample correlation heat map between the TB-31 and ΔBcfrp1, pearson>0.97.

hydrolases (Bcin08g02110, Bcin16g03950, Bcin03g08710, and Bcin14g00480) were upregulated at both the transcription and translation levels in ΔBcfrp1 compared with those of TB-31 ($p<0.05$). Moreover, the genes that encoded a glycosyl hydrolase (Bcin10g05710), an α-galactosidase (Bcin03g02710) and a β-galactosidase (Bcin06g04500) were upregulated at the translation levels, while a galactose oxidase (Bcin09g04410) was upregulated at both the transcription and translation levels. These enzymes could be involved in the degradation of starch, sucrose, cellulose, and lactose, respectively. However, the level of translation of the genes that encoded the enzymes for glycogen degradation, such as a glycogen debranching enzyme (Bcgdb1), a glycogen phosphorylase (Bcgph1), and an ADP-sugar bisphosphatase (Bcin08g01920) were downregulated in ΔBcfrp1 compared with TB-31 ($p<0.05$).

3.7. DEGs and DEPs involved in ABA biosynthesis-related pathways

We analyzed the DEGs and DEPs involved in ABA biosynthesis-related pathways in *B. cinerea* TB-31 and ΔBcfrp1 (Figure 6; Supplementary Table S4).

The carbon flux from glucose to pyruvate *via* catabolic glycolysis and pentose phosphate pathway (PPP), and the genes that encoded hexokinase (Bcglk), transaldolase (Bcin09g03850)

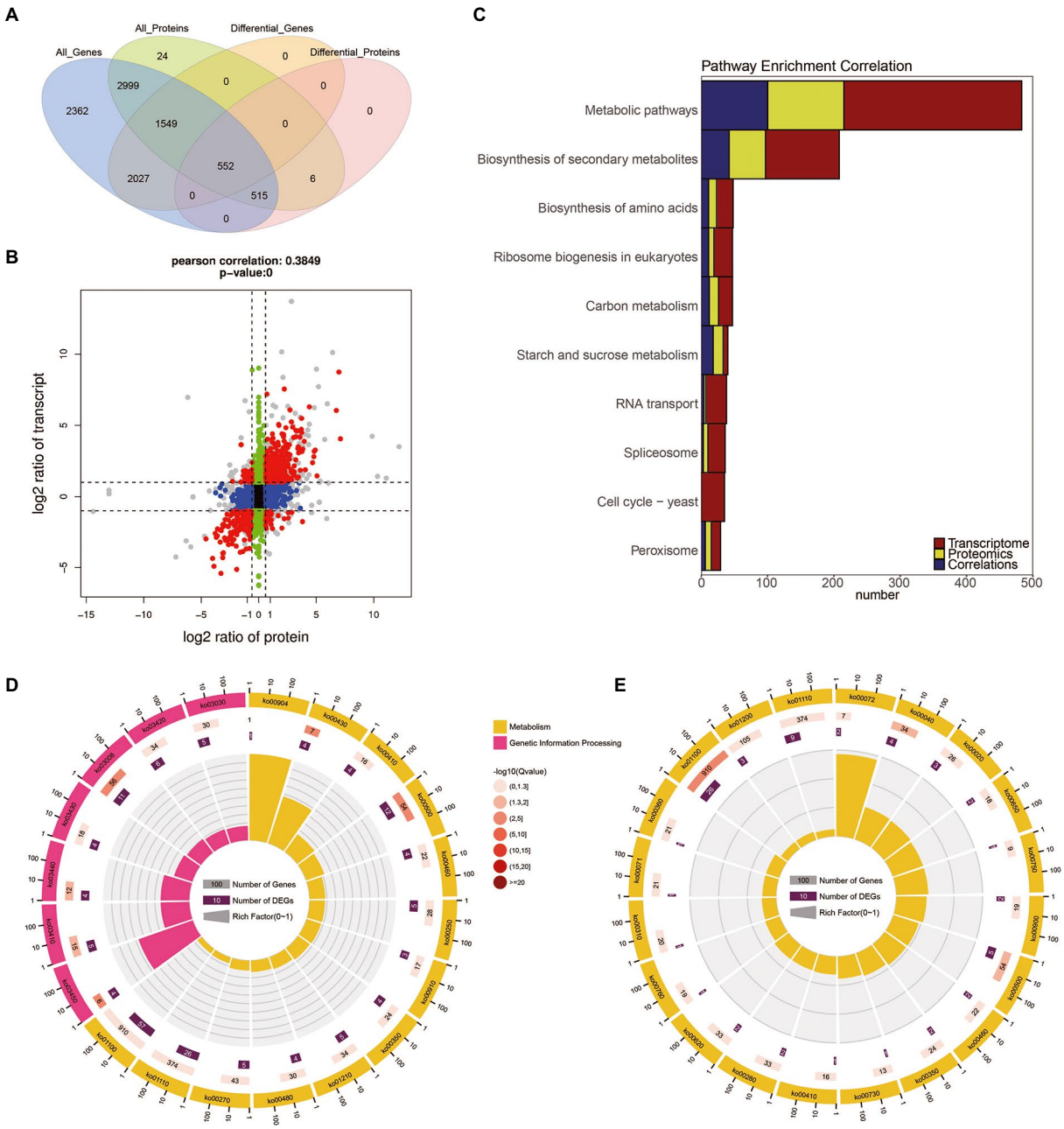

FIGURE 4
The correlation of transcriptome and proteome between the *B. cinerea* TB-31 and ΔBcfrp1. **(A)** Venn diagram of the number of all mRNAs and proteins between TB-31 and ΔBcfrp1. **(B)** The nine-quadrant graph of TB-31 and ΔBcfrp1 (considering the statistical significance, p). [The abscissa is the fold change of the protein (take ratio>1.5), the ordinate is the fold change of the transcription (take ratio>2), and at the top of the figure is the Pearson correlation and statistical significance, p, associated with the transcription and proteomic data. Each dot represents a gene/protein: the black dots represent non-different proteins and genes, and the red dots represent the same or opposite trend of changes in genes and proteins, and the gray dots indicate the differential expression of genes but non-differential expression of proteins]. **(C)** Histogram of the number of genes on the pathway overlapped by TB-31 and ΔBcfrp1 [The number of differentially expressed mRNA (red), protein (yellow), and associated genes (blue) is annotated on the pathway, respectively]. **(D)** The circular plot of the pathway overlapped in the quadrant 3 of the nine-quadrant map between TB-31 and ΔBcfrp1. **(E)** The circular plot of the pathway overlapped in the quadrant 7 of the nine-quadrant map between TB-31 and ΔBcfrp1.

and DAHP synthetase I (Bcin01g10330) were upregulated at both the transcription and translation levels in ΔBcfrp1 compared with TB-31 ($p < 0.05$). However, the levels of translation of two genes that encoded triosephosphate isomerase (Bcin08g05220) and glyceraldehyde-3-phosphate dehydrogenase (Bcin15g02120) were downregulated, respectively. Moreover, one gene that encoded fructose-bisphosphate aldolase (Bcin07g03760); was downregulated at the transcription level in ΔBcfrp1 compared

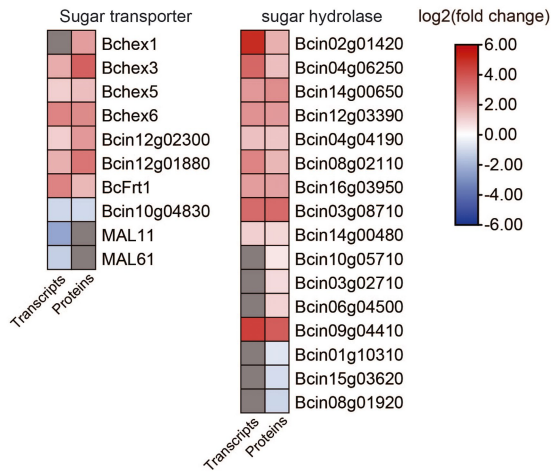

FIGURE 5
Heat map of DEGs and DEPs in sugar transport and degradation between the *B. cinerea* TB-31 and ΔBcfrp1. The heat map was generated with the software TBtools (Toolbox for Biologists) V1.0971. The gray color means no significant difference at the transcription or translation level.

with TB-31 ($p < 0.05$). The levels of transcription of genes that encoded pyruvate decarboxylase (Bcin02g06580) and aldehyde dehydrogenase (Bcin13g05810) were upregulated in ΔBcfrp1 compared with that of TB-31 ($p < 0.05$). The results may lead to increase the production of cytosolic acetyl-CoA by the pyruvate dehydrogenase bypass. On the other hand, the genes of pyruvate dehydrogenase complex (PDH) were not significantly changed between ΔBcfrp1 and TB-31, and only one gene that encoded dihydrolipoamide dehydrogenase (Bcin02g06400) was downregulated at the translation level. Moreover, as shown in Figure 6, three genes were downregulated at the transcription and translation levels in the tricarboxylic acid (TCA) cycle. The gene that encoded ATP citrate lyase, succinate dehydrogenase, and phosphoenolpyruvate carboxykinase Bcpck1 were downregulated in ΔBcfrp1 compared with TB-31 ($p < 0.05$). In addition, a gene that encoded isocitrate lyase1 (Bcicl1) in the glyoxylate cycle (GYC) was upregulated at the translation level ($p < 0.05$).

In *B. cinerea*, acetyl-CoA can be converted to isopentenyl pyrophosphate (IPP) *via* the mevalonate (MVA) pathway, which includes seven enzymatic steps. As shown in Figure 6, three genes that encoded the acetyl-CoA synthase (Bcerg10) and 3-hydroxy-3-methylglutaryl coenzyme A synthase (Bcerg13) were downregulated at both the transcription and translation levels and mevalonate kinase (Bcerg12) was downregulated at the translation level in ΔBcfrp1 compared with TB-31 ($p < 0.05$). In addition, the level of transcription of the gene encoding MVA kinase (Bcmvd1) was also downregulated. What's more, the expression of the ABA biosynthetic gene cluster *bcaba1-4* was also identified in the transcriptome and proteome of TB-31 and ΔBcfrp1. As shown in Figure 6, *bcaba1-3* was downregulated at the levels of translation in ΔBcfrp1 compared with TB-31 ($p < 0.05$). This suggests different levels of expression of genes involved in the MVA pathway and the ABA biosynthetic gene cluster, which may lead to ABA deficiency in ΔBcfrp1 strain.

3.8. DEGs and DEPs involved in secondary metabolism

We analyzed the DEGs and DEPs involved in secondary metabolism in *B. cinerea* TB-31 and ΔBcfrp1 (Figure 7; Supplementary Table S5).

In addition to the genes related to ABA synthesis, we also analyzed genes involved in secondary metabolism. As shown in Figure 7, five polyketide synthase (PKS) genes and one gene for a non-ribosomal peptide synthase (NRPS) were differentially expressed in ΔBcfrp1 compared with TB-31 ($p < 0.05$). Two genes that encoded Bcpks8 and Bcpks13 were downregulated at both the transcription and translation levels, and Bcpks13 was involved in the synthesis of dihydroxynaphthalene (DHN)-type melanin (Zhang et al., 2015). However, the Bcpks21 gene was upregulated at the translation level. The other two genes that encoded Bcpks11 and Bcpks20 were also upregulated at both the transcription and translation levels. However, their corresponding compounds are unknown. In addition, the gene for the non-ribosomal peptide synthase Bcnrps6 was upregulated at the transcription and translation levels.

The gene for sesquiterpene cyclase (Bcstc1, also designated Bcbot2) was decreased significantly at the transcription level in ΔBcfrp1 compared with that in TB-31 ($p < 0.05$). In addition, the other four genes (*bcbot1* and *bcbot3-5*) were significantly downregulated at both the transcription and translation levels in the botrydial (BOT) synthetic gene cluster. The results showed that the bocinic acid (BOA) synthetic genes of *bcboa3-5*, *bcboa10-12* and *bcboa15-17* were significantly downregulated at the transcription level. Moreover, the translation level of *bcboa2* also decreased, suggesting that *bcfrp1* could regulate the level of expression of the entire cluster.

3.9. DEGs and DEPs involved in development

We also analyzed the DEGs and DEPs involved in development based on the transcriptome and proteome data (Figure 7; Supplementary Table S6).

Leyronas et al. (2015) reported that *B.cinerea* is a heterothallic species, so there are two mating types (MAT1-1 and MAT1-2; Leyronas et al., 2015). In this study, we found that the transcription level of a characteristic MAT1-1 α-domain gene (Bcin01g02150), which also existed in the B05.10 (mating type MAT1-1), was downregulated in ΔBcfrp1 compared with that in TB-31 ($p < 0.05$). In addition, the translation levels of the probable gene for dipeptidyl-aminopeptidase B (Bcin15g01570) and G protein α-subunit Bcg1, which could be involved in the mating process and signaling, were downregulated in ΔBcfrp1. It was reported

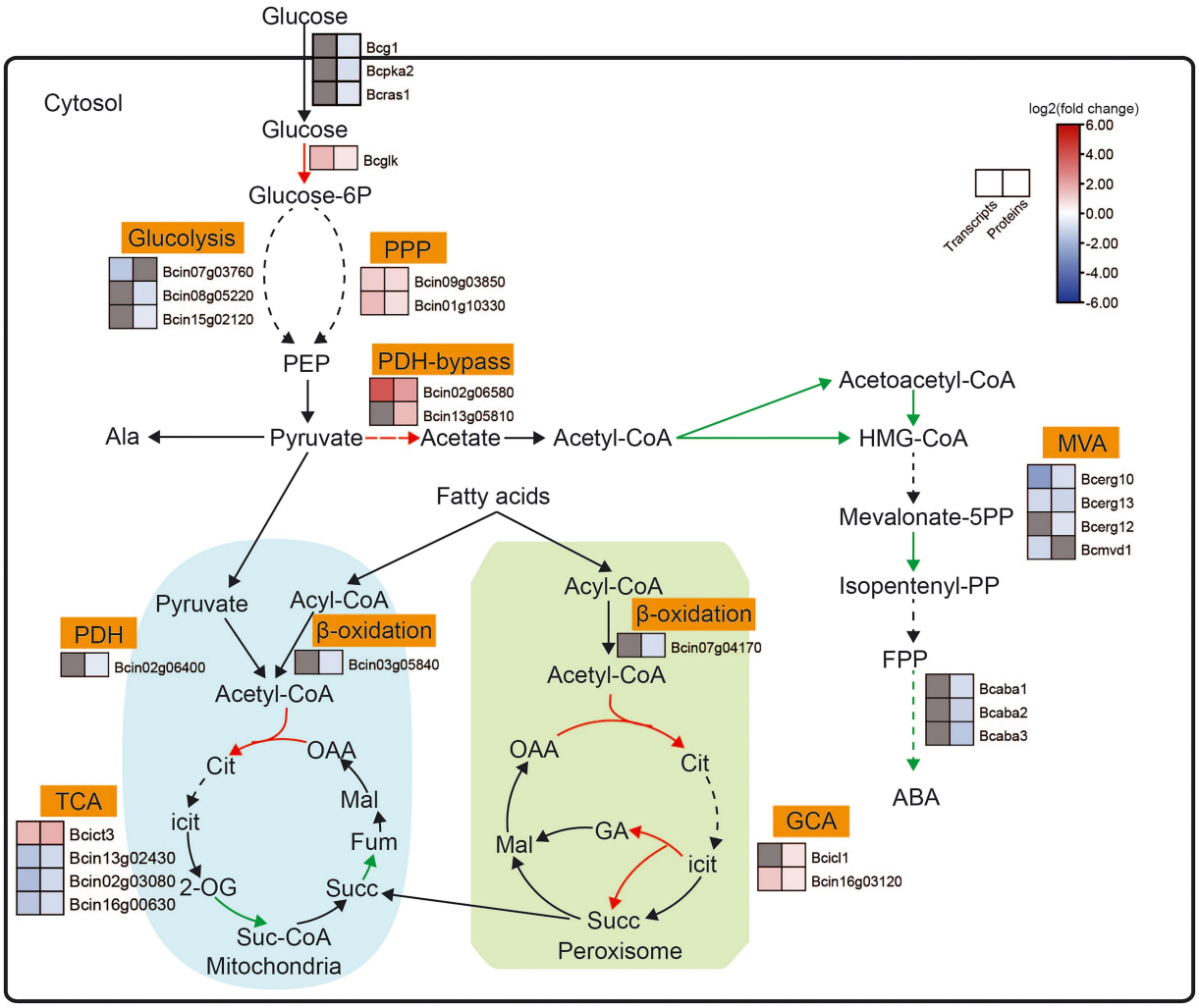

FIGURE 6
Expression pattern of key genes involved in ABA biosynthesis-related pathways between the *B. cinerea* TB-31 and ΔBcfrp1. The heat map was generated with the software TBtools (Toolbox for Biologists) V1.0971. The gray color means no significant difference at the transcription or translation level.

that three polyketide synthase genes including Bcpks13, hydroxynaphthalene reductase dehydrates (Bcbrn1) and scytalone dehydratase (Bcscd1) were involved in the synthesis of DHN melanin (Zhang et al., 2015). In this study, the *bcpks13* and *bcbrn1* genes were downregulated at both the transcription and translation levels in ΔBcfrp1 compared with those in TB-31 ($p < 0.05$), while the *bcscd1* gene was upregulated at both the transcription and translation levels.

3.10. DEGs and DEPs involved in plant cell wall degradation and the generation of reactive oxygen species

It was reported that the gene *fofrp1* is required for pathogenicity in *Fusarium oxysporum* (Jonkers et al., 2011). We analyzed the transcriptome and proteome data between *B. cinerea* TB-31 and ΔBcfrp1, and the results showed that; except for the genes involved in the synthesis of BOA and BOT toxins, there were also a considerable number of genes involved in pathogenicity that were differentially expressed (Figure 8; Supplementary Table S7).

While invading their hosts, many phytopathogenic fungi synthesize plant cell wall degrading enzymes (CWDE), for example xylanases, pectinases, and arabinanase (Amselem et al., 2011). Extracellular enzymes have been selected as potential virulence factors due to promoting the growth of hyphae. Three genes that encoded an endopolygalacturonase (Bcpg4), a galacturonate reductase (Bcgar1), and a glyoxal oxidase (Bcgo1) were downregulated at both the transcription and translation levels in ΔBcfrp1 compared with those in TB-31 ($p < 0.05$). Moreover, the two genes that encoded α-1,5-L-endo-arabinanase (Bcara1) and pectin methylesterase (Bcpme1), were downregulated at the translation level.

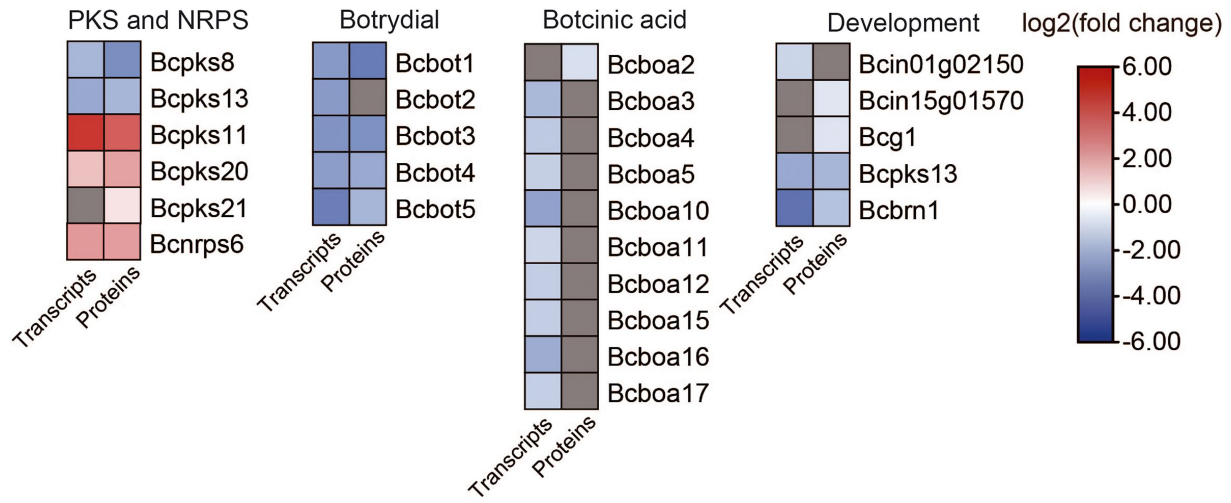

FIGURE 7
Heat map of DEGs and DEPs in secondary metabolism key enzymes encoding genes and development between the *B. cinerea* TB-31 and ΔBcfrp1. The heat map was generated with the software TBtools (Toolbox for Biologists) V1.0971. The gray color means no significant difference at the transcription or translation level.

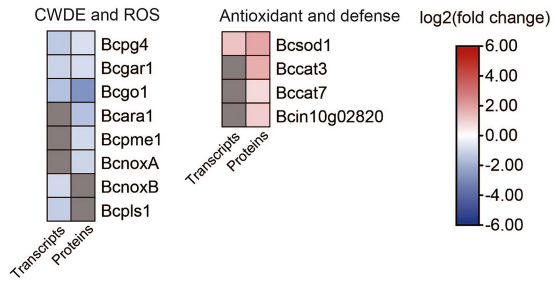

FIGURE 8
Heat map of DEGs and DEPs in plant cell wall degradation and reactive oxygen species generation between the *B. cinerea* TB-31 and ΔBcfrp1. The heat map was generated with the software TBtools (Toolbox for Biologists) V1.0971. The gray color means no significant difference at the transcription or translation level.

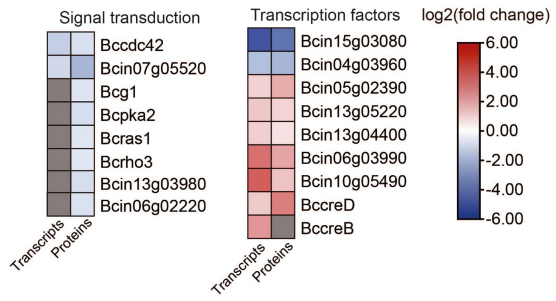

FIGURE 9
Heat map of DEGs and DEPs in transcription factors and signal transduction between the *B. cinerea* TB-31 and ΔBcfrp1. The heat map was generated with the software TBtools (Toolbox for Biologists) V1.0971. The gray color means no significant difference at the transcription or translation level.

Botrytis cinerea is a necrotrophic pathogen that can generate reactive oxygen species (ROS) by enzymes. NADPH oxidases (Nox) are major enzyme systems that produce ROS, which can contribute to the virulence of the fungus. Siegmund et al. (2013) reported that the Nox including a tetraspanin (BcPls1) and two catalytic transmembrane subunits (BcNoxA, BcNoxB) were required for the virulence involved in the process of penetration in *B.cinerea* (Siegmund et al., 2013). In this study, the translation levels of *bcnoxA* were downregulated, while transcription levels of *bcnoxB* and *bcpls1* were downregulated in ΔBcfrp1 compared with TB-31 ($p < 0.05$), which could affect the penetration of ΔBcfrp1. In addition, the antioxidant enzymes can protect fungi by degrading the ROS produced by plants. In this study, the superoxide dismutase gene (Bcsod1) was upregulated at both the transcription and translation levels, and the catalase (Bccat3 and Bccat7) and glutathione S-transferase kappa 1 (Bcin10g02820) genes were upregulated at the translation level in ΔBcfrp1 compared with that of TB-31 ($p < 0.05$). Thus, we speculated that the upregulation of antioxidant enzymes could protect the fungal cell from the ROS.

3.11. Analysis of transcription factors and other genes associated with signal transduction

Eight genes that are involved in signal transduction were differentially expressed in ΔBcfrp1 compared with TB-31 ($p < 0.05$; Figure 9; Supplementary Table S8). Two genes that encode the cell division control protein 42 (Bccdc42) and calmodulin (Bc4) were downregulated at both the transcriptional and translational levels. In addition, six genes were downregulated at the translational level, including the genes that encode

heterotrimeric G α-subunit (Bcg1), PKA catalytic subunit (Bcpka2), medium Ras-like GTPase (Bcras1), small GTPase (Bcrho3), MAPK p21-activated kinase (Bcste20), and serine/threonine protein phosphatase pzh1.

In addition, nine genes that encode transcription factors (TFs) were differentially expressed in ΔBcfrp1 compared with TB-31 ($p < 0.05$; Figure 9; Supplementary Table S8). Of them, two genes that encode cutinase A (BccutA) and the regulatory subunit of protein phosphatase 1 Bcglc8, respectively, were downregulated at both the transcriptional and translational levels. Six genes that encoded TFs (Bcsfp1, Bctma46, Bcin13g04400, Bcku70, Bcku80, and BccreD) were upregulated at both the transcriptional and translational levels. In addition, a gene that encoded BccreB, a TF that is involved in the process of deubiquitinating CreA, was upregulated at the transcriptional level.

4. Discussion

The ubiquitin-proteasome system (UPS) is the main pathway for the degradation of intracellular protein in eukaryotes, which is composed of ubiquitin, ubiquitin-activating enzyme E1, ubiquitin-conjugating enzyme E2s, ubiquitin ligase E3s, 26S proteasome, and deubiquitinates (DUBs; Willems et al., 2004; Wu et al., 2022). SCFs complexes constitute a new class of E3 ligases, in which F-box protein is responsible for regulating its downstream target proteins by specific recognition and ubiquitination of protein substrates (Cardozo and Pagano, 2004; Johnk et al., 2016). The fungal F-box protein was initially found in *Saccharomyces cerevisiae*, and has been shown to play an important role in regulating a variety of cellular functions, including cell cycle regulation, nutritional sensing and fungal morphogenesis in fungi (Jonkers and Rep, 2009a; Sharma et al., 2021; Wu et al., 2022). For example, MUS-10 of *Neurospora crassa* is involved in cell senescence (Kato et al., 2010), Fbx23 and Fbx47 of *Aspergillus nidulans* participate in carbon catabolite repression (CCR), and Fbx50 (GrrA) is required for production of mature ascospores (De Assis et al., 2018). The F-box proteins are also required for virulence, like Fbx15 of *Aspergillus fumiga* and Fbp1 of *Cryptococcus neoformans* (Liu et al., 2011; Johnk et al., 2016). Frp1 is an F-box protein, which was initially found in *Fusarium oxysporum,* and its homologous proteins seem to show different functions in different fungi. Jonkers et al. (2011) reported that the F-box protein that encoded the gene *fofrp1* is necessary for virulence and carbon catabolism in *Fusarium oxysporum*, and the *B. cinerea* Bcfrp1 complemented into the ΔFofrp1 mutant restored pathogenicity (Jonkers et al., 2011). However, there is no effect on pathogenicity and sexual reproduction was impaired in the ΔBcfrp1 mutant produced by *B. cinerea* B05.10 (Jonkers et al., 2011). In our study, we found that a novel function of *bcfrp1* is required for the biosynthesis of ABA in *B. cinerea* TB-31. In this research, the mutant E154 that produced lower amounts of ABA revealed that the T-DNA insertion site was 1806 bp upstream of the predicted start codon of Bcfrp1. In addition, the deletion of Bcfrp1 had a significant effect on the biosynthesis of ABA in *B. cinerea* TB-31, and its yield decreased by 97% compared with TB-31 at 12 days. ABA yield of both E154-C and ΔBcfrp1-C restored to more than 80% by the complementation of *bcfrp1* gene. Although it did not reach the level of the control strain TB-31, which may be owing to the promoter sequence of *bcfrp1*, it was obvious that BcLAE1 was essential for ABA synthesis. To date, no reports have been published on the impact of F-box proteins on secondary metabolic regulation in *B. cinerea*.

To understand the evolution of Bcfrp1, we analyzed the conserved domain of F-box. The exact location of the F-box is 169–209 aa, defined as a receptor for ubiquitination targets (Supplementary Figure S3). A phylogenetic tree was constructed using the amino acids of the full length (Supplementary Figure S4), and resulted in the conclusion that orthologs of Bcfrp1 are present in fungi from six classes (Leotiomycetes, Sordariomycetes, Dothideomycetes, Eurotiomycetes, Pezizomycetes, and Xylonomycetes) belonging to the Pezizomycotina, and what's interesting is that these fungi are pathogenic fungi, such as *Sclerotinia sclerotiorum*, *Hyaloscypha bicolor*, *Venustampulla echinocandica*, *Neurospora crassa*, *Trichoderma reesei*, *Fusarium graminearum*, *Fusarium oxysporum f.* sp. *lycopersici*, *Trematosphaeria pertusa*, *Xylona heveae*, *Tuber melanosporum*. Bcfrp1 orthologs were relatively close to *Botrytis porri*, *Botrytis byssoidea*, *Botrytis sinoallii*, *Botrytis fragariae* and *Sclerotinia sclerotiorum*, which might share an ancestor. It is not clear whether these strains have the capability to produce ABA. These homologous proteins were not characterized in the present study but may be involved in functional gene regulation related to pathogenicity in these pathogenic fungi. The mechanism underlying the functions of Bcfrp1 and its homologues are still to be elucidated.

It is apparent that different *frp1* mutant have phenotypic variations which indicate that Frp1 targets different proteins in different fungi. However, Jonkers and Rep (2009a,b) speculated that the main function of Frp1 does not depend on ubiquitination of targets (Jonkers and Rep, 2009a). They found Frp1 of *F. oxysporum* can bind to Skp1 in yeast two-hybrid and pull-down assays, but mutations in the F-box domain of Frp1 that impair binding to Skp1 do not affect the phenotype. Therefore, in order to better understand the downstream genes affected by Frp1, a stringent comparative transcriptome and proteome analysis was performed to identify differentially expressed genes between TB-31 and ΔBcfrp1, which would be very useful for novel target genes discovery. We found about 627 upregulated DEPs and 446 downregulated DEPs between TB-31 and ΔBcfrp1, and 552 proteins were shared between both DEPs and DEGs, suggesting the changes in the transcriptomic and proteomic level is very notable. This study will help us find targets that may be regulated by *bcfrp1* and expand our knowledge of the molecular basis by which *bcfrp1* regulates ABA biosynthesis in *B. cinerea*.

We first compared data from the transcriptome and proteome to analyze the DEGs related to the ABA biosynthetic pathway. In ΔBcfrp1 mutant, several genes involved in the biosynthesis of

pyruvate and acetyl-CoA were upregulated at the transcription and/or translation level, which definitely favor the synthesis of acetyl-CoA. However, the levels of transcription and/or translation of the genes involved in IPP synthesis (MVA pathway), and the *bcaba1-4* genes involved in ABA synthesis from FPP were severely downregulated. As a result, we hypothesized that this is an important reason for the decrease of ABA biosynthesis in ΔBcfrp1 mutant. As Wang et al. (2018) reported the TF BcabaR1 directly regulate the promoter of ABA gene cluster (Wang et al., 2018). In this study, we found that the levels of transcription and translation of *bcabaR1* in ΔBcfrp1 did not change significantly when compared with TB-31. However, the levels of transcription of the entire ABA gene cluster were downregulated, so we speculated that there are other undiscovered regulatory mechanisms participating in the biosynthesis of ABA.

In addition to ABA, we also closely examined the other enzymes in secondary metabolism. The levels of transcription and translation of five key genes for enzymes were altered, including Bcpks8, Bcpks11, Bcpks13, Bcpks20, and Bcnrps6. The corresponding compounds of Bcpks8, Bcpks11 and Bcpks20 have not been identified. The level of translation of the sesquiterpene cyclase Bcbot2 gene was also downregulated, which is required for the virulence factor botrydial (BOT) biosynthesis. The biosynthetic gene cluster of BOT was similar to ABA, the remaining four genes in the BOT synthesis gene cluster (*bcbot1–5*) were downregulated at the levels of transcription and translation, while had no effect on TF Bcbot6. However, the deletion of Bcfrp1 resulted in the downregulation of Bcbot1-5 genes but not BcBot6, implying that Bcfrp1-induced clustering regulation could have another mechanism to bypass the TF. In addition, the level of transcription of nine genes in the bocinic acid (BOA) gene cluster decreased. In a previous study, we found that the regulator BclaeA is essential for the biosynthesis of ABA, which could affect the levels of transcription of the ABA, BOT, and BOA clusters (Wei et al., 2022). In this study, the levels of transcription and translation of *bclaeA* in ΔBcfrp1 did not change noticeably compared with TB-31, indicating that there are different regulatory mechanisms for BclaeA to synthesize ABA.

The downregulation of the BOA and BOT gene clusters may affect the virulence of *B. cinerea*. Dalmais et al. (2011) knocked out two genes, Bcbot1 and Bcbot2, involved in BOT production in the wild-type strain T4, which resulted in reduced virulence. In addition, they simultaneously knocked out the key genes that encode the enzymes Bcboa6 or Bcboa9 of BOA in the strain B05.10 led to the reduction of virulence (Dalmais et al., 2011). In this study, the level of expression for Bcboa6 or Bcboa9 did not change in ΔBcfrp1 compared with TB-31. However, several genes that encoded plant CWDE and NADPH oxidase enzymes, were downregulated at the transcription and/or translation levels in ΔBcfrp1, suggesting that Bcfrp1 plays key roles in regulating the level of expression of these genes.

Simultaneously, we found that the radial growth was decreased in the Bcfrp1 mutants. The mycelia of the ΔBcfrp1 transformants appeared white when compared with that of TB-31 owing to decreased expression of the key synthetic genes of melanin. The dihydroxynaphthalene (DHN) melanin biosynthetic pathway in *B. cinerea* comprises of the polyketide synthase PKS12 and PKS13, the hydrolase YGH1, tetrahydroxynaphthalene (TNH) reductase BRN1 and BRN2, and the scytalone dehydratase SCD1(Cheung et al., 2020). In our study, the *bcpks13* and *bcbrn1* genes are downregulated while the *bcscd1* is up-regulated in ΔBcfrp1. It was reported that deletion of the *bcpks13* gene resulted in albino conidia in *B. cinerea* (Zhang et al., 2015), and the *bcbrn1* deletion mutants was deficient in melanin biosynthesis, indicating the disruption of melanogenesis. Meantime, deletion of the *bcscd1* gene mutant also exhibited strong reduction in melanogenesis with no effects on other cellular processes. It was reported that the ΔBcscd1 mutant accumulated scytalone in the culture filtrate rather than the mycelium, and excessive scytalone appears to be self-inhibitory to the fungus (Chen et al., 2021). Therefore, the biological significance of up-regulation of *bcscd1* in ΔBcfrp1 is worth discussing, which may cause the decrease of scytalone accumulation. Some scientists believe that fungal melanin could also be perceived as a molecular pattern of pathogens by their hosts. In ascomycete rice blast fungus *Magnaporthe grisea*, DHN-melanin is a necessary component of the functioning appressorium (Jacobson, 2000). In human-pathogenic fungi *Aspergillus fumigatus*, DHN melanin specifically interferes with functions of host phagocytes, thus ensuring the virulence of the pathogen. Heinekamp et al. (2013) reported that DHN melanin and its precursors, like T4HN, and 1,8-DHN are also able to scavenge host-derived ROS in *A. fumigatus* (Leavitt et al., 2013). In TB-31, the effects of Bcfrp1, Bcpks13, Bcbrn1 and Bcscd1 on pathogenicity remains unclear. Jonkers et al. (2011) observed no effect on pathogenicity when Bcfrp1 in *B. cinerea* B05.10 was targeted for disruption (Jonkers et al., 2011). The *pks13* mutants also did not exhibit any changes in development or pathogenicity, and the effects of BRN1 deletion would be similar to other melanin biosynthesis genes and is nonessential for fungal development and pathogenicity. Therefore, the effect of Bcfrp1 and the functional genes regulated by Bcfrp1 on pathogenicity of *B. cinerea* TB-31 merits further study. In fact, *B. cinerea* TB-31 with substantially increased ABA yields have undergone many rounds of mutagenesis from a wild-type strain TBC-6, which was originally isolated from wheat stem, and leaf (Gong et al., 2014; Ding et al., 2016). Through observation, the mycelial growth of TB-31 is obviously weaker than that of TBC-6, B05.10 and T4, which may affect its colonization on the plant surface (data not shown). Thus, how to design experiments to evaluate the toxicity of TB-31 and ΔBcfrp1 mutant is the next challenge to consider.

Jonkers et al. (2011) compared the growth phenotypes of the ΔFrp1 mutants of *F. graminearum*, *F. oxysporum*, and *B. cinerea* on different carbon sources using a Biolog FF assay (Jonkers et al., 2011). The *F. oxysporum* ΔFofrp1 mutant grew significantly less on non-sugar carbon sources, which was very close to the previous growth phenotype on solid plates (Jonkers et al., 2009). In addition, the cell wall degradative genes and isocitrate lyase1 *icl1* were downregulated in the ΔFofrp1 mutant (Jonkers and

Rep, 2009b). On the other hand, the ΔFgfrp1 mutant could normally grow on agar plates that contained various non-sugar carbon sources and polysaccharides. The *B. cinerea* B05.10 ΔBcfrp1 mutants grew well on any carbon source. The 'cross-species' complementation experiment with the Bcfrp1 of *B. cinerea* to replace the Fofrp1 of *F. oxysporum*, which led to the growth damage on non-sugar carbon source in ΔFofrp1 changed to the growth damage of sugar carbon source in the complementary mutant ΔFofrp1+ Bcfrp1. Jonkers et al. (2011) postulate that this difference is owing to the promoter sequence of *frp1* (Jonkers et al., 2011). In this study, we compared the colony diameters of TB-31, ΔBcfrp1, and ΔBcfrp1-C on CDA media for 6 days with several carbon sources (Figure 2D). As is shown in Figures 2D,E, after cultivation on CDA medium containing D-glucose and maltose for 6 days, the colony diameter of ΔBcfrp1 was significantly reduced to 25, and 37% of that of TB-31, respectively. Moreover, ΔBcfrp1 could not grow on CDA plates that contained sucrose. It is obvious that different *frp1* mutants have different phenotypes upon utilising different carbon sources, which is worthy of further study. We have also considered whether there is such a possibility that *bcfrp1* knockout affected the basic metabolism including carbon metabolism, and then indirectly affected the biosynthesis of ABA in TB-31. According to our observation, the different levels of expression of genes involved in the MVA pathway and the ABA biosynthetic gene cluster may lead to ABA deficiency in the ΔBcfrp1 strain. But we also found some genes involved in putative sugar transport and degradation, and the gene encoded hexokinase (Bcglk), were upregulated. Thus we do not know whether some products of sugar metabolism inhibit the pathway of ABA synthesis. Therefore, it is necessary to expand the screening range of carbon sources, detect ABA yields and the expression patterns of related genes under different carbon sources, and jointly analyses to gain insights into the carbon metabolism and the regulation of ABA synthesis in TB-31 and ΔBcfrp1.

In this research, we found that eight genes were downregulated in the signal transduction pathways, including *bcg1*, *bcras1*, *bcrho3*, *bccdc42*, *bcpka2*, *pzh1*, *bcste20*, and *bc4*. The function of the two genes that encoded serine/threonine-protein kinase Bcste20 and Calmodulin Bc4 remains unknown. As reported, the inactivation of *bcg1* (heterotrimeric Gpa2 homolog) caused a decrease in colonies on poor medium with sucrose as carbon source (Gronover et al., 2001), and inactivation by *bcras1* resulted in stunted hyphal growth (Minz Dub et al., 2013). Furthermore, when the *bcras1* gene from another small GTPase family was inactivated, the fungus grew less effectively (An et al., 2015), and the inactivation of *bccdc42* also caused a decrease in hyphal growth (Kokkelink et al., 2011; An et al., 2015). In this study, the *bcg1*, *bcras1*, *bcrho3*, and *bccdc42* genes were downregulated in ΔBcfrp1, which suggests that the decrease in hyphal growth could be related to the decrease in level of expression of these four genes. Fekete et al. (2004) reported that the metabolism of D-galactose except for *via* the Leloir pathway exists as an alternative pathway for hydrolytic D-galactose metabolism with L-sorbose as an intermediate in *A. nidulans* (Fekete et al., 2004). In this study, the glucose/galactose transporter gluP resulted in the downregulation of β-galactosidase, which catalyzes the conversion of lactose to galactose, and α-galactosidase, which catalyzes the conversion of D-galactose to sorbose, suggesting that the colony diameter of ΔBcfrp1 grown on lactose was similar to that of TB-31 and could be related to the alternative pathway of D-galactose metabolism. Ariño et al. (2019) reported that glycogen metabolism and cell cycle control in eukaryotes was regulated by the protein phosphatase PP1 (Ariño et al., 2019). In this study, the genes that encoded protein phosphatase pzh1 (glc7 homolog) and the regulatory subunit Bcglc8 were downregulated, suggesting that downregulation of the genes of glycogen metabolism could be related to the decreased expression of *pzh1* and *bcglc8*. In addition, carbon catabolite repression (CCR) is a global regulatory mechanism that is ubiquitous in microorganisms. In filamentous fungi, CCR is involved in catabolite responsive elements (*CreA*, *CreB*, *CreC*, and *CreD*) as well as the genes of cAMP and Protein Kinase (PKA) signal pathway (Adnan et al., 2017). The mutation of *cre1* in the *fofrp1* deletion mutant restored the impairments in the ΔFofrp1 mutant (Jonkers and Rep, 2009b), which indicates that the Fofrp1 and Cre1 proteins are both involved in the regulation of the CCR gene in *F. oxysporum*. In this study, we discovered that the regulation of *bccreA* and *bcsnf1* did not change significantly, whereas the expression of *bccreB and bccreD* increased in the ΔBcfrp1 generated from *B. cinerea* TB-31. Adnan et al. (2017) hypothesised that CreD was involved in the ubiquitination of CreA and CreB was involved in the deubiquitination of CreA, respectively (Adnan et al., 2017). The effect of *bccreB and bccreD* on the interaction of *bccreA* in *B. cinerea* requires further investigation.

In this study, 30 DEPs with unknown functions were revealed in the signal transduction pathways. We found about 2,661 upregulated DEGs and 1,647 downregulated DEGs, we also found about 627 upregulated DEPs and 446 downregulated DEPs between TB-31 and ΔBcfrp1, suggesting that the changes in the transcription and translation level is very notable. We hypothesise that the effect of Bcfrp1 on the change of expression level of a large number of genes may be amplified by regulating some signal transduction pathway.

In conclusion, we found that a novel function of *bcfrp1* is required for the biosynthesis of ABA in *Botrytis cinerea* TB-31. The deletion of *bcfrp1* resulted in the downregulation of the level of expression of the ABA biosynthetic gene cluster and the genes that participate in the mevalonic acid pathway. This study discovered the same regulatory pattern of Bcfrp1 targeting botrydial (BOT) and bocinic acid (BOA) gene clusters. In addition, DEGs and DEPs participating in the growth and carbon catabolite repression (CCR), and signal transduction in *B. cinerea* were identified based on the transcriptome and proteome data. Our future research will study the DEPs that are regulated by Bcfrp1 in more detail and search for potential targets in *B. cinerea*.

Data availability statement

The data presented in the study are deposited in the ScienceDB (https://www.scidb.cn/detail?dataSetId=bf230977945c4b4785ec355293b23d79) and accession number (doi: 10.57760/sciencedb.06985).

Author contributions

DC contributed to designing and performing the experiments, data analysis, and writing the manuscript. ZW helped with the data analysis. DS and HT helped with revision of the manuscript. All authors contributed to the article and approved the submitted version.

Funding

This research received financial support from the National Natural Science Foundation of China (32070059). We acknowledge funding from the Technology Innovation Project of Chengdu Science and Technology Bure (2021-YF05-01197-SN) and Natural Science Foundation of Sichuan (2022NSFSC1634).

Conflict of interest

The authors declare that the research was conducted in the absence of any commercial or financial relationships that could be construed as a potential conflict of interest.

Publisher's note

All claims expressed in this article are solely those of the authors and do not necessarily represent those of their affiliated organizations, or those of the publisher, the editors and the reviewers. Any product that may be evaluated in this article, or claim that may be made by its manufacturer, is not guaranteed or endorsed by the publisher.

Supplementary material

The Supplementary material for this article can be found online at: https://www.frontiersin.org/articles/10.3389/fmicb.2022.1085000/full#supplementary-material

References

Adnan, M., Zheng, W., Islam, W., Arif, M., Abubakar, Y. S., Wang, Z., et al. (2017). Carbon catabolite repression in filamentous fungi. *Int. J. Mol. Sci.* 19:48. doi: 10.3390/ijms19010048

Alazem, M., and Lin, N.-S. (2017). Antiviral roles of abscisic acid in plants. *Front. Plant Sci.* 8:1760. doi: 10.3389/fpls.2017.01760

Amselem, J., Cuomo, C. A., Van Kan, J. A., Viaud, M., Benito, E. P., Couloux, A., et al. (2011). Genomic analysis of the necrotrophic fungal pathogens *Sclerotinia sclerotiorum* and *Botrytis cinerea*. *PLoS Genet.* 7:E1002230. doi: 10.1371/journal.pgen.1002230

An, B., Li, B., Qin, G., and Tian, S. (2015). Function of small Gtpase Rho3 in regulating growth, conidiation and virulence of *Botrytis cinerea*. *Fungal Genet. Biol.* 75, 46–55. doi: 10.1016/j.fgb.2015.01.007

Ariño, J., Velázquez, D., and Casamayor, A. (2019). Ser/Thr protein phosphatases in fungi: structure, regulation And function. *Microb. Cell* 6, 217–256. doi: 10.15698/mic2019.05.677

Cardozo, T., and Pagano, M. (2004). The Scf ubiquitin ligase: insights into a molecular machine. *Nat. Rev. Mol. Cell Biol.* 5, 739–751. doi: 10.1038/nrm1471

Chen, X.-L., Yang, J., and Peng, Y.-L. (2011). Large-scale insertional mutagenesis in *Magnaporthe oryzae* by agrobacterium tumefaciens-mediated transformation. *Methods Mol. Biol.* 722, 213–224. doi: 10.1007/978-1-61779-040-9_16

Chen, X., Zhu, C., Na, Y., Ren, D., Zhang, C., He, Y., et al. (2021). Compartmentalization of melanin biosynthetic enzymes contributes to self-defense against intermediate compound scytalone in *Botrytis cinerea*. *MBio* 12, E00007–E00021. doi: 10.1128/mBio.00007-21

Cheung, N., Tian, L., Liu, X., and Li, X. (2020). The destructive fungal pathogen *Botrytis cinerea*—insights from genes studied with mutant analysis. *Pathogens* 9:923. doi: 10.3390/pathogens9110923

Choquer, M., Robin, G., Le Pêcheur, P., Giraud, C., Levis, C., and Viaud, M. (2008). Ku70 or Ku80 deficiencies in the fungus *Botrytis cinerea* facilitate targeting of genes that are hard to knock out in a wild-type context. *FEMS Microbiol. Lett.* 289, 225–232. doi: 10.1111/j.1574-6968.2008.01388.x

Dalmais, B., Schumacher, J., Moraga, J., Le Pecheur, P., Tudzynski, B., Collado, I. G., et al. (2011). The *Botrytis cinerea* phytotoxin botcinic acid requires two polyketide synthases for production and has a redundant role in virulence with botrydial. *Mol. Plant Pathol.* 12, 564–579. doi: 10.1111/j.1364-3703.2010.00692.x

De Assis, L. J., Ulas, M., Ries, L. N. A., El Ramli, N. A. M., Sarikaya-Bayram, O., Braus, G. H., et al. (2018). Regulation of *Aspergillus nidulans* crea-mediated catabolite repression by the F-box proteins Fbx23 and Fbx47. *MBio* 9, e00840–e00818. doi: 10.1128/mBio.00840-18

De Simone, N., Pace, B., Grieco, F., Chimienti, M., Tyibilika, V., Santoro, V., et al. (2020). *Botrytis cinerea* and table grapes: a review of the main physical, chemical, and bio-based control treatments in post-harvest. *Foods* 9:1138. doi: 10.3390/foods9091138

Ding, Z. T., Zhang, Z., Luo, D., Zhou, J. Y., Zhong, J., Yang, J., et al. (2015). Gene overexpression and RNA silencing tools for the genetic manipulation of the S-(+)-abscisic acid producing ascomycete *Botrytis cinerea*. *Int. J. Mol. Sci.* 16, 10301–10323. doi: 10.3390/ijms160510301

Ding, Z., Zhang, Z., Zhong, J., Luo, D., Zhou, J., Yang, J., et al. (2016). Comparative transcriptome analysis between an evolved abscisic acid-overproducing mutant *Botrytis cinerea* Tbc-A and its ancestral strain *Botrytis cinerea* Tbc-6. *Sci. Rep.* 6:37487. doi: 10.1038/srep37487

Dou, T., Wang, J., Liu, Y., Jia, J., Zhou, L., Liu, G., et al. (2022). A combined transcriptomic and proteomic approach to reveal the effect of mogroside V on ova-induced pulmonary inflammation in mice. *Front. Immunol.* 13:919. doi: 10.3389/fimmu.2022.800143

Dulermo, T., Rascle, C., Billon-Grand, G., Gout, E., Bligny, R., and Cotton, P. (2010). Novel insights into mannitol metabolism in the fungal plant pathogen *Botrytis cinerea*. *Biochem. J.* 427, 323–332. doi: 10.1042/BJ20091813

Duyvesteijn, R. G. E., Van Wijk, R., Boer, Y., Rep, M., Cornelissen, B. J. C., and Haring, M. A. (2005). Frp1 is a *Fusarium oxysporum* F-box protein required for pathogenicity on tomato. *Mol. Microbiol.* 57, 1051–1063. doi: 10.1111/j.1365-2958.2005.04751.x

Fang, C., Ye, Z., Gai, T., Lu, K., Dai, F., Lu, C., et al. (2021). Dia-based proteome reveals the involvement of cuticular proteins and lipids in the wing structure construction in the silkworm. *J. Proteome* 238:104155. doi: 10.1016/j.jprot.2021.104155

Fekete, E., Karaffa, L., Sándor, E., Bányai, I., Seiboth, B., Gyémánt, G., et al. (2004). The alternative D-Galactose degrading pathway of *Aspergillus nidulans* proceeds via L-sorbose. *Arch. Microbiol.* 181, 35–44. doi: 10.1007/s00203-003-0622-8

Gabriel, R., Thieme, N., Liu, Q., Li, F., Meyer, L. T., Harth, S., et al. (2021). The F-box protein gene Exo-1 is a target for reverse engineering enzyme hypersecretion in filamentous fungi. *Proc. Natl. Acad. Sci.* 118:E2025689118. doi: 10.1073/pnas.2025689118

Gietler, M., Fidler, J., Labudda, M., and Nykiel, M. (2020). Abscisic acid—enemy or savior in the response of cereals to abiotic and biotic stresses? *Int. J. Mol. Sci.* 21:4607. doi: 10.3390/ijms21134607

Gill, A., and Patranabis, S. (2021). Phytohormones as potential anticancer agents. *Int. J. Res. Appl. Sci. Biotechnol.* 8, 37–43. doi: 10.31033/ijrasb.8.3.7

Gong, T., Shu, D., Yang, J., Ding, Z. T., and Tan, H. (2014). Sequencing and transcriptional analysis of the biosynthesis gene cluster of abscisic acid-producing *Botrytis cinerea*. *Int. J. Mol. Sci.* 15, 17396–17410. doi: 10.3390/ijms151017396

Gronover, C. S., Kasulke, D., Tudzynski, P., and Tudzynski, B. (2001). The role of G protein alpha subunits in the infection process of the gray mold fungus *Botrytis cinerea*. *Mol. Plant-Microbe Interact.* 14, 1293–1302. doi: 10.1094/MPMI.2001.14.11.1293

Heinekamp, T., Thywißen, A., Macheleidt, J., Macheleidt, J., Keller, S., Valiante, V., et al. (2013). Aspergillus fumigatus melanins: interference with the host endocytosis pathway and impact on virulence. *Front. Microbiol.* 3:440. doi: 10.3389/fmicb.2012.00440

Hewage, K. A. H., Yang, J. F., Wang, D., Hao, G. F., Yang, G. F., and Zhu, J. K. (2020). Chemical manipulation of abscisic acid signaling: a new approach to abiotic and biotic stress management in agriculture. *Adv. Sci.* 7:2001265. doi: 10.1002/advs.202001265

Jacobson, E. S. (2000). Pathogenic roles for fungal melanins. *Clin. Microbiol. Rev.* 13, 708–717. doi: 10.1128/CMR.13.4.708

Jia, R., Hou, Y., Feng, W., Li, B., and Zhu, J. (2022). Alterations at biochemical, proteomic and transcriptomic levels in liver of tilapia (*Oreochromis niloticus*) under chronic exposure to environmentally relevant level of glyphosate. *Chemosphere* 294:133818. doi: 10.1016/j.chemosphere.2022.133818

Johnk, B., Bayram, O., Abelmann, A., Heinekamp, T., Mattern, D. J., Brakhage, A. A., et al. (2016). Scf ubiquitin ligase F-box protein Fbx15 controls nuclear co-repressor localization, stress response and virulence of the human pathogen *Aspergillus fumigatus*. *PLoS Pathog.* 12:e1005899. doi: 10.1371/journal.ppat.1005899

Jonkers, W., and Rep, M. (2009a). Lessons from fungal F-Box proteins. *Eukaryot. Cell* 8, 677–695. doi: 10.1128/EC.00386-08

Jonkers, W., and Rep, M. (2009b). Mutation of Cre1 in *Fusarium oxysporum* reverts the pathogenicity defects of the Frp1 deletion mutant. *Mol. Microbiol.* 74, 1100–1113. doi: 10.1111/j.1365-2958.2009.06922.x

Jonkers, W., Van Kan, J. A. L., Tijm, P., Lee, Y. W., Tudzynski, P., Rep, M., et al. (2011). The Frp1 F-box gene has different functions in sexuality, pathogenicity and metabolism in three fungal pathogens. *Mol. Plant Pathol.* 12, 548–563. doi: 10.1111/j.1364-3703.2010.00689.x

Jonkers, W., Rodrigues, C. D. A., and Rep, M. (2009). Impaired colonization and infection of tomato roots by the Deltafrp1 mutant of Fusarium oxysporum correlates with reduced CWDE gene expression. *Mol Plant Microbe Interact.* 22, 507–518. doi: 10.1094/MPMI-22-5-0507

Kato, A., Kurashima, K., Chae, M., Sawada, S., Hatakeyama, S., Tanaka, S., et al. (2010). Deletion of a novel F-box protein, Mus-10, in *Neurospora crassa* leads to altered mitochondrial morphology, instability of Mtdna and senescence. *Genetics* 185, 1257–1269. doi: 10.1534/genetics.110.117200

Kim, D., Langmead, B., and Salzberg, S. L. (2015). Hisat: a fast spliced aligner with low memory requirements. *Nat. Methods* 12, 357–360. doi: 10.1038/nmeth.3317

Kokkelink, L., Minz, A., Al-Masri, M., Giesbert, S., Barakat, R., Sharon, A., et al. (2011). The small Gtpase Bccdc42 affects nuclear division, germination and virulence of the gray mold fungus *Botrytis cinerea*. *Fungal Genet. Biol.* 48, 1012–1019. doi: 10.1016/j.fgb.2011.07.007

Leavitt, S. D., Fernández-Mendoza, F., Pérez-Ortega, S., Sohrabi, M., Divakar, P. K., Vondrák, J., et al. (2013). Local representation of global diversity in a cosmopolitan lichen-forming fungal species complex (Rhizoplaca, Ascomycota). *J. Biogeogr.* 40, 1792–1806. doi: 10.1111/jbi.12118

Leyronas, C., Bardin, M., Duffaud, M., and Nicot, P. C. (2015). Compared dynamics of grey mould incidence and genetic characteristics of *Botrytis cinerea* in neighbouring vegetable greenhouses. *J. Plant Pathol.* 97, 439–447. doi: 10.4454/JPP.V97I3.003

Li, B., and Dewey, C. N. (2011). Rsem: accurate transcript quantification from RNA-Seq data with or without a reference genome. *BMC Bioinform.* 12:323. doi: 10.1186/1471-2105-12-323

Lievens, L., Pollier, J., Goossens, A., Beyaert, R., and Staal, J. (2017). Abscisic acid as pathogen effector and immune regulator. *Front. Plant Sci.* 8:587. doi: 10.3389/fpls.2017.00587

Liu, T.-B., Wang, Y., Stukes, S., Chen, Q., Casadevall, A., and Xue, C. (2011). The F-box protein Fbp1 regulates sexual reproduction and virulence in *Cryptococcus neoformans*. *Eukaryot. Cell* 10, 791–802. doi: 10.1128/EC.00004-11

Long, S., Yang, Y., Shen, C., Wang, Y., Deng, A., Qin, Q., et al. (2020). Metaproteomics characterizes human gut microbiome function in colorectal cancer. *NPJ Biofilms Microbiomes* 6, 1–10. doi: 10.1038/s41522-020-0123-4

Love, M. I., Huber, W., and Anders, S. (2014). Moderated estimation of fold change and dispersion for RNA-Seq data with Deseq2. *Genome Biol.* 15, 1–21. doi: 10.1186/s13059-014-0550-8

Marumo, S., Katayama, M., Komori, E., Ozaki, Y., Natsume, M., and Kondo, S. (1982). Microbial production of abscisic acid by *Botrytis cinerea*. *Agric. Biol. Chem.* 46, 1967–1968.

Masso-Silva, J., Espinosa, V., Liu, T.-B., Wang, Y., Xue, C., and Rivera, A. (2018). The F-box protein Fbp1 shapes the immunogenic potential of *Cryptococcus neoformans*. *MBio* 9, E01828–E01817. doi: 10.1128/mBio.01828-17

Miesel, L., Greene, J., and Black, T. A. (2003). Genetic strategies for antibacterial drug discovery. *Nat. Rev. Genet.* 4, 442–456. doi: 10.1038/nrg1086

Minz Dub, A., Kokkelink, L., Tudzynski, B., Tudzynski, P., and Sharon, A. (2013). Involvement of *Botrytis cinerea* small Gtpases Bcras1 and Bcrac in differentiation, virulence, and the cell cycle. *Eukaryot. Cell* 12, 1609–1618. doi: 10.1128/EC.00160-13

Modi, A., Vai, S., Caramelli, D., and Lari, M. (2021). The Illumina sequencing protocol and the Novaseq 6000 system. *Methods Mol. Biol.* 2242, 15–42. doi: 10.1007/978-1-0716-1099-2_2

Nambara, E., and Marion-Poll, A. (2005). Abscisic acid biosynthesis and catabolism. *Annu. Rev. Plant Biol.* 56, 165–185. doi: 10.1146/annurev.arplant.56.032604.144046

Rolland, S., Jobic, C., Fevre, M., and Bruel, C. (2003). Agrobacterium-mediated transformation of *Botrytis cinerea*, simple purification of monokaryotic transformants and rapid conidia-based identification of the transfer-DNA host genomic DNA flanking sequences. *Curr. Genet.* 44, 164–171. doi: 10.1007/s00294-003-0438-8

Sadat, M., Ullah, M., Bashar, K. K., Hossen, Q. M., Tareq, M., and Islam, M. (2021). Genome-wide identification of F-box proteins in *Macrophomina phaseolina* and comparison with other fungus. *J. Genet. Eng. Biotechnol.* 19, 1–14. doi: 10.1186/s43141-021-00143-0

Sakthivel, P., Sharma, N., Klahn, P., Gereke, M., and Bruder, D. (2016). Abscisic acid: a phytohormone and mammalian cytokine as novel pharmacon with potential for future development into clinical applications. *Curr. Med. Chem.* 23, 1549–1570. doi: 10.2174/0929867323666160405113129

Sharma, M., Verma, V., and Bairwa, N. K. (2021). Genetic interaction between Rlm1 and F-box motif encoding gene Saf1 contributes to stress response in *Saccharomyces cerevisiae*. *Genes Environ.* 43, 1–15. doi: 10.1186/s41021-021-00218-x

Shu, D., Tan, H., Zhou, J., Luo, D., Yang, J., Ding, Z. T., et al. (2018). New sesquiterpene cyclase BcABA3 useful for synthesizing 2Z, 4E-alpha-ionylideneehane or abscisic acid, preferably D-abscisic acid, comprises amino acid sequence. CHN Patent No.: CN108753744B. Beijing, China: China National Intellectual Property Administration.

Siegmund, U., Heller, J., Van Kann, J. A., and Tudzynski, P. (2013). The Nadph oxidase complexes in *Botrytis cinerea*: evidence for a close association with the Er and the Tetraspanin Pls1. *PLoS One* 8:E55879. doi: 10.1371/journal.pone.0055879

Siewers, V., Kokkelink, L., Smedsgaard, J., and Tudzynski, P. (2006). Identification of an abscisic acid gene cluster in the grey mold *Botrytis cinerea*. *Appl. Environ. Microbiol.* 72, 4619–4626. doi: 10.1128/AEM.02919-05

Siewers, V., Smedsgaard, J., and Tudzynski, P. (2004). The P450 monooxygenase Bcaba1 is essential for abscisic acid biosynthesis in *Botrytis cinerea*. *Appl. Environ. Microbiol.* 70, 3868–3876. doi: 10.1128/AEM.70.7.3868-3876.2004

Takino, J., Kozaki, T., Sato, Y., Liu, C., Ozaki, T., Minami, A., et al. (2018). Unveiling biosynthesis of the phytohormone abscisic acid in fungi: unprecedented mechanism of core scaffold formation catalyzed by an unusual sesquiterpene synthase. *J. Am. Chem. Soc.* 140, 12392–12395. doi: 10.1021/jacs.8b08925

Wang, Y., Zhou, J., Zhong, J., Luo, D., Li, Z., Yang, J., et al. (2018). Cys_2his_2 zinc finger transcription factor Bcabar1 positively regulates abscisic acid production in *Botrytis cinerea*. *Appl. Environ. Microbiol.* 84, e00920–e00918. doi: 10.1128/AEM.00920-18

Wei, Z., Shu, D., Sun, Q., Chen, D. B., Li, Z. M., Luo, D., et al. (2022). The BcLAE1 is involved in the regulation of ABA biosynthesis in Botrytis cinerea TB-31. *Front. Microbiol.* 13:969499. doi: 10.3389/fmicb.2022.969499. PMID: 35992717; PMCID: PMC9386520.

Willems, A. R., Schwab, M., and Tyers, M. (2004). A hitchhiker's guide to the cullin ubiquitin ligases: Scf and its kin. *BBA-Mol. Cell. Res.* 1695, 133–170. doi: 10.1016/j.bbamcr.2004.09.027

Wu, T., Fan, C.-L., Han, L.-T., Guo, Y.-B., and Liu, T.-B. (2022). Role of F-box protein Cdc4 in fungal virulence and sexual reproduction of *Cryptococcus neoformans*. *Front. Cell. Infect. Microbiol.* 11:806465. doi: 10.3389/fcimb.2021.806465

Yu, J. H., Hamari, Z., Han, K. H., Seo, J. A., Reyes-Domínguez, Y., and Scazzocchio, C. (2004). Double-joint Pcr: a Pcr-based molecular tool for gene manipulations in filamentous fungi. *Fungal Genet. Biol.* 41, 973–981. doi: 10.1016/j.fgb.2004.08.001

Zhang, C., He, Y., Zhu, P., Chen, L., and Xu, L. (2015). Loss of Bcbrn1 and Bcpks13 in *Botrytis cinerea* not only blocks melanization but also increases vegetative growth and virulence. *Mol. Plant-Microbe Interact.* 28, 1091–1101. doi: 10.1094/MPMI-04-15-0085-R

Frontiers in Microbiology

Explores the habitable world and the potential of microbial life

The largest and most cited microbiology journal which advances our understanding of the role microbes play in addressing global challenges such as healthcare, food security, and climate change.

Discover the latest Research Topics

See more →

Frontiers

Avenue du Tribunal-Fédéral 34
1005 Lausanne, Switzerland
frontiersin.org

Contact us

+41 (0)21 510 17 00
frontiersin.org/about/contact